INSULATION MATERIALS

4th Volume

Testing and Applications

André O. Desjarlais
Robert R. Zarr
EDITORS

STP 1426

STP 1426

Insulation Materials: Testing and Applications: 4th Volume

André O. Desjarlais and Robert R. Zarr, editors

ASTM Stock Number: STP1426

ASTM International
100 Barr Harbor Drive
PO Box C700
West Conshohocken, PA 19428-2959

Printed in the U. S. A.

ISBN: 0-8031-2898-3
ISSN: 1058-1170

Photocopy Rights

Peer Review Policy

Each paper published in this volume was evaluated by two peer reviewers and at least one editor. The authors addressed all of the reviewers' comments to the satisfaction of both the technical editor(s) and the ASTM Committee on Publications.

To make technical information available as quickly as possible, the peer-reviewed papers in this publication were prepared "camera-ready" as submitted by the authors.

The quality of the papers in this publication reflects not only the obvious efforts of the authors and the technical editor(s), but also the work of the peer reviewers. In keeping with long-standing publication practices, ASTM maintains the anonymity of the peer reviewers. The ASTM Committee on Publications acknowledges with appreciation their dedication and contribution of time and effort on behalf of ASTM.

Printed in Bridgeport, NJ
October 2002

Foreword

The Fourth Symposium on Insulation Materials: Testing and Applications was held in Charleston, South Carolina on 21–22 Oct. 2002. ASTM Committee C-16 on Thermal Insulation served as its sponsor. The symposium chairs and co-editors of this publication were André O. Desjarlais, Oak Ridge National Laboratory, and Robert R. Zarr, National Institute of Standards and Technology.

Contents

Overview

Since its founding in 1938, ASTM Committee C16 on Thermal Insulation has hosted over a dozen symposia pertaining to thermal insulation and its use to increase energy efficiency in residential, commercial, and industrial applications. This Special Technical Publication is the latest product of the most recent of these symposia.

Since the last symposia held in 1997 in Quebec City, significant advances have been made in many aspects of thermal engineering. On the materials side of the ledger, vacuum panel insulations have been developed and a materials specification covering these unique insulation products is now available. The cellular plastic insulation industry has been asked once again to re-engineer their products to address global climate change issues associated with their blowing agents. On the experimental side, we continue to test how good our test methods are through round robins so that we can continue to improve them. Finally, we are developing keen interests in moisture-related material properties as a greater number of building envelope failures appear to be caused by improper moisture control.

The existence of this STP is due to the tremendous efforts of many people. In particular, we would like to thank the symposium organizing committee, the session chairpersons, and all of the authors and reviewers that donated their time to this effort. Special thanks are due to Dorothy Fitzpatrick and Crystal Kemp at ASTM for the organizational skills and their support.

Finally, the editors would like to dedicate this STP to their colleague and close friend David McElroy. Throughout his long association with ASTM Committee C16 on Thermal Insulation, Dave has inspired us with his immeasurable contributions. When he spoke, we all listened because we knew that his comments were well thought out and without bias. There was hardly a ballot item that did not benefit from Dave's critical examination and review. Thankfully, he was always the gentleman and only submitted comments! He will be sorely missed both during and after the business portion of the meetings. Dave, we wish you the best of luck and happiness in whatever endeavor you pursue.

André O. Desjarlais
Oak Ridge National Laboratory
Oak Ridge, TN

Robert R. Zarr
National Institute of Standards and Technology
Gaithersburg, MD

Session 1: Thermal, Mechanical, and Hygric Properties

Robert R. Zarr[1] and James J. Filliben[1]

An International Study of Guarded Hot Plate Laboratories Using Fibrous Glass and Expanded Polystyrene Reference Materials

---

Reference: Zarr, R. R. and Filliben, J. J., **"An International Study of Guarded Hot Plate Laboratories Using Fibrous Glass and Expanded Polystyrene Reference Materials,"** *Insulation Materials: Testing and Applications: 4th Volume, ASTM STP 1426*, A. O. Desjarlais and R. R. Zarr, Eds., ASTM International, West Conshohocken, PA, 2002.

Abstract: Thermal conductivity measurements of four thermal insulation reference materials are presented. The measurements were obtained from an international study of guarded-hot-plate laboratories in Canada, France, Japan, the United Kingdom, and the United States. For each reference material, the study requires five independent replicate measurements at a fixed temperature of 297.15 K, and single-point measurements at 280 K, 290 K, 300 K, 310 K, and 320 K. An important finding from the replicate analysis is the existence of a laboratory-material interaction; that is, there are laboratory-to-laboratory differences in both location and variation that change from material to material. The major underlying source for the variability (both within- and between-laboratory) in the replicate data is discussed. The analysis of the multi-temperature (280 K to 320 K) data supports the laboratory-material interaction as exhibited in the fixed-temperature replicate data. The multi-temperature analysis also reveals an increasing difference between laboratories as the temperature departs from 297.15 K.

Keywords: certified reference material, guarded hot plate, interlaboratory, reference materials, thermal insulation, thermal conductivity, SRM

Introduction

In 1996, an ASTM C-16 Workshop on thermal insulation Standard Reference Materials (SRMs) identified concerns with the transference of national reference materials across international borders [*1*]. Responding to similar concerns in Europe, the National Physical Laboratory began to organize an international study of guarded-hot-plate apparatus in national standards laboratories in Canada, France, Japan, United Kingdom, and United States in 1997. The purpose of the study was to assess the measurement variability among test results of five laboratory participants: the National

[1] Mechanical Engineer and Mathematical Statistician, respectively, National Institute of Standards and Technology, 100 Bureau Drive, Gaithersburg, MD, 20899-8632.

Research Council Canada (NRCC), Laboratoire National d'Essais (LNE), Japan Testing Center for Construction Materials (JTCCM), the National Physical Laboratory (NPL), and the National Institute of Standards and Technology (NIST). The study investigated one regional and three national reference materials. Ten specimens of each material were distributed to the participants by an issuing organization (or delegate laboratory).

This study requested two sets of data: 1) five replicate measurements of each specimen at 297.15 K (24 °C); and 2) individual (single-point) measurements at 280 K, 290 K, 300 K, 310 K, and 320 K. The test results were conducted in accordance with either International Standard Thermal Insulation–Determination of Steady-State Areal Thermal Resistance and Related Properties–Guarded Hot Plate Apparatus Test Method (ISO 8302) or ASTM Test Method for Steady-State Heat Flux Measurements and Thermal Transmission Properties by Means of the Guarded Hot Plate Apparatus, (C 177). A detailed analysis of the resulting data has been provided to the laboratory participants [*2*] and a summary of the results has been recently presented [*3*]. The present paper focuses primarily on the replicate thermal conductivity data at 297.15 K (24 °C).

Reference Materials

The reference materials were selected to test a wide – yet manageable – variety of insulation materials from Asia, Europe, and North America. Table 1 summarizes the reference materials by designation, description, density (ρ), thickness (L), temperature range (T), source, and reference. Materials 1 through 3 were fibrous in composition, ranging from 13 kg/m^3 to 200 kg/m^3. Material 4 was a molded-beads, expanded polystyrene board (38 kg/m^3). Material 3, which is a mixture of glass and mineral oxides fibers having high-temperature capabilities, is currently undergoing an internal review process for certification. Each issuing laboratory was responsible for characterizing and distributing 10 specimens of the reference material to the laboratory participants [*2*]. The European Commission Institute for Reference Materials and Measurements (IRMM) agreed to provide specimens of Certified Reference Material IRMM-440 to NPL for characterization and distribution to the participants. As a side note, the NIST Standard Reference Material Program has officially designated SRM 1451 as obsolete due to historically low customer demand. (Although obsolete, SRM 1451 is available from the Building and Fire Research Laboratory at NIST.) Comparisons of the test results with predicted values of the NIST Standard Reference Materials have been presented previously [*2,3*].

Table 1 – *Reference Materials*

ID	Designation	Description	ρ (kg/m^3)	L (mm)	T (K)	Source and Reference
1	SRM 1451	Fibrous glass blanket	13	25	100 to 330	NIST [*4*]
2	IRMM-440	Resin-bonded glass fibre board	70	35	263 to 323	IRMM [*5*]
3	JTCCM candidate	Mineral-oxide fiberboard	200	25	---	JTCCM
4	SRM 1453	Expanded polystyrene board	38	13	285 to 310	NIST [*6*]

Laboratory Apparatus

Table 2 summarizes the major parameters of the guarded-hot-plate apparatus used in this study. Each laboratory determined values for their relative expanded uncertainty (U), *independently* of this study, based on international guidelines [7]. The relative expanded uncertainties reported here for a coverage factor of $k = 2$ represent a level of confidence of approximately 95% [7]. The expanded uncertainty defines an interval about the result of a measurement that may be expected to encompass a large fraction of the distribution of values that could reasonably be attributed to the measurand (λ).

Table 2 – *Laboratory Guarded-Hot-Plate Apparatus*

Parameter	JTCCM	LNE	NIST	NPL	NRCC
ID	1	2	3	4	5
Plate, mm	300×300	610×610	1016 ϕ	610×610	610×610
Meter plate, mm	150×150	300×300	406.4 ϕ	305.2×305.2	250×250
Plate emittance	0.9	0.86 ± 0.05	0.89	>0.9	0.89
Edge guarding	Condition air	[1]	Condition air	[2]	Glass-fiber
Type of heater	Distributed	Distributed	Line source	Distributed	Distributed
Temperature sensor	Type T	Type K	PRT[3]	Type E	Type T
Operation mode	2-sided	2-sided	2-sided	1-sided	2-sided
U (k=2) (%)	Not reported	1.5	1.5 (IRMM-440) 1.0 (others)	1.2	1.0

[1] Edge insulation, temperature controlled peripheral guard and additional outer edge insulation
[2] Linear temperature gradient edge guard and 100 mm expanded polystyrene
[3] Platinum resistance thermometer

Test Protocol

Under steady-state conditions, measurements of thermal conductivity[2] (λ) for the pair of specimens are determined using the following equation:

$$Q = \lambda \, 2A \frac{\Delta T}{L} \tag{1}$$

where Q is the heat flow (W) through the meter area of the specimens; $2A$ is the meter area normal to direction of heat flow (m^2); ΔT (K) is the temperature difference across the specimen hot (T_h) and cold surfaces (T_c); and, L (m) is the in-situ thickness of the pair of specimens. Values of λ are reported at the mean temperature, $T_m = (T_h + T_c)/2$.

For a single-sided mode of operation (Table 2), a single specimen is placed between the hot and cold plates of the apparatus. The other specimen is replaced with an auxiliary piece of insulation. The auxiliary guard plate is maintained at the same temperature as

[2] The thermal transmission properties of heat insulation determined from standard test methods typically include several mechanisms of heat transfer, including conduction, radiation, and possibly convection. For that reason, some experimentalists will include the adjective "apparent" when describing thermal conductivity of thermal insulation. However, for brevity, the term thermal conductivity will be used in this paper.

the hot plate. For determining λ in the single-sided case, Eq 2 is modified slightly by taking a meter area (A) coefficient of unity.

Each participant was requested to conduct five replicate measurements for each pair of specimens at 297.15 K (24 °C) and a temperature difference of 20 K (100 observations). The operator was requested to remove the specimens from the apparatus after each measurement and re-install the specimens after sufficient conditioning. After completion of the replicate measurements, thermal conductivity measurements were conducted for each material at 280 K, 290 K, 300 K, 310 K, and 320 K and a temperature difference of 20 K (100 observations). The multi-temperature tests were conducted in random order; however, the specimens were not removed from the apparatus between temperature settings.

Except for SRM 1451, the materials were tested at thicknesses determined by each laboratory with the only provision that the clamping pressure exerted on the specimens by the measuring equipment was limited from 1000 Pa to 2000 Pa. For SRM 1451, the test thickness was limited to 25.4 mm by utilizing spacer stops placed at the perimeter of the specimen to prevent over-compression of the material during testing. The use of spacer stops for the other materials (for example, limiting plate movement due to specimen creep, if any) was left to the operator's discretion. The test data were recorded in SI units on "official" data forms and returned to NIST for analysis.

Fixed Temperature (297.15 K) Replicate Data

Figure 1 plots the measurements of λ (297.15 K) versus laboratory (identified[3] in Table 2) for each of the four materials (Table 1). For each laboratory, the replicate observations are offset along the x-axis to assess trends in the run-sequence of an individual laboratory. For laboratories 2, 3, 4, and 5, the data points include symmetric error bars representing the respective laboratory's estimate of expanded uncertainty (U) for λ (Table 2). The major conclusions from Figure 1 are as follows:

1) For materials 1, 2, and 3, the laboratories differed in average response.
2) In contrast, for material 4, the average laboratory responses were essentially the same.
3) For materials 1 and 2, laboratory 1 had a significantly high average response.
4) For materials 1, 2, and 3, laboratory 2 was consistently higher than laboratory 3.
5) For material 3, laboratory 4 was significantly low.
6) The differences between the five laboratories changed from material to material – that is, there is a laboratory-material interaction.

[3] While planning this study, the laboratory participants decided that the international user communities would derive maximum benefit by open presentation of the data; hence, the data are *not* presented anonymously.

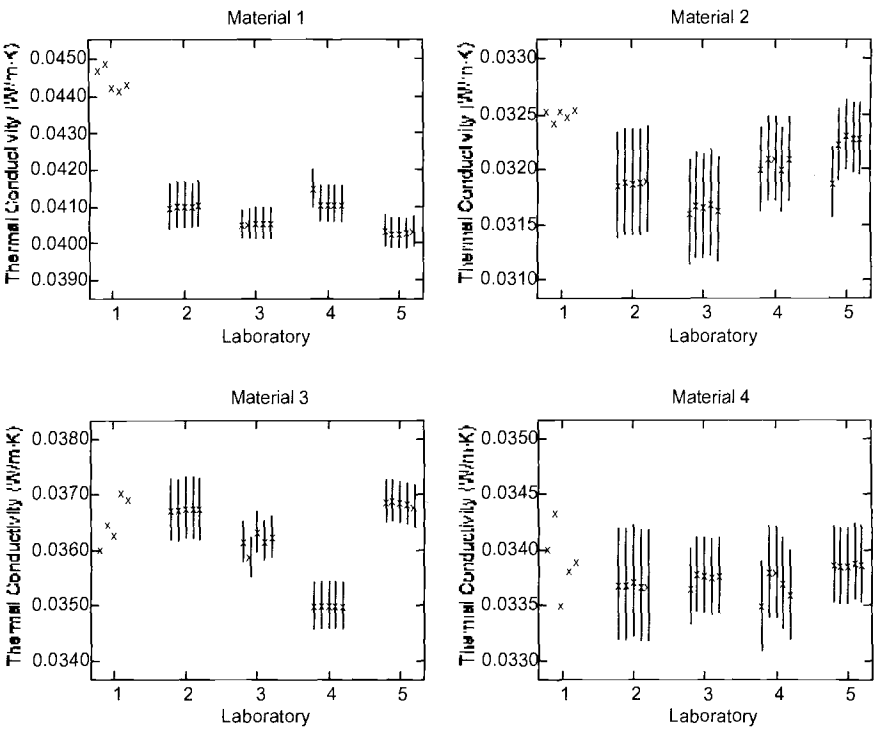

Figure 1 – *Replicate data (297.15 K) versus laboratory. Error bars equal laboratory expanded uncertainty (Table 2).*

Summary Statistics

The statistical treatment of interlaboratory data typically involves determining location and variation parameters based on an assumed underlying model for the data. For the fixed temperature (297.15 K) replicate data, there are two primary factors: laboratory (5 levels) and reference material (4 levels). Thus, the underlying model for these data is assumed to have the following form:

$$y = a_{ij} + \varepsilon \tag{2}$$

where y is the response variable λ, a_{ij} is a constant for laboratory i and material j, and ε is error. The effect of temperature as a primary factor, from 280 K to 320 K, is discussed later.

Table 3 summarizes the mean values (location) and standard deviations (variation) for the replicate data (100 observations). Each entry represents the local (5 observations) mean ($\bar{\lambda}$) or standard deviation (SD(λ)), respectively, for a particular laboratory. The last column provides the respective grand or "pooled" statistic (25 observations) for each

laboratory (across all materials). The last row in each table provides the respective grand or "pooled" statistic (25 observations) for each material (across all laboratories).

Table 3a – *Means for Replicates (297.15 K)*

Lab	Material 1 $\bar{\lambda}$ (W/m K)	Material 2 $\bar{\lambda}$ (W/m K)	Material 3 $\bar{\lambda}$ (W/m K)	Material 4 $\bar{\lambda}$ (W/m K)	Lab Average (W/m K)
1	0.04448	0.03251	0.03655	0.03391	0.03686
2	0.04104	0.03189	0.03675	0.03369	0.03584
3	0.04055	0.03166	0.03616	0.03375	0.03553
4	0.04118	0.03206	0.03500	0.03368	0.03548
5	0.04032	0.03220	0.03686	0.03387	0.03581
Average	0.04151	0.03206	0.03626	0.03378	0.03591

Table 3b – *Standard Deviations for Replicates (297.15 K)*

Lab	Material 1 SD (λ) (W/m K)	Material 2 SD (λ) (W/m K)	Material 3 SD (λ) (W/m K)	Material 4 SD (λ) (W/m K)	Pooled SD (W/m K)
1	0.00032	0.00005	0.00043	0.00030	0.00031
2	0.00003	0.00002	0.00002	0.00002	0.00002
3	0.00002	0.00004	0.00017	0.00005	0.00009
4	0.00018	0.00005	0.00000	0.00013	0.00011
5	0.00003	0.00018	0.00004	0.00001	0.00009
Pooled SD	0.00016	0.00009	0.00021	0.00015	0.00016

The last column in Table 3a reveals that the average of laboratory 1 across all four materials is consistently higher than the other laboratories. On the average across all four materials, laboratories 2 and 5, and 3 and 4, are closely paired and each pair of laboratories differs by about 0.8%. The last column in Table 3b reveals that laboratory 1 is consistently noisy across all four materials. Laboratories 3, 4, and 5 exhibit similar levels of variability while laboratory 2 is extremely precise (by nearly a factor of 5 in comparison to the other three laboratories) across all four materials.

Treatment of Anomalous Data

The results from Figure 1 and Table 3 reveal that the test results for materials 1 and 3 from laboratories 1 and 4, respectively, are significantly different than the other laboratories. In general, the treatment of anomalous (or outlying) data can be handled either by retaining, correcting, or deleting the data. Obviously, none of these options are completely satisfactory; however, the third option (deletion) is acceptable when a physical cause can be identified to explain the behavior of the data. For interlaboratory studies, it is extremely helpful (and inevitably necessary) for the laboratories in question to present their own explanations for the behavior of the test results. To their credit, laboratories 1 and 4 did provide explanations for their anomalous data.

After submission of their test data, laboratory 1 reported that the surface temperatures for determinations of specimen ΔT were measured using 0.2-mm-diameter

thermocouples placed directly on the surface of the specimen with adhesive tape. In contrast, the other laboratories utilized temperature sensors permanently mounted in the heating and cooling surfaces.[4] It is surmised that much of the variability observed in Figure 1 could be attributed to the technique of affixing thermocouples to the specimen surface. An early comparison of guarded hot plates [*8*] noted that discrepancies could result between conductivity values obtained using temperatures from plate surfaces and those measured using surface thermocouples. These data for laboratory 1 and material 1 were considered sufficiently different from the others to warrant rejection as an outlying observation and were omitted in further analyses of the replicate data.

For material 3, laboratory 4 reported values of λ that are 3.5% below the grand mean for material 3. In the comment section of their official test report form, laboratory 4 reported that, "this material had completely delaminated on arrival so that the test specimen consisted of two pieces which were always aligned in the same orientation with respect to each other whilst testing." Unfortunately, although laboratory 4 made a notable effort to test material 3, the specimens received by laboratory 4 were physically different than those received by the other laboratories. Since no other laboratories reported similar experiences, this set of data for material 3 was considered sufficiently different from the other specimens to warrant rejection as an outlying observation and was omitted in further analyses of the replicate data.

Laboratory-to-Laboratory Differences

Ideally, interlaboratory studies are designed to investigate within- and between-laboratory variability of the primary factors by minimizing the effects of secondary laboratory factors. Thus, the resulting variability in the test data may then be attributed to unavoidable random errors present in every experiment. In actuality, however, lab-to-lab differences reflect a confusing mixture of random and systematic errors. As noted above, the presence of relatively large lab-to-lab differences offer easier targets for identifying plausible physical explanations. Unfortunately, as lab-to-lab differences approach some minimum level of engineering significance, separating the random and system effects becomes difficult, if not impossible. An underutilized technique for examining lab-to-lab differences is the cause-and-effect chart.

Figure 2 categorizes 19 secondary factors that could affect the test result of an individual laboratory. The major categories of variation examined in this study include: 1) procedure; 2) specimen; 3) equipment; and, 4) measurement, among others. Here, procedure refers to a particular technique utilized by a laboratory. For example, the technique utilized to determine the ΔT across the test material. Specimen refers, in this case, to the effect of bulk density within a material. Other material effects, although desirable, were not investigated in this study. Equipment covers the component differences noted in Table 2, and measurement covers all properties measured in-situ in

[4]Temperature sensors such as thermocouples are typically installed in grooves cut in the surfaces of the plates. For laboratory 3, a platinum resistance thermometer is actually installed in the guard-gap on the perimeter of the meter plate in accordance with ASTM Practice for Guarded-Hot-Plate Design Using Circular Line-Heat Sources practice (C 1043).

the guarded-hot-plate apparatus for the determination of λ. Obviously, this list is not all-inclusive – the effects associated with operator and environment are not considered.

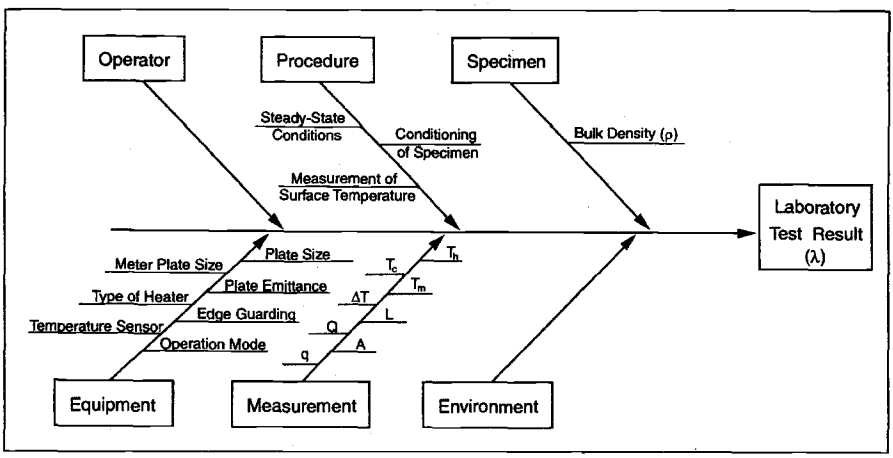

Figure 2 – *Cause-and-effect chart for secondary factors.*

An analysis of variance (ANOVA) for λ is useful in determining whether there are factor effects on λ. Specifically, values of the ANOVA cumulative probability near 100 % are indications of factor significance. Significance, however, does not necessarily imply causation – especially given the fact that many correlations exist among the factors themselves. For example, if T_h is significant and/or T_c is significant, then it is not surprising that T_m and/or ΔT would also be significant.

Table 4 summarizes whether a factor is statistically significant. The term *FCDF* (F-cumulative distribution function) is the percent point of the F-distribution [9]; only *FCDF* values above 95% are considered significant (i.e., at the 5% level). It is important to note that values of *FCDF* are based on the assumption that the variances of the treatments[5] are constant across treatments – this is decidedly *not* the case for many analyses. An advantage of the ANOVA analysis is that it is applicable to both types of data: quantitative (numeric) or qualitative (categorical).

From Table 4, the single most important conclusion is that, for material 4, the primary factor laboratory is *not* statistically significant. This is not the case for materials 1, 2, and 3 – there is statistically significant difference across the five laboratories. Further examination of Table 4 above indicates that many of the 19 (secondary) laboratory factors are significant. Finding the root significant factor(s) is done by using results from Table 4 in conjunction with engineering judgment (and possibly additional tests) by the participating laboratories.

The nearly homogeneous behavior of the laboratories for material 4 is noteworthy. One possible explanation is material composition. Material 4 is a molded-beads, expanded polystyrene board [6]; the three others are (essentially) fibrous glass and

[5] A treatment is a particular combination of levels of the factors involved in an experiment.

binder, having nominal densities ranging from 13 kg/m^3 to 200 kg/m^3 (Table 1). The cellular nature of polystyrene board, consisting primarily of small spheres, would have different anisotropic properties and specimen/plate contact characteristics than the fibrous materials. Another possible explanation is that the relatively thin specimen (13 mm) would have less effect on edge heat losses, if present.

Table 4 – *Is a Factor Statistically Significant? (FCDF > 95 %? Yes/No)*

Laboratory Factors	Material 1	Material 2	Material 3	Material 4
0) Laboratory (primary)	Y	Y	Y	N
1) Steady-state conditions	Y	Y	Y	N
2) Conditioning of specimen	Incomplete	Incomplete	Incomplete	Incomplete
3) Measurement technique for surface temperatures	Y	Y	N	Y
4) Bulk density (ρ)	Y	Y	Y	N
5) Plate size	Y	Y	N	N
6) Meter plate size	Y	Y	Y	N
7) Plate emittance	Y	Y	Y	N
8) Type of heater	N	Y	N	N
9) Edge guarding	Y	N	Y	N
10) Temperature sensor	N	Y	Y	Y
11) Operation mode	N	N	Y	N
12) T_h	Y	N	Y	Y
13) T_c	Y	N	Y	Y
14) T_m	Y	N	Y	Y
15) ΔT	Y	Y	Y	Y
16) L	N	Y	Y	N
17) Q	Y	Y	Y	N
18) A	Y	Y	Y	N
19) q	Y	Y	Y	N

Laboratory Equivalence

Two sets of laboratory data (material 1, laboratory 1 and material 3, laboratory 4) have been identified that are sufficiently different to warrant rejection as outlying observations based physical causes. Excluding these 10 observations, laboratory *relative* means and the grand *relative* standard deviations are re-computed and summarized in Table 5.

The laboratory relative standard deviation represents the relative variation of data about the local laboratory mean. A low value represents a "tight" or quiet laboratory; correspondingly, a high value for the relative standard deviation represents a "noisy" laboratory. From Table 5, laboratory 2 is tight for all four materials. In some cases, as noted in Table 5, the laboratory variation is high (above 1%) or marginally high (approaching 0.5%). With regards to laboratory variation, ISO 8302 specifies a reproducibility[6] limit of better than 1% for independent replicate measurements near room temperature. With the exception of one set of data (material 3, laboratory 1), the laboratory standard deviations are all less than 1% (Table 5).

[6] ASTM defines this quantity as repeatability.

Table 5 – *Relative Means and Standard Deviations for Replicates (297.15 K) Excluding Outlying Data (Material 1-Lab1 and Material 3-Lab 4)*

Lab	Material 1		Material 2		Material 3		Material 4	
	Mean (%)	SD (%)	Mean (%)	SD (%)	Mean (%)	SD (%)	Mean (%)	SD (%)
1	----	----	1.4	0.16	−0.1	1.19[1]	0.39	0.89[1]
2	0.7	0.07	−0.6	0.06	0.5	0.04	−0.26	0.05
3	−0.5	0.04	−1.3	0.11	−1.1	0.47[2]	−0.09	0.13
4	1.0	0.43[2]	0.0	0.17	----	----	−0.30	0.39[2]
5	−1.1	0.06	0.4	0.56[1]	0.8	0.11	0.27	0.04
Grand	----	0.91	----	0.95	----	0.95	----	0.49
Range	1.8	----	2.7	----	1.9	----	0.69	----
Half-Range	± 0.9	----	± 1.4	----	± 1.0	----	± 0.35	----

[1]High; [2]Marginally high

The laboratory relative mean represents the relative differences of the laboratory mean from consensus values (i.e., the grand mean) for each material. As observed earlier in Figure 1, the differences for many of the laboratories in Table 5 change sign from material to material. It is important to note that the laboratory relative means represent relative differences currently utilized in key comparisons as part of the international Mutual Recognition Agreement [*10*]. From Table 5, the ranges of laboratory means for materials 1, 2, 3, and 4 are 1.8%, 2.7%, 1.9%, and 0.69%, respectively. The corresponding half-ranges (last row of Table 5) for materials 1, 2, 3, and 4 are ± 0.9%, ± 1.4%, ± 1.0%, and ± 0.35%, respectively.

Are the relative differences among laboratories at 297.15 K significant? The answer depends on the uncertainty metric considered, and there are several metrics that can be used for comparison, including:

1) An international comparison of a large population (nearly 50) of international guarded-hot-plate laboratories from Africa, Asia, Australia, Europe and North America [*11*];
2) C 177 imprecision statements;
3) ISO 8302 uncertainty statements;
4) NIST SRMs 1451 and 1453 uncertainty limits;
5) The minimum difference (Δ) accepted as significant from an engineering perspective;
6) Individual laboratory expanded uncertainties as reported in Table 2; and,
7) Laboratory statistical significance, ANOVA, 95% as reported in Table 4.

The first metric is from a study that was intended to determine the worldwide state-of-the-art in guarded hot plate measurements prior to the development of ISO standards [*11*]. Participants measured the thermal conductivity of fibrous glass board at mean temperatures of 283 K, 297 K, and a third temperature within the range from 273 K to 313 K. The results indicated that the relative standard deviation of the data from the fitted curve is 2.4%, although several data points deviated from the curve by more than 5% and some by more than 10% [*11*]. The metrics for 2) to 4) are well known and summarized in Table 6.

The participants have agreed to accept 1.5% as the minimum engineering significance difference (Δ) for the above comparison of national standards laboratories. In other words, for national standards laboratories, any difference less than 1.5% from the consensus mean is considered insignificant from an engineering perspective.

Table 6 summarizes the responses (yes or no) by material for the seven different uncertainty metrics and their corresponding estimate (in parentheses) at the two standard-deviation level. Note that only for material 4 are the laboratories considered equivalent for all the uncertainty metrics. For the other materials, however, the laboratories are considered equivalent with respect to the minimum engineering difference of 1.5% (as well as the first four uncertainty metrics). For the individual laboratory expanded uncertainty (at k =2) metric, the laboratories are not equivalent for materials 1, 2, and 3. Particular combinations of laboratories, however, are equivalent as shown in Table 6 and these combinations change for materials 1, 2, and 3.

Table 6 – *Are the Laboratories Equivalent at 297.15 K? (Yes/No)*

Uncertainty Metrics (2 × Standard Deviation)	Material 1 (± 0.9%)	Material 2 (± 1.4%)	Material 3 (± 1.0%)	Material 4 (± 0.35%)
1) International GHP Study (4.8%) [*11*]	Y	Y	Y	Y
2) ASTM C 177 (2% to 5%)	Y	Y	Y	Y
3) ISO 8302 (2% to 5%)	Y	Y	Y	Y
4) SRMs 1451 (3%) and 1453 (1.3%)	Y	---	---	Y
5) Minimum Engineering Significance Δ (1.5%)	Y	Y	Y	Y
6) Laboratory Uncertainty (1.0% to 1.5%)	N:(2,4)(3,5)	N:(2,3)(4,5)	N:(1,2,5)(3)	Y
7) Statistical Significance (ANOVA, 95%)	N	N	N	Y

Multi-Temperature Data (280 K to 320 K)

For the multi-temperature data, there are three primary factors: laboratory (5 levels), reference material (4 levels), and temperature (5 levels). Although the single data-point at each temperature precludes a rigorous statistical analysis, the analyses are driven by the same central theme considered for the fixed-temperature replicate data: How do the laboratories behave across the four materials? In particular, what are the location and variation estimates for each material? Examination of these questions is provided by a linear regression analysis of the multi-temperature data using the following model:

$$\lambda = b_0 + b_1 T_m \tag{3}$$

where $\hat{\lambda}$ is the predicted value for Eq 3 based on least-squares estimates for b_0 and b_1.

Figure 3 plots the relative deviations from the fitted curve for each data point. As observed with the replicate data, the principal conclusion from Figure 3 is that the behavior of the laboratories does, in fact, change from material to material. For the four plots, the location and variation of each set of laboratory data changes from material to material. Further examination of the slopes reveals that there is a change in slope for several laboratories (most notably for laboratories 1, 2, and 5). A final conclusion of Figure 3 is that the relative deviations among the laboratories are affected substantially as

the mean temperature decreases from room-temperature conditions. This conclusion is less evident if data from laboratory 1 are omitted.

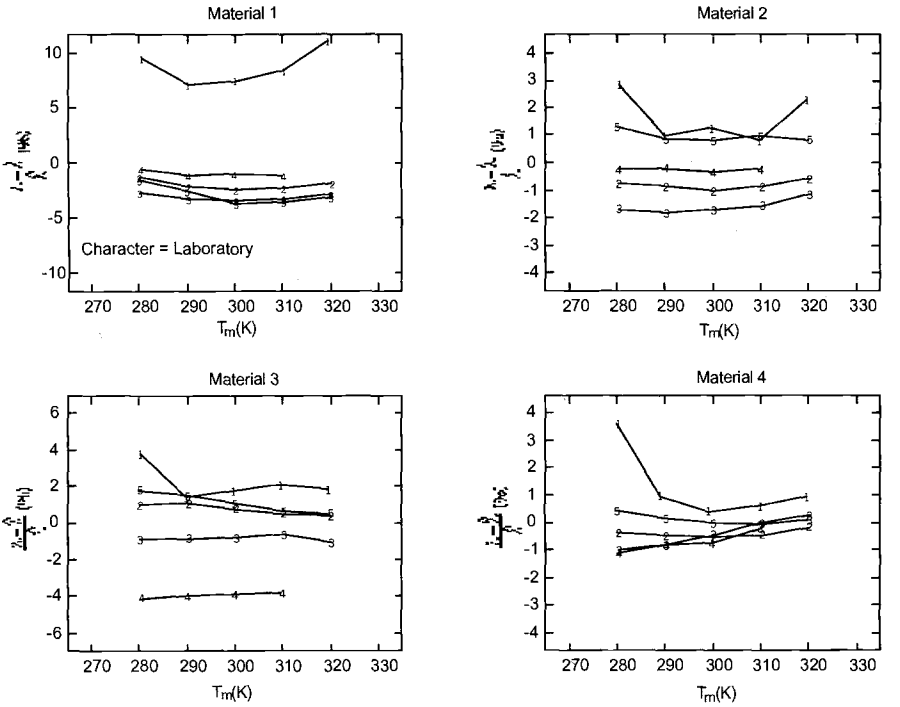

Figure 3 – *Multi-plot of relative deviations versus mean temperature.*

Conclusions

This international comparison investigated the variability in thermal conductivity results among guarded hot plate laboratories in Canada, France, Japan, the United Kingdom, and the United States using four regional/national reference materials. The reference materials were SRM 1451 (fibrous-glass blanket), IRMM-440 (resin-bonded glass fibre board), JTCCM "candidate" mineral-oxide fiberboard, and SRM 1453 (expanded polystyrene board). The collaboration assessed the effects of two primary factors – laboratory and material – for five replicate measurements at 297.15 K (24 °C), and included a third primary factor – temperature – for single-point measurements at 280 K, 290 K, 300 K, 310 K, and 320 K.

The thermal conductivity test data (Figures 1 and 3) indicate that there is a laboratory-to-laboratory difference for each of the materials, except SRM 1453. As expected, there is a material-to-material difference – material 1 (SRM 1451) was the highest thermal conductivity; material 2 (IRMM-440) was the lowest. This material-to-material difference was greater than the laboratory-to-laboratory difference. Ranking the

materials by variability (all data included) yields the following order (lowest to highest): material 4 (SRM 1453), material 2 (IRMM-440); material 3 (JTCCM "candidate"); and, material 1 (SRM 1451). The results of the multi-temperature (280 K to 320 K) data were consistent with the results observed for the fixed-temperature (297.15 K) replicate data. In addition, the results indicated that disagreement among the laboratories tended to increase as mean temperatures decreases from 297.15 K.

Two of the replicate data sets (at 297.15 K) were identified as anomalous and later excluded after the laboratories in question identified physical causes for the behavior of their data. After exclusion of the anomalous data, the half ranges for materials 1, 2, 3, and 4 were ± 0.9%, ± 1.4%, ± 1.0%, and ± 0.35%, respectively. These laboratory-to-laboratory differences are considered small by many different uncertainty metrics, including ISO 8302 uncertainty statements, C 177 precision indices, and NIST SRM uncertainty statements, among others. For this comparison, the laboratory participants have accepted a minimum engineering significance difference of 1.5% from the consensus mean for national standards laboratories. In other words, laboratory differences less than 1.5% from the consensus mean are currently considered insignificant based on an engineering perspective.

One of the most plausible factors affecting the test data was procedural in nature. In particular, a significant difference in average value and variation was experienced by one laboratory that affixed temperature sensors directly to the specimen surface rather than using permanent sensors affixed to the apparatus plates. The approach of adhering fine-diameter temperature sensors to the specimen surface appears to have contributed to measurement differences and may be an *unintended* extension of the test procedures specified in ISO 8302 and C 177. Further measurements comparing different techniques for determining the temperature difference across a test specimen would be extremely useful. With regard to ISO 8302 and C 177, the appropriate sections on determination of the temperature difference should be reexamined for clarity and revised, if necessary.

Acknowledgments

The authors appreciate the cooperation, openness, professionalism, and hard work of the following individuals and laboratories: Masayoshi Uezono (JTCCM), Gianni Venuti (LNE), David Salmon (NPL), Ronald Tye (NPL), Kumar Kumaran (NRCC), and Fitsum Tariku (NRCC). The authors appreciate the donation of one material (IRMM-440) by the European Commission Institute for Reference Materials and Measurements through the efforts of Jean Pauwels, Andrée Lamberty, and Chris Ingelbrecht. We gratefully acknowledge the efforts of Eric Lagergren, who developed the test plan utilized in this collaboration.

References

[1] McCaa, D. J., "Standard Reference Materials: C 518 Heat Flow Meter," *Standard Reference Materials: Issues and Concerns for the Future, ASTM C-16 Workshop*, New Orleans, LA, 1996.

[2] Zarr, R. R. and Filliben, J. J., "International Comparison of Guarded Hot Plate Apparatus Using National and Regional Reference Materials," *NIST Technical Note 1444*, U.S. Government Printing Office, Washington D.C., 2002.

[3] Zarr, R. R. and Filliben, J. J., "Collaborative Thermal Conductivity Measurements of Fibrous Glass and Expanded Polystyrene Reference Materials," *Proceedings of the 26th ITCC/14th ITES Conferences*, 2001 (in publication).

[4] Hust, J. G., "Standard Reference Materials: Glass Fiberblanket SRM for Thermal Resistance," *NBS Special Publication, 260-103* U.S. Government Printing Office, Washington D.C., 1985.

[5] Quin, S. Venuti, G., DePonte, F., and Lamberty A., "Certification of a Resin-Bonded Glass Fibre Board for Thermal Conductivity between −10 °C and +50 °C: IRMM-440," *EUR 19572 EN*, 2000.

[6] Zarr, R. R., Davis, M. W., and Anderson, E. H., "Room-Temperature Thermal Conductivity of Expanded Polystyrene Board for a Standard Reference Material," *NISTIR 5838*, 1996.

[7] ISO, "Guide to the Expression of Uncertainty in Measurement," ISBN 92-67-10188-9, 1st Edition, *ISO*, Geneva, Switzerland, 1993; see also Taylor, B. N. and Kuyatt, C. E., "Guidelines for Evaluating and Expressing the Uncertainty of NIST Measurement Results," *NIST Technical Note 1297*, U.S. Government Printing Office, Washington D.C., 1994; available at http://physics.nist.gov/Pubs/.

[8] Robinson H. E. and Watson, T. W., "Interlaboratory Comparison of Thermal Conductivity Determinations With Guarded Hot Plates," *ASTM STP 119*, 1951, pp. 36-44.

[9] Snedecor, G. W. and Cochran, W. G., Statistical Methods, 6th Edition, Iowa State University Press, Ames, Iowa, USA, 1967, p. 117.

[10] Mutual Recognition Arrangement (MRA): JCRB and BIPM Key Comparison Database, URL: http://www.bipm.fr/enus/8_Key_Comparisons/introduction.html, Bureau International des Poids et Mesures, Sèvres, France, 28 February 2001.

[11] Smith, D. R. "Thermal Conductivity of Fibrous Glass Board by Guarded Hot Plates and Heat Flow Meters: An International Round-Robin," *International Journal of Thermophysics*, Vol. 18, 1997, pp. 1557-1573.

John R. Mumaw[1]

Calculating Thermal Test Results – The History and Use of ASTM Standard Practice C 1045

Reference: Mumaw, J. R., "**Calculating Thermal Test Results – The History and Use of ASTM Standard Practice C 1045,**" *Insulation Materials: Testing and Applications: 4th Volume, ASTM STP 1426*, A. O. Desjarlais and R. R. Zarr, Eds., ASTM International, West Conshohocken, PA, 2002.

Abstract: Thermal property data have historically been used to compare the thermal performance of insulation systems. Accurate calculation and presentation of those data is critical to not only the laboratory performing those tests and the final user of the results, but also to the developers of product and building design specifications. ASTM Practice for Calculation of Thermal Transmission Properties under Steady-State Conditions (C 1045) was developed as a means of standardizing the calculation and presentation of these results across the many test methods within the C 16 Thermal Insulation umbrella. In this paper, a brief history of the development of the practice through the current version is first presented. A discussion of the current practice follows including an example of its use and an outline of its use in product specifications.

Keywords: Calculations, Thermal Results, History

Introduction

Every test procedure ever developed within the ASTM C 16 Thermal Insulation Committee has required a section which contains some manipulation of test data to provide a test result. Thermal test methods are no exception. Most measurements included within the thermal insulation test methods, especially those involving thermal measurement of conductivity, resistance and transmittance values, require the determination of such parameters as voltage drops, electrical resistance, current flow, temperatures and dimensions as the fundamental measures of the test process. The desired results are calculated from these measured values using standardized equations that are based upon fundamental laws of physics such as Fourier's Law of Heat Transfer. Since these equations are the basis of all the thermal test procedures and since they are used in most of the test methods, it would appear reasonable that a need would arise to standardize the basic equations for use in all the test procedures. Until the early 1980's, the calculation sections of the principle ASTM heat transfer test methods such as Test Method for Steady-State Heat Flux Measurements and Thermal Transmission Properties

[1] Manager, Global Insulation Standards, Owens Corning, 2790 Columbus Road, Granville, Ohio 43023

by Means of the Guarded Hot Plate Apparatus (C 177), Test Method for Steady-State Thermal Performance of Building Assemblies by Means of a Guarded Hot Box (C 236), and Test Method for Steady-State Thermal Transmission Properties by Means of the Heat Flow Meter Apparatus (C 518) all contained the same duplicate calculation equations.

Another influence in spurring the development of a new standard was the growth of the size and complexity of the revised ASTM procedures. This transition, which occurred during the late 1970's, changed the overall purpose of the test methods. These test methods began as procedures having a short, simple cookbook style format. The thermal test method format entering the 1980's was a detailed, almost tutorial, collection of all knowledge on the test method subject. This new format, while greatly expanding the flexibility of application of the test methods also created a massive, detailed, sometimes difficult to follow, test method structure. In addition, much of the common, basic calculations were repeated in each method to exacting detail. As more methods were developed and revised, the sheer volume of the written text became burdensome. Recognizing this problem, a few of the early members of Subcommittee C 16.30 organized an effort to investigate the possibility of gathering the common sections of the test methods into separate practices that could be referenced by each of the test methods. This concept would not only save space and duplication but also provide a mechanism where all calculations could be updated quickly and easily without balloting every test method. This effort was the genesis for the development of Standard C 1045.

The History of C 1045 Development

Initial Development

Between 1976 and 1982, the membership of ASTM Subcommittee C 16.30 was struggling with the expansion of the C 177 and C 518 test methods and with a reconfiguration of these procedures to be consistent with those developed by the International Standards Organization. An outgrowth of this work was the recognition of the need to reorganize the existing test standards. The popular thought at that time was to subdivide the methods into topical areas that had similar structures within all the test methods. Some of the areas identified for extraction and organization as separate methods included definitions, Terminology Relating to Thermal Insulation (C 168), calibration, Practice for Calibration of the Heat Flow Meter Apparatus (C 1132), and calculations, C 1045.

The first reported actual work on the development of a calculations document was in the minutes of the March 16, 1983 meeting in Lake Buena Vista, Florida. Here, a task group led by Jerry Hust and Dave McCaa, reported that: "It was the consensus of the task force that C177 and C 518 should be simplified, and that it would be considerably clearer, if all the sections in the current drafts relating to specimen classification and interpretation of test results were removed and placed in a new document that would stand alone, and could be referenced by other methods." During the Fall 1983 meeting in Philadelphia, the subcommittee reported that "Copies of a second draft of the New Standard Practice on Deriving The Thermal Properties from Heat Flow Measurements was distributed. Comments on those drafts were requested by the end of December

1983." Thus the wheels of motion were in place and work was proceeding on the new standard.

Further progress was made on this new procedure during the winter of 1983-1984. A subcommittee ballot was conducted on a third draft and the ballot resulted in five negatives and one set of comments. At the April 1984 meeting in San Antonio, the negatives and comments were discussed in preparation for a fourth draft. The fourth draft was again balloted at subcommittee during the summer of 1984 and received two negatives. At the Fall 1984 meeting in Minneapolis, those two negatives were resolved by editorial comments and the fifth draft was forwarded for main committee ballot. During that next winter, the latest draft of the new standard completed main committee ballot and was forwarded, after some minor editorial changes, to ASTM Society Ballot for final approval. In July 1985, the new standard, now given the designation ASTM C 1045, was balloted at the society level and received one negative because of the title. This negative was withdrawn by editorial change and the standard was published in 1985 as "Standard Practice for Thermal Transmission Properties Calculated from Steady State Heat Flux Measurements." Thus the practice completed its first cycle of the development. As the following paragraphs outline, this was just the beginning of a long history of development of this practice.

Further Refinements

The first published version of the C 1045 was published in Volume 04.06 of the ASTM Book of Standards in November of 1985. As stated in the original scope: "This practice provides requirements and guidelines for the determination of thermal transmission properties based upon heat flux measurements under a variety of conditions. The practice is directed particularly toward a description of the heat flux and associated measurements necessary to obtain useful properties that are applicable to end-use conditions." As stated above, the standard was initially developed as a way to consolidate the common background discussion that had been included in several test methods. This single document would then be referenced in those methods and others being developed. The original concept was to have the theoretical basis for the calculation of thermal properties, including the limitations associated with those properties, in this practice and retain the equations in the test methods. The use of this standard for its original purpose was limited. For the large part, the major thermal test procedures being developed at this time largely repeated the information in their own documents, thus voiding the original purpose of this new document.

The first revision of the 1985 document, published as ASTM C 1045-90, did not substantially change the Practice but added text to help with it's understanding. The primary addition was an Appendix that gave some mathematical definitions of the equation variables and an example of how the practice could be used. Again, it was largely under-utilized.

The second revision of the standard practice was approved in July 1997. This revision was motivated by the complaints from many users of C 1045-90 that the previous versions of the standard was difficult, if not impossible, to understand and of no practical use. In this revision, much of the educational information was moved to the Appendix portion of the document so that only the "cookbook" materials necessary to

make the fundamental calculations in support of the thermal test methods remained in the body of the standard. Unfortunately, some of the educational information, thought to be too theoretical and not practical, was dropped in this editing.

During the 1990's, many major users of the data generated by the insulation producers were demanding input data on the many available products that covered a wide range of temperatures. Increased use of heat loss and surface temperature computer analysis programs conforming to the Practice for Determination of Heat Gain or Loss and the Surface Temperatures of Insulated Pipe and Equipment Systems by Use of a Computer Program (C 680) and the safety concerns relative to the burn hazards from the insulation surfaces drove the need for better data. Also, the manufacturer's finally realized that the data previously listed in materials specifications were incorrect due to errors in how the data was treated in developing representative product thermal curves. Because of this mishandling of data, products were over-designed for thermal values, especially at the high temperatures, due primarily to the method of test and the test conditions selected.

The latest revision, started in 1998 and finally approved as C 1045-01, was aimed at reaching a compromise between the "theoretical" and the "practical" factions on the task group. While each side had strong arguments for their version of the practice, compromise was necessary and finally available. The current method attempts to clearly define how the data from the ASTM thermal test methods should be analyzed. It provides not only the handling of simple thermal test data but also the complex conversion of multiple test data sets into representative thermal curves. The principles presented there are applicable for a wide range of products and systems, so long as they can be mathematically described in some fashion.

The following paragraphs describe the current C 1045-01 Practice, including an example of the analysis. Beyond the example, a discussion of some of the technical issues still surrounding the Practice is included.

The Use of C 1045-01 – An Example

In order to understand the limitations of use of C 1045 we must first outline its capabilities. The equations in C 1045 provide a means of calculating the thermal properties values from the data provided by the thermal test method. As currently configured, the test method provides output of temperatures, heat flux rate and dimensions. In its simplest form, use of C 1045 provides the user a means of calculating the temperature averaged thermal parameter result for the individual test. Note that each test data set provides an averaged value for the parameter. Often, when meeting a specification or other requirement this form of the result is adequate.

The true power of the C 1045 practice is its use in reducing multiple thermal test results into a curve or equation that defines the thermal property over a range of temperatures, independent of the surface test conditions. The output from this type analysis provides the necessary input to analysis tools such as C 680, used for calculation of heat loss and surface temperatures for operating systems. The example in the following paragraphs shows how one can take test results from a series of thermal tests and develop a product thermal curve using the principles of C 1045.

Problem statement

Four thermal tests have been conducted in an apparatus conforming to Test Method for Steady-State Heat Transfer Properties of Horizontal Pipe Insulation (C 335) for development of a thermal curve to describe the product. The data available from the test is shown in Table 1. The need from the C 1045 analysis is a thermal curve covering the temperature range from about 25 °C to 400 °C that is independent of the temperature difference across the material.

Table 1 – Example Thermal Test Apparatus Output Data

Hot Plate Temperature, °C	Cold Plate Temperature, °C	Test Thickness, mm	Test Density, (kg/m3)	Test Average Conductivity, (W/m K)
72.82	26.18	50	58.3	0.03506
237.49	38.18	50	58.3	0.05210
344.42	49.81	50	58.3	0.06884
451.12	64.79	50	58.3	0.09049

Analysis

The first step in the C 1045 analysis is to specify a thermal curve equation form. This equation form may have any number of terms but it is important that the equation:

1. Be continuous and defined over the temperature range
2. Be kept as simple as possible (least number of terms.)
3. Physically representative of the heat transfer process.

For our example, the equation form presented in Eq. 1 has been chosen.

$$\lambda = A + B * T + C * T^3 \quad (1)$$

This equation is generally applicable for porous insulation products. This equation provides a physically representative model by including a linear temperature parameter representative of the conductivity variation with temperature of solid and gaseous materials and a third power temperature term representative of the radiation component of the apparent conductivity in porous materials. Note: For simplification purposes, the prefix "apparent" has been dropped from the rest of this discussion. The next step in the process is to obtain the equation for the integrated average thermal conductivity for the test temperature range. This is the test value recorded in Table 1 that must be processed to obtain the final equation coefficients. Integrating Eq. 1 over the range from the hot surface temperature T_h to cold surface temperature T_c yields Eq. 2 for our example.

$$\lambda_{test} = A + B * T_{mean} + 0.5 * C * T_{mean} * (T_h^2 + T_c^2) \quad (2)$$

Where: $T_{mean} = (T_h + T_c)/2$

From examination of Eq. 2, the regression for the test results must be for the test thermal conductivity as a function of the average value of the surface temperatures and the product of that average temperature times the sum of the squares of the hot and cold surface temperatures divided by 2. Since this example has only three unknowns, the regression analysis requires only four data sets for a curve fit. For this analysis, we have four data sets so the analysis should be easily performed using one of the available programs. For our example, a common spreadsheet analysis provided the following statistical analysis of regression results.

Table 2 - Multiple Regression Analysis Results Output

SUMMARY OUTPUT

Regression Statistics	
Multiple R	0.99993
R Square	0.99987
Adjusted R Square	0.99962
Standard Error	0.00046
Observations	4

ANOVA

	df	*SS*	*MS*	*F*	*Significance F*
Regression	2	0.00168	0.00084	4017.89	0.011154
Residual	1	2.09E-07	2.09E-07		
Total	3	0.00168			

	Coefficients	*Standard Error*	*t Stat*	*P-value*	*Lower 95%*	*Upper 95%*
Intercept	0.026857	0.000786	34.15759	0.018632	0.016866	0.036847
X Variable 1	0.000161	8.37E-06	19.27874	0.032992	5.50E-05	0.000267
X Variable 2	8.23E-10	6.31E-11	13.04799	0.048695	2.15E-11	1.62E-09

As configured for this example, the analysis results presented in Table 2, for the data of Table 1, yields the following thermal equation, Eq. 3, where the thermal conductivity is presented independent of test surface temperatures. As prescribed in C 1045, this analysis is valid for the temperature range from 25 °C to 450 °C.

$$\lambda = 0.0268570 + 0.0001615 * T + 8.237E\text{-}10 * T^3 \quad (3)$$

where: T = temperature °C.

With this resulting equation, the user can develop product thermal conductivity table, Table 3 or product thermal conductivity curve, Figure 1, that are representative of this

data. One word of advise, however, is that this curve is valid only for the data it represents. If the purpose of this analysis is to generate a product curve, multiple test data sets should be processed to make the resulting thermal equation more statistically representative.

Table 3 – Typical Analysis Output Thermal Properties Table

Temperature (°C)	lambda (W/mK)	RSI (m^2K/W)	Resistivity (mK/W)
25	0.0309	1.62	32.35
75	0.0393	1.27	25.43
125	0.0487	1.03	20.55
175	0.0595	0.84	16.80
225	0.0726	0.69	13.78
275	0.0884	0.57	11.31
325	0.1076	0.46	9.29
375	0.1309	0.38	7.64
425	0.1587	0.32	6.30
475	0.1918	0.26	5.21

Note also in Figure 1, the difference between the test thermal conductivity value, plotted as triangles, and the regressed thermal conductivity curve values. Resolution of this difference is the justification for using this Practice.

A Guide to the C 1045-01 Practice – What It Is and What It Is Not

The new ASTM C 1045 Practice for Calculating the Thermal Transmission Properties Under Steady-State Conditions is a tool that is valuable in performing an accurate analysis of a series of thermal test results. It contains valuable information that can be referenced by users of other test methods and specifications within the ASTM framework to simplify their work. It provides the needed analysis tools for a single test or a complete product data set. When followed closely, the resulting C 1045 thermal properties are in a form usable to any and all users. However, the use of C 1045 does have its limitations. The following paragraphs discuss some of those limitations and other frequently asked questions.

Quality of Data

The first, and fundamentally the most important, limitation for the use of C 1045 is that the results of the prescribed data analysis are only as good as the heat transfer test data derived from the test method. That is, if a test method precision and bias are only good to within +/- 10 percent of the true answer, the analysis can be expected to be no better. Granted, the "averaging" of the data obtained from a least-squares fit of an equation to a set of test results can improve the analysis somewhat. However, the old adage of "garbage in, garbage out" still applies. Therefore, it is still necessary that the apparatus used to generate the input thermal test results be as accurate and as precise as possible.

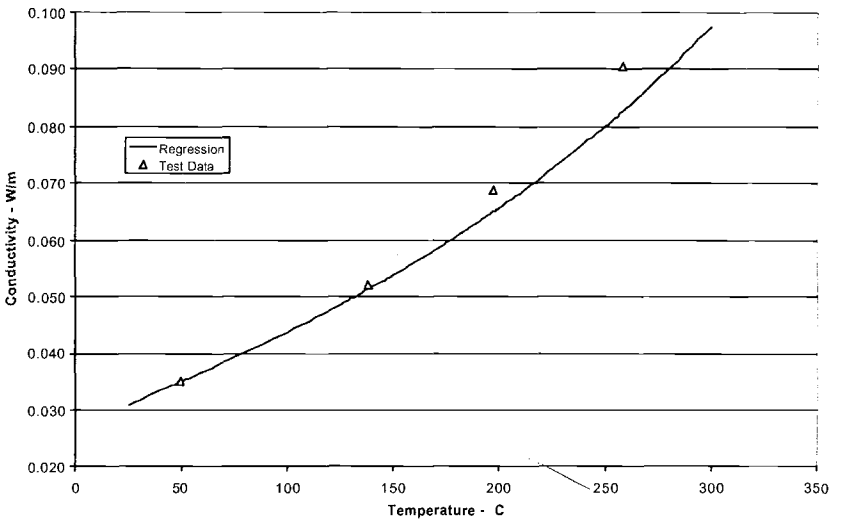

Figure 1 – *Typical Graphical Representation of a Thermal Curve Comparison of Test Data to Regression Analysis*

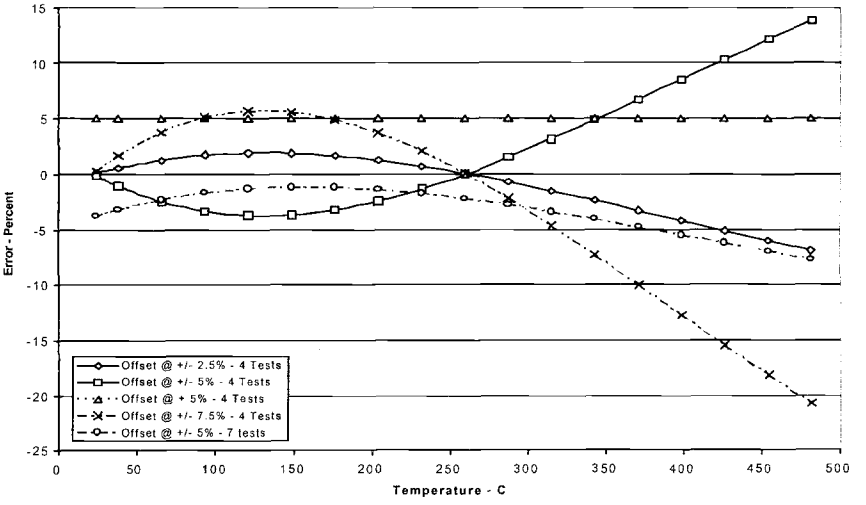

Figure 2 – *Study of the Impact of Quality of Data – Errors in Input Data Sets*

Figure 2 has been generated to illustrate this point. Here possible cases of data variation are presented. All these test conditions represent the expected errors that result from the analysis of five test data sets obtained at evenly distributed temperature points for a simulated C 335 Guarded Hot Pipe test setup. All calculations are for the same basic data set. The new thermal curves were calculated from the offset data using the C 1045 analysis. The plotted values are the differences between the values of the "new" curve and those of the "original" thermal curve plotted versus temperature.

The first curve shows what happens if the second and fourth data points are offset from the real "test" result by +/- 2.5 percent. For this example, the second data point is offset by plus 2.5 percent and the fourth point is offset by minus 2.5 percent. Note the cyclic nature of the difference curve and that the percent offset at 482 °C is more than double the initial 2.5 % offset of the last data point.

The second curve shows what happens if the second and fourth data points are offset from the real "test" result by +/- 5 percent. For this curve however, the second data point is offset by minus 5 percent and the fourth point is offset by plus 5 percent. Note the same cyclic nature of the difference curve and that the percent offset at 482 °C is also more than double the initial 2.5 % offset of the last data point. Note also that the sign of the offset is in the same direction as the offset of the highest temperature data point.

The third curve shows what happens if the data is biased by a fixed 5 % for all data points. For this case, the new calculated thermal curve and the base data curve values are simply offset by the same 5 percent. This would be the case for a test apparatus with good precision but a 5 percent bias.

The fourth curve of Figure 2, offset by 7.5 percent shows the same relative behavior as in the first curve but the differences increase with the magnitude of the offset. Note however, that the error in this simple example is now nearly 21 percent at the 482 °C level.

The final curve of Figure 2 shows the effect of holding the offset error at +/- 5 percent but compensating for the imprecision by increasing the number of test points from four to seven. For this case, the magnitude of the resulting regression is about equal to that of the +/- 2.5 percent offset curve. This last curve suggests that the imprecision of the apparatus can be somewhat compensated for by increasing the number of test points.

Similar analysis using a greater number of data sets and a random numbers generated offset demonstrated a similar result to the last curve. In cases where the test results variation is truly random and a greater number of test data sets are used, the net offset error approaches zero. This analysis shows that care should be observed in selecting the number of test data sets used to describe a product's thermal curve. When using the curve to describe a product offering, multiple specimens should be used to cover the expected range of density and other product variations. The bottom line of this analysis shows the importance of having good test accuracy. If the errors are random, then it is critical that the level of precision be minimized. The bias, while critical to the absolute result, may not be as critical, percentage wise, as the imprecision.

Equation Form

A second limitation, is that the form of the curve fit equation must be representative. Anyone who has conducted this type of data analysis realizes that the same data set can

be represented by a large variety of thermal equation forms. For data to be useful in explaining why and how the thermal behavior of a product performs, the form of the equation must be representative. A good example from the past is the equation form used to represent the variation of product thermal conductivity for mineral fiber insulations. During the 1980's, several manufacturers used an equation for given in Eq. 4. Other manufacturers used an equation of the form given in Eq. 5.

$$\lambda = A * e^{B*T} \tag{4}$$

$$\lambda = A + B * T + C * T^3 \tag{5}$$

In reality, both equation forms provided approximately equal representation for the thermal test results from a mathematical basis. However, if the criteria were to be physically representative, then the equation form of Eq. 5, can be shown to be superior. Equation 5 shows that, for mineral fiber, there are two components of the temperature relationship. The first is a function of the conductivity of the insulation principle component, i.e. the air. The second component of the temperature relationship is proportional to the cube of the temperature. This cubic relationship is the component of the heat transfer that is due to radiation exchange. While both equations can be shown to equally represent the thermal results over the limited range, there is no question that the more physically representative model is superior.

Independent of the type of insulation represented, the equation used as the model must be appropriate for the temperature range of interest. For example, for a cellular foam material having a condensable gas in the cells, the equation form must follow the changing thermal conductivity values as the heavier molecular gas in the cells condense and the level of heat flux is controlled by a different gas mix. When analyzing data for these materials using C 1045, the temperature range is generally divided up where a simple equation can be used to describe each portion of the curve between the inflection points of the data. Thus, the real problem for the user is matching the equations at the inflection points to provide a continuous relationship.

Applicable Temperature Range

A third, and very controversial, limitation is the temperature range of the heat flux data in relationship to the useful temperature range of the thermal conductivity curve. It is obvious that the temperature range of the derived curve cannot exceed the range of the λ data. However, the question is: "How close do the end of range data points need to be to the extreme of the range to yield a full temperature range thermal curve?" The obvious answer is that if the temperature differences for each test are kept small enough, then the range is no problem. This is because the temperature difference is not significant for most insulation products if it is below 30 K. (The notable exception is a product having inflection points in the temperature range of interest.) This temperature difference limit may be valid but it is also not practicable. For example, what about pipe insulation testing? The C 335 thermal test method does not provide for an elevated outside surface temperature above that of the ambient. Often, a second layer of insulation is used to elevate the temperature of the cold surface. Frequently, a second layer is not adequate to

yield the needed temperature range. For example consider problems with testing mineral fiber pipe insulation up to 650 °C. Therefore, a specification that requires the mean temperature of the end thermal test points to be within 50 K of the end points of the temperature range is ridiculous. A second place where this problem exists is for products with a finite upper temperature limit. For example, take polystyrene insulation of any form. According to the Specification for Rigid, Cellular Polystyrene Thermal Insulation (C 578), the maximum use temperature for this product is 74 °C. If a thermal test is limited to a minimum temperature difference of 20°C, how does the user get thermal data to cover that range of 53 °C to 74 °C if the temperature limit on the hot side of the test is 74 °C?

The more appropriate question is does it make a difference? The answer is no. As C1045 states clearly, so long as the thermal test data covers the temperature range of interest, the analysis results are as accurate as the test data. A simple analysis to study this question was performed on a fictitious material having a thermal conductivity in the range of typical products. Figure 3 presents the results of the analysis. The three sets of results shown by the graph are for the same material. The first curve is developed from the actual thermal curve used in the analysis. The second curve, identified by the square symbols, was developed from "test results" based on a principle of large temperature difference tests. The temperature differences used here are similar to that used in a C 335 test for the temperature range. The third curve, symbolized by the triangles, is based on small temperature differences for the "tests". It uses temperature differences recommended by Practice for Selecting Temperatures for Evaluating and Reporting Thermal Properties of Thermal Insulation (C 1058). It should be noted here that the "test" data was calculated using an ASTM C 680 analysis. After the thermal curve analysis for each data set, the subsequent thermal conductivity curves versus temperature are plotted in Figure 3. Interestingly, the resultant curves plot, for practical purposes, the same curve over the entire range of data. In fact, the thermal curve equation coefficients are almost identical. From this analysis, the answer is still clearly that it makes no difference how close the mean temperature is to the end points of the range. This discussion must be tempered by the fact, demonstrated previously, that if the test device is inaccurate or imprecise the effects on the final result can be significant.

Test Temperature Difference

Another concern is the effect of test temperature difference on the test result. This concern is the justification for using a C 1045 analysis of the heat flux data from the tests. A series of simulated test results were calculated using C 680 to evaluate the effect of test temperature difference on the test result. Figure 4 contains the results of these calculations. For this graph, each test result was calculated for our theoretical material using a different test temperature difference. All calculations were for a mean temperature of 232 °C. By lowering the cold side temperature and increasing the hot side temperature by equal amounts for each calculation, the simulated test result can be calculated. Note, in Figure 4, as the test temperature difference becomes larger, the difference between the "test" result and the conductivity at 232 °C becomes greater. The reason that the measured conductivity is greater is that the test result is a temperature

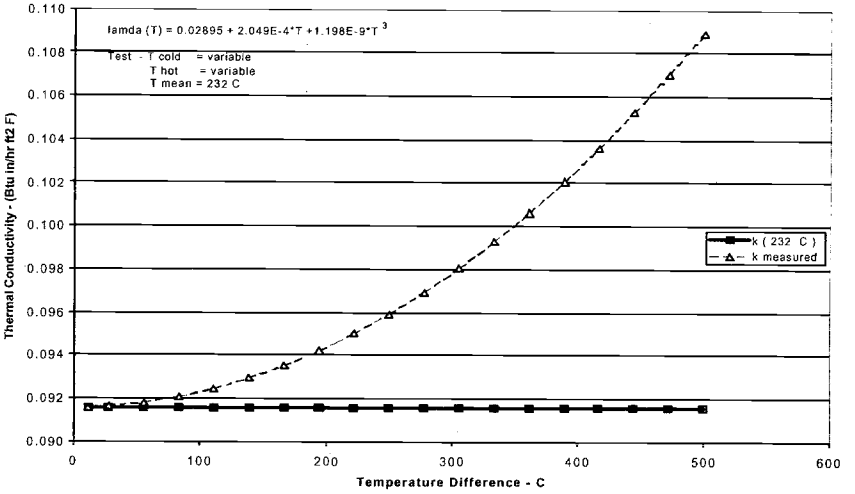

Figure 3 – *Regression Results for Different Temperature Differences*

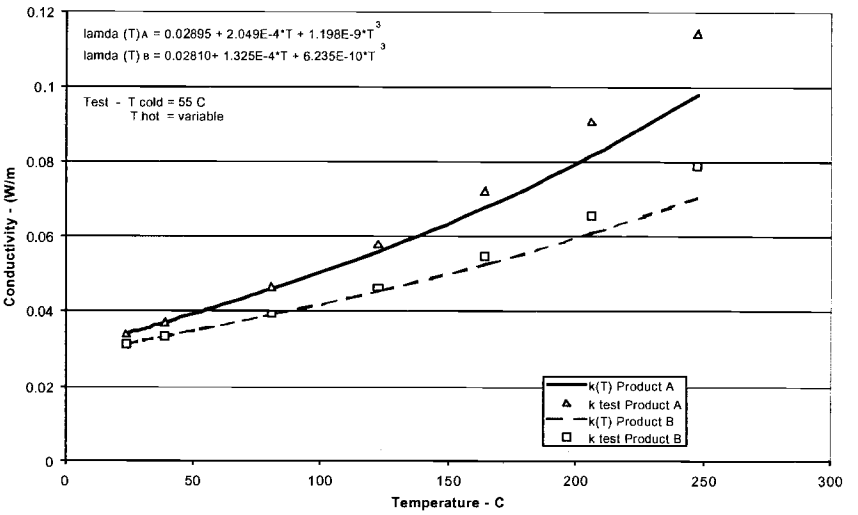

Figure 4 – *Effect of Test Temperature Difference at Constant Mean Temperature*

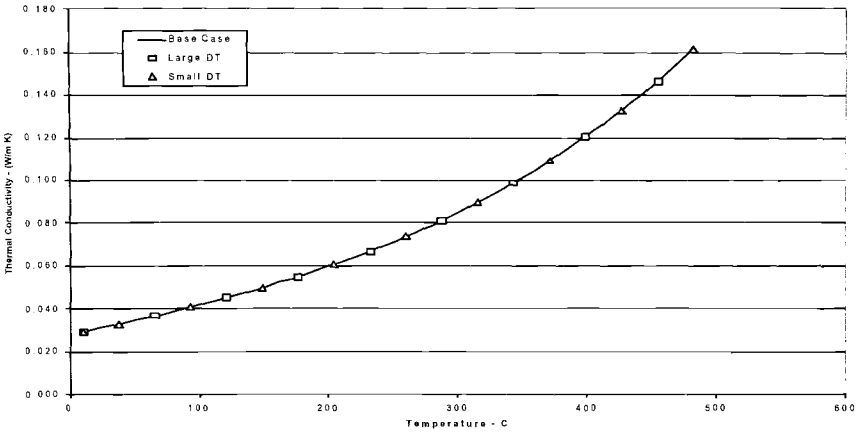

Figure 5 – *Comparison of Actual vs. Measured Conductivity – Effects of Test Temperature Difference – Product Effects*

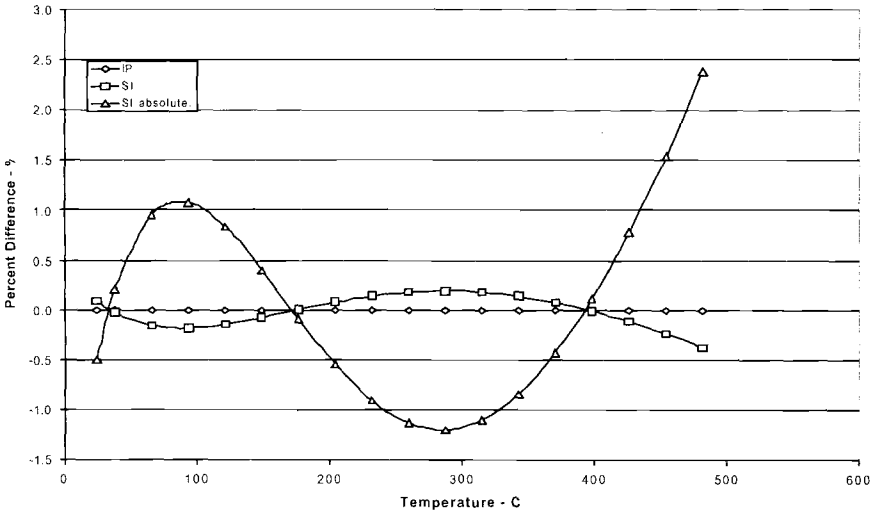

Figure 6 – *Comparison of the Impact of Units Selection for the Analysis*

integrated average of the conductivity over the temperature range of the test. This difference is the reason that the C 1045 analysis is critical. Use of the C 1045 tool permits the user to "reverse" the integration process to obtain the "true" thermal conductivity versus temperature curve.

In Figure 5, a similar analysis is presented. These data simulate Test Method C177 test results. Here the cold side is fixed at 13 °C and the hot side is increased until the final result is for a test mean temperature of 246 °C. For this figure, the analysis is repeated twice for thermal curves having approximately double the variation with temperature. Note that the difference between the test result and the conductivity curve value at the same temperature is proportional to the ratio of the slopes of the respective thermal conductivity curves. Also observe in Figure 5 that the difference in results increases from near zero for a temperature difference up to 56 °C to approximately 15 percent of the actual value at 246 °C mean or a 470 °C. temperature difference.

Analysis Units

The final topic answers the question: " Does it make a difference which system of units is used in the analysis?" Figure 6 presents the results of an analysis conducted on a single four test data set. In this analysis, the form of the regression equations was identical in all cases. The difference between the generated curves is due to the system of units used in the regression. Three units systems were compared. They were IP(°F), SI(°C) and SI absolute (°K). The resulting equations are presented on Figure 6 for comparison. The final result is that the calculated values are, within practical limits, equal. However, the choice of the analysis system of units must be established by the needs of the analysis and the need for a physically accurate model and not simply by a concern for accuracy of the results.

Application of C 1045-01 in Material Specifications

The quality of material specifications can benefit from the use of C 1045 in specifying the apparent thermal conductivity relationship desired. It is important that the material be specified by intrinsic properties that are independent of test conditions to insure that the method of test, or the conditions used during the test do not influence the results. Practice C 1045 provides that method of identifying the material's relationship between temperature and thermal properties independent of temperature difference. To insure that C 1045 is used properly, C 1045-01 Section 9, presents a series of recommendations for inclusion of C 1045 in material specifications.

The recommendations include: (1) Definition of the test methods to be used for the data generation; (2) Use of the C 1058 for test temperature difference selection; (3) Limiting range of hottest hot and coldest cold surface temperatures for the analysis; (4) Analysis format and results presentation format; and (5) Adding a precautionary note for the user on comparing the results of a C 1045 analysis with existing specifications requiring fixed temperature difference tests. The use of these recommendations is already has been demonstrated in several material specification rewrites.

Summary

The use of Practice C 1045 is a valuable tool in the development of accurate and useful information for an insulation product's thermal properties. As with most standard practices, the quality of the results is dependent upon the quality of the input data from the thermal test method and how well the Practice is followed. Successful use of the procedure documented in C 1045 over the past 20 years by most of the major insulation manufacturers and specifiers, confirms that use of this standard is beneficial to the insulation community. This paper has attempted to document the history of the development of this practice and to answer some of the questions on its use.

Robert J. Rushforth[1]

Normal Variation and Tolerances for Thermal Resistance in Thermal Insulation Specifications

REFERENCE: Rushforth, R. J., "**Normal Variation and Tolerances for Thermal Resistance in Thermal Insulation Specifications**," *Insulation Materials: Testing and Applications: 4th Volume, ASTM STP 1426*, A. O. Desjarlais and R. R. Zarr, Eds., ASTM International, West Conshohocken, PA, 2002.

ABSTRACT: The purpose of this presentation is to explain how specification tolerances are determined for thermal resistance in thermal insulation. Variation in measured test results is an important concept in the determination of specification tolerances. When a test of a product property is repeated, the measured test result isn't exactly the same as in the first test. This normal variation in measured test results is described by the normal probability frequency distribution curve, the bell-curve. A measure of this normal variation is the standard deviation. Specification tolerances are established from a table of probabilities of the normal curve by determining the position of the appropriate confidence level in terms of a constant multiplied by the standard deviation. A similar concept is involved in new ISO standards, in which a double confidence level is used.

KEYWORDS: building insulation, mineral fiber, thermal resistance, R-Value

Nomenclature

σ	Population standard deviation of 30 or more individual specimens
μ	Population average (mean) of 30 or more individual specimens
s	Sample standard deviation of individual specimens
Xbar	Sample average (mean) of individual specimens
X	Lower specification limit
n	Number of specimens
k	Number of standard deviations from the mean to the lower specification limit

[1] Senior Research Engineer, ASQ Certified Quality Engineer, Johns Manville, Technical Center, P.O Box 625005, Littleton, CO 80162-5005.

Introduction

The different thermal requirements for mineral fiber building insulation have caused some confusion among manufacturers and users. There are different thermal requirements for the United States Federal Trade Commission (FTC), ASTM, Canada (CAN/ULC), and the International Standards Organization (ISO). An understanding of the statistics involved in these thermal standards will assist manufacturers and users in sorting out these requirements

Discussion

The first step in sorting out the different thermal requirements for mineral fiber building insulation is to understand the concept of variation. No two items are exactly the same, even if they are manufactured under what appears to be the same conditions. This is because there are many sources of product/process variation, not all of which can be identified. Examples are temperature, humidity, location across machine width, time in a shift and equipment wear. This variation is called product or process variation. Sometimes it is called normal variation.

Even if the two items actually are identical, however, the test results still may be different. This is called test method or measurement variation. As in the case of product/process variation, there are many sources of test method or measurement variation, not all of which can be identified. Examples are reagent aging, apparatus wear, and different operators. When pooled together, these two sources of variation must be taken into consideration when establishing thermal requirements and determining compliance with those requirements.

Normal variation causes the thermal resistance test results to form a normal curve, when plotted on a graph of frequency of occurrence vs. the values of a product property, such as thermal resistance. When the sample size is relatively small, the graph is called a histogram. It has a jagged appearance. When the sample size is sufficiently large to represent the entire population, the curve is smooth and has the shape of the familiar bell-shaped curve. The curve also is called the normal probability curve.

Statistical measures of the normal curve are the mean and the standard deviation. The mean is the average of the test results. It is a measurement of the location of the curve. For the normal curve, 50% of the test results are greater than the mean and 50% are less than the mean. The standard deviation is the measure of variability in the test results or the spread of the normal curve.

The area under the normal curve is called the cumulative probability of all test results. Tables of the cumulative probability of the normal curve are found in most books on statistics, such as *NIST Handbook 91* [*1*]. For thermal requirements a one-tailed normal probability curve is most often used (Figure 1). A one-tailed probability is when there is a specification limit on only one end of the normal curve. For example, the area under the normal curve for test results greater or equal to the mean minus "k" standard deviations is the cumulative probability that the test results are greater or equal to the

lower specification limit. If "k" is 3, the cumulative probability is 99.87%. Only about one test result out of 1000 will fall below the mean minus 3 standard deviations. In other words, there is a 99.87% cumulative probability that a test result will be greater or equal to the mean minus 3 standard deviations or 99.87% of the test results will be greater or equal to the mean minus 3 standard deviations. This is often considered to be certainty for many specification compliance purposes. Therefore, the mean minus 3 standard deviations is usually chosen as the lower specification limit. This is expressed by the following equation.

$$\text{Target (mean)} - k\sigma = X \tag{1}$$

Another way of expressing this equation is as follows.

$$k = (X - \mu)/\sigma \tag{2}$$

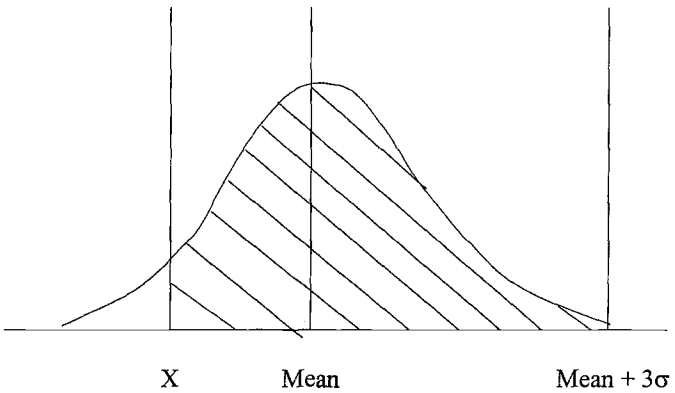

Figure 1 – *Single Tailed Normal Curve*

Sometimes "k" is shown as "z" in statistics books [1]. A population is all of the possible test results. Usually 30 or more test results are needed before a sample is considered to be a population. If the number of test results in a sample is less than 30, the equation becomes as follows.

$$k = (X - \text{Xbar})/s \tag{3}$$

These same principles can be applied to analyzing each of the thermal requirements in this paper.

FTC

United States Federal Trade Commission (FTC) requirements for mineral fiber building insulation are contained in Labeling and Advertising of Home Insulation (16CFR460, 1979). The FTC requirement is that all individual test results meet or exceed 90% of the labeled thermal resistance (R-Value). Based upon thermal testing, the population standard deviation of typical mineral fiber building insulation has been determined. This is represented as 3.33% in the FTC requirements. If the manufacturer targets 100% of the labeled R-Value and the lower specification limit is 90%, the lower specification limit will be at the mean minus 3 standard deviations.

$$\text{Target (mean)} - k\sigma = X \qquad (1)$$

where

$k = 3$
$\sigma = 3.33\%$
$X = 90\%$

$$\text{Target (mean)} - 3(3.33\%) = 90\%$$

$$\text{Target (mean)} = 100\%$$

Therefore, the manufacturer must target as the mean 100% of the labeled R-Value to comply with the requirement.

ASTM

ASTM requirements for mineral fiber building insulation are contained in ASTM Specification for Mineral-Fiber Blanket Thermal Insulation for Light Frame Construction and Manufactured Housing (C665-98). There are two requirements. The first requirement is the same as the 16CFR460 requirement. All individual test results shall meet or exceed 90% of the labeled R-Value. The manufacturer must target as a mean 100% of the labeled R-Value to comply with the first ASTM-C665 requirement.

The second requirement is statistically equivalent to the first. The average of four specimens shall equal or exceed 95% of the labeled R-Value. When determining the standard deviations of the averages of different numbers of specimens, the standard deviation of individual specimens is divided by the square root of the number of specimens.

$$\sigma_{\text{average of n}} = \sigma / \sqrt{n} \qquad (4)$$

where

$n = 4$
$\sigma_{average\ of\ n}$ = population standard deviation of the averages of n specimens
$\sigma = 3.33\%$

$$\sigma_{average\ of\ 4} = (3.33\%)/\sqrt{4} = (3.33\%)/2 = 1.665\%$$

$$\text{Target (mean)} - k\sigma_{average\ of\ n} = X \qquad (5)$$

where

$k = 3$
$n = 4$
$\sigma_{average\ of\ 4} = 1.665\%$
$X = 95\%$

$$\text{Target (mean)} - 3(1.665\%) = 95\%$$

$$\text{Target (mean)} = 100\%$$

Therefore, the manufacturer must target as the mean 100% of the labeled R-Value to comply with the second ASTM-C665 requirement.

The manufacturer must target as the mean 100% of the labeled R-Value to comply with both requirements of ASTM-C665.

CAN/ULC

CAN/ULC requirements for mineral fiber building insulation are contained in Mineral Fibre Thermal Insulation for Buildings (CAN/ULC-S702-97). There are two requirements. The first requirement is that 95% of individual test results meet or exceed the labeled R-Value. Using cumulative probability tables [1] at 95% area under the normal curve, the target (mean) R-Value is determined to be 1.645 standard deviations above 100%.

$$\text{Target (mean)} - k\sigma = X \qquad (1)$$

where

$k = 1.645$
$\sigma = 3.33\%$
$X = 100\%$

$$\text{Target (mean)} - 1.645(3.3\%) = 100\%$$

$$\text{Target (mean)} = 105.5\%$$

Therefore, the manufacturer must target as the mean 105.5% of the labeled R-Value to comply with the first CAN/ULC S702-97 requirement.

The second CAN/ULC S702-97 requirement is the average of 3 specimens tested meet or exceed the labeled R-Value. Again, as with the second requirement of ASTM-C665, the standard deviation of the average of a number of specimens is equal to the standard deviation of individual specimens divided by the square root of the number of specimens.

$$\sigma_{\text{average of n}} = \sigma / \sqrt{n} \qquad (4)$$

where

n = 3

$\sigma_{\text{average of n}}$ = population standard deviation of the averages of n specimens

σ = 3.33%

$$\sigma_{\text{average of 3}} = (3.33\%)/\sqrt{3} = (3.33\%)/1.732 = 1.923\%$$

This means that the average of three specimens equals or exceeds 100% of the labeled R-Value.

$$\text{Target (mean)} - k\sigma_{\text{average of n}} = X \qquad (5)$$

where

k = 3

$\sigma_{\text{average of 3}}$ = population standard deviation of the averages of 3 specimens = 1.923%

X = 100%

$$\text{Target (mean)} - 3(1.923\%) = 100\%$$

$$\text{Target (mean)} = 105.8\%$$

Therefore, the manufacturer must target as the mean 105.8% of the labeled R-Value to comply with the second CAN/ULC S702-97 requirement.

The two requirements of CAN/ULC S702-97 are approximately the same. The manufacturer must target 105.8% R-Value to comply with both requirements.

ISO

ISO requirements for mineral fiber building insulation are contained in Building Materials and Products – Procedures for Determining Declared and Design Values (ISO/FDIS 10456:1999). These requirements are expressed in terms of double probabilities. For example, there is a 90% confidence that 90% of the test results meet or exceeds the labeled R-Value. This is expressed as 90/90. Likewise, 90/50 means there is a 90% confidence that 50% of the test results meet or exceed the labeled R-Value.

Two sets of tables are presented in ISO/FDIS 10456 (Table 1). The section for factor K1 is for use when the population standard deviation is known. About 30 historical test results are needed to qualify it as the population standard deviation before this section of Table 1 is used. The section for factor K2 is for use when the population standard deviation is unknown. This is when less than 30 historical test results are available to determine the standard deviation. More extensive tables for 90/90 and several other combinations are contained in *NIST Handbook 91* [*1*] and *Sandia Corporation Monograph SCR-607* [*2*]. Equations in *Sandia Corporation Monograph SCR-607* [*2*] can be used to calculate an expansion of the 90/50 tables in ISO/FDIS 10456.

Table 1 – *Coefficients for one-sided tolerance intervals (90% confidence)[2]*

Number of Specimens Tested	Factor K1 (σ known) P=50% (% meet)	P=90% (% meet)	Factor K2 (σ unknown) P=50% (% meet)	P=90% (% meet)
3	0.74	2.02	1.09	4.26
5	0.57	1.86	0.69	2.74
7	0.48	1.77	0.54	2.33
10	0.41	1.69	0.43	2.07
12	0.37	1.65	0.40	1.97
15	0.33	1.61	0.35	1.87
20	0.29	1.57	0.30	1.77
50	0.18	1.46	0.18	1.56
Infinity	0.00	1.28	0.00	1.28

Calculations of the targets to comply with the ISO/FDIS 10456 requirements are similar to the method used for the other requirements in this paper.

$$\text{Target (mean)} - (K1)\sigma = X \tag{6}$$

where

K1 = factor for use when population standard deviation is known. It is the number of standard deviations from the mean to the lower specification limit

The section of Table 1 for K1 at 90/50 contained in ISO/FDIS 10456 should be used for mineral fiber building insulation, because the number of test results available to determine the population standard deviation is extremely large. In this case, the population standard deviation is known. When the number of test results used to determine compliance also is extremely large, K1 = 0. The calculation becomes the same as the normal distribution "k" used for 16CFR460 and ASTM-C665 requirements. When the number of test results used to determine compliance is smaller, such as in a specific short time period, K1 is greater than 0. For example, if a week's thermal testing consists of 20 test results, K1 = 0.29. The following equations are used to determine the target (mean) R-Value to comply with the ISO/FDIS 10456 requirements.

$$\text{Target (mean)} - K1\sigma = X \qquad (6)$$

where

K1 = 0.29 where K1 (n, confidence, % compliance), or K1 (20, 0.90, 0.50)
σ = 3.33%
X = 100%

$$\text{Target (mean)} - 0.29(3.33\%) = 100\%$$

$$\text{Target (mean)} = 100.97\%$$

Therefore, the manufacturer must target as the mean 100.97% to comply with the ISO/FDIS 10456 requirement.

In the case where the population standard deviation is known and there is a compliance requirement of 90% confidence that 90% of the test results meet or exceed 100% of the labeled R-Value, factor K1 from the 90/90 section of Table 1 is used. For a week's thermal testing of 20 test results, K1 = 1.57. The following equations are used to determine the target R-Value to be sure of compliance with the requirements.

$$\text{Target (mean)} - K1\sigma = X \qquad (6)$$

where

K1 = 1.57 where K1 (n, confidence, % compliance), or K1 (20, 0.90, 0.90)
σ = 3.33%
X = 100%

$$\text{Target (mean)} - 1.57(3.33\%) = 100\%$$

Target (mean) = 105.23%

Therefore, the manufacturer would target (mean) 105.23% to comply with the ISO/FDIS 10456 requirement.

If a longer time period or higher testing frequency are used, the targets (means) would be closer to 100%. For example, if 50 test results are available, K1 (50,90,90) = 1.46, instead of 1.57. In that case, the manufacturer would target 104.9%, instead of 105.23%. Also, if the manufacturer's population standard deviation is less than 3.33%, the target (mean) would be closer to 100%.

Comparisons

The targets (means) to comply with each of the thermal requirements of the different mineral fiber building insulation standards are compared in Table 2.

The required targets (means) for compliance with the requirements of 16CFR460, ASTM-C665, and ISO/FDIS 10456 (90/50) are approximately equal, although ISO/FDIS 10456 (90/50) requires a slightly higher target (mean) of 101%, instead of the 100% required for 16CFR460 and ASTM-C665. On the other hand, CAN/ULC S702-97 and ISO/FDIS 10456 (90/90) also are approximately equal and require targets (means) of 105.2%-105.8% to comply.

Table 2 – *Comparisons of targets (means) for compliance*

Specification	Thermal requirement	Target (mean) to comply
16CFR460	Individuals meet/exceed 90%	100%
ASTM-C665	Individuals meet/exceed 90%	100%
	Average of 4 meet/exceed 95%	100%
CAN/ULC-S702	Individuals meet/exceed 95%	105.5%
	Average of 3 meet/exceed 100%	105.8%
ISO/FDIS10456	90%confidence/50% compliance meet/exceed 100% (n=20)	101%
	90% confidence/90% compliance meet/exceed 100% (n=20)	105.2%

Conclusions

The requirements of ISO/FDIS 10456 are calculated in a manner similar to 16CFR460 and ASTM-C665.

ISO/FDIS 10456 shows two sets of factor tables (F1 and F2). Because the population standard deviation for thermal resistance is known for mineral fiber building insulation, based on greater than 30 test results, factor K1 is to be used.

The targets (means) for compliance are approximately equal for 16CFR460, ASTM-C665 and ISO/FDIC 10456 (90/50). For 16CFR460 and ASTM-C665, the target (mean) for compliance is 100% of the labeled R-Value. The target (mean) is slightly higher at 101% of the labeled R-Value for ISO/FDIS 10456 with a 90% confidence that 50% of the test results meet or exceed the labeled R-Value.

The targets (means) for CAN/ULC-S702-97 and ISO/FDIS 10456 with 90% confidence that 90% of test results meet or exceed the labeled R-Value are approximately equal. The targets (means) are 105.2% - 105.8% of the labeled R-Value to comply.

References:

[1] Natrella, M. G., *Experimental Statistics, NIST Handbook 91*, U.S. Government Printing Office, Washington, D.C., 1966.

[2] Owen, D. B., *Factors for One-Sided Tolerance Limits and for Variables Sampling Plans, Sandia Corporation Monograph SCR-607*, 1963.

Torben V. Rasmussen[1]

Creep Tests and Techniques for Predicting Densities Necessary to Prevent Settling of Loose-fill Insulation in Walls

Reference: Rasmussen T. V., **"Creep Tests and Techniques for Predicting Densities Necessary to Prevent Settling of Loose-fill Insulation in Walls,"** *Insulation Materials: Testing and Applications: 4th Volume, ASTM STP1426*, A. O. Desjarlais and R. R. Zarr, Eds., ASTM International, West Conshohocken, PA, 2002.

Abstract: This paper presents a proposal for a standardized method for creep tests and techniques for predicting densities necessary to prevent settling of loose-fill insulation in walls. Experimental techniques and a theoretical framework needed for determining the associated creep parameters are described.

The theoretical framework allows a quantitative approach to the problem of achieving non-settling of a loose-fill insulation material in a given wall.

The theory leads to a set of equations to estimate stresses in a loose-fill insulation material as a function of the geometry of the wall, material parameters for the loose-fill insulation material and friction coefficients between the wall and the loose-fill. A theoretical description of creep and a technique that allows the determination of the relevant material parameters from the proposed creep tests is shown together with the test results. Furthermore, the necessary loose-fill density for long-term stability in a wall exposed to varying relative humidity is predicted.

Keywords: Loose-fill material, thermal insulation, creep, settling, volume stability, cellulosic fibre insulation

A new theory for estimating the necessary density of loose-fill material in walls in order to ensure volume stability has been developed [*1, 2*]. The specific application presented here is loose-fill insulation material placed in walls as thermal insulation. Loose-fill insulation material in a wall is considered to be in a volume-stable state as long as it fills out the internal volume of the wall.

From practice and experimental work it is well known that insulation materials that are loose-filled in walls may settle after installation. For example, loose-fill insulation in a test house exhibited progressive settling which was 0.07 and 0.38 m before and after removal of the gypsum board that served as a wind barrier [*3*].

Today, when loose-fill insulation is used as horizontal insulation in attics, an extra amount is added over and above the level required for insulation to solve the settling problem. When used for walls, settling is reduced by adding an extra amount of the

[1] MSc (CivEng), PhD, Senior Researcher, Danish Building and Urban Research, Building Technology and Productivity Division, P.O. Box 119, DK-2970 Hørsholm, Denmark.

loose-fill material into the wall to increase the density of the loose-fill after installation. This higher density has so far been based on experience.

This paper presents a test method and a theoretical framework that describes creep of loose-fill material. In addition a method is shown that can be used to adjust results from creep tests for predicting long-term densities necessary to prevent settling of loose-fill in walls.

The method is designed to describe and model the creep behaviour of loose-fill materials exposed to a stable environment. In addition, a test procedure to determine the volume-stable density of a loose-fill material exposed to a varying relative humidity (RH) is described.

It is the objective to use short-term tests to model and describe long-term material behaviour. The method is designed for use in the laboratory.

Definitions

A material under instantaneous load will exhibit instantaneous strain, and under a continuous load most materials will exhibit additional strain [*4*]. This time-dependent strain is called creep. Figure 1 shows a typical example of creep as a function of time for a material subjected to a constant load that is subsequently removed.

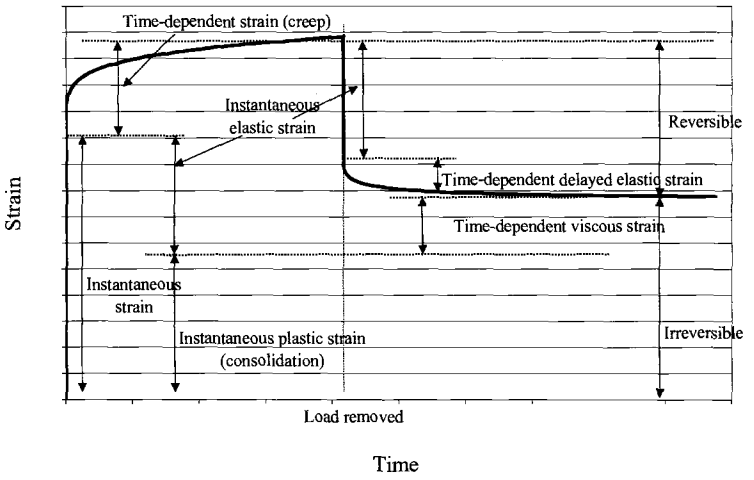

Figure 1-*Typical example of creep as a function of time for a material with a constant load that is subsequently removed.*

Creep is defined as the strain that occurs in a material exposed to a constant load as a function of time. Deformation that occurs during loading is denoted instantaneous strain. Deformation that develops over time is denoted time-dependent strain. A deformation, which recovers when the load is removed, is denoted a reversible deformation. The instantaneous elastic deformation and the time-dependent delayed elastic deformation are reversible. Deformations that remain after the load has been removed are denoted irreversible deformations. The instantaneous plastic deformation,

also called the consolidation, and the time-dependent viscous deformation are irreversible. Instantaneous strain contains an instantaneous elastic part and an instantaneous plastic part. Consolidation as part of the instantaneous strain during loading is not defined as creep. Creep and recovery can be described theoretically [*4 - 9*].

Theoretical Description of Creep

Some materials can be defined as Clouser materials. These materials can be described by applying the theory for a Clouser material [*6*]. The use of the Clouser equation is presented in [*1, 2, 10, 11*]. It should be noted that parameters in the creep functions are theoretically independent of the load state. However, this is only true if the load does not cause damage to the material. The measured creep is adjusted to the Clouser equation.

The resulting strain is given by

$$\varepsilon(t)=\begin{cases}\varepsilon_0+\sigma_1 c(t), & 0\le t<t_1\\ \varepsilon_0+\sigma_1 c(t)-(\sigma_1-\sigma_2)c(t-t_1), & t\ge t_1\end{cases} \tag{1}$$

where $c(t)$ is the Clouser equation given by

$$c(t)=\frac{1}{E}\left[1+\left(\frac{t}{T}\right)^{a_1}\right] \tag{2}$$

and t (s) is time, t_1 is the time (s) at the load relieve, E (Pa) is the elastic modulus, T (s) is a constant called the relaxation time and a_1 (dimensionless) is the creep exponent which is also a constant. In addition, the consolidation denoted ε_0 (dimensionless) is a constant found from experiments. σ_1 (Pa) is the constant load for $t < t_1$ and σ_2 (Pa) is the constant load for $t \ge t_1$.

The creep function $c(t)$ describes the strain that occurs, when the material is subjected to a constant stress, $\sigma = 1$ at the time $t = 0$.

Static Conditions

Stresses in the loose-fill insulation material can be described by applying theories used for describing silos. The application of silo theories is summarized and described in [*12*] and proved to be useful for describing the stress state of dry granular bulk solids in [*13, 14*] and to explore anisotropic properties of dry granular solids in [*15*].

The theory describes the stress state as a function of the height of the loose-fill insulation material in a wall. The load originates from the loose-fill insulation material itself. It is assumed that the insulation material is homogeneously distributed in the wall. The theory includes two material parameters, the coefficient of friction between the wall and the insulation material and the horizontal stress ratio, respectively.

The vertical stress, σ_v (Pa), as a function of the height of the loose-fill insulation material in a wall is given by [*1, 2, 16*]

$$\sigma_v(z) = \frac{A\rho g}{\mu\lambda O}\left[1 - e^{-\frac{\mu\lambda O}{A}z}\right] \quad (3)$$

where the internal horizontal area and perimeter of the wall is denoted A (m^2) and O (m), respectively. ρ (kg/m^3) is the density of the loose-fill insulation material and g (m/s^2) is the gravitational acceleration. z (m) is the distance from the upper surface of the loose-fill insulation material, μ is the coefficient of friction (dimensionless) between the wall and the loose-fill insulation material and λ is the horizontal stress ratio (dimensionless). In the derivation of Equation (3) it is assumed that the horizontal stress ratio is constant in the whole wall, and that the vertical stress, $\sigma_v = 0$ for $z = 0$.

Figure 2 shows calculations of the stresses in a loose-fill insulation material filled in a wall, using Equation (3) for a wall made of gypsum boards. The wall was 2.4 m high, between 0.1 m and 0.5 m thick and 1.0 m wide. Stresses were calculated for densities of the insulation material of 48, 50, 53 and 56 kg/m^3. The coefficient of friction between the wall and the loose-fill insulation material was 0.66. The horizontal stress ratio was 0.42. The coefficient of friction between the wall and the loose-fill insulation material and the horizontal stress ratio were found from tests with loose-fill cellulosic fibre insulation material [*1,17*].

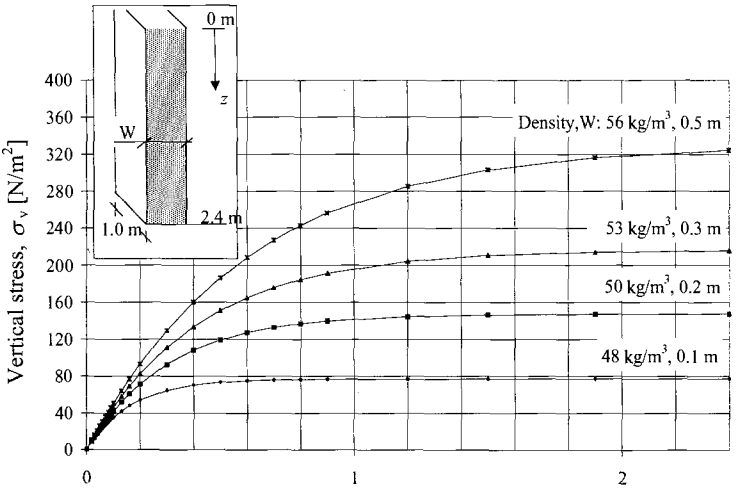

Figure 2-*Stresses in loose-fill insulation material filled in a wall as a function of density, width of the wall and distance from the upper surface of the insulation material. The coefficient of friction between the wall and the loose-fill insulation material was 0.66. The horizontal stress ratio was 0.42.*

Stress-Stable State and Volume Stability

Loose-fill materials loose-filled into a wall will be in a volume-stable state provided the loose-fill remains in a stress-stable state and fills out the volume of the wall.

Constant Relative Humidity

When a wall is in temperature and relative humidity equilibrium in a stable environment, the necessary density of the loose-fill can be found in the following way:

For a predetermined homogeneous density of loose-fill, stresses as a function of the height of the insulation material in the wall is determined from Equation (3). From Equation (3) the stress level for which the loose-fill must be volume-stable is determined as the highest calculated stress level for the wall, called the design stress. For the predetermined density of loose-fill, creep for the design stress as a function of time is determined by using the Clouser equation. From these calculations the irreversible strain is determined. The irreversible strain is defined as the difference between the instantaneous strain plus the creep and the instantaneous elastic strain plus the delayed elastic strain.

If the density of the loose-fill is determined to be in its irreversible state for the design stress, a recalculation has taken place using a higher density of loose-fill. For the loose-fill to be in its reversible state at the design stress, the irreversible strain must be eliminated. The irreversible strain can be calculated as

$$\text{Irreversible strain} = \left(\varepsilon_0 + \sigma_1 c(t)\right) - \left(\sigma_1 c(t - t_1)\right) \leq 0 \qquad (4)$$

from which the critical consolidation can be determined.

That the insulation material is kept inside the wall at a reversible state means that the material will fill out the volume of the wall, i.e. it stays at a volume-stable state.

Varying Relative Humidity

When a wall is exposed to a varying relative humidity, the necessary density of loose-fill is found from two different design principles: 1. using a stress criterion, 2. using an energy criterion.

1, stress criterion – From a strain-time diagram for varying RH, the stable strain-state at different load levels is determined. From the stable strain-state, the associated density for a volume-stable state is determined as a function of the applied stress. A linear function found by the least square fit, which determines the density for volume-stable state, denoted $\rho_{v\text{-}s}$ (kg/m^3) as a function of the associated stress, denoted $\sigma_{v\text{-}s}$ (Pa) is found and given by

$$\rho_{v-s} = a\sigma_{v-s} + b \qquad (5)$$

where a (kg/Nm) is a constant and b (kg/m^3) is a constant.

Hereafter the design stress is determined. The design stress is used to calculate the volume-stable density. The calculated volume-stable density is found when it is equal to the predetermined density. The volume-stable density of loose-fill can be determined as an iterative process that includes the predetermined density and the calculated volume-stable density.

2, energy criterion – Using this design method, the volume-stable state is found by energy optimisation of the loose-fill. The necessary energy is the difference between the required and the available energy for the wall insulated with loose-fill. The required energy is calculated as the integral of the vertical stress in the wall over the height of the wall for the predetermined density of loose-fill. The available energy for the predetermined density of loose-fill is calculated as the integral of the stress associated with the density for the volume-stable state of loose-fill over the height of the wall, denoted h_0. The necessary energy, denoted U_N (J) is given by

$$U_N = \int_0^{h_0} A\sigma_v(z)\mathrm{d}z - \int_0^{h_0} A\sigma_{v-s}(\rho)\mathrm{d}z \geq 0 \qquad (6)$$

When optimizing the necessary energy, it is assumed that the loose-fill is able to make physical use of its energy resource by expanding at stress relieves.

The volume-stable density of loose-fill can be determined as an iterative process involving the predetermined density of loose-fill.

For more elaborate calculations the influence from a vertical load applied on top of the insulation material can be taken into consideration [*1, 2, 17*].

Test Material

The loose-fill material tested was a loose-fill cellulosic fibre material made of recycled paper and used for thermal insulation. In the following it is referred to as cellulose fibre insulation (CFI). The CFI is produced from recycled paper torn to pieces of maximum 2 mm by 3 mm. In total, 5 % by weight of borax and boric acid is added to the CFI to ensure that the cellulose is fire-resistant and resistant to mould growth. The loose-fill material was characterised by being a mass of material consisting of many small separate parts and fibres. These small parts and fibres were not bound together in a fixed predefined form. With a relatively small effort, the CFI could be distributed homogeneously across a predefined area which was large compared with the size of a single particle.

Test Method – Constant Relative Humidity

Sampling

Samples should be randomly chosen. The chosen sample was loosened by pressurized air in a closed box mounted a vent that prevents loss of material prior to conditioning and testing. Samples should be conditioned to test conditions before testing. Especially conditioning to the predetermined relative humidity and the

predetermined temperature is important. The sample should be handled in such a way that the least possible interaction takes place between particles, moisture and additives, and the surroundings.

One test series includes 3 in principle identical specimens of loose-fill loaded to 3 different load levels. One specimen is used for every load level. A sufficient number of specimens should be exposed to allow statistical examination of the results.

Test equipment must be clean, free from static electricity and conditioned before testing. It is important to keep the test set-up vibration free during the test period.

Test Equipment

Test equipment for the creep test included the following:

Test container - An acrylic cylinder with a vertical centreline was placed on a horizontal acrylic plate. The cylinder had an internal diameter of 104.5 mm ± 0.5 mm and was approximately 110 mm in height. The test container also consisted of at plane disc made of acrylic with a diameter 1.5 - 2 mm less than the internal diameter of the cylinder. The plane disk was provided with small drilled, but not riddled-drilled, holes made for grips. The plate was 5.5 mm thick, and the cylinder and the disc are both 3 mm thick. The cylinder was marked on the outside at a horizontal plane at 3 angles (120°) at every 10 mm vertically from the bottom plane. The disc was fixed in a position where the distance from the bottom plane to the underside of the disc was 70 mm. This was done by sticks put through holes drilled in the cylinder.

Weights should be easy to add to and remove from the upperside of the disc in order to introduce only minor disturbances and sources of error to the test. The load was mounted as a steady load on top of the disc. For heavier loads it is convenient to use load discs with load and off-load hangers.

Mounting-stick - An approximately 200 mm stick was mounted perpendicular to a disk. The diameter of the disk was 1.5 - 2 mm less than the internal diameter of the cylinder. For every cm^2 the disk was provided with a hole with a diameter of 1 - 1.5 mm. The disc was made of acrylic and was approximately 5.5 mm thick.

Distance measuring system - A distance measuring system with the capability of at least 12 mm of displacement with an accuracy of ± 0.1 mm. An LVDT displacement transducer on a bridge was mounted on top of the cylinder. The position of the displacement transducer should be flexible. The weight of the displacement transducer stick was included in the load put on the CFI.

Other aid and test facilities - A datalogger for sampling displacement as a function of time and a datalogger control system, for example a PC.

A balance capable of weighing up to 0.5 kg with an accuracy of ± 0.0001 kg.

Plastic gloves and a light form of respirator should be used together with tweezers and containers for handling and storing the material.

Tests were carried out in an environment where the relative humidity and temperature were kept constant with an accuracy of ± 2% and ± 2 °C, respectively.

Test equipment and a test set-up is shown in Figure 3. The height of the sample was restricted so that the loss of stress due to wall friction (originating from the displacement) from the top to the bottom of the loose-fill material was negligible.

Displacements were measured along the vertical centerline of the loose-fill material.

Procedure

The right amount of loose-fill material for obtaining the predetermined overall density in the test container was weighed out. The weighed-out material was divided into 7 parts, with identical weight. The parts were then mounted one by one in the test container in the following way. One part of the CFI was homogeneously distributed over the horizontal plane of the cylinder. When necessary, the tweezers were used.

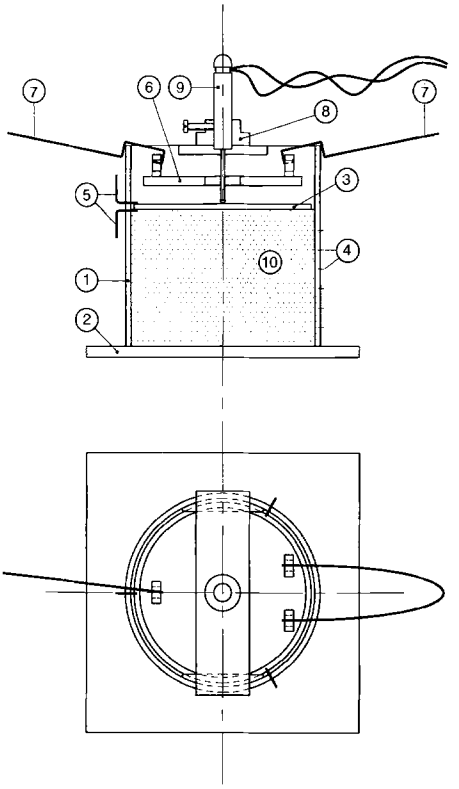

Figure 3-*Test equipment to measure instantaneous strain and creep for loose-fill material. Top: vertical section. Bottom: plan. 1: 104.5 mm Ø; acrylic cylinder of 110 mm height. 2: 5.5 mm thick acrylic plate. 3: 3 mm thick acrylic disc. 4: 10 mm marks. 5: sticks. 6: load disc. 7: load and off-load hangers. 8: bridge. 9: LVDT displacement transducer. 10: loose-fill material.*

When distributed, the mounting-stick was used gently to press the CFI to the predetermined density, marked on the test container as a horizontal plane with spots at 3 angles (120°). When the weighed-out material was filled in the test container, the disc was fixed.

If load hangers are used, they should be mounted at this point. Furthermore, the displacement transducer was put in position.

The test is now ready and logging can begin. When the start position has been noted, the disc is loosened and the predetermined load is mounted on the upperside of the disc.

Loading should not last longer than 20 seconds. If loosening of the disc does result in an expansion of the CFI, the disc must be unfixed first at the underside and then loaded before the sticks at the upperside of the disc are removed carefully.

Initial sampling rate recommended is 1 second increasing to 5 seconds a few minutes after loading and finally to be increased to 1 hour after 2 hours from the time of loading.

The vertical displacement of the disc is measured as a function of time. After some time, for example 3 days, the added load is carefully removed and hereafter only the disc and the displacement transducer stick will load the CFI. When unloading, it is recommended to use the same sample rate scheme as when loading. The test was finished 2 hours after unloading.

Test Method-Varying Relative Humidity

Tests were carried out as described in the test method above. However, it was made possible for air to flow through the CFI. The horizontal acrylic plate, which formed the base of the test container; see Figure 3 (2) and the plane disc; see Figure 3 (3), were provided with small drilled holes. Holes 1 - 1.5 mm in diameter were drilled at approximately every cm^2. During testing 10 - 20 Pa of the mounted load is put on to the CFI as a low pressure mounted the base of the test container. In this way the relative humidity around the test set-up was used to change the moisture condition in the CFI.

Results from Creep Tests

Constant Relative Humidity

Strain-time diagrams have been determined for CFI of various densities exposed to a constant load of 78, 202 and 499 Pa, respectively until the time denoted t_1, and subsequently relieved of 20, 68 and 87% of its load. The CFI tests have been carried out with densities of 30, 42, 50 and 60 kg/m^3 at 23 °C and 50 % RH. Additionally, tests have been carried out with a density of 42 and 50 kg/m^3 at 23 °C and 80 % RH. The nominal density is related to the density of the insulation material at 23 °C and 50 % RH.

Table 1 shows strain components determined from strain-time diagrams for CFI. Table 1 includes the measured instantaneous strain, measured instantaneous elastic strain determined from the load relieved at the time t_1 and instantaneous plastic strain. The instantaneous plastic strain is defined as the difference between the instantaneous strain and the instantaneous elastic strain. Figure 4 shows measured strain-time in a diagram for CFI.

Table 1-*Strain components for CFI with densities of 30, 42, 50, and 60 kg/m^3 determined from creep tests at 23 °C and 50 % RH and 80 % RH.*

Relative humidity [%]		50				80	
Density [kg/m^3]		30	42	50	60	42	50
Strain	Load level, σ_1						
Instantaneous	78 Pa	0.092	0.062	-0.010	-0.068	0.060	-0.008
strain,	202 Pa	0.201	0.131	0.010	-0.018	0.120	0.004
$\varepsilon_0+\sigma_1/E$	499 Pa	0.307	0.22	0.100	0.038	0.210	0.060
Instantaneous	78 Pa	0.005	0.003	0.003	0.010	-	-
elastic strain,	202 Pa	0.020	0.021	0.022	0.022	0.010	0.008
σ_1/E	499 Pa	0.047	0.056	0.054	0.057	0.019	0.022
Instantaneous	78 Pa	0.088	0.059	-0.013	-0.078	0.060	-0.008
plastic strain	202 Pa	0.181	0.110	-0.012	-0.040	0.110	-0.004
(consolidation), ε_0	499 Pa	0.260	0.164	0.046	-0.019	0.192	0.038

Table 2 shows the elastic modulus for CFI at a density of 30, 42, 50 and 60 kg/m^3 at 23 °C and at 50 % RH and 80 % RH. The elastic modulus has been determined from the 2 highest load levels. The elastic modulus is the linear elastic modulus and represents the capability of the material to regain its volume when relieved of its load.

Table 2-*Elastic moduli (average from load level 202 and 499 Pa) for CFI at a density of 30, 42, 50 and 60 kg/m^3 at 23 °C and at 50 % RH and 80 % RH.*

Density [kg/m^3]	RH [%]	Elastic modulus [Pa]
30	50	10690
42	50	8650
50	50	9850
60	50	9900
42	80	31330
50	80	29385

Varying Relative Humidity

The strain-time diagram for CFI with a density of 50 kg/m^3 exposed for 3 – 4 days at a time alternating between 50 % RH, and 80 % RH; see Figure 5. CFI was exposed to a constant load of 59, 129 and 279 Pa at the upperside of the loose-fill and a suction pressure at the underside of 21 Pa. The start conditions of the material was 23 °C and 50 % RH. Throughout the test period the temperature was kept constant at 23 °C.

Determination of Material Properties

The measured creep that develops in the CFI exposed to constant stress, as a function of time is adjusted by the Clouser equation. Adjusting the creep data to the Clouser equation it is found that the equation can be linear by logarithm; see [*1, 2*]. An extract of the measured creep data, for at least 3 load levels, is adjusted to the linear logarithm

creep equation by the least square method. From the linear logarithm creep equation the constant relaxation time, T and the constant creep exponent, a_1 are found. For adjusted creep data to the linear logarithm creep equation the instantaneous plastic strain must be added to the creep function as a constant and therefore takes no part in the determination of the parameters a_1 and T.

The modulus of elasticity used was the average instantaneous elastic modulus found from unloading the specimens.

Adjusting the Creep Data

Measured versus calculated strain, for CFI with a density of 60 kg/m^3 at 23 °C and 50 % RH is shown in Figure 4. Strain is calculated using equation (1) with E = 9900 MPa, a_1 = 0.1345 and T = 139.6 days. ε_0 is taken from Table 3 according to load level. CFI is exposed to a constant load of 78, 202 and 499 Pa until the time denoted t_1 and subsequently partly relieved of 20, 68 and 87 % of its load, respectively.

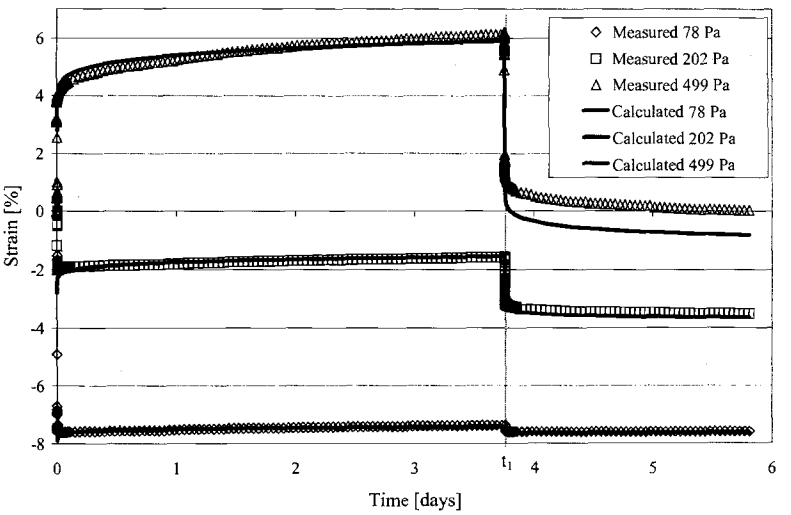

Figure 4-*Strain-time diagram for CFI. CFI is exposed to a constant load until the time denoted t_1 and subsequently partly relieved of its load. Solid lines show strain calculated with the Clouser equation, Equation (1) and (2) for the load level 78, 202 and 499 Pa.*

Table 3 shows the creep parameters a_1 and T describing the Clouser equation for CFI at different densities and different moisture conditions. Furthermore, the strain components used are shown. The creep data have been adjusted to the Clouser equation for the load level of 78, 202 and 499 Pa. Creep tests have been carried out for the densities 30, 42, 50 and 60 kg/m^3 at 23 °C and 50 % RH. Additional tests have been carried out with densities of 42 and 50 kg/m^3 at 23 °C and 80 % RH.

Table 3-*Creep parameters and their associated strain components for CFI.*

RH [%]		50				80	
Density [kg/m^3]		30	42	50	60	42	50
a_1		0.2563	0.2759	0.2612	0.134[illegible]	0.3118	0.3317
T [days]		0.0723	1.9015	17.457	139.63	0.0025	0.0215
Strain	load level, σ_1						
Instantaneous	78 Pa	0.1100	0.0670	-0.0140	-0.0790	0.0850	-0.0120
strain,	202 Pa	0.2200	0.1400	0.0130	-0.0280	0.1450	0.0065
$\varepsilon_0+\sigma_1/E$	499 Pa	0.2700	0.2200	0.1100	0.028[illegible]	0.2000	0.0670

Prediction of Creep at Varying Relative Humidity

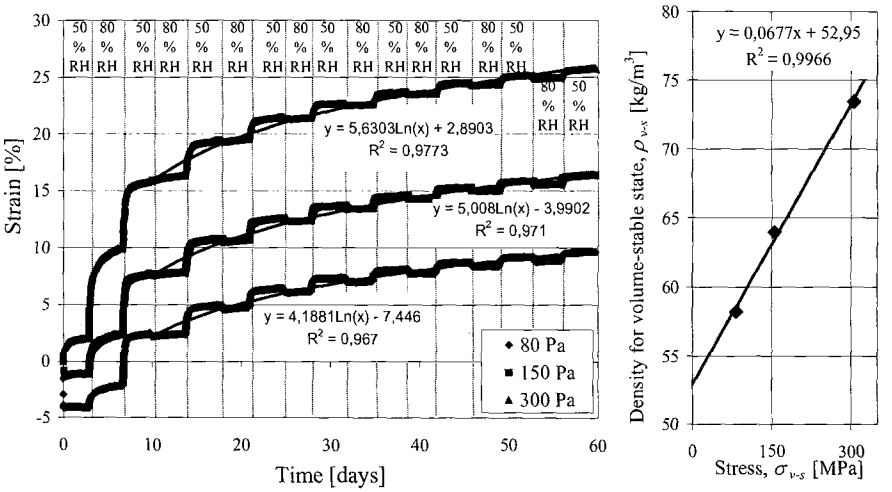

Figure 5-*Strain-time diagram for CFI exposed to 23 °C and a relative humidity alternating between 50 % RH and 80 % RH exposed to a constant load of 80, 150 and 300 Pa, respectively. In addition the density for a volume-stable state as a function of stress is shown. Functions found by the least square method are shown.*

Figure 5 shows the strain-time diagram for varying relative humidity. In addition an exponential function given by $\varepsilon(t) = c\ln(t) + d$ is found by the least square method and shown for each load level. c and d are regression constants. Test data from the 4th RH cycle were used to find exponential functions. Furthermore, the density of the CFI related to a stable strain level as a function of the applied stress is shown. From the exponential equation describing strain as a function of time and RH cycles, 175 days corresponding to 25 RH cycles was chosen to represent the stable strain level for these experiments. From these assumptions the density for a volume-stable state of CFI as a

function of the stress is calculated. By the least square method a and b are found, a = 0.0677 kg/Nm and b = 52.95 kg/m^3.

Prediction of Volume Stability

The density of CFI required to ensure volume stability in a wall made of gypsum boards 2.4 m high, 0.2 to 0.5 m thick and 1.0 m wide was determined. The coefficient of friction between the wall and CFI, and the horizontal stress ratio for CFI was 0.66 and 0.42, respectively. The required density was found for 3 different cases; 1) the wall was exposed to 23 °C and 50 % RH; 2) the wall was exposed to 23 °C and 80 % RH; and 3) the wall was exposed to 23 °C and alternately 50 % RH and 80 % RH. Results are shown in Figure 6.

In the case where the wall was in a stable environment of 23 °C and 50 % RH, the necessary density of the CFI is found using Equation (4).

For a design stress, creep as a function of time is determined using the Clouser equation. From these calculations the density for eliminating the irreversible strain is determined. A period of a few days was used as the lifetime for the calculations. However, Figure 4 shows that only minor additional strain develops at the actual load level after a few days.

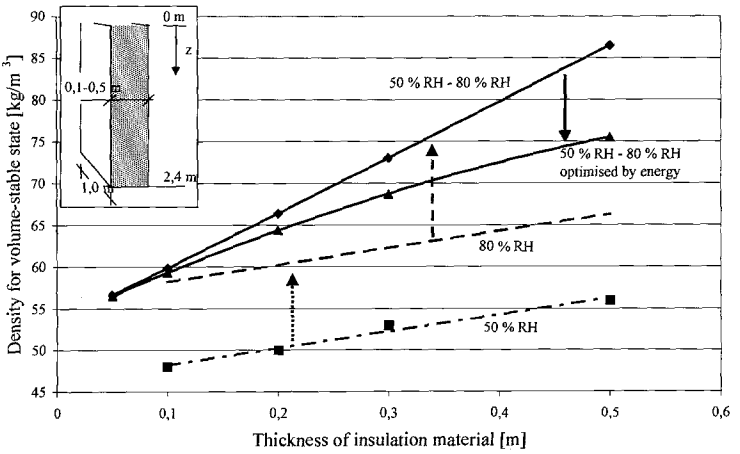

Figure 6-*Calculated necessary density as a function of wall thickness to prevent settling of CFI in a wall.*

Similar calculations have been carried out for the wall exposed to 23 °C and 80 % RH. Moreover, results from CFI used for thermal insulation exposed to 23 °C and 80 % RH are shown for partly extrapolated data.

For the wall exposed to 23 °C alternating between 50 % RH and 80 % RH, the necessary density of CFI is found from two different design principles. First, by using Equation (5). Second, by optimising the necessary energy using Equation (6) combined with the predetermined density.

Discussion

This paper presents a proposal for a standardised method for describing the experimental techniques and theoretical framework needed to determine the associated creep parameters. Furthermore, it is shown how the described creep for CFI can be used by the theory presented to calculate the necessary density of CFI required to prevent settling in a wall. The coefficient of friction between the wall and the insulation material, and the horizontal stress ratio, must be determined in order to use the theory presented. Usable methods to determine the individual parameters are shown in [*1, 2, 17*].

The strain-time components of CFI exposed to a constant load and constant moisture conditions have been shown. Analyses of the creep function allow CFI to be described by the Clouser equation. Stress components determined using the description of the creep function by use of the Clouser equation was found to be in good agreement with strain components determined from the strain-time diagram, see Tables 1 and 3. It was also found that parameters describing the creep functions are theoretically independent of the load level. However, this is only true if the load does not cause damage to the material. The stress analyses of walls showed that the stress state for practical use is well described by the Clouser equation. Additional tests have shown that a range of other loose-fill materials used for thermal insulation can be defined as Clouser materials [*1*].

The elastic modulus is the linear elastic modulus and represents the capability of the material to regain its volume when relieved of its load. The elastic modulus is determined from the strain-time diagram. The capability of the material to regain its volume was found to be related to the relative humidity of CFI. For the actual investigated densities of CFI, the capability to regain volume decreased with increased relative humidity. Similar results are shown in [*1*]. Furthermore, it was found that the capability of the material to regain its volume was not related to the density of the CFI for densities relevant when used for thermal insulation.

For an alternating relative humidity of the insulation material exposed to a constant load, the strain-time diagram shows a progressive strain. This progressive strain stabilised with the number of cycles. This phenomenon is not covered by the creep theory described. However, it is shown how results from the proposed test equipment can be used to predict a volume-stable state for CFI in a wall.

Both the loss of the capability of CFI to regain its volume and an increased strain of CFI exposed to a constant load, when the relative humidity is increased; and increased strain of CFI exposed to a constant load and alternately changing relative humidity, result in an increase in the necessary density to keep CFI in a volume-stable state in a wall.

Conclusion

The paper describes a proposal for a standardized method for describing the experimental techniques and theoretical framework needed to determine the associated creep parameters. The specific application presented here is loose-fill cellulosic fibre insulation material filled in walls and used as thermal insulation. Moreover, it is shown

how the proposed design tool can be used to predict the density needed for a given loose-fill insulation material in order to prevent settling in a wall. The theory and design tool considers stress analysis and the creep of the material. Stress analysis showed that it was possible to set up equations to estimate stresses in loose-fill insulation materials as a function of the height of a wall. These considerations have been combined with theories describing creep of the loose-fill insulation material.

Using the proposed experimental techniques and theoretical framework it was found possible to determine creep analytically with good agreement with test results. The proposed method and theoretical framework can be used for walls exposed to a constant environment and to an environment with an alternating relative humidity.

Calculations have shown that loose-fill material of cellulose in a 0.1-m-thick and 1.0-m-wide gypsum wall 2.4 m in height with a minimum density of 48 kg/m^3 will not settle if kept at a constant relative humidity of 50 % and at a temperature of 23 ^{0}C. A minimum density of 53 kg/m^3 is necessary if the thickness of the wall is increased from 0.1 m to 0.3 m. If changing the constant environment from a relative humidity of 50 % to 80 % and at a temperature of 23 ^{0}C, a minimum density of 63 kg/m^3 is necessary. Furthermore, if the wall is exposed to a temperature of 23 °C and an alternating relative humidity of 50 % and 80 %, the necessary density is increased to 73 kg/m^3. Assuming that the material is able to make use of its energy ressource, the density can be reduced to 68,7 kg/m^3; see Figure 6.

References

[1] Rasmussen, T. V., "Sætningsfri indblæsning af løsfyldsisolering i vægge," (Settling of loose-fill insulation materials in walls; in Danish, summary in English), By og Byg Dokumentation 011, Danish Building and Urban Research, Hørsholm, Denmark, 2001.

[2] Rasmussen T. V., "Modelling Settling of Loose-fill Insulation in Walls, Part I," *Journal of Thermal Envelope & Building Science*, Vol. 25, No. 2, October, 2001.

[3] Andersen, T., Fynholm, P., Hansen, M. H., and Nicolajsen, A., "Fugtsikre træfacader - Fugtindhold i højisolerede træfacader," (Moisture content in highly insulated wood frame walls; in Danish), By og Byg Dokumentation 025, Danish Building and Urban Research, Hørsholm, Denmark, 2002.

[4] Nielsen A., "Rheology of Building Materials," National Swedish Building Research, Stockholm, Sweden, 1972.

[5] Burgers J. M., "Mechanical Considerations, Model Systems, Phenomenological Theories, in Akademie van Wetenschappen, First Report on Viscosity and Plasticity," Amsterdam, Holland, 1935, pp. 21-33.

[6] Clouser W. S., "Creep of Small Wood Beams under Constant Bending Load," U.S. Forest Products Lab. Report 2150, Washington D.C., USA, 1959.

[7] Flügge, W., "Viscoelasticity," Blaisdell Publishing Company, London, 1967.

[8] Nielsen, L. F., "Rheologische Eigenshaften für isotrope linear-viskoelastische Kompositmaterialien." Cement and Concrete Research 3, 1973, pp. 751.

[9] Wesche, K., "Baustoffe für tragende Bauteile 1," Bauverlag GMBH, Wiesbaden und Berlin, Germany, 1977, pp. 68 – 84.

[10] Nielsen, L. F., "Materialemekanik grundkursus II i bygningsmaterialer," (Materials mechanics; in Danish), Technical Report 169/86, Building Materials Laboratory, Technical University of Denmark, 1986.

[11] Nielsen, L. F., "Materialemekanik," (Materials mechanics; in Danish), Technical Report 286/1993, ISSN 0908-3871, Building Materials Laboratory, Technical University of Denmark, 1993.

[12] Wenzel, F., "Untersuchungen über die Druckverhältnisse in Silozellen," Diss. TU Braunschweig, 1962.

[13] Hartlen, J., "The strength parameters of grain, European Symposium on Particle Technology," 3-5 June, Amsterdam, 1980, pp. 9.

[14] Munch-Andersen, J. and Nielsen, J., "Pressures in slender grain silos," CHISA 1990, Second European Symposium on Stress and Strain in Particulate Solids, Prague, 26-31 August, 1990, pp. 9.

[15] Hartlen, J.; Nielsen, J.; Ljunggren, L.; Martensson, G. and Wigram, S. "The wall Pressure in large Grain Silos," Swedish Council for Building Research, Stockholm, Document D2:1984, 1984.

[16] Barfod, N., "En introduktion til partikelteknologi," (An introduction to particle technology; in Danish), Department of Chemical Engineering, Technical University of Denmark, 1982.

[17] Rasmussen T. V., "Modelling Settling of Loose-fill Insulation in Walls, Part II, Determination of Coefficients," accepted for publication in *Journal of Thermal Envelope & Building Science*, 2002.

David R. Salmon,[1] Ray G. Williams,[1] and Ronald P. Tye[2]

Thermal Conductivity and Moisture Measurements on Masonry Materials

Reference: Salmon, D. R., Williams, R. G., and Tye, R. P., **"Thermal Conductivity and Moisture Measurements on Masonry Materials,"** *Insulation Materials: Testing and Applications: 4th Volume, ASTM STP 1426,* A. O. Desjarlais and R. R. Zarr, Eds., ASTM International, West Conshohocken, PA, 2002.

Abstract: A program of work involving measurement of moisture transport properties coupled with guarded hot plate thermal conductivity of some typical masonry materials containing different amounts of moisture has been carried out in support of a large European Union investigation involving the thermal performance of masonry walls. The basic property data were required to assist in both the verification of different hot-box methods and in the development and verification of a simple model that could be used to estimate the thermal performance of moist masonry walls with typical moisture contents.

The five materials studied were an aerated concrete, a high-density hollow concrete block, a hollow clay block and two mortars of widely different density. Measurements were carried out by a number of thermal conductivity laboratories in accordance with appropriate ISO and CEN standards on each material in the dry state and conditioned at 23°C/50%RH and 23°C/90%RH. In addition the moisture absorption/desorption and the water vapor permeability were measured for each material.

The results are discussed with respect to their use and value to the overall program and to previous work on masonry materials. In particular the validity of previous relationships for thermal conductivity with density and for the effects of moisture are also discussed.

Keywords: thermal conductivity, moisture adsorption, moisture desorption, moisture permeability, concrete, mortar, standards

Background and Objectives

During the past ten years there has been a concerted effort by members of the European Union to provide a standardized approach to specifying, testing and applying commonly used materials used for and within the building envelope. This is manifested

[1] Principal Research Scientists, Thermal Metrology Team, National Physical Laboratory, Teddington, Middx. TW11 0LW, UK.
[2] Consultant to Thermal Metrology Team, National Physical Laboratory Teddington, Middx. TW11 0LW, UK.

by the development of standards[3], the adoption of which will be mandatory for member countries within the next year or so. The draft standard prEN 1745 "Masonry and masonry products: Methods for determining design thermal values," produced by CEN/TC125, details methods for determining design values for thermal conductivity and resistance of both masonry and masonry products. These design values for masonry and composite masonry walls refer to "moisture content under service conditions" which may be taken from tabulated design values derived from measurements on test walls or from calculations using numerical methods.

For composite masonry systems the experimental determination of the dependence of thermal performance on moisture content by measurements at several moisture content levels is complicated, time consuming and expensive. At present the design value required at the national level is derived from measured values in different ways in different countries. Thus the above harmonized conversion procedure is required in order to obtain thermal design values of composite masonry systems found under service conditions (these will be defined on a national basis according to nationally varying climatic conditions) from measured values, preferably from a single determination in the dry state.

The desire for standardized test methods to facilitate an open market has prompted the production of a number of standards for the measurement of the thermal resistance of building materials (e.g. walls) in the dry and moist state. These standards (produced by Working Group 8 of CEN/TC89) include:

- ISO 8990:1994 The "classical" hot-box standard for the guarded hot-box (GHB) and calibrated hot box (CHB).
- EN 1934:1995 This is a hot-box measurement procedure that employs a heat flow meter fixed to the test element (HFM/HB). This standard was based mainly on the experience of German, Austrian and Swiss laboratories.

This latter standard has the advantage over the two "classical" hot-box types of being able to deal with a wide range of thickness of masonry structures in a modest sized hot-box. It is now essential to quantify the repeatability and reproducibility of these different measurement procedures in order that the requirements of the Construction Products Directive 89/106/EC (attestation of conformity), in connection with the basic document Nr. 6 (energy conservation and heat insulation) and the guidance paper 1, which deals with "classes and performance levels," can be met.

In order to attain the overall goal, a comprehensive three year project involving a total of twelve organizations undertaking measurements on five materials was initiated in 1998. The properties measured by selected organizations were thermal conductivity, thermal conductance and U Value, water vapor resistance and hygroscopic sorption. The materials selected were an autoclaved aerated concrete, a typical hollow concrete masonry block, a hollow brick block and two types of mortar

The project had six major objectives:

1. Determine the relevant thermal and moisture properties of five basic constituent materials at three different moisture content levels for use in subsequent tasks.
2. Validation of EN 1934.

[3] A list of E.U. Technical Committees and Standards relevant to this project is listed in the Appendix.

3. Determination of the uncertainty, repeatability and reproducibility requirements as defined in ISO 5725-2.
4. Measurement of the thermal resistance of walls fabricated using three different masonry products and two different mortars.
5. Measurement of the thermal resistance of a range of "ideal" wall systems by replacing the mortar with glass sheets to enable final analysis to be verified.
6. Using the measured data to develop a model and conversion procedure which enables the thermal properties of masonry wall systems to be derived from the component properties in the dry state.

The present paper describes and discusses the work carried out in order to satisfy the first objective. The work on the other objectives is ongoing and will be reported elsewhere once it has been completed and analyzed.

Scope

In order to accomplish the task of providing data on the individual objectives the following measurements were made by six individual European organizations:

- Thermal conductivity at 10 °C mean temperature using procedures specified in ISO8302/prEN13009 on the as-dried material and on specimens conditioned at 50% RH and 90% RH respectively to constant weights. (Limited measurements involving different temperature differences and at 24 °C were carried out by one organization).
- Water vapor transmission (permeability) using procedures specified in EN12572 on specimens conditioned at the same levels.
- Hygroscopic sorption and desorption over the total RH range on the as-dried and as-conditioned specimens in accordance with EN12571.

Participants

Table 1 contains details of the seven organizations plus associated contractors that were commissioned to undertake the complete experimental program.

Materials

The following masonry materials were selected for the study and specific lots supplied in sufficient amounts to each participant

- an aerated autoclaved concrete (AAC), Type Planstein PP2 0.45, supplied in the form of 0.5 by 0.25 m rectangular blocks and thicknesses of 0.1, 0.2 and 0.3 m.
- a hollow concrete block (CB), Tonblock, supplied by Lapor in the form of rectangular blocks of size 0.5 by 0.22 by 0.3 m.
- a hollow brick block (BB), Type HLZ Flat brick supplied by Weinberger having dimensions 0.25 by 0.249 by 0.3 m.
- a high density mortar (HDM), Quick-mix K01 – lime cement for internal and external walls. It was supplied in the form of 32kg sacks by Quick-mix D-

Schwagsdorf and stated to be a Mortar Group II (DIN 1053, DIN 18550) with binders (DIN 1164 and 1060) and mineral additives.

Table 1 — *Project participants and their roles.*

Institution, (Short Name), Country	Guarded Hot Box	Hot Plate	Sorption	Vapor transmission	FEA modeling	Supply material	Industrial expertise	Conversion modeling
National Physical Laboratory, (NPL), UK	X	X	X	X				
Fraunhofer-Institut für Bauphysik, (IBP), Germany	X	X	X	X	X	X		
Forschungsinstitüt für Wärmeschutz e.V, (FIW), Germany	X	X	X	X	X	X		
Swedish National Testing and Research Institute, (SP), Sweden	X	X	X	X				X
Technical Research Centre of Finland, (VTT), Finland	X	X	X	X				
Leopold-Franzens-Universität Innsbruck, Institut für Bauphysik, (UI), Austria	X				X			
Laboratoire Federal d'Essai des Materiaux et de Recherches, (EMPA), Switzerland	X	X	X	X	X	X		
H H Celcon, (CELCON), UK							X	
Bautechnische Versuchs- Und Forschungsanstalt, (BVFS), Austria		X	X	X				
Versuchs-und Forschungsanstalt der Stadt Wien Magistratsabteilung 39, (MA39), Austria	X				X			
Versuchsanstalt fur Wärme - und Schalltechnik am Technologischen, (TGM), Austria	X				X			
Quadruple-M Elsaesser GmbH, (4M), Austria						X		

- a low density mortar (LDM) supplied by Sakret D-Dortmund in the form of 32 kg sacks and stated to be Mortar Group IIa (DIN1053) with binders and cement

(DIN1164) with special lightweight aggregates 0/4 (expanded clay) plus special additives plus lightweight additives.

Experimental Details

On receipt of the test materials appropriately sized test-specimens were prepared for the particular test method and apparatus used by a participant. In the case of the block materials this involved slicing the large area faces from one or more blocks and cutting and machining them to the required test size. For the thermal conductivity tests the machining ensured that the thickness was uniform and the surface flat to within the limits specified for the test method. Specimens of the two mortar materials were mixed with recommended amounts of water either by machine or hand mix and cast in appropriate sized moulds, allowed to dry and then machined to the desired surface finish.

Hygroscopic Sorption and Desorption

Measurements were carried out following the procedures outlined in EN ISO12571:2000. This involved conditioning small specimens of the order of 25 grams to constant mass in an enclosure controlled at different relative humidities obtained by the use of different salt solutions. The criteria for constant mass was a change of less than 0.1% in 24 hours. During the course of the investigation one of the participants discovered that after completing the adsorption curve and subjecting the specimen to lower humidity conditions to measure desorption that for one specimen the specimen mass after showing an initial decrease started to slowly increase. This is caused by carbonization that takes place due to the reaction of the cement with the CO_2 in the presence of moisture. As a consequence the constructed moisture content curves do not return to the initial starting point. Thus the participants developed an agreed method of processing of the results.

The standard is based on a constant dry weight only and does not provide any guidance for the present type of behavior. It is known that the process is not linear over the total RH range since at low values there is insufficient water available while above 70% RH, liquid water in the pores reduces the rate of diffusion of CO_2. However for the present study it was agreed that the results would be processed based on the assumption that the effect could be considered to be linear for the complete RH range and thus the mass increase is constant with time and the same at all humidity values. The masses were then corrected accordingly.

Water Vapor Transmission

All measurements were carried out in conformance with procedures specified in EN ISO12572. However the method allows for several possible size options and specimen sealing procedures. A comparison of the specific experimental approach adopted by each organization is listed in Table 2. Diagrams of the cups used are shown in Figure 1.

Thermal Conductivity

For the five materials involved in the study the expected thermal conductivity was in the approximate range $0.1<\lambda<2$ W/m·K and thus in principle can be measured in an

Table 2 — *Water vapor resistance, summary of experimental details.*

	SP	BVFS	VTT	NPL
Specimen size (mms)	125 x 125 x 30 thick		Measurement area 145 diameter	Brick 90 dia. x 7 thick, others 190 dia. x 50 thick
Dry / Wet Cup - Cup design and material	Type c Steel	Type b for AAC Type c for all others Glass	Type d Aluminum	Type c Glass
Sealant	Bitumen + Al foil			Mastic sealer tape
Salt for dry conditions	$CaCl_2$	Silica Gel	$CaCl_2$	P_2O_5
Salt for moist conditions	KNO_3	KNO_3	KNO_3	KNO_3
Chamber conditions	23 °C & 50% RH	23 °C & 50% RH	23 °C & 50% RH	23 °C & 50% RH
Preconditioning			1 month in 50% RH chamber	

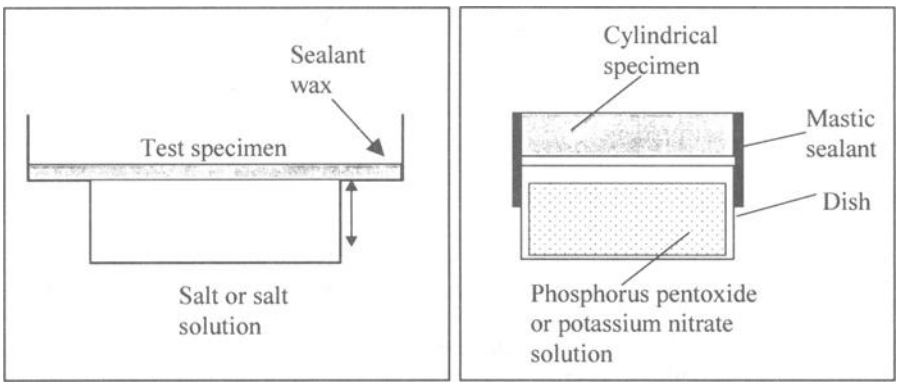

Figure 1 — *Designs of wet/dry cup used on the left type d and on the right type c*

absolute manner using the guarded hot plate method according to ISO 8302. Its application for medium and low resistance specimens and materials containing moisture is also addressed by the standards EN12664 and ISO 10051. For the present program, the majority of the testing was carried out in accordance with the procedures recommended in these standards.

However, the brick material presented a particular problem since the maximum practical thickness of a specimen of the lateral dimensions required for most standard hot plates was only of the order of 6 mm to 7 mm. For its expected thermal conductivity the overall thermal conductance was outside the acceptable range of the method for such a thin specimen. As a result several organizations had to use alternative methods to enable measurements of reasonable precision to be made.
These included:

- NPL measured a 50 mm diameter, 6 mm thick specimen in a guarded heat flow meter apparatus.
- SP and IBP measured the thermal resistance of a 50 mm thick piece of material containing air gaps and then calculated the thermal conductivity from the results using an appropriate model.
- EMPA measured a 25 mm diameter thin specimen in an apparatus similar to NPL.
- FIW and BVFS measured a 6 mm thick specimen by the guarded hot plate. However BVFS contracted the work to *Physikalisch-Technische Bundesanstalt* (PTB) for measurement using their special small hot plate [1] that had been verified in measurements of a Pyrex 7740 European Certified Reference Material.

For the remaining four materials the matter of contact resistances at the specimen and apparatus surfaces coupled with accurate temperature measurement are the most critical factors involved in measurements on hard materials of relatively high thermal conductivity. One of the present authors illustrated these issues with respect to masonry material some years ago [2]. In this study measurements were made on specimens with fine thermocouples embedded in 0.5 mm grooves cut in the specimen surfaces and held in place with a paste adhesive. Results were obtained using both the thermocouples in the apparatus plates and those in the specimen. These indicated significant differences, increasing from 3% to 40% as the thermal conductivity increased from 0.2 to 2 W/m·K, thus illustrating the importance of taking extra care when measuring the surface temperature of high conductivity materials.

As part of the work involved in developing Pyrex 7740 as a European reference material NPL also undertook a program of work to support that of the PTB. This addressed the best means of temperature measurement and minimizing contact resistance in high conductivity materials using a conventional guarded hot plate [3]. The study involved a combination of interface materials and different thermocouple attachment techniques. The technique of embedding the thermocouples in the specimen was found to provide the most consistent and precise measurements. However, the use of 0.075 mm fine gauge thermocouple flattened to 0.03 mm by a rolling technique and fixed directly to the specimen surface, with a thin layer of thermal conducting compound and maintained in place with a thin layer of foamed silicone rubber of known thermal properties was found to provide results almost as good as the embedded sensor technique. Based on this evidence participants agreed to use one of these two techniques for their measurements on the four materials.

For the conditioned specimens, following conditioning to constant weight at 50% and 90% RH in controlled environments the specimens were wrapped in a thin polythene film prior to measurement. A separate study for establishing constant weight for these thicker specimens showed that much longer times were required and that the mass stability criterion had to be extended to less than 0.035% in 24 hours rather than the 0.1% recommended in the standard which is applicable to much thinner specimens. It is assumed that for these low moisture contents there is no moisture movement during thermal conductivity testing.

Results

All results are presented with the individual organizations identified by a number in order to preserve anonymity.

Hygroscopic Sorption and Desorption

The results are summarized in Table 3. Figure 2 contains a comparison of the mean of the values from the three organizations that obtained results for the complete set of conditions. The results illustrate both the overall variability and the effect of the carbonization that takes place during the conditioning procedures, particularly for the concrete block and mortar materials.

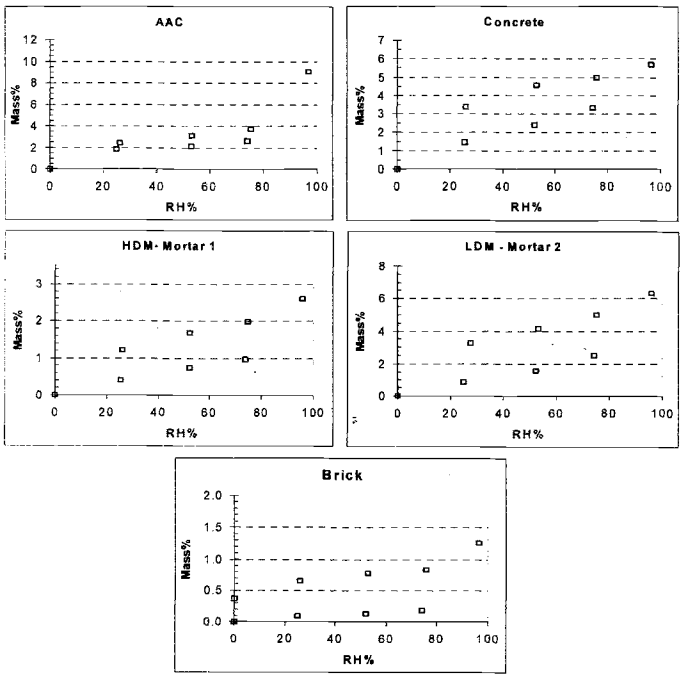

Figure 2 —*Hygroscopic sorption and desorption – Mean values of the three laboratories*

Table 3 — *Summary of hygroscopic sorption and desorption results*

	Lab 1		Lab 5		Lab 4		AVERAGE VALUES		
	RH%	Mass %	RH%	Mass %	RH%	Mass %	RH%	Mass %	Spread
AAC	0	0.00	0.00	0.00	0.00	0.00	0.00	0.00	0.00
	22	1.96	23.00	1.70	29.80	1.72	24.93	1.79	0.26
	55.3	2.40	53.00	2.02	50.10	1.84	52.80	2.08	0.56
	75.8	2.86	75.00	2.65	71.10	2.30	73.97	2.60	0.56
	97.1	4.50	97.00	10.38	95.90	12.26	96.67	9.05	7.76
	76.9	3.19	75.00	3.31	74.40	4.74	75.43	3.75	1.55
	54.4	2.86	53.00	2.84	52.90	3.56	53.43	3.09	0.72
	22.1	2.31	23.00	2.19	34.00	2.73	26.37	2.41	0.54
	0	0.00	0.00	0.00	0.00	0.00	0.00	0.00	0.00
	RH%	Mass %	RH%	Mass %	RH%	Mass %	RH%	Mass %	Spread
CB	0	0.00	0.00	0.00	0.00	0.00	0.00	0.00	0.00
	24.4	1.26	23.00	1.53	29.80	1.53	25.73	1.44	0.27
	53.7	1.96	53.00	2.33	50.10	2.89	52.27	2.39	0.93
	76.4	2.89	75.00	3.08	71.10	4.08	74.17	3.35	1.19
	95.7	4.26	97.00	6.21	95.90	6.57	96.20	5.68	2.31
	77	3.82	75.00	5.36	74.40	5.71	75.47	4.96	1.89
	52.2	3.56	53.00	5.04	52.90	5.11	52.70	4.57	1.55
	21.5	2.79	23.00	3.54	34.00	3.85	26.17	3.39	1.06
	0	0.00	0.00	0.00	0.00	0.00	0.00	0.00	0.00
	RH%	Mass %	RH%	Mass %	RH%	Mass %	RH%	Mass %	Spread
BB	0	0.00	0.00	0.00	0.00	0.00	0.00	0.00	0.00
	22.6	0.07	23.00	0.08	29.80	0.13	25.13	0.09	0.07
	53.2	0.09	53.00	0.16	50.10	0.15	52.10	0.13	0.07
	76.8	0.10	75.00	0.23	71.10	0.19	74.30	0.17	0.13
	97.1	0.21	97.00	1.99	95.90	1.55	96.67	1.25	1.78
	77.3	0.14	75.00	1.69	74.40	0.69	75.57	0.84	1.55
	52.7	0.13	53.00	1.65	52.90	0.56	52.87	0.78	1.52
	20.7	0.14	23.00	1.40	34.00	0.43	25.90	0.66	1.26
	0	0.00	0.00	1.10	0.00	0.00	0.00	0.37	1.10
	RH%	Mass %	RH%	Mass %	RH%	Mass %	RH%	Mass %	Spread
HDM	0	0.00	0.00	0.00	0.00	0.00	0.00	0.00	0.00
	23.8	0.52	23.00	0.08	29.80	0.62	25.53	0.41	0.54
	53.6	0.78	53.00	0.41	50.10	1.05	52.23	0.75	0.64
	75.5	1.09	75.00	0.30	71.10	1.52	73.87	0.97	1.22
	95.2	1.72	97.00	2.52	95.90	3.62	96.03	2.62	1.90
	75.5	1.52	75.00	2.15	74.40	2.30	74.97	1.99	0.78
	51.7	1.33	53.00	1.93	52.90	1.80	52.53	1.68	0.60
	21.3	0.94	23.00	1.46	34.00	1.24	26.10	1.21	0.51
	0	0.00	0.00	0.00	0.00	0.00	0.00	0.00	0.00
	RH%	Mass %	RH%	Mass %	RH%	Mass %	RH%	Mass %	Spread
LDM	0	0.00	0.00	0.00	0.00	0.00	0.00	0.00	0.00
	21.9	0.98	23.00	0.40	29.80	1.14	24.90	0.84	0.74
	53.4	1.79	53.00	0.83	50.10	2.08	52.17	1.57	1.25
	77	3.26	75.00	1.00	71.10	3.27	74.37	2.51	2.27
	95.3	4.80	97.00	6.07	95.90	8.18	96.07	6.35	3.38
	76.4	4.27	75.00	5.07	74.40	5.58	75.27	4.97	1.31
	54	3.78	53.00		52.90	4.56	53.30	4.17	0.78
	25.5	2.61	23.00	3.92	34.00	3.20	27.50	3.25	1.31
	0	0.00	0.00	0.00	0.00	0.00	0.00	0.00	0.00

Water Vapor Transmission

The results are summarized in Table 4 and compared in Figure 3. The large differences in value between the results of the various participants highlights the inherent difficulties with the test method especially for these types of hard, dense materials. An evaluation of the uncertainties due to direct sources including masses, dimensions, relative humidities at different levels, etc. would indicate that an uncertainty of 7 to 10% is possible. However there are additional and unquantifiable sources of error involved including different specimen sizes, densities and forms, methods of sealing plus corrections for air layers between the various surfaces at the different conditions.

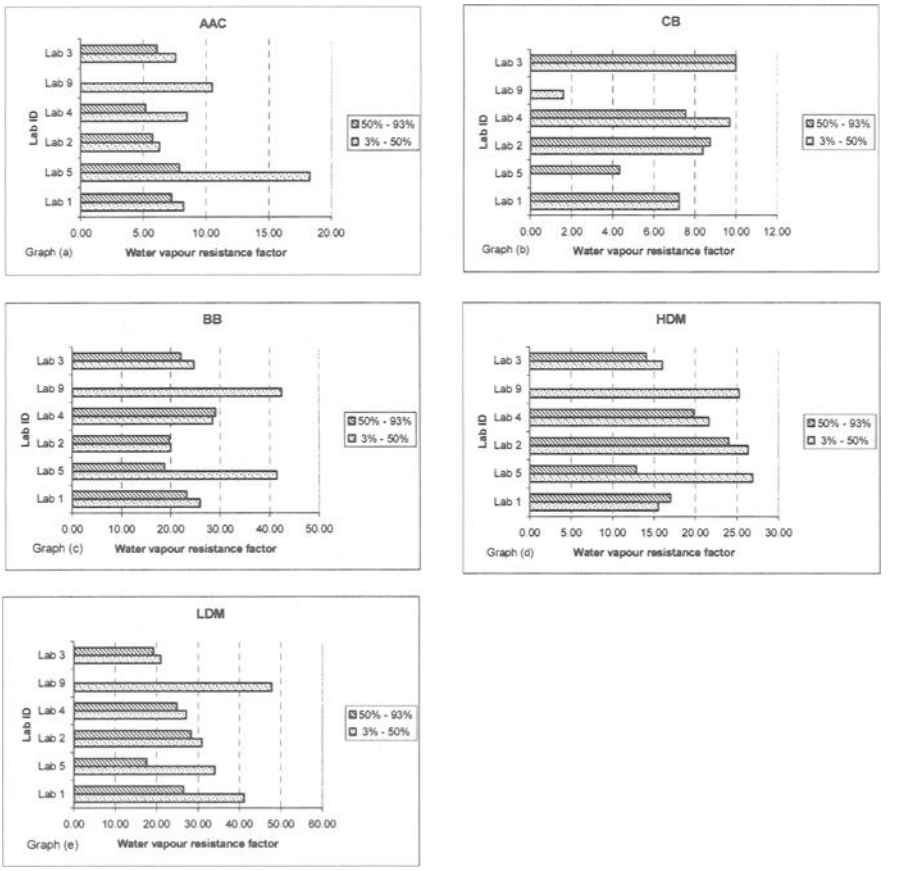

Figure 3 — *Water vapor resistance factor – Comparison of results for wet cup and dry cup humidity levels*

Table 4 — *Summary of water vapor transmission results*

Material	Mean temp °C	RH% Gradient	MEASURED WATER VAPOUR RESISTANCE FACTOR Lab 1	Lab 5	Lab 2	Lab 4	Lab 9	Lab 3	Mean value Note [1]	Standard deviation Note [1]	Standard deviation (%)	Mean of all values 30-50 & 50-90 Note [1]	Standard deviation of all values Note [1]	Standard deviation of all values(%) Note [1]
			Lab 1	**Lab 5**	**Lab 2**	**Lab 4**	**Lab 9**	**Lab 3**						
AAC	23	3% - 50%	8.22	18.30	6.30	8.48	10.48	7.58	8.2	1.52	18.5	7.32	1.57	21.4
	23	50% - 93%	7.26	7.90	5.74	5.18		6.10	6.4	1.12	17.4			
			Lab 1	**Lab 5**	**Lab 2**	**Lab 4**	**Lab 9**	**Lab 3**						
CB	23	3% - 50%	7.24		8.40	9.70	1.60	10.00	8.8	1.27	14.4	8.61	1.19	13.9
	23	50% - 93%	7.24	4.34	8.75	7.56		10.00	8.4	1.26	15.0			
			Lab 1	Lab 5	Lab 2	Lab 4	Lab 9	Lab 3						
Brick	23	3% - 50%	25.96	41.43	20.00	28.46	42.44	24.70	30.5	9.28	30.4	26.89	8.18	30.41
	23	50% - 93%	23.24	18.72	19.67	29.07		22.10	22.6	4.07	18.0			
			Lab 1	**Lab 5**	**Lab 2**	**Lab 4**	**Lab 9**	**Lab 3**						
Mortar 1	23	3% - 50%	15.50	26.91	26.33	21.64	25.28	16.04	22.0	5.13	23.4	19.95	5.15	25.8
	23	50% - 93%	16.98	12.89	24.00	19.76		14.10	17.5	4.48	25.6			
			Lab 1	**Lab 5**	**Lab 2**	**Lab 4**	**Lab 9**	**Lab 3**						
Mortar 2	23	3% - 50%	41.16	34.06	31.00	27.12	47.76	21.03	33.7	9.64	28.6	28.98	9.19	31.7
	23	50% - 93%	26.52	17.62	28.33	24.92		19.22	23.3	4.67	20.0			

Note[1] Values highlighted have been omitted because they are either twice the mean value or half the mean value

Thermal Conductivity

The overall results from the participants indicated that there were large differences in density of the original specimens such that the results could not be critically assessed without some normalization to a common density. The prEN1745 standard provides the means of correcting the measured values for such variations in density via a series of equations for different product types. Table 5 contains the uncorrected results of all measurements by one laboratory for each product. Table 6 contains a summary of the normalized values of each participant. The table also includes details of the equation used in the normalization procedure. Figure 4 contains the collected results for the variation of thermal conductivity with moisture content for each material.

Table 5 — *Laboratory 1- Experimental results for all materials*

Material	Thickness	Conditioning treatment	Moisture start	Moisture finish	Temp diff	Mean temp	Thermal conductivity	Density
	m	%RH	%	%	°C	°C	W/m.K	kg/m^3
AAC	0.0497	90.00	2.88	2.82	10.5	10.6	0.141	507
AAC	0.0497	50.00	2.59	2.55	9.9	9.9	0.136	499
AAC	0.0497	Dry	0.25	0.31	10.0	9.9	0.131	488
AAC	0.0497	Dry	0.25	0.31	9.7	22.6	0.133	488
AAC	0.0497	Dry	0.25	0.31	19.3	9.9	0.131	488
AAC	0.0497	Dry	0.25	0.31	20.2	23.1	0.132	488
BB	0.0091	90.00	1.25	1.22	24.8	9.8	0.398	1568
BB	0.0091	52.00	0.65	0.66	25.3	9.5	0.368	1549
BB	0.0091	DRY	0.01	0.03	25.1	9.7	0.364	1539
BB	0.0091	DRY	0.01	0.03	24.6	23.2	0.371	1539
CB	0.0421	90	3.60	3.55	10.4	9.8	0.208	792
CB	0.0421	50	2.37	2.33	9.7	9.9	0.207	780
CB	0.0421	Dry	0.056	0.16	10.3	10.1	0.194	757
CB	0.0421	Dry	0.056	0.16	10.1	23.0	0.198	757
CB	0.0421	Dry	0.056	0.16	20.6	10.4	0.194	757
CB	0.0421	Dry	0.056	0.16	21.2	23.1	0.198	757
LDM	0.0492	90.00	3.51	3.46	10.0	10.1	0.348	1096
LDM	0.0492	50.00	2.41	2.38	10.3	10.3	0.335	1067
LDM	0.0492	Dry	0.040	0.081	10.2	9.9	0.311	1033
LDM	0.0492	Dry	0.040	0.081	10.4	23.2	0.313	1033
LDM	0.0492	Dry	0.040	0.081	20.4	9.7	0.311	1033
LDM	0.0492	Dry	0.040	0.081	20.6	23.3	0.314	1033
HDM	0.0495	90.00	1.57	1.55	9.7	10.0	1.29	1872
HDM	0.0495	50.00	0.99	0.99	10.3	10.1	1.24	1851
HDM	0.0495	Dry	0.012	0.043	10.0	10.0	1.20	1827
HDM	0.0495	Dry	0.012	0.043	10.0	23.0	1.20	1827
HDM	0.0495	Dry	0.012	0.043	19.6	9.7	1.21	1827
HDM	0.0495	Dry	0.012	0.043	19.7	23.4	1.20	1827

Table 6 — *Summary of normalized thermal conductivity results* [+]

AAC				NORMALISED TO A NOMINAL DRY DENSITY C								LINKED	Mean λ value	Range of λ values	Range as % of mean	Standard deviation
Density	488	Density	488	Density	473	Density	469	Density	484	Density	505					
Moisture %	Lab 1	Moisture %	Lab 4	Moisture %	Lab 2	Moisture %	Lab 3	Moisture %	Lab 9	Moisture %	Lab 5		W/m.K	W/m.K	%	
0.25	0.134	0.00	0.134	0.3	0.132	0.00	0.129	0.00	0.129	0.00	0.133		0.132	0.005	3.79	0.00231
2.59	0.139	2.38	0.137	3.2	0.144	1.30	0.136	1.30	0.133	1.48	0.136		λ = (500-Density x 0,00027)+Measured λ			
2.88	0.145	5.57	0.148	5.2	0.157	2.70	0.142	3.68	0.139							

CB				NORMALISED TO A NOMINAL DRY DENSITY OF								LINKED	Mean λ value	Range of λ values	Range as % of mean	Standard deviation
Density	757	Density	790	Density	715	Density	749	Density	719	Density	799					
Moisture %	Lab 1	Moisture %	Lab 4	Moisture %	Lab 2	Moisture %	Lab 3	Moisture %	Lab 9	Moisture %	Lab 5		W/m.K	W/m.K	%	
0.056	0.194	0.00	0.179	0.00	0.175	0.00	0.187	0.00	0.189	0.00	0.187		0.185	0.019	10.21	0.00700
2.37	0.207	2.33	0.196			2.92	0.196	2.88	0.196	1.61	0.192		λ = (0,000320 x density) - 0,0780			
3.60	0.207	5.05	0.209			4.17	0.202	5.57	0.206	4.21	0.210					

BB				NORMALISED TO A NOMINAL DRY DENSITY OF								LINKED	Mean λ value	Range of λ values	Range as % of mean	Standard deviation
Density	1539	Density	1528	Density	1457	Density	1468	Density	1493	Density						
Moisture %	Lab 1	Moisture %	Lab 4	Moisture %	Lab 2	Moisture %	Lab 3	Moisture %	Lab 9	Moisture %	Lab 5		W/m.K	W/m.K	%	
0.01	0.348	0.00	0.416	0.00	0.371	0.00	0.370	0.00	0.256				0.352	0.159	45.17	0.059
0.65	0.353					0.38	0.343						λ = (0,000370 x density) - 0.12100			
1.25	0.383	1.58	0.454			0.95	0.351									

HDM				NORMALISED TO A NOMINAL DRY DENSITY C								LINKED	Mean λ value	Range of λ values	Range as % of mean	Standard deviation
Density	1827	Density	1837	Density	1700	Density	1680	Density	1657	Density	1744					
Moisture %	Lab 1	Moisture %	Lab 4	Moisture %	Lab 2	Moisture %	Lab 3	Moisture %	Lab 9	Moisture %	Lab 5		W/m.K	W/m.K	%	
0.012	1.081	0.00	0.871	0.00	0.817	0.00	0.828	0.00	0.848	0.00	0.914		0.893	0.264	29.58	0.09841
0.994	1.119	0.66	0.859			1.63	0.831	1.73	0.932	0.78	1.078		λ = (0,001392 x density) - 1,522881			
1.57	1.174	2.39	0.986			2.42	0.882	3.13	0.955	1.12	1.062					

LDM				NORMALISED TO A NOMINAL DRY DENSITY OF								LINKED	Mean λ value	Range of λ values	Range as % of mean	Standard deviation
Density	1033	Density	1079	Density	1000	Density	957	Density	1022	Density	1022					
Moisture %	Lab 1	Moisture %	Lab 4	Moisture %	Lab 2	Moisture %	Lab 3	Moisture %	Lab 9	Moisture %	Lab 5		W/m.K	W/m.K	%	
0.0398	0.306	0.00	0.307	0.00	0.294	0.00	0.280	0.00	0.295	0.10	0.365		0.308	0.085	27.68	0.0297
2.41	0.330	1.77	0.323			3.75	0.289	3.13	0.332	1.53	0.397		λ = (0,000317 x density) - 0,018333			
3.51	0.344	5.72	0.389			5.78	0.300	6.35	0.333	3.12	0.421					

[+] The values are normalized to the original mean dry density of each material using the original dry density (except for AAC where the nominal density is used.)

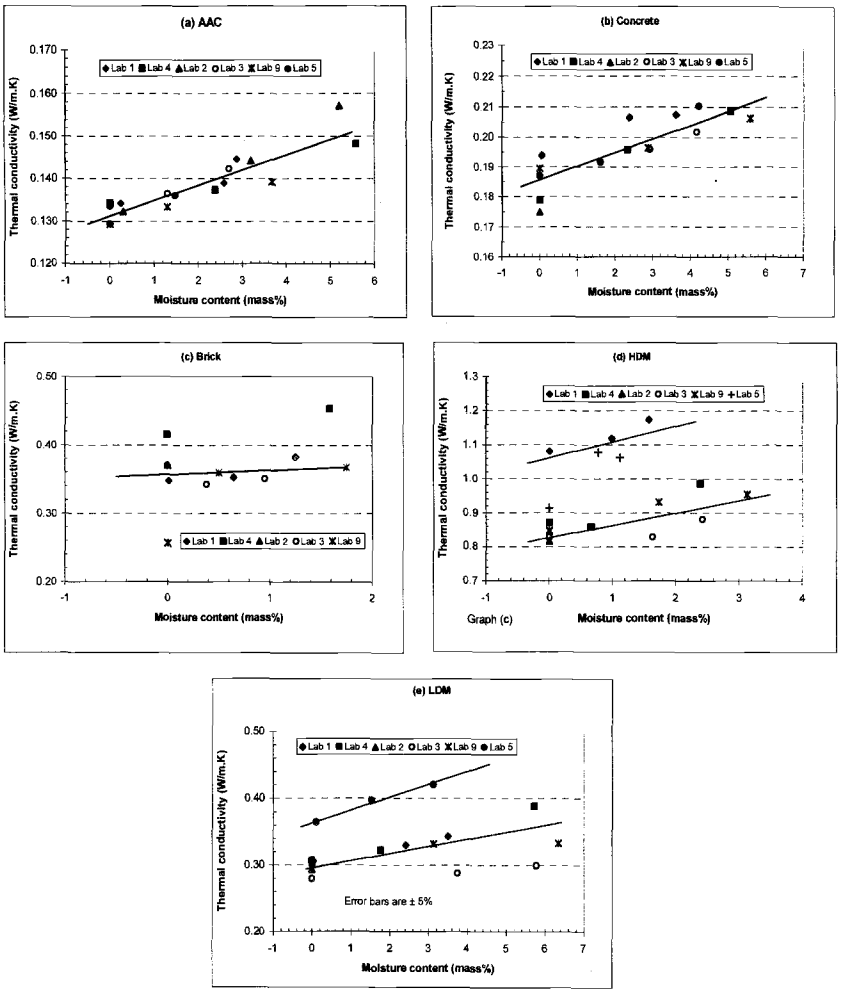

Figure 4 — *Collected thermal conductivity versus moisture content for all materials*

Discussion

This study was carried out with special care taken to use accepted standardized and controlled procedures for individual property measurement. However despite this important factor some surprising results were obtained and are discussed specifically in the context of previous measurements on masonry materials.

Moisture Sorption

While allowing for the overall differences obtained by the individual participants, there appears to be a significant difference in behavior between the results of measurements on the small moisture sorption specimens and the larger thermal conductivity specimens. In most cases this difference is much greater than 30%. It is assumed that it is due to a combination of factors. These include the specimen sizes for the two test procedures being much different with the consequence that the test/conditioning chambers are significantly different in volume and the equilibrium times involved much different.

The carbonization factor is also a phenomenon that is not addressed by the current standard and it would appear that this is a subject for further study in order to evaluate its true effect and significance in the measurements.

Effect of Moisture on Thermal Conductivity

A most surprising result of this controlled study is that the overall increase in thermal conductivity with moisture content is much lower than has been found from previous results on a large number of different masonry products. Valore [4,5] has carried out various critical analyses of thermal conductivity and thermal conductance data from many sources. In general the results overall have indicated that as a minimum a 1% by weight increase in moisture provides an increase of 5% in the thermal conductivity of a masonry material. The present results show that for the materials studied the increase in thermal conductivity is only of the order of 2.5 to 3 % for a 1% by weight increase in moisture. This value is shown consistently for all materials even when there is a difference in absolute value as manifested by the HDM material. However the present values are still lower than the 4% increase for a one percent change in moisture content by mass given in the more recently published EN ISO 10456:2000.

The HDM material is the only one for which there is less agreement in absolute value between the participants. The measurement of the thermal conductivity of masonry materials does present some difficulties due to their form and range of values. However all participants followed recommended proven practices and acceptable agreement was obtained for the other materials. An examination of the water vapor transmission results also indicated a difference in behavior by two participants including Lab 1, which obtained the high thermal conductivity value for HDM. In discussions with the partners about the material it was found that different mixing procedures used different amounts of added water. Both Labs 1 and 3 hand mixed the mortars rather than machine mixing them and this procedure had also involved adding less water per unit mass to obtain a consistent mix. These factors may be a contributing factor to the different behavior and thermal conductivity value.

At present no ready explanation is forthcoming regarding the observed difference in thermal conductivity behavior with increase in moisture content. The present investigation was carried out under carefully controlled parameters and procedures for the various properties whereas the analyses of past data have involved predominately measurements on specimens or composite walls under less controlled conditions.

Thermal Conductivity of Dry Masonry Products

Figure 5 summarizes the results for the five materials in the dry state and shows that the four cementitious products can be represented by one relationship with the high-density brick product some 30% or more off the curve. Valore [5,6] has indicated that there are various specific relationships for different products including clay based products depending on the type and amounts of constituents. The present cementitious products fall well within the limits of these more refined equations, as does the brick for the clay based materials.

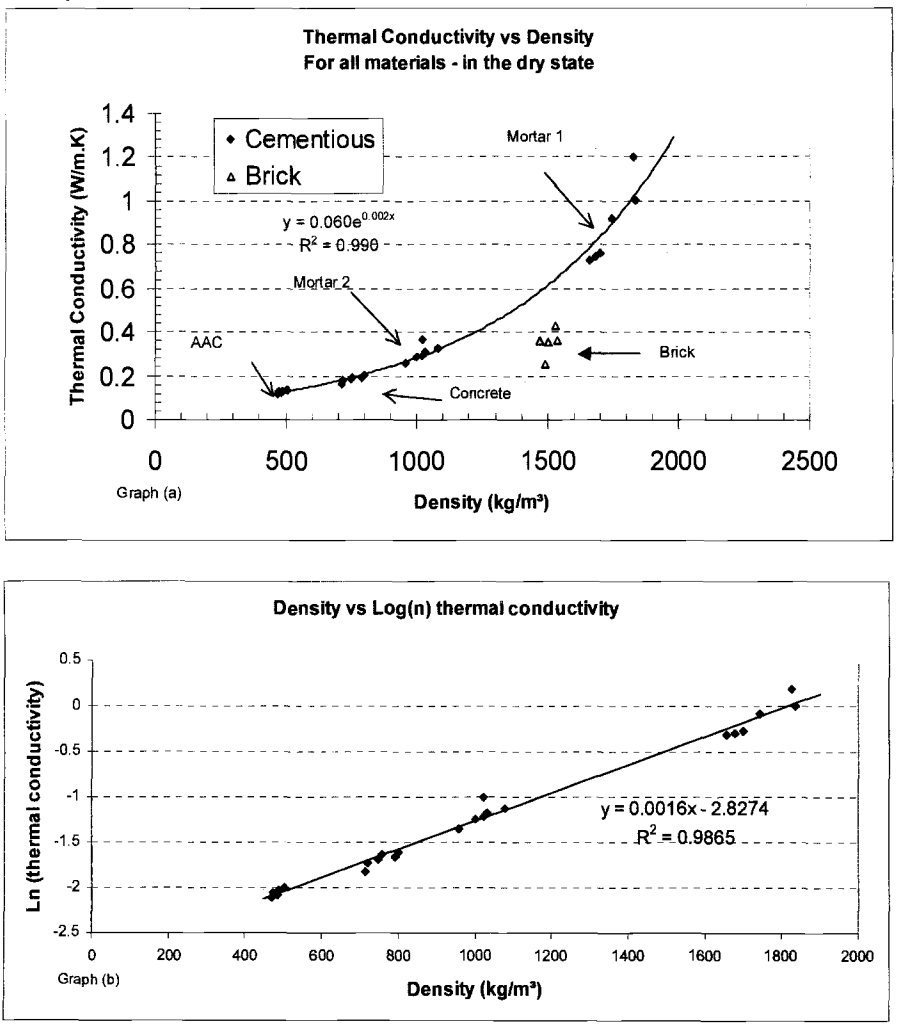

Figure 5 — *Thermal conductivity results – All materials*

Summary

A controlled study of thermal and moisture absorption and transmission properties of masonry materials has been undertaken as part of an overall investigation to provide the European Union with the tools to meet a Construction Products Directive for such products. Measurements have been carried out using the appropriate international or European Standard methods together with recommended practices specifically developed for these material types.

The results indicate that the increase in thermal conductivity with increase in moisture content (3%:1%) is somewhat less than that determined from evaluation of past experimental data (5%:1%). Suggestions are made concerning the needs for improving current experimental methods, particularly those involving moisture absorption and transmission.

References

[1] Hemminger, W. and Jugel, R., "A Guarded Hot Plate Apparatus for Thermal Conductivity Measurement over the Temperature Range –75 to 200 °C," International Journal of Thermophysics, Vol. 6, No. 5, 1985, pp 483.

[2] Tye, R. P. and Spinney S. C., "Thermal Conductivity of Concrete: Measurement Problems and the Effect of Moisture," Proceedings of Commission B1 of International Institute of Refrigeration, Washington DC, Institut International du Froid, Paris, 1976, pp. 119-127.

[3] Corsan, J. M. and Williams, I., "Errors Associated with Imperfect Surfaces in Standard Hot Plate Thermal Conductivity Measurements," NPL Report QU57, February 1980. (See also Williams, I. and Shawyer, R. E., NPL Special Report QUS46, February 1990).

[4] Valore, R. C. Jr., "Insulating Concretes," Journal of American Concrete Institute, Vol. 28 No. 5, 1956, pp 509 – 532.

[5] Valore, R. C. Jr., "Calculation of U-values of Hollow Concrete Masonry," American Concrete Institute, Concrete International – Design and Construction, 1980, pp. 40 – 63.

[6] Valore, R. C. Jr., Tuluca, A. and Caputo, A., "Assessment of the Thermal and Physical Properties of Masonry Block Products," Report number ORNL/Sub/86-22020/1, Oak Ridge National Laboratory, 1986.

Appendix

List of EU technical standards referenced in this project

Title	Number	Date
Masonry and masonry products: Methods for determining thermal design products.	EN 1745	
Thermal performance of buildings: Determination of thermal resistance by hot box method using heat flow meter - Masonry.	EN 1934	1998
Accuracy (trueness and precision) of measurement methods and results: • General principles and definitions • Basic methods for the determination of repeatability and reproducibility of a standard testing method. • Intermediate measures of the precision of a standard measurement method. • Basic methods for the determination of the trueness of a standard measurement method Use in practice of accuracy terms	ISO 5725 Part 1 Part 2 Part 3 Part 4 Part 6	1994
Thermal insulation - Determination of steady state thermal transmission properties - Calibrated and guarded hot box.	ISO 8990	1994
Thermal tests - Assessment of instrument accuracy and personnel competence: Part 4: Calibrated and guarded hot box guidelines and criteria.	EN 1946-4	1998
Thermal insulation - Determination of steady state thermal resistance and related properties - Heat flow meter apparatus	ISO 8301	1991
Thermal performance of building products and components - Specific criteria for the assessment of laboratories measuring heat transfer properties. - Part 3: Measurement by heat flow meter apparatus.	EN 1946-3	1999
Thermal Insulation - Determination of steady state thermal resistance and related properties - Guarded hot plate apparatus	ISO 8302	1991
Thermal performance of building products and components - Specific criteria for the assessment of laboratories measuring heat transfer properties. - Part 2: Measurement by guarded hot plate apparatus.	EN 1946-2	1999
Thermal insulation - Moisture effects on heat transfer - Determination of thermal transitivity of a moist material.	ISO 10051	1996
Thermal insulation products for building applications - Conditioning to moisture equilibrium under specified temperature and humidity conditions.	prEN 12429	Feb 98
Building materials; Determination of Hygroscopic sorption curves *This contains tables of air RH% at a specific temperature over salt solutions.*	EN 12571	2000
Building Materials - Determination of vapor transmission properties	EN 12572	2001
Determination of thermal resistance by means of ghp and hfm methods. – Dry and moist products of medium and low thermal resistance.	EN 12664	2000
Building materials - Determination of hygric expansion coefficient	EN 13009	2000
Determination of water absorption coefficients	prEN 15148	June 96
Hygrothermal performance of building materials and products - Determination of moisture content by drying at elevated temperature.	EN 12570	2000
Methods of tests for masonry units: Determination of net and gross dry density of masonry units (except natural stone).	EN 772-13	1996
Building materials and products – Procedures for determining declared and design thermal values.	EN ISO 10456	1999

Session 2: Testing

William M. Healy[1] and Daniel R. Flynn[2]

Thermal Modeling of Multiple-Line-Heat-Source Guarded Hot Plate Apparatus

REFERENCE: Healy, W. M. and Flynn, D. R., **"Thermal Modeling of Multiple-Line-Heat-Source Guarded Hot Plate Apparatus,"** *Insulation Materials:Testing and Applications:4th Volume, ASTM STP 1426*, A. O. Desjarlais and R. R. Zarr, Eds., ASTM International, West Conshohocken, PA, 2002.

ABSTRACT: The National Institute of Standards and Technology is building a guarded hot plate apparatus of advanced design to provide very accurate thermal transmission properties for specimens of thermal insulation 500 mm in diameter, with thicknesses up to 110 mm, at mean temperatures from 90 K to 900 K. This paper documents some of the extensive thermal modeling and analyses that were carried out in the course of designing this apparatus and characterizing potential errors and uncertainties. In an idealized guarded hot plate apparatus, the effective thermal conductivity is simply computed from the measured power input to the meter plate heater, the effective area of the metering plate, the temperature of the hot plate and the two cold plates, and the specimen thickness. In an actual apparatus, there may be (a) temperature variations in the hot plate and cold plates, (b) radial heat flow within the specimen, and (c) transient temperature fluctuations that add uncertainty to the measured thermal conductivity. For the new 500 mm apparatus, both analytical solutions and finite element analyses were used to model temperature distributions in critical thermal components, heat flows that might affect the measured thermal conductivity values, and the effects of departures from ideal steady-state conditions on test results. This paper focuses on the results of these analyses and computations.

KEYWORDS: finite element analysis, guarded hot plate, heat conduction, heat transfer, insulation, R-value, thermal analysis, thermal conductivity, thermal insulation, thermal resistance

Introduction

The National Institute of Standards and Technology (NIST) is designing a new guarded hot plate to test thermal insulation from 90 K to 900 K. An accompanying paper [*1*] describes the major components and design concepts of this proposed apparatus. The plate design is based on ASTM Test Method for Steady State Heat Flux Measurements and Thermal Transmission Properties (C 177), ASTM Practice for

[1] Mechanical Engineer, Building and Fire Research Laboratory, National Institute of Standards and Technology, Gaithersburg, MD 20899-8632.
[2] President and Chief Scientist, MetSys Corporation, Millwood, VA 22646-0317.

Guarded-Hot-Plate Design Using Circular Line-Heat Sources (C 1043), and ISO International Standard: Thermal Insulation – Determination of Steady-State Thermal Resistance and Related Properties – Guarded Hot-Plate Apparatus (ISO 8302).

Determination of the thermal conductivity of the insulation follows from the applicable approximation to Fourier's Law in one dimension:

$$Q = \lambda A \frac{\Delta T}{\Delta z}, \tag{1}$$

where λ is the thermal conductivity, Q is the time rate of heat flow through the specimen, Δz is the specimen thickness, A is the area through which the heat flows, and ΔT is the temperature difference across the thickness of the specimen. λ is determined by measuring the temperatures, heat flow, and specimen thickness and applying Eq. (1).

The proposed guarded hot plate will add greater range to the measurement capability at NIST. Zarr [*2*] has documented the history of NIST's role in testing heat insulators. Overviews of this procedure and of plates throughout the world have been given by Klarsfeld [*3*] and Pratt [*4*]. A number of articles have been written that describe thermal analyses of guarded hot plates. Hahn et al [*5*] discuss the line-heat source concept, the technique for creating known temperature distributions on a plate that was adopted as part of C 1043. The authors suggest that placing ring heaters in a circular plate leads to more accurate determinations of the plate temperatures because the plate temperatures can be accurately modeled mathematically. Other mathematical analyses of plates are included in [*6-9*]. Recently, numerical methods have played a greater role in the design and evaluation of guarded hot plates. Troussart [*10*] was the first to demonstrate the use of finite element analysis to examine edge losses and the effect of a gap temperature differential in a rectangular plate. Subsequent analyses have become more sophisticated as finite element resources have advanced [*11-13*]. Recently, Virgone et al [*14*] used a three-dimensional finite difference algorithm to model the edge losses and gap effects in a square plate. In all of these works, focus has been placed on the effects of edge losses. The present work examines edge losses in the design of the new guarded hot plate at NIST. Additional results show the expected temperature profiles for a real application of the multiple-line heat source concept and for coolant tubes in the plates.

The purpose of this paper is to discuss the thermal analyses that guided the design process and have helped to identify performance characteristics of the apparatus. The initial designs were typically created with the help of analytical techniques to predict temperature fields within the plates. Finite element analysis, using a commercial software package, was utilized to predict thermal performance in those parts of the plate where analytical techniques would have been excessively cumbersome. Decreasing the uncertainty in the measurements was the ultimate goal in the thermal analyses. The major areas of uncertainty related to the thermal design can be deduced from Eq. (1). Measurement errors can arise from imperfect guarding, inaccurate determination of temperature differences, failure to reach thermal equilibrium, and incorrect determination of the specimen thickness. The thermal analyses have three main objectives: (1) Ensure that the hot and cold plates are nearly isothermal so that the measured temperature is an accurate estimation of the actual average surface

temperatures, (2) determine whether the design minimizes radial heat flow in the meter section of the specimen so that effectively all heat input to the meter plate travels uniaxially through the specimen to the cold plate, and (3) estimate errors associated with non-steady state operation. The investigation of the plate typically involved each component of the plate separately, and the following discussion provides analyses for the major components of the proposed apparatus.

Overview of Design

Figure 1 shows a cross-sectional schematic of the guarded hot plate apparatus. The apparatus consists of round plates with a diameter of 500 mm and accepts cylindrical specimens on both sides of the meter plate. Each cold plate is composed of one single disk, while the hot plate is made up of a disc-shaped meter plate surrounded by an annular guard ring. The metering plate will have a diameter of 200 mm to the center of the guard gap, which will be 1.4 mm wide on the surface. The plates will be oriented vertically, as shown in Fig. 1. Plate temperatures are determined by standard platinum resistance thermometers (SPRTs) inserted in wells in the meter plate and cold plates. A thermopile will be used to measure the temperature differential across the guard gap, and thermocouples will be installed to check the uniformity of the temperature distribution of the plates. An edge guard controlled to the mean temperature of the hot and cold plate will surround the specimen to minimize radial heat flow within the specimens. Electric heaters will be placed in the meter plate, guard ring, cold plates, and edge guards. Coolant tubes will be inserted in the cold plates and the edge guard. Since the plate will be operated at temperatures far from ambient, precautions are needed to prevent heat loss through the SPRT, thermocouple wires, heater leads, and support cables. These protrusions will be thermally grounded to a connection guard block that is maintained at the temperature of each plate. Auxiliary insulation will encapsulate these components, and a water-cooled jacket will form the outside of the apparatus. The entire apparatus will be installed in a bell jar so that variable pressure can be applied to the system. For further detail on the design, the reader is referred to Flynn et al [*1*].

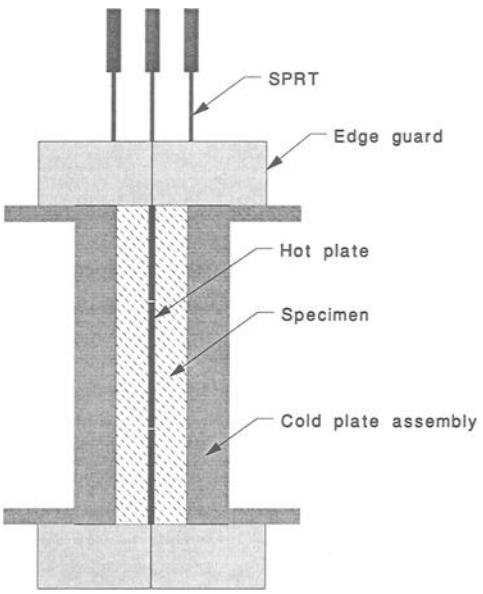

Figure 1 - *Schematic of guarded hot plate cross section.*

Provision of Isothermal Surfaces

Hot Plate

Meter plate – Heating of both the metering plate and the guard ring of the guarded hot plate occurs through the use of multiple line source heaters. Procedures for computing the preferred locations for circular heaters have previously been published in C 1043. These procedures were used to determine the optimal number of circular heaters to produce a surface temperature with sufficient uniformity. The ideal heater layout was then modified to accommodate practical heaters as discussed in C 1043.

Table 1 shows the critical parameters for the hot plate simulations. Five concentric ring heaters are used in each of the meter plate and the guard ring. The plates are 16 mm thick, with the heating elements located at the midplane. Because of symmetry, only one half of each plate thickness is modeled, so all axial locations are measured in reference to the heating elements. Figure 2 shows results both from analytical solutions using series expansions and from finite element analyses for the normalized temperature profile in the meter plate. The local temperature is given as $v(r,z)$ and the average temperature over the top surface is V. In these simulations, it was assumed that no heat transfer occurred from the edges or bottom of the plate, and a constant heat flux was removed from the top surface adjacent to the specimen. The finite element solution overlays the lines depicting the analytical solution, indicating an excellent match between the two techniques. At z = 4 mm, the amplitude of the temperature fluctuations are greater than at z = 8 mm because of the closer proximity to the heaters. More smoothing occurs in the temperature profile further away from the heaters because of lateral heat conduction. The close agreement of these two techniques provided confidence that the finite element analyses would sufficiently simulate millikelvin temperatures. Temperature fluctuations are miniscule with 5 heaters, and the temperature peaks are quite uniform. Similar plots of the predicted temperature distribution in the guard ring due to five circular rings show that the finite element predictions match the analytical predictions.

Table 1 - *Parameters for hot plate.*

Parameter	Value
Material	Nickel
Plate λ	70 W/(m·K)
Radius	250 mm
Thickness	16 mm
Guard Gap Width	1.6 mm
Radial Location of Center of Guard Gap	100 mm
Heater Diameter	3.2 mm

Figure 2 demonstrates the temperature distribution that would result if one were able to place idealized heater rings within the plates. Unfortunately, practical concerns make ring heaters impossible. Heater leads require entry into and out of the plates, and the proposed plates have an SPRT in the middle to measure temperature as shown in Fig. 3. The first attempt at creating a practical heater layout to mimic the performance of the five ring heaters in the meter plate is shown in Fig. 3. The switchbacks between the main loops and the leads are positioned so that each heater length removed from the ideal rings is replaced with an equal length of heater in the switchback or the lead.

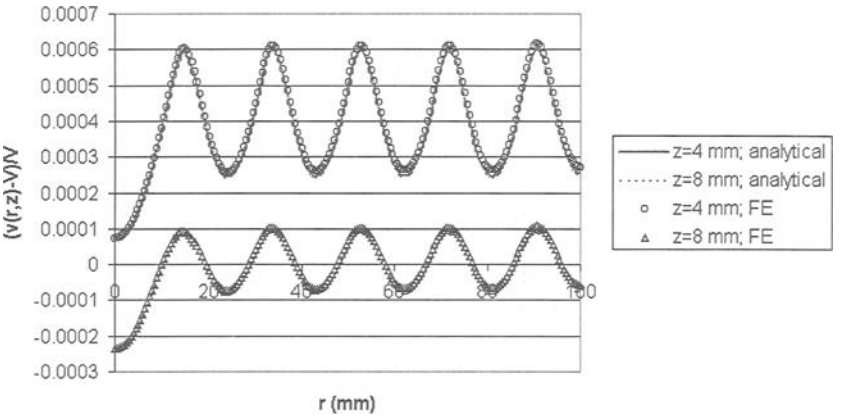

Figure 2 - *Radial temperature profile in meter plate (FE and analytical).*

The temperature distribution within the meter plate was simulated using a three-dimensional finite element analysis. Because of symmetry, only one half of the plate was modeled. The plane of symmetry is an adiabatic boundary, and it is assumed that no radial heat flow occurs at the edge of the meter plate because of the guard gap. From the surface facing the specimen, heat transfer is governed by assuming a specimen thermal resistance of 0.125 m^2·K/W and a cold-plate temperature of 273.15 K. This test specimen is highly conductive and represents a worst-case scenario for the temperature uniformity on the meter plate. By designing for this worst case, the design should perform satisfactorily at all conditions. A constant volumetric rate of heat generation is applied in the heating element to obtain a surface temperature at the meter plate that is approximately 20 K greater than the temperature of the cold surface.

Figure 4 shows the temperature contours on the surface of the meter plate for the heater layout shown in Fig. 3. Overall temperature variations are within 45 mK across the plate surface. Cold spots occur at the top of the plate, where the heater leads do not compensate for the lost heater length at the switchback, and slightly below the center of the plate, where a large gap occurs in the heaters. Hot spots appear where heating elements become too close. While the overall temperature variation is reasonable, the location of the cold spot just below the center of the plate raises a concern for temperature measurement. Recall that the objective in creating a plate with a uniform

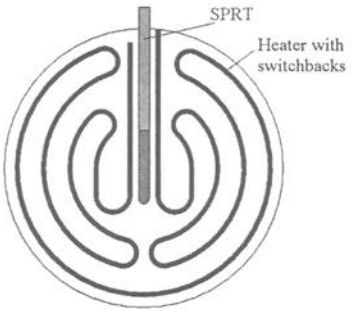

Figure 3 - *Original heater layout in meter plate.*

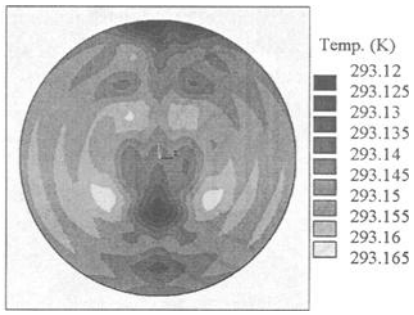

Figure 4 - *Temperature contours on surface of meter plate with original heater layout.*

surface temperature is to ensure that the measured temperature accurately represents the true average surface temperature. For the meter plate, the temperature will be measured using an SPRT inserted in the middle of the plate as shown in Fig. 3. The sensitive region of the SPRT is a 50 mm length at the center of the plate. The concern with the estimated temperature distribution in the meter plate is that the cold spot below the center of the plate lies close to the region of the SPRT. The dip in temperature begins to approach the sensitive region of the SPRT, and potential exists for erroneous readings in the temperature. To avoid this potential problem, the heater layout was redesigned to move this temperature trough away from the SPRT.

Figure 5 shows the revised heater layout in the meter plate, and Fig. 6 displays the resulting surface temperature profile. The temperature range seen on the plate surface is similar to that seen in the previous simulation, but by bringing the heater leads down along the SPRT, the temperature variation along the SPRT has been diminished.

Figure 5 – *Re-designed heater layout in meter plate.*

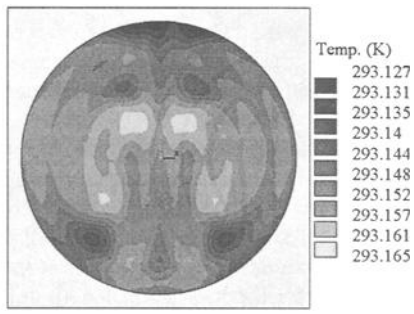

Figure 6 - *Surface temperature contours for revised heater layout.*

Guard Ring – The guard heater layout is based on five concentric rings and is shown in Fig. 7. Note that a lead going to the meter plate heater passes through the guard plate, and heat generated in that piece of wire must be accounted for in determining the location of switchbacks in the guard plate. To model the temperature distribution in the guard plate, adiabatic conditions are applied to the bottom and the edges of the plate (note that a half-thickness is modeled). A specimen with a thermal resistance of 0.125 $m^2 \cdot K/W$ and a cold-plate temperature of 273.15 K was used to model the heat transfer from the surface of the plate. Volumetric heat generation was applied to both the guard-plate heater and the lead to the metering plate. The different generation rates were calculated by assuming that the flux leaving both the meter plate and the guard plate would be identical. Since a greater amount of heater per unit area is present in the metering plate than in the guard plate, the volumetric heat generation rate in the metering plate heater is 64 % of that in the guard-plate heaters. The resulting surface temperature profile is shown in Fig. 8. The estimated temperature span on the surface is 51 mK.

Figure 7 - *Guard plate heater layout.*

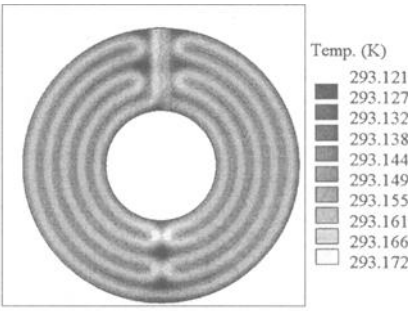

Figure 8 - *Surface temperature profile on the guard plate.*

Cold Plate

The thermal design of the cold plate consisted of both heater layouts and coolant tube layouts. To satisfy space and heater length constraints, nine rings are used as the basis for the design. Analyses of the resulting temperature distribution, however, indicated that a solid plate with nine ring heaters would lead to excessive temperature fluctuations at the surface and at the SPRT location. The simulation involved a 20 mm thick nickel plate (λ=69.7 W/(m·K)) at 900 K. Heat transfer through a specimen with a thermal resistance of 0.125 $m^2 \cdot K/W$ occurred from a hot plate maintained at 920 K, and heat transfer to the ambient at 298 K occurred through auxiliary insulation with a thermal resistance of 0.5 $m^2 \cdot K/W$. The edges of the plate were maintained as adiabatic. With a solid construction, it was found that the maximum temperature variations on the plate surface were 9 mK and those at the depth of the SPRT were 24 mK. While the coolant tubes were not modeled initially, it was believed that temperature variations would be even more dramatic owing to the varying heat flow to the coolant as it passes through the channels. For these reasons, it was decided that a composite construction was needed, and a layer of insulation 0.5 mm thick was placed between the plate

containing the heating elements and the plate touching the specimen and containing the SPRT (hereafter called the "thermometry" plate). Analytical modeling showed that the temperature fluctuations dropped to 0.001 mK at the plate surface and 0.002 mK at the SPRT depth when this composite construction was utilized.

Because the temperature variations indicated by the analytical results were negligible, finite element simulations of the three-dimensional temperature distribution arising from the heating elements were not performed. Instead, the focus of the finite element analysis was on the temperature field resulting from the coolant channels. The temperature distribution resulting from the coolant channels is a concern because, unlike heaters, a constant heat flux is not removed at all points along the channel.

The key parameters in the design of the coolant channel are the geometric configuration (i.e. the hydraulic diameter), the fluid, and the mass flow rate through the channel. While a number of patterns were considered, the final design uses a bifilar spiral through which the fluid flows into the center and then back outward. A rectangular channel will be milled into a solid plate with a width of 20 mm and a depth of 6.5 mm. Several fluids were considered as coolants: nitrogen gas, liquid nitrogen, two-phase nitrogen, and ethanol. Table 2 provides the critical thermal properties for these fluids.

Table 2 - *Thermal properties for coolants of interest*

Coolant	**Density (kg/m^3)**	**λ (W/(m·K))**	**Cp (J/(kg·K))**
Nitrogen gas	4.61	0.00750	1.12
Liquid Nitrogen	808	0.147	2040
Ethanol	790	0.183	2400

Initial analyses were carried out to estimate the amount of cooling, the associated pressure drop, and the frictional power dissipation due to circulating different fluids through a straight, smooth tube. For fully developed laminar flow, the Moody friction factor is inversely proportional to the Reynolds number, and the Nusselt number is a constant. For fully developed turbulent flow, at Reynolds numbers above 3000, a correlation by Petukhov [*15*] was used to compute the friction factor, and a correlation by Gnielinski [*16*] was used to compute the Nusselt number. The fluid temperature at the end of the channel is a function of the mass flow rate through the pipe. A higher mass flow rate increases the enthalpy transfer down the channel, thereby decreasing the temperature at the outlet, but the higher velocity leads to greater frictional losses that raise the fluid temperature. An optimal mass flow rate can be found for each fluid and channel shape that minimizes the temperature rise from the inlet to the outlet. This optimal value was found for each configuration and used as a boundary condition for the finite element analysis.

To obtain temperatures around 90 K on the surface of the cold plate, initial analyses indicated that the eventual design would require liquid nitrogen to be circulated as the coolant to achieve the lowest operating temperatures. Using cooled nitrogen gas was ruled out as an option because vast amounts of gas would be needed to remove the

heat from the plate, and the resulting temperature profile showed large variations on the plate surface. Liquid ethanol could be used to achieve cold plate temperatures from room temperature down to approximately 210 K. To attain cold plate temperatures between the boiling point of nitrogen (77 K) and 210 K, liquid nitrogen will be used in the coolant channels and heat will be provided from the heating element in the cold plate to raise it to the desired temperature. The use of the heater in tandem with coolant in the same metal plate, however, posed a serious control problem. To alleviate this problem, an additional layer of insulation was added between the plate containing the heating elements and the plate containing the cooling channel. A schematic of the cross-section of the cold plate is given in Fig. 9.

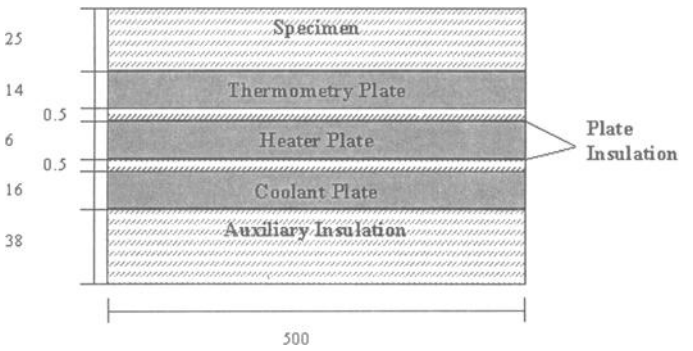

Figure 9 - *Cross section of cold-plate assembly (not to scale; dimensions in mm).*

The first finite element analysis that was performed involved gaseous nitrogen cooled to 90 K. Table 3 displays the key parameters for all simulations. Figure 10 shows the resulting temperature profile on the surface of the cold plate facing the

Table 3 - *Cold plate simulation parameters.*

Parameter	Value
Plate material	Nickel
Plate λ	100 W/(m·K)
Specimen R-value	0.125 m^2·K/W
Hot Plate Temp.	110 K, *or* 270 K
Auxiliary insulation R-value	0.630 m^2·K/W
Environmental Temperature	298 K

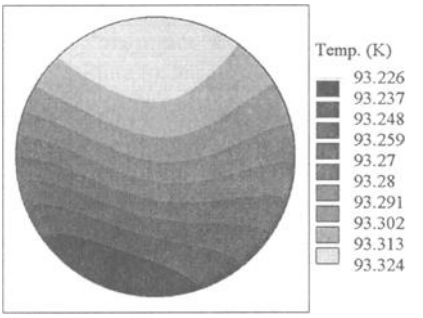

Figure 10 - *Surface temperature profile on cold plate with gaseous nitrogen as coolant.*

specimen. A large asymmetry in the temperature profile exists, and the span of temperatures is estimated as 98 mK.

The next simulation involved the use of ethanol as the coolant. Ethanol can be used down to a temperature of 210 K, so this fluid would be adequate for temperatures slightly below the freezing point of water. The surface temperature contours for this scenario are shown in Fig. 11. The temperature variation over the surface of the plate is estimated to be 4 mK. The temperature of ethanol remains close to the inlet temperature because of its high enthalpy. The shape of the profile is dictated by the geometry of the coolant tubes, as opposed to the case of gaseous nitrogen, where the temperature profile is a function of both tube geometry and the temperature of the fluid within the tubes.

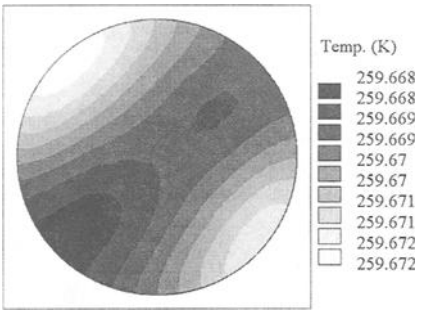

Figure 11 - *Surface temperature profile on cold- plate with ethanol as coolant.*

To attain cold-plate temperatures down to 90 K, liquid nitrogen will be used as the coolant. The temperature distribution on the surface of the cold plate has a similar shape as that shown for ethanol in Fig. 11, albeit at an average temperature of approximately 90 K.

Guarding Against Extraneous Heat Flows

Edge Guard Design

At operating temperatures far from ambient, edge guards became a necessity to minimize heat flow to or from the metering region through the edge of the specimen. An edge guard will be constructed that fits closely around the specimen, as shown in Fig. 1. The first decision that was made concerned the spacing between the edge of the plates and specimen and the edge guard. If the edge guard lies too close, thermal expansion of the plates could lead to contact between the two pieces, and heat transfer between the plates and the edge guard would be quite large. If the guard is too far away, a path for heat conduction to the environment is opened up. As a compromise, a distance of 10 mm was selected as the spacing between the edge of the plates and the edge guard. This gap will be filled with ceramic fiber insulation.

Two different designs were proposed for the edge guard. The first design produces an isothermal edge guard that is maintained at the mean specimen temperature, or the mean of the hot and cold plate temperatures. The second design results in a linear temperature profile along the edge guard to match the temperature distribution through the specimen. Finite element simulations were performed to determine the effectiveness of each edge guard. These analyses examined a two-dimensional axisymmetric cross-section of the guarded hot plate as shown in Fig. 12. Table 4 gives the properties of the materials in these simulations. The case that was examined was a worst case scenario in

which the specimen temperature (910 K) deviated the furthest from ambient and the specimen thickness was greatest (100 mm). Sufficient performance under these conditions would prove that the edge guard would effectively mitigate radial heat flow in the meter section under expected conditions.

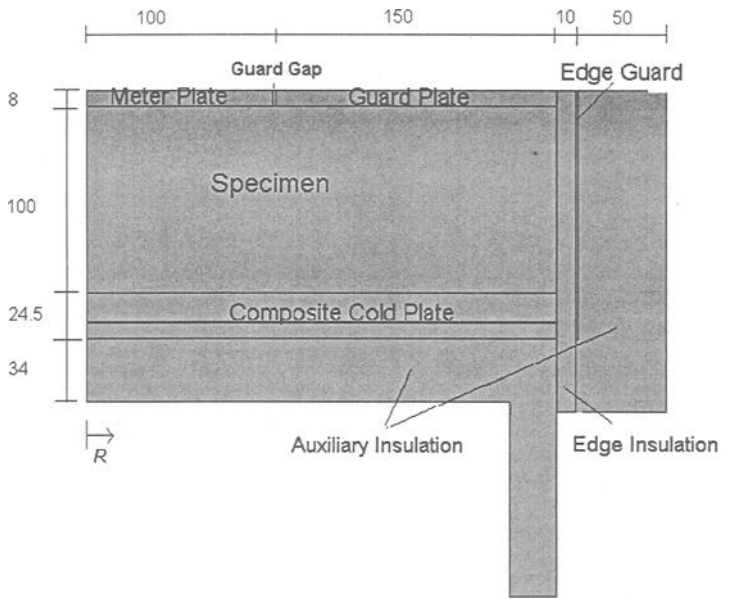

Figure 12 - *Simulation model for edge guard studies (dimensions in mm).*

Table 4 - *Model parameters for edge guard simulations.*

Plate material	Nickel
Plate thermal conductivity	70 W/(m·K)
Edge guard material	Nickel
Edge guard thermal conductivity	20 W/(m·K)
Specimen material	Fiberglass batt
Specimen thermal conductivity	0.0328 W/(m·K) (T = 300 K) – 0.106 W/(m·K) (T = 1000 K)
Aux. insulation material	Alumina board
Aux. insulation thermal conductivity	0.0627 W/(m·K) (T = 297 K) – 0.160 W/(m·K) (T = 1073 K)
Edge insulation material	Ceramic Fiber
Edge insulation thermal conductivity	0.038 W/(m·K) (T = 297 K) – 0.270 W/(m·K) (T = 1023 K)
Edge guard temperature	910 K
Ambient temperature	298 K

In this model, certain simplifying aspects are included. Details of the heaters in all plates are replaced by uniform volumetric heat generation in the plates. The three-part composite construction of the cold plate is replaced by a two-part construction, with the plate holding the coolant tubes being combined with the plate containing the heaters. Additionally, details of the edge guard are omitted and are replaced by a perfect cylinder surrounding the specimen. These simplifications should not affect the result of interest, namely the edge heat losses.

Figure 13 shows temperature contours within the specimen for an isothermal edge guard and a temperature difference of 40 K across the specimen. In the meter section the isotherms are nearly parallel, indicating that the heat is transferred in a one-dimensional manner. At the edge of the specimen, the isotherms diverge because the edge guard is maintained at the mean temperature of the specimen. Figure 14 shows a similar plot for an edge guard with a linear temperature profile. Parallel isotherms are maintained throughout the entire specimen. The linear edge guard thus qualitatively provides superior guarding.

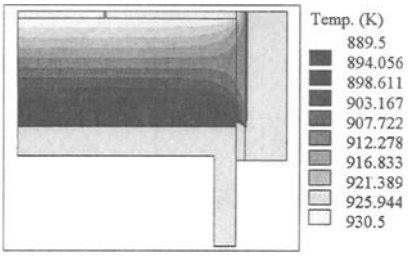

Figure 13 - *Temperature contours within the specimen with an isothermal edge guard.*

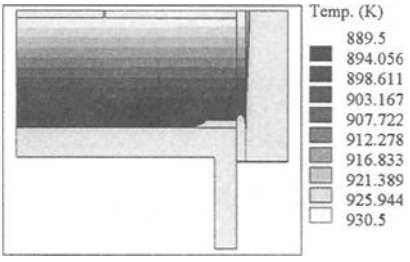

Figure 14 - *Temperature contours within the specimen with a linear edge guard.*

The errors in the thermal conductivity measurements were also computed for both cases. Since the thermal conductivity of the specimen is known in the model, Eq. (1) can be used to determine an experimental thermal conductivity. The surface temperature over the meter plate and the meter section of the cold plate are determined from the model and the heat flow from the meter plate is also determined. In both cases, the error in the thermal conductivity measurement was less than 0.2 % for the 40 K temperature difference. For a $\Delta T = 10$ K, the errors were worse, but errors for both cases lay between 0.5 % and 0.7 %. Within the bounds of the accuracy of the model, negligible differences exist between the two types of edge guards.

While the above analysis indicates that either edge guard will work equally well, that analysis assumes that one knows the true surface temperature. In the actual experiment, uncertainty exists in the temperature measurements. The SPRT measures only the temperature in the center of the plate. With this in mind, it is useful to examine the surface temperature profiles in both cases. Figure 15a shows the profiles along both the hot plate and the cold plate for both simulations, while Fig. 15b shows those same

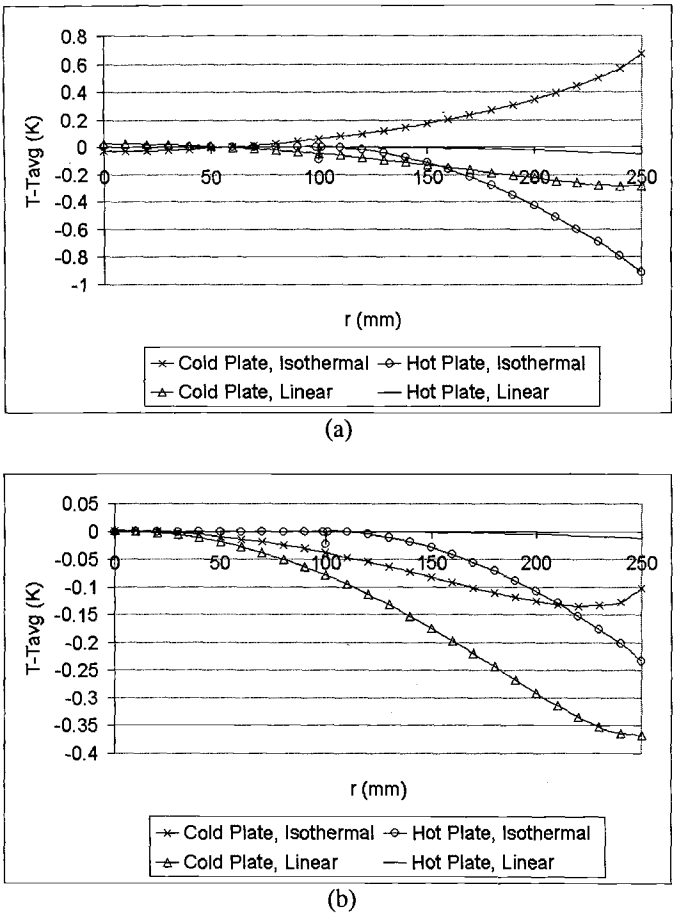

Figure 15 - *Surface temperatures in edge guard simulations with Δz = 100 mm (a) ΔT = 40 K, (b) ΔT = 10 K*

profiles for a ΔT = 10 K. In (a), the temperatures at the edges of all plates deviate from the average. For the isothermal guard, the edge of the cold plate increases in temperature, while the edge of the hot plate decreases in temperature because of heat flow to or from the edge guard, respectively. For the linear edge guard, both the cold plate and hot plate see slight decreases in temperatures at the edge because of heat loss to the environment. For the case where ΔT = 10 K, interesting observations can be made. For the isothermal guard, the behavior of the hot plate is similar to that for the previous case in that its temperature drops as r increases. The cold plate, however, behaves in a different manner when ΔT = 10 K versus the case where ΔT = 40 K. With a difference of only 5 K between the cold plate and the edge guard, heat flow from the edge guard to the cold plate is overwhelmed by heat flow from the cold plate to the environment. Because of the net heat flow out of the cold plate, the temperature at the

edge drops. For the linear case, the hot plate temperature profile is similar to that of the previous case, but the cold plate temperature drops more severely with ΔT = 10 K than with ΔT = 40 K. The reason for this behavior is that the cold plate does not receive as much heat from either the hot plate or the edge guard to make up for the heat lost to the environment. The lesson learned from these plots is that both a linear edge guard and an isothermal edge guard could lead to errors in temperature measurement of the plate, depending upon the operating conditions.

The decision concerning which edge guard to use was dictated more by manufacturing issues than thermal issues. The thermal analyses showed that either guard would provide satisfactory results, so the fact that the isothermal guard would be much easier to fabricate than the linear guard made the choice for an isothermal guard.

Connection Guard Block Design

Key paths for heat flow to or from the hot and cold plates are the SPRT, thermocouple and thermopile wires, heater leads, and support cables. Because the plates will be operated at temperatures far from ambient, precautions need to be made to minimize the heat flow through these entities. To accomplish this guarding, all leads are attached to a connection guard block. Each plate has one connection guard block adjacent to it that will be controlled to be at the same temperature as the plate. The edge guard will also have connection guard blocks to minimize heat loss through the heater and thermocouple leads in that component.

Figure 16 shows a schematic of a connection guard block. Only the SPRT is shown passing through the block, but heater wires and thermocouple leads will also pass through it. The circles on the block are mandrels that hold heater wire or coolant tubes. The location of those mandrels is different on the hot plate connection guard block than on the cold plate connection guard block. The block is removed from each plate by a distance of 10 mm. Finite element analysis was used to determine the temperature distribution within these blocks. Since the blocks are so close to the plates, it was necessary to ensure that the temperature variation along the edge that is near the plate is as uniform as possible. The blocks were modeled in isolation from the surrounding plate under the assumption that adiabatic boundaries existed everywhere except where heat was lost through the connections and where heat was added to the block. Simulations were run with the blocks at 930 K to estimate the worst-case scenario, that where the block's temperature is furthest from room temperature. The effect of the SPRT and wire leads was modeled by estimating the thermal resistance caused by these items between the guard blocks

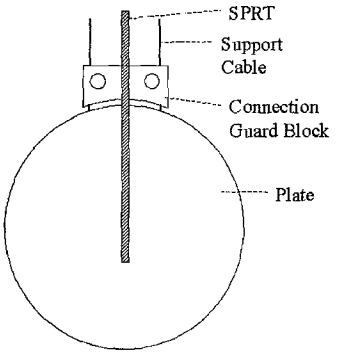

Figure 16 - *Connection guard block schematic.*

and a room temperature block located a known distance from the connection guard blocks. That condition was applied to a small area on the top of the block. The effect of the support cables was modeled in a similar fashion. Table 5 describes critical parameters for the simulations.

Table 5 - *Parameters for connection guard block studies*

Parameter	Value
Block material	Nickel
Block thermal conductivity	70 W/(m·K)
Thermal resistance of support cable	2.62×10^{-3} m^2·K/W
Thermal resistance of SPRT + wires	2.86×10^{-3} m^2·K/W
Environmental Temperature	298 K
Heat flux on each hot plate CGB mandrel	4010.8 W/m^2
Heat flux on each cold plate CGB mandrel	2005.8 W/m^2

Figure 17 shows the temperature contours on the hot plate connection guard block. Figure 17a shows the complete range of temperatures seen on the block in an oblique view. This block has four bosses on it, with two bosses having heating elements and the other two having cooling coils. In this simulation, the high temperature case was of interest, so heat was applied on the front-left boss and the back-right boss. The necessary heat flux needed on those surfaces was calculated to match the heat loss through the cables and SPRT with the block at 930 K. Figure 17b shows a narrower range of temperatures in a front view of the block. The temperature span along the lower portion of the block is approximately 0.56 K. While this temperature span is large compared to those seen in the meter plate, insulation between the plate and the block

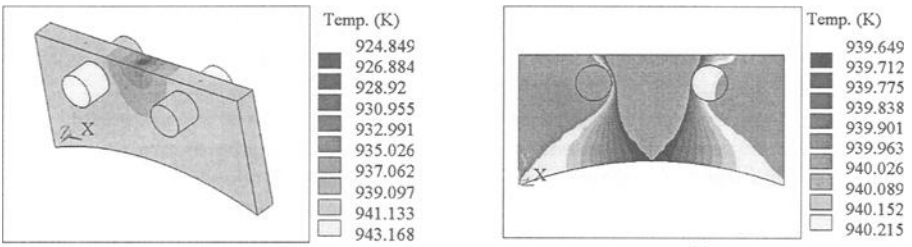

Figure 17 - *Temperature contours on the hot plate connection guard block.*

will prevent those temperature fluctuations from causing any severe problems in the plate itself. While it would have been desirable to decrease that temperature span, packaging issues prevented a better location of the bosses.

Figure 18 shows the temperature contours on the cold plate connection guard block. In both of these figures, symmetry has been used in the model, so only half of the block is shown. The plane of symmetry is on the left-most portion of the model. This block is shaped differently from the hot plate connection guard block so that the two blocks fit together when the entire apparatus is assembled. Each block has two bosses that face the same way. Both heating elements and coolant lines will be wound around each boss. The SPRT and wires emerge from the center portion, and the support cables are connected to the right edge. At these locations, the temperature is lower because of conduction from the ambient. The narrower temperature range shown in the head-on view of Fig. 18b displays the temperature range seen near the cold plate. A temperature span of nearly 2 K is seen along the bottom of this block. While the insulation between the block and the plate should help mitigate those temperature variations, observation will be needed when the plate is built to determine whether this temperature variation affects temperatures within the cold plate.

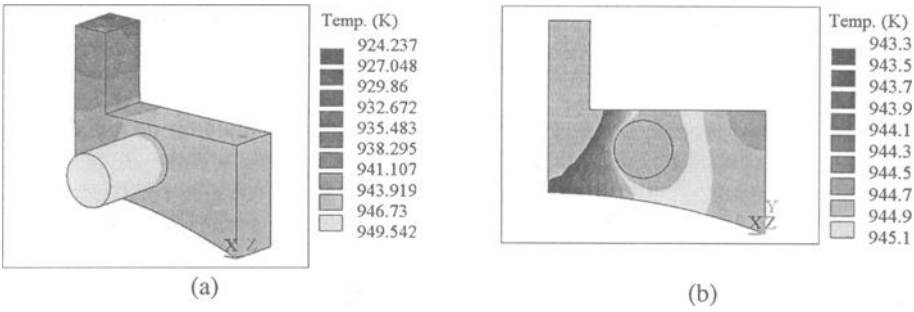

Figure 18 - *Temperature contours on cold plate connection guard block*

Transient Calculations

A guarded hot plate apparatus operates under the assumption that steady-state conditions have been achieved in the apparatus. An analysis was performed to determine the effect of deviations from a steady-state condition on the measured thermal conductivity. Errors will appear in determinations of specimen thermal conductivity if the measured dissipation of heat in the meter plate does not match the heat flowing through the specimens. Such a condition will occur if thermal energy is stored in the meter plate.

The amount of energy transferred through each specimen can be determined by Eq. (1), while the amount of energy stored in the meter plate is given by the following equation:

$$q_{st} = lA\rho C_p \frac{dT}{dt}, \tag{2}$$

where:

q_{st} = stored energy in meter plate
l = thickness of meter plate
ρ = density of meter plate material
C_p = specific heat of meter plate material
dT/dt = time rate of change of average meter plate temperature.

The goal in the design was to keep errors from transient effects to less than 0.1 % of the measured heat flow. The ratio of the stored heat to the heat transferred through two specimens was calculated for three different operating conditions and a temperature difference across the specimen of 10 K. Table 6 gives the maximum allowed temperature change in the meter plate to keep the ratio of the rate of stored energy to the rate of heat flow through the specimen below 0.1 %. For all conditions, temperature fluctuations need to remain very low owing to the thick construction of the meter plate made necessary by the SPRT. When measuring specimens with high R-values (thermal resistance), transient fluctuations in temperature will have a greater effect on the measured thermal conductivity because of the low heat flow through the specimen. At higher ΔT, the allowed temperature fluctuations will be larger because of the greater heat flow through the specimens. Table 6, therefore, represents a worst-case scenario for the operating conditions listed.

Table 6 - *Maximum average temperature fluctuation in meter plate to achieve less than 0.1 % error in measured heat flux through specimen due to transient effects; ΔT = 10 K*

Condition	Specimen R- value [$m^2 \cdot K/W$]	Plate ($l \cdot \rho \cdot C_p$) [$J/(m^2 \cdot K)$]	$\left(dT/dt\right)_{max}$ [K/h]
80 K in air	4	28 300	6.4×10^{-4}
80 K in vacuo	40	28 300	6.4×10^{-5}
934 K in air	2	64 900	5.5×10^{-4}

Conclusions

Thermal modeling of a proposed guarded hot plate apparatus has given a greater understanding of the performance of the apparatus. Analytical techniques were used together with finite element analysis to predict temperature fields within the plates and heat flows within the specimen. Temperature variations across the surfaces of the meter plate and the guard ring were calculated to be approximately 38 mK and 51 mK, respectively, for a typical test involving a 20 K temperature difference across a specimen with a thermal resistance of 0.125 $m^2 \cdot K/W$. These small temperature deviations indicate that temperature measurements of the plate will yield an accurate estimate of the true average surface temperature. Simulations of the temperature distribution along the surface of the cold plate also show that this plate is nearly isothermal when liquid nitrogen or ethanol is used as the coolant.

The proposed plate will have an isothermal edge guard maintained at the mean specimen temperature. Modeling showed that this component effectively guards the meter section from environmental effects, even at a worst-case scenario involving a thick specimen at an operating temperature far from ambient. Errors in thermal conductivity measurements of the specimen are estimated to be less than or equal to 0.7 % at these extreme conditions. Measurements taken on thinner specimens at temperatures closer to room temperature will result in negligible errors due to edge losses. To further guard the plates from the surrounding environment, connection guard blocks will be included in the design to minimize unwanted heat flow through heater and thermometry leads and support mechanisms.

Analyses of the transient performance of the guarded hot plate apparatus revealed the importance of maintaining steady-state conditions throughout each test. It was found that temperature fluctuations in the meter plate need to be kept below 1 mK/h to ensure that errors arising from transient effects are lower than 0.1 % for the cases studied.

The use of finite element analysis in tandem with analytical techniques has provided significant insight into the operation of the proposed guarded hot plate apparatus and will allow better estimates of the uncertainties associated with measurements of the thermal conductivity of thermal insulation.

References

[1] Flynn, D. R., Zarr, R. R., Hahn, M. H., and Healy, W. M., "Design Concepts for a New Guarded Hot Plate Apparatus," *Insulation Materials: Testing and Applications: 4th Volume, ASTM STP 1426*, A.O. Desjarlais and R. R. Zarr, Eds., American Society for Testing and Materials, West Conshohocken, PA, 2002.

[2] Zarr, R. R., "A History of Testing Heat Insulators at the National Institute of Standards and Technology," to appear in *ASHRAE Transactions*, Vol. 107, Pt.2.

[3] Klarsfeld, S., "Guarded Hot Plate Method for Thermal Conductivity Measurements," in *Compendium of Thermophysical Property Measurement Methods, Vol. 2, Recommended Measurement Techniques and Practices*, K.D. Maglic, A. Cezairliyan, and V.E. Peletsky, Eds., Plenum Press, New York, 1992, pp. 99-131.

[4] Pratt, A. W., "Heat Transmission in Low Conductivity Materials," in *Thermal Conductivity*, Col. 1, R.P. Tye, Ed., Academic Press, London, 1969, pp. 301-405.

[5] Hahn, M. H., Robinson, H. E., and Flynn, D. R., "Robinson Line-Heat Source Guarded Hot Plate Apparatus," in *Heat Transmission Measurements in Thermal Insulation, ASTM STP 544*, R.P. Tye, Ed., American Society for Testing and Materials, Philadelphia, 1974, pp. 167-192.

[6] Flynn, D. R. and Gorthala, R., "Thermal Design of a Miniature Guarded Hot Plate Apparatus," in *Insulation Materials: Testing and Applications: Third Volume, ASTM STP 1320*, R.S. Graves and R.R. Zarr, Eds., American Society for Testing and Materials, West Conshohocken, PA, 1997, .

[7] De Ponte, F. and Di Filippo, P., "Thermal Conductivity Measurements of Insulating Materials Down to 100 K," *Proc. Of the XIII Intl. Congress of Refrigeration, Progress in Refrigeration Science and Technology*, 1973 pp. 7-14.

[8] De Ponte, F. and Di Filippo, P., "Some Remarks on the Design of Isothermal Plates," in *Some Thermophysical Properties of Refrigerants and Insulants*, 1973.

[9] De Ponte, F. and Di Filippo, P., "Design Criteria for Guarded Hot Plate Apparatus," in *Heat Transmission Measurements in Thermal Insulations: ASTM STP 544*, Ed. R.P. Tye, American Society for Testing and Materials, Philadelphia, PA, 1974, pp. 97-117.

[10] Troussart, L. R. "Three-Dimensional Finite Element Analysis of the Guarded Hot Plate Apparatus and its Computer Implementation," *J. Thermal Insulation* Vol. 4, 1981, pp. 225-254.

[11] Pham, Q. T. and Smith, C. G. "Thermal Imbalance Errors and Effective Area in Guarded Hot Plates," *Rev. Sci. Instrum.* Vol. 57, 1986, pp. 99-105.

[12] Nicolas, J., Martin, F., Andre, Ph., and Rivez, J. -F. "Finite-Element Design of a Guarded Heating Cylinder to Measure Thermal Properties of Materials," *Rev. Sci. Instrum.* Vol. 61, 1990, pp. 3876-3882.

[13] Ashworth, E. and Ashworth, T. "Finite Element Analysis of Unguarded Hot-Plate Thermal Conductivity Apparatuses," *Thermal Conductivity 18: Proc. Intl. Thermal Conductivity Conference*, 1985, pp 599-609.

[14] Virgone, J., Yezou, R., and Roux, J., "Computer Simulation of the Measurement Error with the Guarded Hot-Plate System," *High Temperatures-High Pressures* Vol. 31, 1999, pp. 275-281.

[15] Petukhov, B. S., "Heat Transfer and Friction in Turbulent Pipe Flow with Variable Physical Properties," in *Advances in Heat Transfer, Vol.6*, T.F. Irvine and J.P. Hartnett, eds., Academic Press, New York, 1970, pp. 503-564.

[16] Gnielinski, V., "New Equations for Heat and Mass Transfer in Turbulent Pipe and Channel Flow," *Intl. Chem. Eng.* Vol. 16, 1976, pp. 359-368.

Daniel R. Flynn,[1] Robert R. Zarr,[2] Mahn Hee Hahn,[3] and William M. Healy[2]

Design Concepts for a New Guarded Hot Plate Apparatus for Use Over an Extended Temperature Range

REFERENCE: Flynn, D. R., Zarr, R. R., Hahn, M. H., and Healy, W. M., **"Design Concepts for a New Guarded Hot Plate Apparatus for Use Over an Extended Temperature Range,"** *Insulation Materials: Testing and Applications: 4th Volume, ASTM STP 1426*, A. O. Desjarlais and R. R. Zarr, Eds., ASTM International, West Conshohocken, PA, 2002.

ABSTRACT: The National Institute of Standards and Technology is building a new guarded hot plate apparatus (GHP) for use at temperatures from 90 to 900 K, with provision to conduct tests in various gases at controlled pressures from 0.013 Pa to 0.105 MPa (≈ 1.04 atm). Important features of the design of the new NIST GHP include: enclosure of the entire apparatus in a vacuum chamber; solid metal hot plates and cold surface plates to provide highly isothermal surfaces in contact with the test specimens; an integral close-fitting edge guard to minimize the effects of edge heat losses or gains; connection guard blocks to minimize the effects of heat conduction along coolant lines, heater leads, thermometry wells, and sensor leads coming from the hot plate and the cold plates; provision of a system to provide a known clamping force between the specimens and the contacting hot and cold plate surfaces; provision of an accurate system for *in-situ* measurement of specimen thickness during a test; and the use of three long-stem standard platinum resistance thermometers to measure the average temperature of the meter plate and the two cold plates.

KEYWORDS: guarded hot plate, heat conduction, heat transfer, insulation, R-value, thermal conductivity, thermal insulation, thermal resistance

Introduction

The guarded hot plate apparatus is generally recognized as the primary absolute method for measurement of the thermal transmission properties of homogeneous insulation materials in the form of flat slabs. This test method has been standardized as ASTM Test Method for Steady-State Heat Flux Measurements and Thermal Transmission Properties by Means of the Guarded-Hot-Plate Apparatus (C 177) and ISO International Standard: Thermal Insulation – Determination of Steady-State Thermal Resistance and Related

[1]President and Chief Scientist, MetSys Corporation, Millwood, VA 22646-0317.
[2]Mechanical Engineer, Building and Fire Research Laboratory, National Institute of Standards and Technology, Gaithersburg, MD 20899.
[3]Mechanical Engineer, Manufacturing Engineering Laboratory, National Institute of Standards and Technology, Gaithersburg, MD 20899.

Thermal Insulation – Determination of Steady-State Thermal Resistance and Related Properties – Guarded-Hot-Plate Apparatus (ISO 8302), with the two test methods being very similar, but not identical. Over the temperature range to which typical building insulations are exposed, interlaboratory comparisons on well-behaved materials have shown that different guarded hot plate apparatus can produce thermal conductivity or thermal resistance values with differences of ±2 or 3 percent. However, interlaboratory comparisons among different guarded hot plate apparatus at higher temperatures (e.g., 400 K to 1000 K), in both North America [*1*] and in Europe [2], have revealed variations in thermal properties ranging from ±12 to 18%. There do not appear to have been similar interlaboratory comparisons for guarded hot plate measurements at cryogenic temperatures but larger uncertainties than near room temperature could be expected there.

The good agreement among different guarded hot plate apparatus near room temperature is believed to be in large part due to the ready availability of certified reference materials that have been measured by one or more national standards laboratories, and that can be used by various laboratories to check out their own thermal transmission measurement equipment. Very few national standards laboratories have guarded hot plate apparatus that are known to provide reliable calibration data at cryogenic temperatures or at high temperatures, so the availability of certified reference materials for use at these more extreme temperatures is quite limited. For many years, ASTM Committee C-16 on Thermal Insulation has been asking NIST to provide suitable reference materials for use over the broad temperature range of interest for various applications of industrial insulations. In addition to there being a need for reference materials for use over a broad temperature range in air, NIST perceives a need for reference materials whose thermal transmission properties are well known when the insulation is evacuated or filled with a gas of high molecular weight, such as might be the case for cryogenic insulations or the advanced insulation panels that are being developed for use in refrigerators, freezers, and refrigerated transport.

In order to have the capability of measuring thermal transmission of commercial products and candidate reference materials over a broad range of temperatures and gas pressures, NIST and MetSys Corporation (under an SBIR contract) have undertaken a project to design, analyze, fabricate, and evaluate a new 500 mm diameter guarded hot plate apparatus for the determination of steady-state thermal transmission properties of insulating and building materials at mean temperatures from 90 K to 900 K. Ultimately, the apparatus will be provided with the capability of carrying out such measurements at controlled gas pressure from 0.01 Pa to 0.105 MPa (≈1.04 atm), with dry air or a selected filler gas.

The present paper includes a summary of some of the perceived problems with previous designs of guarded hot plate apparatus, the performance criteria for the new guarded hot plate to be built at NIST, and the design concepts that will be used to ensure that the new apparatus will be convenient to use and that it will provide accurate thermal conductivity and thermal resistance data over a broad range of temperatures and pressures.

Background

Traditionally, most guarded hot plate apparatus have been constructed using a metal-surfaced laminated design, in which an electrical heater on a central electrically insulating plate is sandwiched between two thin electrically insulating plates which in turn are

sandwiched between two metal surface plates. While such designs can work quite well in air at temperatures in the range of, say, 240 K to 340 K, problems are often encountered at higher or lower temperatures or if it is desired to measure the thermal transmission of specimens under vacuum conditions. At higher temperatures, the meter plate may be constructed as a sandwich of a ceramic plate, with an embedded heater, between two metal plates. Laminated hot plates typically must use materials having different thermal expansion coefficients so that such plates are subject to warping at either low temperatures or high temperatures, with attendant large thermal contact resistances between the surface plates and the specimens. At low temperatures, and particularly under vacuum conditions, thermal contact resistances between the different layers can be quite large, resulting in the meter and guard heaters being considerably hotter than the surface plates, a situation that can result in poor guarding and possible temperature variations over the surface plates. Laminated designs are generally not suitable for use in vacuum since they are subject to severe outgassing and, if a good vacuum is achieved, the thermal contact between the heater plates and the metal plates is poor, particularly at lower temperatures where radiative heat transfer across the thermal contacts is low. Rather than using laminated metal-surface constructions, some high-temperature guarded hot plate designs have used ceramic plates with electrical heaters embedded in them. If the meter, guard, and auxiliary plates are made of ceramic, they typically are made rather thick in order to provide increased lateral thermal conductance; even so, the thermal conductivity of most ceramics is approximately inversely proportional to the absolute temperature so that the plate thermal conductivities become quite low at high temperatures, making it difficult to achieve isothermal plate surfaces. In addition, the electrical resistivity of ceramics drops sharply with increasing temperature so that it can be difficult to avoid electrical leakage from the heaters to the temperature sensors.

In the early 1960s, Robinson conceived the idea of building a circular guarded hot plate as solid metal plates with embedded line heat sources, one in the meter plate and one in the guard plate, rather than to distribute the heating elements over the area of each plate. In an unpublished 1964 paper [*3-5*], he described his concept, developed the mathematical analysis behind his proposed design, and listed some of the virtues he saw for a line-heat-source guarded hot plate, as compared to the conventional distributed-heater design:

"1. There is no danger that a surface temperature thermocouple, or more seriously perhaps, a gap thermocouple, may give an erroneous result because one of its junctions happens to be too close to a wire of one of the heater windings. Difficulties of this kind have occurred in carefully-made hot plates with distributed grid heaters, and are not easily discovered.

"2. Although it is not necessary, it appears that most metal-surfaced hot plates with distributed grid heaters are square in shape. Because of the corners, the problem of getting a good average balance of across-gap temperatures along the entire length of the guard gap is more difficult than it is for the circular design described here.

"3. The guard section of a guarded hot plate operates with practically no heat exchange laterally at the gap separating it from the metering section, but usually some heat exchange occurs at its outer edges. With a uniformly-distributed heater, this means that some radially-directed lateral temperature gradients must exist, which may significantly disturb the uniformity of guard surface temperature near the gap. With the line-source heated guard

described, the radial lateral temperature gradients near the periphery can exist, but do not disturb the temperatures of the inner part of the guard within the radius of the heater.

"4. The flatness, and thickness, of a hot plate made of a solid plate of metal operated at very nearly a uniform temperature are subject to no change except as a result of thermal expansion of the metal, which can be calculated if significant. The flatness, and thickness, of a hot plate made with laminations of electrical insulation, a distributed heater winding on a template, and relatively thin metal face plates, all held together by screws, may both be questionable at various temperatures, or after a period of use. In measurements on thin or quite conductive materials, uncertainties as to thickness or flatness of the hot plate may be important, particularly if specimen thickness is measured in the apparatus, which is desirable if the specimen changes in thickness with temperature."

In the early 1970s, Hahn carried out a thorough mathematical analysis and developed a detailed design for a line-heat-source guarded hot plate apparatus [*6*]. After Robinson's death, a summary of his analysis and of Hahn's analysis and design were presented at an ASTM C-16 conference and published in 1974 [*7*]. In this paper, it was stated that some of the specific problems which may be associated with a distributed heater winding such as typically used include the following:

"1. Construction and repair of the heaters is somewhat complicated and difficult.

"2. The construction by lamination of different materials can lead, because of differential expansion, to warpage of the hot plate, which may result in nonuniform thermal contact with the specimens and difficulty in accurate *in situ* measurements of specimen thickness.

"3. Repeated thermal cycling of the apparatus can lead to permanent deformation of the hot plate.

"4. The need for structural integrity of the laminated design requires excessive material bridging the gap thus resulting in a high thermal conductance between the metering and bridge sections.

"5. It is difficult to locate and install thermocouples so as to determine the average surface temperatures of the metering section.

"6. It is difficult to locate and install a thermopile so as to adequately reflect the average temperature difference across the gap.

"7. The hot plate design is rather unsuitable for vacuum operation because of outgassing problems and uneven temperature distributions due to poor and nonuniform thermal contacts among the elements of the hot plate."

In 1978, construction of a prototype line-heat-source guarded hot plate apparatus, based on Hahn's design, with a diameter of 305 mm was completed [*8-10*]. Hahn then led the design and construction effort that resulted in the completion, in 1980, of a 1016-mm diameter apparatus [*11-14*], that is still in very active use today. Recently Zarr and Hahn documented the detailed designs of both of these apparatus [*15*].

During the 1980s, the key design features for a line-heat-source guarded hot plate were standardized as ASTM Standard Practice for Guarded-Hot-Plate Design Using Circular Line-Heat Sources C 1043). During the mid-1990s, the scope of C 1043 was substantially extended. As part of this effort, consideration was given to the design of line-heat source guarded hot plate apparatus to be used at elevated temperatures or for measurement of the thermal transmission of specimens that have lower thermal resistances than is the case for

thick specimens of good thermal insulations at temperatures near to normal ambient. Analyses were carried out which showed that accurate thermal transmission measurements for higher conductance specimens would benefit from the use of a line-heat-source guarded hot plate apparatus with multiple circular line heat sources, rather than just one or two, in the meter plate and in the guard plate. Accordingly, in the revision of C 1043, an annex was added that provides guidance on how and where to locate the heaters in such apparatus. Since that annex was written, substantial additional analyses relative to the location of heaters in a guarded hot plate apparatus have been carried out [*16*].

Problems With Prior Designs

Some of the problems that have been encountered with guarded hot plates for use at cryogenic temperatures or high temperatures are summarized in Table 1. The difficulties with the design of the hot plate have been discussed above in some detail. Similar concerns apply to the design of the cold plates when it is necessary that they be equipped with heaters, rather than just coolant coils, as is the case for many GHPs for use near room temperature.

Edge Guarding

In many guarded hot plate apparatus used at moderate temperatures, the equipment is inside an environmental chamber whose temperature can be adjusted to be nearly equal to the average temperature of the test specimens. By this means, with or without the use of edge insulation, the effect of heat gains to or losses from the edge of the guard plate and the specimens can be kept acceptably small. In many high-temperature guarded hot plate apparatus, a cylindrical edge guard is used to control the temperature of the outside of the edge insulation to be close to the specimen mean temperature. Figure 1 shows the overall layout (not necessarily to scale) of a typical high-temperature guarded hot plate apparatus. The (usually cylindrical but sometimes square) "stack" is symmetrical about the mid-plane of the apparatus. All of the electrical power input to the meter plate heater ideally flows through the meter area (i.e., an area equal to the area of the meter plate plus half of the area of the guard gap between the meter plate and the guard plate) of the specimens.

The guard plate temperature is controlled by a thermopile across the guard gap so that there is, again ideally, no heat flow across the guard gap. Each auxiliary plate, which is the "cold plate" as far as the specimen is concerned, is provided with an electrical heater and is controlled to the desired cold-side temperature. The auxiliary insulation between each auxiliary plate and the corresponding coolant plate keeps the heat load to the auxiliary plate heater to a reasonable value. Each coolant plate is cooled by circulating water or some other liquid. The edge guard, which is significantly larger in inside diameter than the outer diameter of the stack, is usually controlled at a temperature close to the mean temperature of the specimens so as to minimize edge heat losses. There frequently is a cooled shroud (not shown) outside of, and coaxial with, the edge guard. The space between the stack and the edge heater, and that between the edge heater and the shroud are filled with loose-fill insulation. Permanently installed thermocouples are located in the meter plate, guard plate, auxiliary plates, and edge guard.

Table 1 – *Design Concerns for GHPs for Use Over Extended Temperature Ranges*

Component	Concerns
Hot and Cold Plates	
• Laminated construction with metal surface plates	Warpage, poor thermal contact between layers, lateral temperature variations, outgassing
• Ceramic plates with embedded heaters	Low thermal conductivity at high temperatures, electrical leakage at high temperatures
Edge Guarding	
• Guard design	Spatial temperature variations, shunting heat flows
• Fill insulation	Messy, not suitable for vacuum
Heaters and Sensors	
• Connection leads	Parasitic heat flows
Temperature Measurement	
• Alloy thermocouples	Calibration uncertainties
• Pure element thermocouples	Inadequate sensitivities at cryogenic temperatures
Thickness Measurement	
• Room temperature only	Thickness may change due to variable compressive force and/or thermal expansion
• *In situ*	Difficult to achieve desired accuracy

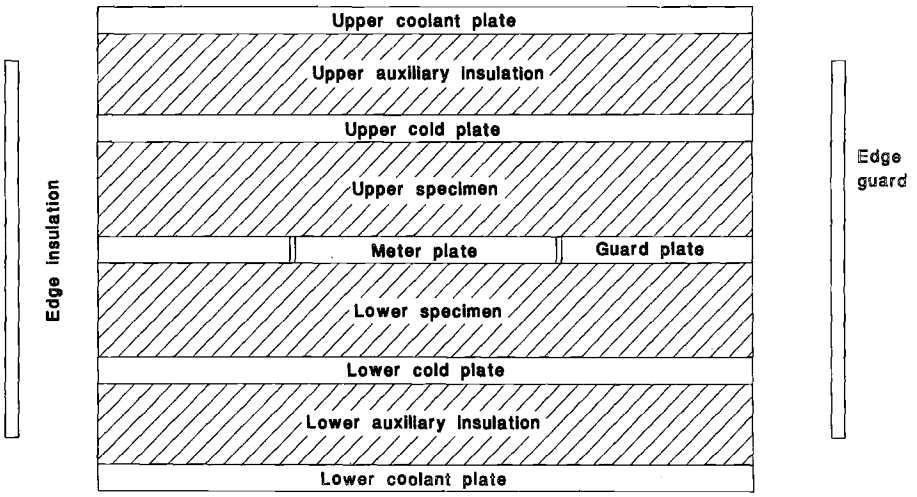

Figure 1 – *A typical high-temperature guarded hot plate apparatus*

The type of edge guard shown in Figure 1 can lead to very serious errors. For some designs, the edge guard is not sufficiently conductive, or the heater is not properly distributed, to ensure that the edge guard is uniformly maintained at the desired average temperature. Even if the guard is isothermal, for tests at a high mean temperature, the edges of the guard plate, the two specimens, and the two auxiliary plates will be much hotter than the coolant plates, with the resultant effect that there are very large longitudinal heat flows in the insulation that fills the annulus between the stack and the edge guard. The longitudinal heat flow near the stack in this annulus must be provided by radial heat losses from the edges of the auxiliary plates, the edges of the specimens, and even, for thin specimens, from the edge of the guard plate. The analysis which was carried out shows that there can be large net heat losses from the edges of the specimen, even when the edge guard is at the mean temperature of the specimen [*16*].

Heaters and Sensors

As indicated in ISO 8302, it is important that heater and sensor leads be thermally tempered so that heat conduction along such connections does not contribute parasitic heat flows to the heat flow through the meter section of the specimens and does not significantly perturb the temperature uniformity of the hot plate or the cold plates. Such thermal tempering is not adequate in many guarded hot plate apparatus designs.

Temperature Measurement

In order to obtain accurate thermal transmission data, it is necessary to know accurately the average temperature difference across the meter area of the specimens. This need requires that the surfaces of the meter plates be uniform and stable in temperature and that the temperature sensors adequately sample the meter area if there are significant temperature variations. Most guarded hot plate apparatus use thermocouples to measure hot and cold plate temperatures. Of the standardized thermocouple types, the noble-metal thermocouples (Types B, R, and S) do not have adequate sensitivities to be used at cryogenic temperatures, and the base-metal thermocouples that use iron, copper, or copper-nickel alloys (Types E, J, and T) cannot be used, for long periods of time with fine wire sizes, at the higher temperatures of interest for the new NIST GHP. Thus, of the standardized thermocouples, it would appear to be necessary to select Type K or Type N thermocouples – but both of these thermocouple types have instabilities that limit the accuracy to which temperatures can be measured. (Note that thermocouple departures from calibration do not constitute a serious problem for thermopiles used to control the guard temperature since they are used as null sensors so their actual sensitivity is not critical.) NIST calibrations of Type K and Type N thermocouples, by comparison to a reference thermocouple or a standard platinum resistance thermometer, have expanded uncertainties ($k = 2$) of 0.4 K at 77 K, dropping to near zero at the ice point, and increasing to 0.6 K at 930 K [*17-18*]. Recently NIST has shown that thermocouples fabricated from pure elements, either gold versus platinum or platinum versus palladium, can be calibrated against fixed point standards with expanded uncertainties ($k = 2$) as small as 10 mK at the highest temperatures of interest for the new NIST GHP [*19-21*]. Unfortunately, these thermocouples have a very low sensitivity at cryogenic temperatures.

Performance Specifications

The performance specifications for the new NIST GHP are summarized in Table 2. The hot plate will be 500 mm in diameter, which is one of the sizes recommended by ISO 8302 for new apparatus. The meter plate will be 200 mm in diameter to the center of the guard gap, which will be 1.4 mm wide at the hot-plate surfaces. The apparatus will be located in a vacuum chamber that can be filled with dry air or other gases and controlled at constant pressures from a fairly soft vacuum to 1.05 atm. The hot and cold plates will be hung vertically so that the heat flow will be horizontal. The apparatus will accommodate a pair of specimens, each of which can be 10 mm to 110 mm thick, and can be operated in either a 1- or 2-sided mode. The apparatus will be designed to measure the ranges of thermal conductivities and thermal conductances shown in Table 2 at mean temperatures from 90 K to 900 K, with the precisions and uncertainties shown at the bottom of Table 2. In preparing these performance specifications, the highest priorities were assigned to the specimen size, the typical ranges of thermal conductivity and thermal conductances, the temperature range, and the precisions and uncertainties of measurement.

Summary of Design Approach

In response to the design limitations of previous GHPs (Table 1) and the performance specifications (Table 2) that were developed, the following design features were included:

- The hot plate will be of all-metal construction with a multiple-turn swaged meter heater and a multiple-turn swaged guard heater embedded in it. The meter plate and the guard plate will be separated by a diamond-shaped guard gap.
- Each cold plate will be laminated, with a surface plate containing the temperature sensors, a middle plate with a multi-turn swaged heater, and a back plate with a bifilar coolant channel embedded in it, with the three plates separated by thin layers of thermally insulating material.
- Based on the advice of the NIST Thermometry Group, long-stem platinum resistance thermometers (SPRTs) will be used as the primary temperature sensors in the hot plate and the two cold plates. Swaged Type N thermocouples will be provided as secondary temperature sensors. The thermopile across the guard gap will also be of swaged construction, with the thermoelements being Type NP wire versus a 65 % Au/35 % Pd alloy.
- Two integrated edge guards will be provided, one for each specimen. These edge guards will provide an isothermal environment, nominally at the mean temperature of each specimen.
- Connection guard blocks will be provided to temper the thermometer wells and the heater and sensor leads coming from the hot plate and from both cold plates.
- The hot plate, the two cold plates, and the two edge guards will be suspended vertically from linear ball bushings on rails so that they can be easily moved back and forth to install specimens of various thicknesses.
- Provision will be made to apply a known axial force to the cold plates.
- Provision will be made to measure the thickness of the test specimens *in situ*.
- The entire apparatus will be cantilevered from a vertical vacuum base plate, with a vacuum enclosure that can be rolled into place so that the apparatus can be operated in a vacuum, or operated at a controlled pressure with whatever filler gas is desired. Provision

Table 2 – *Design Specifications for the NIST 500 mm Guarded Hot Plate Apparatus*

Parameter	Specification		Comment
	Minimum	Maximum	
Hot Plate Size	500 mm round		Per ISO 8302
• Meter Plate	200 mm		Center of gap
• Gap Width	1.4 mm		diamond profile
• Thickness	16 mm		
Specimen			
• Thickness	10 mm	110 mm	
• Conductance	0.1 W/(m^2·K)	50 W/(m^2·•K)	Design
	0.8 W/(m^2·K)	8 W/(m^2·K)	Typical
• Conductivity	0.001 W/(m·K)	0.5 W/(m·K)	Design
	0.01 W/(m·K)	0.2 W/(m·K)	Typical
Temperature			
• Mean	90 K	900 K	
• Hot Plate	95 K	915 K	
• Cold Plate	85 K	885 K	
• Difference	0 K	40 K	
Gas Pressure	0.013 Pa	0.105 MPa	10^{-4} to 790 torr
Operational Mode	1 or 2 sided		
Orientation	Horizontal heat flow		
Precision (90 to 900 K)			
• Single run	0.2 %		k = 2 coverage
• Replicate	0.5 %		k = 2 coverage
Uncertainty			
• 90 K	2 %		k = 2 coverage
• 300 K	1 %		k = 2 coverage
• 900 K	2 %		k = 2 coverage

will be made to clamp the vacuum enclosure to the base plate so that the apparatus can be operated with the chamber pressure somewhat higher than the local barometric pressure.

The proposed overall design of the NIST 500 mm guarded hot plate apparatus, excluding the supporting structure and the vacuum enclosure, is shown in Figure 2. The hot plate itself consists of the 200 mm diameter (to the center of the guard gap) meter plate and the surrounding 500 mm o.d. guard plate. The two specimens are shown cross-hatched. The two cold plate assemblies each move as an integrated unit as do the two donut-shaped edge

guards. The Standard Platinum Resistance Thermometers (SPRTs) used to measure the hot and cold plate temperatures are shown extending to the top of the drawing.

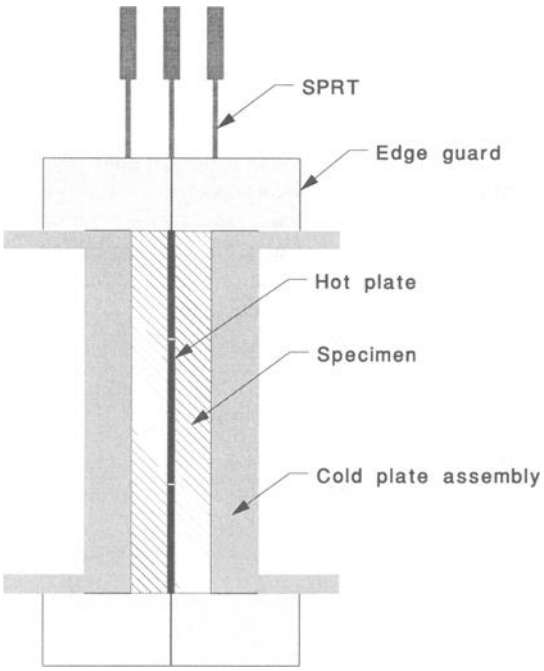

Figure 2 – *Configuration of the NIST 500 mm guarded hot plate apparatus*

Selection of Plate and Guard Materials

The materials used for the construction of the hot plates, the cold plates, and the edge guards need to have suitable thermal and mechanical properties, good oxidation resistance over the temperature range of interest, and be amenable to the selected method of fabrication. The plates also need to be able to accept and retain a suitable high-emittance coating, as required by C 177 and ISO 8302.

Material Properties

It is desirable for the thermal conductivity of the plate and edge guard material to be as high as possible. In order to achieve thermal equilibrium more rapidly, it is desirable for the plate material to have a low volumetric heat capacity. In general, constructing the plates from a material with a very high thermal conductivity would allow the plates to be thinner, thus further reducing the thermal capacity. However, for the present design, the use of SPRTs as temperature sensors precludes the use of thin hot and cold plates. Some of the advantages and disadvantages of potential plate and guard construction materials are summarized below:

Silver – Silver has the highest thermal conductivity and the lowest volumetric heat capacity of any metal. Its cost would not be excessive when compared with the overall costs of designing, fabricating, and verifying the performance of this new GHP. The strength of silver is rather low but would appear to be adequate. A major problem with silver, for the higher temperatures of interest in this project, is that it forms a volatile oxide so that any high-emittance coating would not continue to adhere to the plates. In principle, silver could be protected from oxidation by applying a heavy electroplated coating of, e.g., gold or nickel.

Copper – Copper has a thermal conductivity similar to that of silver, but has a significantly higher volumetric heat capacity and, in addition, would have to be heavily coated, e.g., by nickel, silver, or gold plating, to provide protection against oxidation. Consultations with NIST metallurgists did not achieve consensus as to whether or not copper could be adequately protected against oxidation for long periods at elevated temperatures, or consensus as to the best means of providing oxidation protection.

Gold – Gold has a thermal conductivity somewhat lower than that of silver and copper and a volumetric heat capacity essentially identical to that of silver and copper. Gold is impervious to oxidation. It apparently is very difficult to get high-emittance coatings to adhere to gold. In any case, gold is too expensive to be used for this project.

Aluminum – Aluminum has a thermal conductivity about half that of silver and copper, and could be used only to about 700 K (the melting point of aluminum is 933 K).

Nickel – Nickel has a thermal conductivity much lower than those of the other pure metals discussed above, but it could be used in air over the temperature range of interest.

Metallic Oxides – Below about 800 K, the thermal conductivity of beryllium oxide is higher than that of nickel, and below about 200 K its thermal conductivity is as high or higher than that of silver and copper. However, at higher temperatures, the thermal conductivity of beryllium oxide is quite low compared to the pure metals. Aluminum oxide is even worse. In addition, metallic oxides would require quite different fabrication techniques from those described below for use with metals.

Means of Fabrication

As discussed below and in the companion paper [*16*], it is important to have the heaters located accurately in the hot and cold plates in order to obtain optimally isothermal conditions. After reviewing alternative methods of fabrication that would ensure accurate positioning, it was decided to make the hot plate from two halves brazed together, with swaged heater elements brazed into grooves machined in one half. This type of construction should provide excellent conductive heat transfer while avoiding outgassing problems. The cold plate heaters will be brazed into grooves in a "heater plate," as described further below. Alternative means of fabrication that would result in a swaged heater being embedded in a plate include casting, electroforming, electrical deposition, or hot isostatic pressing.

Selected Material

The final candidates for the material from which to fabricate the hot and cold plates and the edge guards were (1) nickel and (2) nickel-plated copper. If the SPRTs were not being used, the plates could have been made thinner and the higher thermal conductivity of copper would have helped ensure that the plates were adequately isothermal. However, the use of SPRTs mandated the use of thick plates that, with appropriate heater design, will have sufficient lateral thermal conductance to be adequately isothermal even when fabricated from nickel, with its much lower thermal conductivity. The use of nickel avoids the need of providing a thick electroplated coating over copper, with the attendant risks of flaws that could allow potentially serious oxidation of the copper. The plates and the edge guard are thus being fabricated from Alloy 201, a commercially pure nickel with a low carbon content

and good oxidation resistance. The commercial swaged heating elements have an Alloy 600 sheath. The brazing alloy is a nickel-phosphorous eutectic alloy that is known to work extremely well with nickel and to adhere well to Alloy 600.

Hot Plate Design

The geometrical layout of the guarded hotplate is shown in Figure 3. A major difference from the designs of other guarded hot plates is that the thermometer well, heater leads, and thermocouple and thermopile leads are thermally grounded to a "connection guard block" that is provided with a heater and a coolant coil so that it can be maintained at the same temperature as the meter and guard plates. This connection guard block is particularly important in order to avoid perturbing the temperature distribution in the guard plate due to heat conduction along the thermometer well and the swaged leads, which are more conductive than is the case for most previous designs.

Figure 4 shows the type of heater layout that might be used in the meter plate for a guarded hot plate that uses thermocouples as temperature sensors. The switchback bends in this layout are located such that the total length of heater is the same as it would be for five circular heaters, located at the recommended radii from C 1043. Thus there might be local hot and cold spots, relative to the temperature distribution that would be obtained with circular heaters, but the overall temperature uniformity of the meter plate would be similar to what it would be for circular heaters [*16*]. This heater layout is not suitable for use with a long-stem platinum resistance thermometer, however, since the sensitive portion of the SPRT would be located too close to the heater. For the new NIST guarded hot plate apparatus, the heater layout will be as shown in Figure 5. A bifilar swaged heater will be brazed into grooves in one half of the meter plate, as shown at the bottom of Figure 5, and

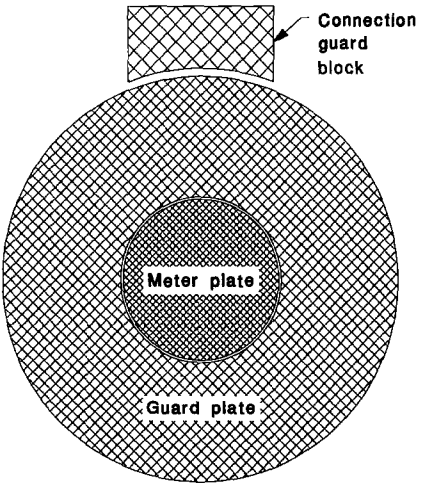

Figure 3 – *Overall layout of hot plate*

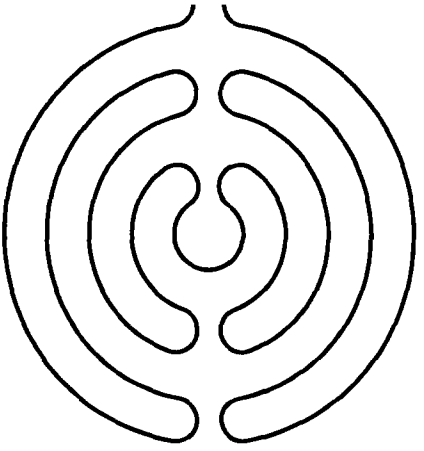

Figure 4 – *Meter plate heater layout for use with thermocouples*

the two halves of the plate will be brazed together. This heater layout provides an open "corridor" for the SPRT, the sensitive portion of which is shown as a darker gray than the insensitive portion [*16*]. A thermometer well will be brazed into the meter and guard plates, with a vacuum-tight O-ring seal at the top. The thermometer well will be provided with a side connection so that it can be filled with helium to provide better thermal coupling to the SPRT.

The layout of the guard plate heater, which is also a bifilar, swaged heater, is shown in Figure 6. The straight section of heater running from the inside of the guard plate to outside the top of the guard plate, just to the right of the centerline, contains the leads to the meter plate heater. The guard heater layout has been designed to allow for the heat generated in the leads to the meter plate heater. There also will be an edge heater, not shown in Figure 6, to compensate for heat loss to the edge guards.

Figure 5 – *Meter plate heater layout for use with SPRTs.*

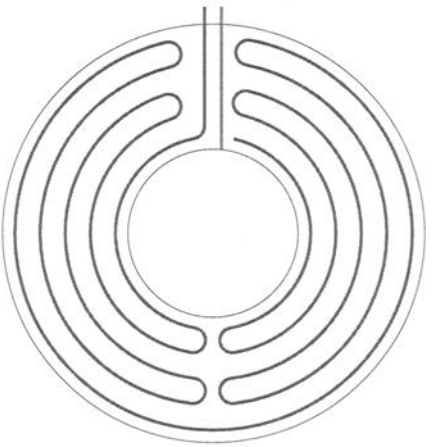

Figure 6 – *Guard plate heater layout*

Cold Plate Design

Each cold plate assembly will be laminated, with a surface plate that accommodates the SPRT, a thin layer of insulation, a heater plate with a swaged heater element similar to that shown in Figure 4, but with more turns, another thin layer of insulation, a coolant plate, with a bifilar channel to accommodate liquid nitrogen or ethanol as a coolant, a thick layer of insulation, and a water jacket to provide a constant temperature environment and to protect personnel from contact with hot or cold surfaces [*16*]. Each cold plate assembly will be provided with a connection guard block, similar to that discussed above for the hot plate. Each cold plate assembly will be an integral unit, so that when installing test specimens, it

will not be necessary to deal separately with the various components or to use loose-fill insulation. As shown in Figure 2, there is an extra annulus of insulation behind the outer edge of each cold plate assembly, in order to provide insulation of the inside surface of the edge guard when thinner specimens are tested.

Thermometry

As stated above, based on discussions with the NIST Thermometry Group, the primary measurements of the hot plate and cold plate temperatures will be made using three long-stem platinum resistance thermometers that have been calibrated by NIST. The bridge used to measure the thermometer resistances is of the same type used for calibrating SPRTs in many national standards laboratories and will provide a resolution of 1 mK.

The hot plate and the two cold plates will also be provided with swaged, Type N thermocouples to provide information as to how accurately plate temperatures could be measured if the SPRTs were not used. This information should be useful to laboratories that might wish to copy aspects of the present design for a guarded hot plate apparatus but that do not wish to incur the expense of SPRTs and a bridge. The edge guards will be provided with the same type of thermocouples. Type T thermocouples will be used to monitor water jacket and support structure temperatures. The leads from all thermocouples will be brought to an isothermal junction box where they will be connected to leads, from the same lot of thermocouple wire, that pass through vacuum seals to an isothermal zone box, whose temperature will be measured using a calibrated capsule platinum resistance thermometer. Thus if it is necessary to replace a thermocouple in the apparatus, it is not necessary to make a new vacuum seal. All thermocouple voltages will be read using a low-thermal-emf switch system and a high-accuracy digital voltmeter.

For the guard gap thermopile, it important to have a high sensitivity but it is not necessary that the sensitivity be accurately known, since the thermopile operates as a null control sensor. Type E (nickel-10% chromium versus nickel-45 % copper) thermocouples have the highest sensitivity of the common letter-designated thermocouples. However, the nickel-45 % copper alloy oxidizes too easily for fine wire sizes to be used at the highest temperatures of interest for this project. For the new NIST guarded hot plate apparatus, the thermopiles will use Type KP (nickel-10 % chromium) wire for the positive leg and a gold-35 % palladium alloy for the negative leg. Such a combination has a sensitivity similar to that of Type E thermocouples but can withstand much higher temperatures. The leads from the guard plate to room temperature will be constructed of a pure element (platinum, gold, or palladium) to minimize spurious thermal emfs that might otherwise arise if an alloy were used for the leads. The two thermopiles across the guard gap will also be of swaged construction and will be brazed into grooves cut in the surfaces of the hot plate.

Edge Guards

For the new NIST GHP, relatively tight-fitting edge guards will be used, with 10 mm of edge insulation between the outer edge of the hot and cold plates and the inner surface of the edge guards[*16*]. As indicated in Figure 2, there will be two doughnut-shaped edge guards, one surrounding each specimen. Each edge guard will have a "bite" taken out of it

at the top where the connection guard blocks are located (see Figure 3). Each edge guard will consist of an inner nickel ring with a swaged heater brazed into it, a thin layer of insulation, a second nickel ring provided with cooling coils, a thick layer of insulation, and an outer water jacket to keep the exposed surface of the edge guard at room temperature. The nickel rings will be wider than the thickest specimens for which the apparatus is designed.

Secondary Systems

Suspension System

The vacuum base plate will be vertically oriented, with three pairs of horizontal rails cantilevered from it to support the key components of the guarded hot plate apparatus. The hot plate is suspended from pillow blocks with bearings that ride on the innermost pair of rails. The two cold plate assemblies are similarly suspended from the second pair of rails and the two edge guard assemblies hang from the outer pair of rails.

Force Application

The cold plate assembly that is furthest from the vertical baseplate will be fixed in place by a stanchion that can be moved along a slide to accommodate specimens of different thickness and then locked down. A system of weights and a lever arm will be used to apply a known force to the back of the other cold plate assembly. Conceptually, the force-application system will be similar to a mechanical beam balance, with lever arms to amplify the force and apply it to the back of the moveable cold plate assembly.

Thickness Measurement

Specimen thickness will be measured using displacement sensors at room temperature, with the positions of the cold plates being brought out to room temperature using fused quartz rods in a manner analogous to single pushrod dilatometry. Two displacement transducers will be used, each being mounted on a stanchion provided with kinematic mounts such that the stanchion can be removed and replaced in the same location within about 1 μm. The bases to which the stanchions are attached ride on an invar U-frame that is not subjected to external forces. In use, the movable stanchion base will be clamped down to the invar frame at a position appropriate for the specimen thickness to be tested. Gage blocks of length similar to that of the specimens to be tested would be inserted between the hot plate and each of the cold plates, providing a calibration of the combined tare for the two displacement transducers. The stanchions will be removed while the specimens are installed and then replaced at the same position, thus allowing determination of any changes in combined specimen thickness as a function of test temperature.

Environmental Control System

The NIST 500 mm guarded hot plate apparatus ultimately will be enclosed in a chamber consisting of a vertical metal baseplate, to which the apparatus is attached, and a cylindrical

metal bell jar that lies on its side, in a movable cart, so that the flange holding the captive O-ring is in a vertical plane. The requirements for this atmospheric control system include:

- Capability to pump the system down to 0.01 Pa, starting with any of a range of gases in the chamber
- Capability to pump down very slowly with the mechanical vacuum pump so that powdered or fibrous specimens will not be sucked out of the chamber
- Fully automated pump-down of the chamber
- Capability to clamp the bell jar to the baseplate so that the system can be pressurized up to 0.105 MPa absolute, regardless of the ambient barometric pressure
- Capability to backfill the chamber with various gases, and to control the chamber pressure at any desired pressure from 0.01 Pa to 0.105 MPa while the temperatures inside the guarded hot plate apparatus vary.

Summary

The new NIST 500 mm GHP that is described in this paper provides new design concepts for a guarded hot plate apparatus that complies with the requirements of C 177 and ISO 8302, while offering several design advantages, relative to prior designs, that will result in very good measurement accuracy over a broad temperature range and under controlled gas pressure. These design concepts include:

- A solid nickel guarded hot plate with embedded meter plate and guard plate heaters designed so that the temperature distribution in the plates can be calculated and the average temperature in the meter plate can be accurately determined.
- A laminated cold plate construction with the heaters and coolant lines in different nickel plates (from the surface plate) so as to minimize temperature variations across the cold plates.
- Rugged swaged heaters and thermocouples in all components of the apparatus, and a swaged thermopile across the guard gap.
- The use of long-stem platinum resistance thermometers as the primary temperature sensors in the hot plate and the two cold plates, thus providing greatly improved accuracy in temperature measurement, relative to what could be attained with thermocouples.
- The use of integrated edge guards that have been designed to minimize errors due to edge heat loss or gain.
- The use of connection guard blocks to minimize the effects of parasitic heat flows along thermometer wells and heater and sensor leads.
- Provision to provide a controlled, accurately known force to the cold plates.
- Provision to make accurate *in situ* measurements of specimen thickness, while using kinematic mounts to allow removal of the displacement sensors during specimen installation.
- Enclosure of the GHP inside a vacuum enclosure so that the apparatus can be operated in a vacuum, or operated at any desired controlled pressure with whatever filler gas is desired.
- An overall design that allows accurate measurements from 90 K to 900 K, without any need to open up the apparatus or to change components.

References

[1] Hust, J. G., and Smith, D. R., "Round-robin Measurements of the Apparent Thermal Conductivity of Two Refractory Insulation Materials, Using High-Temperature Guarded-Hot-Plate Apparatus," Report No. NBSIR 88-3087, National Bureau of Standards, Boulder, CO, April 1988, 27 pp.

[2] Salmon, D. R., and Tye, R. P., "A High Temperature Guarded Hot Plate Intercomparison," to be published in *Thermal Conductivity 26 / Thermal Expansion 14*, R. Mannello, Ed., Technomic Publishing Co, Lancaster, PA, 2002.

[3] Robinson, H. E., "Line Heat Source Hot Plates for Measuring the Thermal Conductivity of Insulations," unpublished paper presented at the Thermal Conductivity Conference held at the National Physical Laboratory, United Kingdom, in July 1964.

[4] Tye, R. P., "Thermal Conductivity," *Nature*, vol. 204, 1964, pp. 636-637.

[5] Flynn, D. R., Robinson, H. E., and Watson, T. W., "Progress Report: National Bureau of Standards," in *Proceedings 4th Conference On Thermal Conductivity* (Limited distribution), U.S. Naval Radiological Defense Laboratory, San Francisco, CA, October 1964, pp. VIII-NBS-1 to VIII-NBS-14.

[6] Hahn, M. H., "The Line Source Guarded Hot Plate for Measuring the Thermal Conductivity of Building and Insulating Materials," Ph.D. Dissertation, Catholic University of America, Washington, DC, 1971.

[7] Hahn, M. H., Robinson, H. E., and Flynn, D. R., "Robinson Line-Heat-Source Guarded Hot Plate Apparatus," in *Heat Transmission Measurements in Thermal Insulation, ASTM STP 544*, R. P. Tye, Ed., American Society for Testing and Materials, Philadelphia, 1974, pp. 167-192.

[8] Powell, F. J. and Siu, M. C. I., "Development of the Robinson Line-Heat-Source Guarded-Hot-Plate Apparatus for Measurement of Thermal Conductivity," in *Proc. XIV International Congress of Refrigeration*, Vol. 2, International Institute of Refrigeration, Paris, France, 1975, pp. 536-542.

[9] Siu, M. C. I. and Bulik, C., "National Bureau of Standards Line-Heat-Source Guarded-Hot-Plate Apparatus," *Rev. Sci. Instrum.* Vol. 52, 1981, pp.1709-1716.

[10] Siu, M. C. I., "Comparison of Results of Measurements Made on a Line-Heat-Source and a Distributed-Heat-Source Guarded-Hot-Plate Apparatus," in *Thermal Conductivity 17*, J. G. Hust, Ed., Plenum Press, New York, 1983, pp. 413-426.

[11] Powell, F. J. and Rennex, B. G., "The NBS Line-Heat-Source Guarded Hot Plate for Thick Materials," *Proceedings ASHRAE/DOE Conference On Thermal Performance of Exterior Envelopes of Buildings II, ASHRAE SP 38*, American Society of Heating, Refrigerating and Air-Conditioning Engineers, Atlanta, GA, 1983, pp. 657-672.

[12] Rennex, B. G., "Error Analysis for the NBS 1016 mm Guarded Hot Plate," *J. Thermal Insulation*, Vol. 7, 1983, pp. 18-51.

[13] Rennex, B., "Summary of Error Analysis for the National Bureau of Standards 1016-mm Guarded Hot Plate and Considerations Regarding Systematic Error for the Heat Flow Meter Apparatus," in *Guarded Hot Plate and Heat Flow Meter Methodology, ASTM STP 879*, C. J. Shirtliffe and R. P. Tye, Eds., American Society for Testing and Materials, Philadelphia, 1985, pp. 69-85.

[14] Rennex, B. G., "An Assessment of the NBS 1-m Guarded-Hot-Plate Limits," Rept. No. NBSIR 85-3221, National Bureau of Standards, Gaithersburg, MD, August 1985, 97 pp.

[15] Zarr, R. R. and Hahn, M. H., "Line-Heat-Source Guarded-Hot-Plate Apparatus," Adjunct to ASTM C 1043-97, December 1995. (Available from American Society for Testing and Materials, 100 Barr Harbor Drive, West Conshohocken, PA 19438-2959. Request PCN No. 12-310430-61.)

[16] Healy, W. M. and Flynn, D. R., "Thermal Modeling of a New Guarded Hot Plate Apparatus," *Insulation Materials: Testing and Applications:4th Volume, ASTM STP 1426*, A. O. Desjarlais and R. R. Zarr, Eds., ASTM International, West Conshohocken, PA, 2002.

[17] Ripple, D. Burns, G., W,. and Scroger, M. G., "Assessment of Uncertainties of Thermocouple Calibrations at NIST," Report No. NISTIR 5340, National Institute of Standards and Technology, Gaithersburg, MD, January 1994, 34 pp.

[18] Mangum, B. W., Furukawa, G. T. K., Kreider, G., Meyer, C. W., Ripple, D. C., Strouse, G. F., Tew, W. L., Moldover, M. R., Johnson, B. Carol, Yoon, H. W., Gibson, C. E., and Saunders, R. D., "The Kelvin and Temperature Measurements," *J. Res. Natl. Inst. Stand. Technol.*, Vol. 106, 2001, pp. 105-149.

[19] Burns, G. W., Strouse, G. F., Liu, B. M., and Mangum, B. W., "Gold versus Platinum Thermocouples: Performance Data and an ITS-90 Based Reference Function," in *Temperature: Its Measurement and Control in Science and Industry*, Vol. 6, J. F. Schooley, Ed., American Institute of Physics, New York, NY, 1992, pp. 531-536.

[20] Burns, G. W. and Ripple, D. C., "Techniques for Fabricating and Annealing Pt/Pd Thermocouples for Accurate Measurements in the Range 0 °C to 1300 °C," in *Proceedings of TEMPMEKO '96, 6th International Symposium on Temperature and Thermal Measurements in Industry and Science*, P. Marcarino, Ed., Levrotto & Bella, Turin, Italy, 1997, pp. 171-176.

[21] Burns, G. W., Ripple, D. C., and Battuello, M., "Platinum versus Palladium Thermocouples: An Emf-Temperature Reference Function for the Range 0 °C to 1500 °C," *Metrologia*, Vol. 35, 1998, pp. 761-780.

Mark A. Albers [1]

A Round Robin Interlaboratory Comparison of Thermal Conductivity Testing Using the Guarded Hot Plate up to 1000°C

Reference: Albers, M. A., "**A Round Robin Interlaboratory Comparison of Thermal Conductivity Testing Using the Guarded Hot Plate up to 1000°C** ," *Insulation Materials: Testing and Applications: 4th Volume, ASTM STP 1426,* A. O. Desjarlais and R. R. Zarr, Eds., ASTM International, West Conshohocken, PA, 2002.

Abstract: A round robin interlaboratory comparison of thermal conductivity measurements was performed using the Guarded Hot Plate apparatus at temperatures from about 0°C to 1000 °C. There were twelve participating laboratories including four national laboratories in three different countries. A statistical analysis was performed and the variation in measurement results is discussed. Both within laboratory and between laboratory variability is analyzed. A definite conclusion of this comparison is that measurement variation increases progressively with increasing temperature. As a result there is a need for the U.S. national laboratory, the National Institute of Standards & Technology, to develop high temperature testing capability and then high temperature thermal conductivity reference standards.

Keywords: Interlaboratory comparison, round robin, thermal conductivity, thermal measurements, Guarded Hot Plate, C 177, ISO-8302, high temperature, C 1114

Introduction

It has long been discussed and realized that thermal conductivity (k) measurements by Guarded Hot Plate (GHP) apparatuses at higher temperatures (>100°C) can lead to greater errors and larger deviations in test results between laboratories. All these GHP apparatuses meet the ASTM Test Method for Steady-State Heat Flux Measurements and Thermal Transmission Properties by Means of the Guarded Hot Plate Apparatus (C177). A previous investigation into the magnitude of these differences occurred in the 1980s with a final report by Hust and Smith [*1*] (at NIST) in April 1988. That interlaboratory comparison between high temperature GHPs was a "quick look" in that it used different specimens for each participant. The authors then used a series of tests to create models in order to remove as much of the material variability as possible. There still remained relatively large deviations between laboratories. This prompted a desire in the early 1990s to perform a "true" round robin, in that the *same* specimen set would be circulated to the participating laboratories. Therefore an international interlaboratory comparison round robin was started in 1993 with twelve laboratories participating. Most of the National Laboratory apparatus were not true high temperature GHP but their inclusion was for a reference at the lower temperatures. In addition, an apparatus that meets

[1] Research Scientist, Research and Development Division, Johns Manville Technical Center, 10100 W. Ute Ave., Littleton, CO 80127.

ASTM Test Method for Steady-State Thermal Transmission Properties by Means of the Thin-Heater Apparatus (C 1114) was also included for the same reason. Of the national laboratories, only the National Physical Laboratory participated at the higher temperatures.

Twelve Participants

The twelve participants, four National Laboratories and eight private laboratories are listed below intentionally in no particular order:
NIST – National Institute of Standards & Technology
ORNL – Oak Ridge National Laboratory (used C 1114 apparatus)
NRCC – National Research Council of Canada
NPL – National Physical Laboratory (United Kingdom)

JM – Johns Manville International Inc.
OC – Owens Corning Fiberglas
Knauf Fiber Glass GmbH
CSG – Certainteed San Gobain
Holometrix
CTL – Construction Technology Laboratories
Unifrax (Carborundum)
Fiberglas Canada (Owens Corning)

Types of ASTM C 177 Guarded Hot Plates Participating

Below are brief descriptions of the participating GHP in order of testing:
100 cm circle
185 cm unguarded Thin-Heater "screen" apparatus (C 1114)
61 cm square
60 cm square brass and aluminum with black paint
46 cm square
30 cm by 36 cm stainless steel, (ISO-8302) ,1 sided design and construction
30 cm square dull steel
30 cm circle alumina with no coating
30 cm circle Inconel coated with Pyromark 2500, (ISO-8302)
20 cm circle ceramic with Inconel face plates
20 cm circle ceramic with Inconel face plates
20 cm circle with black paint
20 cm circle ceramic with Inconel face plates

The test material chosen for this comparison was very similar to one of the two materials used in the previous 1988 investigation. The material was a refractory ceramic fiber alumina-silica board of about 300 kg/m^3 density. All the material was heat-treated to over 1000°C before testing began. The order of testing was chosen so the specimens could be successively cut down to fit the smaller plates. Specimens were cut from the centers of previous test specimens as needed to properly fit the next apparatus. Test

results were sent to a single laboratory upon test completion where alphabetical letters were assigned to represent each laboratory. There were no communications between laboratories as to their results, and the various participants were not informed of the other laboratories assigned letters.

The laboratories participating in the comparison were asked to test at 5 mean temperatures spanning the full range of operation of their GHP. One of the five test points had to be at 325°C with a 50°C temperature difference. This rule obviously did not apply to the lower temperature plates that couldn't reach 325°C. In the list above, the smaller plates were the higher temperature units and tested in the latter part of the round robin when the specimens were cut down in size.

Results and Discussion

Test laboratories will be referred to by letters A through M for all of this discussion.

Variations in Operation

All of the participating laboratories followed the ASTM C 177 testing procedures, however there are some variations in their operational methods worth mentioning here.

Almost all laboratories mounted their temperature measurement thermocouples (TC) in the surface of the apparatus plates. The exception was laboratory E which mounted the hot surface TC in the plate but the auxiliary or "cold" surface TC on the test specimens.

Only two laboratories do any correction for apparatus dimensional changes with temperature or thermal expansion. Laboratory A corrects for both metering area and specimen thickness changes although it is only for a lower temperature apparatus. Only one truly high temperature apparatus, laboratory G, corrects for the change in meter area with temperature. A correction for thickness is not made by laboratory G.

Due to power limitations laboratory F was only able to achieve less than half their usual temperature difference across the specimens on the highest temperature test point. This point ended up being considered an outlier with a thermal conductivity (k) which was too high.

There was some variation in the use of the imbalance detectors, or gap thermopile (gap pile) used to measure the temperature difference between the metering area and the guard region. All but two of the laboratories mount the gap pile in the plates, on the gap, staggered on opposite sides. Laboratory H mounts their gap pile "within the heater" and 5 mm from the gap center on each side. The other variation is by laboratory I which does the same thing except the distance is about 6 mm from the gap center.

Two laboratories, G and J, actually run the ISO-8302 [*2*] version of the GHP. The construction of laboratory J's apparatus only allows testing each specimen of the specimen pair individually (single-sided); these two results were then averaged into a single test point. Laboratory G chose to test each specimen individually in a single-sided mode so these two values were also averaged into a single test point at each temperature for this analysis.

Plots of Data and Curves

The plot in Figure 1 shows all the data with a different letter (A-M) representing the test series for each laboratory. At first glance, there seems to be two obvious outliers, one point from laboratory F and one from laboratory L. These are the highest

temperatures tested for these two laboratories.

All of the laboratories with points that appear to be outliers were contacted to see if they found any errors in their data calculations. The laboratories all reported that they would have to stand with the points they turned in since they could find no errors in their methods. It will be shown later that these points are indeed statistical outliers. As already mentioned, Laboratory F indicated they had power limitations on that point and therefore had to settle for a reduced temperature difference (delta T) that was less than half their usual. Also of possible interest, the Laboratory L outlier was the only point where they switched to a 50% higher delta T than used on all their other points.

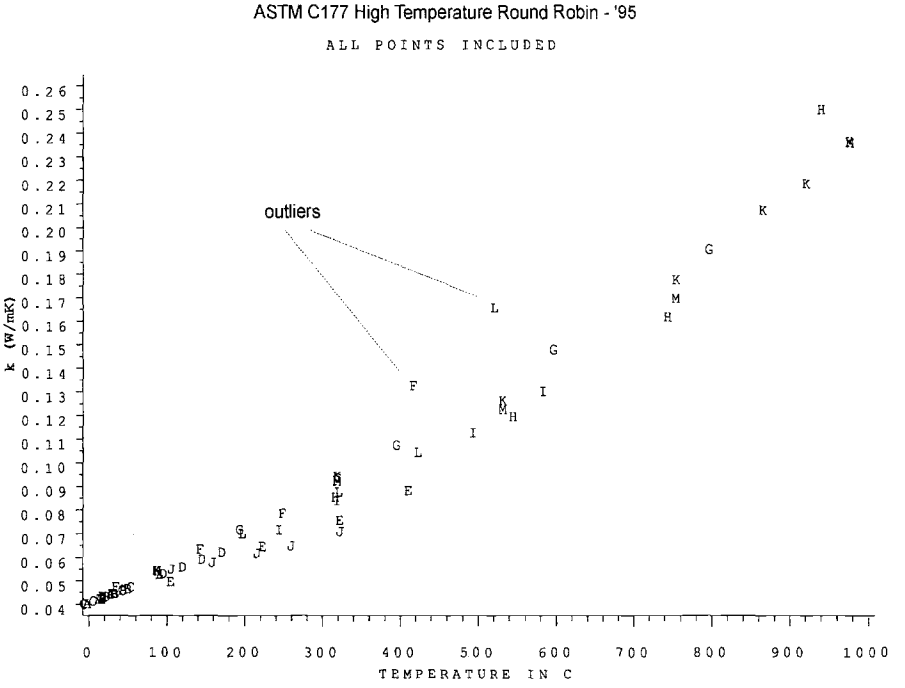

Figure 1

In this analysis laboratory M is the same as laboratory K. The K series was tested when the specimens were first cut to the 20 cm size, whereas the M series was tested last in the round robin. Therefore the laboratory M series is after most of the handling and shipping of the smallest "cut-down" specimens which were exposed to the highest temperatures. Since the points labeled K and M are nearly the same, we can assume that the integrity of the specimens remained intact for at least the highest temperature and most extreme testing of the last four laboratories. Since these last four laboratories represent the most extreme temperatures tested we can therefore also assume there were no changes at the lower less abusive temperatures of the earlier test laboratories. The ceramic fibers making up the test board are designed for considerably higher temperatures than those involved in this study so we would expect no degradation. The

calculated density by each laboratory varied on average less than 1% during all the testing, shipping, and cutting down of specimen size except for one exception. After the testing by laboratory G on the 30 cm specimens and the cutting down to 20 cm specimens and testing by laboratory K, there was a thickness decrease and associated density increase of about 8%. For the highest temperature points in Figure 1 this theoretically could have caused a downward shift of about the height of the identifying letters for laboratories K, M, and H. There was no correction applied to these points.

In order to look more closely at the data in a series of plots it has been separated into different temperature regions. In Figure 2 only the data under 100°C is shown. This plot shows the entire test series of three invited participants that are not high temperature versions of the guarded hot plate apparatus. Two of the series represent the "anchor points" of two national laboratory GHPs. The NIST 100 cm circular plate and the NRCC 60 cm square plate will serve as good references to past round robins of all the other instruments that are not considered "high temperature" GHP, since they represent the American and Canadian national standards generating GHPs. In addition the ORNL "Screen Heater" (ASTM C1114) apparatus shows how tightly this unguarded test method fits with the traditional guarded hot plates.

The plot in Figure 3 shows the data under 325°C, which is the common intermediate temperature that was chosen as the point that all high temperature GHP would test in their series. It is easily recognized that as the temperature increases, the spread in the test data increases.

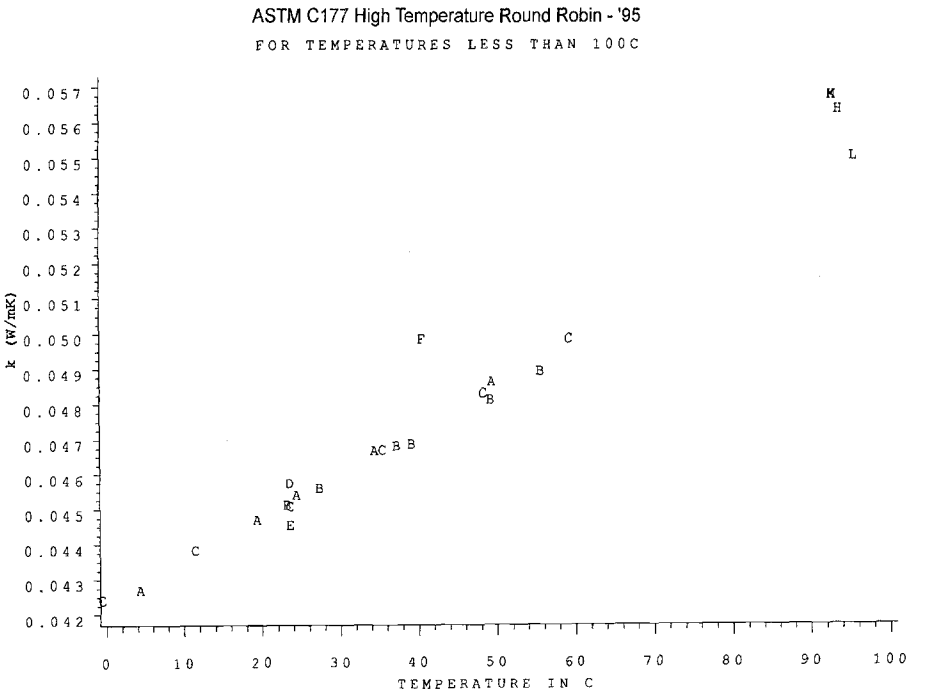

Figure 2

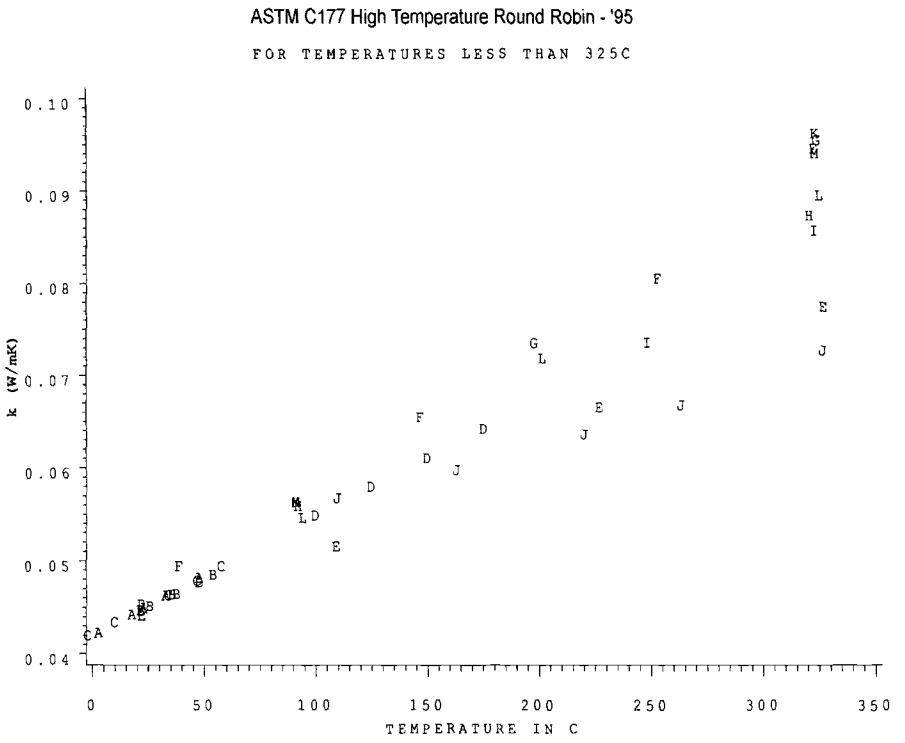

Figure 3

Using all the data, a preliminary regression model line was generated. Figure 4 shows all the data, with 95% upper and lower confidence limits on the individual predicted values. This is statistical terminology stating the error is for both the regression and the individual points. The dashed lines shown on the plot indicate a range or limits such that all current or future points should fall within those limits with a 95% confidence. Notice that the highest points from both series F and L fall outside the limits. This is a common statistical basis for designating outliers, therefore they are considered outliers and were eliminated from further analysis at this point. It is also obvious that the variability is not constant, but is increasing with k and temperature. Consequently, the estimate of the standard deviation (STD) will need to be a function of k and/or temperature.

The separate k vs T curves for each laboratory are shown in Figure 5. With these curves it is noticeable that the highest point of the H series causes a rapid increase in slope, and both J and E have much lower slopes than the rest.

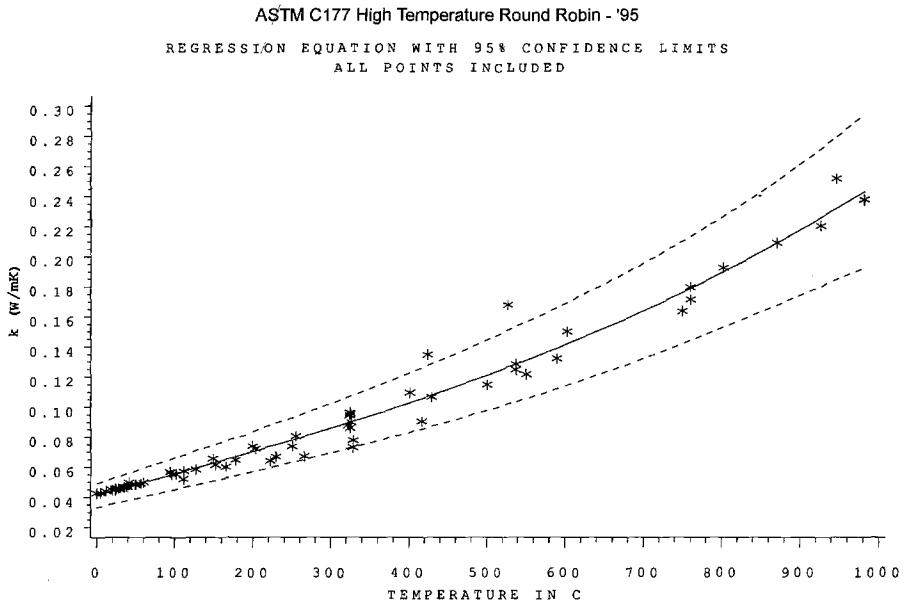

Figure 4

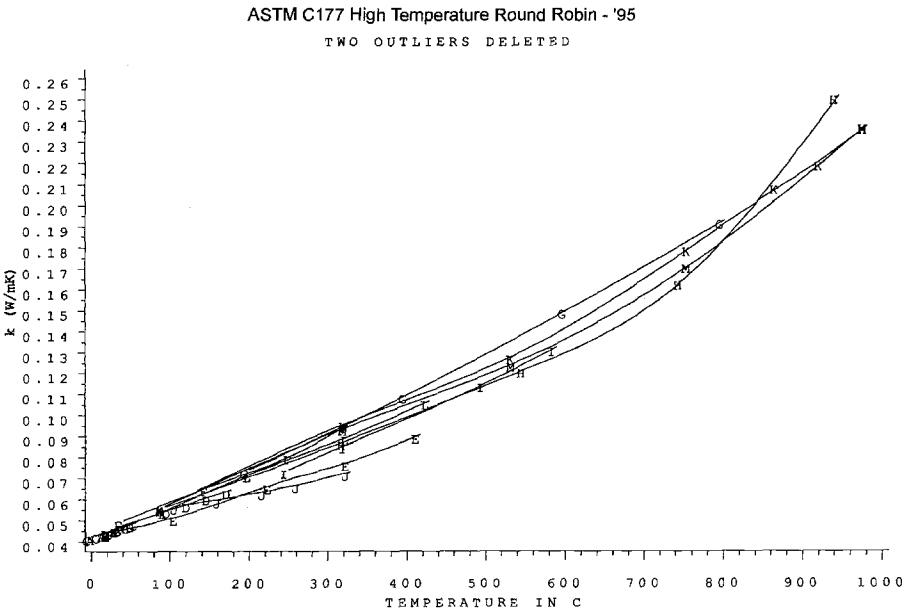

Figure 5

Between-Laboratory Variability

A linear regression of all the data (68 minus the two outliers = 66 points) gives the following results for expressing k (thermal conductivity in W/mK) as a function of temperature (°C):

$$\text{Predicted k} = 0.0421 + 0.000131(\text{Temp}) + 7.804\text{E-}11(\text{Temp}^3) \quad (1)$$

and,

$$s = \text{STD} = \text{standard deviation} = 5.83\% \text{ of predicted k (ie. 0.0583 times the predicted k)}$$
$$= 0.0583\,(0.0421 + 0.000131(\text{Temp}) + 7.804\text{E-}11(\text{Temp}^3)) \quad (2)$$

Results of the regression analysis are shown in Appendix A. The regression equation chosen involving T and T^3 is used extensively by various authors and within ASTM when the data is at high temperatures or has a significant amount of radiation heat transfer. At lower temperatures the T^2 term is usually sufficient, but when more radiation is involved the T^3 term fits better and the T^2 term can be dropped. This regression was also performed, as is usually done, using absolute temperature (°K). The results were indistinguishable so it was chosen to use (°C) for easier understanding. Of course as with any polynomial equation, extrapolation beyond the lowest or highest temperature data points is not suggested. Obviously the equation is useless below 0 °C. The information shown in Appendix A represents the typical computer generated output of a regression routine. Most of the information is annotated and easily understood, however some is beyond the scope of this discussion but was retained for the statistically inclined.

Appendix B contains all the reported thermal conductivity data from each participating laboratory and calculations for each data point of predicted thermal conductivity. The table also shows the error (actual k-predicted k), and the 95% upper and lower limits from the regression equation. This data indicates there are two points from laboratory J that are outside the 95% confidence limits.

The 95% confidence limits on individual points from a regression equation are:

$$predicted\,k \;\pm\; (t_{0.025})\,STD\left[1+\frac{1}{n}+\frac{(T-\bar{T})^2}{\sum_i^n (T_i-\bar{T})^2}\right]^{\frac{1}{2}}, \quad n=66 \quad (3)$$

In this case the student *t* value ($t_{0.025}$) for 95% confidence limits and 63 DF (degrees of freedom) is $t = 1.998$. This is a somewhat complicated statistical equation, but the difference between the upper and lower limits expressed as a percent of k is given in the summary table in Appendix C. It is on average 24.0% of the predicted k, which is very close to +/- 2s since this is a 95% confidence limit. This 24% is slightly more than 4s (4x5.83% = 23.3%) since it contains both error in the data points and error in the regression coefficients, as shown in the bracketed part of equation (3). That means that *the difference in predicted k between two laboratories for a given temperature will be less than 24% of k with 95% confidence.* This difference can also be expressed in terms of temperature, which is also given in the table.

The predicted equation (Eq. 1) with its 95% confidence limits is shown in both Figure 6 and Figure 7 along with the individual data points.

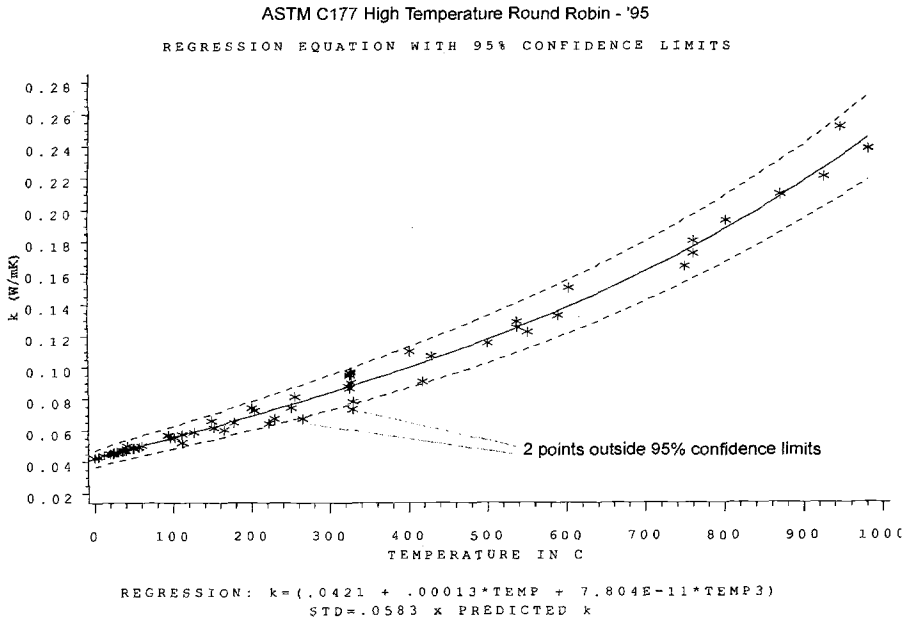

Figure 6

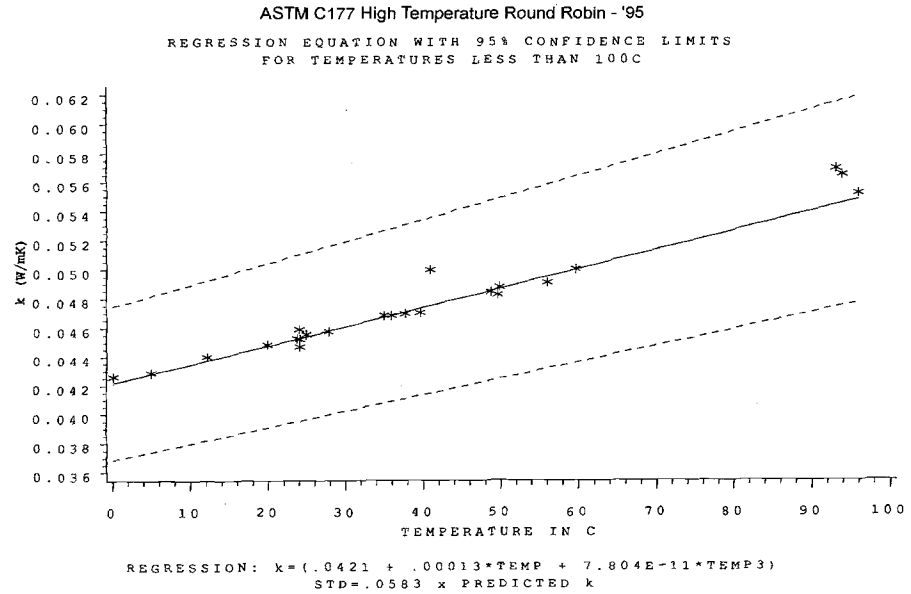

Figure 7

Remember that the difference between the upper and lower limits (dashed lines) is approximately 24% of k. Two points from series J fall just below the lower limit as indicated on the graph. These two points would however be within 90% confidence limits. Information that may be of interest is that laboratory J is the rectangular one of the two ISO-8302 plates.

The equation (Eq. 1) and test points for only the temperatures below 100°C are shown in Figure 7. The 95% confidence limits look extremely wide at these lower temperatures. The explanation is that these points are from national laboratories with specialized apparatus designed only for lower temperatures. Once we go above 100°C we introduce many more laboratories and the variability increases, as is apparent from Figure 8 which shows the next higher temperature region with all data up to 325°C.

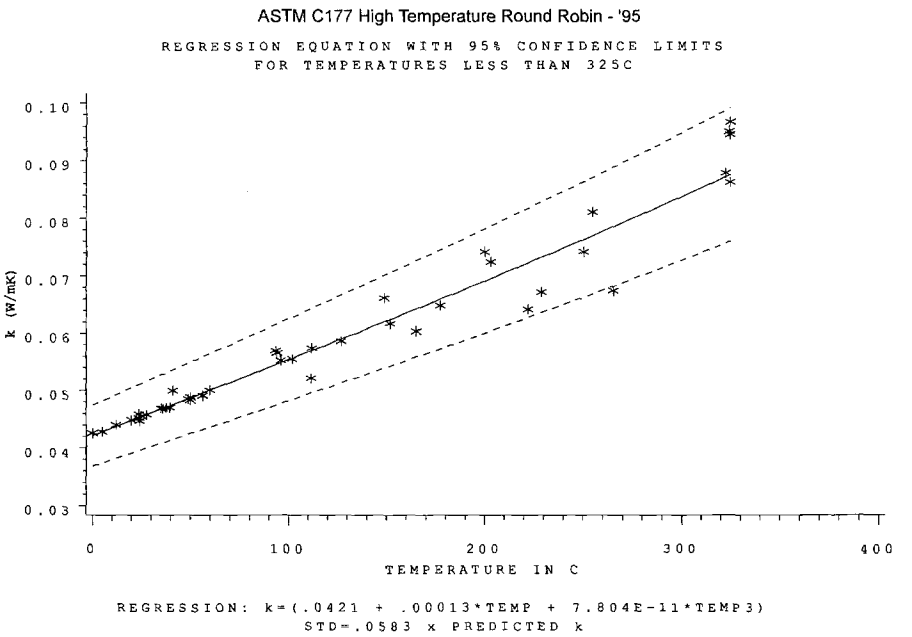

Figure 8

Within Laboratory Variation

The standard deviation within each laboratory is shown in the table below. After an analysis described here of removing outliers, it was determined that the standard deviation within a laboratory should be no larger than 2.5% of the average k. That means that if a laboratory does a regression of the form $k = a + bT + cT^3$ on a k vs T data series, and the (standard deviation)/(mean k) is greater than 0.025 (2.5%), then this is a flag that something is wrong with one or more of the test points. For example, using all their temperature points, laboratories F and L had standard deviations that were 4% and 10% of their mean k respectively. Removing each of their highest temperature points, which have been deemed outliers, dropped their standard deviations down to 1.75% and 1.26%

respectively. The other laboratory that had a standard deviation larger than 2.5% was H with a 5.6% error. The highest temperature point of the H series appears higher than would be expected in analyzing Figure 5. Once again, eliminating its highest temperature point, dropped its error down to 1.47%. There is reason to believe that, as a hot plate approaches its upper limit on temperature, the measured thermal conductivity may increase more than would be expected given the previous test points. This was the case with all three of these laboratories. Consequently, if a laboratory has a standard deviation greater than 2.5% of mean k, then it may have exceeded its reliable temperature range, especially if removing the highest temperature point drops the standard deviation to less than 2.5%.

As a side note, many of the low temperature laboratories (A,B,C,D) had standard deviations much less than 2.5% (around 0.02% to 0.17%). The following table is a summary of within laboratory variations:

WITHIN LABORATORY STANDARD DEVIATIONS

Lab	Standard Deviation as a % of the average k	Standard Deviation when the last temperature point is removed	Comments
A	0.05%		
B	0.15%		
C	0.17%		
D	0.02%		
E	1.7%		
F	3.9%	1.75%	highest point is an outlier
G	0.46%		
H	5.6%	1.47%	highest point is to high
I	0.56%		
J	0.17%		
K	1.6%		
L	10.1%	1.26%	highest point is an outlier
M	2.5%		same as Laboratory K
K&M	2.1%		K&M combined together

Conclusions

There are several things that can be learned from this high temperature round robin. Test specimen material degradation was most likely not an issue. A second test of the specimens at the end of the round robin by the same laboratory that tested near the middle of the circulation indicated that there seemed to be no material degradation during testing at the last group of laboratories. Given that these last laboratories involved the highest temperature testing of the series, it can be assumed there was probably also no degradation during testing at the earlier lower temperature laboratories. This material is very stable and fairly durable and would make a very good SRM (Standard Reference Material).

It appears that testing at the highest test temperatures an apparatus is capable of, could lead to results which are erroneously to high. This seems to occur when the

apparatus is operated beyond it's useful range. Laboratories F, L, and H, would seemed to have reached this limit on their highest points. A laboratory should be able to achieve a within laboratory variation of within a 2.5% standard deviation or they could be running into this problem. Laboratory J would seem to have a totally different problem in that its highest two points were outside the 95% confidence limits on the LOW side, while still having a very good within laboratory standard deviation.

The between-laboratory variability analysis indicated that the difference in predicted k between two laboratories for a given temperature is less than 24% of k with a 95% confidence. This seems higher than the 1988 round robin, which stated 15% (2s) for the very similar alumina-silica board. However, the 1988 comparison covered from 57°C to 428°C (330°K to 701°K), where as this comparison goes from 5°C to 982°C (278°K to 1255°K).

A definite conclusion of this study is that the test result variation increases considerably with increasing temperature. This points out a need for the U.S. national laboratory, the National Institute of Standards & Technology, to develop high temperature testing capability and then high temperature thermal conductivity reference standards. If SRMs were available for these higher temperatures, further recommended studies could involve investigations on where these errors are introduced in tests at high temperatures. There may be problems with the test standard, or a liberal interpretation of the standard, the apparatus, or the procedures used by each laboratory.

References

[1] Hust, J. G., and Smith, D. R., "Round-Robin Measurements of the Apparent Thermal Conductivity of Two Refractory Insulation Materials, Using High Temperature Guarded-Hot-Plate Apparatus," NBSIR 88-3087, 28pp., U. S. National Institute of Standards and Technology, April 1988.

[2] ISO-8302:1991, "Thermal insulation -- Determination of steady-state thermal resistance and related properties -- Guarded hot plate apparatus", TC 163/SC 1, ICS 27.220, (ISO-International Organization for Standardization).

APPENDIX A

REGRESSION ANALYSIS WITH TWO OUTLIERS REMOVED

Model: MODEL (with an intercept, temperature, and temperature cubed terms)
Dependent Variable: k

Analysis of Variance

Source	DF (deg. of freedom)	Sum of Squares	Mean Square	F Value	Prob>F
Model	2	0.19407	0.09704	3010.694	0.0001
Error	63	0.00203	0.00003		
C Total	65	0.19611			

Root MSE	0.00500	R-square	0.9896
Dependent Mean	0.08653	Adjusted R-square	0.9893
Coefficient of Variation (C.V.)	5.83439		

Parameter Estimates

Variable	DF	Parameter Estimate	Standard Error	T for HO: Parameter=0	Prob>|TI|
INTERCEPT	1	0.042108	0.00119841	35.137	0.0001
TEMP	1	0.000131	0.00000553	23.730	0.0001
$TEMP^3$	1	7.803849E-11	0.00000000	11.899	0.0001

MODEL: $k = 0.04211 + 0.000131*TEMP + 7.804E\text{-}11*TEMP^3$

APPENDIX B

SUMMARY OF REGRESSION

LAB	TEMP °C	k	PRED. k	ERROR	UPPER 95% LIMIT	LOWER 95% LIMIT	WITHIN LIMITS?
A	5.000	0.04286	.04276	.00010	.04815	.03737	Y
A	20.000	0.04485	.04473	.00012	.05040	.03907	Y
A	25.000	0.04556	.04539	.00017	.05115	.03963	Y
A	35.000	0.04684	.04671	.00013	.05266	.04076	Y
A	50.000	0.04879	.04868	.00011	.05491	.04246	Y
B	23.790	0.04528	.04523	.00005	.05097	.03949	Y
B	27.900	0.04575	.04577	.0000	.05159	.03996	Y
B	37.780	0.04697	.04707	.0001	.05307	.04107	Y
B	39.690	0.04702	.04732	.0003	.05336	.04129	Y
B	49.780	0.04827	.04865	.0004	.05488	.04243	Y
B	56.160	0.04909	.04950	.0004	.05584	.04315	Y
C	0.105	0.04257	.04212	.00045	.04742	.03682	Y
C	12.130	0.04400	.04370	.00030	.04922	.03818	Y
C	24.200	0.04524	.04529	.0000	.05103	.03954	Y

C	35.980	0.04685	.04684	.00001	.05280	.04087	Y
C	48.860	0.04846	.04853	.0001	.05474	.04233	Y
C	59.760	0.05001	.04997	.00004	.05638	.04356	Y
D	24.090	0.04590	.04527	.00063	.05102	.03953	Y
D	101.900	0.05546	.05557	.0001	.06277	.04837	Y
D	126.910	0.05856	.05893	.0004	.06660	.05126	Y
D	152.010	0.06164	.06234	.0007	.07049	.05420	Y
D	177.190	0.06477	.06581	.0010	.07443	.05718	Y
E	24.200	0.04470	.04529	.0006	.05103	.03954	Y
E	111.300	0.05210	.05683	.0047	.06420	.04946	Y
E	229.100	0.06710	.07313	.0060	.08276	.06350	Y
E	328.800	0.07800	.08806	.0101	.09966	.07645	Y
E	417.100	0.09070	.10254	.0118	.11593	.08915	Y
F	41.000	0.05000	.04750	.00250	.05356	.04144	Y
F	148.900	0.06600	.06192	.00408	.07000	.05383	Y
F	254.900	0.08100	.07687	.00413	.08700	.06674	Y
F	324.500	0.09500	.08738	.00762	.09890	.07587	Y
G	199.830	0.07408	.06897	.00511	.07803	.05991	Y
G	325.770	0.09590	.08758	.00831	.09913	.07604	Y
G	401.245	0.10981	.09984	.00997	.11290	.08677	Y
G	603.058	0.15014	.13841	.01173	.15551	.12131	Y
G	802.353	0.19282	.18777	.00505	.20884	.16670	Y
H	94.140	0.05650	.05453	.00197	.06159	.04748	Y
H	322.710	0.08780	.08710	.00070	.09859	.07562	Y
H	550.800	0.12200	.12747	.0055	.14355	.11140	Y
H	749.790	0.16400	.17346	.0095	.19342	.15349	Y
H	946.870	0.25200	.23269	.01931	.25775	.20763	Y
I	250.300	0.07410	.07620	.0021	.08624	.06615	Y
I	324.900	0.08620	.08745	.0012	.09897	.07592	Y
I	500.000	0.11510	.11752	.0024	.13258	.10245	Y
I	589.600	0.13260	.13552	.0029	.15236	.11868	Y
J	111.688	0.05732	.05688	.00043	.06426	.04950	Y
J	165.045	0.06027	.06413	.0039	.07252	.05574	Y
J	222.011	0.06417	.07211	.0079	.08160	.06262	Y
J	265.473	0.06730	.07843	.0111	.08877	.06808	N
J	328.473	0.07324	.08800	.0148	.09960	.07641	N
K	93.300	0.05690	.05442	.00248	.06146	.04739	Y
K	325.000	0.09660	.08746	.00914	.09899	.07593	Y
K	537.800	0.12870	.12486	.00384	.14068	.10904	Y
K	760.000	0.18000	.17616	.00384	.19633	.15598	Y
K	871.10	0.2095	.20807	.00143	.23079	.18536	Y
K	926.70	0.2207	.22590	.0052	.25026	.20153	Y
K	982.20	0.2383	.24502	.0067	.27148	.21857	Y
L	96.08	0.0552	.05479	.00041	.06188	.04771	Y
L	203.24	0.0724	.06945	.00295	.07858	.06032	Y
L	326.90	0.0900	.08776	.00224	.09932	.07619	Y
L	429.30	0.1069	.10465	.00225	.11829	.09102	Y
M	93.30	0.0569	.05442	.00248	.06146	.04739	Y
M	325.00	0.0945	.08746	.00704	.09899	.07593	Y
M	537.80	0.1250	.12486	.00014	.14068	.10904	Y
M	760.00	0.1720	.17616	.0042	.19633	.15598	Y
M	982.20	0.2380	.24502	.0070	.27148	.21857	Y

Removed outliers:

F	424.00	0.135
L	527.10	0.1681

APPENDIX C

SUMMARY TABLE

TEMP °C	PRED. k	ESTIMATED STANDARD DEVIATION	STD. DEV. AS % OF TEMP.	UPPER 95% LIMIT OF k	LOWER 95% LIMIT OF k	DIFF. IN LIMITS AS % OF k	DIFF. IN LIMITS AS % OF TEMP
25	.0454	.0026	.01059	.0508	.0400	23.7	.04307
50	.0487	.0028	.00568	.0544	.0429	23.7	.02303
75	.0520	.0030	.00404	.0581	.0459	23.6	.01636
100	.0553	.0032	.00322	.0618	.0488	23.6	.01303
125	.0587	.0034	.00274	.0656	.0518	23.5	.01104
150	.0621	.0036	.00241	.0694	.0548	23.5	.00973
175	.0655	.0038	.00218	.0732	.0578	23.5	.00880
200	.0690	.0040	.00201	.0771	.0609	23.5	.00811
225	.0725	.0042	.00188	.0811	.0640	23.5	.00758
250	.0762	.0044	.00178	.0851	.0672	23.5	.00717
275	.0798	.0047	.00169	.0893	.0704	23.6	.00685
300	.0836	.0049	.00162	.0935	.0737	23.6	.00658
325	.0875	.0051	.00157	.0978	.0771	23.7	.00637
350	.0914	.0053	.00152	.1022	.0806	23.7	.00619
375	.0955	.0056	.00148	.1068	.0841	23.7	.00604
400	.0996	.0058	.00145	.1115	.0878	23.8	.00592
425	.1039	.0061	.00143	.1163	.0915	23.8	.00582
450	.1083	.0063	.00140	.1212	.0954	23.9	.00574
475	.1128	.0066	.00138	.1263	.0994	23.9	.00567
500	.1175	.0069	.00137	.1316	.1035	23.9	.00562
525	.1223	.0071	.00136	.1370	.1077	23.9	.00558
550	.1273	.0074	.00135	.1426	.1121	23.9	.00554
575	.1324	.0077	.00134	.1483	.1166	24.0	.00552
600	.1377	.0080	.00134	.1542	.1212	24.0	.00550
625	.1432	.0084	.00134	.1604	.1261	24.0	.00549
650	.1489	.0087	.00134	.1667	.1311	24.0	.00549
675	.1547	.0090	.00134	.1733	.1362	23.9	.00549
700	.1608	.0094	.00134	.1800	.1415	23.9	.00550
725	.1670	.0097	.00134	.1870	.1470	23.9	.00552
750	.1735	.0101	.00135	.1943	.1527	24.0	.00554
775	.1802	.0105	.00136	.2018	.1586	24.0	.00558
800	.1871	.0109	.00136	.2096	.1646	24.0	.00562
825	.1943	.0113	.00137	.2177	.1708	24.1	.00568
850	.2016	.0118	.00138	.2261	.1772	24.2	.00575
875	.2093	.0122	.00139	.2348	.1838	24.4	.00583
900	.2172	.0127	.00141	.2439	.1904	24.6	.00594
925	.2253	.0131	.00142	.2534	.1973	24.9	.00607
950	.2338	.0136	.00143	.2633	.2042	25.3	.00622
975	.2425	.0141	.00145	.2736	.2113	25.7	.00639
1000	.2515	.0147	.00147	.2845	.2184	26.3	.00661

Clark Stacey[1]

NPL Vacuum Guarded Hot-Plate for Measuring Thermal Conductivity and Total Hemispherical Emittance of Insulation Materials

Reference: Stacey, C., **"NPL Vacuum Guarded Hot-Plate for Measuring Thermal Conductivity and Total Hemispherical Emittance of Insulation Materials,"** *Insulation Materials: Testing and Applications: 4th Volume, ASTM STP 1426,* A. O. Desjarlais and R. R. Zarr, Eds., ASTM International, West Conshohocken, PA, 2002.

Abstract: The National Physical Laboratory has developed a Vacuum Guarded Hot-Plate (VGHP) for measurement of both the total hemispherical emittance and thermal conductivity of insulating materials in a vacuum or gas atmosphere. This paper describes the principles of operation of the VGHP and practical issues associated with the design and construction. Also described are features that make it a versatile and convenient device for measuring the thermal properties of a wide range of construction products.

Measurement results are presented on fumed silica powder of the type used in evacuated insulation panels, measured in a specially designed and instrumented container. Also presented are results of total hemispherical emittance measurements on reference materials of known emittance and on a low-emittance reflective insulation product. The VGHP emittance measurements are compared with the results by a spectrophotometric method, which is often not suitable for measuring insulation materials.

Keywords: thermal conductivity, total hemispherical emittance, evacuated insulation, reflective insulation, guarded hot-plate

Introduction

The need for efficient energy use for both commercial and environmental reasons has led to an increasing number of alternative insulation products, such as evacuated insulation panels and reflective foil products. Accurate thermophysical property data are needed for these new products, to facilitate fair competition between material manufacturers when quoting thermal performance.

[1] Research Scientist, Thermal Metrology Team, National Physical Laboratory, Teddington, Middlesex, TW11 0LW, United Kingdom.

The most accurate and reliable apparatus for measuring thermal conductivity of insulation and poor thermal conductors is the guarded hot-plate. The National Physical Laboratory (NPL) has developed a Vacuum Guarded Hot-Plate (VGHP) that is an enhancement of this technique, intended to meet the growing requirement to characterize a wide range of insulation products in terms of total hemispherical emittance and thermal conductivity.

Details of the initial design and testing have been published in a previous paper [*1*]. However, it was found that the achieved vacuum of 10^{-2} mbar was insufficient to allow measurements on low emittance surfaces. Since that publication the vacuum capability has been improved to 9×10^{-5} mbar and the measurement of emittance has been validated using reference materials of known emittance. Many additional features have been added and the measurement of thermal conductivity has also been improved.

The measurement of thermal conductivity has been validated using the European reference material IRMM-440 [*2*] (resin-bonded glass fiber board, -10 °C to 50 °C) and with polymethylmethacrylate (Perspex), NPL Batch 7/81 (0 °C to 60 °C). The VGHP now conforms to the European standard ISO 8302:1991 "Thermal insulation – Determination of steady-state thermal resistance and related properties – Guarded hot plate apparatus".

Apparatus Design

The VGHP is a 305 mm square, single specimen, guarded hot-plate apparatus incorporating a linear temperature gradient edge-guard, all mounted in a vacuum chamber.

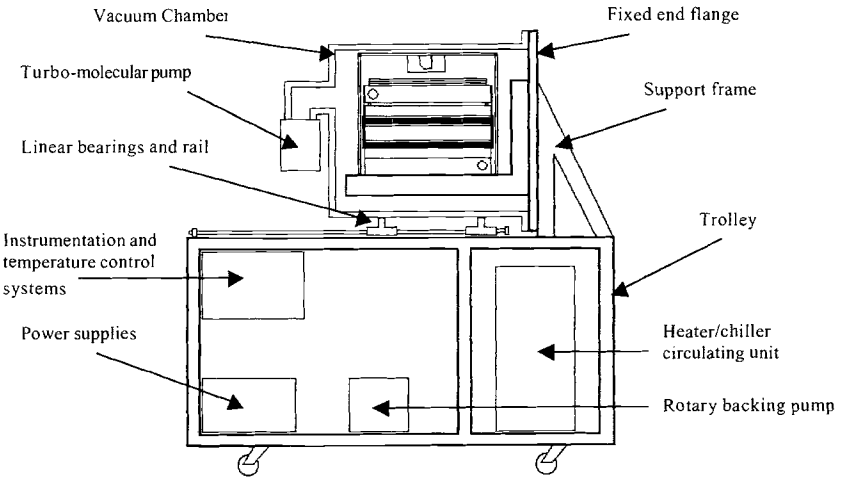

Figure 1 – *Vacuum Guarded Hot-Plate*

The VGHP can measure the thermal conductivity of a single 305 mm square specimen in air, other gases or at reduced pressure. Specimens are less than 65 mm thick having a conductivity of less than 2 W/(m· K) and thermal resistance greater than 0.025 (m²· K)/W. The apparatus can be operated with an evacuated gap between a specimen and the cold-plate of known emittance, thus allowing the total hemispherical emittance of a specimen surface to be measured.

The mean specimen temperature range of thermal conductivity measurement is -50 °C to 70 °C, typically with a 20 K temperature drop across the specimen. There is a reduced temperature range for measurement of emittance that is dependent on the type of specimen. The cold-plate temperature is controlled by a unit that is designed solely as a re-circulator, rather than a bath with an additional pump. This has the advantage that the silicone oil, which is used as the heat transfer medium, is not exposed to the air where it can adsorb moisture. It also offers a high flow-rate for increased stability and uniformity of the cold-plate temperature. The unit has a heat extraction capacity of 1 kW at -60 °C.

The vacuum system includes a rotary backing pump and a turbo-molecular pump. The achievable vacuum of 9×10^{-5} mbar is mainly limited by outgassing of the specimen and the materials in the heater stack. A separate valve is incorporated in the system to allow the chamber to be back-filled with gases other than air.

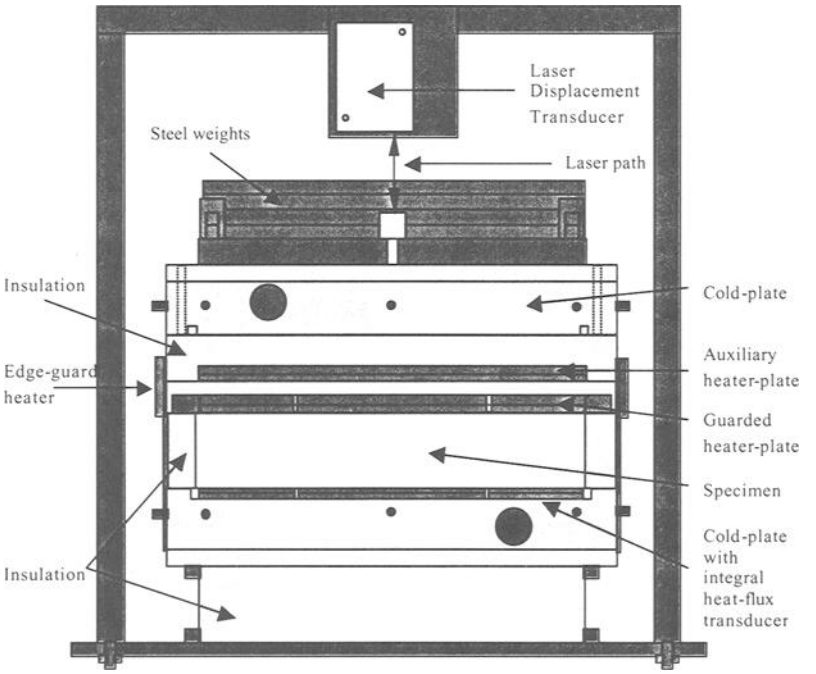

Figure 2 – *Guarded Hot-Plate Stack*

Single Specimen, Reversible Heat-Flux Configuration

The VGHP is a single-specimen design with an auxiliary heater plate behind the guarded heater plate, and maintained at the same temperature (normally within ± 0.01 °C when measuring insulations) as the guarded heater plate to prevent any net heat flow from its back surface. The auxiliary plate temperature is controlled by a differential thermocouple mounted on the adjacent surfaces of each plate. A layer of rigid closed cell foam insulation is placed between the plates to reduce the net heat flow for a given temperature difference, and thereby increase the effectiveness of the control.

The guarded plate, auxiliary plate and surrounding insulation can be removed from the apparatus as a single unit for reinsertion in the apparatus the other way up. This allows the specimen to be mounted either above or below the heater-plate and is useful in assessing the effect of convection within very low density specimens.

E-type thermocouples are mounted on the specimen surface to ensure accurate temperature measurement for specimens that have a thermal resistance less than 0.33 ($m^2 \cdot K$)/W, as recommended in ISO 8302:1991. Thermal contact sheets (foamed silicone rubber) are used to ensure even thermal contact with specimens by eliminating air gaps caused by either thermocouples or bowing of the specimen arising from differential expansion.

Guarded Heater-Plate

The design of the guarded heater plate is based on the recommendations of the European standards EN 12667 "Thermal performance of building materials and products – Determination of thermal resistance by means of guarded hot plate and heat flow meter methods – Products of high and medium thermal resistance" and ISO 8302:1991. The plate is 305 mm x 305 mm with a central metering area of 152.5 mm x 152.5 mm.

The heater-plate is constructed from two 5 mm thick plates of an aluminum alloy tooling plate chosen for its stability when subject to repeated temperature cycling.

Sandwiched between the aluminum plates is a custom-designed, printed circuit board (pcb) heater. The heater has two circuits of copper track on each side, which can be used to provide up to 90 W in the central region and 240 W in the outer guard region. The potential drop across the circuit in the central metering area, on each side of the pcb, is measured and used in the heat-flux calculation. The heater is electrically isolated from the aluminum plates by thin laminate sheets of cloth impregnated with resin (Tufnol) and the whole heater plate is held together with an adhesive suitable for the temperature range -60 °C to 120 °C.

The heater-plate has five E-type thermocouples mounted in grooves, in the central metering area, and their temperature values are used in the calculation of thermal conductivity. There are two thermocouples in the lateral guard area, and the thermocouples in the underside of the heater-plate are used to form a differential with those in the adjacent surface of the auxiliary plate.

Across the 2 mm wide guard-center gap is a 64-junction differential thermocouple, which has 32 junctions on each side of the plate. The junctions are positioned in a groove, at a depth of 2.5 mm below the plate surface. The legs of the junction remain parallel to the gap for 15 mm before crossing it. The plate surfaces were machined flat to

better than 0.05 mm and sprayed with a black paint having a total hemispherical emittance of 0.90.

Edge-Guard System

An edge-guard system is used because the sides of the specimen cannot be adequately insulated within the confines of the chamber and because the air cannot easily be controlled at the mean specimen temperature. The edge-guards can be attached to either of the cold-plates, depending on the specimen/heater orientation. They consist of four copper plates (1 mm thick) that are clamped to the edges of the cold-plate. At the other end of the copper plates is a strip-heater whose width matches the combined width of the main heater, the auxiliary heater and the insulation between them. This edge heater is controlled to match the temperature of the heater-plates to minimize heat losses from the main heater and auxiliary guard.

The section of the edge guard adjacent to the specimen will have a similar temperature gradient and will therefore minimize net heat flow from the edge of the specimen. Compressible insulation of 25 mm thickness is placed between the specimen edge and the edge-guard to stop convection currents from forming in the gap. When the apparatus is running in vacuum, the edge-guard's outer surfaces are covered with a thermally reflecting foil, to minimize heat transfer by radiation with the inside of the chamber walls. When running in air, insulating blanket is wrapped around the stack and 25 mm of flexible foam insulation covers the outside of the chamber.

This system allows thermal conductivity measurements in air, over the whole temperature range, without the need for controlling the air temperature within the chamber, as the specimen and heater edges are thermally isolated from the external environment.

Cold-Plate Heat-Flux Transducer

A heat-flux transducer is incorporated into the lower cold-plate to allow the heat flux on the cold side of the specimen to be measured. This will allow rapid measurements (2-3 hours) of specimens with conductivities greater than about 0.2 W/(m· K).

The transducer was custom made by Isover Saint Gobain in France and is a 0.6 mm thick glass-reinforced plastic substrate with 900 thermocouple junctions covering an area matching the central metering area of the VGHP heater plate. It is mounted in a recess in the cold-plate, with a 4 mm thick high-pressure laminate sheet of cloth impregnated with resin (Tufnol) between the heat-flux transducer and the cold-plate, to damp out small rapid temperature fluctuations caused by the liquid passing through the plate. On the other side of the transducer is an aluminum alloy cold surface which is in contact with the specimen, and in which the cold-plate thermocouples are mounted in 1.5 mm grooves. This surface plate has a 2 mm gap similar to the heater-plate, to reduce lateral heat flow between the edges and the central region.

This unit is calibrated by placing a thin thermal contact sheet between the lower cold surface and the heater plate. When the apparatus is in thermal equilibrium, it can be assumed that there is the same heat-flux in the transducer as leaving the heater. Thus by

applying different heat fluxes at different temperatures, a calibration can be made between transducer output and heat flux, at different temperatures.

Thickness Measurement (Displacement Transducer)

Specimens with a high coefficient of thermal expansion may change thickness over the full temperature range of the apparatus. Also, the thickness of semi-compressible insulations may vary with time as they settle under the load, applied by means of calibrated weights on the upper cold-plate. To enable the thickness of the specimen to be accurately monitored during a series of measurements, a laser displacement transducer is mounted above the upper cold-plate. The transducer operates by measuring the angle of scattered light from a white surface mounted on the cold-plate, and gives a signal that is proportional of the displacement.

The transducer output is calibrated against the specimen thickness by setting up the guarded hot-plate stack with sets of calibrated gauge blocks, of different thickness, in place of the specimen. The calibration is also carried out at several temperatures to take account of expansion or contraction of the plates and insulation in the rest of the stack. The transducer output is monitored during thermal conductivity measurements to give the specimen thickness value used in calculating the thermal conductivity.

Validation of Thermal Conductivity Measurements

The VGHP measurement of thermal conductivity in air has been evaluated according to the performance checks specified in ISO 8302:1991. They have also been validated using the European reference material IRMM-440 [*2*] (Table 1) and with NPL reference material Perspex Batch 7/81 (Table 2).

The IRMM-440 is a resin-bonded glass fiber board, certified over the temperature range -10 °C to 50 °C, and with a quoted uncertainty of ± 1 %. In addition to their measurements that contributed to the certified reference values, the Istituto di Fisica Tecnica in Italy also made measurements down to -170 °C.

Table 1 – Measured Thermal Conductivity of IRMM-440 Reference Material

Mean Specimen Temperature, °C	VGHP Measured Thermal Conductivity	IRMM Thermal Conductivity Reference	Difference (Measured - Reference)
-50.0	0.0248	0.0244 [1]	1.6 %
-30.9	0.0266	0.0264 [1]	0.8 %
-10.9	0.0286	0.0283	1.0 %
9.3	0.0305	0.0304	0.3 %
29.7	0.0329	0.0327	0.6 %
50.0	0.0357	0.0352	1.4 %

[1] These values are not part of the official material certification.

The VGHP values for the IRMM-440 glass fiber board have an estimated uncertainty of ± 1.5 % and are in agreement with the IRMM-440 reference values within the combined measurement uncertainty.

The NPL Perspex Batch 7/81 reference material is polymethylmethacrylate, certified over the temperature range 0 °C to 60 °C, with an uncertainty of ± 3 %.

Table 2 – Measured Thermal Conductivity of NPL Perspex (7/81)

Mean Specimen Temperature, °C	VGHP Measured Thermal Conductivity	Perspex Thermal Conductivity Reference	Difference (Measured - Reference)
-0.8	0.1860	0.1877	-0.9 %
19.6	0.1878	0.1904	-1.4 %
39.6	0.1904	0.1931	-1.4 %
59.5	0.1937	0.1958	-1.1 %

The VGHP values for the Perspex (7/81) have an estimated uncertainty of ± 3 % and are in agreement with the NPL reference values within the combined measurement uncertainty.

Measurements on Powder in Vacuum

Evacuated Insulation Panels

With the increasing use of evacuated insulation in refrigeration and also in specialized applications, there is a growing need to evaluate these products. The panels consist of filler material, generally fumed silica or aerogels, which are evacuated and surrounded by a laminated gas barrier of different plastics and an aluminum foil. They can have a thermal resistance that is ten times greater than a conventional insulation of the same thickness. Better characterization of the filler material will allow further development and comparison of various panel designs.

Evacuated-Powder Container

To measure powders in vacuum, an instrumented container was constructed to hold the powder in the form of a 305 mm square specimen. The container is placed as a specimen in the VGHP and its contents are evacuated along with the vacuum chamber.

The container is made of a 4 mm thick high-pressure laminate sheet of cloth impregnated with resin (Tufnol), so as to provide a rigid reusable box. The laminate sheet has a thermal conductivity of about 0.3 W/(m· K), which minimizes lateral heat-flow through the base, lid, and vertically through the sides. The 25 mm high sides consist of two layers, the inner bolted and glued to the base, while the outer is bolted to the inner. A layer of "vacuum cleaner bag" paper is sandwiched between the inner and outer layers, both of which have large cutouts in them. These cutouts and the paper form windows, allowing the inside of the container to be evacuated, while keeping the powder contained.

The temperatures on either side of the powder are measured with five thermocouples mounted on the inner surface of the base and lid. They are made from E-type wire of 0.2 mm diameter, which have been rolled flat to less than 0.1 mm (the calibration is not significantly altered by this process). The inner surface of the container is sprayed with a black paint with a total hemispherical emittance of 0.90.

Evacuated-Powered Measurements

Trial measurements (Table 3) were carried out on typical fumed silica used in evacuated panel insulations. The absolute pressure inside the chamber was less than 10^{-3} mbar.

Table 3 - *Measured Thermal Conductivity of Fumed Silica (69 kg/m^3)*

Mean Specimen Temperature, °C	Thermal Conductivity, W/(m· K)
49.5	0.0067
19.2	0.0044
-17.1	0.0026

There is very little data on this fumed silica product, but the values obtained by NPL are similar to those published by the manufacturer. The NPL measurements are also in good agreement with measurements carried out at the Oak Ridge National Laboratory on similar types of fumed silica [*3*], using a radial heat-flow apparatus with vacuum capability. The Oak Ridge measurements show similar temperature dependencies as those in the VGHP. They were in the range 0.003 W/(m· K) to 0.008 W/(m· K) at temperatures between 27 °C and 57 °C, at pressures of 2 x 10^{-2} mbar to 4 x 10^{-2} mbar.

Discussion

The uncertainty for measurements on evacuated specimens will be higher than the ± 1.5 % for measurements on conventional insulations in air. This is due to the power required to create the desired temperature drop through the specimen (20 K) being much smaller (100-200 mW), so that the uncertainty on the power could be up to ten times greater. The guard-center balance will also be far more critical and any heat gain or loss from the edges of the specimen will have a greater effect. Although further performance evaluation is required before a detailed uncertainty budget can be produced, the uncertainty is estimated to be about ± 10 %.

Due to the extremely low thermal conductivity of the evacuated specimens, the VGHP took much longer than normal to reach thermal equilibrium. The measurements given above were taken after the test had been running for 48 hours. The long drift-time and small heat-fluxes involved suggest that some fine-tuning is required to determine the optimal tuning of temperature controllers and the equilibrium criteria. Variations due to guard/center off-balance and the optimum temperature drop also need to be investigated.

Measurements of Total Hemispherical Emittance

Conventional apparatus that measure near-normal total emittance are generally not suitable for the dusty, inhomogeneous materials commonly used in building construction and it is necessary to obtain these values using a different technique. The method chosen was to measure the total hemispherical emittance by measuring the net radiation interchange between the specimen surface and a colder surface of known emittance. Total hemispherical emittance relates to the integration of the radiation over all angles and all wavelengths that the surface is radiating. This is often more directly applicable than normal total emittance, which must be corrected before it can be used in heat transfer calculations of building elements.

This technique has previously been used with an air-filled gap [*4, 5*]. It is generally carried out with the air gap under the heater to reduce convection. It is also often used to measure the emittance of heater-plates that have a high emittance, as described in ISO 8302:1991, using a varying gap thickness to avoid significant corrections for air conduction. However, when this technique is used for surfaces with a low emittance, the radiative flux is small compared with that conducted through air, which is the reason that an evacuated gap is used in the VGHP. For rough, inhomogeneous materials this method also has the advantage of using a more representative area than is possible using the small samples required for a spectrophotometric apparatus.

Configuration for Emittance Measurements

The effective emittance of a specimen surface is determined by measuring the radiant heat transfer across a gap between the heated specimen and the cold plate. The surface of the cold plate has been sprayed with the same black paint as the heater-plate, whose emittance, 0.90 at 20 °C, has been measured at NPL using a spectrophotometric apparatus [*6, 7*].

To suppress heat transferred across the gap by air conduction and convection, the apparatus has been mounted in a vacuum chamber. For gaseous conduction to become negligible with a 3 mm gap requires a pressure of the order of 10^{-4} mbar. Once this level of vacuum is achieved, the radiative heat transfer across the gap is assumed to be equal to the electrical power into the central heater, as the lateral and edge guarding minimize net lateral heat transfer.

Small Tufnol spacers at each corner of the lateral guard area maintain the gap between the specimen surface and the top cold plate. The spacers are 3 mm long tubes of 5 mm diameter and 2 mm wall thickness. By keeping this gap small and by covering the edge guards with a reflective aluminum foil, the net radiant heat emitted by the central metering area to the edge guard is reduced to a negligible level.

The surface temperature of the cold plate is measured by thermocouples embedded in grooves in the surface of the plate before it was sprayed. The specimen's surface temperature is measured by a thermocouple of 0.2 mm diameter wire, rolled flat to 0.1 mm and taped to the specimen surface. A tape is selected with similar emittance to the specimen and just enough is used to ensure good thermal contact between the thermocouple and specimen.

Principle of Emittance Measurements

The specimen and top cold plate surfaces are assumed to be diffuse reflectors and emitters, and have thermal radiative properties that do not vary with wavelength, i.e. they are gray. The expression for the net radiative heat exchange Q between two infinite parallel flat plates in terms temperatures T_{hot} and T_{cold}, emittance ε_{hot} and ε_{cold}, area A, and Stefan Boltzmann constant σ, 5.67 x 10^{-8} W/($m^2 \cdot K^4$), is then given by [8]

$$Q = \frac{A\sigma(T_{hot}^4 - T_{cold}^4)}{\frac{1}{\varepsilon_{hot}} + \frac{1}{\varepsilon_{cold}} - 1} \tag{1}$$

Rearranging equation (1) we obtain an equation for the specimen emittance ε_{hot}.

$$\varepsilon_{hot} = \frac{1}{\frac{A\sigma(T_{hot}^4 - T_{cold}^4)}{Q} - \frac{1}{\varepsilon_{cold}} + 1} \tag{2}$$

Hence, measuring the net radiant heat transfer Q from the metering area A, measuring the surface temperatures and knowing ε_{cold}, the specimen emittance ε_{hot} can be calculated.

Comparison with NPL Spectrophotometric Standard

In order to validate the performance of the new VGHP apparatus, the emittance of polymethylmethacrylate (Perspex) and a coated glass were measured by the NPL Optical Radiation Measurement Group using a spectrophotometric apparatus. This apparatus can measure both diffuse and regular (spectral) components of reflectance and transmittance, from which the spectral emittance can be calculated. Knowledge of the spectral emittance over the thermal infrared spectrum enables near-normal total emittance to be calculated. This method requires small specimens and is generally not suitable for inhomogeneous materials or materials with a low heat capacity. This method also has large uncertainties for highly reflective materials.

To compare the near-normal total emittance values produced by the NPL spectrophotometric technique with measurements made in the VGHP, the near-normal values need to be converted into a total hemispherical emittance. This can only be achieved to high-accuracy if the emission and reflection properties of both surfaces are known, and it involves complex calculations. However, for the purposes of this comparison, tables of "corrected" emittance in the European standard EN 673:1998 "Glass in building – Determination of thermal transmittance (U value) – Calculation method", will provide sufficiently accurate conversion factors.

Emittance of Polymethylmethacrylate

The near-normal total emittance of a sample of polymethylmethacrylate thermal conductivity reference material (NPL batch 7/81) was measured using the NPL spectrophotometric technique, converted to total hemispherical emittance, and compared with measurements made in the VGHP (Table 4).

Table 4 – Measured Thermal Emittance of Polymethylmethacrylate

Specimen Surface Temperature, °C	VGHP Measured Emittance	Spectrophotometric Reference Emittance [9]	Difference (Measured -Reference)
-24.7	0.949	0.896	0.054
-6.7	0.917	0.897	0.021
12.6	0.939	0.898	0.041
22.3	0.951	0.898	0.052
32.8	0.974	0.899	0.075

The temperature difference between the specimen (hot) surface and the calibrated cold-plate surface was 12 K to 15 K.

Emittance of a Coated Glass

The near-normal total emittance of a sample of glass with a low emittance semi-conducting coating of tin oxide doped with fluorine atoms, was measured using the NPL spectrophotometric technique. These results were then converted to total hemispherical emittance, and compared with measurements made in the VGHP (Table 5).

Table 5 – Measured Thermal Emittance of Coated Glass

Specimen Surface Temperature, °C	VGHP Measured Emittance	Spectrophotometric Reference Emittance [10]	Difference (Measured -Reference)
-19.2	0.208	0.167	0.041
1.3	0.187	0.169	0.018
21.4	0.180	0.171	0.009
21.8	0.184	0.171	0.013
43.9	0.201	0.173	0.027
63.5	0.208	0.175	0.032

The temperature difference between the specimen (hot) surface and the calibrated cold-plate surface was 20 K to 25 K.

Emittance of a Reflective "Aluminized" Insulation

There has been a recent emergence in the UK construction industry of "reflective insulation" products being used inside cavity walling as an alternative to conventional insulations. The principle on which they are marketed is that they reduce heat transfer by radiation, which can be a significant component of the thermal transmittance of an un-insulated cavity wall. Products such as "aluminized bubble-wraps," consist of a layer of plastic and air cavities, of nominally 5 mm to 10 mm thickness, with reflective aluminum foil on one or both surfaces. The single foil products are nailed to the inner leaf of a cavity wall, while the double foil products are hung centrally within the cavity.

The performance of these products are currently evaluated by NPL using thermal transmittance measurements made in a Hot Box, with the product mounted in a reference cavity. However, Hot Box tests are expensive and time consuming. The VGHP offers a more economic approach and can provide direct measurements of both emittance and resistance. This will enable investigation into some of the issues surrounding these products, which include the transparency of plastics used to coat the aluminum foil and the reduction of performance due to dirt, dust and tarnishing.

The near-normal total emittance of a sample of reflective "aluminized" insulation was measured using the NPL spectrophotometric technique, converted to total hemispherical emittance, and compared with measurements made in the VGHP (Table 6).

Table 6 – Measured Thermal Emittance of Aluminized Insulation

Specimen Surface Temperature, °C	VGHP Measured Emittance	Spectrophotometric Reference Emittance	Difference (Measured -Reference)
-1.0	0.040	0.073	-0.033
20.2	0.038	0.074	-0.036

The temperature difference between the specimen (hot) surface and the calibrated cold-plate surface was 20 K.

Discussion

The agreement between the VGHP total hemispherical emittance measurements and the spectrophotometric values are of accuracy acceptable for many construction industry applications. The VGHP measurement uncertainty is higher than the spectrophotometric method. However, further refinements should lead to improved accuracy and it is a good alternative for materials that are not suitable for the spectrophotometric method.

The uncertainties of the measured values for temperature difference and the heat-flux both have a significant effect on the overall uncertainty of the measured emittance. The emittance of the cold-plate has far less effect as long as the painted surface is well maintained. Examples of the estimated effect of each of these measured parameters are given for high emittance specimens (Table 7) and low emittance specimens (Table 8).

Table 7 – Estimated Effect of Measured Parameters on the Uncertainty in Emittance for a Specimen of High Emittance (0.95)

Measured Parameter	Estimated Uncertainty	Effect on Emittance Value	Emittance Uncertainty, %
Temperature difference	0.5 K	0.047	4.9
Heat-flux	2 %	0.021	2.2
Cold-plate emittance	0.005	0.006	0.6

Table 8 – Estimated Effect of Measured Parameters on the Uncertainty in Emittance for a Specimen of Low Emittance (0.18)

Measured Parameter	Estimated Uncertainty	Effect on Emittance Value	Emittance Uncertainty, %
Temperature difference	0.5 K	0.004	2.2
Heat-flux	2 %	0.004	2.2
Cold-plate emittance	0.005	negligible	0.1

The temperature drop is measured by a thermocouple taped to the specimen surface, with heat sink compound used to aid thermal contact, and another in embedded in a groove on the cold-plate surface. Future improvement in the performance of the VGHP may be achieved by alternative approaches to mounting the specimen thermocouple.

While the electrical power into the central heater of the guarded heater plate can be measured to about 0.03 %, the resulting net radiative heat flux between the specimen surface and the cold-plate, will be affected by the amount of additional heat gained or lost to the environment. This heat gain or loss will depend on the effectiveness of the lateral, auxiliary and edge guards, and will have a greater influence the further the surface temperature is from ambient.

Summary and Planned Developments

The NPL VGHP provides a versatile measurement facility for characterizing a wide range of insulation products. The thermal conductivity of a filler material used in evacuated insulation panels has been measured under vacuum conditions in an instrumented container. The values are in good agreement with those from other sources with similar filler materials. Future enhancements may include some form of control over the pressure within the chamber to allow determination of a relationship between thermal conductivity and pressure. It is also intended that the VGHP will make measurements on insulations in gases other than air and at elevated pressures.

The total hemispherical emittances of polymethylmethacrylate, a coated glass and a reflective insulation product have been measured with accuracy acceptable for many construction industry applications. Further work on evaluating the performance of the apparatus will allow a detailed uncertainty budget to be produced. Practical problems still need to be overcome to allow measurement of low-density insulations, as temperature

gradients within the evacuated insulation can be much greater than across the evacuated gap.

Acknowledgements

My colleagues John Redgrove, David Salmon and Ray Williams at NPL, provided valuable comments.

The standards work of the NPL Thermal Metrology Team is supported and funded by the UK Government's Department of Trade and Industry, and is an essential part of the UK National Measurement system ensuring consistency and traceability of measurement throughout the UK.

References

[1] Stacey, C. and Williams, R., "Development of the NPL Guarded Hot-Plate Emissometer," *Proceedings of the 24th Conference on Thermal Conductivity*, Pittsburgh, PA, October 26-29, 1997, pp. 755-763.

[2] Quin, S., Venuti, G., De Ponte, F. and Lamberty, A., "Certification of a Resin Bonded Glass Fibre Board for Thermal Conductivity between –10 °C and +50 °C," IRMM Report EUR 19572 EN, 2000.

[3] Yarbrough, D. W., Weaver F. J., Graves, R. S. and McElroy, D. L., "Development of Advanced Thermal Insulation for Appliances, Progress Report for the Period July 1984 Through June 1985," Oak Ridge National Laboratory Report ORNL/CON-199, May 1986, p. 37, Table C.4.

[4] Hager, N. E., Jr., "Methods for Measuring Total Hemispheric Emissivity of Plane Surfaces with Conventional Thermal Conductivity Apparatus," *Proceedings of the 7th Conference on Thermal Conductivity*, Gaithersburg, MD, November 13-16, 1967, pp. 241-246.

[5] Jaouen, J-L. and Klarsfeld, S., "Heat Transfer Through a Still Air Layer," *Thermal Insulation, Materials and Systems, ASTM STP 922*, Powell and Matthews Eds., Dallas, TX, 1984, pp. 283-294.

[6] Clarke, F. J. J. and Larkin, J. A., "Emissivity Determined from Hemispherical Reflectance and Transmittance throughout the Thermal Infrared Spectrum," *High Temperature – High Pressure*, 1985, 17, pp. 89-96.

[7] "Hemispherical Diffuse and Regular IR Spectral Reflectances and Emittances of a Black Painted Sample," *NPL Calibration Certificate, CEM/27/98/017/Q321AS*, 1998.

[8] Incropera, F. P. and De Witt, D. P., "Fundamentals of Heat and Mass Transfer," 3rd edition, John Wiley & Sons, 1991, p. 815.

[9] "Spectral Regular Reflectance, Spectral Transmittance and Total Emittance of One Sample," *NPL Calibration Certificate, CEM/27/96/024*, 1996.

[10] "Spectral Regular Reflectance, Spectral Transmittance and Total Emittance of One Pilkington K-Glass Sample," *NPL Calibration Certificate, CEM/27/96/023*, 1996.

Session 3: Building Systems I

Jan Kosny[1] and Phil Childs[2]

Accuracy of Hot Box Testing of Steel Stud Walls

REFERENCE: Kosny J. and Childs P., **"Accuracy of Hot Box Testing of Steel Stud Walls,"** *Insulation Materials: Testing and Applications: 4th Volume: ASTM STP 1426*, A. O. Desjarlais and R. R. Zarr, Eds., ASTM International, West Conshohocken, PA, 2002.

ABSTRACT: A new procedure was developed to increase the accuracy of hot box testing of walls containing strong thermal bridges. Since steel is about one thousand times more conductive than wood, steel-framed walls are very good examples of structures containing strong thermal bridges. The traditional analysis method of hot-box test data (as described in the ASTM C1363 standard) is relatively accurate for hot box testing of conventional wood-famed walls. However, this methodology is significantly less accurate for heavily thermally bridged steel-framed walls. In the proposed new method, three sources of inaccuracies were identified for steel stud assemblies:

- zone of influence for the thermally bridged areas,
- distribution of surface temperatures for locations of strong thermal bridges, and
- thermal conductivity of foam used in the surround panel.

All three factors are important in that they may reduce the accuracy of the hot box testing on thermally bridged walls

KEYWORDS: steel framing, heat transfer, hot-box tests, wall R-value

[1] Research Engineer, [2] Research Support Staff Member, Engineering Science & Technology Division, Oak Ridge National Laboratory, Oak Ridge, TN.

Introduction

During hot-box experiments, average wall surface temperatures are traditionally calculated based on the geometrical distribution of the internal wall structure. In the case of steel-framed walls, the wall area is normally divided into three zones: cavity, stud/flange, and track. The geometric average temperature is calculated by combining the appropriate average temperatures in an area-weighted manner based on the percentage of the total wall surface area of each individual wall component is comprised. While the geometric average method of temperature calculation is sufficient for wooden structures, the application of steel framing makes such calculations much less practical. A method was determined that allows an improved method of computing temperature averages for more accurate analysis in situations where hot box test results are utilized to calibrate computer models.

A new method of surface temperature calculation was implemented to address this uncertainty. In traditional practice, the average surface temperature calculations were accomplished by assigning a zone of influence for individual thermocouples based on the area of the wall element to which this thermocouple is affiliated. In the new procedure, for each thermocouple location the zone of influence is estimated based on temperature maps generated by detailed three-dimensional computer modeling.

A second potential source of errors in R-value calculations of steel structures is the fact that surface temperatures in locations of strong thermal bridges are not uniform. For example, the temperature difference across a steel flange can reach 1.12° C (for 28° C gradient across the wall), necessitating the precise positioning of each thermocouple in thermally bridged areas and then accurately defining and including its effect during temperature calculations.

A third additional source of inaccuracies in hot box testing is the potential misinterpretation of the thermal properties of insulation used for the surround panel. During hot box tests, it is a common practice to use foam surround panels where the foam fill materials are installed between the edge of the tested specimen and the edge of the hot box frame. In the hot box energy balance calculations, a nominal value of the apparent thermal conductivity for this foam is used to account for heat flow through the surround panel. Unfortunately, this area is highly bridged, and these thermal bridges (studs or tracks) influence the localized heat transfer. Because of this, the nominal apparent thermal conductivity of the surround foam should not be used for heat transfer calculations in these areas.

Thermal Analysis Method

Three-dimensional heat conduction, finite difference computer code Heating 7.2 [*1*], was used for this analysis. The resultant isotherm maps were used to calculate average heat fluxes, and wall system R-values. The generalized heat conduction code developed by ORNL, Heating 7.2, was used to analyze the thermal fields in steel-framed walls and was used to solve steady-state heat conduction problems in two or three dimensions using Cartesian coordinates. The surface-to-environment boundary conditions were specified for both surfaces of the simulated walls. Exterior and interior air temperatures were simulated at -6.7 ^{0} C and 21.1 ^{0} C, respectively and an exterior wind velocity of 25 km/h

was assumed. For the computer modeling thermal resistances of the wall surfaces were taken from the *ASHRAE Handbook of Fundamentals* [*2*] and were set at 0.03 m^2K/W for the outside wall and 0.12 m^2K/W for the inside wall. Maps of temperatures obtained from the modeling were used to calculate average heat fluxes and wall R-values .

The ability of Heating 7.2 to accurately predict wall system R-values was verified by comparing simulation results with published test results for twenty-eight masonry, wood frame, and metal stud walls. Ten empty two-core 30.5cm units reported by Valore [*3*], Van Geem [*4*], and James [*5*] were modeled with accuracy better than ±4 percent [*6*]. Similar eight filled two-core 30.5cm units reported by Valore, Van Geem, and James were modeled with an accuracy better than ±6 percent.

A 2x4 wood stud wall reported by James was modeled with accuracy better than ±2 percent. For three metal stud walls tested at ORNL [*7*], the average accuracy of computer modeling was within 2.3 percent. Considering that the precision of the guarded hot box test method is reported to be approximately 8 percent [*8*], the ability of Heating 7.2 to reproduce the experimental data is adequate to generate the desired analysis.

Description of the Test Wall and Methodology of Wall Thermal Measurement

A hot box experiment was undertaken to validate theoretical assumptions of the improved measurement technique [*9*]. A conventional steel stud wall with nominal 2 x 4 standard steel-framing was considered. This wall was finished with 1.27 cm thick gypsum drywall on the warm side and 1.27 cm thick oriented strand board (OSB) on the cold side. Full-width R-13 fiberglass batt insulation was installed in the cavities.

The R-13 batts used in the 2 x 4 walls were kraft paper faced. The drywall and OSB materials were fastened to the framing using standard #8 drywall and OSB screws, respectively. The screws were spaced on-center at 15.24-cm intervals around the perimeter of the wall and at 30.5-cm intervals on the center studs. Table 1 shows the configuration of the tested wall.

Table 1 - *Hot-box test wall configuration*

Nominal Stud Size	Web Design		Cavity Insulation	Sheathing	
	Stud	Track		Interior	Exterior
8.9-cm	solid	solid	R-13 batt	1.27 cm drywall	1.27 cm OSB

The specimen wall built for this test measured 239.4 x 236, 9-cm short of filling the metering chamber opening both horizontally and vertically. Additional fill material was needed to make up the difference in size. The wall was positioned in the test frame such that the wall was centered both vertically and horizontally over the metering chamber opening. The area surrounding the test wall panel was filled with a thermally resistive foam insulation material, expanded polystyrene (EPS) to the same thickness as the tested wall. The 2 x 4 steel-framed test wall was subjected to a nominal climate side air temperature setting of -6.7° C and a nominal meter side air temperature of 21.1° C.

An array of thermocouples was installed on both sides of each wall and a geometric area weighting method was used to determine an overall average surface temperature. The weighting factors used for the individual components will be discussed later in this paper. Figures 1 and 2 show the typical thermocouple layouts.

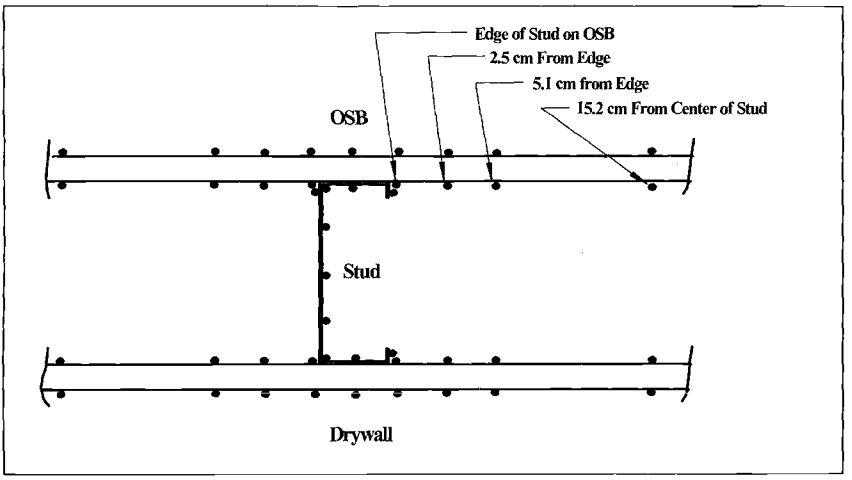

Figure 1. *Map of thermocouples in location of steel stud.*

The fiberglass batts were carefully installed in the cavities to minimize gaps between the insulation and the stud/track interface. The insulation used on the 2 x 4 framed wall was kraft paper faced and the seams were taped with masking tape to provide a tight air barrier.

Table 2. *Thermal conductivities of wall materials measured using ASTM C 518-98 test method.*

Name of wall material	Thermal conductivity Wm/K
Gypsum board	0.16
R-13 Fiberglass Batt	2.52
OSB	5.55
EPS foam	1.63

In addition to testing the steel-framed wall system in the Rotatable Guarded Hot Box (RGHB), samples were taken from each of the materials used in the test wall. These samples were submitted to the Materials Thermal Analysis Group at the Oak Ridge National Laboratory, where the thermal resistance of each sample was measured in accordance with ASTM C 518-98, "Standard Test Method for Steady-State Thermal Transmission Properties by Means of the Heat Flow Meter Apparatus." The specimens were subjected to mean temperatures of 10° C and 23.8° C. Table 2 shows measured thermal conductivities of wall materials.

Hot Box Test Results

The temperatures and heat flows recorded during the hot–box test were averaged for the time interval when steady-state had been achieved. A warm surface temperature profile recorded during the hot box test is presented on Figure 3.

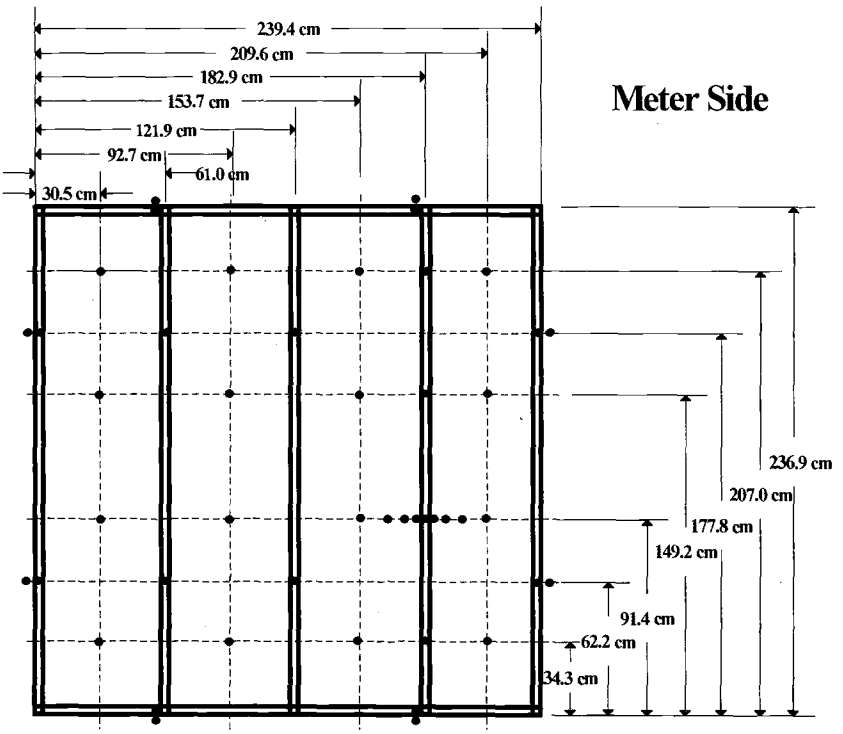

Figure 2. *Wall surface thermocouple detail*

The profile of surface temperatures depicted on Figure 3 suggests that the zone of influence of the steel stud is much wider than the actual size of the stud flange of 3.8 cm. To calculate the meter side and climate side average surface temperatures, the appropriate average temperatures are combined in a geometric area-weighted manner. At first, the traditional method was utilized for average surface temperature computations. The overall surface area of the individual test walls was 5.6 m^2. To area weight the surface temperature, the percentage of the total wall surface area that each individual wall component comprised was determined. For the steel framed wall specimens, the average temperature was computed by area-weighting the average cavity, stud, and track surface temperatures. The weighting factors (calculated in traditional way) used for these areas were 0.8819, 0.0913, and 0.0268, respectfully [*9*]. For the 2 x 4 steel-framed wall tested

for this study, the calculated R-value using methods from ASTM C 1363-97 was 1.43 m^2K/W.

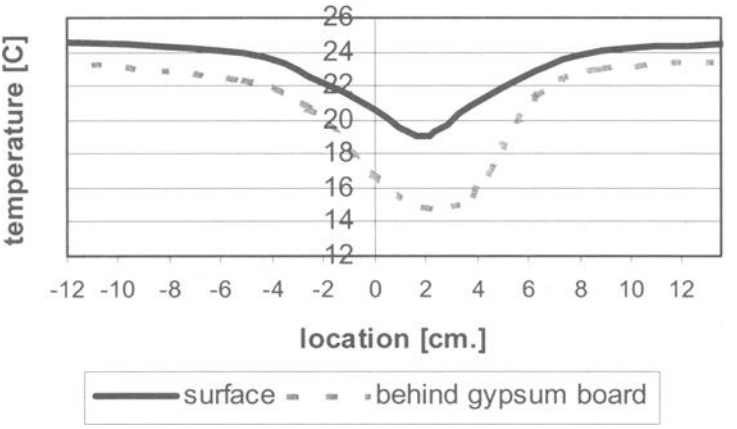

Figure 3. *Temperature map for warm surface of the wall recorded during the hot-box test (location of the stud flange is between 0.0 and 3.8-cm).*

Zone of Influence of Thermally Bridged Area

Since the experimental data suggests that the zone of influence of the steel stud is much wider than the actual size of the stud flange, the zone of influence for each thermocouple location is estimated based on temperature maps generated by detailed three-dimensional computer modeling from the proposed calculation procedure. These zones of influence generated from the finite difference simulations are used in the calculation of influence factors for each group of thermocouples (studs, tracks, and cavities). Weighted average wall surface temperatures are then calculated using measured local temperatures multiplied by their zones of influence rather than simply geometric areas representing centers between studs or stud and track flanges.

Figure 4.depicts simulated temperatures on the cross section of 2x4 steel stud wall. This simulation shows that the zone of influence of the temperature assigned to the center of the stud flange is larger than the actual width of the stud flange.

Modified zones of influence (based on computer modeling) are used in the calculation of weighting factors for each group of thermocouples (studs, tracks, and cavities). For the tested 2x4 steel-framed wall specimens, the simulation generated weighting factors for cavity, stud, and track surfaces areas are 0.83, 0.12, and 0.05, respectively.

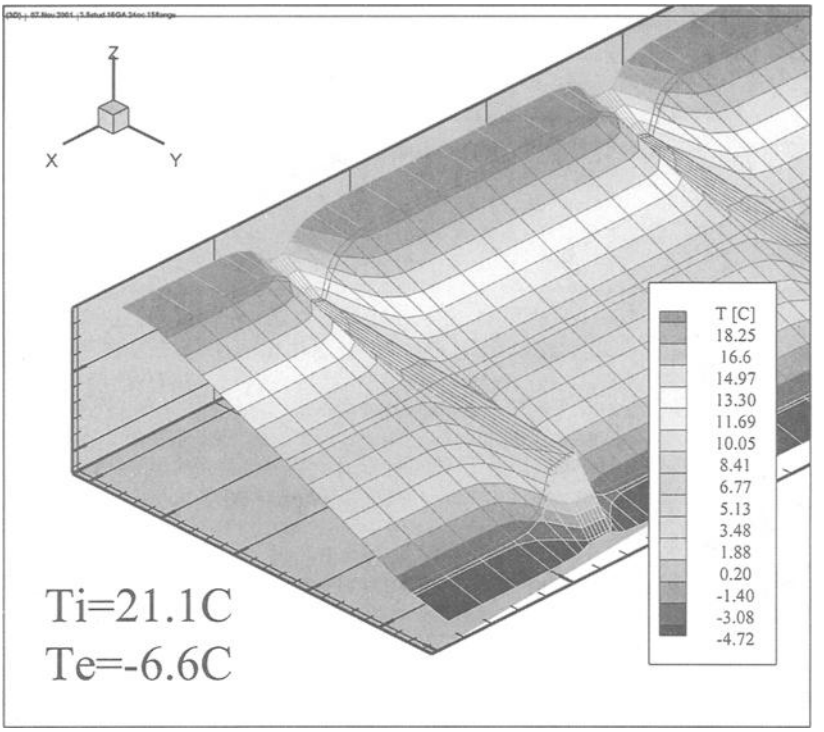

Figure 4. *Simulated temperature fields on the horizontal cross section of 2x4 steel stud wall.*

Variation of Local Surface Temperatures in Areas of Strong Thermal Bridges

Since the wall surface temperatures on the stud or track flanges are not uniform, precisely locating each temperature sensor during hot box experiments is consequently a very important factor determining the accuracy of test results. In traditional C-shaped steel stud wall systems, these surface temperatures vary along the width of the flange. Figure 4 depicts cross sectional temperature profiles for a conventional 8.9 cm deep steel-framed wall with R-11 batt insulation and a temperature difference of 27.8° C across the wall. For the cold surface, the maximum temperature difference across the stud flange location is 0.1°C and for the warm surface, the maximum temperature difference in similar locations is 0.5° C. For the track flange locations, corresponding temperature differences are 0.5 and 1.1° C, respectively.

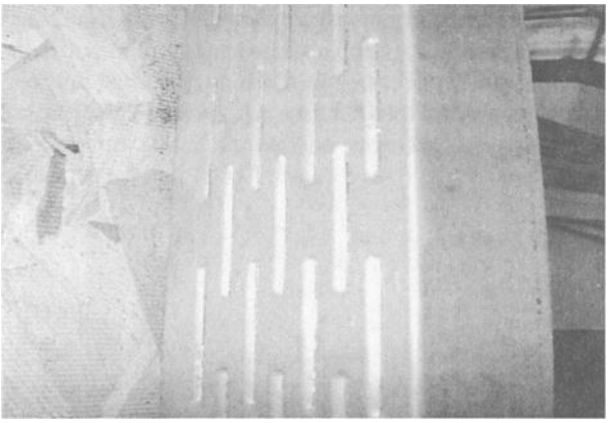

Figure 5. *Slit stud with series of vertical perforations along the length of the stud web*

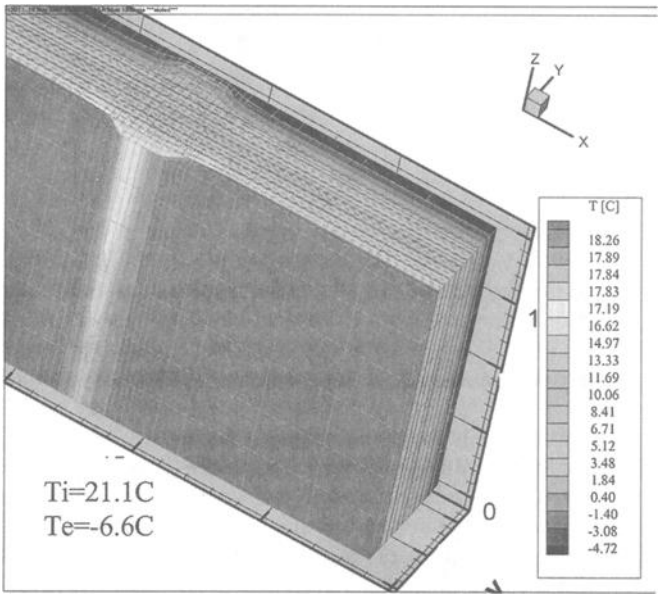

Figure 6. *Surface temperature fields for 8.9 cm deep slit steel-stud wall with R-11 batt insulation and a temperature difference of 27.7° C across the wall.*

Temperature fields at locations of perforated studs are much more complex. Figure 5 shows a slit stud with a series of vertical perforations along the length of the stud web. For a 2x4 slit steel-framed wall, the surface temperature is changing in both vertical and horizontal directions and in the webbing between the flange area. Figure 6 depicts surface

temperature fields for 8.9 cm deep slit steel-framed wall with R-11 batt insulation and a temperature difference of 27.8° C across the wall. For the cold surface, the maximum temperature difference across the stud flange location is 0.1° C and for the warm surface, the maximum temperature difference in similar locations is 0.5° C. For the track flange locations, corresponding temperature differences are 0.4 and 0.8° C, respectively.

Consequently, for walls containing strong thermal bridges, locations of the temperature sensors must be precisely located around thermal bridged areas and taken into account during the average surface temperature calculations. If this practice is not followed, the R-value calculated from the test results of the hot box experiment can be inaccurate.

Surround Panel Areas

Surround panels are used to minimize the so-called edge effects on the boundaries of measured specimens during the hot box experiments. Usually, thick foam panels are installed between the edge of the tested wall and the edge of the hot box frame. Traditionally, during the hot box energy balance calculations, a nominal value of the apparent thermal conductivity for this foam is used to account for heat flow through the surround panel. Unfortunately, heat transfer in this area is highly bridged by neighboring studs or tracks. That is why, nominal apparent thermal conductivity should not be used for heat transfer calculations in these areas. Three dimensional computer modeling clearly provides more accurate representation of the heat transfer in these areas.

Described above corrections in the size of the area of the zone of influence effect only the area of the metering box. However, some additional thermal bridge effects can be also observed in surrounding panels. Since they are made of highly insulating materials (foam), potential for errors in heat flow estimates for surround panels is relatively high. That is why, separate R-value adjustments were proposed for this area. They incorporate the effects of transversal heat transfer in the edge between the wall specimen and surround panels.

In our hot box experiment, the R-value of the foam surround panel using the ASTM C 518-98 test standard procedure was 3.75 m^2K/W. After performing a series of three-dimensional simulations on the surround panel/steel frame interface area, the effective R-value of the surround foam became 1.35 m^2K/W. This R-value reflects the effects of thermal bridging on the local heat transfer. Because of the heavy thermal bridging affecting the foam located around the steel framing, the heat transfer through this area is actually three-dimensional. Therefore, higher heat flow rates should be used in hot box energy balance calculations when measuring walls with strong thermal bridging. Thermal conductivity values measured using one-dimensional ASTM C 518 techniques need to be adjusted for this purpose.

Hot-box Test Results and Application of Improvements to Traditional Hot-Box data Analysis

A current practice of analyzing hot box test generated data may be a potential source of errors in R-value calculations for wall assemblies containing strong thermal bridges.

Currently, average wall surface temperatures are calculated based on the geometrical distribution of the internal wall structure. In the case of steel framed walls, the wall area is normally divided into three zones: cavity, stud/flange, and track.

In this work, a zone of influence for each thermocouple location is estimated in the traditional geometrical way and then again based on temperature maps generated by detailed three-dimensional computer modeling. The reason is that in the case of conventional C-shape studs where thermal bridges are strong, the zone of influence of temperatures measured at the center of the stud flange is larger than the nominal width of this flange. Similar zones of influence are used in the calculation of influence factors for other groups of thermocouples (tracks, and cavities). As a result, weighted average wall surface temperatures are calculated using measured local temperatures multiplied by simulation-generated zones of influence rather than using simple geometric areas.

The proposed experimental correction procedure was utilized on one typical steel-framed wall discussed previously in this paper. The following example shows the potential for generation of errors in R-value calculations when applying current standard hot box procedures.

Corrections in the wall R-value computations were started from analyzing heat flow rates in foam surround panel. New simulation generated weighting factors for cavity, stud, and track surfaces areas of 0.83, 0.12, and 0.05 were used in calculations. Also, after performing modeling on the surround panel/steel frame interface area and determining the effects due to thermal bridging, the effective R-value of the surround foam became 1.35 m^2K/W.

The new procedure was also applied to determine the potential errors in temperature measurement due to placement of the thermocouples across the face of the stud flange on the same 2 x 4 test wall. Potential error values of $\pm 0.1°$ C on the cold side and $\pm 0.4°$ C on the warm side were considered. The temperature variation across the face of the track flange was calculated to be $\pm 0.5°$ C on the cold side and $\pm 1.1°$C on the warm side.

Using the R-value measured by ASTM C 518 techniques for the surround foam (R-3.75) and the maximum potential temperature errors across the face of the stud and track flanges, the R-value of the wall becomes 1.4 m^2K/W. With the minimum potential temperature errors and the C 518 foam R-value, the R-value of the wall becomes 1.39 m^2K/W.

Applying the surround panel R-value calculated after accounting for the thermal bridging effects (R-1.35 m^2K/W), and the maximum and minimum potential temperature errors across the face of the stud and track flanges, the R-values of the wall become 1.46 and 1.45m^2K/W, respectively.

The difference between the lowest and highest R-values, obtained with the new method on this 2 x 4 standard steel-framed wall, is about 4.4 percent. This spread of R-values indicates a potential for errors in R-value computations using the ASTM C 1363-97 hot-box measurement procedure.

While this example shows the potential for errors in hot box testing, this value cannot be arbitrarily applied to other wall configurations. It is expected that potential error of ASTM C 1363-97 method of hot-box measurements may increase with increased thickness of the tested specimen. Application of highly resistant cavity insulations may also effect this error. Further modeling on multiple wall systems is needed to develop a more comprehensive error analysis.

Conclusions

This new experimental correction procedure was used on one typical 8.9 cm steel-framed wall to improve R-value computations on hot-box testing results. In the proposed new method, three sources of inaccuracies were identified for steel stud assemblies:

- zone of influence for the thermally bridged areas,
- distribution of surface temperatures for locations of strong thermal bridges
- thermal conductivity of foam used in the surround panel.

All the above factors were found important and each may reduce the accuracy of the hot box testing of thermally bridged walls. The difference between the lowest and highest R-values obtained with the new method on this 2 x 4 standard steel-framed wall was about 4.4 percent. This value indicates a potential for errors in R-value computations based on ASTM C 1363-97 method of hot-box measurements. However, it has to be remembered that for most of conventional assemblies ASTM C 1363-97 method of hot-box measurements yields relatively accurate result. A new procedure applies only for highly bridged structures.

A simple example presented in this paper shows the potential for errors in hot box testing of highly thermally bridged structures. This specific value of error cannot be arbitrarily applied to the other wall configurations. Further modeling on multiple wall systems is needed to develop a more comprehensive error analysis.

Acknowledgment

This paper was prepared by Buildings Technology Center, at the Oak Ridge National Laboratory, Oak Ridge TN. The Oak Ridge National Laboratory is managed by UT-Battelle LLC. For U.S Department of Energy under contract No. DE-ACO500OR22725.

References

[1] Childs, K. W., HEATING 7.2 Users' Manual, *Oak Ridge National Laboratory, ORNL/TM-12262*, ORNL, February 1993.

[2] ASHRAE, ASHRAE Handbook of Fundamentals, ASHRAE, 2000.

[3] Valore, R. C., "Thermophysical Properties of Masonry and Its Constituents, Part II," *Thermal Transmittance of Masonry*, International Masonry Institute, Washington, 1988.

[4] Van Geem, M. G., Thermal Transmittance of Concrete Block Walls with Core Insulation, *Journal of Thermal Insulation*, Vol. 9, January 1986.

[5] James, T. B., Manual of Heat Transmission Coefficients for Building Components, Department of Mechanical Engineering, University of Massachusetts, Amherst, Massachusetts, November 1990.

[6] Barbour E., Godgrow J., Kosny J., Christian J.E. Thermal Performance of Steel-Framed Walls, NAHB Research Center. Nov. 1994.

[7] Kosny, J., Desjarlais, A. O., Influence of Architectural Details on the Overall Thermal Performance of Residential Wall Systems, *Journal of Thermal Insulation and Building Envelope*, July 1994

[8] ASTM C 236-89, Standard Test Method for Steady-State Thermal Performance of Building Assemblies by Means of Guarded Hot Box, Vol. 04.06, pp. 53-63.

[9] ORNL Internal report - An Evaluation of the Steady-State Thermal Performance of Thermally Efficient Steel Frame Wall Systems (Phase I) - *OAK RIDGE NATIONAL LABORATORY Contract No. DE-AC05-96OR22464*. January Oak Ridge TN, 2000

Thomas W. Petrie,[1] Jan Kośny,[2] Jerald A. Atchley,[3] and André O. Desjarlais[4]

Effect of Steel Framing in Attic/Ceiling Assemblies on Overall Thermal Resistance

Reference: Petrie, T. W., Kośny, J., Atchley, J. A., and Desjarlais, A. O., **"Effect of Steel Framing in Attic/Ceiling Assemblies on Overall Thermal Resistance,"** *Insulation Materials: Testing and Applications: 4th Volume, ASTM STP 1426*, A. O. Desjarlais and R. R. Zarr, Eds., ASTM International, West Conshohocken, PA, 2002.

Abstract: Experiments have been performed to assess the impact of cold-formed-steel framing on the thermal performance of attic/ceiling assemblies. Test configurations duplicated features of full-sized, truss-based and conventional joist-and-rafter assemblies away from the edges of the ceiling. Steady-state tests were done at winter conditions in a climate simulator. In truss systems, strong thermal bridges due to framing members that penetrated through the insulation to the bottom chords persisted as the insulation level increased. Without penetrations, the effect of steel framing eventually disappeared as insulation level was increased. For negligible effect of the framing, framing spaced 41 cm oc required greater insulation depth than did framing spaced 61 cm oc. Without penetrations but with enough insulation to cover framing with depths of 8.9 cm, 20.3 cm and 30.5 cm, greater framing depth yielded slightly poorer thermal performance. In some tests, a continuous layer of extruded polystyrene foam insulation was placed between the C-shaped bottom chords of trusses and the gypsum board ceiling. System R-values improved slightly more than the R-value of the foam insulation. A three-dimensional model of the thermal behavior of the assemblies was used to extend the test results to the entire range of steel-framed attic/ceiling configurations. Equations generated from this and related work can be the basis for changes in codes and standards that reflect the effect of steel framing on the thermal performance of attic/ceiling assemblies and discourage allowing steel framing to extend beyond insulation in the assemblies.

Keywords: thermal bridges, steel framing, residential attics, hot box tests, system R-value, code support

[1-4] Research Engineer, Research Engineer, Research Support Staff Member and Group Leader, respectively, Engineering Science & Technology Division, Oak Ridge National Laboratory, Oak Ridge, TN.

Introduction

Cold-formed-steel framing (also called light-gauge-steel framing) in residential building envelopes has the potential to create more severe thermal bridges than does wood framing. The situation during steady-state heat transfer by conduction illustrates the potential problem. The rate of heat flow by conduction is directly proportional to the product of a material's thermal conductivity and its cross-sectional area perpendicular to the direction of heat flow. The thermal conductivity of steel is at least two orders of magnitude larger than that of wood. Smaller cross-sectional areas are possible for steel to support the same mechanical load as wood because of steel's higher mechanical strength. However, areas with steel are not two orders of magnitude smaller and do not offset the effect of steel's higher thermal conductivity. Intense heat flow per unit area is possible through steel if materials in series with the steel can support it.

The *ASHRAE Fundamentals Handbook* [*1*] summarizes methods for estimating the overall thermal resistance of one-dimensional building components without thermal bridges. Isothermal plane and parallel path methods are explained. The thermal performance of curtain-wall and stud-wall constructions containing metal is also addressed. For ceilings and roofs with wood framing, the thermal resistance of a ceiling can be obtained by techniques that apply to flat construction. The thermal resistance of ventilated attic spaces under pitched roofs is more complicated. Under winter conditions, the thermal resistance of the attic space is small. Under summer conditions, a table is presented for the effective resistance of the attic space that accounts for varying ventilation air temperature, air flow direction and rate, ceiling thermal resistance, roof or sol-air temperature and surface emittance. These methods are applied in current codes and standards.

The current *ASHRAE Fundamentals Handbook* does not address the overall thermal resistance of attic/ceiling assemblies with steel framing. Therefore, it is not surprising that current codes and standards do not address them either. The problem is that their thermal resistance cannot be estimated with confidence by procedures that work for wood framing because of the potential for more severe thermal bridges with steel framing. Techniques for steel-framed walls are also of doubtful accuracy when applied to steel-framed attic/ceiling assemblies. Conventional joist-and-rafter assemblies do not have the sandwich-like construction of wall assemblies. Insulation, not construction materials, usually covers the joists. In some cases, the joists may not be completely covered and severe thermal bridges are created across all the joists. A further complication happens occasionally in conventional assemblies and regularly in truss-based assemblies. Support braces attached to the joists or bottom chords penetrate the insulation. Each one creates a persistent thermal bridge because a highly thermally conducting element communicates directly with the attic air regardless of the level of insulation.

The Oak Ridge National Laboratory's Buildings Technology Center did steady-state tests and analysis of them from September 2000 through mid-February 2001. The objective of this project was to address the lack of any information on steel-framed attic/ceiling assemblies in current codes and standards. Results of the tests are presented. The tests provided data to validate a model of the thermal behavior of steel-framed attic/ceiling assemblies away from the edges. Direct comparisons between the experiments and model are presented. Codes and standards that address attic/ceiling

assemblies are the International Code Council's (ICC) International Energy Conservation Code (IECC), formerly the Model Energy Code (MEC), and the American Society of Heating, Refrigerating and Air-Conditioning Engineers, Inc.'s (ASHRAE) Standard 90.1, Energy Standard for Buildings Except Low-Rise Residential Buildings and Standard 90.2, Energy Efficient Design of New Low-Rise Residential Buildings. This paper concludes with presentation of simple but accurate relationships that will allow inclusion of information on steel-framed attic/ceiling assemblies in codes and standards.

Apparatus and Procedures

The tests were done in the Large Scale Climate Simulator (LSCS) at the Oak Ridge National Laboratory's Buildings Technology Center according to ASTM C1363, Standard Test Method for the Thermal Performance of Building Assemblies by Means of a Hot Box Apparatus. Attic/ceiling assemblies were constructed especially for the tests. The C-shaped steel framing from 1.9-mm-thick stock had 3.8-cm-wide flanges and was 8.9 cm, 20.3 cm or 30.5 cm deep. Gypsum board that was 1.27 cm thick formed the ceiling. Horizontal framing to which the gypsum was attached was spaced 41 cm oc or 61 cm oc. Various depths of full-width fiberglass batt insulation were placed in layers between and over the horizontal framing. Given the number of tests that were needed, fiberglass batts were a good choice over loose-fill material in terms of ease of removal and ability to be reinstalled quickly and to a consistent R-value. For a few tests, 2.5-cm-thick extruded polystyrene foam insulation with a nominal R-value of 0.88 $m^2 \cdot K/W$ was placed between the bottom flanges of the horizontal framing and the gypsum board ceiling.

In some of the tests with the 8.9-cm-deep joists and in all of the tests with 20.3-cm-deep and 30.5-cm-deep joists, only batt insulation was placed between and over the joists. These configurations simulated conventional joist-and-rafter designs. With the 8.9-cm-deep framing, tests were also done with one to nine pieces of the framing attached vertically to each piece of the horizontal framing. The pieces extended upward through the insulation. These configurations simulated typical steel truss designs.

Up to three layers of fiberglass batt insulation were used. Two of the layers had nominal thickness of 15.9 cm. The third layer had nominal thickness of 8.9 cm. Thermal conductivity from 0.046 to 0.048 $W/(m \cdot K)$ is a typical range for fiberglass at room temperature. By dividing thickness by thermal conductivity, the nominal R-value of the 15.9-cm-thick batt is 3.4 $m^2 \cdot K/W$. The nominal R-value of the 8.9-cm-thick batt is 1.9 $m^2 \cdot K/W$. The four configurations of insulation that were tested had nominal R-values of 3.4, 5.3, 6.7 and 8.6 $m^2 \cdot K/W$.

The actual R-value of the fiberglass insulation for each layer in each test was produced from the average installed thickness and density and from the thermal conductivity as a function of mean temperature and density. Thickness and density were determined according to ASTM C167, Standard Test Methods for Thickness and Density of Blanket or Batt Thermal Insulations, and thermal conductivity according to ASTM C518, Standard Test Method for Steady-State Heat Flux Measurements and Thermal Transmission Properties by Means of the Heat Flow Meter Apparatus. Temperatures measured on the top and the bottom of each layer during the tests were averaged to yield its mean temperature. Installed thickness of a layer divided by its thermal conductivity at

test temperature yielded its R-value at test conditions. The effect of temperature on insulation R-value was particularly important in the tests with foam insulation on top of the ceiling. The foam insulation shielded the fiberglass insulation from 21°C conditions below the assemblies more than the gypsum alone did. Therefore, the mean temperature of the fiberglass insulation was lower and its R-value was higher in the tests with foam insulation than without foam insulation, adding to system R-value.

Figure 1 shows an example test configuration that simulated a truss. For each horizontal framing member under the nominal R-3.4 $m^2 \cdot K/W$ insulation, except the two at the outer edges of the test section, three truncated braces extend upward through the insulation. Spacing between horizontal members is 41 cm oc. The center 2.44 m x 2.44 m area of the test section is the area that is metered in the LSCS for heat flow through the attic/ceiling assembly. During a test, the cover boards leaning against the back wall of the LSCS were placed on top of the assembly on a frame that fit into the brackets around the perimeter of the assembly. The cover boards formed a 0.61-m-deep unventilated attic space above the insulation.

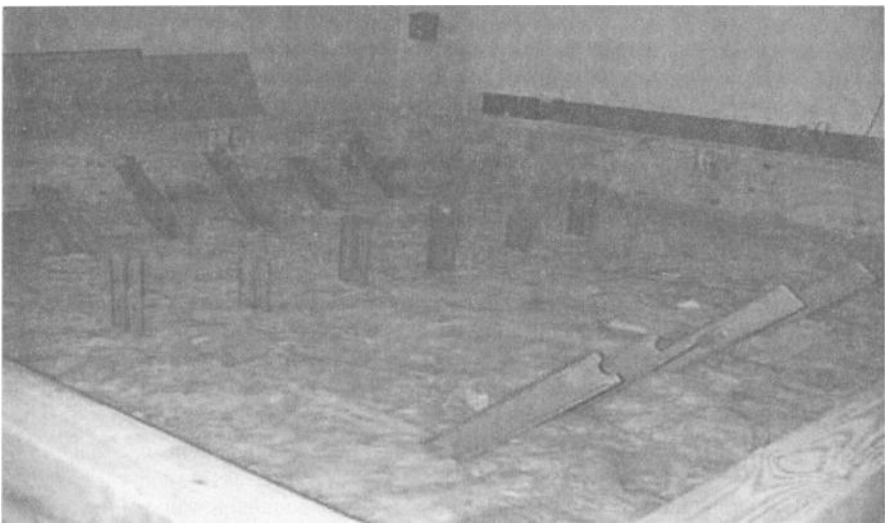

Figure 1. *Example truss test configuration with three truncated braces attached to each bottom chord. Chords are spaced 41 cm oc and braces penetrate the nominal R-3.4 $m^2 \cdot K/W$ insulation.*

For the results presented in this paper, air temperature in the chamber above the attic/ceiling assembly was held at -18°C. Air flowed over the top of the assembly at a velocity of 0.5 to 0.8 m/s. Air temperature in the attic space was a few degrees warmer. The attic space was sealed against ventilation. Air temperature in the metering chamber under the ceiling was 21°C and air passed over the bottom of the ceiling at a velocity of 0.8 to 0.9 m/s. Results are reported in terms of an air-to-air system R-value obtained by the formula:

$$R_{system} = \frac{A \bullet \Delta T}{Q} \quad (1)$$

where

R_{system} is the air-to-air R-value in units of $m^2 \cdot K/W$,

A is the area of the ceiling through which heat flows out of the metering chamber. It is equal to the 5.95 m^2 opening of the metering chamber for thin specimens. Here it was increased by 8.5% to 10.6%, depending upon insulation R-value, to account for two-dimensional heat flow around the perimeter through the relatively thick insulation,

ΔT is the temperature difference between the air below the ceiling and the air above the insulation, in K or °C, and,

Q is the net heat flow out of the metering chamber, obtained from an energy balance on the metering chamber, in W.

The air handling system in the metering chamber of the LSCS includes a water-cooled cooling coil, an electric resistance heating coil and circulation fans to move air over them. The ability to use cooling in the metering chamber is a unique feature that allowed us to test over the wide range of insulation R-values given above. For some tests, the heat added to the metering chamber by the fans was more than the heat flow out through the ceiling. Even at severe winter conditions, additional cooling was necessary to do the tests at the desired 21°C in the metering chamber. If cooling is sufficient, temperature control is done with the fast-responding electric resistance heating coil.

Measurement of the amount of cooling, Q_{cool}, is difficult over a long series of tests due to very slow drift in the calibration of the instrumentation used to sense the cooling water flow rate and its temperature rise when it flows though the metering chamber. For several cases in which net heat flow out of the metering chamber was sufficient for control without metering chamber cooling, tests were done with and without cooling to establish the appropriate correction, ΔQ_{cool}, for the metering chamber energy balance. The correction varied from a minimum of 6.8 W at the start of the tests to a maximum of 13.6 W near the end of the tests. The correction was 7% to 29% of the net heat flow.

With no cooling in the metering chamber, the bias and precision of the LSCS was established and has been checked periodically with a calibration panel fabricated from a 10.2-cm-thick piece of expanded polystyrene foam insulation. Figure 2 shows results from 1990 through 2001 with no cooling in the metering chamber (solid symbols). Also shown are results from 1998 through 2001 since cooling has been available in the metering chamber (open symbols). The fit of the data with no cooling and the limits of the 95% confidence interval about these data have been extended to the range of mean calibration panel temperatures when cooling was needed in the metering chamber. When net heat flow into the metering chamber was greater than 45 W, the amount of cooling was corrected with a linear function of the net heat flow to produce the R-values shown as the open symbols. As evidence of the goodness of this correction, note the distribution of these corrected R-values about the solid line. They fall generally within the limits of the 95% confidence interval that is shown by the dashed lines: ±1.8% to ±2.3% of the expected R-value [*2*]. Our experience with other test sections with higher R-value than the calibration panel is that uncertainty doubles as R-value doubles.

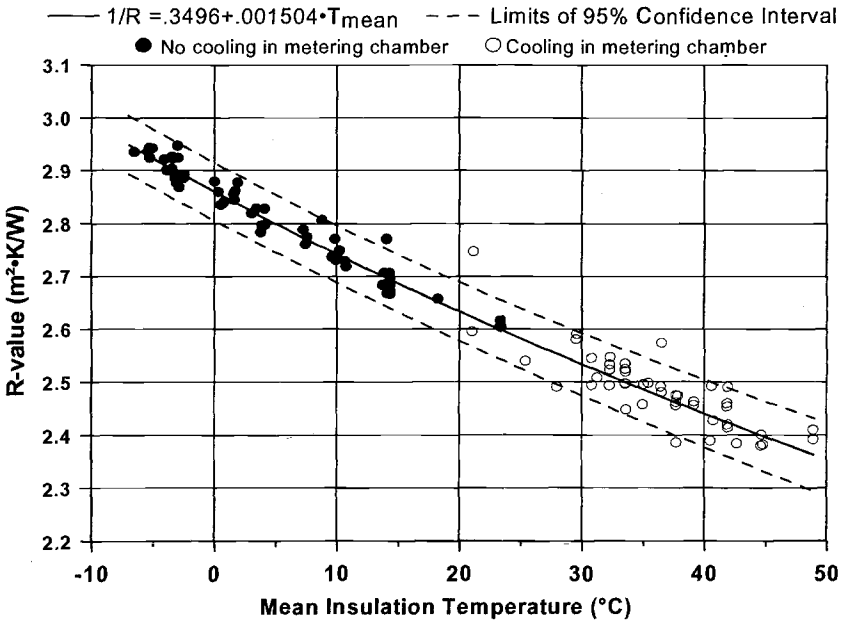

Figure 2. *Results with a calibration panel to monitor the bias and precision of the Large Scale Climate Simulator.*

Test Results and Discussion

Two working graphs have been prepared from the results with air temperature above the attic/ceiling assemblies at -18°C and air temperature below the ceiling at 21°C. Actual insulation R-values are used in the abscissas while system R-values as determined from Eq 1 are used in the ordinates. The graphs show trends in the experimental results that should be reflected in the model. They also show how internally consistent the test results are. This is of special concern because of the handling of the fiberglass batts from test to test that was required to change configurations in a timely manner.

Figure 3 shows the system U-value as a function of insulation U-value for tests with 8.9-cm-deep framing and various numbers of support braces to simulate trusses. U-value is the inverse of R-value. It is useful in this figure because the origin for insulation U-value represents infinitely thick insulation. Plotting U-values clearly shows how close the behavior is to that of insulation without any effects of steel framing. This situation is the bold line labeled No Steel in the figure. Solid symbols and light solid curves depict results for framing spaced 61 cm oc. Open symbols and light dashed curves show results for framing spaced 41 cm oc. Curves were hand drawn with a French curve through the data for each framing configuration that was tested at several insulation depths.

The configurations with 0 braces are expected to behave like framing-free assemblies as U-value approaches 0 (thick insulation depth). The assemblies with both 61 cm oc and 41 cm oc spacing of framing have this behavior. Performance for large

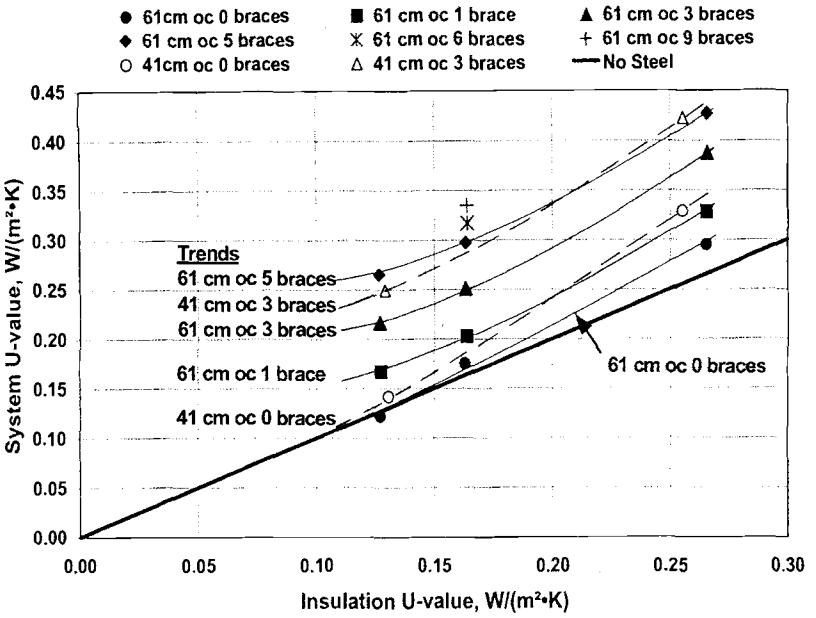

Figure 3. *Test results and trends for simulations of steel trusses with various numbers of support braces.*

insulation U-values (thin insulation depth) is worse for the 41 cm oc spacing than for the 61 cm oc spacing because 41 cm oc spacing causes more thermal bridges per unit area than 61 cm oc spacing. This is true for 0 braces and especially for 3 braces. Similarly, as the number of braces increases with framing spaced 61 cm oc, there are more thermal bridges per unit area of test section. Therefore, the curves and points for progressively more braces show progressively higher system U-values.

All braces were attached to the horizontal member that supported them within ±0.9 m of length from the center of the horizontal member. Thus, all attachments were within the 2.44 m x 2.44 m metered area for Eq 1. For framing spaced 61 cm oc, the increase in system U-value from 6 to 9 braces is no more than the increase from 5 to 6 braces. This indicates that the thermal bridge caused by each of the 9 braces is not as severe as it is for each of the 6 braces. The thermal bridges are interfering with one another.

The braces extended upward through the insulation as shown in Fig. 1. Cold-formed-steel members penetrating from the attic air space through to the bottom chords will continue to cause thermal bridges no matter what the depth of insulation. The data in Fig. 3 with 1, 3 and 5 braces and framing spaced 61 cm oc suggest that the effect of these thermal bridges eventually dominates. If so, the curves for braces should become parallel to the abscissa, not the No Steel line, as insulation U-value approaches 0.

Figure 3 does not show the results of three tests in which a continuous layer of extruded polystyrene foam insulation having nominal R-value of 0.88 $m^2 \cdot K/W$ was placed between the ceiling and the bottom chords. Nominal R-5.3 fiberglass batt

insulation was between each pair of bottom chords. The framing was spaced 61 cm oc. No braces, 1 brace and 5 braces penetrated the fiberglass insulation in the tests. There was relatively little thermal bridging in the tests with no braces and 1 brace, but the foam insulation did add its R-value to the system R-value. System R-value also increased (system U-value decreased) a small amount because the fiberglass insulation was colder when it was above the foam insulation and gypsum than when it was above the gypsum only. Because the continuous layer of foam insulation broke the many thermal bridges, it significantly improved the results with 5 braces. U-value with the foam insulation under this assembly fell on the curve drawn in Fig. 3 for framing 61 cm oc with 3 braces.

Figure 4 displays all data from tests without braces and includes results for framing with depths of 8.9 cm, 20.3 cm and 30.5 cm. There are two cases with three tests each that allow observation of trends. If system R-value is indeed linear with insulation R-value for each case, scatter is greater for 8.9-cm-deep framing spaced 61 cm oc than for 20.3-cm-deep framing spaced 41 cm oc relative to straight lines through the data for each case. The deviation from the line for the data with 8.9-cm-deep framing is at most -0.26 $m^2 \cdot K/W$ at system R-value of 5.7. This is within ±5% of R-5.7, where ±5% is the uncertainty expected at this level of R-value in the Large Scale Climate Simulator. Uncertainty masks whether or not system R-value is linear with insulation R-value.

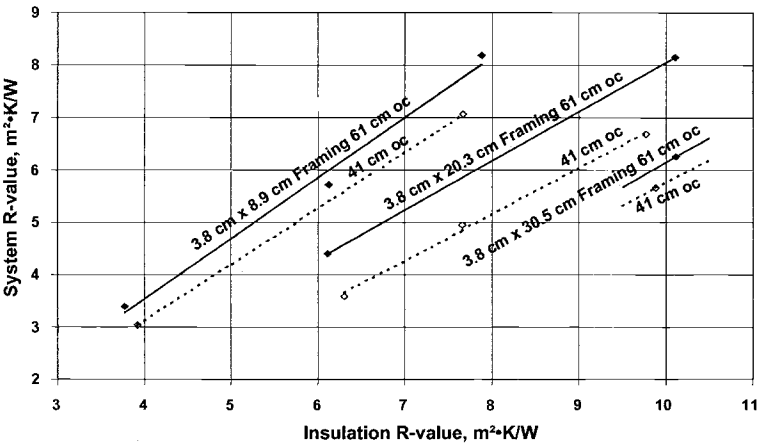

Figure 4. *Test results and trends for simulations of steel-framed joist-and-rafter constructions.*

When results for framing with depths of 8.9 cm, 20.3 cm and 30.5 cm are compared at about the same insulation R-values, the deeper the framing the lower the system R-value. Separation between the straight lines drawn through the data for framing spaced 61 cm oc and 41 cm oc is less for 8.9-cm-deep framing and 30.5-cm-deep framing than it is for 20.3-cm-deep framing. The slopes of the lines for the 20.3-cm-deep framing were used to draw lines through the data with 30.5-cm-deep framing. Differences in slopes among the three framing depths and two spacings are within expected uncertainty. The slight inconsistency in spacing is further discussed in the next section.

Development and Validation of the Computer Model

A finite difference computer code HEATING 7.3 [*3*] was utilized to model sections of steel-framed truss-based and conventional joist-and-rafter attic/ceiling assemblies. The model enabled data to be generated directly from principles of heat transfer for all steel-framed attic/ceiling configurations of interest without the need to interpolate or extrapolate experimental results. Trends that occur as parameters are varied are not subject to experimental uncertainty. In this paper, HEATING results represent "ideal" installation of insulation wherein no gaps exist between insulation and framing. In the field, some gaps will exist with all insulation products. The simulation results give maximum credit for the thermal insulation used in all configurations.

HEATING 7.3 is a multidimensional, general-purpose heat transfer code. Models in it may include multiple materials. The thermal conductivity, density, and specific heat of each material may be both time-dependent and temperature-dependent. Constant properties were used herein but they varied with the type of material and, for validation of the model, with the mean temperature of each layer of fiberglass batt insulation. Experimental values were used for the mean temperatures. HEATING allows boundary conditions that are known temperatures or any combination of prescribed heat flux, forced convection, natural convection, and radiation. For this paper, constant air temperatures were imposed at boundaries with solid materials. Constant values of heat transfer coefficients acted between solid materials and surrounding air.

Computer simulations of conventional joist-and-rafter attic/ceiling configurations were done for framing spaced 41cm oc and 61 cm oc. The joists with various depths were located in the middle of each section. In several cases where insulation with nominal R-values of 3.4 and 5.3 $m^2 \cdot K/W$ was used, steel was exposed above the top layer of fiberglass batts. The area exposed to the air, including both sides of the top flange, caused a severe thermal bridge through the assembly.

In the case of roof trusses, two models were used. One was the same as the conventional joist-and-rafter model for 61 cm oc spacing. In it, 1.22-m-long by 0.61-m-wide sections had only insulation and a steel bottom chord. In the other, 1.22-m-long by 0.61-m-wide sections of attic/ceiling assemblies also contained one, two or three vertical braces. The overall R-value of the truss assemblies was calculated by the following:

$$\frac{1}{R_{overall}} = \frac{fnb}{Rnb} + \sum_i \frac{fb_i}{Rb_i} \qquad (2)$$

where

fnb is the fraction of ceiling area occupied by the non-braced portion of the assembly,

Rnb is the R-value of the non-braced portion of the assembly from HEATING,

fb_i is the fraction of ceiling area occupied by each braced portion of the assembly (i = 1, 2, 3 for one, two or three braces, respectively), and,

Rb_i is the R-value of the each braced portion of the assembly from HEATING.

Very detailed modeling was used to accurately account for the thermal influence of the steel framing, especially the vertical braces. Figure 5 shows, for insulation with R-value of 5.3 $m^2 \cdot K/W$ and a single brace extending vertically from the bottom chord, typical temperature variations throughout the 1.22-m-long by 0.61-m-wide section. For one vertical steel brace, as well as two and three vertical steel braces, the zone wherein

temperatures are disturbed by the braces is smaller than ±0.61 m along the truss from the brace. The 1.22-m-long components used for modeling are long enough that the zones of disturbance from thermal bridges due to braces in adjacent components do not overlap. Therefore, parallel-path R-value calculations are justified for the overall R-value of steel-framed truss assemblies comprised of 1.22-m-long components. The parallel-path approximation is not valid within the components.

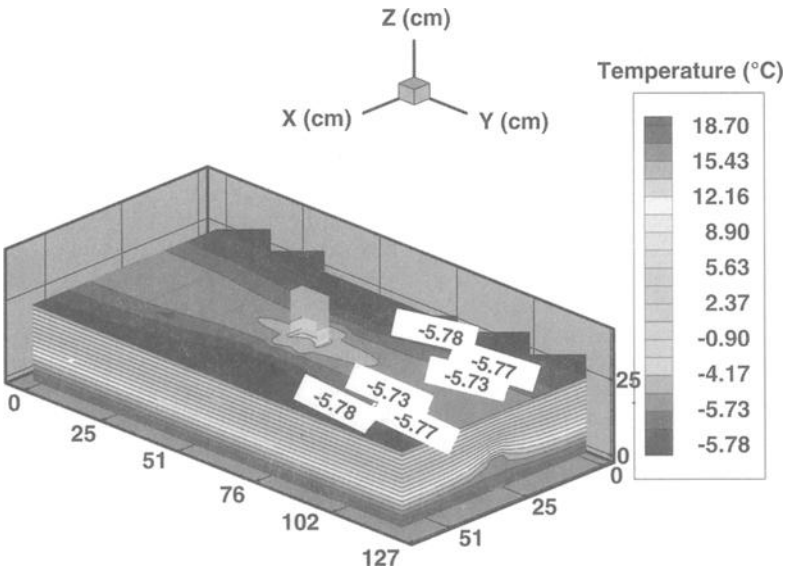

Figure 5. *Detailed temperatures from model of 1.22 m x 0.61 m section of truss with 1 brace penetrating R-5.3 m²·K/W insulation.*

No attempt was made to model the effect of any small gaps between the insulation and framing. Results from the model with no gaps between insulation and framing were compared with results from measurements with as-installed fiberglass batt insulation. See Figs. 6, 7 and 8. It was apparent from these comparisons that uncertainty in the test data masked any effects of the small gaps where the insulation did not conform exactly to the C-shaped steel framing members.

Figures 6, 7 and 8 provide evidence that the model is accurate and produces correct trends as parameters are varied. Direct comparison is made to results at the winter conditions of the tests. Mean insulation temperatures from our ASTM C1363 tests were available for the nominal 8.9-cm-thick layer and the two 15.9-cm-thick layers that were used in the various configurations. Apparent thermal conductivity at these temperatures from our ASTM C518 measurements was imposed in the model.

Figure 6 compares results from the model and the experiments for a simple truss system with one king post in the middle of the span. The comparison is done for the range of insulation R-values from the tests. This is the only truss system that we

simulated experimentally for which there was no doubt that zones of thermal disturbance from vertical braces were inside the metered area and did not overlap. Five spans from 2.4 m to 4.9 m were modeled. Spacing between trusses was 61 cm oc. In the model, these systems are combinations of two components. One is 1.2 m long and has a single vertical brace and R-value equal to Rb_1. The other is long enough to complete the span and has no vertical braces and R-value equal to Rnb. R-value for each component was combined with its respective fractional area for each span using Eq 2.

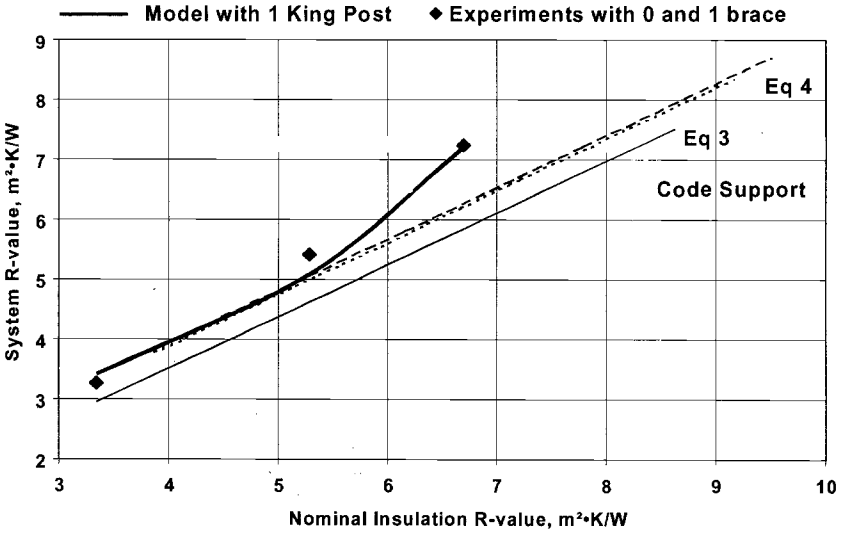

Figure 6. *Comparison of truss system air-to-air R-values averaged over all spans from the experiments and the model with 1 king post.*

The heavy solid curve in Fig. 6 shows the average for all spans from the model. System R-value is less than 2% higher for the longest span and less than 3% lower for the shortest span. The model was configured to yield the thermal resistance from the bottom of the ceiling to the top of the insulation including the effect of the framing. Thermal resistances of the air films measured in the experiments were added to yield the air-to-air system R-values shown for the model. The light lines labeled Code Support are explained in the next section after discussion of Eqs 3 and 4.

Results from the experiments with 8.9-cm-deep framing spaced 61 cm oc are shown as symbols in Fig. 6. The system R-values for the 61 cm oc 0 braces system in Fig. 3 were inserted directly for Rnb in Eq 2. The system R-values for the 61 cm oc 1 brace system in Fig. 3 were interpreted as $R_{overall}$ in Eq 2. Using the 0 brace experimental values as Rnb for a 1.2-m-long component with no braces, Eq 2 was solved for experimental values of Rb_1 for a 1.2-m-long component with one brace. These values of Rnb and Rb_1 were then used to estimate experimental R-values for the five spans with one king post. The average for all five spans at each insulation R-value is plotted.

Figure 6 shows that results from the model agree with the experiments within the uncertainty of measuring system R-values at high insulation R-values. It also shows that a model is very valuable for displaying correct trends when uncertainty masks their display from experiments. If a curve had been drawn on Fig. 6 through the experimental results, it would have shown almost linear increase of system R-value with nominal insulation R-value. We expect what the model shows, that the effect of the single king post on system R-value is less severe as insulation R-value increases. Therefore, system R-value should increase faster than insulation R-value.

Figures 7 and 8 display air-to-air system R-values for joists that are not thermally bridged by braces. Figure 7 is for 61 cm oc spacing and Fig. 8 is for 41 cm oc spacing. Solid symbols show experimental results from test sections wherein the joists were always covered by insulation. An additional open symbol in each figure is from results with an earlier test section constructed to support ASHRAE Technical Research Project 981 [*4*]. In that project, a few tests were done with joists not covered by insulation. That project also addressed effects of connections between joists, rafters and wall top plates.

Results from the model are shown as heavy curved lines in Figs. 7 and 8. For them, the sum of the thermal resistances of the air films above and below the assemblies was the average sum observed in the experiments. The lines are drawn smoothly through the air-to-air R-values that were predicted by the model at the four nominal insulation R-values for each joist depth. Thermal conductivity of the various layers was inserted at the mean temperature of each layer that was observed in the experiments. Modeled system

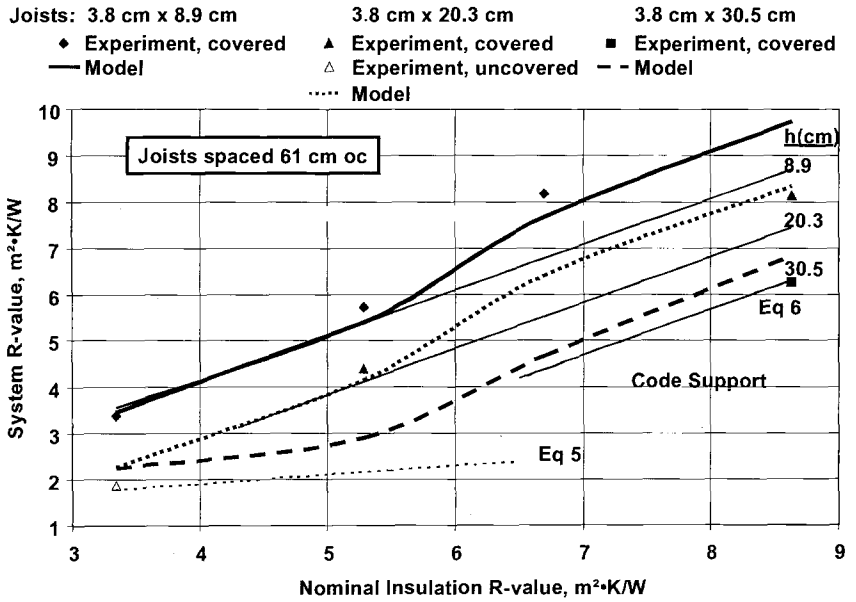

Figure 7. *Comparison of experiment and model for conventional joist-and-rafter steel-framed assemblies with framing 61 cm oc.*

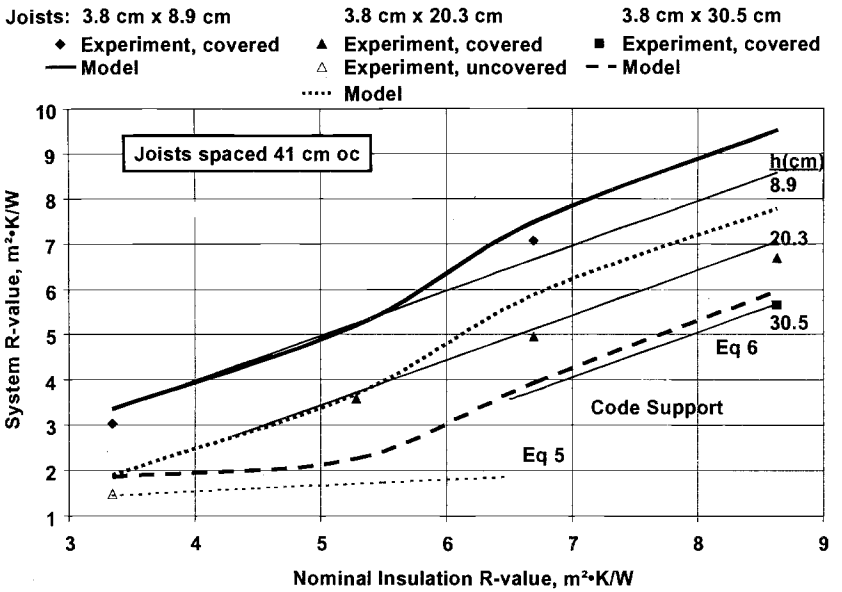

Figure 8. *Comparison of experiment and model for conventional joist-and-rafter steel-framed assemblies with framing 41 cm oc.*

R-values do not vary with nominal insulation R-value as smoothly as expected. However, as expected for a particular insulation thickness and framing depth, the modeled system R-values with framing spaced 41 cm oc are slightly smaller than with 61 cm oc. The light lines in Figs. 7 and 8 labeled Code Support are explained in the next section after discussion of Eq 5 for uncovered joists and Eq 6 for covered joists and the three framing depths, h.

In general, experimental values fall within experimental uncertainty above and below the appropriate curves from the model. The results with 20.3-cm-deep joists spaced 41 cm oc at the nominal insulation R-values of 6.7 and 8.6 m²·K/W are exceptions. Recall that data on Fig. 4 for the 20.3-cm-deep framing spaced 41 cm oc were not consistent with the rest of the data. System R-values for this case are far enough below model values in Fig. 8 to suspect flaws in the insulation configuration.

In the model, the insulation does not always cover completely the 20.3-cm-deep and 30.5-cm-deep framing. The top flange of the 20.3-cm-deep framing is above the R-3.4 insulation (with about 15.9 cm depth). The top flange of the 30.5-cm-deep framing is above both the R-3.4 insulation and the R-5.3 insulation (with about 24.8 cm depth). For uncovered joists, the model predicts a system R-value of about 2.3 m²·K/W for framing spaced 61 cm oc and about 1.9 m²·K/W for framing spaced 41 cm oc at a nominal R-value of 3.4 m²·K/W. These values are slightly higher than the values obtained in the earlier project.

In summary, the system R-values from the model display the expected trends as the insulation R-value and framing configuration are varied. There are enough reliable

test results to confirm that the trends are correct. More importantly, there are enough reliable test results to ensure that system R-values from the model are accurate within experimental uncertainty.

Results with the Model for Support of Codes and Standards

Modeled configurations of attic/ceiling assemblies with steel framing were those that are likely to be built. Since assemblies in the field see both summer and winter conditions, properties were input at room temperature. We used 0.29 $m^2 \cdot K/W$ for the sum of air film thermal resistances and gypsum ceiling thermal resistance. The effect of going from winter to summer conditions is not large. For example, our ASTM C518 measurements on fiberglass batt insulation yielded nominal R-value of 3.4 $m^2 \cdot K/W$ at 24°C. They further showed that R-value of the insulation alone increased to R-3.8 at 4°C (winter conditions) and decreased to R-3.0 at 41°C (summer conditions). The effect of thermal bridges due to steel framing would not have much temperature dependence because the thermal conductivity of steel is very high relative to that of insulation at all temperatures. System R-values are expected to have less temperature dependence than insulation R-values, especially in highly thermally bridged situations.

We analyzed the results keeping in mind what is required to support development of codes and standards. For codes, simple relationships are needed that allow code officials to easily determine compliance. For standards, accurate relationships are needed to allow comparisons among alternatives and support energy efficient use of steel framing.

We addressed only truss systems made from 3.8 cm x 8.9 cm steel framing and installed 61 cm oc. The model showed that system R-value, within ±6%, was described for spans up to 15 m, with the appropriate number of braces, by an average over all spans. The number of support braces per unit length of span was such that thermal bridging did not vary much from the average situation.

We limited analysis of the effects of continuous extruded polystyrene foam insulation between the gypsum ceiling and the bottom chords to thickness from 1.3 cm to 2.5 cm. In this range, system R-value with foam insulation was 1.05 to 1.10 times the R-value of a system with the same amount of insulation R-value but with all of the insulation between and over the bottom chords. The continuous foam insulation made the extent of the thermal bridging slightly less severe in the fiberglass insulation. Temperature changes in the attic insulation due to the foam insulation and their effects on system R-value were neglected to approximate average behavior over all seasons.

The following equations describe air-to-air system R-values of truss systems made from 3.8 cm x 8.9 cm cold-formed-steel framing installed 61 cm oc. With no extruded polystyrene foam insulation between the ceiling and the bottom chords,

$$R_{system} = 0.864 \cdot R_{insulation} + 0.0581 \quad (3)$$

With 1.27 cm to 2.54 cm of foam insulation between the ceiling and bottom chords,

$$R_{system} = 0.864 \cdot R_{insulation\ (including\ foam)} + [\,0.36 + 0.050 \cdot t] \quad (4)$$

where

R_{system} is the air-to-air system R-value, in $m^2 \cdot K/W$,

$R_{insulation}$ is the nominal insulation R-value, including R-value of the foam insulation if present between the ceiling and bottom chords of the trusses, in m²·K/W, and,

t is the thickness of the foam insulation if present, in cm.

The system R-value from these equations is plotted in Fig. 6 against insulation R-value, including R-value of the foam insulation if present. Fiberglass insulation R-values were as high as 8.6 m²·K/W. Hence, insulation R-values for the equations extend to higher values than they do for the results of the truss tests and model validation on Fig. 6. The latter had lower depths of fiberglass insulation and no foam insulation. Equation 3 gives results that are conservative relative to results at winter conditions from the tests and model. This is desirable for year-round applications.

Two lines are shown for Eq 4. The short-dashed line is for 1.3-cm-thick foam insulation. The long-dashed line is for 2.5-cm-thick foam insulation. Thicker foam insulation does not improve system R-value very much at a particular value of total insulation R-value compared to the significant improvement from the situation with no foam insulation that is shown by the solid line for Eq 3. The 1.3-cm-thick foam insulation is thick enough to break the thermal bridges. Once continuous insulation breaks thermal bridges, more thickness adds little more than its R-value to the system R-value.

For conventional joist-and-rafter systems, 3.8-cm-wide steel framing with depths of 14.0 cm, 20.3 cm, 25.4 cm and 30.5 cm are of interest. We added 8.9-cm-deep framing because of its use for trusses. Spacings of interest are 41 cm, 49 cm and 61 cm oc. The usual situation is to cover the joists completely with insulation. However, it is possible that some attic applications call for joists that protrude beyond the insulation despite the severe thermal bridges that result when parts of the joists are exposed to attic air temperatures. This is a common situation for floors, for which parts of the joists are often exposed to more moderate basement or crawlspace air temperatures.

The need to address joists covered by insulation and joists not covered by insulation complicates development of codes and standards. The relationship between system R-value and insulation R-value is different for the covered and not covered situations. Also, a decision must be made about which situation is true for a particular application.

The amount of insulation that is installed is usually specified by R-value. In addition to R-value, the thermal conductivity or thermal resistivity is needed in order to estimate the installed thickness. For the fiberglass batt insulation used in the tests for this project, nominal thermal conductivity is 0.047 W/(m·K). To cover an 8.9 cm-deep joist requires R-1.9 m²·K/W. To cover a 20.3-cm-deep joist requires R-4.3 m²·K/W. To cover a 30.5-cm-deep joist requires R-6.5 m²·K/W.

The following equations describe air-to-air system R-values of conventional joist-and-rafter systems made from 3.8-cm-wide cold-formed-steel framing. Joist depth can range from 8.9 cm to 30.5 cm. Spacing can be from 41 cm oc to 61 cm oc. If the insulation thickness is such that parts of the joists are uncovered, the following relationship applies:

$$R_{system} = [0.00374 \cdot s - 0.028] \cdot R_{insulation} + [0.00295 \cdot s + 0.923] \quad (5)$$

If the insulation thickness is such that the joists are completely covered by insulation, then

$$R_{system} = 0.993 \cdot R_{insulation} + [0.00113 \cdot s - 0.180] \cdot h + [-0.00338 \cdot s + 1.333] \quad (6)$$

where

R_{system} is the air-to-air system R-value, in $m^2 \cdot K/W$,

$R_{insulation}$ is the nominal R-value of the insulation, in $m^2 \cdot K/W$,

s is the spacing between adjacent joists, in cm, and,

h is the depth of the joists, in cm.

Figures 7 and 8 include the straight lines that these equations produce when values for the relevant parameters are inserted. The dashed line for Eq 5 at all values of joist depth and the solid line for Eq 6 at joist depth of 30.5 cm that are drawn on both figures clearly illustrate the abrupt change in system R-value that is implied by these equations. A 30.5-cm-deep joist undergoes the transition from being uncovered to being covered near an insulation thickness corresponding to R-6.5 $m^2 \cdot K/W$ for the insulation used in the tests. The curve for the model of the 30.5-cm-deep joist was drawn smoothly between predictions made at the four nominal insulation R-values of 3.4, 5.3, 6.7 and 8.6 $m^2 \cdot K/W$. Modeling for a typical case at additional R-values above and below the insulation R-value for the transition showed that the system R-value change is indeed gradual. Using the low values from Eq 5 should discourage the practice of exposing steel framing beyond insulation. The values from Eq 6 for covered joists at nominal conditions are conservative with respect to the modeled values at winter conditions with high levels of insulation. This is desirable for year-round applications.

Conclusions

Experiments have been performed to assess the impact of cold-formed-steel framing on the thermal performance of attic/ceiling assemblies. Test configurations duplicated features of full-sized, truss-based and conventional joist-and-rafter assemblies away from the edges of the ceiling. Steady-state tests were done at winter conditions in a climate simulator. In truss systems, strong thermal bridges due to framing members that penetrated through the insulation to the bottom chords persisted as the insulation level increased. Without penetrations, the effect of steel framing eventually disappeared as insulation level was increased. For negligible effect of the framing, framing spaced 41 cm oc required greater insulation depth than did framing spaced 61 cm oc. Without penetrations but with enough insulation to cover framing with depths of 8.9 cm, 20.3 cm and 30.5 cm, greater framing depth yielded slightly poorer thermal performance. A continuous layer of extruded polystyrene foam was placed between the C-shaped bottom chords of trusses and the gypsum board ceiling for a few tests. System R-values improved by slightly more than the R-value of the foam insulation.

A three-dimensional model of the thermal behavior of the assemblies was validated by direct comparison with the test results. Agreement between model and experiment was generally within experimental uncertainty. The model showed trends due to effects of parameter variations more consistently than the test data. The model allowed us to extend the test results to the entire range of cold-formed-steel-framed attic/ceiling configurations. Four linear equations were generated to summarize all results. Two reflected the behavior of truss systems with and without foam insulation between the ceiling and the bottom chords of the trusses. Two reflected the behavior of joist-and-rafter assemblies away from edges when the joists were not covered by insulation and when they were. The equations can be the basis for changes in codes and standards that

reflect the effect of steel framing on the thermal performance of attic/ceiling assemblies and discourage allowing steel framing to extend beyond the insulation.

Acknowledgment

This paper was prepared by the Buildings Technology Center at the Oak Ridge National Laboratory, Oak Ridge, Tennessee. The Oak Ridge National Laboratory is managed by UT-Battelle, LLC for the U.S. Department of Energy under contract No. DE-AC05-00OR22725. The American Iron and Steel Institute provided technical assistance, construction materials and funding. Owens-Corning Corporation's Science and Technology Center provided additional technical assistance and construction materials.

References

[*1*] 2001 ASHRAE Handbook Fundamentals, "Calculating Overall Thermal Resistance; Constructions Containing Metal; Zone Method of Calculation; Modified Zone Method for Metal Stud Walls with Insulated Cavities; Ceilings and Roofs," American Society of Heating, Refrigerating and Air-Conditioning Engineers, Inc., Atlanta, GA, 2001, pp. 23.8, 25.9-25.12.

[*2*] Wilkes, K. E., Petrie, T. W., and Childs, P. W., "Precision and Bias of the Large Scale Climate Simulator in the Guarded Hot Box and Cold Box Modes," *Thermal Conductivity 23, Proceedings of the Twenty-Third International Thermal Conductivity Conference,* K. E. Wilkes, R. B. Dinwiddie and R. S. Graves, Eds., Technomic Publishing Company, Lancaster, PA, 1996, pp. 395-406.

[*3*] Childs, K. W., "HEATING Users' Manual," Report ORNL/TM-12262, Oak Ridge National Laboratory, Oak Ridge, TN, 1993.

[*4*] Steven Winter Associates, Inc., "Thermal Performance of Cold-Formed Steel Ceiling/Roof Framing Assemblies," Final Report on ASHRAE Research Project 981-TRP, Submitted to American Society of Heating, Refrigerating and Air-Conditioning Engineers, Inc., Atlanta, GA, July 1999.

John R. Mumaw[1]

A Test Protocol for Comparison of the Moisture Absorption Behavior of Below-Ambient Piping Insulation Systems Operating in Hot-Humid Environments

Reference: Mumaw, John R., "**A Test Protocol for Comparison of the Moisture Absorption Behavior of Below-Ambient Piping Insulation Systems Operating in Hot-Humid Environments,**" *Insulation Materials: Testing and Applications: 4th Volume, ASTM STP 1426*, A. O. Desjarlais and R. R. Zarr, Eds., ASTM International, West Conshohocken, PA, 2002.

Abstract: The value of adding insulation to piping systems operating at below ambient temperatures has been demonstrated by many successful installations. For other systems operating at these temperatures, the adverse impact of moisture migration into the insulation system during operation has caused many premature failures. The objective of this paper is to propose a standard test protocol for evaluating an insulation system's moisture adsorption response when exposed to a design combination of ambient temperature and relative humidity. Test results, developed using this protocol, for eight chilled water piping insulation systems are presented and compared to simplified model results.

Keywords: Piping, Insulation, Moisture, Below Ambient, Hot-Humid Environment

Introduction and Objective

Background

Most industrial and commercial buildings contain process piping and equipment that requires the installation of an insulating system to isolate those process systems from the environment. A majority of the process systems operate at temperatures that are greater than that of their surroundings. Equipment and piping systems of this type require insulation systems that reduce heat loss, increase system durability, provide personnel protection, provide freeze prevention, and provide ease of installation, maintenance and repair. However, a significant number of process systems are operating at temperatures below the ambient temperature. These include: air conditioning ducts, refrigeration and freezer rooms, gas liquefaction, chilled water piping, and refrigeration equipment. Design goals for these systems include: 1) energy efficiency; 2) personnel protection; 3) reduced surface condensation; 4) extended service life; but also, 5) ease of installation, maintenance and repair. Some of the process systems, for example, air distribution ducts,

[1] Manager, Global Insulation Standards, Owens Corning, 2790 Columbus Road, Granville, Ohio 43023

operate a portion of the year below the ambient, but may also operate a portion of the year at temperatures above the ambient. These systems have a chance to drive off any moisture that has accumulated during the cold cycle operation. Many cold systems, especially distribution lines carrying chilled brine or water, operate at below ambient conditions for months, if not years, without exceeding the ambient temperature. For these systems, the vapor flow is unidirectional, and these are the systems that need special design consideration.

The successful insulation system must deal with the unidirectional vapor drive by either a) providing a continuous and effective vapor retarder to limit the quantity of water vapor flowing to the equipment surface or b) providing a means to remove the condensed water. Traditionally, most designs have utilized a low permeance vapor retarder and/or a low permeance insulation material in conjunction with appropriate sealants and tapes to minimize the water vapor flow.

Objective and Approach

The overall objective of the original research project was to develop relative performance data on several insulation systems operating at below ambient temperatures. The approach involved fabricating samples of a number of insulation systems and exposing these samples to controlled environmental conditions for an extended period of time. The samples were periodically weighed to quantify the amount of water gained.

The objective of this paper is to propose a test protocol for use in determining the relative performance of insulation systems on pipe operating at sub ambient temperatures in hot humid environments. This protocol was developed as a sub-objective of the research program. Two significant sub-objectives were accomplished in the course of this work. These steps included:

1. Developing a "standard" test section that was representative of piping insulation systems in general, and yet simple enough to be easily handled and reproduced.

2. Developing a measurement procedure that allows discrimination between the various systems tested.

This paper presents a summary of the information gained in this portion of the overall project. Some experimental data is also presented that demonstrates the usefulness of the experimental protocol. The report on the experimental results of the original test program is available **[1].**

Experimental Design and Equipment

Test Module Design and Assembly

For an experiment to provide results that are representative of actual installations, the insulation system must be installed in the same fashion as in the field. Installations should be representative from both a dimensional and operational manner. To accomplish this, each insulation specimen must be assembled in a reproducible facility called a test

module. For our tests, the module is assembled on a section of 1 inch (25 mm) nominal diameter copper tubing. This size copper tubing was chosen for several reasons. One, it represents a size used extensively for below ambient systems. Two, it provides a sample small enough to handle easily, yet large enough to absorb sufficient moisture from the environment to be measurable. And three, the copper tubing provides excellent thermal conductance to the coaxial, stainless steel test module support tube which is the source of sample cooling. Details for the specimen assembly are presented in Figure 1. Note that the end caps are made of 0.13 inch (3 mm) inch plastic sheet. This material provides a good seal to the moisture and yet reduces the condensation on the end-cap surface.

Once the insulation material has been pre-conditioned in the laboratory, the assembly of the test specimen begins. The insulation is assembled, following the manufacturer's instructions such that there is a single butt joint in the system at the center of the 36-inch (0.91 m) specimen and at least one lateral joint passing for the entire length. For insulation systems having multiple layers, the joints are staggered but at least one butt joint is required for each layer. Note that for some systems, the manufacturer recommends the application of joint sealant directly to the internal surface of the pipe insulation prior to its application. This effectively glues the insulation directly to the pipe surface. For those systems requiring sealant at the joints, the sealant was also applied at the end cap locations. For all systems, a second end cap was installed at the opposite end of the tube and sealed in place so the total insulated system measures 36 inches (0.91 m) in length. Finally, when the vapor retarder is in place, the ends of the vapor retarder surface are sealed to the end caps using silicone caulk. This completes the assembly of a test module. After conditioning for several days in the laboratory to ensure cure of the mastics and caulk, the modules are weighed and ready for installation on the test support facility. An example of an assembled module is presented in Figure 2.

Test Module Support Facility

The support facility is intended to support the test modules in such a fashion that they are all exposed to the same environmental conditions. The supports for the test modules must be cooled to a temperature that permits the inside tube of the test modules to be cooled to the desired pipe operating temperature. The rack must have uniform flow through each support so uniform temperatures can be maintained at each position.

Our test module support rack, Figure 3, consists of 16 parallel tubes mounted on a steel support rack measuring approximately 6 feet (1.83 m) high and 40 inches (1.02 m) wide. Figure 4 provides a view of one of the 44 inch (1.12 m) long stainless steel support tubes that are the source of cooling and are spaced in a stacked pattern so that the insulated modules are spaced approximately 11 inches (0.28 m) apart. This permits adequate airflow between and around the test modules.

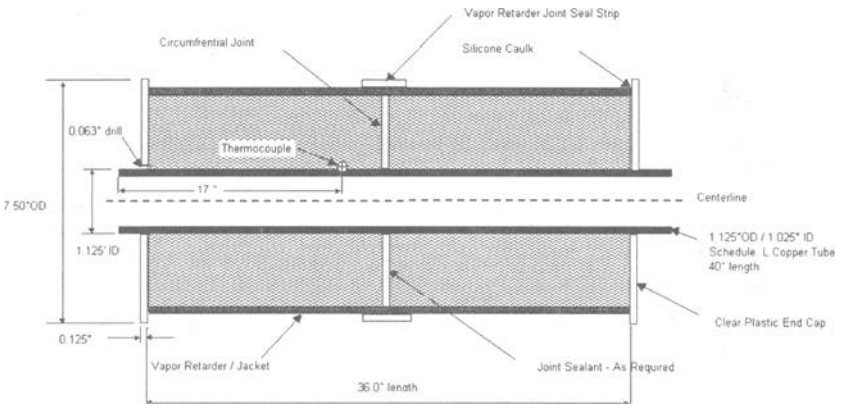

Figure 1 – *Insulated Test Module – Section View*

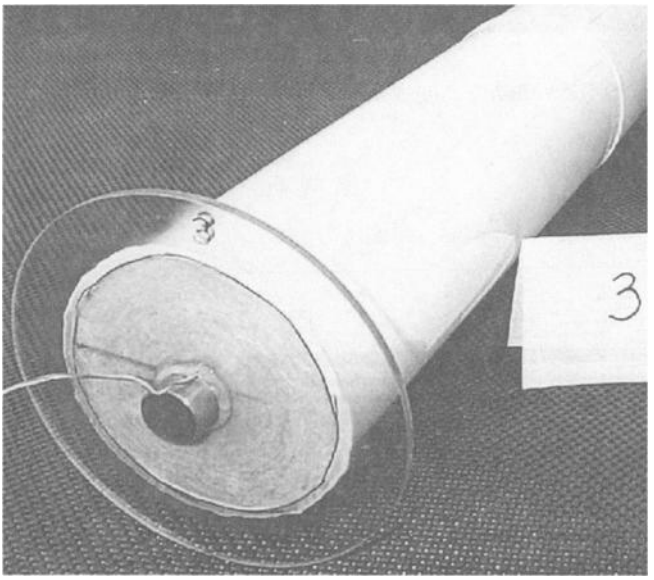

Figure 2 – *An Example of an Assembled Test Module*

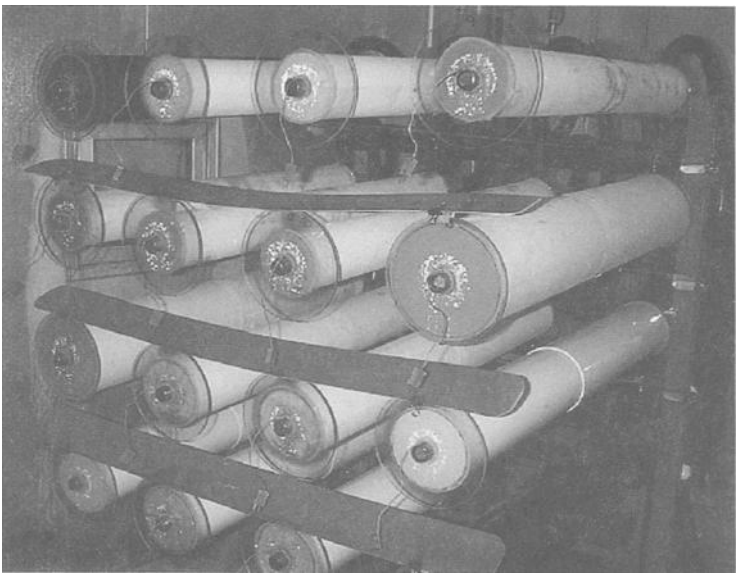

Figure 3 – Test Module Support with Specimen Modules Installed

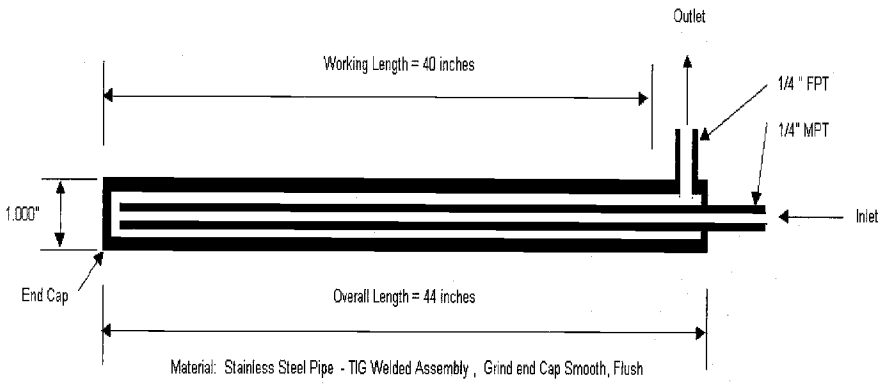

Figure 4 – *Test Module Support Tube – Section View*

A manifold connects the chilled water supply to the tube banks on the support structure. The assembly is fabricated so that the water enters the center tube, passes to the other end and then returns to the outlet installed near the original entry. With this configuration, the end of the tube support is cooled to the operating temperature and the overall end to end temperature difference is very small. The external diameter of the support provides a tight fit to the test module tube, but permits easy removal of the test modules for weighing.

One caution must be observed during design of the support facility. If, during the conditioning condensation occurs on the surface of a specimen, then precautions (end wings in Figure 3) must be in place to insure that the condensation from the tube ends does not drip onto adjacent specimens.

Cooling Facility - Cold Water Supply

The supply of cooling fluid, usually a mixture of antifreeze and water, is pumped through the stainless steel pipe modules by a refrigerated recirculator. For our experiment, the unit provided water at 34 °F +/- 0.2 °F (1 °C +/- 0.1 °C) at a flow rate of approximately 10 gpm (38 l/m) at 40 psi (273 kP). This flow rate coupled with the 15 gallon (57 liter) reservoir provides excellent temperature stability during the testing.

Conditioning Facility – Environmental Chamber

A large temperature and humidity controlled room is required to provide the conditioning environment for these tests. The dimension required for this facility is a function of the number of specimens to be tested at one time. Our room provided a clear 12 by 12 by 11 foot (3.7 by 3.7 by 3.4 m) interior chamber dimension for testing. Repeated monitoring of the room temperature and humidity during the conditioning will show the uniformity of the control. For our experiment, the temperatures, measured in the proximity of the test frame, were within ±1.0 °F (0.5 °C). Relative humidity control was demonstrated to be about ±4% RH)

Insulation Thickness Determination

The selection of the test thickness for each insulated system is based upon a calculation of the expected operating surface temperature. The design criterion is to avoid condensation on the outer surface of the insulation systems. In other words, the calculated surface temperature must be above the dew point temperature of the environmental chamber air. All specimens must begin the test with a dry surface condition. If changes to the conductivity of the system after installation caused condensation to form at the surface, then that should be part of the conditioning process.

A computer program that conforms to the ASTM Practice for the Determination of Heat Gain or Loss and The Surface Temperatures of Insulated Pipe and Equipment Systems by the Use of a Computer Program (C 680) was used to determine the surface temperature of the piping systems as a function of its operating conditions, the insulation thermal properties and the significant dimensions. To compensate for variations in apparatus control, the design temperature conditions used for specifying the insulation

thickness can be adjusted to account for the anticipated variations. The local air velocity chosen for the calculation was 0 mph. Thermal conductivity values used for the thickness design should come from the available product literature, when available, or from those values found in existing ASTM Product Specifications. Adjustments for available sizes and thicknesses must be made during the selection process so that the actual product thickness, when accounting for ASTM Specification dimensional tolerance around the nominal thickness, is equal to or greater than the minimum calculated thickness.

Measurements and Data Analysis

Measurement Protocol

The objective of this experimental procedure is to measure the absorption of moisture into the operating insulation system as a function of time. The frequency of measurement is determined from test results obtained as the samples are exposed. If the weight gain is rapid, measurement frequency should be increased. If gains are slow, the frequency can be extended. Based on some initial testing done on similar systems, the frequency of our measurements was fixed at seven days. Since the weight change for most samples was small, this frequency was adequate to record the changes. The established weighing procedure was followed for each specimen. Each specimen was removed from the rack to be weighed and, at the same time, visually observed. After measurement and examination, the specimen was returned to the conditioning rack and the next specimen was examined. For our experiments, the total time to remove, measure and return each specimen averaged about 5 minutes.

Specifically, the measurement procedure to be used for each specimen were as follows:

a) remove a specimen from exposure rack;
b) wipe dry the interior of the copper tube;
c) cap the open ends to prevent additional condensation;
d) wipe dry the end guard areas;
e) weigh the specimen to the nearest gram;
f) wipe dry any specimen surface condensation, if any, from specimen;
g) weigh again, if necessary;
h) remove end caps and replace on the exposure rack;
i) Note that any weight should not include the weight of the end caps.

Adjustment of Exposure Positioning

One concern with the rack setup for the specimens was the variation of exposure caused by the close proximity of the adjacent specimens. To overcome this concern, each specimen was moved to a new position after weighing. All the specimens were moved after weighing in a similar pattern. With this rotation, all specimens were cycled through all the positions during the ninety-day period of testing. Thus, all specimens were exposed to the same conditions.

Expected Results

Model Development

Whenever an experimental program is undertaken, there is the need to look at the experiment using the available modeling tools to see if the experimental results make technical sense. For this procedure, a model is used in an attempt to understand the important parameters influencing the level of moisture accumulation. The physical model for moisture is similar to that used to describe the heat transfer through the system. The difference for the moisture calculation is that the driving force is the vapor pressure gradient across the system and the resistance to moisture flow is related to the water vapor permeability of the materials. Since our test module is a straight piece of pipe, the geometry of the model can be a simple one-dimensional moisture transfer in the radial direction. One simplifying assumption of the moisture model is that the moisture accumulated at the pipe surface is assumed to stay at that surface and not migrate into the insulation. A second assumption for this model is that the moisture flow is caused only by diffusion. This neglects the effects of leakage through joints and seals. The impact of these assumptions is that the model underestimates the total moisture flow for real systems. The basic form of one model is given in Equation 1 below.

$$m = \frac{2 \bullet \pi \bullet L \bullet \Delta P}{\sum_{i=1}^{i=n} [\ln(r_{i+1} / r_i) / K_i]} \qquad (1)$$

where:

m	=	flow rate, (grains / hour)
r_n	=	system outside radius, inches
r_i	=	layer inside radius, inches
r_{i+1}	=	layer outside radius, inches
n	=	number of layers
K_i	=	layer water vapor permeability,(grains inch / hr ft^2 inHg)
ΔP	=	water vapor pressure gradient, (in Hg)
L	=	length of the pipe system, feet

Note that the model is dependent upon each layer's thickness, moisture permeance and water vapor pressure drop. By multiplying the model result by the length of the test module and the time of exposure, an anticipated total moisture accumulation over time can be estimated. It is also important to note here that the model only assumes continuous layers of different materials. The predicted performance neglects any joint failure, cracks, sealers or other accessory factors found in a real system.

Moisture Model Results

Using the model above and the vapor permeance properties for the insulation and jacketing materials provided by ASHRAE [2] and the applicable ASTM material

specifications, the estimated moisture accumulation over a 90 day period was calculated for our test conditions. (See Table 1, Column 2) Note that the moisture accumulation for most of the systems is relatively small. However, the ASTM Test Method for Water Vapor Transmission of Materials (E 96) "dry cup" properties of the jacketing materials were used in these calculations. Exercising the model a second time, but using the "wet cup" properties shows a significant increase in the predicted moisture flow. (See Table 1, Column 3). A comparison of the two sets of results shows predicted differences as great as 6 times. Clearly, the selection of material vapor permeance properties is significant to the amount of predicted moisture.

A review of Table 1, Column 3 shows that the estimated moisture accumulation for our test systems during the ninety day test period ranges from virtually zero (for the cellular glass system) to nearly 102.

Table 1 - Comparison of Predicted and Experimental Moisture Gain For a 36 inch Insulation Section Operating at 35 °F in a 90 °F / 90% RH Environment after 90 Days

Sample	Predicted Weight Gain Dry Cup, g	Predicted Weight Gain Wet Cup, g	Measured Weight Gain, g	Specimen to Specimen Test Variation (percent of average)
1	3	4	60	133
2	3	4	37	40
3	5	5	87	17
4	13	79	60	50
5	12	60	150	27
6	10	37	288	50
7	0	0	35	29
8	16	102	273	97

Experimental Program Results

The test insulation systems were selected to represent a cross section of insulation systems used throughout the insulation industry. Note that for each sample, two identical specimens were constructed and tested. This was intended to allow a rough estimate of the variability of the measured results. (See Table 1, Column 5). Each system was assembled using accessories recommended by the manufacturer of the particular insulation material and supplied by their local fabricator.

Selected Test Conditions

The conditions for our tests were intended to be "realistic" yet provide for an accelerated exposure for the tested systems. For this purpose, the fluid temperature circulated to the cold piping was selected to be that required to maintain the insulated

pipe surface at 35 °F (1.7 °C). During the experiment, the thermocouples located at the pipe surface were monitored to insure that the proper temperature was maintained.

For the test chamber environment, the exterior exposure condition was specified to be a constant 90 °F (32.2 °C) and 90% relative humidity. This condition was selected to be a "worst case" condition in order to maximize the vapor drive to the cold surface. For this experiment, no attempt has been made to correlate this exposure to real, in service conditions other than to say that this exposure should be more severe than seen in most applications, including US Gulf Coast exposure.

Testing was completed over a three-month period of time between May 2000 and August 2000.

Moisture Gain Results

Figure 5 presents a plot of the average moisture accumulation versus time. For this figure, the average moisture accumulation of the two identical specimens is plotted. Note that all of the specimens showed a measurable weight gain. Measured values after 90 days conditioning for the individual specimens ranged from a low of 20 grams to 405 grams.

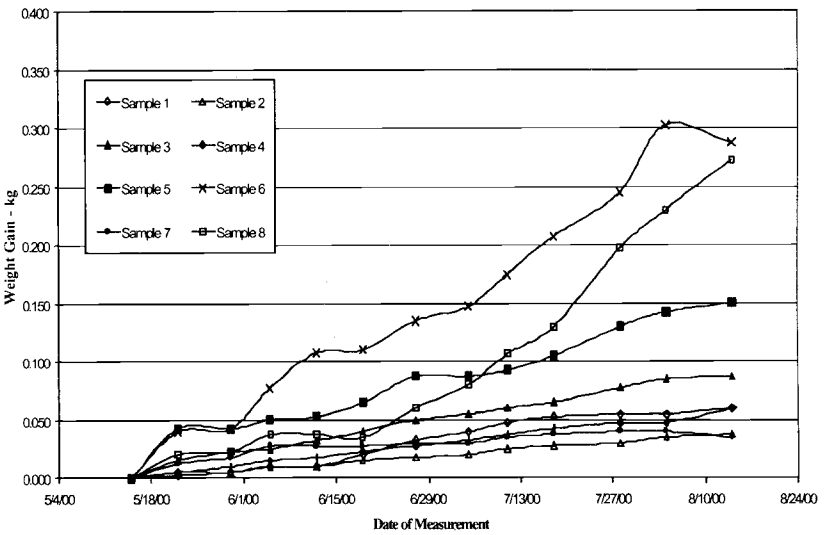

Figure 5 - *Average Specimen Weight Gain vs. Time of Exposure*
For a 36" long, 35 °F Pipe at 90 °F / 90% RH after 90 Days

A comparison of expected and measured moisture can be made from the data in Table 1, Columns 3 and 4. In all cases, the observed moisture accumulation was significantly larger than that predicted by the simple model. This fact is not surprising since the simplified model does not account for known leakage paths such as longitudinal joints, butt joints, and lap seals in the vapor retarders. There was also a significant difference in

moisture gain between specimens of the same material system. (See Table 1 Column 5). This shows the difficulty in fabricating repeatable specimens. It should be noted that all specimens were prepared using laboratory assembly techniques that followed the manufacturer's recommended instructions. From the standpoint of workmanship, we believe that the assembly techniques used were probably better than typical installations found in the field.

Physical Examination

In addition to the changes in weights during the conditioning period, physical observations during and after conditioning are important in understanding the test results. Photographs should be taken during the exposure to document the testing. Photographs taken during the specimen assembly and the post-test dissection are also helpful. For our experiments, the specimens were dissected at the end of the ninety-day exposures in an attempt to understand what changes had occurred in the systems that might explain the weight gain results. Our observations included: discoloration of the foam insulation due to moisture penetration; changes to the sealant material such as water absorption and lack of curing; location of moisture accumulation and shrinkage of the insulation material away from the joints.

Conclusions:

The results obtained and reported have demonstrated the success of this test protocol in discriminating between alternate insulation systems. The results also show that additional work remains (possibly at other laboratories) to improve this protocol. It is obvious from the experiments described that many questions remain. The following is a brief list of several areas that must be researched before this method can be fully implemented.

1. The precision and repeatability of this protocol must be defined by additional testing on specimens similar to those used in this report.
2. The experimental work should be repeated on other systems used for below ambient conditions in hot humid environments.
3. This study should be extended to other temperature, humidity and exposure time conditions to prove the applicability of the results at a range of conditioning combinations.
4. An improved model that attempts to include some treatment of the joint and seal leakage should be developed and verified.

BIBLIOGRAPHY AND REFERENCES

[1] Mumaw, J.R., "Below Ambient Piping Insulation Systems", *Insulation Outlook*, National Insulation Association, September 2001, pp. 19-30.
[2] "Thermal and Water Vapor Transmission Data", *ASHRAE Fundamentals Handbook – Chapter 22*, American Society of Heating , Refrigeration and Air Conditioning Engineers, 1993.

Session 4: Building Systems II

Shanzhong Yuan, [1] G. Albert Russell, [2] and William P. Goss [2]

Uncertainty Analysis of A Calibrated Hot Box

REFERENCE: Yuan, S., Russell, G. A., Goss, W. P., "**Uncertainty Analysis of a Calibrated Hot Box,**" *Insulation Materials: Testing and Applications: 4th Volume, ASTM STP 1426*, A. O. Desjarlais and R. R. Zarr, Eds., ASTM International, West Conshohocken, PA, 2002.

ABSTRACT: The accuracy of the thermal transmittance, or U-factor, of a fenestration system measured in a building assembly thermal test facility depends upon the test apparatus, test conditions, operating procedure, and the specimen properties. By conducting the uncertainty analysis of a specific thermal test facility, the measurement uncertainty can be identified and quantified. The estimation procedure for the uncertainty associated with the U-factor result for a test apparatus should be established and reported with the measurement of the U-factors of fenestration products. In a study on the University of Massachusetts Research Calibrated Hot Box, detailed analyses of the elemental uncertainties associated with the basic measurements and uncertainty propagation on U-factor results have been performed. In the analysis of uncertainty propagation, the Root Sum Square (RSS) method was used extensively. The procedure for uncertainty analysis used for this test apparatus can be used in any ASTM C 1363 hot box thermal test facility including those also using ASTM C 1199 for fenestration U-factor measurements. Using the uncertainty analysis procedure described in detail in this paper, a plastic-faced Calibration Standard Transfer (CTS) is analyzed. The results show a reasonable uncertainty level for the U-factor measurement made using ASTM C 1199. The improvement of the U-factor uncertainty can be achieved by reducing the uncertainties associated with the test specimen flanking heat transfer and the metering chamber extraneous heat transfer in the hot box test apparatus.

KEYWORDS: calibrated hot box, uncertainty, fenestration, thermal transmittance, thermal test, measurement, heat transfer, thermal transmittance, thermal resistance, extraneous heat transfer

[1] Director of Thermal and Materials Testing Labs, ETC Laboratories, Inc., 297 Buell Road, Rochester, NY 14624.

[2] Professor Emeritus, Department of Mechanical and Industrial Engineering, University of Massachusetts, Amherst, MA 01003.

Nomenclature

A_S Specimen projected area (m^2)
A_{SP} Surround panel projected area (m^2)
H_S Specimen height (m)
H_{SP} Surround panel height (m)
k Thermal conductivity (W/m·K)
k_{SP} Surround panel thermal conductivity (W/m·K)
L Thickness, depth (m)
L_S Specimen thickness (depth) (m)
L_{SP} Surround panel thickness (depth) (m)
P Confidence level (%)
Q_{EXTR} Extraneous heat transfer in the metering chamber (W)
$Q_{FL,S}$ Specimen flanking heat transfer (W)
Q_{IN} Total power input to the metering chamber (W)
Q_S Heat transfer through the test specimen (W)
Q_{SP} Heat transfer through the surround panel (W)
R Dependent variable
s_y Sample standard deviation of measured values of variable y
t Temperature (°C)
t_{AMB} Ambient air temperature (°C)
t_c Cold side (climatic chamber) air temperature (°C)
t_h Warm side (metering room) air temperature (°C)
$t_{v,P}$ t value of v's degree of freedom and P's confidence level
U_{CTS} CTS thermal transmittance ($W/m^2 \cdot K$)
U_S Specimen thermal transmittance ($W/m^2 \cdot K$)
U_{ST} Standardized specimen thermal transmittance ($W/m^2 \cdot K$)
V *Metering chamber wall thermopile voltage (mV)*
W_S Specimen width (m)
W_{SP} Surround panel width (m)
x_i Independent variable, $i = 1, 2, \ldots, N$
y_c Calculated value of dependent variable y
z Independent variable
$\theta_{me,sur}$ Surround panel mean temperature (°C)
σ Stefan-Boltzmann constant, 5.669×10^{-8} ($W/m^2 \cdot K^4$)
Δ Uncertainty, difference
δt Temperature difference (°C)
δt_{hc} Air temperature difference between warm and cold side chambers (°C)
∂ Partial derivative
v Degree of freedom
δt_{SP} Surround panel surface temperature difference (°C)

Symbols [Superscripts]
$\bar{}$ Average value (mean)

Introduction

Uncertainty analysis, as defined by Kline and McClintock [*1*] and Airy [*2*], refers to the process of estimating the effect of uncertainties in individual measurements on the final calculated experimental result.

Due to economic and time constraints, in most engineering experiments it is not practical to statistically estimate the overall measurement uncertainty. Experiments in which the uncertainty is not found by repetition are called single-sample experiments. Several engineering experimentation textbooks (e.g., [*3-5*]) present the basic methods of uncertainty analysis and discuss their importance in planning, evaluating and reporting experiments. Moffat [*6-8*] explored many aspects of the techniques of single-sample uncertainty analysis. A more general discussion on uncertainty analysis is given in Yuan [*9*].

According to Moffat [*7*], and Kline and McClintock [*1*], the value of a variable is specified by giving the mean of the readings and an uncertainty interval at a particular confidence level. The uncertainty propagation from variables to result may be analyzed by the method of the second power equation presented by Kline and McClintock [*1*]. Moffat [*7*] refers to this technique as the "Root-Sum-Square" (RSS) method. Using the RSS method (sometimes called "quadrature addition"), the propagation of uncertainty can be analyzed for a specific measurement facility and test procedure. Large uncertainties in any of the measured variables result in large uncertainties of the final calculated result. Therefore, a reduction in a larger uncertainty is far more important than the same percent reduction in a smaller uncertainty. Thus, uncertainty analysis is a useful tool for the selection of instrumentation [*1*].

Uncertainty analysis of thermal tests for fenestration systems have been carried out by Klems [*10*], Harrison and Dubrous [*11*], and Elmahdy [*12*] who presented methods for determining the uncertainty of U-factor measurements for their specific test facilities. Van Dijk [*13*] proposed a guidance of uncertainty analysis based on ISO Test Method: Thermal Insulation – Determination of Steady State Thermal Transmission Properties – Calibrated and Guarded Hot Box (8990) for "an idealized situation: the uncertainty when measuring a homogeneous specimen".

This paper presents detailed analysis procedures for the estimation of the uncertainty of Hot Box tests using the current ASTM and ISO Hot Box fenestration test method. It should be noted that the uncertainty analysis procedures presented here applies to all chamber designs (Guarded, Calibrated or Hybrid). The only difference would be in the magnitude of the uncertainty components and the instruments utilized to make the fundamental measurements.

Measured U-Factor Uncertainty Presentation

The measurement of the thermal transmittance or U-factor of a fenestration system in a hot box test yields a single numerical value; however, equally as important as the U-factor value are the uncertainty and the confidence level of the measurement. Therefore, the proper way to express the measured U-factor is:

$$U_S = \overline{U}_S \pm \Delta^P U_S \qquad (conficence\ \ level\ \ P\%) \tag{1}$$

where $\overline{U_S}$ is the best estimate for a specimen's U-factor, and $\Delta^P U_S$ is the uncertainty at a specified level P (e.g., $P = 95$ %) . Taken together these three quantities indicate that there is a P % probability that the true U-factor value lies within the $(\overline{U_S} \pm \Delta^P U_S)$ range. It should be noted that the uncertainty and the confidence level are closely related, the larger the level (e.g., 99 %) the larger the resulting uncertainty. The method used to quantify $\Delta^P U_S$ in Equation (1) is called uncertainty analysis.

The uncertainty or $\Delta^P U_S$ term in Equation (1) can be estimated for a given test apparatus and test procedure, and the general procedure for doing this should be developed before any measurement is carried out. Doing so indicates the critical aspects of the measurement procedure and the limitations of the particular test apparatus being used. Since the design and instrumentation used in a specific hot box are usually unique, the uncertainties associated with each component in the specific test apparatus will be different from other test apparatuses. The general uncertainty analysis procedure, however, is similar for all Hot Box designs and instrumentation.

In both fenestration test methods ASTM C 1199 and ISO Thermal Performance of Doors and Windows – Determination of Thermal Transmittance by Hot Box Method (12567-1), the test specimen thermal transmittance, U_S, is the fundamental measured result from the thermal test using the Hot Box. In order to compare test results with other U-factor results such as computer calculated thermal transmittance values, the results must be standardized. In such a procedure, more measured values such as the specimen's total surface heat transfer coefficients (ASTM C 1199), or the specimen's total surface thermal resistances (ISO 12567-1) have to be obtained and used to calculate the standardized U-factor, U_{ST}. So far, there is no standardization method that correctly reproduces the actual thermal performance of the fenestration product. The additional measured values introduced by the standardization procedure can significantly increase the uncertainty of the U_{ST} result in comparison with the uncertainty of the more fundamental U_S result. It is important to improve the current computer models to use variable local heat transfer coefficients on warm and cold side surfaces, and glazing cavity to more accurately model the Hot Box conditions. This would allow future calculated U-factors to be directly compared with the actual measured thermal transmittance, U_S, instead of the two U_{ST} values defined in ASTM C 1199 or the modified U_S value from ISO 12567-1. This direct validation would permit the computer models to be more reliably used over a wider range of fenestration heat transfer conditions. Therefore, this paper will focus on the investigation of uncertainty elements and their propagation to the basic test results (i.e., the thermal transmittance of the test specimen, or U_S value).

In the study of the University of Massachusetts Research Calibrated Hot Box, a detailed investigation of the uncertainty elements associated with the temperature measurement, power measurement, calibration procedure, and material properties will be conducted. Then the Root-Sum-Squares (RSS) method will be used to determine the propagation of uncertainty components to the measured U-factor results. Particular attention is given to the techniques and equations used to evaluate the various heat transfer terms in the total energy balance of the test apparatus.

Uncertainties of Fundamental Measurements

The individual uncertainty associated with a fundamental measurement is referred to as an element of uncertainty. Each measurement element uncertainty will combine with other uncertainties to increase the uncertainty of the fundamental measurement. Before considering the uncertainty propagation to the U-factor results, the uncertainty of the elements associated with a specific Hot Box test apparatus must be investigated.

For the University of Massachusetts Research Calibrated Hot Box, the uncertainty elements can be obtained by either specifications supplied by the manufacturer or the calibration results using calibration data traceable to some national standards. The uncertainty associated with the measurement of length, temperature, temperature difference, power and thermal conductivity measurements, are listed in Table 1.

In Table 1, the uncertainties in length, temperature and power were obtained directly from the suppliers of the tape measure, the 30-gage Type T thermocouple wire, and the watt/watthour transducer [*14*]. The thermocouples used for measuring temperature differences were from the same manufacturer's lot. The uncertainty value was obtained from calibration results for the temperature difference measurement in the Hot Box as given in Gatland [*14*]. The thermal conductivity of materials and the associated uncertainty should be obtained using either ASTM Standard Test Method for Steady-State Heat Flux Measurements and Thermal Transmission Properties by Means of the Guarded-Hot-Plate Apparatus (C 177) or ASTM Standard Test Method for Steady-State Thermal Transmission Properties by Means of the Heat Flow Meter Apparatus (C 518).

Table 1 - *Uncertainty Elements*

Uncertainty Element	Symbol	Unit	Uncertainty at $P = 95$ %
Length	$\Delta^P L$	m	±0.0005
Temperature	$\Delta^P t$	°C	±0.5
Temperature Difference	$\Delta^P \delta t$	°C	±0.05
Voltage	$\Delta^P V$	MV	±1.0 %
Power	$\Delta^P Q_{IN}$	W	±(0.09 %·Q_{IN} + 0.125)
Thermal Conductivity	$\Delta^P k$	W/(m·K)	±1 % *

* Note: Uncertainty in ASTM C 177 measurements. Use 2 to 3% for ASTM C 518 measurements.

Uncertainty Propagation on the U-Factor

Each of the above uncertainty elements listed in Table 1 is incorporated into the total uncertainty of the U-factor, U_S. The uncertainty propagation is based on the RSS method as described by Kline and McClintock [*1*]. If a result R is based on quantities x_i ($i = 1, 2, \ldots, N$), as given in the expression below:

$$R = R(x_i), i = 1, 2, \ldots, N$$

where x_i are known with uncertainties $\Delta^P x_i$, each with the same confidence level, P(e.g., $P = 95$ %):

$$x_i = \bar{x}_i \pm \Delta^P x_i \qquad (confidence\ \ level\ \ P\%)$$

Then the uncertainty in the computed result R is given by:

$$\sum_{i=1}^{N}\left(\frac{\partial R}{\partial x_i}\Delta^P x_i\right)^2 \tag{2a}$$

or in percentage of R,

$$\frac{\Delta R}{R} = \sqrt{\sum_{i=1}^{N}\left(\frac{\partial R}{\partial x_i}\frac{\Delta^P x_i}{R}\right)^2} \tag{2b}$$

Using this methodology, the uncertainties for some intermediate components and for the final U-factor will be obtained.

Using the Hot Box method (ASTM C 1199 or ISO 12567-1), the U-factor of a specimen can be obtained by Equation (3):

$$U_S = \frac{Q_S}{A_S \cdot \delta t_{hc}} \tag{3}$$

where $\delta t_{hc} \equiv t_h - t_c$. Using the RSS method, we can obtain $\Delta^P U_S/U_S$:

$$\frac{\Delta^P U_S}{U_S} = \sqrt{\left(\frac{\Delta^P Q_S}{Q_S}\right)^2 + \left(\frac{\Delta^P A_S}{A_S}\right)^2 + \left(\frac{\Delta^P \delta t_{hc}}{\delta t_{hc}}\right)^2} \tag{4}$$

Using Equation (4), one can estimate the uncertainty of the U-factor with respect to its estimated experimental value. In this equation, the uncertainty of the temperature difference, $\Delta^P \delta t_{hc}$is given in Table 1. In the next two sections, the equations for the calculation of the uncertainty of$\Delta^P A_S$ and$\Delta^P Q_S$ are presented.

Uncertainty Propagation on the Specimen Area

The projected area of a test specimen can be calculated from the measured width and height measurements using Equation (5):

$$A_S = H_S \times W_S \tag{5}$$

Using the RSS method, $\Delta^P A_S/A_S$ is:

$$\frac{\Delta^P A_S}{A_S} = \sqrt{\left(\frac{\Delta^P H_S}{H_S}\right)^2 + \left(\frac{\Delta^P W_S}{W_S}\right)^2} \tag{6}$$

Uncertainty Propagation on the Specimen Net Heat Transfer

All of the above analysis applies to ASTM C 1363, ISO 8990, ASTM C 1199 and ISO 12567-1 Hot Box test procedures. However, methodology for determining the value and uncertainty in the test specimen heat transfer rate, Q_S, differs for the basic Hot Box (ASTM C 1363 and ISO 8990) test methods and the two fenestration Hot Box (ASTM C 1199 and ISO 12567-1) test methods. This is due to the various calibrated heat transfer rates that have to be subtracted from the basic heat transfer in, Q_{IN}, measurement. In this section, the uncertainty of the measured specimen heat transfer rate, Q_S, for a Hot Box following either the ASTM C 1199 or ISO 12567-1 fenestration test methods developed. In addition, the uncertainty of the surround panel heat transfer rate, Q_{SP}, and the test specimen flanking heat transfer rate, $Q_{FL,S}$, must also be determined.

The net heat transfer through a test specimen is obtained by an energy balance on the metering chamber shown in Figure 1. The result is:

$$Q_S = Q_{IN} - Q_{SP} - Q_{EXTR} - Q_{FL,S} \tag{7}$$

Equation (7) includes the specimen flanking heat transfer and therefore it is applicable to specimens with thickness less than that of the surround panel in the Hot Box. For a specimen with a thickness the same as or slightly larger than that of the surround panel, the last term, $Q_{FL,S}$, should be dropped from Equation (7).

Using the RSS method, the uncertainty of the net heat transfer $\Delta^P Q_S/Q_S$ through the specimen is:

$$\frac{\Delta^P Q_S}{Q_S} = \sqrt{\left(\frac{\Delta^P Q_{IN}}{Q_S}\right)^2 + \left(\frac{\Delta^P Q_{SP}}{Q_S}\right)^2 + \left(\frac{\Delta^P Q_{EXTR}}{Q_S}\right)^2 + \left(\frac{\Delta^P Q_{FL,S}}{Q_S}\right)^2} \tag{8}$$

Equation (8) can be used to calculate the percentage of the uncertainty of the net heat transfer through the specimen once the uncertainty of each of the four terms inside the square root sign are known. The uncertainty of the power input to the metering box, ΔQ_{IN}, can be obtained from the elemental uncertainty value given in Table 1. For the remaining three terms, additional analysis needs to be conducted.

The ideal one-dimensional heat transfer through the projected area of the surround panel can be calculated using Equation (9) as follows:

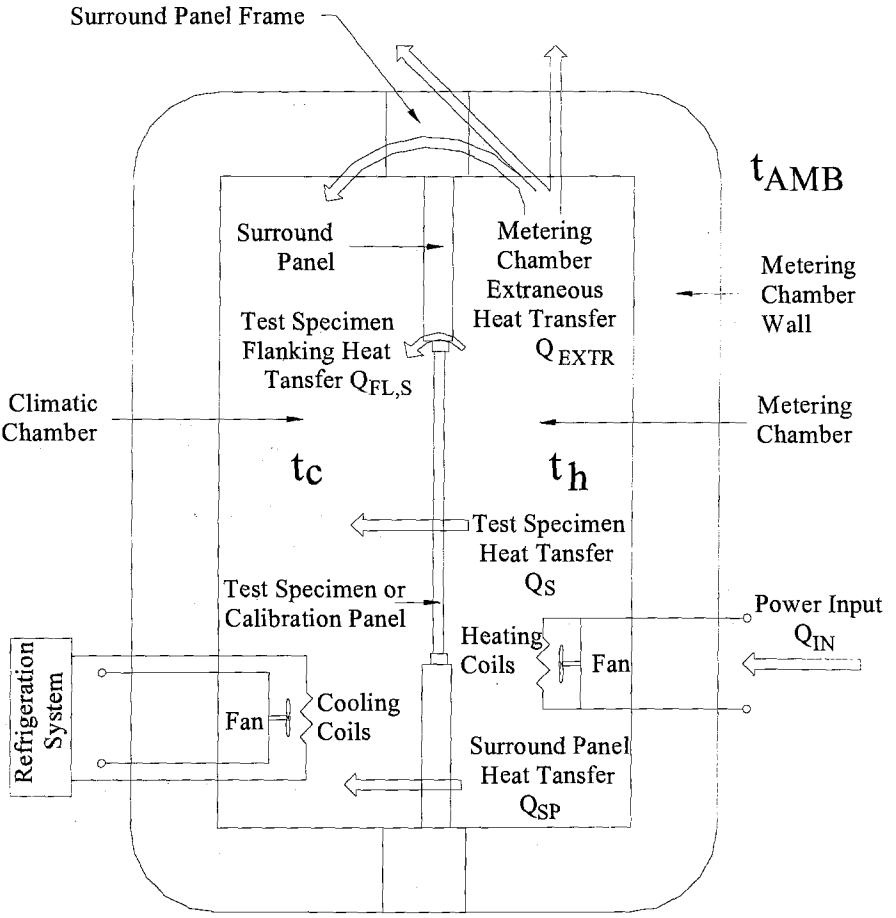

Figure 1 - *Schematic Setup for the Hot Box Metering Chamber Energy Balance*

$$Q_{SP} = k_{SP}\left(\frac{A_{SP}}{L_{SP}}\right)\cdot \delta t_{SP} \tag{9}$$

Using the RSS method, the uncertainty for $\Delta^P Q_{SP}$ can be shown to be:

$$\frac{\Delta^P Q_{SP}}{Q_S} = \left(\frac{Q_{SP}}{Q_S}\right)\left(\frac{\Delta^P Q_{SP}}{Q_{SP}}\right) = \left(\frac{Q_{SP}}{Q_S}\right)\sqrt{\left(\frac{\Delta^P k_{SP}}{k_{SP}}\right)^2 + \left(\frac{\Delta^P A_{SP}}{A_{SP}}\right)^2 + \left(\frac{\Delta^P \delta t_{SP}}{\delta t_{SP}}\right)^2} \tag{10}$$

Using Equation (10) together with the results of uncertainty element analysis given in Table 1, the uncertainty associated with the heat transfer through the surround panel can be determined. This result is then used in Equation (8) for the uncertainty estimate of the net heat transfer through the test specimen.

The extraneous heat transfer from the Hot Box metering chamber during the test of a specimen include the metering chamber wall heat transfer to the ambient room, the heat transfer from the metering to climatic chambers through the surround panel frame (called surround panel flanking heat transfer in ASTM C 1199), and any other unwanted heat transfer as shown schematically in Figure 1. This extraneous heat transfer, Q_{EXTR}, should be accounted for by using an empirical correlation obtained through separate calibration experiments. In the calibration procedure, a homogeneous surround panel (with no test specimen) is mounted in the surround panel frame of the Hot Box shown in Figure 1. The calibration experiments are performed using ASTM C 1199 and ISO 12567-1 standards. In these calibration experiments, since there is no test specimen installed, the test specimen net heat transfer, Q_S, and the test specimen flanking heat transfer, $Q_{FL,S}$, which appear in Equation (7), are both zero. For this situation, solving for extraneous heat transfer in Equation (7), gives the following results:

$$Q_{EXTR} = Q_{IN} - Q_{SP} \tag{11}$$

After setting the ambient and metering chamber air temperatures at different levels, the metering wall thermopile temperature difference voltage, the surround panel average temperature difference and the power input are measured. Using the ASTM C 1199 test method, the empirical calibration correlation for the extraneous heat transfer, $Q_{EXTR,ASTM}$, was obtained using a least squares multiple regression technique given in Yuan [9]. The result for nine calibration experiments is:

$$Q_{EXTR,ASTM} = 0.9391\delta t_{SP} + 1.3319V - 0.4827 \tag{12}$$

Similarly, following the ISO 12567–1 test method, the empirical calibration correlation for the extraneous heat transfer, $Q_{EXTR,ISO}$, was obtained as shown in Yuan [9]. The result for nine calibration experiments is:

$$Q_{EXTR,ISO} = 0.9269\delta t_{SP} + 1.2667V - 0.5068 \tag{13}$$

For a given δt_{SP}, which is related to δt_{hc}, the thermopile temperature difference voltage contribution should be minimized by making the ambient temperature, t_{AMB}, as close to the metering chamber air temperature, t_h, as possible.

The specimen flanking heat transfer, $Q_{FL,S}$, can be determined by calibration by mounting several calibration panels, with different thickness and the same known thermal properties, in the surround panel. This flanking heat transfer for a given thickness surround panel can be obtained by the following equation:

$$Q_{FL,S} = Q_{IN} - Q_{SP} - Q_{EXTR} \tag{14}$$

where, Q_{SP} can be obtained using Equation (9) and Q_{EXTR} is obtained from calibration (i.e., Equation (12) for ASTM C 1199 conditions and Equation (13) for ISO 12567-1 conditions).

For a given thickness surround panel, $Q_{FL,S}$ is a function of the thickness of the specimen, and the least-squares regression fit correlation procedure for ASTM C 1199 fenestration test method is given in Yuan [*9*] and Yuan et al [*15*]. The result for the 102.2 mm surround panel used is:

$$Q_{FL,S;ASTM} = 40.798 - 0.8475L_S + 0.0044L_S^2 \qquad (0 < L_S < 102.2mm) \tag{15}$$

where, L_S is the thickness of the specimen.

The least square regression curve fit correlation for the ISO 12567-1 fenestration test method is given in Yuan [*9*] and Yuan et al [*15*]. The result for the same surround panel is:

$$Q_{FL,S;ISO} = 38.974 - 0.7566L_S + 0.0037L_S^2 \qquad (0 < L_S < 102.2mm) \tag{16}$$

The difference between Equations (15) and (16) are due to the different metering and climatic temperatures used in ASTM C 1199 and ISO 12567-1.

It should be noted that ISO 12567-1 has tables of idealized calculated $Q_{FL,S}$ values. Calibrated $Q_{FL,S}$ values are used in this paper since they include the characteristics of a specific Ho Box design. In addition, in ASTM C 1199, $Q_{FL,S}$ values are not required. This is a problem since the previously mentioned two-dimensional fenestration heat transfer calculation programs that ASTM C 1199 results are often compared with assume that $Q_{FL,S}$ is zero.

The sample standard deviation for each of these two calibrated heat transfer rates, Q_{EXTR} and $Q_{FL,S}$, is determined not only by the measurement errors but also by the imperfect structure of the correlation formula chosen to describe the dependence. Therefore, each least-squares fit with its precision interval is:

$$y = y_c \pm t_{v,P} s_y \qquad (confidence\ \ level\ \ P\%) \tag{17}$$

where, y is either Q_{EXTR} or $Q_{FL,S}$; y_c is the value of y calculated using Equations (15) or (16) for Q_{EXTR} and $Q_{FL,S}$; $t_{v,P}$ is the t value of the v's degree of freedom and P's confidence level (e.g., $P = 95$ %); s_y is the standard deviation of the least square curve fit

y value as described in Neter et al [16]. Based on the calibration measurements described in Yuan [9] and Yuan et al [15], the uncertainty results listed in Table 2 are obtained. It should be noted that additional calibration measurements for Q_{EXTR} and $Q_{FL,S}$ should be made to reduce their uncertainty.

Table 2 - *Uncertainty Results of the Calibrated Heat Transfer of Q_{EXTR} and $Q_{FL,S}$*

Calibration Item	Degrees of Freedom ν	Student-t $t_{\nu,P}$	Standard Deviation s_y (W)	Uncertainty $\Delta^P y = t_{\nu,P} \cdot s_y$ (W)
$Q_{EXTR;ASTM}$	6	1.943	0.904	1.756
$Q_{FL,S;ASTM}$	3	2.353	0.818	1.924
$Q_{EXTR;ISO}$	6	1.943	0.971	1.887
$Q_{FL,S;ISO}$	1	6.314	0.145	0.918

By substituting the appropriate uncertainty values of $\Delta^P Q_{EXTR}$, and $\Delta^P Q_{FL,S}$ into Equation (8), $\Delta^P Q_S/Q_S$ can now be calculated. Finally, using Equation (4), the uncertainty value for $\Delta^P U_S/U_S$ can be estimated.

Results of A CTS Measurement Uncertainty Analysis

A Calibration Transfer Standard (CTS) was used to calibrate the specimen surface heat transfer coefficients for fenestration Hot Box tests. The plastic (polycarbonate) faced CTS was constructed in accordance with ASTM C 1199 and ISO 12567-1. Table 3 shows the summary of the measurement results using ASTM C 1199. More detailed calibration data and results are presented in Yuan [9]. Using the uncertainty data and uncertainty analysis procedures described in the previous sections of this paper, the U-factor uncertainty of the CTS and the intermediate calculation results were obtained and are given in Tables 3 and 4.

From Table 4, the U-factor and its uncertainty from this CTS at the $P = 95$ % confidence level is:

$$U_{CTS,ASTM} = 1.598 \pm 0.093 \quad W/(m^2 \cdot K) \qquad (P = 95\%) \tag{18}$$

This represents an estimated 5.8 % uncertainty in the rounded off measured U-factor value of 1.6 W/(m^2·K).

For comparison purposes, the ASTM C 177 (surface to surface) resistance of the CTS expanded polystyrene core was combined with the two polycarbonate face resistances and the standardized cold and warm side surface heat transfer resistances to give a predicted CTS U-factor of 1.595 W/(m^2·K). This value is within the experimental uncertainty range [1.505 to 1.691 W/(m^2·K)] given in Equation (18) and is only 0.16 % from the measured value.

Among the three uncertainty components of Equation (4), the uncertainty of the specimen heat transfer, ΔQ_S, as shown in Table 4, dominated the U-factor uncertainty. The uncertainty of ΔQ_S is mainly influenced by the uncertainties of $\Delta Q_{FL,S}$ and ΔQ_{EXTR}.

These two quantities were calculated using statistical techniques described previously and based on a limited number of calibration experiments. Therefore, in order to decrease the overall U-factor uncertainty, additional calibrations for the extraneous heat transfer and additional thickness calibration panels for the specimen flanking heat transfer are necessary.

Further examples of fenestration product uncertainty analysis and results for an IEA Round Robin Insulated Glazing Unit (IGU) and an ISO Round Robin PVC window are presented in Yuan [*9*].

Conclusions and Recommendations

A general uncertainty analysis procedure for the Hot Box measurement of fenestration thermal transmittance has been presented in this paper. After all fundamental uncertainties associated with basic or direct measurements such as temperature, power, and dimensions are known, the RSS method is used extensively in the uncertainty propagation analysis. Also, specific statistical error analysis of calibration procedures is conducted in order to complete this propagation analysis.

The metering chamber extraneous heat transfer calibration is an important component in the net heat transfer through the test specimen. Its value has a significant effect on the measurement of the net test specimen heat transfer. It should be minimized by maintaining low metering chamber wall temperature thermopile voltage values. More importantly, the uncertainty associated with its calibration procedure should be minimized as well. At least nine calibration experiments are required to achieve reasonable accuracy as shown in Yuan [*9*]. Since the calibration correlation equations for this extraneous heat transfer is obtained by using regression methods, a corresponding statistical error analysis technique should also be used. Additional calibrations for the extraneous heat transfer and specimen flanking heat transfer are recommended to reduce the uncertainty of the specimen U-factor.

In order to fully account for all of the heat transfer that does not occur directly through the test specimen, the specimen flanking heat transfer should be subtracted from the total heat input to the metering chamber. It should be noted that the ISO 12567-1 fenestration test method requires this calculation, while ASTM C 1199 does not. When this correction is made, measured U_S value, rather than one of the larger uncertainty standardized U_{ST} values, can be shown (Yuan [*9*]) to be 1% off the numerically calculated U-factor for thermally well designed relatively non-projecting fenestration products. It is recommended that changes be made in ASTM C 1199 to include the subtracting out of the test specimen flanking heat transfer. Since the specimen flanking heat transfer in a Hot Box measurement is a relatively small quantity, care needs to be taken during the associated calibration experiments. To achieve accurate U-factor measurements, the uncertainty of the specimen flanking heat transfer calibration should be kept below 5%. It is further recommended that idealized numerically calculated specimen flanking heat transfer results, such as those given in tables in ISO 12567-1, should not be used when reliable specimen flanking heat transfer physical calibration measurement results exist.

Table 3 - *Measured Values and Estimated Uncertainties at the P = 95 % Confidence Level for a Plastic-faced CTS Calibration Panel*

Quantity	Symbol	Unit	Measured Value	Uncertainty Based on Table 1
specimen height	H_S	m	1.219	0.0005
specimen width	W_S	m	0.609	0.0005
specimen thickness	L_S	m	0.021	0.0005
hot side air temperature	t_h	°C	20.99	0.5
cold side air temperature	t_c	°C	-17.89	0.5
surround panel conductivity	k_{SP}	W/m·K	0.032	0.00032
surround panel outer height	H_{SP}	m	2.44	0.0005
surround panel outer width	W_{SP}	m	2.44	0.0005
surround panel hot side surface temperature	t_{SP1}	°C	19.16	0.5
surround panel cold side surface temperature	t_{SP2}	°C	-17.41	0.5
metering chamber wall thermopile voltage	V	mV	7.41	0.07
hot side power input	Q_{IN}	W	168.55	0.277

Table 4 - *Calculated Values of Intermediate Quantities and the U-factor for the CTS*

Quantity	Symbol	Unit	Calculated Value	Calculated Uncertainty	Percent Uncertainty
specimen projected area	A_S	m^2	0.744	0.0007	0.09%
surround panel projected area	A_{SP}	m^2	5.203	0.0010	0.04%
extraneous heat transfer	Q_{EXTR}	W	43.74	1.756	3.8%
surround panel heat transfer	Q_{SP}	W	57.46	0.580	1.0%
specimen flanking heat transfer	$Q_{FL,S}$	W	21.16	1.924	9.1%
specimen heat transfer	Q_S	W	46.19	2.683	5.8%
specimen U-factor	U_S	$W/m^2 \cdot K$	1.598	0.093	5.8%

References

[1] Kline, S. J., and McClintock, F. A, "Describing Uncertainties in Single Sample Experiments," *Mechanical Engineering 75*, 1953, pp. 3-8.

[2] Airy, Sir George Biddle, *Theory of Errors of Observation*, Macmillan, London, 1879.

[3] Schenck, H., *Theory of Engineering Experimentation*, third edition, McGraw Hill, New York, NY, 1979.

[4] Figliola, R. S., and Beasley, D. E., *Theory and Design for Mechanical Measurements*, second edition, John Wiley & Sons, Inc., New York, 1995.

[5] Taylor, John R., *An Introduction to Error Analysis*, second edition, University Science Books, Sausalito, California, 1997.

[6] Moffat, R. J., "Describing the Uncertainties in Experimental Results," *Experimental Thermal and Fluid Science*, 1988, Vol. 1, pp. 3–17.

[7] Moffat, R. J., "Contributions to the Theory of Single Sample Uncertainty Analysis," *ASME Transaction, Journal of Fluids Engineering*, 1982, Vol. 104, pp. 250–260.

[8] Moffat, R. J., "Using Uncertainty Analysis in the Planning of an Experiment," *ASME Transaction, Journal of Fluids Engineering*, 1985, Vol. 107, pp. 173–178.

[9] Yuan, S., "Experimental and Analytical Heat Transfer Analyses for a Calibrated Hot Box and Fenestration Systems," Ph. D. dissertation, University of Massachusetts, Amherst, MA, 2001.

[10] Klems, J. H., "Method of Measuring Nighttime U-Value Using the Mobile Window Thermal Test Facility," *ASHRAE Transactions*, 1992, Vol. 98, Part 2, pp. 619–629.

[11] Harrison, S. J., and Dubrous, F. M., "Uncertainties in the Evaluation of Window SHGC and U-Values Measured Using an Indoor Solar Simulator Facility," *ASHRAE Transactions*, 1992, Vol. 98, Part 2, pp. 638–645.

[12] Elmahdy, H., "Heat Transmission and R-value of Fenestration Systems Using IRC Hot Box: Procedure and Uncertainty Analysis," *ASHRAE Transactions*, 1992, Vol. 102-2.

[13] Van Dijk, Dick, "Interim Report on U-Value Measurements," TNO-BOUW, P. O. Box 29, 2600 AA Delft, The Netherlands, 1997.

[14] Gatland, Stanley D. II, "The Design, Fabrication, Calibration, and Operation of a Second Generation Research Calibrated Hot Box," M. S. thesis, University of Massachusetts, Amherst, MA, 1996.

[15] Yuan, S., Gatland, S.D. II, Goss, W. P., "Calibration Procedures for Hot Boxes", *Insulation Materials: Testing and Applications: 4th Volume, ASTM STP 1426*, A. O. Desjarlais and R. R. Zarr, Eds., ASTM International, West Conshohocken, PA, 2002.

[16] Neter, John, Kutner, Michael H., Nachtsheim, Christopher J., and Wasserman, William, *Applied Linear Statistical Models*, fourth edition, WCB/McGraw-Hill, New York, NY, 1996.

Daniel J. Wise[1] and Bipin V. Shah[2]

An Assessment of InterLaboratory Repeatability in Fenestration Energy Ratings: 2001 NFRC InterLaboratory Test Round Robin

Reference: Wise, D. J. and Shah, B. V. **"An Assessment of InterLaboratory Repeatability in Fenestration Energy Ratings: 2001 NFRC InterLaboratory Test Round Robin,"** *Insulation Materials: Testing and Applications: 4th Volume, ASTM STP 1426,* A. O. Desjarlais and R. R. Zarr, Eds., ASTM International, West Conshohocken, PA, 2002.

Abstract: This paper presents the results from the 2001 Testing Round Robin. The tested fenestration thermal performance ratings (U-factors) were acquired in accordance with *NFRC 100 (1997): Procedures for Determining Fenestration Product U-factors* and *NFRC Test Procedure for Measuring the Steady-State Thermal Transmittance of Fenestration Systems (April 1997).* A total of 8 NFRC-accredited testing laboratories participated in the 2001 test round. This paper presents results from the testing laboratory round robins.

The National Fenestration Rating Council conducts a Laboratory Accreditation Program (LAP) designed to promote accuracy and uniformity among the independent laboratories providing energy rating services (simulations or tests) in accordance with NFRC procedures. NFRC has conducted annual interlaboratory round robins since 1994. The continuance of interlaboratory round robins permits the continued evaluation of the repeatability and variance among the participating laboratories when evaluating the same product. This information is also made available to ASTM C16 for precision and bias.

The round robin testing consisted of each laboratory conducting a thermal performance test on a thermally improved aluminum fixed window with high performance glazing. Each participating testing laboratory received the identical window product to be tested for thermal transmittance. Every laboratory was directed to keep all test results confidential. All questions pertaining to the testing round robin were to be directed to NFRC staff only. The testing began in February of 2001 and was completed in June of 2001. The results of each thermal test performed were reviewed and placed in a spreadsheet for analysis and comparison

[1] Program Director, National Fenestration Rating Council, 1300 Spring Street, Suite 500, Silver Spring, MD 20910.

[2] Program Manager of Engineering, National Fenestration Rating Council, 1300 Spring Street, Suite 500, Silver Spring, MD 20910.

of data. No laboratory was provided with expected results or the relative position of their data with respect to all data presented.

Results were compiled for all participating laboratories in the test round robin. Specific data regarding various measured and calculated performance values as required by the NFRC Procedures and Program Documents are presented herein.

NFRC will continue to conduct annual interlaboratory testing round robins and simulation round robins as an on-going component of the NFRC Laboratory Accreditation Program. The round robins assist in the evaluation of the laboratories to the conformance to the procedures, repeatability between laboratories and the variance between laboratories.

Key Words: U-factor, standardized U-factor, area-weighted method, calibration transfer standard (CTS) method, standardized film coefficient, coefficient of variance, reproducibility, round robin, National Fenestration Rating Council (NFRC).

Background

The National Fenestration Rating Council (NFRC) conducts annual interlaboratory round robin evaluations as part of its Laboratory Accreditation Program (LAP) for NFRC-accredited simulation and testing laboratories. This report presents the findings and comparison of the 2001 test round robin of all NFRC-accredited testing laboratories.

A total of 8 different thermal testing laboratories participated in these testing round robins. Each participating testing laboratory was accredited by NFRC to conduct thermal performance testing using *NFRC 100: Procedures for Determining Fenestration Product U-factors* and *NFRC Test Procedure for Measuring the Steady-State Thermal Transmittance of Fenestration Systems (April 1997).* The participating laboratories are identified in the Acknowledgement section of this paper.

NFRC has specific requirements documented in the NFRC Test Procedure ('97) that is intended to increase the ability to compare the results between test labs. Variances are expected due to differences in design construction, wind direction and the geometry of the hot boxes at each test lab. A summary of the NFRC specified test conditions are as follows:

- Interior ambient temperature of 70 °F (±0.5 °F), 21.1 °C (±0.25 C°C).
- Exterior ambient temperature of 0 F °F (±0.5 F °F), -17.8 °C (±0.25 C°C).
- Interior relative humidity shall be maintained at or below 15%.
- Interior measured film coefficient (h_i) during CTS panel calibration testing of 1.35 Btu/hr-ft^2-°F (8.29 W/m^2-°C) (±5%).
- Exterior measured film coefficient (h_{ii}) during CTS panel calibration testing of 5.1 Btu/hr-ft^2-°F (28.97 W/m^2-°C) (±10%).
- Each glazing corner edge thermocouple shall be placed at a point 0.5 in. (12.5 mm) from the adjacent framing member(s).
- Attachment of specimen surface thermocouples shall be performed parallel to the thermocouple wire.

The area-weighted method of calculation shall be used if the measured thermal transmittance, U_s, is equal to or greater than 0.60 Btu/hr-ft^2-F°F (3.4 W/m^2-K°C) or the ratio of the test specimen projected area to wetted area on either side of the test specimen is less than or equal to 0.8. In all other cases, the CTS calculation method shall be used to determine the standardized thermal transmittance, U_{st}..

Laboratories were required to present the thermal transmittance (U-factor) data using three different analytical techniques - U_s (the air to air measured U-factor), $U_{st[aw]}$ (the area weighted calculation approach referred to as Method A), and $U_{st[cts]}$ (referred to as Method B, which uses calibration data from the CTS specimen). Based upon the requirements stipulated in the NFRC Test Procedure ('97), NFRC- accredited testing laboratories are required to report one U_{st} number. For the purposes of this paper, all three results are reported and evaluated.

ASTM E691, E177 and Inter-laboratory Data Analysis Software were used to determine a level of statistical agreement for U_s and each U_{st} value between laboratories.

Terminology

U-factor - thermal transmittance in Btu/hr-ft^2-°F (W/m^2-°C).

U_s - the measured air-to-air U-factor in Btu/hr-ft^2-°F (W/m^2-°C). This value may vary, dependent on each laboratory's ability to control temperature and environmental conditions within the required tolerances and standard conditions during testing of the thermal transmittance of the test specimen. The variation may be also due to the differences in thermal hot box design and construction in NFRC-accredited laboratories.

$U_{st[AW]}$ - thermal transmittance; the area-weighted calculation approach for standardizing U-factor reporting, referred to as Method A, assigns areas to each surface temperature measurement to calculate interior and exterior area weighted average temperature. The area weighted average temperature is used for the calculation of the interior and exterior film coefficients. The actual measured film coefficients determined during the testing of a fenestration product are subtracted, or stripped, from the measured U_s: then calculated standardized film coefficients are added to the measured U_s. This standardization process of removing actual measured film coeeficients and replacing them with standardized film coefficients allows comparison of results between laboratories.

$U_{st[CTS]}$ - thermal transmittance; uses the calculation approach for standardizing U-factor reporting based on film coefficient and temperature from calibration of homogeneous planner Calibration Testing Panel (CTS) in the hot box chamber.

Testing Methods

The following applicable test standards are used:

NFRC Test Procedure for Measuring the Steady-State Thermal Transmittance of Fenestration Systems (April 1997).

Additional referenced ASTM Standards:
ASTM: Test Method for Steady-State Thermal Performance of Building Assemblies by Means of a Guarded Hot Box *(C 236).*

ASTM: Standard Test Method for the Thermal Performance of Building Assemblies by Means of a Hot Box Apparatus (C 1363).

ASTM: Standard Test Method for Measuring the Steady-State Thermal Transmittance of Fenestration Systems Using Hot Box Methods (C 1199).

ASTM: Test Method for Steady-State Thermal Performance of Building Assemblies (C 976)

Planning and Schedules for Round Robin Testing

As part of the NFRC Laboratory Accreditation Program (NFRC LAP), each laboratory is required to participate in an annual round robin. Each NFRC-accredited testing laboratory is notified by letter explaining the details of the round robin testing prior to the actual start of physical testing. Time periods are established for data submittal and issuance of a final report to NFRC.

Reporting and Information Materials

All participants, to help ensure accuracy and uniformity in data reporting and subsequent analysis, provided standardized report forms and data sheets for use. Laboratories were invited to provide any other supporting materials and information that were deemed useful to the round robin. Each testing laboratory was provided with a set of identical product drawings and bill of materials for use in the data calculation and report generation.

Test Sample Description

The product selected for use in the test round robin was a product that can be utilized in either a commercial or residential application. The product was a fixed window (O) with thermally broken aluminum frame and dual-glazed with high performance glazing. The glazing unit was made out of two sheets of AFG E2 Low emissivity "e" glass (NFRC spectral data ID # 907) with Heat Mirror SC75 (NFRC spectral data ID # 1510). The low "e" coatings were on surfaces 2, 4 and 5. A fenestration manufacturer supplied the test specimen. See Appendix D for product information submitted to each laboratory.

The product description of the round robin specimen requested was reported to be as follows: a nominal 40 inch by 40 inch (1016 mm x 1016 mm) thermally broken aluminum fixed (O) window with high performance glazing.

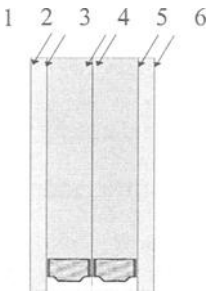

Fig 1: The insulated glazing (IG) pane surfaces are numbered starting from the outside to inside. Surfaces 2, 4 and 5 are Low-e coated surfaces and mid pane is a heat mirror film.

Product Performance Support Data

The product for the round robin testing was simulated to determine the thermal transmittance rating using NFRC-approved software tools WINDOW and THERM. The product was simulated with and without a radiation enclosure model. Additionally, two different liquid urethane conductivity values were used to signify the difference in results based upon a generic value for liquid urethane: 0.1791 Btu/hr-ft-F (0.31 W/m-°C, default value used in software tool), and 0.0702 Btu/hr-ft-F (0.12 W/m-°C, value provided by liquid urethane manufacturer in accordance with ASTM C518). The results are listed below:

	U-Factor (Liq. Urethane 0.1791 Btu/hr-ft-°F)	U-Factor (Liq. Urethane 0.0702 Btu/hr-ft-°F)
Without Radiation Enclosure model	0.43	0.41
With Radiation Enclosure model	0.41	0.40

Confidentiality

All participating testing laboratories were directed to keep all testing files, questions, correspondences and any other issue relating to the round robin thermal test confidential. NFRC conducts these round robins to evaluate each laboratory individually, and any prior knowledge of results could possibly bias the data. Any and all correspondences were to be directed to NFRC staff only.

Test Specimen Control Procedures

Each laboratory was instructed to keep a record of the condition of the test specimen upon arrival at their facility and prior to shipment. Upon arrival at its final destination, the window was in good condition with no apparent damage to any component. No modification or alterations were made to the test specimen during the round robin except for the sealing of the test product to prevent air leakage as required by the NFRC test procedure.

Reported Results and Data Analysis

The final data analysis of the 2001 test round robin is discussed in detail. Each section of the required data submission is reviewed, with any anomalies or comments recorded. Each laboratory is required to determine three thermal transmittance values, U_s, $U_{st[aw]}$ and $U_{st[cts]}$. As per NFRC Test Procedure and ASTM C1199 requirements, the laboratory standardizes the U_s (air-to-air) value using either the area-weighted method or the calibration transfer standard (CTS) method. The criteria for determination of which method is used has been stated in the background section. The three different U-factor results from each participating laboratory were compared to the averaged test results of the product. The U_s, or air-to-air U-factor, was compared to the average U_s value for all participating laboratories testing to *NFRC Test Procedure.* The standardized U-factors were analyzed in the same fashion. The $U_{st[aw]}$ and $U_{st[cts]}$ were compared using two standard deviations to the averaged results, respectively, for the individual calculation methods.

ASTM E691 and E177 test procedures were used to perform statistical analyses of the round-robin test data U-factor results for each NFRC-accredited testing laboratory. While this data set is smaller than specified by these ASTM procedures for a conclusive summation for the individual laboratory data comparison, several important observations can be made and are reported herein for inter-laboratory comparison for which the data set was adequate. Recommendations for future round robins and laboratory investigations are also made. The Appendix of this paper contains the data both in Inch-Pound and Metric units.

Table 1a and 1b show the final test round robin results for 2001 having IP and SI units respectively:

Table 1a - *Test Results (Btu/hr-ft^2-^{o}F)*

	Laboratory ---Reported U-factors---			percent difference from averaged U-factor		
Laboratory	U_s	$U_{st[AW]}$	$U_{st[CTS]}$	U_s	$U_{st[AW]}$	$U_{st[CTS]}$
1	0.40	0.39	0.39	2.4	2.5	4.9
2	0.43	0.41	0.43	-4.9	-2.5	-4.9
3	0.39	0.39	0.39	4.9	2.5	4.9
4	0.41	0.40	0.41	0.0	0.0	0.0
5	0.45	0.41	0.43	-9.8	2.5	-4.9
6	0.42	0.40	0.42	-2.4	0.0	-2.4
7	0.39	0.38	0.39	4.9	4.5	4.6
8	0.39	0.39	0.39	4.9	2.5	4.9
Average:	0.41	0.40	0.41	0.61	0.88	0.88
High:	0.45	0.41	0.43	4.9	4.5	4.9
Low:	0.39	0.39	0.39	-9.8	-2.5	-4.9
Std. Deviation:	0.02	0.01	0.02			

Note: The percentage values are derived using two decimal place accuracy.

Table 1b - *Test Results (W/m^2-^{o}C)*

	Laboratory ---Reported U-factors---			percent difference from averaged U-factor		
Laboratory	U_s	$U_{st[AW]}$	$U_{st[CTS]}$	U_s	$U_{st[AW]}$	$U_{st[CTS]}$
1	2.27	2.21	2.21	2.4	2.5	4.9
2	2.44	2.33	2.44	-4.9	-2.5	-4.9
3	2.21	2.21	2.21	4.9	2.5	4.9
4	2.33	2.27	2.33	0.0	0.0	0.0
5	2.56	2.33	2.44	-9.8	-2.5	-4.9
6	2.38	2.27	2.38	-2.4	0.0	-2.4
7	2.21	2.17	2.22	4.9	4.5	4.6
8	2.21	2.21	2.21	4.9	2.5	4.9
Average:	2.33	2.25	2.31	0.61	0.88	0.88
High:	2.56	2.33	2.44	4.9	4.5	4.9
Low:	2.21	2.17	2.21	-9.8	-2.5	-4.9
Std. Deviation:	0.13	0.06	0.10			

Note: The percentage values are derived using two decimal place accuracy.

Reported Result Summary

The reported results are analyzed using a two standard deviation limit of the average reported results as determined from the average of the eight

laboratories as calculated using an EXCEL 7.0 spreadsheet. This tolerance was established by the NFRC Accreditation Policy Committee prior to the start of the round robin and has been the accepted tolerance for NFRC test laboratory round robins.

Analysis of Heat Flow Test Data

Additional analyses were conducted on a variety of reported data. These analyses allowed further investigation of possible sources of error and helped to identify specific measurements or procedures that might need improvements at each laboratory.

Heat Flows

Each laboratory was requested to provide data for five different categories pertaining to power measurement and heat loss attributes. Total power measurement (Q_{total}) varied from each laboratory. This would be expected because of the differing design characteristics of each thermal chamber test facility. The surround panel and metering box wall heat flows are also variable due to construction techniques, materials used, and overall area of the surround panel exposed to the metering chamber.

One laboratory reported 0.0 Btu/hr for the flanking loss, the loss attributed to heat loss around the perimeter of the surround panel. The laboratory reporting a flanking loss of 0.0 Btu/hr has a guarded hot box, and not a calibrated hot box. For this laboratory, it is assumed that any flanking loss associated with the thermal test is being attributed to the surround panel heat loss. Of the other 7 laboratories, the reported flanking loss values ranged from -6.61 Btu/hr to 58.11 Btu/hr. Flanking loss also varies due to chamber design characteristics.

Net specimen heat loss, or Q_s of the specimen, which is the amount of heat flow attributed to the test specimen, should be fairly consistent between laboratories. The range of values reported was from a low of 301.76 Btu/hr to a high of 346.74 Btu/hr. The difference between all laboratories reporting these values is 44.98 Btu/hr. The average of all 8 laboratories is 318.89 Btu/hr, with a standard deviation of 16.13 Btu/hr. All the participating laboratories reported Q values within the ± 10% tolerance range of 287.00 Btu/hr to 350.78 Btu/hr, as applied to the average Q. Using the average Q (318.89 Btu/hr) and dividing by the averaged area of the specimen (11.11 ft^2) and an ambient air temperature difference of 70.10 °F, the averaged U_s of the specimen would calculate to be 0.41 Btu/hr-ft^2-°F, and is in good agreement with the averaged measured value.

Although all 8 participating laboratories met the ±10% tolerance requirement, removing the highest and lowest values allows further analysis of the data. Laboratory #5 reported the highest net specimen heat loss, that being 346.74 Btu/hr. Laboratory #3 reported the lowest net specimen heat loss of 301.76 Btu/hr. If these two reported values are removed from the reported data, the remaining 6 laboratories reported Q_s values ranging from 304.57 Btu/hr to 331.73 Btu/hr. The spread of all eight reported values is reduced from 44.98 Btu/hr to 27.16 Btu/hr using the remaining six labs. This is a reduction of

approximately 40% of the range of reported Q_s, but < 1% of the average Q_s of the six remaining laboratories, so it is not considered to significantly affect the data and corresponding results.

Table 2a - *Net Specimen Heat Loss Reported - 2001*

Laboratory	Net Specimen Heat Loss Reported (Q) Btu/hr	W
1	308.8	90.5
2	331.7	97.2
3	301.8	88.4
4	322.2	94.4
5	346.7	101.6
6	329.2	96.5
7	306.1	89.7
8	304.6	89.4
Average:	318.9	93.4
High:	346.7	101.6
Low:	301.8	88.4
Std. Deviation:	16.1	4.7

Extraneous Heat Loss

Another factor that was investigated is the amount of extraneous heat loss that was attributed by each laboratory to the total heat input (Q). The reported data showed that for the 8 laboratories, the percentage of heat loss attributed to extraneous losses varied from a low of 24.2% to a high of 40.6%, or nearly half of the total heat input to the metering box. Means to reduce the percentage of extraneous heat loss to the total heat input needs to be investigated by all the participant laboratories. The amount of extraneous losses may increase the probability of potential error of the final result. Table 2b illustrates the results as submitted by each laboratory.

Table 2b - *Percentage of Extraneous Heat Loss Determination – 2001*

	Total Heat Loss Reported (Q)		Net Specimen Heat Loss Reported (Q)		Extraneous Heat Loss		Percent Of Extraneous Heat Loss Compared To Total Heat Loss
Laboratory	Btu/hr	(W)	Btu/hr	(W)	Btu/hr	(W)	
1	407.3	(119.3)	308.8	(90.5)	98.5	(28.9)	24.2%
2	558.6	(163.7)	331.7	(97.2)	226.9	(66.5)	40.6%
3	503.2	(147.4)	301.8	(88.4)	201.4	(59.0)	40.0%
4	465.1	(136.3)	322.2	(94.4)	142.9	(41.9)	30.7%
5	560.1	(164.1)	346.7	(101.6)	213.4	(62.5)	38.1%
6	529.7	(155.2)	329.2	(96.5)	200.5	(58.8)	37.9%
7	419.4	(122.9)	306.1	(89.7)	113.3	(33.2)	27.0%
8	401.9	(117.8)	304.6	(89.2)	97.3	(28.5)	24.2%
Average:	491.9	(144.1)	320.9	(94.0)	171.0	(50.1)	34.1%
High:	560.1	(164.1)	346.7	(101.6)	226.9	(66.5)	40.6%
Low:	407.3	(119.3)	301.8	(88.4)	98.5	(28.9)	24.2%
Std. Deviation:	63.0		16.3		51.8		

Test Conditions

All laboratories reporting data were in compliance with the requirements of being within ±0.5 °F (± 0.2 °C) of the interior ambient temperature of 70.0 F °F (21.1 °C) and the exterior ambient temperature of 0.0 °F (-17.8 C°C).

The average warm side baffle surface temperature for each laboratory was recorded on the data information sheets. The current requirement of warm side baffle temperatures is described on page 7 of NFRC Test Procedure, Section 3.2.2. The warm side baffle temperature must be within ± 2 °F (± 0.9 °C) of the interior ambient surface temperature. All laboratories reporting average warm side baffle temperatures did comply with this requirement.

Calculated Test Data

Method A (Modified) Procedure - Area-weighted

The warm side and cold side surface conductances, as well as the surface-to-surface conductance of the test specimen, are calculated from the actual temperature measurements. The 2001 room side and cold side surface conductances, as well as the averages, can be found in Tables 3a and 3e respectively. The standardized warm side surface conductances reported from all participating laboratories are presented in Table 3c. The exterior coefficients are standardized and are not in tabular form. The test specimen surface-to-surface conductance values are given in Table 3g.

Note: The use of the Method A (Modified) results in this report are for comparative purposes only. Although the final result per the NFRC Test Procedure would be performed using the CTS Method, both methods are evaluated for compliance to the respective methods by the participating laboratories.

Method B Results - Equivalent CTS Method

The warm side and cold side surface film heat transfer coefficient, as well as the surface to surface conductance of the test specimen, are calculated from equations found in *NFRC Test Procedure.* The actual measured room side and cold side surface coefficients can be found in Tables 3b and 3f respectively, while the calculated standardized warm side coefficients are recorded in Table 3d. The exterior coefficients are standardized and are not in tabular form. The test specimen surface-to-surface conductance values are provided in Table 3h.

The Convection Constant 'K', which is used in the calculations, is derived from CTS panel calibration testing, a requirement for NFRC laboratory accreditation, which is performed by each NFRC-accredited laboratory. The "K" numbers reported are given in Table 3i.

The U_{st} results from $U_{st[cts]}$ CTS Method were discussed in a previous section of this report, Reported Results and Data Analysis.

Table 3a - *Interior Measured Film s Coefficients*
Area-weighted Method

Laboratory	Btu/hr-ft^2-F	W/m^2-K
1	1.42	8.03
2	1.46	8.30
3	1.37	7.79
4	1.44	8.18
5	1.59	9.03
6	1.53	8.69
7	1.43	8.09
8	1.31	7.44
Average:	1.44	8.19
High:	1.59	9.03
Low:	1.31	7.44
Std. Deviation:	0.09	0.50

Table 3b - *Interior Measured Film Coefficients*
CTS Method

Laboratory	Btu/hr-ft^2-F	W/m^2-K
1	1.44	8.15
2	1.29	7.32
3	1.42	8.05
4	1.36	7.71
5	1.38	7.84
6	1.40	7.95
7	1.42	8.05
8	1.45	8.22
Average:	1.39	7.91
High:	1.45	8.22
Low:	1.29	7.32
Std. Deviation:	0.05	0.29

Table 3c - *Interior Standardized Film Coefficients*
Area-weighted Method

Laboratory	Btu/hr-ft^2-F	W/m^2-K
1	1.38	7.82
2	1.35	7.67
3	1.38	7.82
4	1.38	7.84
5	1.32	7.50
6	1.38	7.84
7	1.38	7.81
8	1.38	7.85
Average:	1.37	7.77
High:	1.38	7.85
Low:	1.32	7.50
Std. Deviation:	0.02	0.13

Table 3d - *Interior Standardized*
CTS Method

Laboratory	Btu/hr-ft^2-F	W /m^2-K
1	1.38	7.81
2	1.35	7.67
3	1.37	7.77
4	1.39	7.88
5	1.34	7.61
6	1.39	7.89
7	1.38	7.82
8	1.37	7.80
Average:	1.37	7.78
High:	1.39	7.89
Low:	1.34	7.61
Std. Deviation:	0.02	0.10

Table 3e - *Exterior Measured Film Coefficients*
Area-weighted Method

Laboratory	Btu/hr-ft^2-F	W/m^2-K
1	5.24	29.73
2	6.36	36.13
3	5.84	33.14
4	6.75	38.32
5	5.28	29.98
6	5.62	31.91
7	6.54	37.11
8	6.40	36.35
Average:	6.00	34.08
High:	6.75	38.32
Low:	5.24	29.73
Std. Deviation:	0.59	3.33

Table 3f - *Exterior Measured Film Coefficients*
CTS Method

Laboratory	Btu/hr-ft^2-F	W/m^2-K
1	5.40	30.66
2	5.00	28.39
3	5.00	28.39
4	5.06	28.73
5	4.99	28.33
6	5.62	31.91
7	4.87	27.65
8	4.80	27.26
Average:	5.09	28.92
High:	5.62	31.91
Low:	4.80	27.26
Std. Deviation:	0.28	1.57

Table 3g *Exterior Measured Film Film Coefficients* **Area-weighted Method**

Laboratory	Btu/hr-ft^2-F	W/m^2-K
1	0.62	3.50
2	0.67	3.78
3	0.60	3.40
4	0.63	3.57
5	0.67	3.80
6	0.63	3.56
7	0.59	3.36
8	0.61	3.47
Average:	0.63	3.55
High:	0.67	3.80
Low:	0.59	3.36
Std. Deviation:	**0.03**	**0.16**

Table 3h *Exterior Measured Coefficients* **CTS Method**

Laboratory	Btu/hr-ft^2-F	W/m^2-K
1	0.61	3.47
2	0.73	4.15
3	0.59	3.36
4	0.67	3.79
5	0.71	4.03
6	0.68	3.84
7	0.61	3.47
8	0.60	3.43
Average:	0.65	3.69
High:	0.73	4.15
Low:	0.59	3.36
Std. Deviation :	**0.05**	**0.30**

Table 3i - *Convection Coefficient (K)* **CTS Method**

Laboratory	Btu/hr-ft^2-F	W/m^2-K
1	0.31	1.74
2	0.30	1.70
3	0.33	1.87
4	0.28	1.57
5	0.33	1.87
6	0.30	1.72
7	0.29	1.66
8	0.32	1.83
Average:	0.31	1.75
High:	0.33	1.87
Low:	0.28	1.57
Std. Deviation:	0.02	0.11

Note: Certain data tables represented in the body of this paper can also be found in the Appendix.

Potential Outlier Data Analysis

For the standardized U-factors of $U_{st[aw]}$ and $U_{st[cts]}$, the reported values from each laboratory are within acceptable tolerances of the established two standard deviations for the 2001 testing round robin.

Note: Data sheets providing the results are contained in the Appendix.

ASTM E691 Data Analysis

Statistical analysis of the round robin test data U-factor results for each NFRC-accredited testing laboratory was performed. A total of three analyses were performed on the following reported results: U_s, $U_{st[aw]}$, $U_{st[cts]}$. The following table summarizes the analysis of the data:

Table 4a - 2001 Results

	Average of Cell Averages Btu/hr-ft^2-°F (W/m^2-°C)	Std. Deviation between Cell Averages
U_s	0.41 (2.33)	0.02
$U_{st[aw]}$	0.40 (2.27)	0.01
$U_{st[cts]}$	0.41 (2.29)	0.02

Precision and Bias Statement

The National Fenestration Rating Council (NFRC) has conducted the 2001 inter-laboratory comparisons for this procedure. These inter-laboratory comparisons are between the eight NFRC-accredited laboratories that participated in the round robin, with some laboratories having parallel weather side airflow, and others having perpendicular weather side airflow in the thermal chamber. All of the laboratories were required to test the specimen at specified environmental conditions.

Precision

The precision values are presented as an average (mean value from all participating laboratories) thermal transmittance, U_s or U_{st}, and a 95% coefficient of variation. The type of precision described for this round robin is a Reproducibility Precision Statement. Reproducibility deals with the variability between single test results obtained in different laboratories, each of which has applied the test method to a given test specimen. The summary of interlaboratory comparison results is provided in the following tables:

Reproducibility – 8 labs **Table 5a**

No	Year	Test Specimen	Number of Labs	U_s	Ust_{aw}	Ust_{cts}	U_{st} Reported
1	2001	Thermally-broken Fixed (O)	8	14.74%	8.92%	13.78 %	13.78%

Note: Reproducibility variation in percent (between laboratories).

Coefficient of Variance – 8 labs **Table 5b**

No	Year	Test Specimen	Number of Labs	CV% (U_s)	CV% (Ust_{aw})	CV% (Ust_{cts})	CV% (U_{st} Reported)
1	2001	Thermally-broken Fixed (0)	8	5.27%	3.19%	4.92%	4.92%

Note: CV%= reproducibility coefficient of variation in percent (between laboratories).

Bias

This method has no bias statement, as there is no accepted reference value available for comparison.

Acknowledgments

NFRC-accredited Testing Laboratories - AIR-INS – Varennes, Quebec, Canada; E.T.C. Laboratories, Inc. - Rochester, NY; Architectural Testing, Inc. - Fresno, CA; Intertek Testing Services - Middleton, WI; Architectural Testing, Inc. - New Brighton, MN; Architectural Testing, Inc. - York, PA; Quality Testing, Inc. - Everett, WA; National Certified Testing Laboratories, Inc. - York, PA

NFRC Accreditation Policy Committee Members -
John Mumaw, Chair, Dr. Dragan Curcija, Andre Desjarlais, John McFee, Christian Kohler

Summary

The primary objective of this inter-laboratory round robin test program was to test an aluminum type product that has both residential and commercial applications to the NFRC Test Procedure (97') at all NFRC-

accredited laboratories. The results of this required test round robin were compiled into an NFRC evaluation report per NFRC Laboratory Accreditation Program requirements and submitted to the NFRC Accreditation Policy Committee for review and approval. Upon approval by the APC of the 2001 annual test round robin report, the intention is to draft a peer review paper for presentation, showing both the reproducibility and coefficient of variance of the NFRC-accredited testing laboratories.

The results of this effort, as presented and compiled in this paper, indicate that there is evidence that the NFRC-accredited testing laboratories, when testing using the NFRC Test Procedure (1997) and referenced ASTM standards such as ASTM C1199 and ASTM C1363, provide results that are expected to have a reproducibility limit of 13.98% from the average value, at a 95% level of confidence. The standard deviation of cell averages was calculated to be 0.0096. NFRC staff and the APC shall undertake an investigation as to the possible reasons that the results are not within one standard deviation limit for U_s, $U_{st(aw)}$ and $U_{st(cts)}$.

References

[1] ASTM: Standard Test Method for Steady-State Heat Flux Measurements and Thermal Transmission Properties by Means of the Guarded-Hot-Plate Apparatus (E 177-97)

[2] ASTM: Standard Practice for Conducting an Inter-laboratory Study to Determine the Precision of a Test Method (E 691-99)

[3] NFRC 100: Procedures for Determining Fenestration Product U-factors (1997)

[4] NFRC Test Procedure for Measuring the Steady-State Thermal Transmittance of Fenestration Systems (April 1997)

APPENDIX – INCH-POUND/METRIC DATA SHEET

NFRC 2001 Thermal Test Round Robin Test Evaluation

INCH-POUND

Final Test Results

Lab #	1	2	3	4	5	6	7	8			Minimum	Maximum	Average	Std. Dev.
Data Information														
Heat Flows														
Total Measured (Qtotal)	407.27	558.58	503.16	465.11	560.10	529.70	419.45	401.90	Btu/hr		401.90	560.10	480.66	
Surround Panel Loss (Qsp)	76.41	168.18	201.39	134.99	200.36	201.90	82.79	77.86	Btu/hr		76.41	201.90	142.99	
Metering Box Wall Loss (Qmb)	12.03	0.57	-0.21	-18.09	19.52	-3.50	20.38	7.17	Btu/hr		-18.09	20.38	4.73	
Flanking Loss (Qfl)	10.06	58.11	0.00	7.88	-6.61	2.00	10.17	12.29	Btu/hr		-6.61	58.11	11.74	
Net Specimen Heat Loss (Qs)	308.78	331.73	301.76	322.23	346.74	329.20	306.11	304.57	Btu/hr		301.76	346.74	318.89	16.13
Areas														
Projected Area (As)	11.11	11.11	11.11	11.09	11.09	11.11	11.11	11.11	Ft2		11.09	11.11	11.11	0.01
Interior 3-D Area (Ain)	13.15	12.96	12.96	12.99	12.93	12.38	12.94	13.01	Ft2		12.38	13.15	12.91	0.23
Exterior 3-D Area (Aext)	11.31	12.06	11.48	11.56	11.20	11.22	11.60	11.18	Ft2		11.18	12.06	11.45	0.30
Metering Box Opening (Amb)	36.47	64.00	64.00	42.71	61.84	54.39	36.20	36.11	Ft2		36.11	64.00		
Metering Box Baffle (Ab1)	32.13	54.00	53.65	35.97	58.11	46.44	32.13	32.13	Ft2		32.13	58.11		
Surround Panel Int. Area (Asp)	25.36	64.00	52.89	31.62	50.75	43.28	25.09	25.00	Ft2		25.00	64.00		
Interior specimen to AW ratio (2)	0.84	0.86	0.86	0.84	0.84	0.90	0.84	0.85			0.84	0.90	0.85	0.02
Exterior specimen to AW ratio (2)	0.98	0.92	0.97	0.90	0.91	0.99	0.92	0.99			0.90	0.99	0.95	0.04
Test Conditions														
Metering Room Ambient (ti)	70.01	69.71	70.13	70.34	69.98	70.40	70.22	70.00	F		69.71	70.40	70.10	0.22
Cold Room Ambient (to)	0.01	-0.32	0.25	-0.34	-0.04	0.10	0.03	-0.05	F		-0.34	0.25	-0.04	0.20
Guard Room Ambient	71.25	68.16	69.53	68.30	68.98	72.10	71.50	72.00	F		68.16	72.10	70.23	1.66
Metering Room RH	5.75	12.90	13.49	14.22	13.45	11.00	8.89	4.69	%		4.69	14.22	10.55	3.71
Exterior Wind Velocity	15.27	15.00	16.00	15.00	5.60	14.30	14.78	14.68	mph		5.60	16.00	13.83	3.36
Static Pressure Difference	0.10	0.00	0.01	0.20	0.00	0.04	0.08	0.08	psf		0.00	0.20	0.06	0.07
Surround Panel Thickness	4.00	4.00	4.00	4.00	4.00	4.38	4.00	4.00			4.00	4.38	4.05	0.13
Surface Temperature Data														
Area-weighted Interior Surface	50.38	49.48	50.33	50.16	51.01	51.00	50.89	49.07	F		49.07	51.01	50.29	0.71
Area-weighted Exterior Surface	5.32	4.38	4.90	3.97	5.67	3.86	4.25	4.33	F		3.80	5.67	4.58	0.66
Average Interior Frame	45.30	44.10	44.68	44.12	46.49	45.10	45.16	42.77	F		42.77	46.49	44.72	1.09
Average Exterior Frame	7.01	6.94	7.24	5.71	8.43	5.70	6.04	6.33	F		5.70	8.43	6.88	0.92
Average Interior Edge Glass	42.85	42.16	42.62	43.98	43.79	43.50	43.57	42.15	F		42.15	43.98	43.06	0.73
Average Exterior Edge Glass	7.06	6.32	6.45	5.30	7.39	5.90	5.53	5.55	F		5.30	7.39	6.19	0.75
Average Interior Center Glass	56.69	56.08	56.75	56.50	56.34	57.40	57.20	56.11	F		56.08	57.40	56.63	0.46
Average Exterior Center Glass	3.98	2.10	3.37	2.70	3.89	2.30	3.00	2.87	F		2.10	3.98	3.03	0.68
Avg. Surf-Surf Temp Difference (AW)	45.06	45.11	45.43	46.20	45.34	47.20	46.64	44.74	F		44.74	47.20	45.71	0.87
Int-Ext Glass Surf. Temp. Difference	52.71	53.98	53.38	53.79	52.45	55.10	54.19	53.24	F		52.45	55.10	53.60	0.85
Thermal Transmittance Test Results														
Air-to-Air (Us)	0.40	0.43	0.39	0.41	0.45	0.42	0.39	0.39	Btu/hr-ft2-F		0.39	0.45	0.41	0.02
Area-weighted Method A (Ust) (3-D)	0.39	0.41	0.39	0.40	0.42	0.40	0.38	0.39	Btu/hr-ft2-F		0.38	0.42	0.40	0.01
Equivalent CTS Method B (Ust)	0.39	0.43	0.39	0.41	0.43	0.42	0.39	0.39	Btu/hr-ft2-F		0.39	0.43	0.41	0.02

Calculated Test Data														
Method A (Modified) Procedure														
Room Side Surface Conductance (hi)	1.42	1.46	1.37	1.44	1.59	1.53	1.43	1.31	Btu/hr-ft2-F		1.31	1.59	1.44	0.09
Cold Side Surface Conductance (hii)	5.24	6.36	5.84	6.75	5.28	5.62	6.54	6.40	Btu/hr-ft2-F		5.24	6.75	6.00	0.59
Specimen Thermal Conductance (Cs)	0.62	0.67	0.60	0.63	0.67	0.63	0.59	0.61	Btu/hr-ft2-F		0.59	0.67	0.63	0.03
Standardized Values														
Thermal Transmittance (Ust)	0.39	0.41	0.39	0.40	0.41	0.40	0.39	0.39	Btu/hr-ft2-F		0.39	0.41	0.40	0.01
Room Side Surface Conductance (hi)	1.38	1.35	1.38	1.38	1.32	1.38	1.38	1.38	Btu/hr-ft2-F		1.32	1.38	1.37	0.02
Cold Side Surface Conductance (hii)	5.10	5.10	5.10	5.10	5.10	5.10	5.10	5.10	Btu/hr-ft2-F		5.10	5.10	5.10	0.00
Method B (Equivalent CTS Method)														
Room Side Surface Conductance (hi)	1.44	1.29	1.42	1.36	1.38	1.40	1.42	1.45	Btu/hr-ft2-F		1.29	1.45	1.39	0.05
Cold Side Surface Conductance (hii)	5.40	5.00	5.00	5.06	4.99	5.62	4.87	4.80	Btu/hr-ft2-F		4.80	5.62	5.09	0.28
Specimen Thermal Conductance (Cs)	0.61	0.73	0.59	0.67	0.71	0.68	0.61	0.60	Btu/hr-ft2-F		0.59	0.73	0.65	0.05
Standardized Values														
Thermal Transmittance (Ust)	0.39	0.43	0.39	0.41	0.43	0.42	0.39	0.39	Btu/hr-ft2-F		0.39	0.43	0.41	0.02
Room Side Surface Conductance (hi)	1.38	1.35	1.37	1.39	1.34	1.39	1.38	1.37	Btu/hr-ft2-F		1.34	1.39	1.37	0.02
Cold Side Surface Conductance (hii)	5.10	5.10	5.10	5.10	5.10	5.10	5.10	5.10	Btu/hr-ft2-F		5.10	5.10	5.10	0.00
Convection Coefficient (K)	0.31	0.30	0.33	0.28	0.33	0.30	0.29	0.32	Btu/hr-ft2-F		0.28	0.33	0.31	0.02
Radiative Specimen Heat Flow (Qr1)	170.53	134.04	154.80	180.76	190.63	176.40	172.73	190.69	Btu/hr		134.04	190.69	171.32	19.01
Convective Specimen Heat Flow (Qc1)	138.10	167.69	146.97	141.47	156.11	152.80	133.38	123.88	Btu/hr		123.88	167.69	145.05	13.96
Equivalent Warm Surface Temp.	50.65	46.55	50.97	48.94	48.20	49.24	50.78	51.07	F		46.55	51.07	49.55	1.62
Equivalent Cold Surface Temp.	5.16	5.66	5.68	5.40	6.00	5.37	5.69	5.67	F		5.16	6.00	5.58	0.26
Warm Side Baffle Temp.	70.10	68.82	68.41	69.78	69.83	69.30	70.54	69.79	F		68.41	70.54	69.57	0.69
Emittance of Glass (e1)	0.84	0.84	0.84	0.84	0.84	0.84	0.84	0.81			0.81	0.84	0.84	0.01
Warm Side Baffle Emittance (eb1)	0.92	0.93	0.95	0.90	0.91	0.93	0.92	0.92			0.90	0.95	0.92	0.01
Surf-Surf Temp Difference (AW)	52.71	53.96	53.38	53.79	52.45	55.10	54.19	53.24	F		52.45	55.10	53.60	0.85
Surf-Surf Temp Difference (CTS)	45.50	40.89	45.29	43.54	42.20	43.87	45.09	45.41	F		40.89	45.50	43.97	1.70
Test Duration	17.50	30.00	40.50	33.50	25.50	70.00	43.00	22.00	hours		17.50	70.00		

Shanzhong Yuan, [1] Stanley D. Gatland II, [2] and William P. Goss [3]

Calibration Procedures for Hot Boxes

Reference: Yuan, S., Gatland, S. D. II, and Goss, W. P., **"Calibration Procedures for Hot Boxes,"** *Insulation Materials: Testing and Applications: 4th Volume, ASTM STP 1426*, A. O. Desjarlais, and R. R. Zarr, Eds., ASTM International, West Conshohocken, PA, 2002.

Abstract: A complete calibration on any Guarded or Calibrated Hot Box is critical for improving the accuracy of *U*-factor measurements of fenestration products. Any heat transfer that does not occur directly through the test specimen should be determined from the results of detailed calibration experiments. In addition, appropriate test conditions should be verified using national laboratory traceable calibration standards. In this paper, complete sets of calibration procedures using the University of Massachusetts Research Calibrated Hot Box under both the ASTM and ISO test methods are presented. Both the ASTM and ISO procedures include calibrations of the metering chamber extraneous heat transfer and the test specimen flanking heat transfer. The metering chamber extraneous heat transfer includes the metering chamber wall heat transfer, an insulated surround panel flanking heat transfer and other heat losses such as those through gaskets, mechanical fasteners, and less obvious heat transfer paths through the metering chamber wall or surround panel edges. The calibration procedure was conducted under ASTM and ISO test conditions. The calibrated heat transfer rates were characterized by the resulting surface temperature difference of the surround panel and the metering chamber the chamber wall thermopile voltage. In addition, the ASTM calibration procedures included the surface heat transfer coefficients calibrated using a plastic-faced Calibration Transfer Standard (CTS), and the ISO calibration procedures included the total surface thermal resistance calibrated using two Calibration Panels (CP).

Keywords: calibrated hot box, calibration, measurement, fenestration, heat transfer, thermal transmittance, thermal resistance, extraneous heat transfer

[1] Director of Thermal and Materials Testing Labs, ETC Laboratories, Inc., 297 Buell Road, Rochester, NY 14624.

[2] Manager of Building Science Technology, Insulation Group, CertainTeed Corporation, 750 East Swedesford Road, Valley Forge, PA 19482.

[3] Professor Emeritus, Department of Mechanical and Industrial Engineering, University of Massachusetts, Amherst, MA 01003.

Nomenclature

A_{SP} Surround panel projected area (m^2)
$C_{CTS,P}$ CTS polycarbonate thermal conductance ($W/m^2 \cdot K$)
$C_{CTS,EPS}$ CTS EPS thermal conductance ($W/m^2 \cdot K$)
e_1 CTS polycarbonate emissivity
e_{b2} Baffle emissivity
F_{1b} Room side radiative factor
F_c Convection fraction
$F_{c,i}$ Room side convection fraction
$F_{c,e}$ Cold side convection fraction
K_c Room side convective coefficient of test specimen ($W/m^2 \cdot K^{-1.25}$)
k_{EPS} EPS (expanded polystyrene) thermal conductivity ($W/m \cdot K$)
$k_{CTS,P}$ CTS polycarbonate thermal conductivity ($W/m \cdot K$)
L_S Specimen thickness (depth) (m)
h_h Warm side specimen overall surface heat transfer coefficient ($W/m^2 \cdot K$)
h_c Cold side specimen overall surface heat transfer coefficient ($W/m^2 \cdot K$)
h_{STh} Warm side standardized overall surface heat transfer coefficient ($W/m^2 \cdot K$)
h_{STc} Cold side standardized overall surface heat transfer coefficient ($W/m^2 \cdot K$)
q Heat Flux (Density of heat flow rate) through the test specimen (W/m^2)
Q_{BW} Heat transfer through the box (metering chamber) wall (W)
Q_{EXTR} Extraneous heat transfer in the metering chamber (W)
$Q_{EXTR,ASTM}$ Extraneous heat transfer in metering chamber under ASTM conditions (W)
$Q_{EXTR,ISO}$ Extraneous heat transfer in metering chamber under ISO conditions (W)
$Q_{FL,S}$ Specimen flanking heat transfer (W)
$Q_{FL,S;ASTM}$ Specimen flanking heat transfer under ASTM conditions (W)
$Q_{FL,S;ISO}$ Specimen flanking heat transfer under ISO conditions (W)
$Q_{FL,SP}$ Surround panel flanking heat transfer (W)
Q_{IN} Total power input to the metering chamber (W)
Q_{r1} Room side radiative heat transfer of test specimen (W)
Q_{c1} Cold side heat transfer of test specimen (W)
Q_S Heat transfer through the test specimen (W)
Q_{SP} Heat transfer through the surround panel (W)
$R_{eq.h}$ Warm side equivalent overall surface resistance ($m^2 \cdot K/W$)
$R_{eq.c}$ Cold side equivalent overall surface resistance ($m^2 \cdot K/W$)
$R_{eq.tot}$ Total equivalent overall surface resistance ($m^2 \cdot K/W$)
R_c Cold (climatic chamber) side overall surface resistance ($m^2 \cdot K/W$)
R_h Warm side overall surface resistance ($m^2 \cdot K/W$)
R_{SP} Surround panel thermal resistance ($m^2 \cdot K/W$)
$R_{s,tot}$ Total surface thermal resistance ($m^2 \cdot K/W$)
R_{sur} Surround panel thermal resistance ($m^2 \cdot K/W$)
t_1 Warm side specimen surface temperature (°C)
t_2 Cold side specimen surface temperature (°C)
t_{AMB} Ambient air temperature (°C)
t_c Cold side (climatic chamber) air temperature (°C)

t_h Warm side (metering room) air temperature (°C)
t_{mean} Mean temperature (°C)
t_{SP1} Warm side surround panel surface temperature (°C)
t_{SP2} Cold side surround panel surface temperature (°C)
$U_{CTS,C}$ Theoretically calculated CTS thermal transmittance ($W/m^2 \cdot K$)
$U_{CTS,M}$ Measured CTS thermal transmittance ($W/m^2 \cdot K$)
$U_{ST,CTS}$ Standardized CTS thermal transmittance ($W/m^2 \cdot K$)
V_c Climatic chamber air velocity (m/s)
V_h Metering chamber air velocity (m/s)
V_{BW} Metering chamber wall thermopile voltage (mV)
Δt_{SP} Surround panel surface temperature difference (°C)
$\theta_{me,sur}$ Surround panel mean temperature (°C)
σ Stefan-Boltzmann constant, 5.669×10^{-8} ($W/m^2 \cdot K^4$)

Introduction

Hot boxes must be calibrated for any extraneous heat transfer that does not flow through the test specimen. Rucker and Mumaw [*1*], and Lavine et al [*2*] developed calibration procedures and compared their calibration results with numerical calculations to determine the metering chamber wall and test specimen flanking losses. Goss and Olpak [*3*] discussed the design and calibration of a "first generation" calibrated hot box at the University of Massachusetts and Gatland et al [*4*] described the design and fabrication of the "second generation" research calibrated hot box that was used in this research.

One method of calibration often used to determine the metering chamber wall heat transfer is to maintain the same temperature in the climatic chamber (usually the cold side) as in the metering chamber to minimize any flanking heat transfer and then to systematically vary the guard room (or guard box) temperature above and below the metering chamber temperature. This is often difficult to do since it requires that the guard room and climatic chamber environments to be either heated and/or cooled and the climatic chamber has to operate at a temperature way above its design conditions. In addition, since almost all of the heat transfer from the metering chamber goes to the guard room, the electrical energy input to the metering chamber becomes relatively small and may even be less than the metering chamber circulation fan energy requirements which necessitates the use of smaller fans not used in the actual testing or cooling in the metering chamber. All of this adds to the uncertainty in the calibrated metering chamber wall and test specimen flanking heat transfer rates.

In addition, both current ASTM Standard Test Method for Measuring the Steady State Thermal Resistance of Fenestration Systems Using Hot Box Methods (C 1199-00), and ISO Thermal Performance of Doors and Windows – Determination of Thermal Transmittance by Hot Box Method (12567-1)] fenestration thermal transmittance standard test methods require additional calibration measurements to ensure that suitable test conditions are set up. In the ASTM C 1199-00 test method, an additional calibration procedure has to be performed to characterize the surface heat transfer coefficients of a Calibrated Transfer Standard (CTS) before testing actual fenestration products. As described in ISO 12567–1, the total surface thermal resistance calibration procedure has

to be conducted using two calibration panels with different thicknesses. It should also be noted that the ASTM C 1199-00 and ISO 12567-1 fenestration thermal transmittance test methods each have an underline basic hot box test methods. For ASTM C 1199-00, this is ASTM Standard Test Method for the Thermal Performance of Building Assemblies by Means of a Hot Box Apparatus (C 1363-97), and for ISO 12567-1, this is ISO Test Method: Thermal Insulation – Determination of Steady State Thermal Transmission Properties – Calibrated and Guarded Hot Box (8990).

The net heat transfer through a fenestration test specimen in a hot box is obtained from the power input to the metering chamber as shown in Figure 1. This power input includes heat transfer through the metering chamber (box) wall, the surround panel, the surround panel flanking region, and the specimen flanking region. So the net heat transfer through the test specimen can be calculated as:

$$Q_S = Q_{IN} - Q_{SP} - Q_{BW} - Q_{FL,SP} - Q_{FL,S} \tag{1}$$

The last term of Equation (1), $Q_{FL,S}$, is the specimen flanking heat transfer shown in Figure 1. The calibration of specimen flanking heat transfer becomes necessary when the specimen is thinner than the surround panel. ASTM C 1199-00 does not have this calibration procedure, while ISO 12567–1 specifies the use of tables to interpolate the specimen flanking loss. These tables contain calculated results rather than empirical data. In this paper, the experimental calibration procedure for the specimen flanking heat transfer was conducted and an empirical calibration equation was used for fenestration product testing.

In Equation (1) the metering chamber wall heat transfer and the surround panel flanking loss heat transfer are obtained from separate calibration experiments. In reality, however, these losses are difficult to separate. As described previously, the metering chamber wall heat transfer requires the metering and climatic chamber air temperatures to be kept at the same setting which differs by a few degrees Celsius from the ambient air temperature surrounding the hot box. However the air temperatures within the metering and climatic chambers usually differ by 20 °C during an ISO 12567-1 test of a fenestration system and by 38.9 °C during an ASTM C 1199-00 test. Therefore, these calibration experiments are difficult to conduct because of the unrealistic settings.

In this paper, a revised calibration procedure which combines both the metering chamber wall heat transfer and surround panel flanking loss heat transfer is presented. The heat transfer from these two losses was combined into term called the extraneous heat transfer, Q_{EXTR}, and it is shown in Equation (2) and Figure 2.

$$Q_S = Q_{IN} - Q_{SP} - Q_{EXTR} - Q_{FL,S} \tag{2}$$

In the complete calibration procedure for the University of Massachusetts Research Calibrated Hot Box, the following components were calibrated:

1. Metering chamber extraneous heat transfer based on both ASTM C 1199-00 and ISO 12567-1nominal test conditions.
2. Specimen flanking heat transfer using two expanded polystyrene panels with different thickness.

3. Total surface heat transfer coefficients using a polycyanurate faced CTS and following the ASTM C 1199-00 procedure.
4. Total surface thermal resistance using two calibration panels and following the ISO 12567-1 procedure.

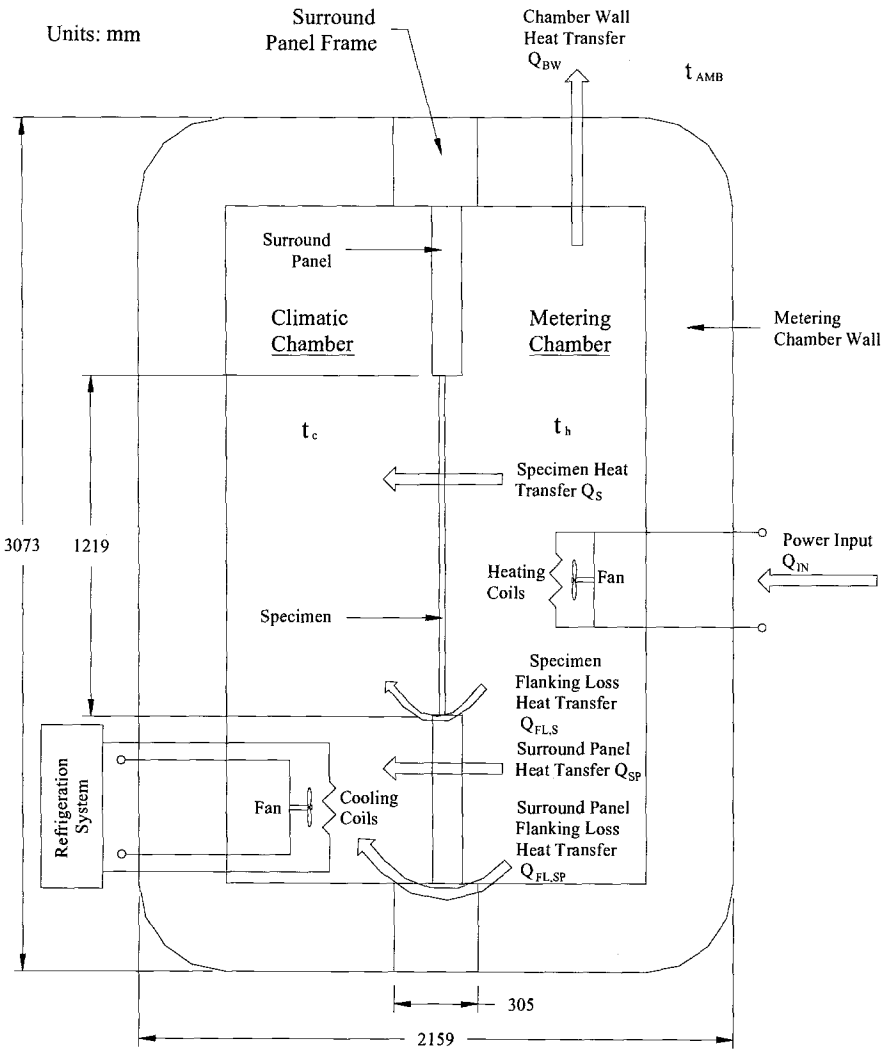

Figure 1 - *Heat Transfer in the Calibrated Hot Box*

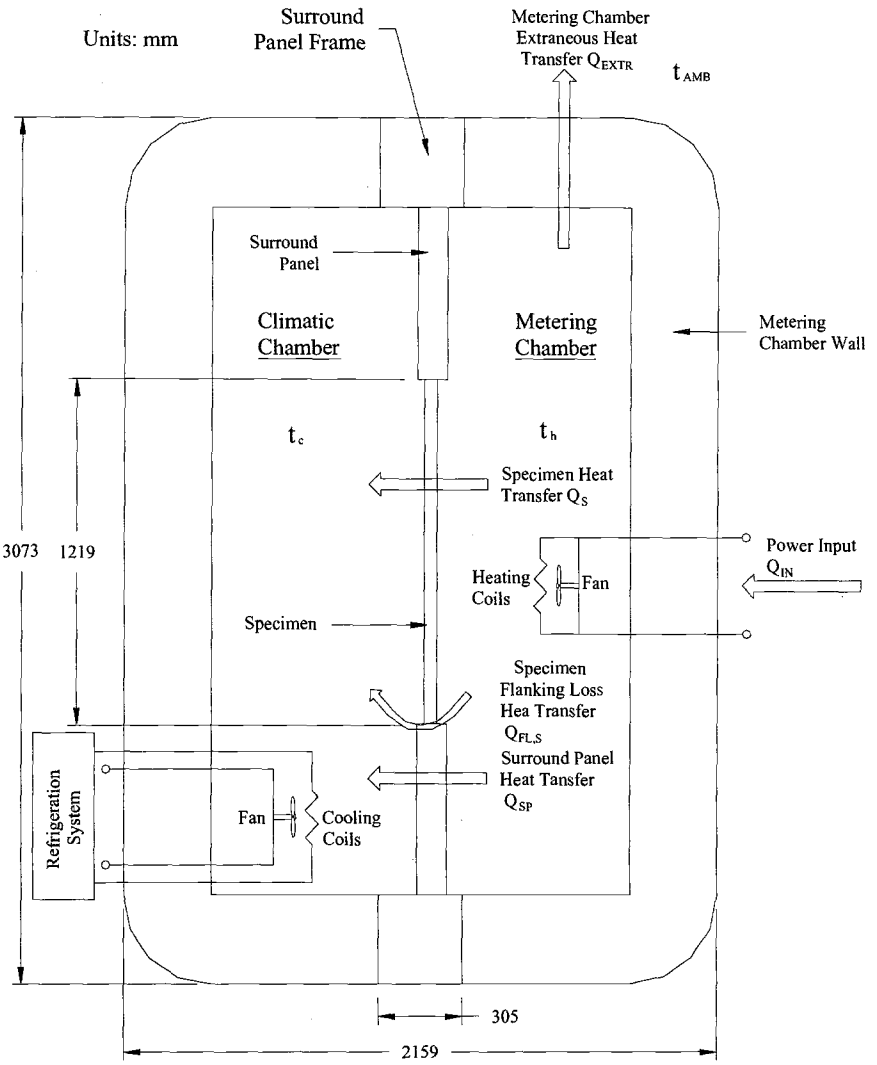

Figure 2 - *Schematic Setup for Calibration Experiments of the Hot Box Metering Chamber Extraneous Heat Transfer Q_{EXTR}*

Metering Chamber Extraneous Heat Transfer Calibration Experiments

By combining the metering chamber wall heat transfer, Q_{BW}, and the surround panel flanking heat transfer, $Q_{FL,SP}$, into the extraneous heat transfer, Q_{EXTR}, the net heat transfer through the test specimen can be obtained from Equation (2). The extraneous heat transfer, Q_{EXTR}, also includes other heat losses such as those through gaskets, pipes, tubing, wires, mechanical fasteners, and any other less obvious heat transfer through the metering chamber wall and/or surround panel frame. The calibration of Q_{EXTR} uses a continuous (homogeneous) surround panel. The experimental conditions approximate the nominal test conditions specified for the testing of fenestration products according to ASTM C 1199-00 and ISO 12567-1. Two sets of calibration experiments must be performed. In these calibration experiments, since there is no test specimen installed, the test specimen net heat transfer, Q_S, and the test specimen flanking heat transfer, $Q_{FL,S}$, are both zero. Another way to look at this is that these two heat transfer terms are now part of the surround panel heat transfer. For this situation, solving for the extraneous heat transfer, Q_{EXTR}, from Equation (2) results in the following equation:

$$Q_{EXTR} = Q_{IN} - Q_{SP} \tag{3}$$

Based on the nominal test conditions specified in ASTM C 1199-00 and ISO 12567–1, calibration experiments are conducted at several ambient and climatic chamber temperature settings. By measuring the power input and temperatures for each calibration experiment, the extraneous heat transfer is obtained. Using linear regression, an empirical calibration correlation for the extraneous heat transfer is then obtained. The following sections present this procedure in detail.

ASTM Extraneous Heat Transfer Calibration

A continuous surround panel with no test specimen was used in the surround panel frame section, and calibration conditions were set according to nominal test conditions. All conditions were maintained constant except the weather side and ambient air temperatures. The weather air temperature was varied three times around the nominal -17.8 °C (0 °F) when the ambient air temperature was set at each level of three different levels. Therefore, a total of nine calibration experiments were conducted. The calibration conditions are summarized in Table 1.

After the steady-state conditions were achieved, all surface and air temperatures were measured. The voltage for the metering chamber box wall thermopile was also measured as well as the total power input to the metering room. Detailed measurement data and calculation results are presented in Yuan [*5*].

Using multi-variant regression statistical technique, the extraneous heat transfer, Q_{EXTR}, of the hot box was obtained. The resulting empirical equation for Q_{EXTR} is:

$$Q_{EXTR,ASTM} = 0.9391\Delta t_{SP} + 1.3319V_{BW} - 0.4827 \tag{4}$$

It should be noted that the number of significant figures in Equation (4) and subsequent empirical correlation equations given in this paper are not reflective on the

actual experimental accuracy. An uncertainty analysis for these equations that ultimately yields an experimental uncertainty of the final founded off *U*-factor is given in Yuan [*5*] and Yuan, Russell and Goss [*6*].

Table 1 - *ASTM Experimental Conditions for the Calibration of* Q_{EXTR}

Condition	Units		Settings	
V_h	m/s (mph)		≤ 0.3 (0.67)	
V_c	m/s (mph)		6.67 (15)	
h_{STh}	W/(m^2·K) [Btu/(h·ft^2·°F)]		7.7 (1.36)	
h_{STc}	W/(m^2·K) [Btu/(h·ft^2·°F)]		29.0 (5.11)	
t_h	°C (°F)		21.1 (70.0)	
t_{AMB}	°C (°F)	19.4 (67.0)	21.1 (70.0)	22.8 (73.0)
		-20.6 (-5.0)	-20.6 (-5.0)	-20.6 (-5.0)
t_c	°C (°F)	-17.8 (0.0)	-17.8 (0.0)	-17.8 (0.0)
		-15.0 (5.0)	-15.0 (5.0)	-15.0 (5.0)

ISO Extraneous Heat Transfer Calibration

Following the ISO 12567-1 test method and the calibration conditions listed in Table 2, another nine calibration experiments were conducted. The experimental results are listed in Yuan [*5*]. The same regression technique was used and the resulting the empirical equation is:

$$Q_{EXTR,ISO} = 0.9269\Delta t_{SP} + 1.2667V_{BW} - 0.5068 \quad (5)$$

The differences between the ASTM C 1199-00 and ISO 12567-1 results given in Equations (4) and (5) are primarily due to experimental uncertainties and changes in the thermal properties of the metering box air and climatic chamber temperatures.

Table 2 - *ISO Experimental Conditions for the Calibration of* Q_{EXTR}

Condition	Units		Settings	
V_h	m/s (mph)		≤ 0.3 (0.67)	
V_c	m/s (mph)		≤ 10.0 (22.37)	
R_h	(m^2·K)/W [(h·ft^2·°F)/Btu]		0.13 (0.74)	
R_c	(m^2·K)/W [(h·ft^2·°F)/Btu]		0.04 (0.23)	
t_h	°C (°F)		20.0 (68.0)	
t_{AMB}	°C (°F)	18.3 (65.0)	20.0 (68.0)	21.7 (71.0)
		-2.8 (27.0)	-2.8 (27.0)	-2.8 (27.0)
t_c	°C (°F)	0 (32.0)	0 (32.0)	0 (32.0)
		2.8 (37.0)	2.8 (37.0)	2.8 (37.0)

Test Specimen Flanking Heat Transfer Calibration

The specimen flanking heat transfer is the heat transfer around the interface of the test specimen and the surround panel as shown in both Figures 1 and 2. It is caused by the non-homogeneity of the materials for the interface between the surround panel and test specimen. The difference in heat transfer conditions across the test specimen is the driving force. This flanking heat transfer exists when the test specimen has a thickness less than the surround panel. Therefore, for many fenestration products thinner than the surround panel, the specimen flanking heat transfer needs to be subtracted from the total power input to the metering chamber to obtain the net heat transfer for the specimen. The metering chamber heat transfer components and the calculation of net specimen heat transfer are shown in Figure 2 and Equation (2). Two expanded polystyrene (EPS) calibration panels were used for the test specimen flanking heat transfer calibration experiments conducted under ASTM C 1199-00 and ISO 12567-1 test conditions.

ASTM Test Specimen Flanking Heat Transfer Calibration

Based on the ASTM C 1199-00 test conditions, two calibration experiments were conducted using two homogeneous calibration panels. These two unpainted, expanded polystyrene (EPS) panels have different thickness. One is 20 mm and the other 60 mm. In each experiment, one of the calibration panels was installed in the middle of the test section, with one face set back from the climatic side of the surround panel by 25.4 mm as per the requirements of ASTM C 1199-00.

During each experiment, steady-state metering and climatic chamber conditions were maintained for at least four hours. In the metering chamber, the warm air was 21 °C and 0.2 m/s (70 °F and 0.5 mph) while in the climatic chamber, the cold air was controlled to –17.8 °C and 6.7 m/s (0 °C and 15 mph). The total power input to the metering chamber and the temperatures were recorded for the entire steady-state test period. Using these data, the specimen flanking heat transfer, $Q_{FL,S}$, was obtained according to the following equation:

$$Q_{FL,S} = Q_{IN} - Q_{SP} - Q_{EXTR} \tag{6}$$

where

$$Q_{SP} = \frac{A_{SP}(t_{SP1} - t_{SP2})}{R_{SP}} \tag{7}$$

Table 3 lists measurement results for two calibration runs under the ASTM C 1199-00 conditions. On the same hot box and under the same conditions, Gatland [7] made two calibration experiments using calibration panels with the same EPS material used in the CTS but different thicknesses. One was 25.4 mm (1 inch) and the other 50.8 mm (2 inches). Gatland's [7] results are also listed in Table 3 and used for regression analysis.

The regression curve is shown in Figure 3. The specimen flanking heat transfer under ASTM conditions is:

$$Q_{FL,S;ASTM} = 40.798 - 0.8475L_S + 0.0044L_S^2 \qquad (0 < L_S < 102.2mm) \qquad (8)$$

The differences between the ASTM C 1199-00 and ISO 12567-1 results given in Equations (8) and (9) are primarily due to experimental uncertainties and the changes in the thermal properties of the metering box walls and the surround panel frame due to changes in the ambient air and climatic chamber temperatures if the temperature dependent properties of the surround panel and calibration panels are accounted for.

Table 3 - *Specimen Flanking Heat Transfer Calibration Results*

Thickness L_S (mm)	Specimen flanking heat transfer $Q_{FL,S}$ (W)
20.0	25.305
25.4	22.712
50.8	7.766
60.0	6.852
102.2	0

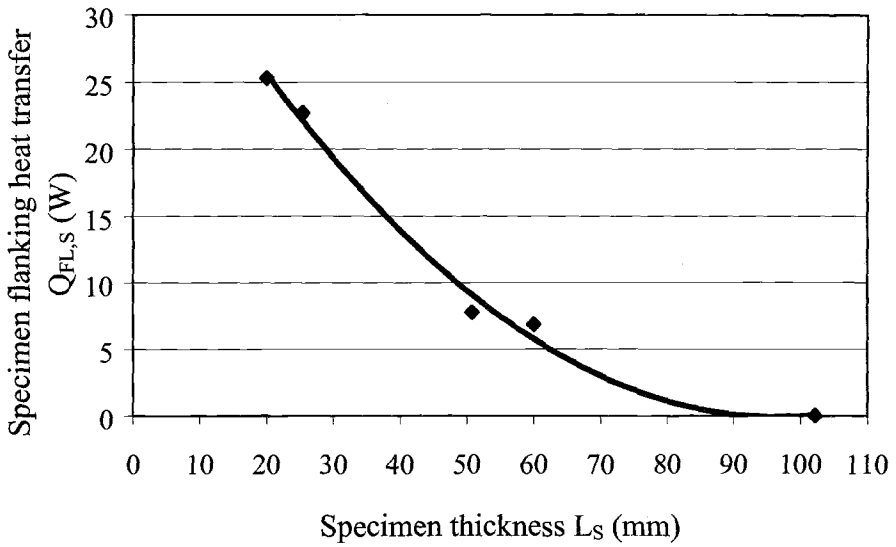

Figure 3 - *Specimen Flanking Heat Transfer Calibration Result*

ISO Test Specimen Flanking Heat Transfer Calibration

The same two EPS calibration panels used in the ASTM specimen flanking calibration experiments were used in the ISO calibrations. Following the ISO 12567-1, standard test conditions were established for the calibrated hot box. Each calibration panel was installed with one face flush with the metering side surround panel surface as per the requirements of the ISO 12567-1. The calibration data and results are documented in Yuan [*5*]. Table 4 shows the final calibration results. The correlation for the ISO specimen flanking heat transfer is given by Equation (9) that turned out to be similar to Equation (8):

$$Q_{FL,S;ISO} = 38.974 - 0.7566L_S + 0.0037L_S^2 \qquad (0 < L_S < 102.2mm) \qquad (9)$$

It should be noted here that using the ISO 12567-1 calculated specimen flanking heat transfer tables gives $Q_{FL,S;ISO}$ values an order of magnitude less than those given in Equation (9) (see Yuan [*5*]). This is probably due to the fact that the ISO calculated table values are for ideal heat transfer conditions, while the measured values in Table 4 are for the actual non-ideal heat transfer conditions. It should also be noted that the heat transfer rates (in W) are quite small relative to the other heat transfer rates (Q_{IN}, Q_S, Q_{EXTR}) and the experimental uncertainty (see Yuan, Russell and Goss [*6*]) for the smaller $Q_{FL,S;ISO}$ values in Table 4 are higher than those for the other heat transfer rates.

Table 4 - *ISO Specimen Flanking Heat Transfer Calibration Results*

Thickness L_S (mm)	Specimen flanking heat transfer $Q_{FL,S;ISO}$ (W)
20.0	25.311
60.0	6.797
102.2	0

ASTM Surface Heat Transfer Coefficients Calibration

The surface heat transfer coefficients on a test specimen indicate the heat transfer effects induced by the room and weather side chamber environments. These two overall coefficients are comprised of both the convective and radiative surface heat transfer coefficients. The radiative component is approximately equal to the natural convective component on the warm side of the specimen surface. On the weather side, the radiative component is relatively small due to the dominant convective heat transfer established by the forced, parallel or perpendicular, air flow. To establish the same standardized surface heat transfer conditions for different fenestration products, a calibration should be conducted to determine the correct operating parameters of the circulation fans, heaters and coolers in the metering side and weather side chambers.

According to ASTM C 1199-00, the surface heat transfer coefficients must be calibrated using a Calibrated Transfer Standard (CTS). Following Annex A1 of ASTM C 1199-00 Annex A of ISO 12567-1 and Goss et al [*8*], a plastic CTS was built and used in

the calibration of the University of Massachusetts Research Calibrated Hot Box. The EPS core material of this CTS has the same thermal conductivity as the surround panel core. It has the following temperature correlation [*5*, *7*]:

$$k_{EPS} = 0.03079 + 0.000123 t_{mean} \tag{10}$$

where, k_{EPS} is the thermal conductivity in W/(m·K) and t_{mean} is the mean temperature of the CTS EPS core in °C.

The total thickness of the CTS is 20.88 mm, consisting of a 12.88 mm thick EPS core sandwiched between two 4 mm polycarbonate sheets. The calibration experiment was conducted in accordance with ASTM C 1199-00. The calibration data and intermediate calculation values are documented in Yuan [*5*]. Table 5 lists the final calculation results.

Table 5 - *Calculations of CTS surface heat transfer coefficients and U-factors*

CTS heat transfer coefficients calibration Results		Unit	Data
$k_{CTS,P}$	(Conductivity of CTS plastic face)	W/m·K	0.192
$C_{CTS,P}$	(Conductance of CTS plastic face)	W/m²·K	48.000
$C_{CTS,EPS}$	(Conductance of CTS EPS core)	W/m²·K	2.373
e_1	(Emissivity of CTS polycarbonate face)	—	0.93
e_{b2}	(Emissivity of baffle)	—	0.90
F_{1b}	(Room side radiative factor)	—	0.83
σ	(Stefan-Boltzmann constant)	W/m²·K⁴	5.67E-08
t_1	(Room side CTS surface temperature)	°C	12.94
t_2	(Cold side CTS surface temperature)	°C	-15.78
Q_{r1}	(Room side radiative heat transfer)	W	23.46
Q_{c1}	(Room side convective heat transfer)	W	22.72
K_c	(Convection coefficient)	W/m²·K$^{-1.25}$	2.25
h_h	(Room side CTS surface coefficient)	W/m²·K	7.72
h_c	(Cold side CTS surface coefficient)	W/m²·K	29.38
Optional check of surface heat transfer coefficients			
h_{STh}	(Standardized room side surface coefficient)	W/m²·K	7.70
$(h_h - h_{STh})/h_h$		%	0.25
h_{STc}	(Standardized cold side surface coefficient)	W/m²·K	29.00
$(h_c - h_{STc})/h_c$		%	1.30
Optional check of U-factors			
$U_{CTS,M}$	(Measured CTS U-factor)	W/m²·K	1.598
$U_{CTS,C}$	(Theoretically calculated CTS U-factor)	W/m²·K	1.595
$(U_{CTS,M} - U_{CTS,C})/U_{CTS,M}$		%	0.16
$U_{ST,CTS}$	(Standardized CTS U-factor)	W/m²·K	1.596
$(U_{CTS,M} - U_{ST,CTS})/U_{CTS,M}$		%	0.12

Based on the measured power input to the metering chamber, the net heat transfer through the CTS was obtained using the other hot box calibration results presented in previous sections of this paper. Since the thermal conductivity of the CTS EPS core is known, the theoretical one-dimensional heat transfer through the CTS can be calculated.

Using the measurement results and calculated CTS heat transfer, the CTS surface heat transfer coefficients and convective coefficient were obtained. Table 5 presents these calculations and results. Also shown in Table 5 are measured and standardized *U*-factors determined according to ASTM C 1199-00. These *U*-factors and the theoretically calculated *U*-factor were compared with each other, and the good agreement is shown in the last part of Table 5. The validated surface heat transfer coefficients can then be used to determine the appropriate test conditions and the thermal transmittance of fenestration products that are tested using ASTM C 1199-00.

ISO Total Surface Thermal Resistance Calibration

Based on ISO 12567-1, two calibration panels with total thicknesses of 20 mm and 60 mm, respectively, were used in the total surface resistance calibration. The core of the panels was EPS, and the skin was two pieces of 4 mm float glass according to Annex C of ISO 12567-1. The overall dimension of these two calibration panels is the same, 1200 mm by 1200 mm. The thermal properties of the EPS were measured in a hot plate apparatus according to ISO Thermal Insulation – Determination of Steady State Thermal Resistance and Related Properties – Heat Flow Meter Apparatus (8302), while the material properties of surround panel were measured using a hot plate according to ASTM Standard Test Method for Steady-State Heat Flux Measurements and Thermal Transmission Properties by Means of the Heat Flow Meter Apparatus (C 518-98).

Six calibration experiments were conducted on these two panels. The first calibration was used to determine the circulation fan settings in the hot box [*5*]. Once the ISO 12567-1 total surface thermal resistance, $R_{s,t}$, of (0.17 ± 0.01) $m^2 \cdot K/W$ was achieved, the settings were kept constant for the remaining calibration experiments. The results for the ISO 12567-1 calibration experiments are plotted in Figures 4 to 6 along with their corresponding least squares regression curves. The correlations are as follows:

1. Thermal resistance of the surround panel:

$$R_{sur} = 3.254 - 0.0113 \cdot \theta_{me,sur} \tag{11}$$

2. Total surface resistance:

$$R_{s,tot} = 0.179 \cdot q^{(-0.0162)} \tag{12}$$

3. Convective fraction:

$$F_{c,i} = 0.5462 - 0.0008 \cdot q \tag{13}$$

$$F_{c,e} = 0.7055 + 0.002 \cdot q \tag{14}$$

The results given in Equations (11) to (14) can then be used to determine the appropriate test conditions and the thermal transmittance of fenestration products that are tested using ISO 12567-1.

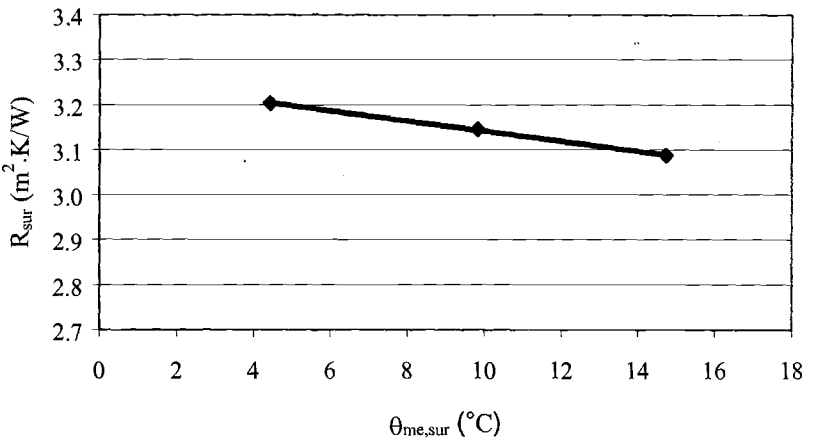

Figure 4 - *Thermal Resistance of the Surround Panel*

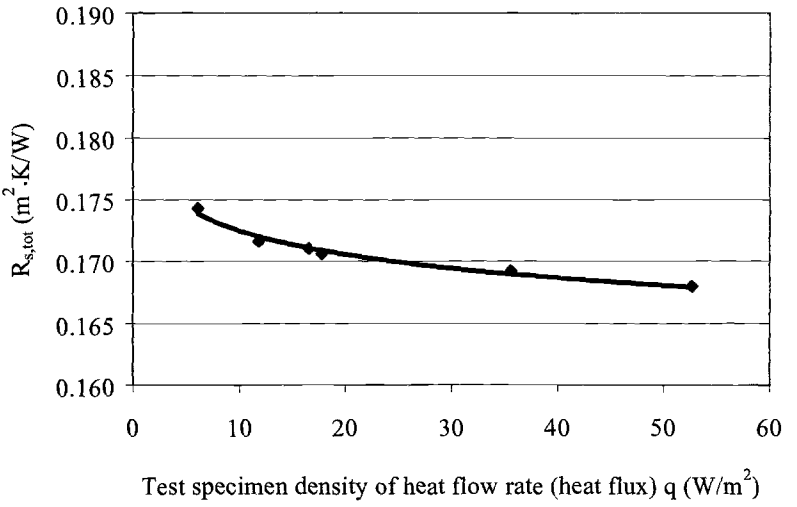

Figure 5 - *Total Surface Resistance*

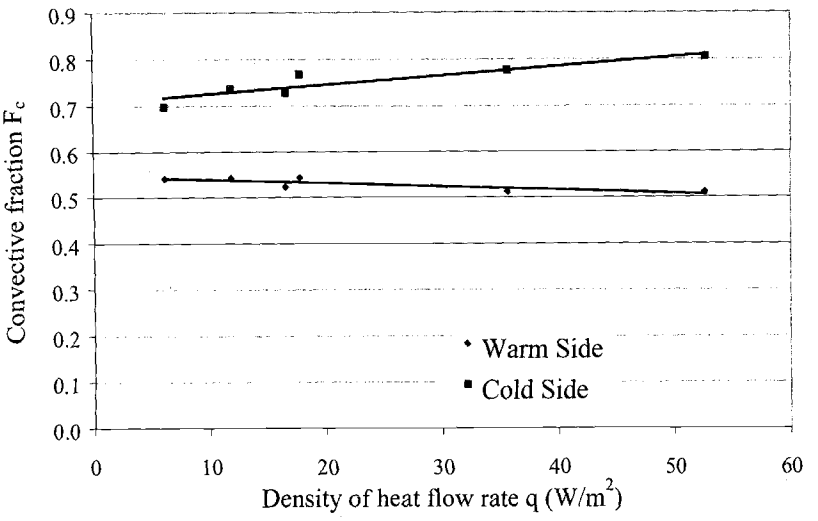

Figure 6 - *Convective Fraction*

Summary of Results

Careful calibration is critical to hot box measurement accuracy and achievement of the proper test conditions. In this paper, a complete hot box calibration procedure using ASTM and ISO standard test methods for fenestration products has been presented.

Metering Box Extraneous Heat Transfer

The traditional metering chamber calibration procedure has been modified to require only one calibrated heat transfer rate, the extraneous heat transfer, Q_{EXTR}, from the metering box. This procedure combines two usually separate calibrations: the metering chamber wall heat transfer and the surround panel flanking heat transfer. Using test conditions that are similar to those used when testing fenestration products, this procedure is more practical and applicable than previously used separate calibration procedures. The extraneous heat transfer calibration results for the University of Massachusetts Research Calibrated Hot Box using ASTM C 1199-00 and ISO 12567-1 are presented in Equations (4) and (5), respectively. The results are similar, with the primary differences due to experimental uncertainties and the different air (climatic, ambient and metering) temperatures in ASTM C 1199-00 and ISO 12567-1. While not shown in this paper, Yuan [*5*] and Yuan, Russell and Goss [*6*], give uncertainty results that show a significant improvement in the overall *U*-factor uncertainty from the usual ±10 % range to the ±5 to 6 % range using this modified calibration procedure.

Test Specimen Flanking Heat Transfer

The thermal transmittance measurements of fenestration systems are more accurate when the specimen flanking heat transfer is taken into account. Since calculated two-dimensional *U*-factors normally assume that no test specimen flanking heat transfer occurs, subtracting out the calibrated specimen flanking heat transfer before determining the measured *U*-factor will tend to make the comparisons between the calculated and measured values more reliable. It is shown in Yuan [*5*] and Yuan, Russell and Goss [*6*] that the uncertainty in the test specimen flanking heat transfer is the largest contribution to the overall *U*-factor uncertainty even though the specimen flanking heat transfer is usually much smaller than the test specimen heat transfer. ISO 12567-1 has tables of theoretically calculated two-dimensional specimen flanking heat transfer values due to the recognition of the difficulty of obtaining experimental calibrated values. It should also be noted that the specimen flanking heat transfer calibration experimental results presented in this paper only apply to the University of Massachusetts Research Calibrated Hot Box while the tables in ISO 12567-1 are intended for use by all hot boxes following that test method. As might be expected, as shown in Yuan [*5*], the experimental results are larger than the ISO 12567-1 table results that are for ideal conditions.

Test Specimen Surface Heat Transfer Coefficients

The ASTM C 1199-00 test method specimen surface heat transfer coefficients are calibrated using a CTS that is used to set up the appropriate metering and weather side fan speed settings. The resulting calibrated surface heat transfer coefficients can also be used to determine standardized test specimen *U*-factors. The results presented in Table 5 illustrated the procedure.

The ISO 12567-1 test method specimen surface heat transfer coefficients are combined into a total surface thermal resistance range that must be set by the use of calibration panels. Equations (11) to (14) and Figures 4 to 6 present the calibrated correlation results for the thermal resistance of the surround panel, the total surface resistance, and the room (metering box) and cold (climatic chamber) side convective fractions.

Yuan [*5*] presents further details on all of the above calibration procedures and also presents the use of these calibration results in determining the ASTM C 1199-00 and ISO 12567-1 overall *U*-factor for glazing unit and PVC window test specimens.

Conclusions and Recommendations

Calibration Procedures for ASTM C 1199-00 and ISO 12567-1 are presented in this paper. The metering box calibration procedure combines the surround panel and the metering box wall heat transfer into a single term, the metering box extraneous heat transfer. This reduces the number of metering box calibration tests, eliminates the need to test at significant off design conditions for a surround panel flanking heat transfer term and should reduce the metering box heat transfer uncertainty. It is recommended that future versions of ASTM C 1199-00 (and/or ASTM C1363-97) and ISO 12567-1 (and/or

ISO 8990) include the metering box extraneous heat transfer calibration procedure given in this paper.

Test specimen flanking heat transfer calibration tends to be more uncertain than the metering box extraneous heat transfer due to the smaller amount of heat transfer. It is recommended that future versions of ASTM C 1199-00 include this heat transfer calibration so that test specimen overall *U*-factors are more consistent with theoretical calculated values. Is is also recommended that future versions of ISO 12567-1 consider requiring experimental calibrated specimen flanking heat transfer results rather than the idealized calculated values currently in use.

The difference in ASTM C 1199-00 and ISO 12567-1 test methods for calibrating the specimen surface heat transfer coefficients has been presented. It is recommended that future versions of ASTM C 1199-00 either adopt or include the ISO 12567-1 specimen surface heat transfer coefficients calibration procedure.

Improvements in the overall *U*-factor uncertainty from ±10 % to ±5 to 6 % are possible by using some of the calibration procedures given in this paper.

References

[*1*] Rucker, J. L., and Mumaw, J. R., "Calibration Procedures and Results for a Large Calibrated Hot Box," *Thermal Performance of the Exterior Envelopes of Buildings, ASHRAE STP 28*, American Society of Heating, Refrigerating and Air-Conditioning Engineers, GA, 1981, pp. 237–249.

[*2*] Lavine, A. G., Rucker, J. L., and Wilkes, K. E., "Flanking Loss Calibration for a Calibrated Hot Box," *Thermal Insulations, Materials, and Systems for Energy Conservation in the 80's, ASTM STP 789*, American Society for Testing and Materials, West Conshohocken, PA, 1983, pp. 234–247.

[*3*] Goss, W. P., and Olpak, A., "Design and Calibration of a Rotatable Thermal Test Facility," *Thermal Insulations, Materials, and Systems for Energy Conservation in the 80's*, ASTM STP 789, F. A. Govan, D. M. Greason and J. D. McAllister, Eds., American Society for Testing and Materials, 1983, pp. 215–233.

[*4*] Gatland, S. D. II, Goss, W. P., and Curcija, D., "The Design and Fabrication of a Calibrated Hot Box Apparatus," *Insulation Materials: Testing and Application*, Third Volume, ASTM STP 1320, R. S. Graves and R. R. Zarr, Eds., American Society of Testing and Materials, 1997, pp. 73–90.

[*5*] Yuan, S., "Experimental and Analytical Heat Transfer Analyses for a Calibrated Hot Box and Fenestration Systems," Ph.D. dissertation, University of Massachusetts, Amherst, MA, 2001.

[*6*] Yuan, S., Russell, G. A., Goss, W. P., "Uncertainty Analysis of a Calibrated Hot Box," *Insulation Materials: Testing and Applications: 4th Volume, ASTM STP*

1426, A. O. Desjarlais and R.R. Zarr, Eds., ASTM International, West Conshohocken, PA, 2002.

[*7*] Gatland, Stanley D. II, "The Design, Fabrication, Calibration, and Operation of a Second Generation Research Calibrated Hot Box," M.S. thesis, University of Massachusetts, Amherst, MA, 1996.

[*8*] Goss, W. P., Elmahdy, H. H., and Bowen, R. P., "Calibrated Transfer Standards for Fenestration Systems," *In-Situ Heat Flux Measurements in Buildings: Applications and Interpretation of Results*, *CRREL Special Report 91-3*, S. N. Flanders, Ed., 1991, pp. 251-260.

Session 5: Industrial Insulations

Kenneth E. Wilkes,[1] Andre O. Desjarlais,[1] Therese K. Stovall,[1] David L. McElroy,[1] Kenneth W. Childs,[1] and William A. Miller[1]

A Pipe Insulation Test Apparatus for Use Below Room Temperature

Reference: Wilkes, K. E., Desjarlais, A. O., Stovall, T. K., McElroy, D. L., Childs, K. W., and Miller, W. A., **"A Pipe Insulation Test Apparatus for Use Below Room Temperature,"** *Insulation Materials: Testing and Applications: 4th Volume, ASTM STP 1426*, A. O. Desjarlais and R. R. Zarr, Eds., ASTM International, West Conshohocken, PA, 2002.

Abstract: Several ASTM material standards for pipe insulations require thermal performance data for systems in which pipe surface temperatures are below room temperature. ASTM Test Method for Steady-State Heat Transfer Properties of Horizontal Pipe Insulation (C 335) and ASTM Test Method for Steady-State Heat Transfer Properties of Pipe Insulation Installed Vertically (C 1033) are the only ASTM pipe insulation test methods, but these are used above room temperature. This paper describes proof-of-concept tests near room temperature on a new pipe insulation tester for evaluating pipe systems operating below room temperature.

The pipe insulation test specimen is inside an electrically heated cylindrical screen which is guarded by a fluid-cooled copper shell with intervening insulation. The main heat flow is radially inward through the test specimen to a central fluid-cooled tube. By matching the temperature of the heater to that of the guard, unwanted radial heat flow to or from the screen heater is minimized. Assuming only inward radial heat flow, a preliminary combined uncertainty was estimated at about ±0.8%.

The new tester has yielded results on three types of pipe insulation: fiberglass, polyisocyanurate foam, and elastomeric foam. Results on the latter two types were compared with results on board specimens of similar materials using ASTM Test Method for Steady-State Thermal Transmission Properties by Means of the Heat Flow Meter Apparatus (C 518).

Finite difference thermal modeling using the HEATING7 program was performed to assess the potential for systematic errors due to deviation from purely radial heat flow. The modeling results showed this type of error to be less than 0.5% for the prototype tester. Modeling was also used to identify design parameters for future testers that would accommodate different pipe sizes and insulation thicknesses and would operate at other temperatures. Designs are in progress to allow use of the tester to pipe surface temperatures as low as -190 °C (-310 °F).

Keywords: pipe insulation, test apparatus, below room temperature

[1] Senior Researchers, Oak Ridge National Laboratory, Oak Ridge, TN 37831.

Introduction

Several ASTM material standards for pipe insulation require thermal performance data below room temperature. There are two ASTM pipe insulation test methods, C 335 and C 1033. Both of these are based on a heated pipe, with heat flow outwards, and both are generally for use above room temperature. Even if these methods were adapted for use below room temperature, the heat flow would still be in the direction opposite to that for flow of a cold fluid through the pipe.

This paper describes a new pipe insulation tester for use below room temperature, wherein the heat flow is inwards towards a cold pipe. Results of proof-of-concept tests with the new apparatus operated near room temperature are given. Results are given of computer modeling that was used to examine systematic errors due to deviation from purely radial heat flow. Modeling was used to assess this type of error in the prototype apparatus and also to assist in design of future testers that would accommodate different pipe sizes and insulation thicknesses and that would be operated at different temperatures. The new apparatus may be suitable for inclusion in C 335 and/or C 1033, or in a new standard test method.

Apparatus

An apparatus was constructed that allows measurements on pipe systems operating below room temperature. Figure 1 shows an axisymmetric schematic of the apparatus. Starting from the inside, the apparatus consisted of a tube through which cold fluid circulated, the test specimen, a thin screen heater, guard insulation, a temperature-controlled guard shell, and outer insulation. The temperatures of the heater and shell were matched so that the heat generated in the thin heater passed radially inwards through the test insulation to the cooled inner tube. The central section of the apparatus served as a metered section with end regions forming a passive guard.

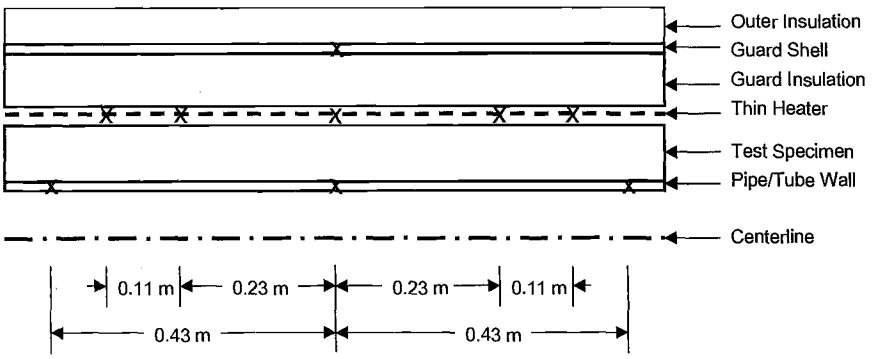

Figure 1 - *Schematic of Pipe Insulation Test Apparatus for below Room Temperature. Crosses denote thermocouple locations.*

A cold pipe or tube was located at the axis of the apparatus. The initial setup used a copper tube with an outside diameter of 34.9 mm (1.375 in.) and a length of 1.5 m (60 in.). Reducers and 12.7 mm (0.5 in.) outside diameter copper tubes were soldered at each end for attachment by rubber tubing to a constant temperature bath which circulated an ethylene glycol mixture through the tube. Initially, the tube was bare, but was later coated with black paint. The total hemispherical emittance of the paint was measured previously and was found to vary linearly with temperature from 0.75 at 50 °C to 0.79 at 150 °C [*1*].

The thin heater was made of a nichrome screen having a 40 by 40 mesh (wires per 25.4 mm) of 0.25-mm-diameter wire (0.010 in. wire). This is the same type of heater that has been used for a flat thin-heater apparatus [*1*]. The screen was rolled into a cylinder with an inside diameter of 88.9 mm (3.50 in.), an outside diameter of 90.2 mm (3.55 in.), and a length of 0.946 m (37.25 in.). Heavy brass flanges were bolted to each end to provide distribution of a direct electrical current from a regulated D.C. power supply.

The outer shell was made from a Type M copper tube (see ASTM Specification for Seamless Copper Water Tube (B 88)) that had an outside diameter of 155.6 mm (6.125 in.), a wall thickness of 3.18 mm (0.125 in.), and a length of 0.914 m (36 in.). The tube was split lengthwise in half for convenience in assembly of the apparatus. Copper tubing with an outside diameter of 15.9 mm (0.625 in.) was soldered to the outside surfaces of the shell. The copper tubing was placed in a lengthwise serpentine pattern with four lengths of tubing on each half of the shell. The copper tubing was connected to a second constant temperature bath which circulated an ethylene glycol solution through the tubing. Initial tests were done with a bare copper inner surface, but a coating of black paint was added later.

Glass fiber pipe insulation wrapped with silicone rubber sheets filled the space between the thin heater and the outer shell. Foil-faced glass fiber duct insulation about 25 mm thick was wrapped around the outside of the outer shell assembly. Finally, glass fiber batt insulation was placed around the portions of the cold tube that protruded from the ends of the test specimen.

Temperatures in the system were measured with Type E (chromel-constantan) thermocouples made from spools of calibrated 36 AWG (0.13 mm, 0.005 in. diameter) wire. An ice-water bath was used as a reference junction, and emfs were read from a calibrated digital voltmeter. On the 0.1V range, the voltmeter had an uncertainty of $\pm$ (0.08 μV + 0.0013%). Thermocouples were bonded to the copper surfaces using thermally conductive epoxy and were spot-welded to platinum wire studs that had been spot-welded to the thin heater. For the initial setup, thermocouples were mounted on the inner tube 0.43 m (17 in.) on each side of the midplane. After the inner tube was coated with black paint, a thermocouple was added at its midplane. Five thermocouples were mounted on the heater: at the midplane, 0.23 m (9.0 in.) on each side of the midplane, and 0.34 m (13.5 in.) on each side of the midplane. One thermocouple was mounted on the inner surface of each half of the outer copper shell.

Power input to the thin heater was measured using voltage taps spot-welded at 0.23 m (9.0 in.) on each side of the midplane. The voltage taps were made of 22 AWG (0.64 mm, 0.025 in. diameter) nichrome wire. Use of nichrome wire essentially eliminated Seebeck emfs due to differences in temperature on the heater between the locations of the voltage taps. The current through the heater was measured by the voltage drop across a

precision 0.01 ohm standard resistor in series with the heater. The power input to the 0.46 m (18.0 in.) long metering section was calculated as the product of the voltage drop and the current.

The apparent thermal conductivity (λ) of the test insulation was calculated from the following equation,

$$\lambda = \frac{P \ln(D_2/D_1)}{2\pi L (T_2 - T_1)} \quad (1)$$

where P is the power dissipated in the central 0.46 m (18.0 in.) metering section of the heater, L is the length of the metering section, 0.46 m (18.0 in.), D_1 and D_2 are the inside and outside diameters of the test insulation, respectively, and T_1 and T_2 are the inside and outside temperatures of the insulation, respectively. The temperature of the inside of the insulation was taken as the average of the readings of the thermocouples on the inner tube. When the test insulation fitted snugly inside the thin heater, the temperature of the outside of the insulation was taken as the average of the three middle thermocouples on the screen heater. If the test insulation did not fit snugly within the heater, additional thermocouples were taped to the outer surface of the test specimen at the same axial locations as the thermocouples on the heater.

The measured power was corrected for small heat exchanges between the heater and the outer copper shell. The average thermal conductivity of the insulation between these two components was measured in calibration tests by matching the temperature of the inner copper tube to that of the heater and then running the outer copper shell at a lower temperature. The measured value of apparent thermal conductivity was 0.0369 W/m•K, and this value was used for calculating corrections. Correction for this radial heat flow was less than 3%. No corrections were made for axial conduction along the heater since modeling described later in this paper shows this effect to be negligible.

The prototype apparatus was placed in a laboratory, where the dew point was typically above -1 °C. Since the apparatus was not contained in a low humidity environment, the lowest pipe test temperatures were selected to avoid condensation on the pipe or within the insulation. To enable tests at lower pipe temperatures, plans call for placement of the apparatus inside a commercially available glove box, where the dew point can be maintained as low as -76 °C by using molecular sieve desiccants.

A preliminary uncertainty analysis was performed for the quantities in Eqn. 1, using the typical case of an insulation with outside and inside diameters of 88.9 mm (3.50 in.) and 34.9 mm (1.375 in.), respectively, and a temperature difference of 20 °C. A conservative estimate of the combined uncertainty, obtained by summing the absolute values of individual uncertainties, was ±1.7%. Use of the law of propagation of uncertainties (square root of the sum-of-the-squares) gave a combined uncertainty of ±0.8%. These uncertainties will be different for other insulation sizes and temperature differences. (Most of the individual uncertainties were estimated such that, for all practical purposes, there was a 100% probability that the true value was within that uncertainty range. With this method of estimation of individual uncertainties, combined

standard uncertainties could be calculated that would be a factor of $\sqrt{3}$ lower than those just stated. See Taylor and Kuyatt [2] for more details on expressions of uncertainty.)

Test Results

Glass Fiber Insulation

The first set of measurements was made on a molded glass fiber pipe insulation that was obtained from the ORNL insulation shop. The insulation had outside and inside diameters of 88.9 mm (3.50 in.) and 34.9 mm (1.375 in.), respectively. The density was 56 kg/m^3 (3.5 lb/ft^3). One set of tests was performed with bare copper surfaces on the central tube and on the outer shell, while the second set was performed after both of these surfaces had been blackened. Also, the midplane thermocouple was added to the inner tube during the painting operation. All subsequent testing on other types of insulation was performed with blackened surfaces, and with three thermocouples on the inner tube.

Tests were performed with a temperature difference of 10 or 20 °C, and the results are shown in Figure 2. Blackening the tube resulted in an increase in the measured

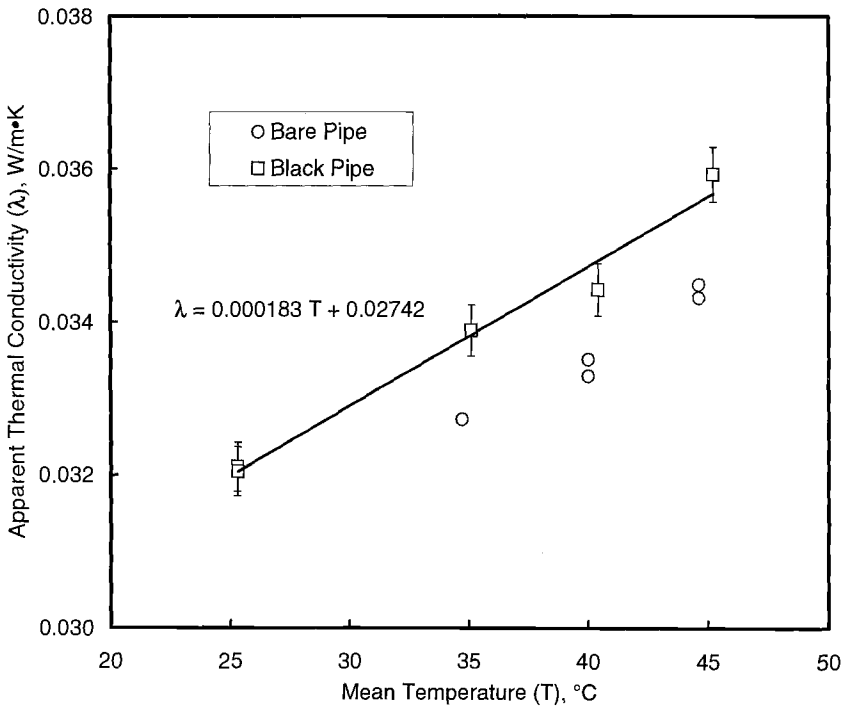

Figure 2 - *Apparent Thermal Conductivity of Glass Fiber Pipe Insulation Specimen with Density of 56 kg/m^3 (3.5 lb/ft^3), Outside Diameter of 88.9 mm (3.50 in.), and Inside Diameter of 34.9 mm (1.375 in.). The bars on the data points for the black pipe are ± 1% of the corresponding λ value.*

apparent thermal conductivity of about 4 to 5%. The data for the black tube were fitted to a relationship linear in temperature and the resulting equation is given on Figure 2 (it is recognized that thermal conductivity generally varies more strongly with temperature, but a linear variation is adequate over the small temperature range shown in Figure 2). The individual data points are all within 1% of the regression line. ASTM Specification for Mineral Fiber Pipe Insulation (C 547) lists the maximum apparent thermal conductivity at 37.8 °C for Type I pipe insulation (minimum 48 kg/m^3, 3 lb/ft^3) as 0.0361 W/m•K. The linear regression of the data with the black tube is less than 5% below this value.

It was also observed that blackening the tube produced more uniform temperatures within the system. Before blackening, temperature variations on the inner tube ranged from 0.30 to 0.92 °C (the larger variations corresponded to larger temperature differences across the test insulation). After blackening, these variations were reduced to 0.21 to 0.50 °C. Similarly, temperature variations on the screen varied from 0.10 to 0.24 °C before blackening, and from 0.02 to 0.10 °C after blackening.

Polyisocyanurate Foam Insulation

The second series of tests was performed on polyisocyanurate foam insulation furnished by an insulation manufacturer. The two-piece pipe insulation had outside and inside diameters of 88.9 mm (3.50 in.) and 34.9 mm (1.375 in.), respectively. Three companion flat slabs about 23.8 mm (0.937 in.) thick were cut from the same piece of foam that was used for the pipe insulation. The density of both types of specimens was 33 kg/m^3 (2.1 lb/ft^3). The apparent thermal conductivity of the flat slabs was measured using C 518 to provide a basis for comparison with results from the pipe insulation tester.

Since the foam was still aging, apparent thermal conductivity measurements were made over a time period of six to eight months. Measurements were made at a mean temperature of 25 °C (77 °F) with a temperature difference of 20 °C. Figure 3 shows the normalized apparent thermal conductivity versus time for the average of the three boards and for the pipe insulation. The data were normalized by dividing the actual thermal conductivity values by the first value that was measured for the pipe insulation. The aging time was estimated by the time of receipt of the specimens. Over the time period of the measurements, the apparent thermal conductivities of both the board and pipe insulations increased by about 8%. Figure 4 shows the apparent thermal conductivity plotted versus a scaled time, which was obtained by dividing the aging time by the square of either the board thickness or the square of the pipe insulation wall thickness. Plotting the data versus scaled time brings the two curves closer together. When compared this way, the two conductivities are within about 2% initially and then converge to within about 1%.

The level of agreement between the two sets of data is considered to be very good, especially considering that the previous aging history of the specimens and their relative locations within the piece from which they were cut were not known. In addition, the different geometries of the specimens may produce differences in aging. For the board specimens, diffusion of air into the specimen and diffusion of the blowing agent out should be one-dimensional in the central location where the apparent thermal

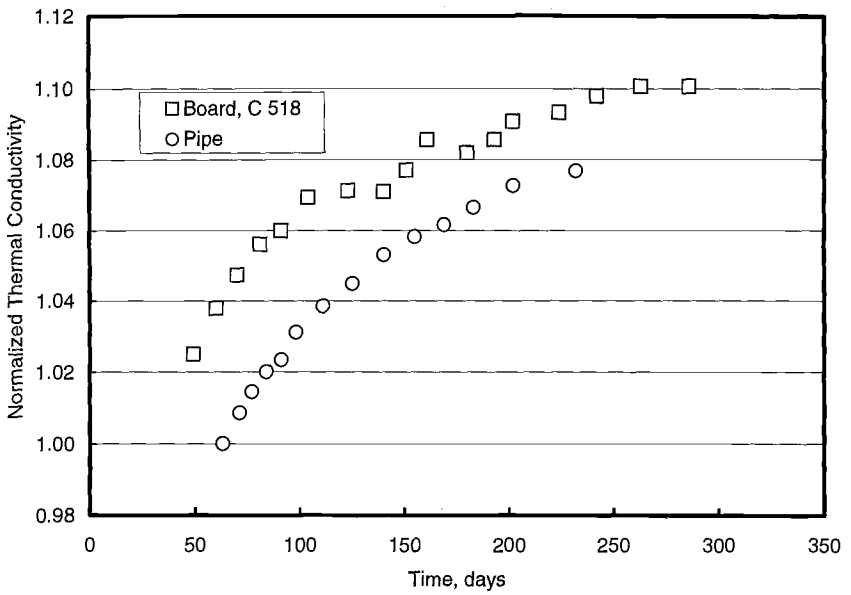

Figure 3 - *Apparent Thermal Conductivity of Polyisocyanurate Foam Insulation. The pipe insulation had an outside diameter of 88.9 mm (3.50 in.) and an inside diameter of 34.9 mm (1.375 in.). The board specimens were 23.8 mm (0.937 in.) thick. The density of both types of specimens was 33 kg/m^3 (2.1 lb/ft^3). The mean temperature was 25 °C. The data have been normalized by dividing each data point by the first data point for the pipe insulation.*

conductivity was measured. For the pipe specimen, however, two-dimensional diffusion should occur because of the cut radial surfaces. Further study is needed to determine the impact of the two-dimensional diffusion on the average apparent thermal conductivity of pipe insulation specimens.

Elastomeric Foam Insulation

The third set of measurements was performed on elastomeric foam pipe insulation. The pipe insulation was obtained from the ORNL insulation shop. The insulation had outside and inside diameters of 80.4 mm (3.167 in.) and 28.6 mm (1.125 in.), respectively. The density was 66 kg/m^3 (4.1 lb/ft^3). The previously used inner copper tube was replaced with a blackened copper tube having an outside diameter of 28.6 mm (1.125 in.) to accommodate the new specimen. Three thermocouples were taped to the outside surface of the insulation, at the midplane and at 0.23 m (9 in.) on each side of the midplane. Silicone rubber sheets were wrapped around the specimen to fill the remaining space between the thin heater and the specimen. The thermal resistances of the specimen and silicone rubber were such that about 90% of the 25 °C temperature difference between the heater and the inner tube occurred across the test specimen.

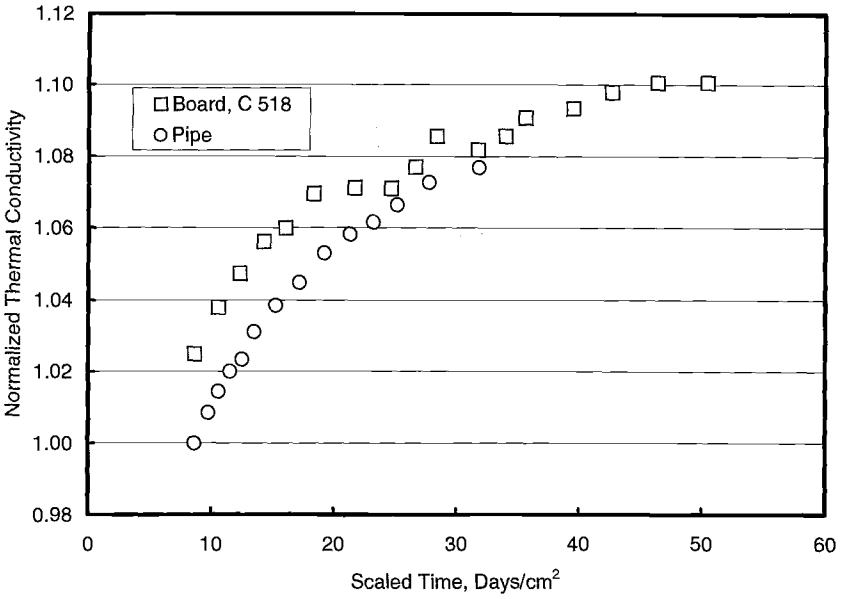

Figure 4 - *Apparent Thermal Conductivity of Polyisocyanurate Foam Insulation. The pipe insulation had an outside diameter of 88.9 mm (3.50 in.) and an inside diameter of 34.9 mm (1.375 in.). The board specimens were 23.8 mm (0.937 in.) thick. The density of both types of specimens was 33 kg/m^3 (2.1 lb/ft^3). The mean temperature was 25 °C. The data have been normalized by dividing each data point by the first data point for the pipe insulation. The scaled time is the aging time divided by the square of the board thickness or the square of the pipe insulation wall thickness.*

To form a basis for comparison, C 518 heat-flow-meter apparatus measurements were performed on flat sheets of similar elastomeric foam insulation from which the skins had been removed. The sheets were about 7.6 mm (0.3 in.) thick, and four sheets were stacked to make up a test specimen. The density of the sheet material was 61 kg/m^3 (3.8 lb/ft^3), which was within 10% of the density of the pipe insulation.

Results of the measurements on the pipe insulation are given in Table 1, in the order in which the tests were performed. Table 1 lists the deviation from a linear regression of the apparent thermal conductivity versus mean temperature. This shows that repeat tests at a given temperature agree within about 1%. Generally, slightly lower apparent thermal conductivities were obtained after performing tests at colder pipe temperatures.

Figure 5 compares the apparent thermal conductivity of the pipe insulation with that of the sheet material, and also with values listed in ASTM Specification for Preformed Flexible Elastomeric Cellular Thermal Insulation in Sheet and Tubular Form (C 534). The regression curves for the two types of insulation agree within 1.5% and 2.5% at mean temperatures of 25 °C and 10 °C, respectively. This is considered good agreement, since the two materials are not identical. Also, the apparent thermal conductivities of both types of materials are well below the maxima allowed by C 534.

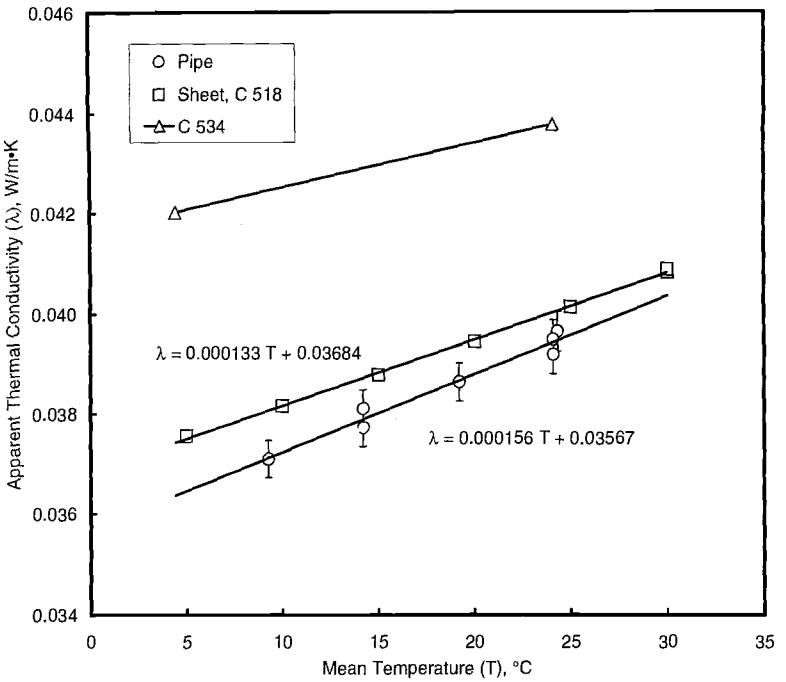

Figure 5 - *Apparent Thermal Conductivity of Elastomeric Foam Insulation. The pipe insulation had a density of 66 kg/m³ (4.1 lb/ft³), an outside diameter of 80.4 mm (3.167 in.), and an inside diameter of 28.6 mm (1.125 in.). The sheet insulation had a density of 61 kg/m³ (3.8 lb/ft³), and consisted of a stack of four sheets, each about 7.6 mm (0.3 in.) thick. The bars on the data points are ± 1% of the corresponding λ value.*

Table 1 - *Results of Measurements on Elastomeric Foam Pipe Insulation. The data are listed in the order in which they were measured.*

Pipe Temp., °C	Mean Temp., °C	λ, W/m·K	Deviation from Regression, %
15.8	24.3	0.03966	+0.5
5.5	14.2	0.03811	+0.6
15.3	24.1	0.03950	+0.1
10.4	19.2	0.03865	-0.07
0.6	9.3	0.03710	-0.06

Design Modeling

One-dimensional radial heat transfer is assumed when the specimen thermal conductivity is calculated using Eqn. 1. The magnitude of errors that could be introduced by axial heat transfer was estimated using a series of two-dimensional (radial (R) and axial (Z)) finite difference models. The first two phases of this effort were based on a preliminary apparatus design that called for a second screen heater instead of the temperature-controlled guard shell described previously; this geometry is shown in Figure 6. The third phase of the modeling task used a constant temperature boundary to represent the guard shell. Additionally, the Phase II model was expanded to three dimensions to explore angular variations in the temperature distribution that could be caused by imperfections in the thin-screen heater's lengthwise joint.

Model Construction and Boundary Conditions

The finite-difference models were created and run with the general-purpose heat conduction code HEATING [*3*]. To consider a broad range of possible insulation specimen properties and apparatus configurations, a number of physical dimensions, temperatures, and material properties were varied parametrically, as shown in Table 2.

Figure 6 shows the components included in the Phase I and II finite-difference models with the radial dimension shown on the vertical axis and the axial dimension shown on the horizontal axis. The cold pipe itself was not modeled, but was represented by a constant-temperature boundary condition. The boundary conditions on the ends and outer surfaces were those of natural convection to an environment at 23 °C. The boundary condition on the midplane (left in Figure 6) was one of symmetry. The guard

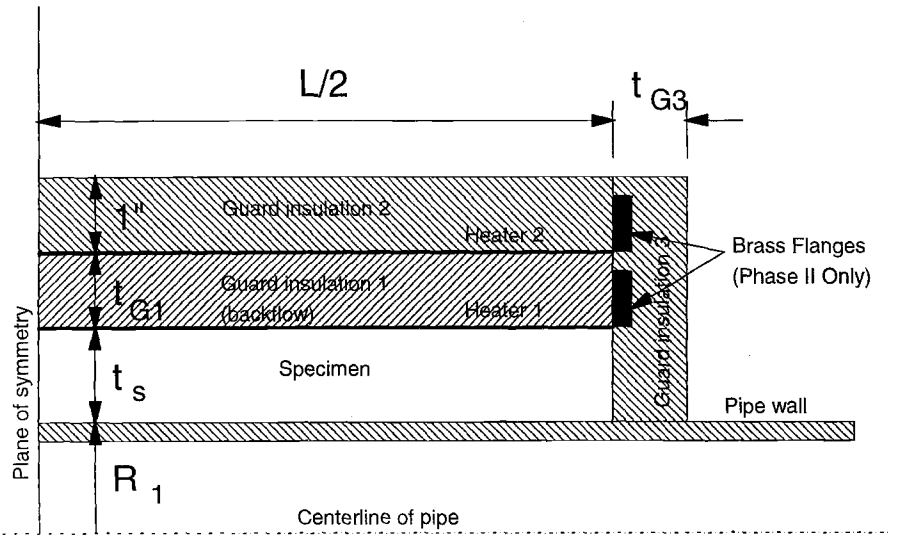

Figure 6 - *Construction of Two-Dimensional (R-Z) Finite Difference Model.*

Table 2 - *Finite Difference Model Parameter Values.*

Phase I		Phase II		Phase III	
Radial Specimen dimensions (inner and outer diameters)*(cm)*					
ID	OD	ID	OD	ID	OD
2.0	8.9	2.0	8.9	2.0	8.9
3.2	8.9	3.2	8.9	3.2	8.9
7.6	12.7	7.6	12.7	7.6	12.7
		7.6	17.8	7.6	17.8
		15.2	35.6	15.2	35.6
Specimen length *(m)*					
0.5, 1.0, 1.5, or 2.0		1.0, 2.0, or 3.0		1.0 or 2.0	
Guard insulation 1 thickness *(cm)*					
2.5 or 5.1		2.5 or 5.1		2.5 or 5.1	
Guard insulation 3 thickness *(cm)*					
0 or 20		5		10 or 20	
Specimen thermal conductivity *(W/m•K)*					
0.02, 0.04, 0.06, or 0.08		0.02 or 0.08		0.08	
Pipe temperature *(°C)*					
-200, -30, or 20		-200, -30, or 20		-200, -100, 0, or 10	

insulation was assumed to have an apparent thermal conductivity of 0.06 W/m•K. Guard insulation 2 was given a thickness of 25.4 mm (1.0 in.). The thin screen heater was taken to be 0.66 mm (0.026 in.) thick and to have an effective thermal conductivity of 2 W/m•K (1/7 that of solid nichrome). Nominal grid spacing in all of the models was 1 mm (0.04 in.) in the radial direction and 5 mm (0.20 in.) in the axial direction. The grid spacing was altered from the nominal values in order to accommodate the actual dimensions of components of the apparatus being modeled.

The Phase II model more closely simulated the conceptual design and the hardware prototype that was under development by including the heavy brass flanges used to bring power to the screen heaters and the insulation covering these flanges. Also, larger pipe sizes and insulation thicknesses were added for this part of the analysis, as shown in Table 2.

One important design consideration of the test apparatus is ensuring that all the heat produced by the thin screen heater flows inward, through the test specimen. This is accomplished by placing a layer of guard insulation outside the screen heater and controlling the temperature on the other side of this guard to the same temperature as the screen heater, so that the heat flow through the guard insulation is as close to zero as possible. In the Phase I and II models, it was assumed that this would be accomplished via the use of a second screen heater. In reality, the temperature will vary somewhat over the length of both heaters. In order to model the control scheme of the conceptual apparatus, the power level for the outer screen heater was selected by an iterative process that matched the two heater temperatures at the center of the long dimension (i.e., along

the plane of symmetry) to within a very small tolerance (typically on the order of 0.01 °C or less). In the Phase III model, the second screen heater was replaced by a constant temperature boundary condition, representative of the heavy copper shell that had by then been constructed for the proof-of-concept test apparatus.

The screen heater power level was set to produce the specified temperature difference across the specimen. In typical cryogenic applications the temperature difference will be large because the outside of the insulation will be at ambient conditions. In other situations, such as a pipe or tube carrying chilled brine, the temperature difference will be less. And in some of the initial proof-of-concept tests, the interior cold fluid temperature would be only slightly below room temperature. The cases modeled consider all these conditions. To ensure inward heat flow, even under near-room temperature conditions, a minimum temperature difference across the insulation specimen was set to 30 °C. Also, to ensure no inward heat flow from the environment across the heater, the heater temperature was set to no less than 2 °C above room temperature. In other words, the screen heater target temperature was set to equal the maximum of either: (1) the pipe temperature plus 30 °C, or (2) the room temperature plus 2 °C.

An expanded, three-dimensional version of the Phase II finite difference model was constructed to examine the influence of a longitudinal seam in the screen heater. The use of a thin-screen heater wrapped around the test specimen allows accurate measurement of the heat input, but does require a seam where the two edges of the screen meet. The thermocouples are placed opposite this seam to minimize the effect of any imperfections, but there was a question about the possible magnitude of any errors the seam might cause in the test results. There are two possible seam defect configurations, first the screen edges could overlap slightly, causing an elevated heat production along the seam (and causing the average heat generation used in the calculations to overstate the heat production on the opposite side). Second, there could be a slight gap between the screen edges, causing a reduced heat production along the seam (and causing the average heat generation used in the calculations to understate the heat production on the opposite side). A three-dimensional model was required to examine this effect because the parameters would then vary in angular, radial, and axial directions.

Model Results

From each steady state solution, the temperature of the thin-screen heater was used to represent the experimentally-measured temperature at the outer surface of the insulation specimen. As Figure 7 shows, this temperature varies along the axial dimension due to axial heat flow. Most cases were like those shown in Figure 7, with the temperature near the midplane relatively unaffected by the axial heat flow. The apparent thermal conductivity as calculated from Equation 1 using these temperatures also varies along the axial dimension. For the selected Phase II cases shown in Figure 7, and considering the thermocouple locations at 0.23 m from the midplane, the model predicts that the temperatures will be relatively unaffected by the axial heat flow and that any errors in the calculated apparent thermal conductivity due to such axial heat flow will be less than 1%, even for insulation thicknesses up to 10 cm.

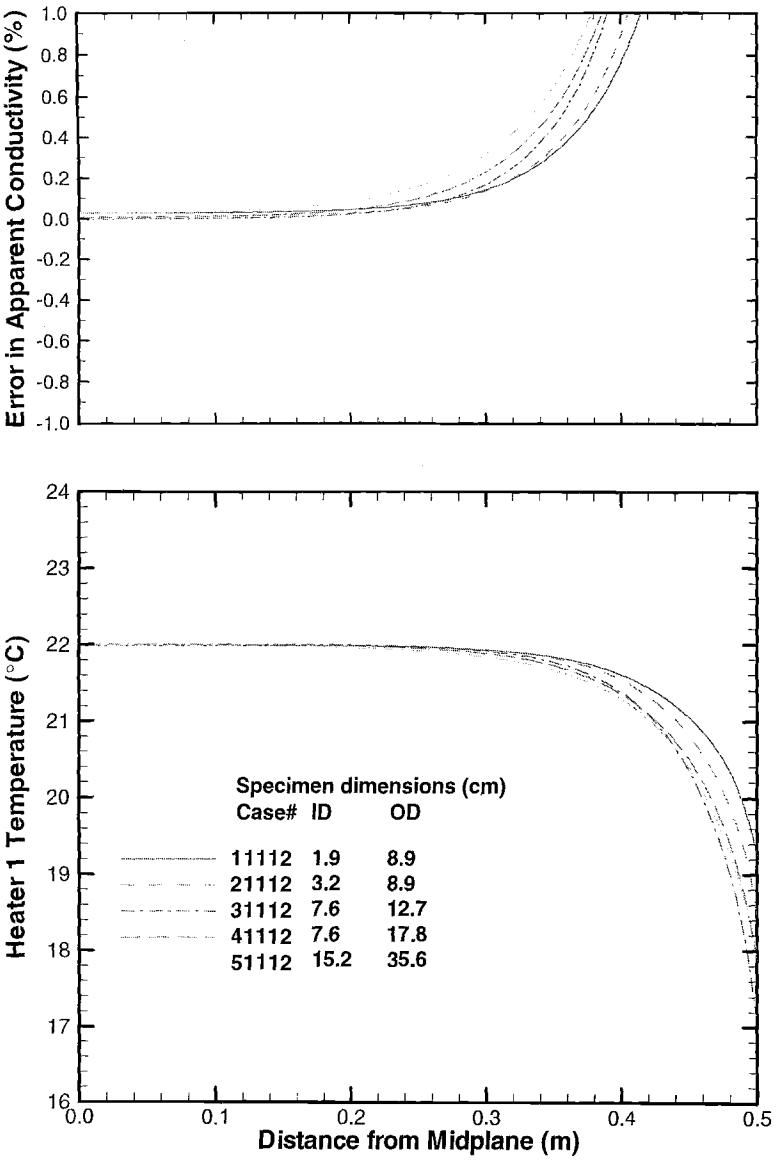

Figure 7 - *Predicted Heater Temperatures and Errors in Apparent Thermal Conductivity along the Test Apparatus Length, for a One Meter Long Apparatus with a 2.5 cm Guard Insulation Thickness, 0.02 W/m•K Specimen Conductivity, -30 °C Pipe Temperature, and Various Specimen Dimensions.*

For all the Phase I cases, the difference between the calculated and the input apparent thermal conductivities ranged from near-zero up to about 7% at these same thermocouple locations. The larger errors all occurred at the warmest interior fluid temperature of 20 °C and with the shortest pipe length of 0.5 m. The majority of the results were similar to those shown in Figure 7, with relatively flat temperature profiles on the screen heater to about halfway between the midplane and the end of the apparatus. The deviation was larger for greater Guard 1 thicknesses. For the range of test specimen conductivities considered (from 0.02 to 0.08 W/m•K), this parameter had a negligible effect on the shape of the temperature profiles.

The more detailed Phase II model was then used to explore the effect of the large brass flanges on the axial heat flow, and the resulting temperature profiles. The scope of the parametric analysis for this phase was adjusted to reflect the understanding gained from the Phase I analysis, as shown in Table 2. These adjustments included the elimination of the shortest pipe length because of the large errors shown for this case in the Phase I results. The thermal conductivity was calculated using temperatures at 0.2 and 0.3 m from the midplane. Again the calculated and input apparent thermal conductivity values were compared to derive estimates of the errors that would occur due to axial conduction. The results from the Phase II analysis can be summarized in terms of the L/D parameter, that is, the length of the specimen divided by its outer diameter, as shown in Figure 8. (The -200 °C results are not included in this figure for clarity, but these errors were always much less than those shown for the -30 °C cases.) These results show errors up to 3.5% at 0.3 m from the midplane, but all errors are $\leq 1\%$ at 0.2 m from the midplane.

When the second screen heater is replaced with a constant temperature guard, the axial temperature variations are greatly reduced. The Phase III analysis considered this improvement along with thicker end guards. The results of this analysis show all the errors reduced to less than 0.05%, even 0.3 m from the midplane, as shown in Figure 9.

Based on an examination of the results, greater Guard 1 thicknesses reduce the accuracy of any measurements along the length of the pipe. Considering the results of these analyses, the prototype sub-ambient pipe insulation test apparatus should be equipped with a guard heater of no more than 25 mm (1-in.) thickness. Considering the use of the constant temperature guard, these analyses show the errors due to axial conduction should be negligible at the proposed thermocouple locations.

The physical parameters were also varied for the three-dimensional version of the Phase II finite difference model, as shown in Table 2 for Phase II. The seam imperfection was varied from a 7.5° gap to a 15° overlap, much larger than any expected defects. For a near-to-ambient cold-side temperature (shown previously to be one of the more challenging test conditions), with a 25 mm (1 in.) guard insulation thickness, the modeled temperature measurements opposite the seam were well within $\pm 1\%$ of those expected with a perfect seam, for all the seam descriptions considered.

Summary

A prototype apparatus for measurements of the apparent thermal conductivity of pipe insulation systems at temperatures below ambient has been constructed and

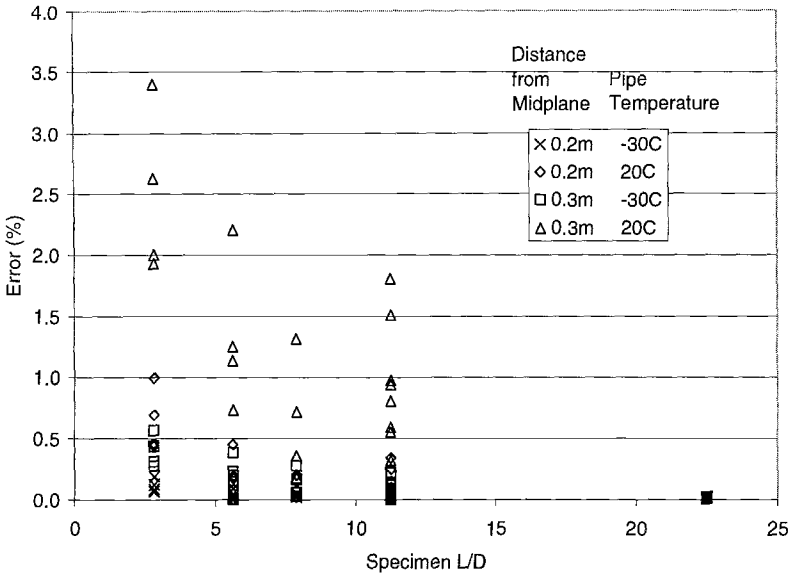

Figure 8 - *Error in Thermal Conductivity Measurement Due to Deviation from Pure Radial Heat Flow at Locations 0.2 and 0.3 m from the Midplane for a Screen-Heater Guard Prototype Design.*

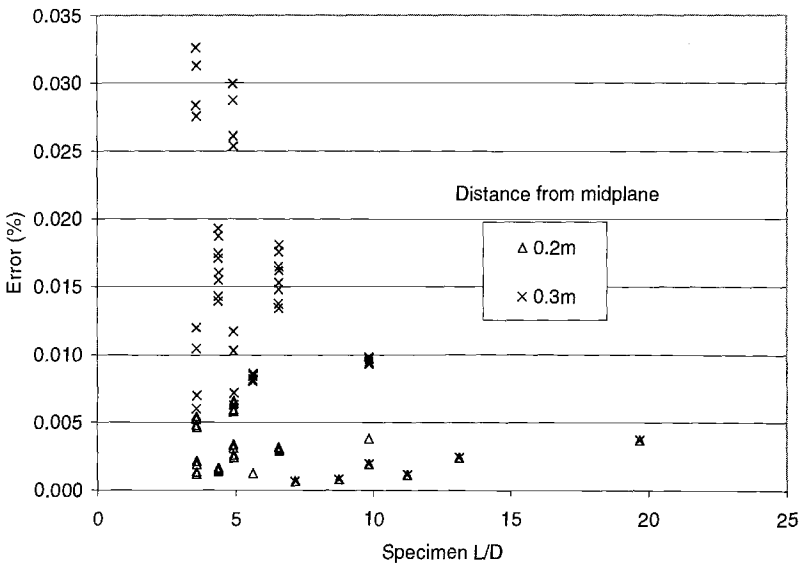

Figure 9 - *Error in Thermal Conductivity Measurement Due to Deviation from Pure Radial Heat Flow at Locations 0.2 and 0.3 m from the Midplane for a Constant Temperature Guard Prototype.*

demonstrated by measurements on specimens of three types of pipe insulation. Measurements on glass fiber insulation demonstrated the need to have a high emittance for the pipe. The measured conductivities were within 5% of the maxima allowed by C 547. Measurements on polyisocyanurate foam insulation were performed both on boards, using C 518, and on pipe-shaped insulation cut from the same material. The two types of measurements agreed within about 1% after aging of both materials had been nearly completed. Measurements on both sheet and tubular specimens of elastomeric foam insulation agreed within 1.5 to 2.5%. This level of agreement on these three types of insulation is considered to be a demonstration that the prototype apparatus is capable of accurate thermal conductivity measurements.

Measurements on the elastomeric foam insulation were extended down to a pipe temperature of 0.6 °C. This was accomplished without condensation because of the unusually low relative humidity in the laboratory during this test. Measurements with pipe temperatures this low or lower will generally require that the apparatus be placed within a low relative humidity enclosure to prevent condensation on the pipe or within the insulation. Plans are underway to acquire a glove box for this purpose. With the use of molecular sieve desiccants, dew point temperatures as low as -76 °C (-105 °F) can be maintained.

Assuming only inward radial heat flow, a preliminary combined uncertainty was estimated at about ±0.8%. A finite-difference model was used to explore errors due to axial heat transfer. The model predicted this error to be less than 0.5% for the prototype apparatus.

It is recommended that the new apparatus be considered for inclusion in C 335 and C 1033, or that a new standard test method be developed based on it.

Acknowledgment

Funding for this project was provided by the U.S. Department of Energy, Office of Building Technology, State, and Community Programs under contract number DE-AC05-00OR22725 with the Oak Ridge National Laboratory, managed by UT-Battelle, LLC.

References

[1] McElroy, D. L., Graves, R. S., Yarbrough, D. W., and Moore, J. P., "A Flat Insulation Tester That Uses an Unguarded Nichrome Screen Wire Heater," *Guarded Hot Plate and Heat Flow Meter Methodology, ASTM STP 879*, C. J. Shirtliffe and R. P. Tye, Eds., American Society for Testing and Materials, Philadelphia, 1985, pp. 121-139.

[2] Taylor, B. N., and Kuyatt, C. E., "Guidelines for Evaluating and Expressing the Uncertainty of NIST Measurement Results," *NIST Technical Note 1297*, U.S. Government Printing Office, Washington, 1994.

[3] Childs, K. W., HEATING 7.2 User's Manual, ORNL/TM-12262, Oak Ridge National Laboratory, Oak Ridge, Tennessee, February 1993.

Efim Litovsky,[1] Jacob I. Kleiman,[2] and Naftaly Menn[3]

Thermal Physical and Optical Properties of Fiber Insulation Materials in the Temperature Range 200 – 1800 °C

REFERENCE: Litovsky, E., Kleiman, J. I., and Menn, N., **"Thermal Physical and Optical Properties of Fiber Insulation Materials in the Temperature Range 200 – 1800 °C,"** *Insulation Materials: Testing and Applications: 4th Volume ASTM STP 1426,* A. O. Desjarlais and R. R. Zarr, Eds., ASTM International, West Conshohocken, PA, 2002.

ABSTRACT: Thermal physical (thermal diffusivity and conductivity) and optical (attenuation, absorption and scattering) properties of alumina fiber insulation materials were measured. The measurements of apparent thermophysical properties are based on the method of heating of plate specimens at a constant rate. The determination of the conductive and the radiative components of apparent properties is based on the combined radiative-conductive heat transfer theory (RCHT) and the measurement of optical properties.

The significant influence of the heat radiation component on the apparent thermal physical properties is demonstrated. Other heat transfer mechanisms that affect the apparent thermal conductivity are also analyzed. Limitations of standard methods for measurement of apparent thermal physical properties of semitransparent fiber materials, including anisotropic materials, are discussed.

KEYWORDS: fiber insulation materials, thermal physical properties, apparent, conductive, radiative, thermal diffusivity, thermal conductivity, optical properties, scattering, absorption, attenuation

[1] Senior Research Associate, Head of Thermophysical Properties Division, Integrity Testing Laboratory Inc., 80 Esna Park Drive, Units 7-9, Markham, ON, Canada, L3R 2R7.

[2] President, Integrity Testing Laboratory Inc., 80 Esna Park Drive, Units 7-9, Markham, ON, Canada, L3R 2R7.

[3] President, LUMINOS Computerized Systems Ltd., Carmel Business Park, Tavor Bldg., Tnufa Str. 3, P.O. Box 104,Tirat Carmel, 39101, Israel.

Introduction

Highly porous insulation materials are mostly semitransparent for thermal radiation and require the knowledge of both thermophysical and optical properties that include absorption and refraction indices and radiation scattering properties [*1-10*]. Presently, the standard testing methods and instruments for measurement of thermal physical properties are based on Fourier's equation that does not take into account that materials could be transparent to heat radiation [*2-10*]. Application of a number of modern ASTM standards (ASTM E 1225-93 Standard Test method for Thermal Conductivity of Solids by Means of the Guarded-Comparative-Longitudinal Heat Flow Technique, ASTM E1461-01 Standard Test method for Thermal Diffusivity of Solids by the Flash method) to semitransparent materials is therefore limited. Similar limitations apply in application of Hot Wire Method and a number of other ASTM and ISO standards [*9-10*]. Most of the instruments measure only the apparent thermal conductivity or diffusivity. Considerable errors in calculation of temperature fields using the apparent properties and the Fourier's equation instead of RCHT theory were shown to exist in a number of investigations [*1- 5*]. Therefore, development of new experimental methods and instruments for measurement of true thermal physical properties of semitransparent materials remains an acute problem in thermal physics.

An expansion of measurement possibilities should be based on radiative conductive heat transfer (RCHT) theory rather than differential Fourier's equations [*1-10*]. The required basic information in the RCHT approach includes the apparent thermal conductivity/diffusivity and certain optical characteristics of the material.

Based on the principles discussed above, a system for determination of the apparent, the radiative, and the conductive thermal conductivity and diffusivity and optical characteristics of radiation attenuation and scattering in semitransparent materials was developed in our group.

The developed instrument for measurement of thermal conductivity is based on the plate steady state method ASTM E 1225-87 and was discussed in [*6*]. In this paper a new thermal diffusivity measurement instrument will be described. The new instrument is not limited by low level of thermal conductivity, minimizes the influence of the radiative component on apparent properties, and can be used for both micro and macro disperse materials. Another important advantage of our method and developed instrumentation lies in it's capability to investigate anisotropic materials. This feature is very important since the theory of standard hot wire method (widely used for testing of insulating materials) that is based on an assumption of cylindrical symmetry of the temperature field, can not be used for anisotropic materials [7].

Apparent Thermal Diffusivity

The main features of the new method and the instrument are associated with the capability to measure not only the apparent thermal diffusivity α_{app}, but also its radiative component α_{rad}, allowing one to calculate the true value α_{cond}.

The usual method for measurement of apparent thermal diffusivity α_{app} is based on Fourier's differential equation, as follows:

$$\alpha_{app} \nabla^2 = \partial T/\partial \tau \tag{1}$$

Apparent thermal conductivity λ_{app} can be calculated as

$$\lambda_{app} = \alpha_{app} \times \rho \times C_p \tag{2}$$

where

ρ = volume density of the material
C_p = heat capacity per unit mass.

The developed here experimental technique is based on the transient plain-flow specimen heating method [*7-8, 15*]. Apparent thermal diffusivity, is determined by measuring the average temperature difference, υ, between thermocouples placed in the center and at a distance $\pm X$ from the center. Additional thermocouples (to estimate the errors associated with the three-dimensional non-uniformity of temperature field) can be arranged near the other four surfaces of the specimen. Using the "small temperature differences" approach at almost constant heating rate, equation (1) can be solved and the following expression for apparent thermal diffusivity can be obtained:

$$\alpha_{app} = bX^2/\upsilon\,(1 + \Delta_{y,z} + \Delta_{\lambda,c}) \tag{3}$$
$$\upsilon = \upsilon_{+X} + \upsilon_{-X}$$

where

υ_{+X}, υ_{-X} = temperature differences between points near the surface and the center of the sample
$b = dT/d\tau$ = the heating rate in the center of the sample
$\Delta_{y,z}$ = correction for non-dimensional temperature field that is calculated based on measurement of temperature differences in the direction perpendicular to the heat flow $\Delta_{\lambda,c}$ = correction associated with temperature dependence of thermophysical properties and nonlinear heating rate.

The equations for calculations of corrections $\Delta_{y,z}$ are $\Delta_{\lambda,c}$ can be found in [*7-8*].

Radiative Thermal Diffusivity

Calculation of the radiative component of thermal diffusivity is based on the solution of non-steady RCHT equation of heat transfer. It can be shown that heat radiation is described

by two heat sources of an elementary volume: positive, if resulted from absorption, and negative if resulted from self –emission of the element of the volume. Heat transfer equation in one-dimensional case becomes:

$$\frac{\partial}{\partial x}\left(-\lambda\frac{\partial T}{\partial x}\right)=-c\rho\frac{\partial T}{\partial t}+\int_0^{\infty}\left\{k_\nu\int_{4\pi}I_\nu d\omega-4\pi j_\nu\right\}d\nu \qquad (4)$$

where the incoming radiation $I_\nu(x, \mu)$ is integrated over all directions in the spatial angle $\omega = 4\pi$; $j_\nu(T)$ is the thermal radiation emitted by an element of volume according to it's temperature $T(x)$ and integration is carried out over all wavelengths ν.
Assuming that local thermodynamic equilibrium takes place, one can get:

$$j_\nu = k_\nu n^2{}_\nu I_B(\nu,T) \qquad (5)$$

For isothermal media where thermodynamic equilibrium exists anywhere and not only locally we get

$$k_\nu\int_{4\pi}I_\nu d\omega=4\pi j_\nu(T) \qquad (6)$$

Radiation intensity, $I_\nu(x, \mu)$ follows the radiation transfer equation that for absorbing, scattering and emitting media has the following form ($\mu = cos\ \theta$; $\mu' = cos\ \theta'$):

$$\mu\frac{dI_\nu(x,\mu)}{dx}=-(k_\nu+\gamma_\nu)I_\nu(x,\mu)+j_\nu\ (T)\frac{\gamma}{4\pi}+\frac{\gamma_\nu}{2}\int_{-1}^{1}I_\nu(x,\mu')P(\mu,\mu')d\mu' \qquad (7)$$

where

k_ν = the true absorption,
γ_ν = the scattering factor
$P(\mu, \mu')$ = the angular function of scattering

From equations (4-6) it is obvious that when true absorption is very low ($k_\nu \rightarrow 0$), the emitted radiation j_ν, as well as absorbed radiation are both approaching zero, meaning that the integral term in (4) is not relevant and temperature distribution in the specimen is not affected by heat radiation at all.

In general case ($k_\nu > 0$,), we define I_ν^+ and I_ν^- as radiation intensity in positive ($\mu = cos\theta > 0$) and negative ($\mu = cos\theta < 0$) directions and express each one of them as a sum of two parts:

$$I_\nu^+ = I_{\nu 1}{}^+ + I_{\nu 2}{}^+;\ I_\nu^- = I_{\nu 1}{}^- + I_{\nu 2}{}^-; \qquad (8)$$

where $I_{\nu 1}{}^+, I_{\nu 1}{}^-$ obey the equations

$$\left.\begin{aligned}\mu\frac{dI_{\nu 1}^{+}}{dx} &= -(k_\nu+\gamma_\nu)I_{\nu 1}^{+} + j_\nu(T)\\ \mu\frac{dI_{\nu 2}^{-}}{dx} &= -(k_\nu+\gamma_\nu)I_{\nu 1}^{-} + j_\nu(T)\end{aligned}\right\} \tag{9}$$

with the following boundary conditions

$$\begin{aligned} I_{\nu 1}{}^{+}(-L,\mu) &= \varepsilon n^2{}_\nu I_B(\nu,T_1) + R\, I_{\nu 1}{}^{-}(-L,\mu)\\ I_{\nu 1}{}^{-}(-L,\mu) &= \varepsilon n^2{}_\nu I_B(\nu,T2) + R\, I_{\nu 1}{}^{+}(L,\mu)\end{aligned} \tag{10}$$

and $I_{\nu 2}{}^{+}, I_{\nu 2}{}^{-}$ obey the equations

$$\left.\begin{aligned}\mu\frac{dI_{\nu 2}^{+}}{dx} &= -(k_\nu+\gamma_\nu)I_{\nu 2}^{+} + \frac{\gamma_\nu}{2}F_{+} + \frac{\gamma_\nu}{2}\int_0^1\left[I_{\nu 2}^{+}P_{+}(\mu,\mu') + I_{\nu 2}^{-}P_{-}(\mu,\mu')\right]d\mu'\\ \mu\frac{dI_{\nu 1}^{-}}{dx} &= -(k_\nu+\gamma_\nu)I_{\nu 2}^{-} + \frac{\gamma_\nu}{2}F_{-} + \frac{\gamma_\nu}{2}\int_0^1\left[I_{\nu 2}^{+}P_{-}(\mu,\mu') + I_{\nu 2}^{-}P_{+}(\mu,\mu')\right]d\mu'\end{aligned}\right\} \tag{11}$$

with the following boundary conditions

$$\begin{aligned} I_{\nu 2}{}^{+}(-L,\mu) &= R\, I_{\nu 2}{}^{-}(-L,\mu)\\ I_{\nu 2}{}^{-}(L,\mu) &= R\, I_{\nu 2}{}^{+}(L,\mu)\end{aligned} \tag{12}$$

In eq. (11) the radiation sources, F_+ and F_- are defined by functions $I_{\nu 1}{}^{+}$ and $I_{\nu 1}{}^{-}$ from equations (10) and angular functions of scattering as follows:

$$F_{+} = \int_0^1\left(I_{\nu 1}^{+}\cdot P_{+} + I_{\nu 1}^{-}\cdot P_{-}\right)d\mu'; \quad F_{-} = \int_0^1\left(I_{\nu 1}^{+}\cdot P_{-} + I_{\nu 1}^{-}\cdot P_{+}\right)d\mu'; \tag{12a}$$

Now we consider the case of a heterogeneous specimen of thickness $H=2L$, heated at a constant heating rate, b. If the temperature drop $\upsilon(x)=T_1-T(x)$ at each point is much smaller than the absolute temperature of the sample, the following integral-differential equation for $\upsilon(x)$ can be obtained

$$\frac{d}{dx}\left(\lambda\frac{d\upsilon}{dx}\right) = -\rho c_p b + \frac{d^2}{dx^2}2\pi\int_0^\infty k_\nu n_\nu^2\frac{\partial I_B}{\partial T}\left(-\Delta T_S\frac{E_4\left[(k_\nu+\gamma_\nu)(l-x)\right]}{(k_\nu+\gamma_\nu)^2} - \frac{\gamma_\nu}{2}\frac{\Delta T_S\cdot V_1(x)}{(k_\nu+\gamma_\nu)^2} - \frac{1}{(k_\nu+\gamma_\nu)^2}\times\right. \tag{13}$$

$$\left.\times\int_{-L}^{L}k_\nu\vartheta\left\{E_3\left[(k_\nu+\gamma_\nu)|x-\xi|\right] - \frac{\gamma_\nu}{k_\nu}(k_\nu+\gamma_\nu)|x-\xi| - \frac{1}{2}\right\}d\xi - \frac{\gamma_\nu}{2(k_\nu+\gamma_\nu)^2}\int_{-L}^{L}k_\nu\vartheta V_2(x,\xi)d\xi\right)d\nu$$

where

ΔT_s = the temperature difference between two boundaries of the specimen (for symmetrical heating $\Delta T_s=0$)

E_n = the integral-exponential functions of order n, and functions V_1 and V_2 are expressed as follows:

$$\left.\begin{aligned}\frac{1}{(k_\nu+\gamma_\nu)^2}\frac{d^2}{dx^2}V_{1(x)} &= \int_{-L}^{L} E_2\left[(k_\nu+\gamma_\nu)(L-\xi)\right]+E_1\left[(k_\nu+\gamma_\nu)x-\xi\right]d\xi \\ \frac{1}{(k_\nu+\gamma_\nu)^2}\frac{d^2}{dx^2}V_{2(x,\xi)} &= \int_{-L}^{L} E_1\left[(k_\nu+\gamma_\nu)z-\xi\right]+E_1\left[(k_\nu+\gamma_\nu)x-\xi\right]dz\end{aligned}\right\} \quad (14)$$

In this approach one can get the following expression for the radiative component:

$$\alpha_{rad}=2\pi\int_0^\infty \frac{k_\nu}{(k_\nu+\gamma_\nu)^2}n^2\nu\frac{\partial I_B}{dT}\left(\alpha^{(1)}{}_{rad,\nu}+\alpha^{(2)}{}_{rad,\nu}+\alpha^{(3)}{}_{rad,\nu}+\alpha^{(4)}{}_{rad,\nu}\right)d\nu \quad (15)$$

$$\alpha^{(1)}_{rad,\nu}=\frac{\Delta T_s}{\Delta T}\left\{E_4\left[(k_\nu+\gamma_\nu)L\right]-\frac{1/3+E_4\left[(k_\nu+\gamma_\nu)L\right]}{2}+\frac{\gamma_\nu}{2}\left[V_1(0)-\frac{V_1(L)+V_1(-L)}{2}\right]\right\} \quad (16)$$

$$a^{(2)}_{rad,\nu}=\frac{k_\nu}{k_\nu+\gamma_\nu}\left\{\begin{aligned}&\frac{2}{3}-\frac{1}{2L(k_\nu+\gamma_\nu)}-\frac{2}{5L^2(k_\nu+\gamma_\nu)^2}+\frac{4E_5\left[(k_\nu+\gamma_\nu)L\right]}{(k_\nu+\gamma_\nu)L}- \\ &\frac{2E_5\left[2(k_\nu+\gamma_\nu)L\right]}{(k_\nu+\gamma_\nu)L}+\frac{4E_6\left[(k_\nu+\gamma_\nu)L\right]}{(k_\nu+\gamma_\nu)^2L^2}-\frac{2E_6\left[2L(k_\nu+\gamma_\nu)\right]}{L^2(k_\nu+\gamma_\nu)^2}\end{aligned}\right\} \quad (17)$$

$$\alpha^{(3)}_{rad,\nu}=\gamma_\nu(k_\nu+\gamma_\nu)\frac{L^2}{3} \quad (18)$$

$$\alpha^{(4)}_{rad,\nu}=\frac{\gamma_\nu k_\nu}{2}\int_{-L}^{L}\left(1-\frac{\xi^2}{L^2}\right)\left[V_2(0,\xi)-\frac{V_2(L,\xi)+V_2(-L,\xi)}{2}\right]d\xi \quad (19)$$

where

$\alpha^{(1)}_{rad,\nu}$ = the component related to the non-symmetry of heated surfaces,
$\alpha^{(2)}_{rad,\nu}$ and $\alpha^{(3)}_{rad,\nu}$ = the components related to absorption and scattering of direct radiation and component, and
$\alpha^{(4)}_{rad,\nu}$ = the component that takes into account the multiple scattering effects inside the specimen.

It should be mentioned here that due to the complexity of the derived equations they were written here for the case R=0 and isotropic scattering $P(\mu, \mu')$=1.

In order to evaluate the conductive term of thermal diffusivity, we have to measure the apparent thermal diffusivity and to calculate the radiative thermal diffusivity of the sample for which the optical properties must be known.

Optical Properties

In order to estimate the radiative component of thermal conductivity/diffusivity it is necessary to know the following properties of the specimen material:

(1) pure absorption coefficient, κ, m^{-1};
(2) scattering coefficient, γ, m^{-1};
(3) angular function of scattering, $P(\theta)$, where θ-is an angle between the incident and the scattered beam.

All these parameters are spectrally dependent, so that they should be known in the wavelength range relevant to the radiative heat transfer. Since our thermal measurements address the temperature range up to 2000 K, it means that the measurement of optical properties should cover the visible and near IR ranges.

Multiple scattering is the major phenomena that may influence the measurements when radiation is propagated in ceramics and refractory materials. The interpretation of obtained results (that actually amounts to solving of an inverse problem of radiation transfer in scattering media) is based on repeated solution of the complete radiation transfer equation below,

$$\mu \frac{dI(x,\mu)}{dx} = -(k+\gamma)I(x,\mu) + I_0 e^{-(k+\gamma)\frac{x}{\mu}} + \frac{\gamma}{2}\int_{-1}^{1} I(x,\mu')P(\mu,\mu')d\mu \qquad (20)$$

where

$I(x,\mu)$ = the intensity of radiation at point x in direction μ ($\mu = \cos\theta$).

Experimental

The measurement of thermophysical properties are based on the mathematical models described by equations (3) for apparent thermal diffusivity. The apparent thermal conductivity was calculated using equation (2). The radiative component of the thermal diffusivity, a_{rad}, was determined from equation (15), and the radiative component of thermal conductivity was calculated using the following equation

$$\lambda_{rad} = \alpha_{rad} \times \rho \times C_p \qquad (21)$$

The conductive component of the apparent thermal conductivity was determined from the following equation

$$\lambda_{cond} = \lambda_{app} - \lambda_{rad} \tag{22}$$

The optical properties that provide basic information for calculation of radiative and conductive components of the apparent thermal diffusivity were determined on the basis of equation (20).

The thermal diffusivity system is similar to the instrument described in ref. [*15*] and was designed on the basis of a fast heating furnace with Super Kanthal heaters that can cover a range of temperatures 100 –1800 °C. The dimensions of the specimens in the present set-up were approximately in the range 110×110×30 - 140×140×40 (mm). The Platinum-Rhodium Pt-Rh 20/40 thermocouples were used in all measurements. The main difference between the present experimental set-up and the one in ref. [*7, 15*] lies in the design of the measurement cell. The present design includes a side refractory heating plate with known and stable optical properties. The reflecting and scattering properties of the heating plates were measured and controlled.

Among the optical parameters measured in our study were the intensity of transmitted (I_t) and reflected (I_R) radiation at several observation angles, θ. For each of the studied materials these parameters were measured for specimens of two different thicknesses, H_1 and H_2. Two approximations for the angular function of scattering have been considered, i.e. an isotropic scattering, where $P(\mu) = 1$ and an anisotropic scattering, with $P(\mu) = 1 + X_1 \cos\theta$, where X_1 is the first coefficient of the expansion of $P(\mu)$ in a series of Legendre polynomials.

The specimen (normally 16 mm in diameter and from 0.9 mm to 5 mm thick) was illuminated using an expanded parallel beam so that the whole specimen surface was covered by radiation. Collecting optics included a small aperture (1 mm in diameter) through which only the central part of the specimen surface was imaged. During the measurements, the position of collecting optics' set-up was changed so that the data could be collected in the range ±75° of the normal to the surface of the specimen for both transmitted and reflected light.

Two light sources were used: the He-Ne laser for the visible range (0.63 μm) and a tungsten halogen lamp for the near IR range. A silicon calibrated sensor head (for the range from 0.5 to 1.163 μm) and a Hamamatsu tube camera (up to 1.9 μm) were used as sensors.

It should be mentioned that no noticeable difference was found in the scattering parameters measured in the visible and the near IR regions. Also, very low pure absorption that was much lower than the scattering (albedo of scattering, $\gamma/\gamma+\alpha$, was about 0.9) was observed. The uncertainty in estimation of absorption may reach 30-50%.

Results and Discussion

A high temperature alumina fiber insulation with density 0.48 g/cm^3 (open porosity ~ 84%) and a diameter of 1-5 μm was investigated. An example of data that was obtained using the described above set-up is presented in Fig. 1. Apparent thermal diffusivity was measured by the described above method. The apparent thermal conductivity was calculated (the black diamonds in Fig. 1) on the basis of measured apparent thermal diffusivity and known data on thermal capacity according to eq. (2) [7]. The radiative component of thermal diffusivity has been measured as described above using eq. (15). The radiative and conductive components

of thermal conductivity (the squares and triangles in Fig. 1) were calculated using equations (21) – (22). Thermal conductivity values (apparent ,radiative and conductive) are plotted in Fig.1 because it is more convenient to operate with thermal conductivitites while analyzing the heat transfer mechanisms [*3, 7, 11-14*].

For optical properties the following value was obtained for the attenuation coefficient ($k+\gamma$) = 970 m^{-1}. The pure absorption data for Al_2O_3 crystals has been approximated in the wavelength range from 0.6 μm to 11 μm by a 6-step function (k values varied from 0.1 m^{-1} to 3760 m^{-1}) and used in calculations.

As can be seen from Fig. 1, the radiative component calculated in this work constitutes only ~ 25% of the apparent value (in the temperature range 1500 – 1800 °C). This is due, primarily, to symmetrical heating of the specimen and low pure absorption in the material.

The significant increase of the conductive component of thermal conductivity of the fiber insulation in the temperature range 1500-1800 °C is quite unexpected (see Fig. 1). This behavior may be explained by sintering of the fibers during the high temperature heating. A similar high temperature sintering mechanism and associated increase in thermal conductivity/diffusivity was detected in experiments with quartz ceramics [*8*] where the material was sintered, originally, at 1100 °C. In an attempt to verify this mechanism we conducted a number of experiments on the same specimen trying to reproduce the data.

In these repeat experiments, the data did reproduce with a scatter of ±5% (within the measurement error limit), a fact that made us to reject the above mechanism.

The effect of thermal expansion mismatch between the fibers and the binder and its influence on the apparent thermal conductivity, on other hand, may be considered as a more viable mechanism that can explain the apparent conductivity curve behavior [*12-14*]. In addition, appearance of a liquid phase at the fibers' boundaries supplements and supports the thermal expansion theory [*3, 7*].

To shed more light on the effect of thermal mismatch during the heating-cooling cycle on the behavior of the apparent thermal conductivity, we investigated the composition and structure of the interfaces between fibers using scanning electron microscopy (SEM). Our analysis had shown that the binder between the sintered fibers is composed of an alumina-silica material, the phase composition of which can be associated with one or more structures like corundum, mullite, cristobalite, quartz glass, etc. [*3*]. The thermal expansion coefficients of these phases, if present in the binder, may differ 3-10 times. Moreover, the cristobalite has a series of phase transformations at 250°C, 1470°C and 1710 °C. In systems mullite-silica and cristobalite-silica a liquid phase appears at temperature above 1600°C [*3*]. Microcracks and nanocracks can arise in such heterogeneous systems after material sintering during the cooling, due to a mismatch between thermal expansion coefficients of the different phases composing the material, or due to the anisotropy of thermal expansion coefficient of randomly oriented grains [3, 7, 12-14]. The SEM analysis of cross-sectioned samples that underwent the heating-cooling cycles had shown that a large number of microcracks, 0.1 – 1.0 μm in size and smaller, indeed exists in the binder. Existence of even a large number of thin nanocracks can be implied from such analysis. As a result, the heat barrier parameters (that are dependent on the width of microcracks and the contact area between the fibers) will change with temperature, and will affect the thermal conductivity of the material.

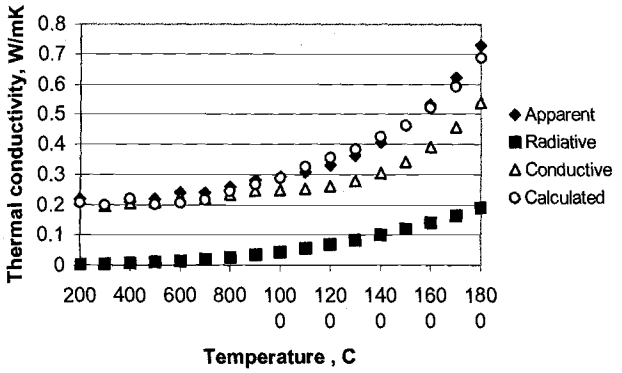

Figure 1- *Thermal conductivity of highly porous alumina (with admixture of silica) fiber insulation: apparent, radiative and conductive.*

Upon cooling the created microcracks will grow, upon heating the microcracks will close [*12-14*]. The total area and the degree of opening of the microcracks will depend on the temperature. At temperatures over 1600 °C the appearance of a liquid phase in the binder and on the surface of the fibers will cause the closing and/or disappearance of micro and nanocracks. Unfortunately, there are no direct methods for analysis of changes of micro and nanocrack geometry at high temperature. These effects can be estimated only on the basis of the thermal conductivity data, as a fitting parameter. To gain a better understanding of the influence of crack opening mechanism onto the behavior of the thermal conductivity, we shall estimate below what should be the value of required area of opening at different temperatures to explain the measured data on the conductive component of thermal conductivity.

The effect of heat barrier resistance on λ_{app} is basically modeled in [*7-8*] by calculating the temperature field within two adjacent particles or grains, viewed as solid slabs with cross sectional area πr^2 and contact area πa^2.

$$\lambda_{app} = \lambda_{cond} M(1 - \Pi)^{3/2} + \lambda_{gas}\Pi^{1/4} + \lambda_{rad} \tag{21}$$

where Π is porosity.

The HBR coefficient M may be calculated from the following expressions:

$$M = \frac{\dfrac{R\Pi}{1-\bar{a}^2} + \dfrac{R_b}{\bar{a}^2} + \dfrac{\Phi^2}{\Phi - 1}}{\left(\dfrac{R\Pi}{1-\bar{a}^2} + \dfrac{\Phi}{\Phi - 1}\right)\left(\dfrac{R_b}{\bar{a}^2} + \Phi\right)} \tag{22}$$

$$\Phi \bar{a}^2 = 1 - \frac{16}{\pi^2} \sum_{n=1,3,5,\ldots} \frac{I_1(n\pi b/L)}{n^2 I_1(n\pi r/L)} [I_1(n\pi r/L) K_1(n\pi b/L) - K_1(n\pi r/L) I_1(n\pi b/L)]. \quad (23)$$

In the above

$$R_{\Pi} = \frac{d/l_P}{L/l_S} = \frac{l_S}{l_P}\frac{d}{L} \quad \text{and} \quad R_b = \frac{d/l_b}{L/l_S} = \frac{l_S}{l_b}\frac{d}{L} \quad (24)$$

are the non-dimensional thermal resistances of the crack and the contact layer of inter fiber material, respectively, where

δ = microcrack width
L = distance between the microcracks
b and r = the effective radii of the contact area and of the microcrack (or grain boundary)
$\bar{a} = b/r$
λ_b = thermal conductivity of the intergrain material
I_1 and K_1 = the modified Bessel functions of the first and the second kind, respectively.

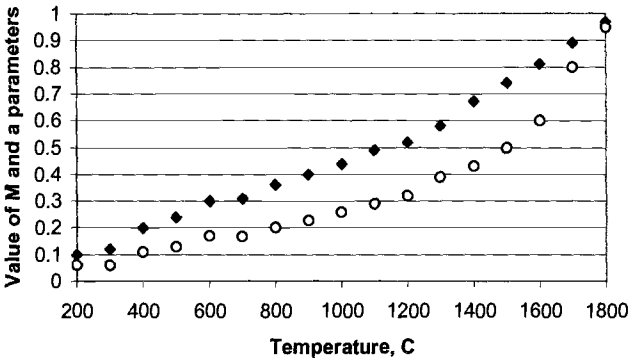

Figure 2- *Dependence of non-dimensional heat barrier resistance parameter (black diamonds) and contact area (open circles) on temperature*

Assuming the M(T) dependence shown in Fig. 2, a good agreement is achieved then for the measured effective thermal conductivity, as shown in Fig. 1.
The dependence of the non-dimensional contact radii, $\bar{a}$ on temperature, according to changes of the M parameter is also shown in Fig. 2. The linear increase in the value of of the contact radii in the range 200-1400°C can be explained by closing of micro and nano cracks between fibers [*12-15*]. The steeper slope in *M* parameter at temperatures 1600-1800 °C can be explained by the appearance of a liquid phase in the system Al_2O_3-SiO_2 [*3*] and increase of the contact area $\bar{a}$.

Conclusions

A measurement system has been developed for measurement of thermal physical and optical properties of porous semitransparent materials like high temperature insulation, refractories, etc. The developed system includes an instrument, based on the method of monotonic heating of plate specimens, that allows to measure thermal diffusivity up to 1800 °C and an instrument for measurement of relevant optical properties (absorption and scattering in visible and near IR wavelengths).

Optical properties of studied material have been measured and the radiative components of apparent thermal conductivity and diffusivity using the RCHT theory, were calculated.

Based on the measured apparent thermal diffusivity/conductivity and the radiative component, the conductive (true) thermal conductivity has been determined for the first time.

Thermal conductivity/diffusivity values of insulating alumina fiber material were measured. It was shown that the radiative component of heat transfer grows significantly with temperature, but not enough to explain the temperature dependence of the true (conductive) thermal conductivity component. Additional mechanisms must be taken into account in the overall heat transfer process.

The grain-binder system thermal expansion mismatch and the appearance of a liquid phase between fibers at temperatures over 1600 °C can explain the behavior of the conductive component of thermal conductivity.

Acknowledgements

The work described in this paper was conducted under a grant from the Canada-Israel Industrial Research and Development Foundation (CIIRDF). The authors wish to acknowledge Dr. H. Rothschild from CIIRDF for his enthusiastic support and guidance in this study. Mr. V. Kon's help in the scanning electron microscopy investigations is also acknowledged with thanks.

References

[1] Siegel R. and Howell J. R., "*Thermal Radiation Heat Transfer*", Hemisphere Publishing, Washington, 1992, pp. 3-760.

[2] Viskanta R., "Combined Conduction and Radiation in Semitransparent Substances", *Thermal Conductivity 19,* D. W. Yarbough, ed., Plenum Press, New York, 1988, pp. 5-20.

[3] Kingery W. D., Bowen H. K. and Uhlmann D. R., "*Introduction to Ceramics*", John Wiley, New York, 1976, pp. 3- 620.

[4] Sergeev O. A. and Menn N. (Men A. A.), "*Thermophysical Properties of Semitransparent Materials*", Standards Publishing, Moscow, 1977, pp. 3-287.

[5] Menn N. (Men A. A.) and Sergeev O. A., "Radiative and Conductive Heat Transfer in an Anisotropic Scattering Medium", presented at the 5th International Heat Transfer Conference, September 3-7, Tokyo, 1974, pp. 67-71.

[6] Litovsky E., Kleiman I.J. and N. Menn, "Measurement of Thermal Physical and Optical Properties of Semitransparent Materials in the Temperature Range 20 -

1800C", *26th International Thermal Conductivity Conference*, R. Mannello, P. R. Ricci, S. E. Smith, R. Campbell, Eds., MA, 2001 (in print).

[7] Litovsky E.Ya. and Puchkelevich N.A.. "*Thermophysical Properties of Refractories.* Reference book". Moscow. Metallurgy, 1982, pp. 3-150.

[8] Litovsky E. Ya, "Thermophysical Properties of Refractories in the Wide Temperature, Pressure and Gas Composition ranges", Doctor of Sciences Thesis, Institute for High Temperatures, Academy of Sciences of the USSR, Moscow, 1985, pp. 3-498.

[9] Andre S. and Degovanni A., "A Theoretical Study of the Transient Coupled Conduction and Radiation Heat Transfer in Glass: Phonic Diffusivity Measurement by the Flash Technique", *Int. J. Heat Mass Transfer.* 18(38), 1995, pp. 3401-3412.

[10] Ebert H.-P., Ebele W., Nilsson O. and Fricke J., "Errors From Radiative Heat Transfer in the Determination of Thermal Conductivity in Semitransparent Media Using The Hot-Wire Method", presented at the EUROTHERM, Heat Transfer in Semi-Transparent Media, Seminar No. 21, Sacadura and F. Allard, eds., February 3-5, Villeubranne France, 1992, pp. 259-269.

[11] Litovsky E., Shapiro M. and Shavit A., "Gas Pressure and Temperature Dependencies of Thermal Conductivity Porous Ceramic Materials. Part II." *J. American Ceram. Soc.*, 79/5, 1996, pp. 1366-1376.

[12] Litovsky E., Gambaryan-Roisman T., Shapiro M. and Shavit A., "Effect of Grain Thermal Expansion Mismatch on Thermal Conductivity of Porous Ceramics", *J. American Ceram. Soc.* , Vol. 82, No 4, 1999, pp. 994-1000.

[13] Litovsky E., Gambaryan-Roisman T., Shapiro M. and Shavit A, "Heat Transfer Mechanisms Governing Thermal Conductivity in Porous Materials", *Trends in Heat, Mass & Momentum Transfer, Research Trends,* Vol. 3, 1997, pp. 147-167.

[14] Litovsky E., Gambaryan-Roisman T., Shapiro M. and Shavit A., "Novel Heat Transfer Mechanisms in Porous Ceramic Materials", 15th European Conference on Thermophysical Properties, September 5-9, 1999, in Wurzburg, Germany and *High Temperatures-High Pressures*, 1(33): 2001, pp. 27-34.

[15] Litovsky E., Litovsky T., Shapiro M.and Shavit A., "Thermal Conductivity Dependence of MgO Heat Insulation on Porosity in Temperature Range 500-2000K" *Third Symposium on Insulation Materials: Testing and Applications, ASTM STP 1320,* R. S. Graves and R.R. Zarr, eds. May 15-17, Quebec, Canada, 1997, pp. 292-306.

Paul A. Hough,[1] Thomas W. Fritz,[2] Peter L. Hunsberger,[2] and Douglas C. Reed[2]

Evaluating the Fire Performance of Thermal Pipe Insulation Systems by Use of the Vertical Pipe Chase Apparatus

Reference: Hough, P. A., Fritz, T. W., Hunsberger, P. L., and Reed, D. C., **"Evaluating the Fire Performance of Thermal Pipe Insulation Systems by Use of the Vertical Pipe Chase Apparatus,"** *Insulation Materials: Testing and Applications: 4th Volume, ASTM STP 1426,* A. O. Desjarlais and R. R. Zarr, Eds., ASTM International, West Conshohocken, PA, 2002.

Abstract: Evaluation of the fire performance of thermal pipe insulations is required by all mechanical codes in the United States. This paper describes a recently developed test to evaluate flame spread, heat release, and smoke generation when pipe insulation systems are exposed in a vertical pipe chase apparatus. This apparatus allows the testing of composite pipe insulation systems, including the core insulation, adhesives, jacketing materials, sealants, tapes, and all other components that are used to field apply these insulation systems.

The method simulates a small, growing fire which escalates into a fully involved fire that may be anticipated when combustible materials burn within a vertical chase or a confined ceiling cavity or plenum. The initial fire exposure is 20kW for three minutes followed by a 70kW exposure for seven minutes. The specimen is comprised of three 2-inch NPS pipes insulated with thermal insulation and accessories. The pipe chase is made up of a 4-foot (1.22 m) horizontal pipe run connected to a 6.5-foot (1.98 m) vertical run. A square gas burner is located 14 inches (0.35 mm) from the vertical rise to ensure that flames will propagate from the horizontal to the vertical pipe section. The fire performance of the insulation system is evaluated by the following: vertical flame spread, heat release determined by oxygen consumption calorimetry, and smoke measurement in the exhaust duct. The vertical configuration ensures that the specimen will remain in the flame exposure area for the duration of the test.

Keywords: pipe insulation, fire test, vertical pipe chase fire test, heat release rate, smoke obscuration

[1] Technical Manager, Armstrong World Industries, Inc., 2500 Columbia Avenue, Lancaster, PA, 17604.

[2] Manager, Product Fire Performance, Technical Specialist, and Research Scientist, respectively, Armstrong World Industries, Inc., 2500 Columbia Avenue, Lancaster, PA, 17604.

Introduction

All U.S. model building codes and mechanical codes require the evaluation of thermal pipe insulation. Currently, this evaluation is accomplished through the use of the *ASTM Test Method for Surface Burning Characteristics of Building Materials (E 84)*, or through the use of a full-scale fire test such as *National Fire Protection Association (NFPA) - Methods of Fire Tests for Evaluating Contribution of Wall and Ceiling Interior Finish to Room Fire Growth (286)*, or *Uniform Building Code (UBC) Room Fire Test Standard for Interior of Foam Plastic Systems (26-3).* There are problems with all of these tests when they are used to evaluate the burning behavior of thermal pipe insulation [*1*]. All of these tests are designed to evaluate materials in a flat orientation and are not capable of evaluating thermal pipe insulation systems which often include core insulation, adhesives, jacketing materials, sealants, tapes, and other components. Pipe insulation has a cylindrical geometry and is always part of a system, which includes other components. The burning behavior of these other components must currently be evaluated separately from the insulation material and thus does not assess any synergistic effects between the various components of the system. There has also been a growing amount of cellular foam materials used in many pipe insulation applications, which may not be accurately evaluated using methods such as E 84. Another standard that is used to evaluate thermal pipe insulation is *Factory Mutual Research Pipe Chase Test (Standard 4924).* This is a large-scale horizontal test, which tends to be expensive and has limitations. This test does not measure heat release rate or smoke but does measure the horizontal spread of flame.

Full scale testing indicates that the overall performance of the system may be radically different from the performance of the individual components. Efforts have been made to develop other full-scale room tests, which may more accurately predict the fire performance of the system [*1*].

The following method simulates a relatively small fire which escalates into a fully involved fire which may be encountered when combustible materials burn within a confined chase or space such as a ceiling cavity or a plenum. Typical plenum spaces contain a growing amount of combustible materials, which may or may not be related to the mechanical system being insulated. In areas such as these, materials which exhibit a high rate of heat release may contribute significantly to the spread of fire both within these confined spaces and to other adjacent or connected spaces. Specification and code writers such as the National Fire Prevention Association's Air Conditioning Committee in *NFPA Standard for the Installation of Air-Conditioning and Ventilating Systems (90A),* have a concern about the increasing use of combustibles in these spaces, but do not always have test methods available to evaluate these materials. The vertical pipe chase apparatus offers a new tool, which may be helpful in these types of evaluations.

This test is being proposed as a new test method which, when approved, will be known as NFPA 274. This method is still under development and may change before the final acceptance and issuance of this method.

Experimental

Equipment

The pipe chase (Figure 1) is an enclosed space constructed of ½ inch (13 mm) thick calcium silicate board with a height of 80 inches (2.03 m) and a width of 24 inches (0.61 m). The vertical section is 18 inches (0.46 m) deep while the horizontal section is 18 inches (0.46 m) high and 48 inches (1.22 m) deep. Three 2-inch NPS (60DN) iron pipes are hung from a steel rod centered across the top of the vertical chase.

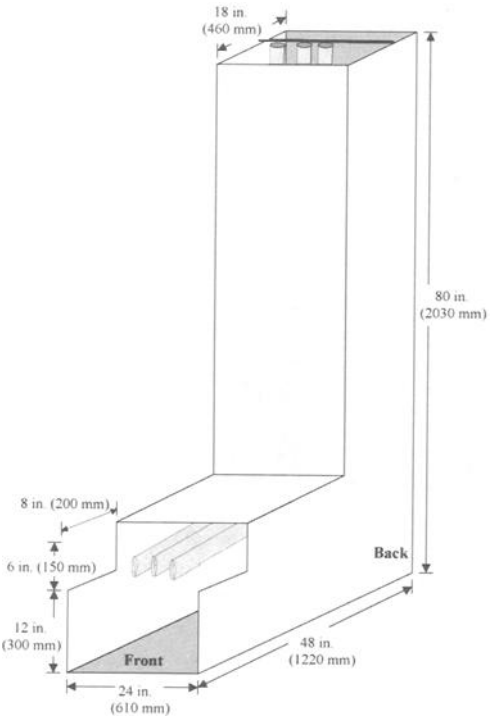

Figure 1- *Pipe Chase Apparatus*

The ignition source for the test is a gas burner with a nominal 12 in. x 12 in. (305 mm x 305 mm) surface. Either a porous refractory material or a layer of sand can be used as a horizontal surface of the burner. Gas flow to the burner is regulated with a mass flow controller. Spark ignition and safety features are included in the burner system.

A computer based data collection system collects data at 3-second intervals. Oxygen (O_2), carbon dioxide (CO_2), carbon monoxide (CO), differential pressure and gas temperature are monitored in the duct from the hood above the pipe chase.

Specimen Mounting

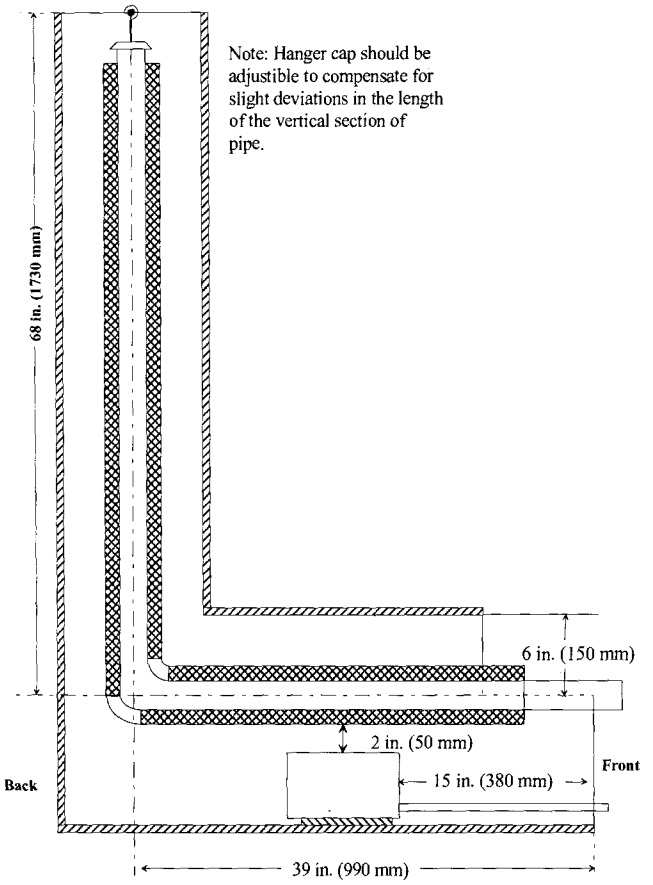

Figure 2

A 1-inch (25 mm) thickness of 2-inch NPS (60 DN) pipe insulation system including supplemental materials (core insulation, jackets, adhesives, tapes, sealants and fitting covers) is mounted on 2-inch NPS (60 DN) iron pipe that is capped at the top and hooked over a bar running across the top of the chase (Figure 2).

Three specimens are centered front to back in the vertical section of the chase and have a 2-inch (50 mm) surface to surface space between the center specimen and the

specimens on either side. Horizontal portions of the L shaped specimens are positioned with the plane of their horizontal centerline 6 inches (150 mm) below the top of the horizontal chase. The lower ends of the pipes are clamped to the bottom of the cutout in front of the chase with steel straps formed to fit over the pipes.

The burner is centered 3 inches (75 mm) below the specimen and 15 inches (380 mm) from the front edge of the horizontal chase. The positioning of the burner will affect the fire exposure to the specimen. This burner position covers the largest horizontal surface area of the pipes and exposes the elbows to the flame.

Other pipe sizes and thicknesses of insulation systems can tested as long as the spacing between the pipes and the burner is maintained per the description above.

Instrumentation and Measurement Analysis

Details for all instrumentation in the hood, exhaust duct, sampling line, gas sampling and analysis and smoke measuring techniques are detailed in NFPA 286. The hood should be as specified in NFPA 286 or equivalent.

Test Procedure

Two minutes of baseline data are collected. The burner is ignited and immediately set to an output level of 20 kW. A level of 20 kW is maintained for three minutes at which time the level is increased to 70 kW for an additional 7 minutes. Observations are taken during the test of flame extension above the top of the chase and other visual events. Ten minutes after the burner is ignited it is extinguished. Post-test observations of the specimens are recorded, heat release and smoke generation are calculated from the raw data.

Calculations

All formulas and equations for determining heat release and smoke obscuration can be found in NFPA 286.

Results and Discussion

A number of commercial insulation pipe insulation systems were tested which included the following:

- Polyolefin tubular foam insulation in a 1-inch (25 mm) thickness with standard contact adhesive, without additional vapor barrier jacketing. Elbows were fabricated from miter cut tubular insulation. (Series A-PEF)

- Elastomeric tubular foam insulation in a 1-inch (25 mm) thickness with standard contact adhesive, without additional vapor barrier jacketing. Elbows were fabricated from miter cut tubular insulation. (Series B-FEF)
- Fiberglass tubular insulation in a 1-inch (25 mm) thickness with a factory applied All Service Jacketing (ASJ). The ASJ was sealed with factory applied pressure sensitive adhesive. Butt joints were sealed with ASJ tape and the elbows consisted of pre-fabricated PVC fitting covers. (Series C-MF)
- Polyisocyanurate foam insulation in a 1-inch (25 mm) thickness with a fabricator adhered polyvinylidene chloride (PVDC) jacket sealed with PVDC tape. Elbows were routed materials wrapped with PVDC tape. (Series D-PIR) This material was also tested with the jacketing removed.
- Phenolic foam insulation in a 1-inch (25 mm) thickness with a fabricator adhered ASJ jacket. The ASJ was sealed with contact adhesive. Butt joints were sealed with ASJ tape and the elbows consisted of routed materials wrapped with PVC tape. (Series E-PHN) This material was also tested with the jacketing removed.
- Polyolefin tubular foam insulation in a 1/2-inch (13 mm) thickness with standard contact adhesive, without additional vapor barrier jacketing. Elbows were fabricated from miter cut tubular insulation. (Series A½-PEF)

Table 1 provides baseline data for the burner design and the bare pipe assembly without insulation with a 20/70 kW gas burner. In order to give a comparison to ordinary combustibles, experiments comparing the gas burner to a wood crib were conducted. The gas burners gives approximately the same total heat release as the wood crib while having approximately the same shape of the heat release curve. Testing did not indicate any significant differences in char formation between the gas burner and the crib. Total heat release of the wood crib and the gas burner can be compared by measuring the area under the heat release curves (Figure 3 and 4). The present two-stage (20/70 kW) gas burner has a slightly higher heat release than the wood crib.

Table 1 - *Baseline Data for Apparatus Only*

Assembly ID	Max RHR_{30s} (kW)	$THR_{10\,min}$ (MJ)	SRR_{30s} (m^2/sec)	$TSR_{10\,min}$
Wood Crib	87.6	24.1	0.23	49
Wood Crib	91.2	28.3	0.21	47
20/70 kW Burner with Bare pipes	75	34	0.15	61
20/70 kW Burner with Bare pipes	73	33	0.13	56
20/70 kW Burner with Bare pipes	71	32	0.14	57

All data for subsequent material evaluation has had this baseline data subtracted out so that the values listed are for test specimens only.

Table 2 looks at three different scenarios for burner net heat output. Net heat outputs of 40 kW for 10 minutes, 60 kW for 10 minutes and 20 kW for 3 minutes followed by 70 kW for seven minutes were evaluated. It was determined that the dual-

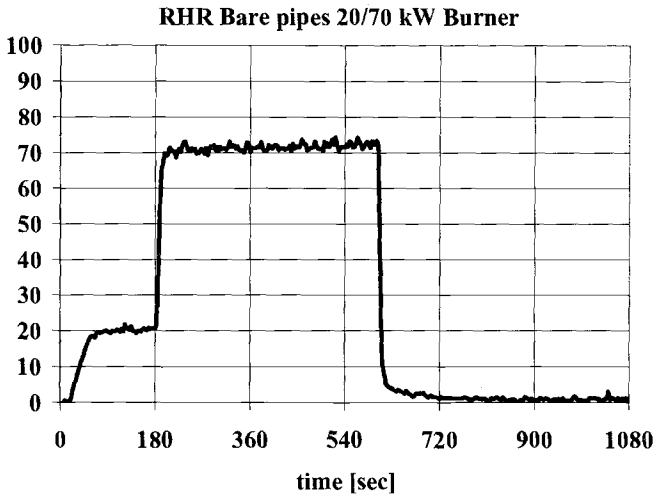

Figure 3 *Heat Release Rate for Bare Pipe Assembly with 20/70 kW Burner*

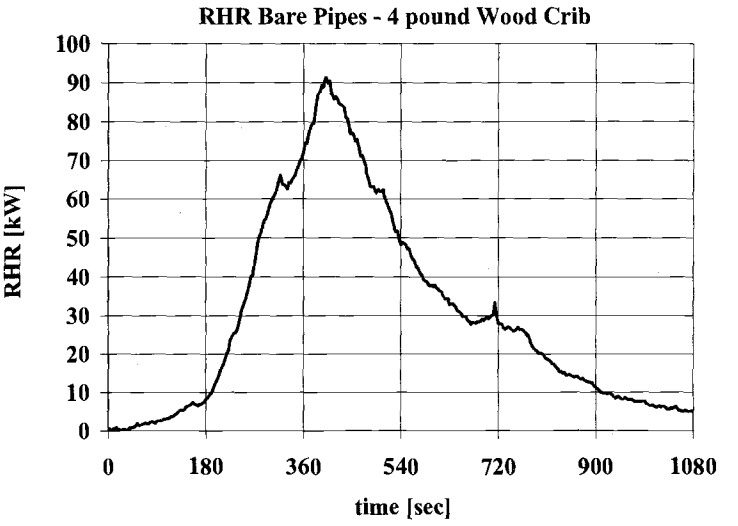

Figure 4 *Heat Release Rate for Bare Pipe Assembly with Wood Crib*

stage 20 kW/70 kW setting produced the most repeatable results and best simulated the shape of the wood crib ignition source.

All of the tables that follow look at insulations types identified by a letter designation. All materials within a type are similar in construction unless otherwise noted in the tables. A number following a letter indicates multiple runs of a similar insulation type and a similar construction.

Table 2 - *Effect of Burner Output*[1]

Material		Burner Output (kW)	Remarks	Max RHR_{30s} (kW)	$THR_{10\ min}$ (MJ)	SRR_{30s} (m^2/sec)	$TSR_{10\ min}$ (m^2)
A	PEF	40	2-1/2" ID X 1" wall – no jacket	612	66.2	8.93	746
A	PEF	60	2-1/2" ID X 1" wall – no jacket	583	62.2	9.73	783
A	PEF	20/70	2-1/2" ID X 1" wall – no jacket	784	33.4	13.07	687
B	FEF	40	2" NPS X 1" wall – no jacket	16.6	6.2	-	-
B	FEF	60	2" NPS X 1" wall – no jacket	39.0	11.2	-	-
B	FEF	20/70	2" NPS X 1" wall – no jacket	42.6	10.6	1.19	301

[1] Burner position of 15 inches (382 mm) and a test duration of 10 minutes.

Table 3 evaluates the position of the burner in relationship to the front opening of the horizontal section of the chase. Locations of 9, 12, 15, and 18 inches (229, 305, 382, and 458 mm) from the opening were evaluated. It was determined that the 15 inch (382 mm) location produced the greatest 30-second average heat release rate and allows the flame to be pulled by the natural draft around the elbows of the insulation thus providing some direct flame exposure to the vertical insulated pipe section.

Table 4 looks at data from typical pipe insulation systems that are commercially available. All specimens were mounted as composite systems utilizing installation procedures as recommended by the various manufactures. These systems include all components that were recommended including insulation material, jacketing where required, adhesives, tapes, and polyvinyl chloride (PVC) fitting covers. In some instances such as with materials like D3 and E2, a portion of the system was removed such as jacketing, to evaluate the effect of an individual component.

Heat Release Rates

Rate of heat release is one of the most important fire performance characteristics associated with a burning product. It describes the size of a fire at any time during a specific fire scenario. This test does an effective job of comparing the performance of insulation systems when exposed to a small developing fire in an enclosed chase or cavity, as simulated by this apparatus.

Table 3 - *Effect of Burner Location*[1]

Material		Burner Position	Remarks	Max RHR_{30s} (kW)	$THR_{10\ min}$ (MJ)	SRR_{30s} (m^2/sec)	$TSR_{10\ min}$ (m^2)
A	PEF	9 (229 mm)	2-1/2" ID X 1" wall – no jacket	711	49.4	8.18	380
A	PEF	15 (382 mm)	2-1/2" ID X 1" wall – no jacket	784	33.4	13.07	687
A	PEF	18 (458 mm)	2-1/2" ID X 1" wall – no jacket	544	59.8	7.33	475
B	FEF	9 (229 mm)	2" NPS X 1" wall – no jacket	35.2	8.5	-	-
B	FEF	12 (305 mm)	2" NPS X 1" wall – no jacket	37.5	10.0	1.17	276
B	FEF	15 (382 mm)	2" NPS X 1" wall – no jacket	44.0	8.1	1.25	213
B	FEF	18 (458 mm)	2" NPS X 1" wall – no jacket	40.7	8.9	-	-

[1] 2-stage burner output of 20 kW for 3 minutes followed by 70 kW for seven minutes with a total test time of 10 minutes.

Heat release is quantified in two manners. The first is the maximum heat release rate for a rolling 30-second average. Based on results from this apparatus, high maximum heat release rates indicate a potential for material to have rapid flame spread and may be an indication of potential flame extension above the top of the chase as indicated by materials A and D in Table 4. Materials D1 & D2 versus D3 in Table 4 also illustrate this. The first two specimens were tested with a fabricator applied jacket adhered with an adhesive while the third sample had the jacket and most of the adhesive removed. Maximum heat release rate may give an indication of how a material will affect other combustible materials in the area.

The second parameter is total heat release over the entire 10-minute test duration. This is an indication of whether a material will cause flashover. Flashover results in extremely high levels of visible smoke, temperature and potentially toxic gases. This is illustrated by material A1 through A3 in Table 4 and Figures 5 and 6. These results are also consistent with modified room corner test flashovers as reported. [*1*]

One way of reducing the heat release rate and total heat release may be to limit the volume of the insulation system being used. This is illustrated with material A and A ½. These are identical materials with the exception that A is a 1-inch (25 mm) wall thickness while A ½ is a ½-inch (13 mm) wall thickness. Increasing the wall thickness from ½-inch (13 mm) to 1-inch (25 mm) more than doubles the volume of insulation used which also more than doubles the amount of combustible material available to burn. In this case, there was sufficient material with a great enough heat release within the chase to change from good fire performance into a material, which will cause a flashover. Limiting the volume of combustible material may have a dramatic effect on heat release values.

Table 4 - *Data from Vertical Pipe Chase Fire Test*[1]

Material		Remarks	Max RHR_{30s} (kW)	THR_{10min} (MJ)	SRR_{30s} (m^2/sec)	TSR_{10min} (m^2)	Flaming Extension above the Chase
A1	PEF	2-1/2" ID X 1" wall – no jacket	814	58.2	9.84	604	Y
A2	PEF	2-1/2" ID X 1" wall – no jacket	784	33.4	13.07	687	Y
A3	PEF	2-1/2" ID X 1" wall – no jacket	631	45.5	11.79	832	Y
B1	FEF	2" NPS ID X 1" wall – no jacket	42.6	10.6	1.19	301	N
B2	FEF	2" NPS X 1" wall – no jacket	44.0	8.1	1.25	213	N
B3	FEF	2" NPS X 1" wall – no jacket	46.0	7.9	1.74	295	N
C1	MF	2" NPS ID X 1" wall –w/jacket	12.7	2.6	0.62	134	N
C2	MF	2" NPS X 1" wall – w/ jacket	25	3.6	1.74	174	N
C3	MF	2" NPS X 1" wall – w/ jacket	23	5.2	1.20	133	N
D1	PIR	2" NPS ID X 1" wall – w/ jacket	173.9	10.4	4.15	242	Y
D2	PIR	2" NPS X 1" wall – w/ jacket	143	10.0	3.68	230	Y
D3	PIR	2" NPS X 1" wall –jacket removed	79.7	7.0	1.84	178	N
E1	PHN	2" NPS X 1" wall – w/ jacket	56.7	10.3	1.19	169	N
E2	PHN	2" NPS X 1" wall – no jacket	89.0	10.9	1.48	73	N
A ½ 1	PEF ½	2-1/2" ID X ½" wall – no jacket	23.0	3.0	0.12	20	N
A ½ 2	PEF ½	2-1/2" ID X ½" wall – no jacket	17.0	3.0	0.16	38	N
A ½ 3	PEF ½	2-1/2" ID X ½" wall – no jacket	12.0	3.0	0.17	33	N

[1] All data has been corrected to subtract out baseline data from the burner for both heat release and smoke production. All testing was done with a 15-inch (382 mm) burner position with a 20/70 kW exposure for 10 minutes.

Max RHR_{30s} is a rolling 30-second average for heat release rate in kilowatts. $THR_{10\ min}$ is total heat release over the 10-minute duration of the test in megajoules.
SRR_{30s} is a rolling 30-second average of smoke release rate in square meters per second. $TSR_{10\ min}$ is total smoke released over the 10-minute duration of the test in square meters.
Flaming Extension Above the Chase is an indication of flame out the top of the chase at some time during the 10-minute test.

The ability of a material to cause flashover is an important consideration in this apparatus as with other larger scale room fire tests. Materials that perform well in this test also perform well in larger scale tests such as the Factory Mutual Research pipe chase and room fire tests (Figures 7 and 8 illustrate a material known to perform well in large scale tests). [*1*] Some materials however perform well in other full-scale tests, but not in the vertical chase.

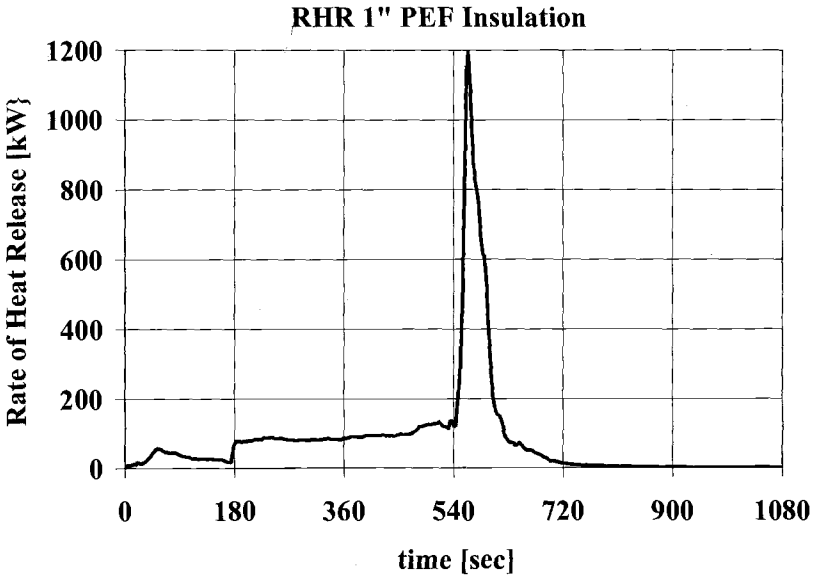

Figure 5 *Rate of Heat Release for 1-inch Polyethylene Foam Insulation*

Smoke generation is measured in two different ways. The first is a rolling 30-second average smoke release rate and the second is total smoke release over the 10-minute test duration. As with the maximum heat release rate, the smoke release rate can be an indication of rapid fire growth during the test while total smoke release is an indication of the total volume of smoke released into the space or building. Using these two numbers together may be useful in evaluating the smoke performance of a system.

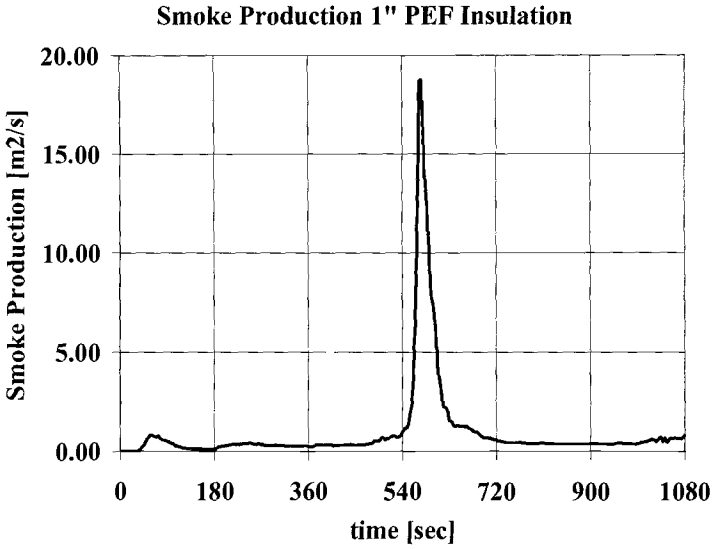

Figure 6 *Smoke Production for 1-inch Polyethylene Foam Insulation*

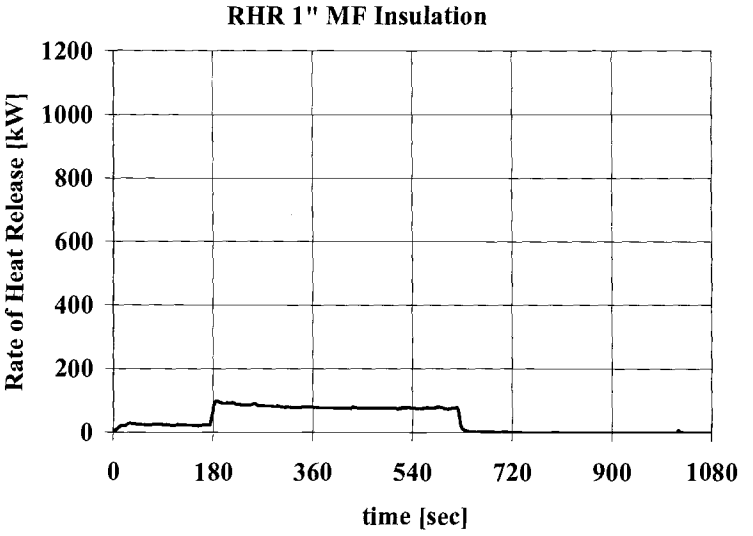

Figure 7 *Rate of Heat Release for 1-inch Mineral Fiber Insulation.*

Some materials do not produce smoke continuously during the test but only produce smoke during ignition while other materials produce smoke continuously throughout the test. As a material approaches flashover both the rate of smoke release and the total smoke release increase dramatically as with material A (See Figure 6).

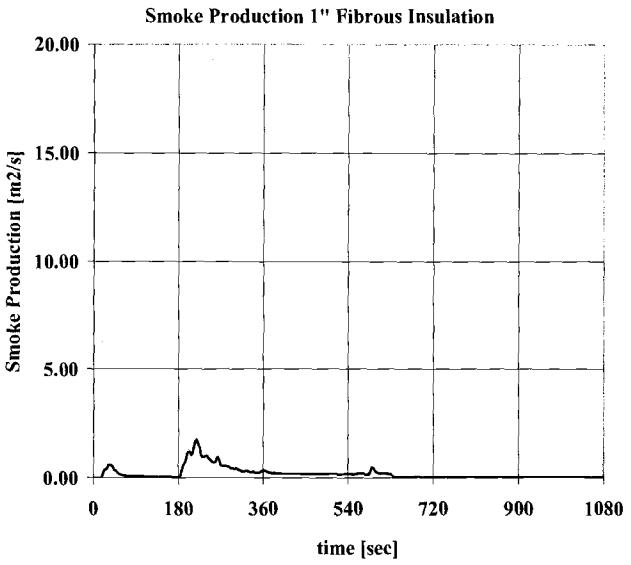

Figure 8 *Smoke Production for 1-inch Mineral Fiber Insulation*

Vertical Flame Spread

Vertical flame spread is a measure of flame extension out the top of the vertical chase. This is the ability of a material to rapidly spread flame between floors or within a confined space, which allows the continued propagation of a self-spreading fire beyond the initial ignition source. Rapid or extensive flame spread is a critical property of a material, which may limit its use in a concealed space and is exhibited by materials A and D.

Post-test Examination

Post-test examination of the materials is a very useful tool in confirming the actual degree of flame spread and to monitor uncontrolled burning of the material. Most examinations of low heat release materials have shown limited damage, which is confined to small sections of the vertical and horizontal insulation sections. Higher heat release materials have shown damage over the entire vertical insulation section. This examination may also be useful in helping to determine the failure mode of a material.

A good example of this is material D in Table 4 in which post-test examination clearly showed that the jacketing caused the failure of the material.

Future Work Anticipated

Additional work, which is anticipated and not yet completed, will be the establishment of material criteria or limits. Once these limits are established this test could be adopted by the Model Codes and 90A as an alternate test method to the currently established tests. Also, additional work must be done to correlate the performance of insulation systems using this new test to other currently accepted test procedures such as E 84 and the larger scale room fire tests. The correlation with other larger scale tests has been difficult due to the inability of most other larger scale tests to test true pipe insulation system composites.

Conclusions

There are potential problems with testing pipe insulation systems with current larger scale tests. These problems may be caused by specimen geometry, specimen orientation, inability to test a composite system, or by the inability of a material to remain in the flame exposure zone. This is supported by the fact that all insulation materials tested currently are advertised as yielding a flame spread of 25 or less and a smoke developed of 50 or less in the E 84 Test. This apparatus has clearly shown that there are potential problems with some of these materials when tested in a different orientation.

The vertical pipe chase apparatus can be a useful tool in evaluating the fire performance of composite pipe insulation systems. This test allows the end user to evaluate all the components of a pipe insulation system in an actual end-use configuration rather than in isolation, as is the case with most other test methods. This test also offers useful information such as heat release and heat release rates, which heretofore have been difficult or impossible to obtain on composite materials. This test does address problems such as testing of thermoplastic materials, which have caused errors and misinterpretation of test results from other accepted test methods such as E 84.

This test may be a useful tool in comparing the relative fire performance of insulation systems, especially when used in conjunction with other intermediate and full-scale fire tests.

References

[1] Bellas, D. W., "Fire Safety in Plenums," *Southern Building*, January/February, 2001, pp. 20-25.

Thomas E. Whitaker[1] and David W. Yarbrough[2]

Review of Thermal Properties of a Variety of Commercial and Industrial Pipe Insulation Materials

Reference: Whitaker, T. E. and Yarbrough, D. W., "**Review of Thermal Properties of a Variety of Commercial and Industrial Pipe Insulation Materials,**" *Insulation Materials: Testing and Applications: 4th Volume, ASTM STP 1426*, A. O. Desjarlais and R. R. Zarr, Eds., ASTM International, West Conshohocken, PA, 2002.

ABSTRACT: A variety of pipe thermal insulation materials has been characterized for thermal properties using the ASTM C 335 Horizontal Pipe Apparatus. The materials represent commercially available pipe insulation that were received and tested between January 1981 through December 1997. These insulation materials are typically used in buildings and industrial manufacturing facilities.

For many materials, there are sufficient replicates to establish a range in the thermal conductivity of the material and an estimate of the material variability. The apparatus used in these measurements was included in a round robin interlaboratory evaluation. The results of that evaluation were published in a previous paper.

Since all commercially available pipe insulation materials experience variation in physical properties such as density, wall thickness, installation methods, etc. there is a corresponding variation in the thermal properties. By evaluating each material over a long time period, the variation in thermal performance can be estimated. This information can be used to determine the proper thermal conductivity for best and worst case scenarios.

Tables and plots of the measured apparent thermal conductivity of various pipe insulation materials is presented showing the range and statistical variability of each materials. All the data has been calculated according to the methods described in ASTM C 335-95 "Standard Test Method of Steady-State Heat Transfer Properties of Horizontal Pipe Insulation" and C 1045-97 "Standard Practice for Calculating Thermal Transmission Properties Under Steady-State Conditions"

KEYWORDS: Thermal Insulation, Calcium Silicate, Mineral Fiber, Cellular Glass, Expanded Perlite, Fiber Glass, Pipe Insulation, Apparent Thermal Conductivity

Introduction

This review is a summary of the thermal properties of a variety of commercially available high-temperature pipe thermal insulations. Thermal measurements were performed between January 1, 1982 through December 31, 1997 on homogenous, inorganic thermal insulations. The mean temperatures in the experimental study ranged

[1] TSRK Enterprises Inc. Grand Junction, CO 81506.
[2] R&D Services Inc, Cookville, TN 38501.

from 100°F (37°C) to 1000°F (537°C).

The pipe insulation materials were grouped by the ASTM material specification that defines the material physical and thermal properties. Within each group, there was more than one manufacturer, except Cellular Glass. The materials included were Calcium Silicate, Expanded Perlite, Mineral Wool, Glass Fiber, and Cellular Glass. In the ASTM C 547-95 material specifications, Mineral Wool and Glass Fiber are not separated. For this review they were reported separately. All the insulation specimens were randomly selected from factory-sealed cartons and were received and tested between the dates of this review. There was no discrimination or elimination of test results if an insulation specimen did not meet the physical property requirements of the appropriate ASTM material specification.

Procedure

The apparent thermal conductivity of each specimen of pipe insulation was measured in accordance with ASTM C335 1981 & 1995 "Standard Test Method for Steady-State Heat Transfer Properties of Horizontal Pipe Insulation." After the insulation specimens were removed from the factory cartons, they were conditioned in an oven at 230°F (110°C) until they reached constant weight. After mounting a specimen on the test apparatus, the test was started as soon as possible to reduce the amount of moisture reabsorbed by the material. In all cases, the apparent thermal conductivity was measured at three or more different mean temperatures to allow a regression analysis. At the end of the test, all the data were saved to a database. In a few cases, the specimens were installed in a double layer configuration to allow measurements on the inner layer at high mean temperatures. The nominal thickness of most of the specimens was two inches (51 mm). In a few cases, the nominal thickness was 1½ inches (38 mm) or 2½ inches (64 mm) depending on the availability of the insulation at the time the specimens were selected.

Apparatus

The test apparatus used in this study was a three-inch (76 mm), schedule 80, stainless steel pipe that was five ft. (1524 mm) long. The pipe was machined to separate the metering area from the guards with only three small bridges for mechanical support. The end guards were 12 inches (305 mm) long, and the metering area was 36 inches (914 mm) long. The pipe was heated with three separate heating circuits, one for each end guard and one for the metering area. The heating circuits were coiled nickel chromium wire in a ceramic core. The outside diameter closely matches the inside diameter of the pipe so there was very little thermal resistance between the heater and the inside of the pipe. Each guard area was heated by 120 VAC power controlled by an electronic controller. The metering area was heated by a regulated DC power supply that supplies a constant voltage. There was a thermopile between each end of the metering area and the guard that was used as the signal input to the guard controllers. There were nine thermocouples on the outside surface of the specimen, nine thermocouples on the surface of the metering area of the pipe and eight thermocouples between the guard area and metering area. The apparatus was operated in a constant temperature room.

All the voltage taps and thermocouples were connected to a data logger that measures each input, converts the signal to engineering units, then transmitted the information to a computer. The computer was used to record the data and determine when equilibrium was reached. The computer was also connected to the guard controllers to allow the program to adjust the controller set point to maintain the temperature difference across the gap. The computer was programmed to collect all the voltage and temperature data every five minutes and make any adjustments to the guard controllers necessary to minimize the gap temperature difference. The data was averaged every 30 minutes and compared to previous averages to determine if equilibrium has been attained. The definition for equilibrium was more rigorous that specified by the C335 test method. The average measured conductivity cannot change by more than 0.25% in a two-hour period and the measured conductivity cannot be consistently increasing or decreasing. An additional requirement was that the average hot surface and average cold surface temperatures cannot change by more than 5% of the average in the same two periods in question.

The metering equipment was calibrated annually by equipment that have calibrations traceable to NIST (National Institute of Science and Technology). An additional check was also made by including a standard specimen of calcium silicate pipe insulation and plotting the results on a control chart. The control chart indicated the apparatus remained consistent within +/- 5% over the period of the project.

This apparatus has been used in an ASTM interlaboratory comparison testing program that were designed to develop the Precision and Bias statements for C 335, [1,2]. In the comparison published in Reference 2, the apparatus used in this review measured the calcium silicate specimens at the beginning and at the end of the project. This was to assure that there had not been a significant change in the specimens and to provide an estimate of the intralaboratory repeatability of the test method. The maximum variation between laboratories in the range of 100°F to 700°F did not vary by more than 6.3% of the average and the intralaboratory repeatability was less than 2%. Since the analysis in this report was based on measurements made on one apparatus, the intralaboratory repeatability was more representative of the testing variation.

Results

Tables 1 through 7 display the results of the regression analysis for each material group. The regression analysis was based on using a second order polynomial. There was little improvement between using a second or third order equation. A second order was chosen because in most of the data sets, the number of points was not equally distributed between the low and high mean temperatures. Using a third order equation in some data sets would cause the regression equation to have an inflection point near the upper end of the curve.

Calcium Silicate Pipe Thermal Insulation

The ASTM specification for this material was C 533-95 "Standard Specification for Calcium Silicate Block and Pipe Thermal Insulation". Table 1 shows a comparison of the data set and the thermal conductivity specification limit at each mean temperature.

The values for the average apparent conductivity (k_a) were obtained from the regression equation:

$$k_a = 2.304 \times 10^{-7} T_m^2 + 2.996 \times 10^{-5} T_m + 0.3456 \quad (1)$$

Table 1 Calcium Silicate Pipe Insulation, ASTM C 533-95, Type 1

Mean Temperature (°F)	Average Apparent Conductivity (Btu in/hr ft^2 °F)	C 533-95 Specification Max (Btu in/hr ft^2 °F)	Upper 95% Confidence Limit of Data
100	0.378		0.406
200	0.415	0.45	0.455
300	0.456	0.50	0.509
400	0.502	0.55	0.571
500	0.553	0.60	0.639
600	0.608	0.66	0.713
700	0.668	0.71	0.794
800	0.733		0.881

The average apparent thermal conductivity of the Calcium Silicate pipe thermal insulation was below the ASTM specification at all the mean temperatures specified in ASTM C 533 as the maximum. Figure 1 shows the 532 individual data points and a line representing the regression equation. The maximum deviation from the average was +22.7 to –26.1%.

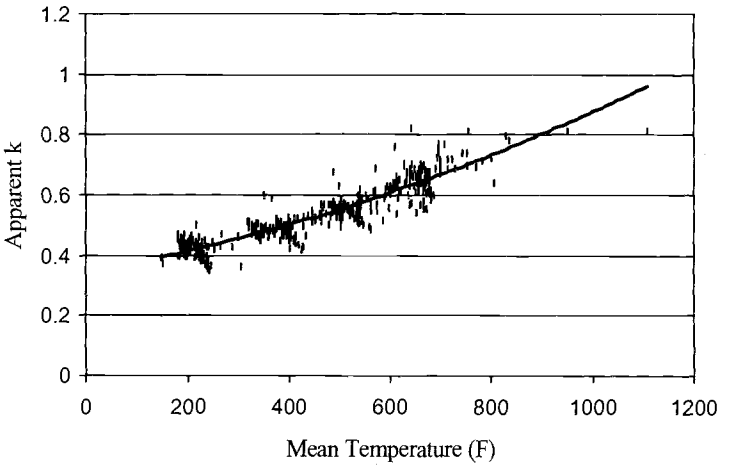

Figure 1 – *Apparent Thermal Conductivity of Calcium Silicate Pipe Insulation*

Cellular Glass Pipe Thermal Insulation

The ASTM specification for this material was C 552-91 "Standard Specification for Cellular Glass Thermal Insulation". The specimens were obtained from a commercial fabricator that prepared pipe insulation by gluing blocks together then machining the larger block to make pipe insulation. This was a common practice for this material and the manufacturer publishes specific instructions on making pipe insulation from flat blocks. Table 2 shows a comparison of the data set and the thermal conductivity specification maximum at each mean temperature. The values for the average apparent conductivity were obtained from the regression equation:

$$k_a = 1.316 \times 10^{-6} T_m^2 + 3.574 \times 10^{-4} T_m + 0.3825 \quad (2)$$

Table 2 - Cellular Glass Pipe Insulation C 552-91, Type II

Mean Temperature (°F)	Average Apparent Conductivity (Btu in/hr ft^2 °F)	C 552-91 Specification Max (Btu in/hr ft^2 °F)	Upper 95% Confidence Limit of Data
100	0.431	0.37	0.733
200	0.507	0.46	0.960
300	0.608	0.56	1.243
400	0.736	0.69	1.582

In all cases, the average apparent thermal conductivity was above the ASTM specification maximum. The Upper 95% confidence limits were influenced by the fact that there were only 10 data points. Figure 2 displays the 10 data points and a line representing the regression equation. The maximum deviation from the average was +4.4 to –2.5%.

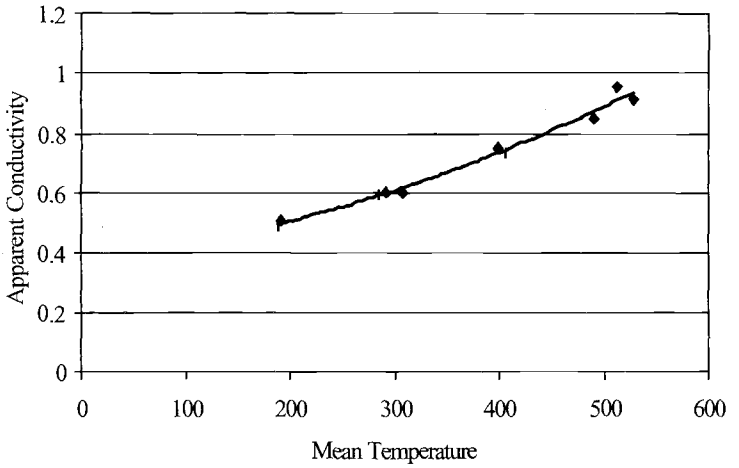

Figure 2 - *Apparent Thermal Conductivity of Cellular Glass Pipe Thermal Insulation*

Glass Fiber Pipe Insulation, Type 1

The ASTM specification for this material was C 547-95 "Standard Specification for Mineral Fiber Pipe Insulation." ASTM C 547-95 does not differentiate between mineral wool and glass fiber. For this analysis, the products were separated for comparison. Table 4 shows a comparison of the data set and the thermal conductivity specification limit. Type 1 was defined as pipe insulation that has a maximum operating temperature of 650°F. The values for the average apparent conductivity were obtained from the regression equation:

$$k_a = 7.787 \times 10^{-7} T_m^2 + 1.921 \times 10^{-4} T_m + 0.2141 \quad (3)$$

Table 3 – Glass Fiber Pipe Insulation C 547-95, Type 1

Mean Temperature (°F)	Average Apparent Conductivity (Btu in/hr ft^2 °F)	C 547-95 Specification Max (Btu in/hr ft^2 °F)	Upper 95% Confidence Limit of Data
100	0.241	0.25	0.47
200	0.284	0.31	0.62
300	0.342	0.40	0.81
400	0.416	0.51	1.04
500	0.505	0.64	1.30

In all cases, the average apparent thermal conductivity was below the specification maximum. Figure 3 displays the 28 measurements and a line representing the regression equation. The maximum deviation from the average was 9.6% to -27.5%.

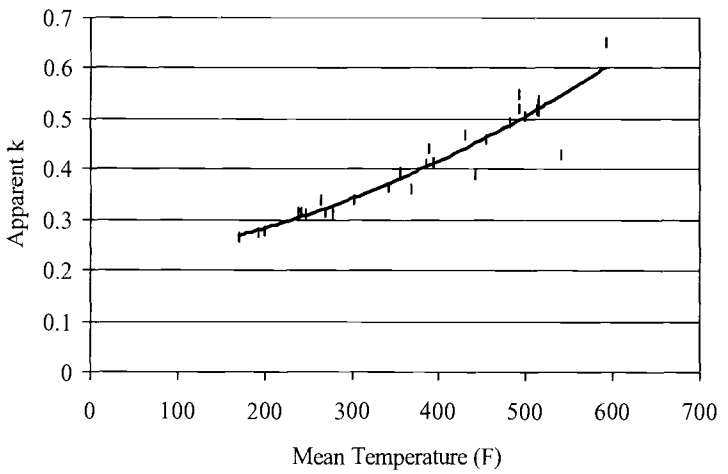

Figure 3 – *Apparent Conductivity of Glass Fiber Type 1 Pipe Insulation*

Glass Fiber Pipe Insulation, Type 2

The ASTM specification for this material was C 547-95 "Standard Specification for Mineral Fiber Pipe Insulation." The difference from the previous group was the maximum temperature rating. Type 2 has a maximum temperature limit of 1200°F. Table 5 shows a comparison of the data set and the thermal conductivity specification limit. The values for the average apparent conductivity were obtained from the regression equation:

$$k_a = 6.728 \times 10^{-8} T_m^2 + 5.118 \times 10^{-4} T_m + 0.3534 \quad (4)$$

Table 4 – Glass Fiber Pipe Insulation C 547-95, Type 2

Mean Temperature (°F)	Average Apparent Conductivity (Btu in/hr ft^2 °F)	C 547-95 Specification Max (Btu in/hr ft^2 °F)	Upper 95% Confidence Limit of Data
100	0.405	0.25	0.455
200	0.458	0.31	0.476
300	0.513	0.37	0.511
400	0.569	0.45	0.558
500	0.626	0.54	0.619
600	0.685	0.65	0.693
700	0.745	0.77	0.780

The average apparent thermal conductivity exceeded the specification maximum in all cases except the value for 700°F. Figure 4 displays the 26 measurements and a line representing the regression equation. The maximum deviation from the average was +8.8% to –13.4%.

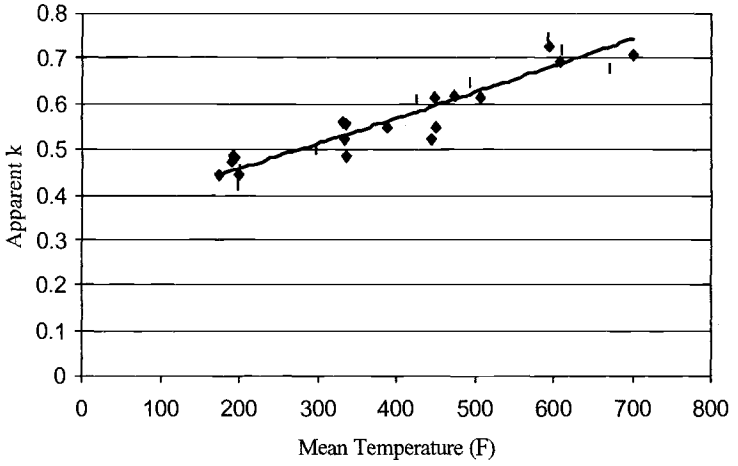

Figure 4 – *Apparent Conductivity of Glass Fiber Type 2 Pipe Insulation*

Mineral Wool (Rock and Slag) Pipe Insulation

The ASTM specification for this material was C547-95 "Standard Specification for Mineral Fiber Pipe Insulation." This was pipe insulation that was molded to fit the actual diameter and has a maximum temperature limit of 1200°F. Table 6 shows the comparison between the data set and thermal conductivity specification limit. Values for the average apparent conductivity were obtained from the regression equation:

$$k_a = 1.059 \times 10^{-6} T_m^2 - 8.210 \times 10^{-5} T_m + 0.3060 \quad (5)$$

Table 5 – Mineral Wool Pipe Insulation C 547-95, Type 2

Mean Temperature (°F)	Average Apparent Conductivity (Btu in/hr ft^2 °F)	C 547-95 Specification Max (Btu in/hr ft^2 °F)	Upper 95% Confidence Limit of Data
100	0.308	0.25	0.455
200	0.332	0.31	0.476
300	0.377	0.37	0.511
400	0.443	0.45	0.558
500	0.530	0.54	0.619
600	0.638	0.65	0.693
700	0.767	0.77	0.780

Only the average apparent conductivity at 400°F mean and above met the requirements of the specification. Figure 5 displays the 91 measurements and a line representing the regression equation. The maximum deviation from the average was +31.5 to –29.7%.

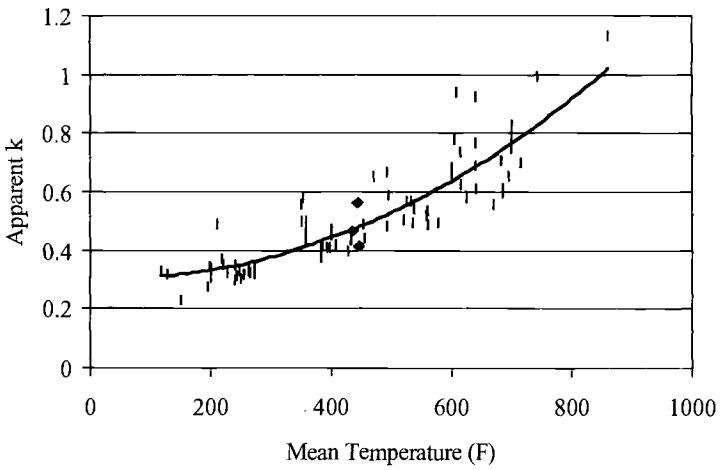

Figure 5 – *Apparent Conductivity of Mineral Wool Type 2 Pipe Insulation*

Grooved Mineral Wool (Rock and Slag) Pipe Insulation

The ASTM specification for this material was C 547-95 "Standard Specification for Mineral Fiber Pipe Insulation". This was pipe insulation that was fabricated from machined board by a precision cutting process and has a maximum temperature limit of 1200°F. The specification defines this as a Type 3 material. Table 7 shows a comparison of the data set and the thermal conductivity specification limit. Values for the average apparent conductivity were obtained from the regression equation:

$$k_a = 1.059 \times 10^{-6} T_m^2 - 8.210 \times 10^{-5} T_m^2 + 0.3900 \quad (6)$$

Table 6 – Grooved Mineral Wool Pipe Insulation C 547-95, Type 3

Mean Temperature (°F)	Average Apparent Conductivity (Btu in/hr ft^2 °F)	C 547-95 Specification Max (Btu in/hr ft^2 °F)	Upper 95% Confidence Limit of Data
100	0.259	0.25	0.348
200	0.307	0.31	0.437
300	0.364	0.37	0.543
400	0.430	0.45	0.666
500	0.504	0.54	0.804
600	0.588	0.65	0.959
700	0.681	0.77	1.131

The average thermal conductivity was very close to meeting the requirements of the material specification. Figure 6 displays the 40 measurements and a line representing the regression equation. The maximum deviation from the average was +12.2 to –18.5%.

Expanded Perlite Pipe Insulation

The ASTM specification for this material was C610-95 "Standard Specification for Molded Expanded Perlite Block and Pipe Insulation". Table 7 shows a comparison of the present data set and the thermal conductivity specification limit. The regression for this data set used a linear equation. Using a higher order regression polynomial did not produce any improvement in the coefficient of determination. The values for the average apparent conductivity were obtained from the regression equation:

$$k_a = 5.744 \times 10^{-4} T_m + 0.39 \quad (7)$$

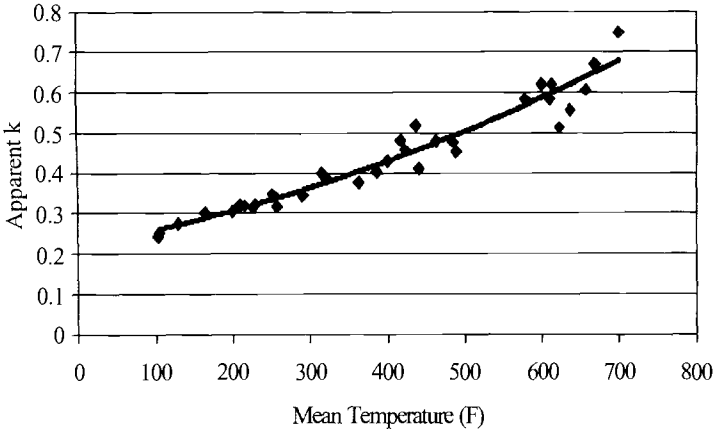

Figure 6 – *Grooved Mineral Wool Pipe Insulation C547 Type 3*

Table 7 – Molded Expanded Perlite Pipe Insulation C610-99

Mean Temperature(°F)	Average Apparent Conductivity (Btu in/hr ft^2 °F)	C610-99 Specification Limits (Btu in/hr ft^2 °F)	Upper 95% Confidence Limit of Data
100	0.447		0.480
200	0.505	0.55	0.544
300	0.562	0.60	0.607
400	0.620	0.66	0.671
500	0.677	0.74	0.734
600	0.735	0.80	0.798
700	0.792	0.88	0.802

The average was well below the specification maximum at all mean temperatures. Figure 7 displays the 170 measurements and a line representing the regression equation. The maximum deviation from the average was +19.5 to –25.4%. The perlite regression equation was the only curve that was not concave up. Notice that the Upper 95% confidence limit and the C 610-99 specification limit are very similar.

Discussion

For each generic material included in this review, there was a considerable variation in the measured thermal conductivity. The variability was related to testing variation and to material variation. The testing variability was relatively small as discussed in the referenced documents. The variability was more related to material variability and the data set includes more than one manufacturer. Since these materials have been selected from commercially available supplies, the data are indicative of what the customer was actually receiving.

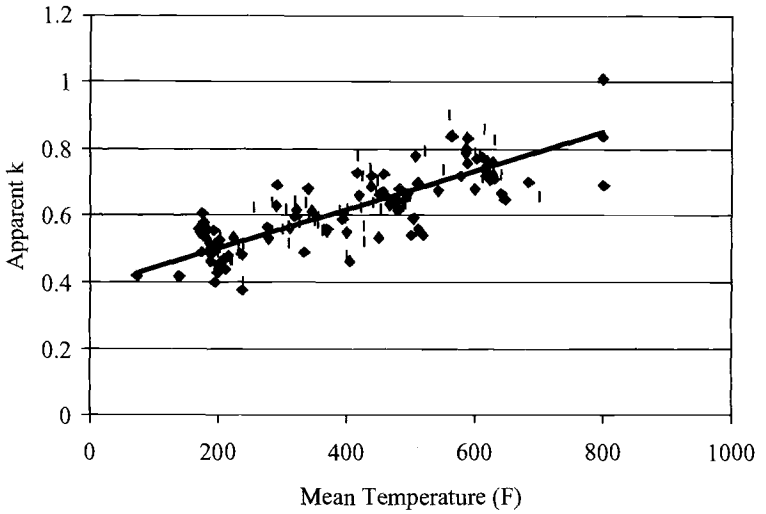

Figure 7 – *Molded Expanded Perlite Pipe Insulation*

Table 8 displays the average density and the range for each of the material groups. The effect of density on the measured thermal conductivity was beyond the scope of this report. The ASTM material specifications typically define a minimum or maximum density for each material and there were data points in this review that were outside those limits. The ASTM C 533-95 and C 547-95 Specifications have multiple Types that are distinguished by the maximum allowable operating temperature. These are shown as different Types.

Table 8 Density Range of Each Material Group

	No of Points	Average Density *	Maximum Density	Min Density	Density Mode	Standard Deviation
Calcium Silicate						
Type 1	532	14.3	20.1	7.2	14.6	1.44
Cellular Glass	10	8.5	8.8	8.3	8.3	0.26
Fiber Glass Type1	28	5.4	9.3	3.4	5.2	2.16
Fiber Glass Type 2	26	12.9	16.4	10.3	12.0	1.98
Grooved Mineral						
Wool	40	9.1	14.4	7.2	8.4	2.06
Mineral Wool	91	9.3	13.6	4.2	9.7	2.85
Expanded Perlite	170	13.5	17.4	8.6	11.3	2.30

* Density in lbs/ft^3

Conclusions

The apparent thermal conductivity of a variety of commercially available pipe thermal insulations was characterized by the generic ASTM material specification for each material. There was a wide variation in the measurements.

The variation is representative of the time period of the program, January 1981 through December 1997, and contains products from several manufacturers. There was no attempt to distinguish between manufactures. This does not imply that any one product or manufacturer does or does not meet the specification requirements, just that as a whole, there is a wide variation in what was commercially available during the period of the program.

The ASTM material specifications denote maximum allowable thermal conductivity. For all the material groups, there were measurements that exceeded these limits. When the average of each material was considered, the correlation averages for Type I Calcium Silicate; Type 1 Glass Fiber; Grooved Mineral Wool; and Expanded Perlite pipe insulation were in compliance with the ASTM material specification in effect at the end of the time period. The correlation average for Mineral Wool satisfied the requirements at 400°F mean and above. The correlation average for Cellular Glass and Type 2 Glass Fiber pipe insulation did not satisfy the material specification maximum limit.

Since the duration of the testing program was 15 years and it ended in 1997, there may be processing or material changes that are not reflected in this review and the pipe insulation products currently produced may come closer to meeting the ASTM material specification limits.

In every case except that of calcium silicate, the analysis of the experimental data indicates significant material with the measured apparent conductivity above the specification maximum. This implies that ASTM Committee C16 should consider changes to their material specifications to better define the specification limits.

References

[1] Smith, David R., 1989. "Interlaboratory Comparison of the Guarded-End Horizontal Test Pipe Apparatus," *NISTIR 89-3913*, National Institute of Standards and Technology, Boulder, CO

[2] Whitaker, T. E., Graves, R. S., McElroy, D. L., and Smith, D. R, 1994, "Interlaboratory Comparison of the Horizontal Pipe Insulation Test Apparatus up to 350°C," *Proceedings of the 22nd International Thermal Conductivity Conference*, Arizona State University, Tempe, AZ

Session 6: Novel Building Systems

Krishpersad Manohar,[1] Jaishree Ramroopsingh,[2] and David W. Yarbrough[3]

Use of Sugarcane Fiber as Building Insulation

Reference: Manohar, K., Ramroopsingh, J., and Yarbrough, D. W., **"Use of Sugarcane Fiber as Building Insulation,"** *Insulation Materials: Testing and Applications: 4th Volume, ASTM STP 1426,* A. O. Desjarlais, and R. R. Zarr, Eds., ASTM International, West Conshohocken, PA, 2002.

Abstract: Low-cost thermal insulations produced as a byproduct of the sugarcane industry are becoming an affordable means of achieving some measure of thermal comfort in buildings located in developing countries. Environmental concerns about solid waste provide additional motivation for the use of sugarcane fiber as a thermal insulation.

Naturally occurring biodegradable sugarcane fibers fall into the category of large diameter fibrous materials with fiber diameters in the range from 0.198 mm to 0.319 mm. Thermal measurements on loose-fill sugarcane fibers show minimum apparent thermal conductivities at 24°C in the range from 0.0468 W/m.K to 0.0496 W/m.K for specimen densities from 100 kg/m^3 to 120 kg/m^3. Additional research on fire resistance and susceptibility to insect attack is underway at the University of the West Indies, Trinidad.

Sugarcane fiberboards with densities near 113 kg/m^3 were produced using cornstarch as the binder. The structural integrity of the boards was tested using a sag test and a breaking strength test. The thermal properties were tested using ASTM Steady State Thermal Transmission Properties by Means of the Heat Flow Meter (C 518). Comparative sag, breaking strength and thermal tests were conducted on commercially available fiberglass and mineral fiber ceiling tiles. Both structural tests show the fiberboard to be between that of the fiberglass and mineral fiber ceiling tiles. The thermal tests show that the minimum apparent thermal conductivity of the sugarcane fiberboard is within the range normally associated with building thermal insulation.

Keywords: thermal insulation, fibrous material, sugarcane fiber, starch, thermal conductivity

[1]Lecturer, Department of Mechanical Engineering, University of the West Indies, St. Augustine, Trinidad, West Indies.

[2]BSc Candidate, Department of Mechanical Engineering, University of the West Indies, St. Augustine, Trinidad, West Indies.

[3]President, R&D Services, Inc., 2594 West Broad Street, Cookeville, TN, USA.

Introduction

In many developing countries in which sugarcane is grown thousands of tons of sugarcane fiber are produced as by-products of the sugar production process. A small percentage is burned as fuel for boilers in the sugar factories and poultry farmers use some as bedding for chickens. However, the major portion goes to landfill where it is sometimes a problem to find space for disposal.

Research on loose-fill sugarcane fiber for use as thermal insulation material showed the fibers consists of diameters ranging from 0.198 mm to 0.319 mm [*1*]. In comparison with fiberglass and mineral fiber insulation for which the fiber diameters are a few microns, sugarcane fiber is looked upon as a large-diameter fibrous material [*1*]. Thermal conductivity tests on loose-fill slab-like specimens showed the material to exhibit a characteristic hooked-shape graph of thermal conductivity with density [*2*]. Minimums in the thermal conductivity curve in the range 0.0468 W/m.K to 0.0496 W/m.K was observed for the density range 100 to 120 kg/m^3. The use of the loose-fill material, however, was limited because handling and uniformity of packing-density proved difficult to control [*1, 3*]. This necessitated the use of a binder to overcome these problems thereby enhancing the potential use of the material. To eliminate the concerns of environmentalist and the long-term effect of hazardous waste disposal the biodegradable property must be maintained. Hence cornstarch was selected.

The binding property of cooked starch depends strongly on the viscosity of the starch at the point of mixing. When starch is cooked, the granule slurry changes from a suspension to a dispersion of swollen granules, partially disintegrated granules and molecular dispersed granule contents. The transition from a suspension of granules to a paste is accompanied by a large increase in apparent viscosity [*4*]. The starch paste is non-newtonian during cooling. Paste consistency increases as molecular association forms a cross-linked network that increases the paste resistance to deformation. In a cooled state paste may remain fluid or form a semi-solid or solid gel showing considerable strength [*4*]. The efficiency of an adhesive to bind together two rough surfaces depends largely on its viscosity. It must be sufficiently fluid to penetrate the interspaces and yet have enough body to give a thin but strong layer of adhesive when the joint is dry.

Fiberboard Manufacture

Cornstarch was boiled in water for approximately 40 minutes. The ratio of dry powder starch to water was varied to optimize the mixture. During the heating process the viscosity was continuously monitored with the Haake VT 550 Viscometer. Continuous stirring of the mixture was necessary to avoid the formation of lumps. The temperature of the starch/water mixture was maintained at approximately 63°C at which the starch gelatinized. The process took approximately 30 minutes for the viscosity of the gel to reach its maximum viscosity of approximately eight poises. This was in accordance with the amylograph for maize starch [*5, 6*]. The viscosity leveled off over the next 10 minutes to about 7 poises and at this point the starch was ready for mixing with the

sugarcane fiber.

Mixing Process

The unique combination of starch gel and sugarcane fiber proved difficult to mix in any conventional commercial mixers readily available. The relatively high-density slush-like starch gel and lightweight sugarcane fiber had to be uniformly mixed. To aid in the mixing process a horizontal drum-like mixer with a centrally located spiked agitator was constructed.

The mixing drum capacity was 3.7 kg of dry sugarcane fiber. The fiber occupied approximately 20 % of the drum volume. The dry fiber was first placed into the mixing drum and the starch was slowly poured in. The agitator and drum was manually activated and sequentially rotated in opposite directions. A drum rotation of 6 RPM and agitator rotation of 24 RPM provided the most effective mixing. At this optimum rotation one batch was completely mixed in three minutes.

Tile Formation

The optimum density (for minimum thermal conductivity) for loose-fill sugarcane fiber is within the density range 100 kg/m^3 to 125 kg/m^3 [*1*]. Therefore, the objective was to form tiles within this density range. The tiles were formed by placing weighed amounts of the mixture in frames with dimensions 300 mm x 300 mm x 25 mm. The tiles were made in batches of four.

After boiling and mixing starch with fiber the mixture was divided into four equal portions by weight and placed in the tile frames. For each tile the starch/fiber mixture was uniformly spread over the frame area and slightly compressed to the 25 mm thickness. The tiles in the frames were dried to constant weight in an oven at 100°C. This process took approximately 12 hours during which the weight was monitored at 2-hour intervals.

Specimen Conditioning

Before testing the oven-dried specimens were allowed to acclimatize to laboratory conditions for one week. During this period the specimen weight was monitored twice per day to determine when equilibrium was reached.

Mechanical Strength Test

Comparative testing was conducted on the sugarcane fiberboard and commercially available fiberglass and mineral fiber ceiling tiles. Modified sag test and transverse strength test were adapted

from ASTM Test Methods for Strength Properties of Prefabricated Architectural Acoustical Tile or Lay-In Ceiling Tile Panels (C 367).

In the sag test two diagonal lines were drawn on 300 mm square specimens to locate the geometric center. Each tile was placed on a square holding frame with a 10 mm edge support. A dial gauge was positioned at the center of the tile and set to zero. A one kg weight was then moved along each diagonal in increments of 40 mm. The central deflection on the dial gauge was noted for each weight position. The average deflection value for the corresponding points along the diagonals for each specimen was calculated and tabulated.

For the strength test, 80 x 300 mm strips were cut from each specimen. The strips were supported at the edges and a dial gauge set to zero placed at the center. The specimens were then centrally loaded until failure occurred. Weights were added in increments of 180 g up to 900 g. If the specimens did not fail up to 900 g larger increment weights were added until failure. Failure was indicated by a continuous increasing deflection without additional weight.

Test Results – Mechanical Strength Test

To investigate the effect of starch/fiber ratio on the tile strength two sets of four batches with each batch consisting of four tiles were prepared with varying amounts of starch. The mass of dry starch powder used were 0.30 kg, 0.40 kg, 0.50 kg and 0.60 kg which were each boiled in 9 L of water to the optimum viscosity of seven poise. Each batch was mixed with one kg of loose-fill sugarcane fiber. With one set of specimens the sag test was conducted. With the next set the breaking strength test was conducted. Respective sag and strength tests were conducted on two specimens each for commercially available fiberglass and mineral fiber ceiling tiles for comparison. The results are given in Tables 1 to 12.

Table 1 – *Sag Test Results (0.30 kg starch)*

Diagonal Point #	Dial Gauge Deflection (Center point) (mm)				Average Deflection (mm)
	Specimen 1	Specimen 2	Specimen 3	Specimen 4	
1	1.016	3.048	1.270	1.905	1.810
2	3.810	5.969	6.096	6.858	5.683
3	10.160	8.763	13.208	13.716	11.462
4	19.939	11.938	20.447	21.082	18.352
5	24.130	13.335	27.178	27.940	23.146
6	19.558	10.668	24.130	25.400	19.939

7	13.462	7.366	20.066	19.558	15.113
8	8.128	4.826	14.224	13.970	10.287
9	5.842	2.794	10.160	9.398	7.049

Table 2 – *Sag Test Results (0.40 kg starch)*

Diagonal Point #	Dial Gauge Deflection (Center point) (mm)				Average Deflection (mm)
	Specimen 1	Specimen 2	Specimen 3	Specimen 4	
1	2.032	2.794	1.778	2.540	2.286
2	4.318	4.572	6.604	6.096	5.398
3	7.874	7.112	11.176	10.160	9.081
4	11.176	10.160	16.764	14.986	13.272
5	14.732	13.716	19.050	18.034	16.383
6	12.954	13.208	15.748	14.986	14.224
7	9.906	10.668	12.192	11.303	11.017
8	7.112	7.747	7.366	8.001	7.557
9	2.794	4.318	4.572	5.207	4.223

Table 3 – *Sag Test Results (0.50 kg starch)*

Diagonal Point #	Dial Gauge Deflection (Center point) (mm)				Average Deflection (mm)
	Specimen 1	Specimen 2	Specimen 3	Specimen 4	
1	0.000	1.016	0.000	0.254	0.318
2	1.016	1.778	1.524	1.778	1.524
3	2.032	2.540	2.540	2.540	2.413
4	3.302	3.175	3.683	3.175	3.334
5	3.556	4.064	4.445	3.429	3.874
6	3.429	3.429	4.572	3.048	3.629
7	2.794	2.794	3.810	2.540	2.985
8	1.143	2.286	2.540	1.905	1.969

9	0.254	1.270	0.127	1.143	0.699

Table 4 – *Sag Test Results (0.60 kg starch)*

Diagonal Point #	Dial Gauge Deflection (Center point) (mm)				Average Deflection (mm)
	Specimen 1	Specimen 2	Specimen 3	Specimen 4	
1	0.762	1.143	0.127	2.540	1.143
2	0.203	1.524	0.635	4.826	1.797
3	3.048	2.159	1.651	8.636	3.874
4	4.572	2.591	3.302	10.922	5.347
5	5.969	3.302	4.064	10.668	6.001
6	5.969	3.048	3.048	9.144	5.302
7	5.207	2.286	2.540	6.858	4.223
8	4.572	1.778	1.651	5.588	3.397
9	3.937	1.016	0.508	4.046	2.377

Table 5 – *Sag Test Result -Commercially Available Fiberglass Ceiling Tile (69.6 kg/m^3)*

Diagonal Point #	Dial Gauge Deflection (Center point) (mm)		Average Deflection (mm)
	Specimen 1	Specimen 2	
1	1.450	1.780	1.615
2	2.290	2.740	2.515
3	4.830	4.620	4.725
4	7.210	6.740	6.975
5	8.140	8.200	8.170
6	7.260	7.030	7.145
7	5.230	4.890	5.060

8	2.330	2.410	2.370
9	1.550	1.660	1.605

Table 6 – *Sag Test Results Commercially Available Mineral Fiber Ceiling Tile (226kg/m^3)*

Diagonal Point #	Dial Gauge Deflection (Center point) (mm)		Average Deflection (mm)
	Specimen 1	Specimen 2	
1	0.110	0.120	0.115
2	0.210	0.280	0.245
3	0.750	0.680	0.715
4	1.050	1.010	1.030
5	1.120	1.130	1.125
6	0.960	1.060	1.010
7	0.600	0.760	0.680
8	0.250	0.350	0.300
9	0.100	0.090	0.095

Table 7 – *Breaking Strength Test Results (0.30 kg starch)*

Central Load (g)	Dial Gauge Deflection (Center point) (mm)				Average Deflection (mm)
	Specimen 1	Specimen 2	Specimen 3	Specimen 4	
180	23.368	11.684	16.637	19.558	17.812
360	Fail	24.384	35.687	24.130	
540		Fail	37.338	Fail	
720			Fail		

Mean breaking load = 540 g

Table 8 – *Breaking Strength Test Results (0.40 kg starch)*

Central Load (g)	Dial Gauge Deflection (Center point) (mm)				Average Deflection (mm)
	Specimen 1	Specimen 2	Specimen 3	Specimen 4	
180	5.969	4.826	6.985	8.763	6.636
360	12.192	9.652	9.779	13.654	11.319
540	18.796	14.224	24.384	32.472	22.469
720	25.476	19.304	37.388	Fail	
903	35.560	25.527	49.530		
997	41.910	27.432	Fail		
1177	57.658	34.290			
1357	Fail	43.180			
1537		56.388			
1717		Fail			

Mean breaking load = 1197.75 g

Table 9 – *Breaking Strength Test Results (0.50 kg starch)*

Central Load (g)	Dial Gauge Deflection (Center point) (mm)				Average Deflection (mm)
	Specimen 1	Specimen 2	Specimen 3	Specimen 4	
180	1.778	2.921	1.778	2.159	2.159
360	3.556	6.223	3.556	5.334	4.667
540	5.588	9.017	5.207	8.128	6.985
720	7.620	12.700	6.858	10.160	9.335
903	9.398	16.637	8.763	11.938	11.684
997	10.160	20.320	9.906	12.827	13.303
1177	11.684	25.654	11.303	14.732	15.843
1357	13.589	34.036	13.208	16.383	19.304
1537	15.367	48.768	14.859	17.907	24.225

1717	18.034	Fail	16.637	20.066
3990	43.627		Fail	47.98
4750	53.628			Fail
5170	Fail			

Mean breaking load = 3906.75 g

Table 10 – *Breaking Strength Test Results (0.60 kg starch)*

Central Load (g)	Dial Gauge Deflection (Center point) (mm)				Average Deflection (mm)
	Specimen 1	Specimen 2	Specimen 3	Specimen 4	
180	2.794	4.699	2.667	1.905	3.016
360	6.858	8.890	7.112	4.064	6.727
540	8.509	13.716	10.668	5.842	9.684
720	10.541	17.780	14.224	7.874	12.605
903	12.573	22.352	17.907	9.906	15.685
997	12.852	24.130	20.574	10.160	16.929
1177	16.383	31.750	24.638	12.573	21.336
1357	19.050	Fail	28.194	14.097	
2650			Fail		
4130	Fail			Fail	

Mean breaking load = 3066.75 g

Table 11 – *Breaking Strength Test Results – Commercially Available Fiberglass Ceiling Tile (69.6 kg/m^3)*

Central Load (g)	Dial Gauge Deflection (Center point) (mm)		Average Deflection (mm)
	Specimen 1	Specimen 2	
30	2.420	1.960	2.190
60	3.990	3.010	3.500
90	4.140	4.900	4.520
120	5.660	6.730	6.195
150	6.070	8.600	7.335
180	6.670	10.450	8.560
210	8.050	12.500	10.275

240	8.970	14.200	11.585
270	9.970	Fail	
300	Fail		

Mean breaking load = 285 g

Table 12 – *Breaking Strength Test Results Commercially Available Mineral Fiber Ceiling Tile (226kg/m^3)*

Central Load (g)	Dial Gauge Deflection (Center point) (mm)		Average Deflection (mm)
	Specimen 1	Specimen 2	
180	0.470	0.081	0.551
360	1.710	1.810	1.760
540	2.030	2.900	2.465
720	2.550	3.240	2.895
903	2.780	3.670	3.225
997	3.000	3.950	3.475
1177	3.500	4.210	3.855
1357	3.790	4.440	4.115
1537	4.250	4.680	4.465
1717	4.480	4.890	4.695
1900	5.020	5.340	5.180
" "			
5600	9.310	10.180	9.745
5800	Fail	11.200	
6000		Fail	

Mean breaking load = 5900 g

Test Results – Thermal Conductivity Measurements

To investigate the thermal insulating properties of sugarcane fiberboard with cornstarch as a binder nine 300 x 300 x 25 mm specimens were prepared. The starch/fiber ratio used for these specimens was 1:2 by weight. This ratio made the best tile in terms of strength. Thermal conductivity measurements were conducted in accordance with ASTM Steady State Thermal

Transmission Properties by Means of the Heat Flow Meter (C 518). Tests were conducted at mean test temperatures of 14°C, 24°C and 34°C with a temperature difference of 20°C in each case. These tests were also conducted on specimens of commercially available fiberglass ceiling tiles for comparison. The test results are given in Table 13.

Discussion

Low cost and the biodegradable property of sugarcane fiber were the driving force for investigating its use as a material for thermal insulation in buildings. Research conducted

Table 13 – *Thermal Conductivity Test Results*

Specimen	Density (kg/m^3)	Thermal Conductivity (W/m.K)		
		14°C	24°C	34°C
1	110.2	0.0474	0.0499	0.0516
2	120.8	0.0487	0.0511	0.0533
3	100.0	0.0481	0.0505	0.0524
4	98.9	0.0481	0.0506	0.0529
5	118.1	0.0477	0.0500	0.0520
6	109.1	0.0469	0.0491	0.0512
7	129.3	0.0490	0.0520	0.0533
8	116.1	0.0475	0.0499	0.0511
9	112.9	0.0467	0.0488	0.0508
Fiberglass Ceiling tile	61.6	0.0318	0.0334	0.0350

on slab-like specimens of the loose-fill material showed minimum thermal conductivity of 0.0469 W/m.K to 0.0496 W/m.K in the density range 100 to 125 kg/m^3 for a mean test temperature of 24°C [*1, 2*]. When compared with existing insulation such as fiberglass with thermal conductivity values of 0.0334 W/m.K at 24°C, sugarcane fiber showed potential use as a possible insulation material.

To overcome the difficulties associated with handling the loose-fill material and to maintain the biodegradable integrity cornstarch was chosen as a binder. However, due to lack of data on the combination of cornstarch and sugarcane fiber preliminary investigation to determine the structural

integrity of the fiberboard were conducted. Due to the porous surface of the fiberboard a modified sag test and breaking strength test was adapted from ASTM C 367. A one kg weight was moved across both diagonals of the tiles and the central point deflection was measured. The values shown in Figure 1 were the mean deflection from the corresponding points of the two diagonals. The results show that the strength of the tiles increased as the starch/fiber ratio increased from 0.3 kg/kg to 0.5 kg/kg as indicated by the decrease in deflection. A significant decrease in strength was seen as the starch/fiber ratio was increased from 0.5 to one to 0.6 to one. The data from Tables 7 to 10 show that as the starch/fiber ratio increased in the proportion 0.3:1, 0.4:1, 0.5:1 and 0.6:1 the mean breaking strength was 540 g, 1197.75 g, 3906.75 g and 3066.75 g, respectively. These results show similar trends with both the sag and breaking strength test in which the tiles with a starch/fiber ratio of 0.5/1 kg/kg were the strongest while there was a decrease in strength with higher or lower starch/fiber ratio.

The lower strength with the starch/fiber ratio less then 0.5/1 kg/kg may be the result of insufficient starch to effectively bind all the fibers. The maximum strength is probably the

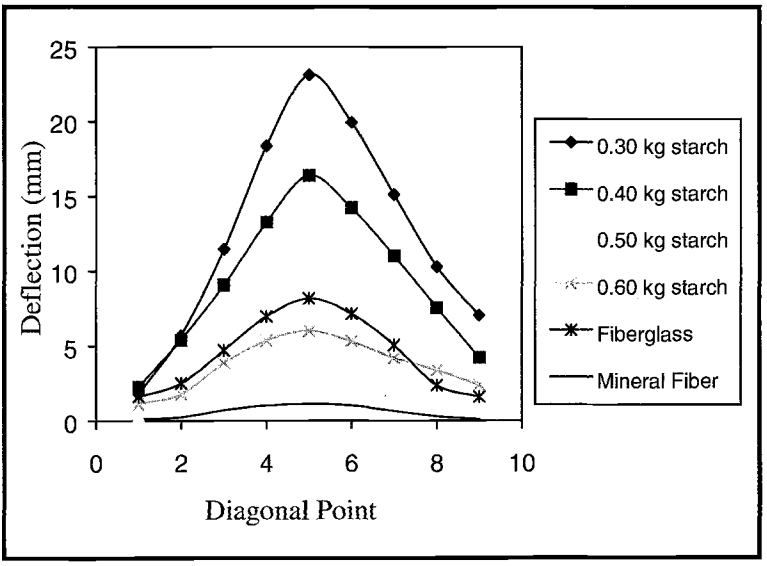

Figure 1 – *Mean Deflection of Tiles Across Diagonals*

result of the optimum amount of starch to cover the fibers with a thin layer. Observations show that specimens with the starch/fiber ratio of 0.6/1 kg/kg had portions of pure starch filling gaps between fibers. This indicated too much starch. Dry starch paste is brittle in nature that could account for the decrease in strength of these tiles.

The comparative sag and strength test with commercially available fiberglass and mineral fiber tiles show that the 0.5/1 kg/kg ratio of starch/fiber tiles was stronger then the fiberglass tiles but

weaker then the mineral fiber tiles. Both structural tests showed that the 0.5/1 kg/kg starch fiber ratio produced the best tiles. This ratio of mixture was used for making the thermal conductivity test specimens.

Variation in packing density resulted in the thermal conductivity test specimens density ranging from 98.9 to 129 kg/m^3. This was slightly larger than the desired 100 to 125 kg/m^3, however it gave a wider than expected test density range. Figure 2 shows a picture of test specimen #6. The thermal conductivity test results for the nine specimens at mean test temperatures of 14°C, 24°C and 34°C are given in Table 13 and shown graphically in Figure 3. The results indicate that the optimum density for minimum thermal conductivity for the fiberboard was approximately 113 kg/m^3. The graphs of thermal conductivity vs. density show the characteristic shape for fibrous materials [*1, 2, 3*]. The best-fit curve for each set of data was determined using the least-square fit method through the data points and are plotted in Figure 3. The trend is in conformance with the characteristic behavior of fibrous materials [*2, 3*].

The comparative thermal conductivity tests at 14°C, 24°C and 34°C between the optimum density sugarcane fiberboard and commercially available fiberglass ceiling tiles show

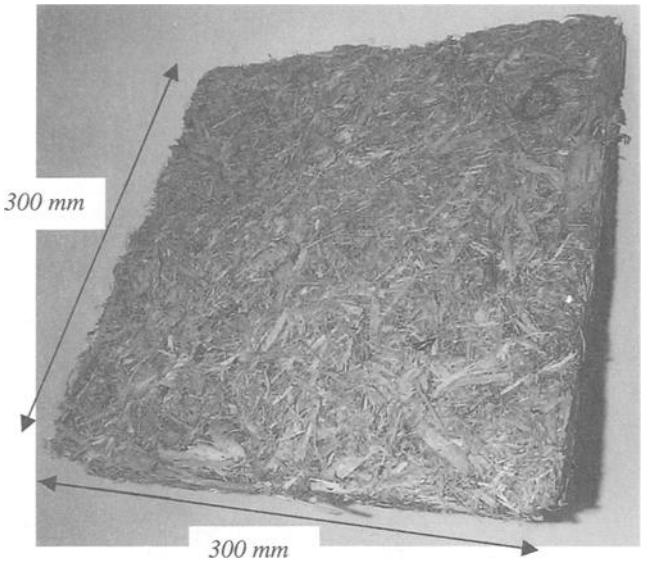

Figure 2 – *Picture of Test Specimen #6*

thermal conductivity values of 0.0467, 0.0318 W/m.K (14°C), 0.0488, 0.0334 W/m.K (24°C) and 0.0508, 0.0350 W/m.K (34°C), respectively. These results show that the thermal conductivity of the fiberboard is comparable with commercially available material and is within the range normally used for building thermal insulation.

Conclusions

Low-cost biodegradable building thermal insulation can be produced using a combination of sugarcane fiber and cornstarch.

A starch/fiber ratio of 1:2 produces the strongest structural tile and is comparable in strength with commercially available ceiling tiles.

At the optimum density of 113 kg/m^3 the thermal insulation property of the sugarcane fiberboard is within the range normally used for building thermal insulation.

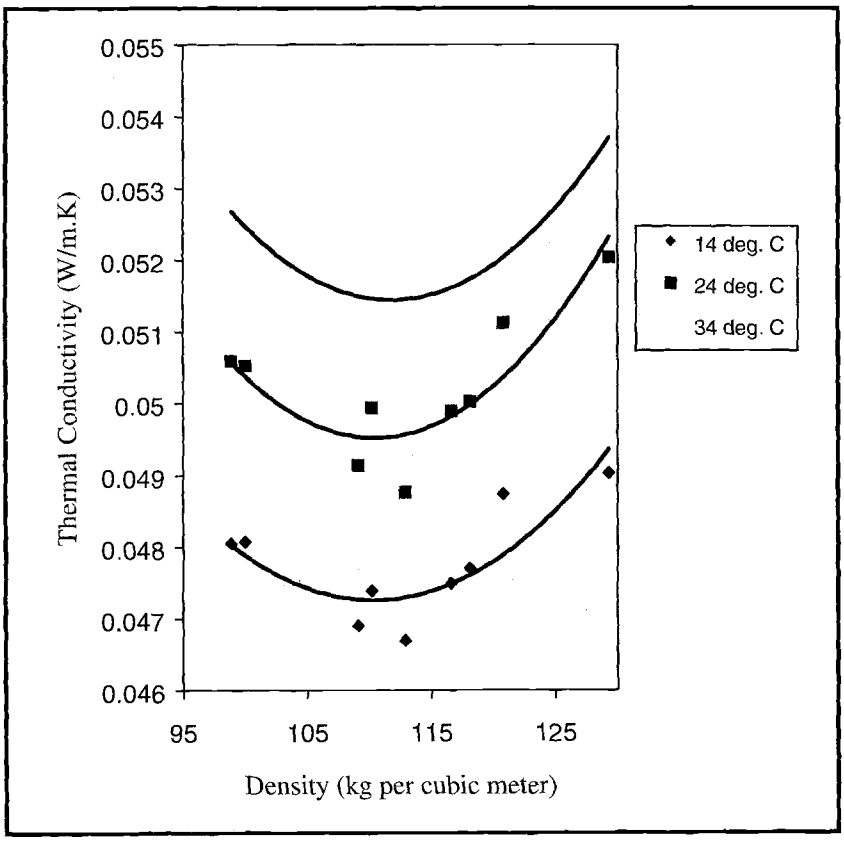

Figure 3 – *Thermal Conductivity Test Results – Sugarcane Fiberboard*

Future Research

The fire resistance property and susceptibility to insect attack is of concern with the use of sugarcane fiber. Research on these properties is currently underway at The University of the West Indies to determine the extent of the problem, if any, and to recommend suitable methods and materials for treating the fiber.

References

[1] Manohar, K., "Heat Transfer Mechanisms in Biological Fibrous Materials," Ph.D. Thesis, Mechanical Engineering Department, The University of the West Indies, Trinidad, West Indies, 1998.

[2] McElroy, D. L., Yarbrough, D. W., and Graves, R. S., "The Thickness and Density of Loose-Fill Insulations After Installation in Residential Attics," *Thermal Insulation: Materials and Systems, ASTM STP 922,* F. J. Powell and S. L. Matthews, Eds., American Society for Testing and Materials, Philadelphia, 1978, pp. 493-505.

[3] Manohar, K., Yarbrough, D. W., and Kochhar, G. S., "Building Thermal Insulation – Biodegradable Sugarcane and Coconut Fiber," *Journal of Thermal Envelope and Building Science,* Vol. 23, No. 3, 2000, pp. 263-276.

[4] Radley, J. A., "Industrial Use of Starch and its Derivatives," Applied Publishers Ltd., London, 1976, pp. 1-30.

[5] Kerr, R. W., "Chemistry and Industry of Starch," Academic Press Inc., New York, N. Y., 1944, pp. 430-440.

[6] Radley, J. A., "Starch and its Derivatives," Chapman and Hall Ltd., London, 1968, p. 177.

Therese K. Stovall[1] and Andrzej Brzezinski[2]

Vacuum Insulation Round Robin to Compare Different Methods of Determining Effective Vacuum Insulation Panel Thermal Resistance

---

REFERENCE: Stovall, T. K. and Brzezinski, A., "**Vacuum Insulation Round Robin to Compare Different Methods of Determining Effective Vacuum Insulation Panel Thermal Resistance**," *Insulation Materials: Testing and Applications, 4th Volume, STP 1426*, A. O. Desjarlais and R. R. Zarr, Eds., ASTM International, West Conshohocken, PA, 2002.

ABSTRACT: A round robin was initiated in February of 2000 to compare different methods of determining the effective thermal resistance of vacuum insulation panels. The outcome of this round robin was designed to provide support for the ASTM material specification and the development of a future ASTM test method. Four issues were identified and addressed: (1) calorimetric vs. center-of-panel/barrier conductivity approaches, (2) comparison of available finite difference/element models, (3) appropriate boundary conditions for all measurements/models, and (4) comparison of center-of-panel measurements to provide a preliminary precision estimate. Six conventional vacuum panels were constructed. All six shared the same dimensional configuration, the same core material, the same getter insert, and the same manufacturing techniques and equipment. Two different barrier materials (three panels from each) were used because barrier thermal conductivity is recognized as a key factor in the determination of effective thermal resistance for vacuum panels, and because the different methods used in this round robin comparison should be sensitive to the barrier thermal properties. The getters were included in these panels to help them remain stable throughout the duration of the round robin.

Each of the nine participating laboratories measured the center-of-panel thermal resistivity of each of the six panels as described in the ASTM standard C1484-00 and reported those results along with pertinent information about their transducer(s) size and location. Several laboratories also calculated the whole-panel effective thermal resistance, using specified sets of boundary conditions.

KEYWORDS: Vacuum insulation, evacuated insulation, insulation panels, thermal resistance, effective thermal resistance, round robin

---

[1]Research Engineer, Oak Ridge National Laboratory, Oak Ridge, TN 37831.
[2]Chief Executive Officer, LaserComp Inc., 20 Spring Street, Saugus, MA 01906.

Introduction

Vacuum insulation systems have long been used for cryogenic applications. These systems have historically consisted of multi-layer evacuated jackets with active vacuum systems. In the early 1990s, sealed evacuated panels became commercially available. These panels were filled with either fiberglass or silica powder and had either metal or plastic barriers. An excellent description of these insulation panels, the importance of each component, and the physics of the aging phenomena are given in [*1*]. An interlaboratory comparison of powder-filled panels in sizes ranging from 0.15 x 0.15 x 0.019 m (6 x 6 x 0.75 in.) to 0.55 x 0.55 x 0.019 m (22 x 22 x 0.75 in.) was initiated in 1991 using heat flow meter apparatuses that were commercially available. That comparison used a precisely defined procedure where the panels were sandwiched between two sheets of silicone sponge rubber and the overall thickness of this sandwich configuration was held constant. The overall thermal conductivity measurements showed a 95% confidence level of ±12.9%[*2*].

The continuing design evolution includes open-celled foam and advanced powder fillers, specialty multi-layer films, and the inclusion of new adsorbent systems. In order to help potential users understand the performance of these panels, a task group was formed in 1995 to create an ASTM material specification, which has now been published as ASTM Standard Specification for Vacuum Insulation Panels (C 1484). Due to the complexity of this non-homogenous insulation form, researchers and panel manufacturers developed several evaluation methods. The task group initiated efforts to systematically compare the results of these differing approaches.

The resulting round robin began in February of 2000, with the goal of comparing different methods of determining the effective thermal resistance of vacuum panels. The outcome of this round robin will provide support for the ASTM material specification and the development of a future ASTM test practice. Four issues were identified: (1) calorimetric vs. center-of-panel/barrier conductivity approaches, (2) comparison of available finite difference/element models, (3) appropriate boundary conditions for all measurements/models, and (4) comparison of center-of-panel measurements to provide a preliminary precision estimate. However, due to laboratory scheduling priorities, the calorimetric measurements were not made.

Round Robin Design

Six conventional vacuum panels were constructed in January 2000. All six shared the same dimensional configuration, the same core material, the same getter inserts, and the same manufacturing techniques and equipment. The open-cell foam core specimens were constructed with dimensions of 298 x 298 x 25.4 mm (11.75 x 11.75 x 1 in.). The six foam cores were divided into two sets, labeled 1a, 1b, 1c, and 2a, 2b, and 2c. The two sets were then encased in two different barriers, or skins. Both barriers have a multi-layer construction, and the materials used for these layers cause one barrier to have a higher thermal conductivity than the other. (The same metallic component that leads to this higher thermal conductivity also provides that barrier with lower gas permeability.) The thermal conductivity of each barrier material was estimated during the round robin by two of the participating laboratories, using methods discussed later in this paper. The thermal conductivity of the barrier used on panels 1a, b, and c is greater than 10 W/m-K, while that

used on panels 2a, b, and c is less than 1 W/m-K. Barrier thermal conductivity is recognized as a key factor in the determination of effective thermal resistance for vacuum panels because of the potential for a "short circuit" heat transfer path around the evacuated region. The different methods used in this round robin comparison should be sensitive to the barrier thermal properties because of the geometry of the specimen, i.e., the small panel size chosen.

Aggressive getters, two five-gram CaO desiccant packs and one SAES Combogetter, were placed within each vacuum panel to help them remain stable throughout the duration of the round robin. The vacuum panels were evacuated to an internal pressure of 0.01 torr, and then heat sealed with nominal 1.2 cm (0.5-in.) wide seals, producing panels with dimensions of 30.5 x 30.5 x 2.54 cm (12 x 12 x 1 in.). Late in the test series, a well-characterized stable expanded polystyrene (EPS) foam board of the same size was added to the rotation to provide a baseline comparison of the test apparatus.

The nine participating laboratories were Advantek, Dow Chemical, DuPont, Holometrix, LaserComp, National Physical Laboratory of Great Britain, National Research Council Canada, Oak Ridge National Laboratory (ORNL), and the Product Design Center (PDC). Over a 19-month period, each laboratory measured the center-of-panel thermal resistivity of each of the six panels as described in C-1484 and reported those results. Six of the laboratories reported the measured panel thickness. Several of the laboratories made multiple measurements at different times and/or using different types of apparatus. Four laboratories measured the thermal conductivity of the EPS foam panel as well, and three of those reported its measured thickness. Pertinent information about the test equipment used in this round robin is shown in Table 1. All of the apparatus meet the requirements of ASTM Test Method for Steady-State Thermal Transmission Properties by Means of the Heat Flow Meter Apparatus (C 518), with the exception of Lab B, because that apparatus does not provide an isothermal plate, and thus can permit edge effects. A few of the laboratories reported the calibration tests completed to determine whether their standard instrument calibrations were adequate for the lower heat fluxes measured with vacuum panel insulation. Several laboratories also calculated the whole-panel effective thermal resistance, with multiple sets of boundary conditions.

Table 1. Heat Flow Meter Parameters

Lab	Plate size [cm (in.)]	Central transducer size [cm (in.)]
D2	61 x 61 (24 x 24)	7.6 x 7.6 (3 x 3)
I	61 x 61 (24 x 24)	10 x 10 (4 x 4)
D1	61 x 61 (24 x 24)	10 x 20 (4 x 8)
E2	61 x 61 (24 x 24)	20 x 20 (10 x 10)
A, C, D3, E1,F, G, H	30 x 30 (12 x 12)	10 x 10 (4 x 4)
B	30 x 30 (12 x 12)	3.2 cm diam with 7.6 cm diam guard(1.25 in.diam with 3. in. diam guard)

An examination of Table 1 shows that some of the test devices were the same size as the vacuum panels, 30.5 x 30.5 cm (12 x 12 in.). Other test devices were twice as wide as the vacuum insulation panels. For tests with the larger devices, a high-density fiberglass blanket was sculpted to fit tightly around the vacuum panels and to match the area of the test apparatus plate size. For all of the smaller plate tests and for some of these large plate tests, the vacuum panel was in direct contact with the constant temperature plate. In these devices, the entire surface of the vacuum panel was in direct contact with the controlled temperature plate. This configuration therefore represents a constant temperature boundary condition, where the temperature gradient from the center of the panel to the edge of the panel is minimized and the lateral heat transfer from the center of the panel to the outer edge through the barrier is reduced. For others, an arrangement where the fiberglass blanket also covers the bottom and top of the vacuum panel, creating a sandwich configuration, was used. When the fiberglass blanket was inserted between the constant temperature plates and the vacuum panel, thermocouples were attached directly to the center of the vacuum panel to record the temperature at that location. This last arrangement was typically used with an array of heat flux transducers and was directed more toward measurement of whole panel performance, because it allows a temperature gradient to develop along the face of the barrier material. Despite this limitation, center-of-panel resistivity measurements were also made using this arrangement.

Several labs performed low heat flow calibrations, using a combination of two approaches. First, multiple calibration specimens were measured individually, and then stacked to measure the sum of their thermal resistances. Second, the temperature difference across a single specimen was reduced. Each approach introduces some element of uncertainty. The stacking approach increases edge losses, especially important for a 0.3 x 0.3 m (12 x 12 in.) apparatus. The reduced temperature difference increases the relative error associated with the individual temperature measurements. However, for all the labs reporting such efforts, the heat flow transducers showed acceptable linearity down to the lower flux values measured here, so that no lab saw the need to use non-standard calibration factors.

Results

Center-of-Panel Thermal Resistivity

The center-of-panel thermal resistivity of a vacuum panel should represent the apparent thermal resistivity of the core evacuated region, reflecting both conductive and radiative heat transfer phenomena. The apparent thermal resistivity of similar core materials had been previously measured using a variable pressure device. The results of those tests, made by ORNL following C 518, showed that the apparent thermal resistivity at an internal pressure of 0.03 torr was about 170 m-K/W (24 h· ft^2· °F/Btu-in.). The manufacturer reports values from 170 to 210 (25 to 30 h· ft^2· °F/Btu-in.) for similar foam products at 0.01 torr[*3*].

Ideally, the center-of-panel value should be unaffected by the thermal conductivity of the barrier. That was so for many of the laboratory measurements in this round robin. The measured center-of-panel thermal resistivity values are summarized in Table 2 and Figure 1.

Table 2. *Center-of-Panel Thermal Resistivity Test Results [m-K/W (h· ft²· °F/Btu· in)]*

Lab	1a	1b	1c	2a	2b	2c	Average 1	Average 2	EPS
A	211(30.5)	193(27.8)	215(31.0)	198(28.5)	196(28.3)	207(29.8)	206(29.8)	200(28.9)	
B·	178(25.6)	178(25.6)	193(27.8)	224(32.3)	231(33.3)	224(32.3)	183(26.4)	226(32.6)	
C	210(30.3)	217(31.3)	225(32.5)	209(30.2)	216(31.1)	210(30.3)	217(31.4)	212(30.5)	
D1	178(25.7)	181(26.1)	198(28.5)	212(30.5)	211(30.5)	200(28.9)	186(26.8)	208(30.0)	
D2	201(29.0)			216(31.2)					
D2	191(27.6)	191(27.6)	220(31.7)	210(30.3)	206(29.8)	199(28.8)	201(29.0)	205(29.6)	
D3	177(25.5)	179(25.8)	194(28.0)	182(26.2)	182(26.2)	178(25.6)	183(26.7)	180(26.0)	
E1	189(27.3)	187(27.0)	204(29.4)	192(27.7)	194(28.0)	194(28.0)	193(27.9)	193(27.9)	
E1	191(27.5)	189(27.2)	202(29.2)	191(27.6)	193(27.8)	194(28.0)	194(28.0)	193(27.8)	
E2							97(14.0)		
F	204(29.5)	187(27.0)	213(30.8)	194(27.9)	192(27.7)	206(29.7)	201(29.1)	197(28.4)	20.4(4.38)
G	184(26.6)	190(27.4)	207(29.8)	190(27.4)	193(27.8)	192(27.6)	194(27.9)	191(27.6)	29.2(4.22)
H	200(28.8)	200(28.8)	217(31.4)	189(27.4)	192(27.8)	196(27.6)	206(29.7)	192(27.7)	30.6(4.41)
I	175(25.3)	27(3.9*)	192(27.7)	164(23.6)	167(24.0)	169(24.4)	184(26.5)	167(24.0)	27.5(3.96)

* Reduced thermal resistance evidence of a failed vacuum condition within the panel, value not used in any reported averages.

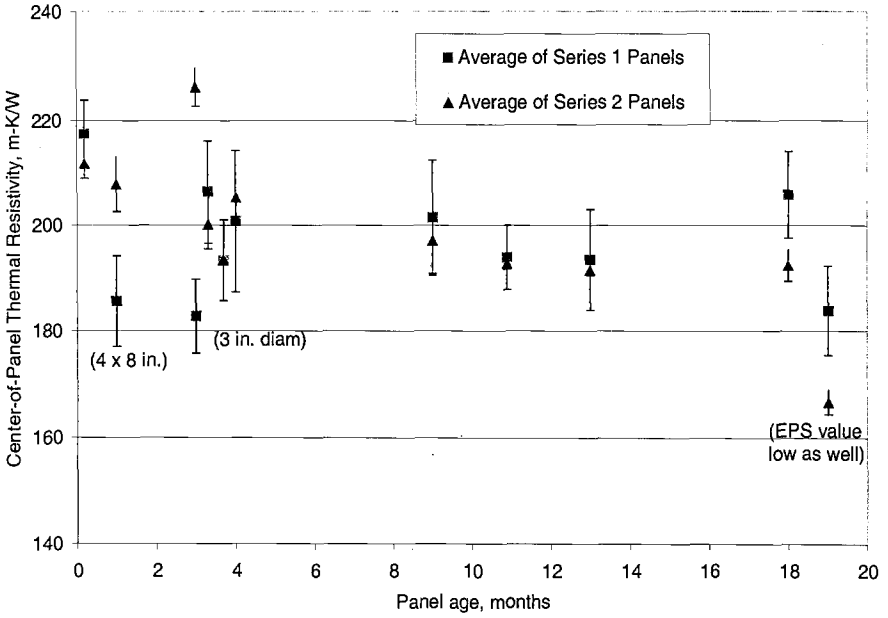

Figure 1 – Measured Values of Center-of-Panel Thermal Resistance

Figure 1 shows the average for each set of three panels for each independent measurement and the standard deviation for that average. For almost every set of measurements, the average center-of-panel thermal resistivities for the two sets of panels are within one standard deviation. The exceptions to this are themselves instructive. Two sets show differences in the early life of the panels. Both of these sets show panels 1a, b, and c to have a significantly lower thermal resistivity, which would be the case if the higher thermal conductivity barrier on these panels were influencing the measurement. Indeed, the first set represents measurements taken on very large transducers, 4 x 8 in. (The influence of transducer size is discussed further below.) The second set is from an older thermal

Table 3. Comparison Of Measured Center-Of-Panel Thermal Resistance To Calculated Effective Whole Panel Resistance For Panel 1

Transducer size [cm (in.)]	Number of measurements	Average [m-K/W (h· ft^2· °F/ Btu· in)]	Standard Deviation (%)
7.6 x 7.6 (3 x 3)	4	201 (29.0)	5.8
10 x 10 (4 x 4)	24	201 (29.0)	6.4
10 x 20 (4 x 8)	3	186 (26.8)	4.6
25 x 25 (10 x 10)	3	97 (14.0)	Not reported
Calculated effective whole panel		76 (11)	

conductivity measurement device. This device uses a 1.25-in. diam transducer set within a 3-in. diam guard. This older device does not have a uniform plate temperature outside that guard area and is therefore more sensitive to lateral heat flow, which becomes more important with the more conductive barrier.

Again looking at Figure 1, after 18 months of age, two sets of measurements show a difference of near or slightly greater than two standard deviations between panels 1 and 2. These differences are measured with the same type of equipment used for the majority of the others, i.e., 10 x 10 cm (4 x 4 in.) transducers, so the difference is not related to the barrier conductivity as it was for those previously discussed. Also, it is now panels from set 2 that show the lower thermal resistivity (although even these lower values are still similar to those measured previously for panels 2a, b, and c), and these are the panels constructed with the less conductive barrier. However, the occurrence of this separation between the two sets of panels after an extended period of time indicates the explanation may lie in the aging phenomena. Over a period of time, atmospheric gas permeates through the barrier and through the barrier seams. (Also, certain materials used for panel components may out-gas as they age.) The getter materials included within the panels will hold the pressure low until those getters are saturated by the permeating gas or vapor. After that point the internal partial pressure for the permeating gas or vapor will increase, which will cause a decrease in the panel's apparent thermal resistivity. Note that it is now panels 2 a, b, and c that have a slightly lower thermal resistivity, consistent with that barrier material's higher gas permeance.

Even considering the possibility of gas permeation, the apparent thermal resistivity reported by Lab I is much lower that reported for any other measurement made using a 10 x 10 cm (4 x 4 in.) transducer. Fortunately, this laboratory participated in the EPS foam measurement as well. As shown in Table 2, their EPS foam apparent thermal resistivity was almost 10% lower than the average for the other three labs, a difference that is consistent with that seen for the vacuum panels. It is possible that the calibration standards used by this laboratory differ from those used by other laboratories. A closer examination of these EPS thermal resistance values shows that the standard deviation doubles, from 2 to 4%when Lab I is included, again indicating the likelihood of some significant difference in the calibration standard used to interpret the results from the heat flow meter apparatus.

Previous modeling work on vacuum panels in the sandwich configuration has shown that the center-of-panel measurement will be more truly representative of the core evacuated region for smaller transducer sizes, as discussed in C 1484. This is most important if the barrier is more conductive, and the results for this round robin show that effect, as seen in Table 3. The effect of lateral heat transfer through the panel barrier becomes more important as the transducer size approaches the panel size. As the center heat flux transducer captures this lateral heat flow, the perceived center-of-panel thermal resistance is reduced. Indeed, the value measured by a 25 x 25 cm (10 x 10 in.) transducer is almost the same as the calculated whole panel effective thermal resistance (as defined in C 1484 and described later in this paper). A summary of the data is shown in Table 4. For the panels with a more conductive barrier (1a,b,c), and excluding the measurement made with the 25 x 25 cm (10 x 10 in.) transducer and the measurement made after panel 1b failed, the standard deviation is 6.8%. For the panels with the less conductive barrier, the standard deviation is 7.4%. Considering the effects of the larger transducers discussed above, and eliminating those measurements made by Lab I because of their significantly lower EPS thermal resistivity, the

Table 4. Measured Center-of-Panel Thermal Resistivity Summary Statistics

	Panels 1a, b, and c		Panels 2a, b, and c	
	Average [m-K/W (h· ft^2· °F/ Btu· in)]	Standard deviation (%)	Average [m-K/W (h· ft^2· °F/ Btu· in)]	Standard deviation (%)
All measurements except 10x10 transducer size and failed panel	198 (28.5)	6.8	199 (28.7)	7.4
Only measurements made using 4x4 and 3x3 transducers, exclude lab I	202 (29.1)	5.9	199 (28.7)	4.2

standard deviations are improved somewhat, to 5.9% and 4.2%, respectively for sets 1 and 2. However, even these values reflect 95% confidence bounds of ±12 and ±8%, respectively.

The center-of-panel thermal resistivity measurements are also highly dependent on the measured thickness of the panel. When the vacuum panel is in direct contact with the heat flow meter's plate, the test apparatus automatically measures the thickness. For other test configurations, especially those that employ a fiberglass blanket above and below the panel, independent measurements are required. Lab D used such an arrangement, and reported panel thickness based on the average panel thickness measured at eight locations over the surface of each panel. A summary of the measured panel thicknesses is given in Table 5 and shows a variation from -7 to +12% relative to the nominal value of 2.54 cm (1 in.). The average of the 42 reported measurements is 2.51 cm (0.99 in)., with a standard deviation of

Table 5. Panel Thickness Measurements (cm)

	1a	1b	1c	2a	2b	2c
Lab C	2.65	2.4	2.49	2.5	2.43	2.64
Lab D, average of 8 locations on panel	2.8	2.48	2.55	2.55	2.54	2.82
Lab D, plate to plate	2.69	2.40	2.51	2.50	2.44	2.72
Lab E	2.62	2.39	2.49	2.5	2.43	2.63
Lab G	2.68	2.39	2.48	2.5	2.42	2.67
Lab H	2.58	2.33	2.44	2.43	2.35	2.55
Lab I	2.54	2.41	2.42	2.44	2.36	2.56
Average	2.65	2.40	2.48	2.49	2.42	2.66
Standard Deviation	0.078	0.041	0.041	0.039	0.058	0.086
Average without Lab D, average 8 locations	2.63	2.39	2.47	2.48	2.40	2.63
Standard Deviation without Lab D	0.053	0.026	0.032	0.031	0.035	0.058

0.12 cm (0.05 in). Considering the direct relationship between measured thermal resistance and measured thickness, this variation (two standard deviations represents 9.4 % of the average thickness) explains much of the variation in the thermal resistivity data discussed above, and therefore provides useful guidance for future efforts to improve the procedures. The variation is likely due to two causes. First, the measurements taken by Lab D that represent an average of eight locations over the surface of the panel are higher than any other measurement for all six panels. If those values are removed from the summary, the standard deviation for each panel is significantly reduced, as shown in Table 5. Second, these panels have a small amount of wrinkles on the surface and are slightly bowed. Depending on the sensitivity of the plate movement drive on each heat flow apparatus, some machines may press on past these imperfections while others may stop on contact.

Whole-Panel Effective Thermal Resistance

Because vacuum insulation panels are non-homogenous, various approaches have been developed to determine their overall thermal effectiveness. One method employs a hotbox technique where mathematical models are used to correct for the effects of materials used to surround the test panel [*4*]. That method has not yet been tested with the round robin specimens.

The other method, used by three of the participating laboratories, employs a finite difference model of the panel. Such models typically require knowledge of the barrier's thermal conductivity, the apparent thermal conductivity of the evacuated region within the panel, and a definition of the thermal boundary conditions for the analysis. These parameters are summarized in Table 6 for the two laboratories that reported this information. Early results from the center-of-panel thermal resistivity tests were used to define the apparent thermal conductivity of the core region. Both laboratories used a combination of measurements and models to determine the barrier conductivity values. One laboratory used a single transducer to measure the heat flow through a barrier-wrapped piece of previously characterized foam insulation (all at atmospheric pressure). This data was then used with a finite element model to calculate the effective thermal conductivity and thickness of the barrier. Another laboratory used an array of transducers to produce a heat flow "map" for a vacuum panel surrounded by previously characterized fibrous glass insulation. A finite difference model (which used the HEATING code) of the heat flow meter apparatus was then created [*5*]. An error function was defined as the sum of the squares of the differences between the predicted heat flow through each transducer on the array and the heat flow actually measured. The thermal conductivity of the barrier was allowed to vary until the minimum value of this error function was achieved. This method had been previously benchmarked using foils and foams of known conductivity and was found to give reasonable results. This laboratory used a micrometer to measure the thickness of each barrier. Although the values shown in Table 6 appear significantly different, the product of the barrier's thickness and conductivity (which represents the ability of the barrier to conduct heat in a lateral direction) differ by only about 30% between the two laboratories. The other materials with their much lower thermal conductivity tend to control the heat flow, so that even this difference has very little effect.

Table 6. Vacuum Panel Parameters Used in Finite Element Analysis

		Lab B	Lab D
Core, Panel 1	Apparent Thermal Conductivity (W/m-K)	0.00447	0.00467
	Thickness (m)	0.0254	0.025
Core, Panel 2	Apparent Thermal Conductivity (W/m-K)	0.00447	0.00467
	Thickness (m)	0.0254	0.025
Barrier, Panel 1	Thermal Conductivity (W/m-K)	189.	16.44
	Thickness (m)	0.000006	0.0000889
Barrier, Panel 2	Thermal Conductivity (W/m-K)	0.202	0.5192
	Thickness (m)	0.000006	0.0000635

Four sets of boundary conditions were considered. The first represents the typical wall or door of a refrigerator. For this configuration, one side of the panel would face a thin sheet of steel (0.0006 m thick, 69. W/m-K) which is in turn exposed to indoor convective transfer to an environment at 21 °C. The other side of the panel would be surrounded by 0.025 m of foam (0.024 W/m-K) and a thin sheet of acrylonitrile-butadiene-styrene (ABS) plastic (0.003 m thick, 0.26 W/m-K) exposed to an air temperature of 4 °C. The second set of boundary conditions represents a wall section of a building. In that wall, one side of the panel would face 0.013 m gypsum board (0.16 W/m-K) exposed to indoor convective conditions (21 °C). The other side would face 1.3 cm of foam (0.03 W/m-K)), followed by a thin cladding (wood, 0.025 m thick, 0.19 W/m-K) exposed to external convection at –7 °C. The third set of boundary conditions represents a heat flow meter apparatus with standard high-density fiberglass surrounding the panel, which is in turn encased within two constant temperature plates. The fourth set of boundary conditions was not reported by that laboratory.

Considering the different mathematical models and the different values used for the element conductivities, there is a surprising degree of agreement in the results shown in Table 7. Even across disparate boundary conditions, the standard deviation for the effective whole panel thermal resistance for the more conductive barrier was 11%, giving a 95% confidence that the effective thermal resistance is between 1.5 and 2.4 m^2-K/W (8.7 and 13.7 h· ft^2· °F/Btu). Again lumping the different boundary conditions together, the standard

Table 7. Finite Difference /Element Model Results for Whole Panel

Lab	Boundary conditions	Whole panel thermal resistance [m^2-K/W (h· ft2· °F /Btu)]	
		Barrier: more conductive	Barrier: less conductive
B	Refrigerator door	1.8(10)	4.6(26)
D	Refrigerator door	1.8(10)	4.1(23)
B	Wall	2.1(12)	5.6(32)
D	Wall	1.8(10)	4.8(27)
D	Test apparatus	1.9(11)	4.8(27)
C	Not available	2.3(13)	4.8(27)

deviation for the whole panel thermal resistance for the less conductive barrier was 12%, giving a 95% confidence that the effective thermal resistance is between 3.5 and 5.8 m^2-K/W (20 and 33 h· ft^2· °F/Btu). (*Note that the small panel size was chosen for its ability to reflect the differences associated with different barrier materials. Normally, panels constructed from the more conductive barrier would be much larger, and the effects of heat flow through the barrier would be much less.*)

Conclusions

This round robin began during the development of a vacuum panel insulation material standard, since published as C 1484. There was at that time only limited formal test practice guidance for vacuum insulation panels, and that situation is unchanged today. This round-robin was therefore exploratory in nature, aimed at better defining the procedures in use, and at determining which of these procedures offer more accurate and consistent results. Examining the results presented here leads to several recommendations.

First, the panel thickness measurement must be improved. Despite the slightly wrinkled surface and/or the slight bow of many vacuum panels, the method of placing the panel directly between the heat flow meter apparatus plates, and allowing that apparatus to measure the whole panel thickness, would appear to be the best choice. That arrangement also appears to give center-of-panel resistivity values that are equal to, or better than, those made between a sandwich of fibrous glass insulation. This recommendation also offers the benefit of favoring the simpler of two approaches used in this round robin. However, there is still a need to address the question of the varying sensitivities of the drive mechanisms of the heat flow apparatus. The previous round robin addressed this issue by circulating thin sheets of silicone rubber to place on each surface, and by prescribing the plate separation distance [2]. However, this approach introduces the need to secure thermocouples to the surface of the vacuum panel, or to otherwise correct for the silicone layer. Whichever approach is selected, it must be uniformly applied and reported in the next round robin.

Second, transducers larger than 0.1 x 0.1 m (4 x 4 in.) should not be used to measure the center-of-panel thermal resistivity for panels 30.5 x 30.5 x 2.54 cm (12 x 12 x 1 in.) or smaller in size. The evaluation of transducer size vs. panel size included in the current version of C 1484 is based on the sandwich configuration, and should be revisited to provide appropriate information for the configuration where the vacuum panel is in direct contact with the apparatus plates.

Third, a standardized finite element model would be useful. Such a model would not replace the special purpose codes necessary for detailed product design. But a standard model could serve a purpose similar to other standard rating conditions and devices. Given the rough agreement for the two models and the various boundary conditions reported here, it is suggested that simple boundary conditions representative of the heat flow meter apparatus be adopted for the standardized model – again choosing the simpler path when the results are similar to those achieved using more complex models. Further development of methods used to define the thermal properties of the barrier materials would also appear to be warranted based on the different values used here. However, it should be noted that these differences appear to have had limited effect on the calculated whole-panel thermal resistance. Indeed, a parametric study of the effect of each variable would give guidance on the accuracy needed for each variable.

Fourth, the methods used in this round robin should be written in the form of a draft test practice, and subjected to a rigorously structured round robin. Certainly, a comparative standard EPS foam board should be included for the duration of that round robin and the low heat flow calibration technique should be addressed as well. The specimens prepared for the next round robin may also be used to further explore other test practices. One such test practice not included here uses a one-sided transient thermal diffusivity measurement apparatus. And one of the most important future efforts will be the addition of calorimetric measurements at a facility dedicated to such work. This will provide a valuable benchmark for the finite element modeling efforts.

Acknowledgments

The authors would like to thank Dow Chemical Company for providing the vacuum panels for this round robin, and LaserComp, Inc. for providing the comparative specimen of EPS foam. This round robin wouldn't have been possible without the active participation of the members of the ASTM task group dedicated to the development of appropriate standards for vacuum panel construction and use. Building Systems and Materials Division, Office of Buildings Energy Research, U.S. Department of Energy sponsored a portion of this research.

References

[1] Yarbrough, D. W. and Wilkes, K. E., "Development of Evacuated Superinsulations," Superinsulations and the Building Envelope Symposium Proceedings, National Institute of Building Sciences, Washington, DC, November 14, 1995.

[2] Graves, R. S. and Kollie, T. G., "Interlaboratory Comparison Measurements of the Thermal Conductivity of Powder-Filled Evacuated Panel Superinsulation," *Thermal Conductivity 22*, Editor Timothy W. Tong, Technomic Publishing Co., Lancaster, PA 1994, pp. 435-446

[3] Dow Chemical Company, Instill™ Foam Product Literature, Form No. 174-01000-698X SMG, Dow Chemical Company, Midland, Michigan.

[4] Ellis, M. W., Fanney, A. H., and Davis, M.W., "Calibration of a Calorimeter for Thermal Resistance Measurements of Advanced Insulation Panels," *HVAC&R Research*, Vol. 6, No. 3, 2000, pp. 273-284

[5] Childs, K. W., *Heating 7.2 User's Manual, ORNL/TM-12262*, Oak Ridge National Laboratory, Oak Ridge, Tennessee, February 1993.

™ Trademark of the Dow Chemical Company

G. Christopher P. Crall[1]

The Use of Wicking Technology to Manage Moisture in Below-Ambient Insulation Systems

Reference: Crall, G. C. P., **"The Use of Wicking Technology to Manage Moisture in Below-Ambient Insulation Systems,"** *Insulation Materials: Testing and Applications: 4th Volume, ASTM STP 1426*, A. O. Desjarlais and R. R. Zarr, Eds., ASTM International, West Conshohocken, PA, 2002.

Abstract: Insulating below-ambient systems presents special challenges due to the possibility of water vapor flow to the cold surface. The traditional approach has been to specify a continuous vapor retarder on the warm side of the insulation to minimize vapor flow. An alternative approach utilizing wicking material to remove condensed water from the system has been in use since 1993. This paper reviews the technical basis for the wicking technology and presents results from laboratory testing and commercial installations of pipe insulation systems.

Keywords: pipe insulation, vapor retarders, wicking

Introduction

Insulation systems for piping and equipment that operate at below-ambient temperatures present special design challenges due the possibility of water vapor movement to the cold surface. If the operating temperature of the system is below the dew point of the ambient air, condensation will occur on the cold surface, creating a vapor pressure gradient through the system. This vapor pressure gradient serves as the driving force for water migration toward the cold surface. If these conditions remain for extended periods of time, a significant amount of liquid water can accumulate in the system. Below-ambient systems therefore require special attention to the design to maintain thermal performance.

The traditional approach has been to specify either a vapor resistant insulation material and/or a continuous vapor retarder on the warm side of the insulation to minimize vapor flow. A variety of facings and jacketing materials are available for use as vapor retarders. These products are designed for low water vapor permeance, with values as low as 0.02 perm achievable under laboratory conditions. In practice, however, this approach requires that the vapor retarder system be continuous at all the joints, elbows, valves and fittings present in real installations. The degree of success therefore depends heavily on the workmanship of the installers. Even with careful installation of

[1] Technical Manager, Industrial and Metal Building Products, Owens Corning, 2790 Columbus Road, Granville, OH 43023.

vapor retarders in conjunction with closed-cell insulation materials, a finite amount of water vapor enters the system and condenses to liquid water on the cold surface [*1*].

The condensed water is undesirable, as it will contribute to increased corrosion rates of metallic pipes. If condensed water is allowed to accumulate, there is a resulting increase in effective thermal conductivity of the insulation system. Depending on the ambient conditions, the resulting decrease in surface temperature can lead to condensation on the exterior surface of the insulation and eventual dripping. The traditional approach is therefore temporary in nature. The system will eventually fail and periodic insulation replacement is required [*2*].

An alternative approach utilizing wicking material to remove condensed water from the system has been in use since 1993 [*3-6*]. The approach accepts the fact that water vapor will enter the system and condense on the cold surface and provides a means to remove it from the system while keeping the insulation material substantially dry.

Theory of Operation

A typical application of wicking technology on a below-ambient pipe is shown in cross section in Figure 1. A thin layer of hydrophilic wicking material is placed around the pipe. A layer of low conductivity insulation material is located around the wick to limit conduction heat transfer to the pipe. A vapor retarder is typically placed on the exterior surface of the insulation to limit the rate of water vapor diffusion into the system. The wicking material is extended downward through a slot in the insulation layer, and the tail of the wick is left exposed to the ambient air to serve as an evaporator section.

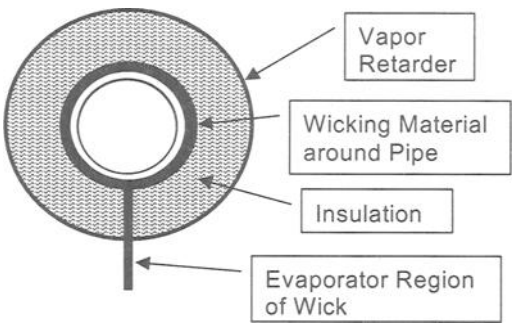

Figure 1 – Schematic of System

Note that the evaporator section of the wick is shown hanging straight down in a vertical position. In practice, this tail portion of the wick may be turned and adhered to the exterior of the vapor retarder. This is done for aesthetics and does not materially effect the operation of the system as long as the exposed area is sufficient to allow adequate evaporation.

In operation, any liquid water that condenses on the pipe surface is absorbed by the wicking material and transported via the combination of capillary forces and gravity through the slot and onto the exposed tail area where it can evaporate to the ambient air.

To help understand the operation of the wicking system, assume that the wick and insulation are initially placed on dry pipe surface when the pipe temperature is in equilibrium with the ambient air. This situation normally exists prior to system start-up. There is no condensation within the system and the partial pressure of water vapor near the pipe surface is equal to the vapor pressure in the ambient air. For this equilibrium condition, there is no driving force and no water vapor flow in the system.

During system startup, the temperature of the fluid in the pipe is reduced, and a temperature gradient is established across the insulation layer. This results in heat flow via conduction through the insulation towards the pipe surface. As long as the pipe surface temperature remains above the dew point of the layer of air nearest the pipe surface, however, no condensation will occur. The water vapor pressure near the pipe remains equal to the vapor pressure in the ambient air, and no water vapor flow occurs.

As the temperature of the fluid in the pipe is further lowered below the dew point of the air near the pipe surface, liquid water will begin to condense on the pipe surface. This reduces the vapor pressure of the layer of air immediately adjacent to the pipe to the saturation pressure, and a vapor pressure gradient is established. This vapor pressure gradient causes water vapor diffusion towards the pipe surface. In this case, there will be energy transport due to the latent heat of condensation as the water vapor condenses on the pipe surface in addition to conduction heat transfer through the insulation layer.

Initially, the condensed water will be absorbed into the wicking material. As the amount of absorbed water increases, the pores in the wick will fill and capillary forces will induce movement of the liquid water towards dry areas of the wick. This capillary force, aided by gravity, will move liquid water through the slot to the evaporator region where it can evaporate to the ambient air.

The advantage of this approach is that the wick material transports condensed water to the outside of the system. The wick keeps the insulation dry, allowing it to maintain its thermal performance over the life of the project.

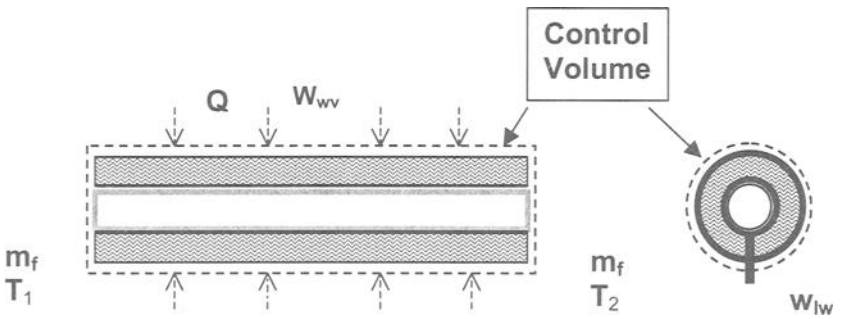

Figure 2 – *Physical Situation*

Steady State Energy Balance

It is recognized that an insulation system for below-ambient conditions must limit the latent loads as well as the sensible loads on the system. An energy balance is helpful in understanding these energy flows. Figure 2 shows the physical situation. A cold fluid flows from left to right within the pipe at a mass flow rate denoted as m_f. Fluid enters the system at location 1 with a temperature denoted as T_1 and enthalpy h_1. Fluid exits at location 2 with temperature T_2 and enthalpy h_2. The dashed line indicates the boundaries of a control volume around the system. For convenience, this boundary is drawn through the tail of the wick as it exits the slot. Hence, the evaporator section is not included in this analysis. Sensible heat transfer across the non-flow boundaries of the control volume is denoted as Q. The rate of water vapor diffusion into the system is denoted as w_{wv}, while the rate of liquid water leaving the control volume at the wick exit is denoted w_{lw}. At steady state, an energy balance yields the following equation:

$$m_f(h_2 - h_1) = Q + w_{wv} \bullet h_{wv} - w_{lw} \bullet h_{lw} \qquad (1)$$

where

m_f = mass flow rate of cold fluid within the pipe
h_1 = enthalpy of the fluid stream entering the system
h_2 = enthalpy of the fluid stream exiting the system
Q = rate of sensible heat transfer across the system boundary
w_{wv} = mass flow rate of water vapor entering the system
w_{lw} = mass flow rate of liquid water leaving the system
w_v = enthalpy of the water vapor entering the system
hl_w = enthalpy of the liquid water leaving the system

At steady state, the flow rate of water vapor into the system (w_{wv}) will equal the flow rate of liquid water leaving the system (w_{lw}), so the energy equation reduces to:

$$m_f(h_2 - h_1) = Q + w(h_{wv} - h_{lw}) \qquad (2)$$

where

w = $w_{wv} = w_{lw}$ = mass flow rate of water at steady state

The quantity of interest is the energy gain to the cold fluid, which is given by the term on the left side of equation (2). The terms on the right indicate that this energy gain comes from two components 1) the sensible heat transfer across the non-flow boundaries and 2) a contribution due to the latent heat of condensation of the water vapor. With some simplifying assumptions, the energy equation can be solved to determine the total load on the fluid stream.

Calculations

The enthalpy of the water vapor entering the system may be determined with knowledge of the ambient conditions. The sensible heat gain (Q), the water flow rate (w) and the enthalpy of the liquid water leaving the system (h_{lw}) are all unknowns that must be determined in order to estimate the total heat gain to the fluid.

As a first approximation, we can neglect any lateral heat transfer from the insulation layer to the liquid stream in the slot area. This "adiabatic slot" assumption is appealing since it simplifies the calculations in several ways. First, it provides us with an estimate of the enthalpy of the liquid water leaving the system since the temperature at this flow boundary (T4) will be nearly equal to the condensation temperature. Second, it allows us to calculate the sensible heat gain (Q) using a simple one-dimensional heat transfer model. Finally, it allows us to neglect any re-evaporation of water in the slot area. We will examine the impact of this assumption later in the paper.

The vapor flow rate can be estimated based on knowledge of the permeance of the vapor retarder. For this calculation, we assume that the driving force is equal to the vapor pressure difference between the ambient air and the saturation vapor pressure at the temperature of the cold pipe. In equation form:

$$w_{wv} = M\, A\, \Delta p_v \qquad (3)$$

where

w_{wv} = water vapor flow rate
M = permeance of vapor retarder
A = area of vapor retarder
Δp_v = vapor pressure difference across the vapor retarder

This approach assumes 1) that the vapor retarder is continuous around the "non-flow" boundary of the control volume and 2) that no water vapor enters the system through the flow boundary where the condensed water exits the control volume.

Using these assumptions, we can calculate the water vapor flow rate for a variety of pipe sizes and insulation thicknesses. The results indicate that the latent component is a small compared to the sensible heat gain. As an example, consider the following severe design conditions:

Cold fluid entering temperature (T_1)	= 35° F (2° C)
Ambient temperature	= 90° F (32° C)
Ambient relative humidity	= 80%
Insulation thermal conductivity	= 0.23 Btu-in/(hr•ft^{2}•°F) (0.033 W/m°C)
Insulation thickness	= 1.0 in. (25mm)
Vapor retarder permeance	= 0.15 perm

Table 1 – *Calculated Energy Gains*

Pipe Size	Pipe OD	Insul OD	Sensible Gain	Latent Gain	Total Heat Gain	Percentage
NPS	in.	in.	Btu/hr/ft	Btu/hr/ft	Btu/hr/ft	(Latent/Sens.)
0.75	1.05	2.88	5.89	0.017	5.91	0.28%
1	1.32	3.50	6.11	0.020	6.13	0.33%
2	2.38	4.50	9.30	0.026	9.33	0.28%
4	4.50	6.62	15.08	0.038	15.12	0.25%
12	12.75	15.00	37.16	0.086	37.25	0.23%

The results of this example calculation indicate that the latent component of the heat gain is very small, less than 0.4% of the sensible component. Calculated water vapor flow rates for this example ranged from 0.0002 to .003 lbs/day per linear foot of pipe (0.5 – 3 g /m/day). These extremely low calculated vapor flow rates represent the idealized situation, and establish a lower limit on the latent contribution.

We know that the simplifying assumptions utilized for these calculations will not be entirely accurate. In real life, any lateral heat transfer in the slot area will tend to increase the temperature of the liquid water leaving the system while simultaneously distorting the temperature field within the insulation layer. Complete understanding of these effects requires numerical modeling of the combined heat and mass transfer problem. More importantly, any gaps or flaws in the vapor retarder or will contribute to increased water vapor ingress, thereby increasing the latent contribution. We will rely on laboratory tests to quantify this effect and establish an upper limit on the latent component.

Laboratory Testing

Samples of pipe insulation were installed on 35 F chilled water lines located within an environmental chamber. Temperature and humidity conditions in the chamber were controlled to a constant 90°F and 80% RH. The test specimens were configured to allow periodic removal and weighing to determine weight gain due to water vapor ingress.

Results of one series of experiments are given in Figure 3, which shows the cumulative weight gain for 3 specimens of ¾" NPS x 1" thick fiberglass insulation sections fitted with wicking material. Note that each section is three feet long. As shown in the figure, there is a rapid weight gain within the first day of testing. Afterwards, the weight of the specimens remains relatively constant. This is consistent with expectations in that an initial period of water accumulation must occur prior to saturation of the wick. During this initial transient period, there is no liquid water at the slot exit, leaving a relatively open path for water vapor to diffuse into the system. This "flaw" in the vapor retarder is narrow (generally less than 0.1" (2 mm) but runs the length of the pipe run.

When the wick becomes saturated, it begins to remove condensed water through the slot to the evaporator area. After this point, the flow rate of water vapor into the system equals the flow rate of liquid water out of the system, and a state of dynamic equilibrium is reached. This particular series of tests were continued for a period of two months without a further increase in weight. Subsequent disassembly and examination of the specimens reveals that liquid moisture is confined to the wick material; the insulation material stays dry.

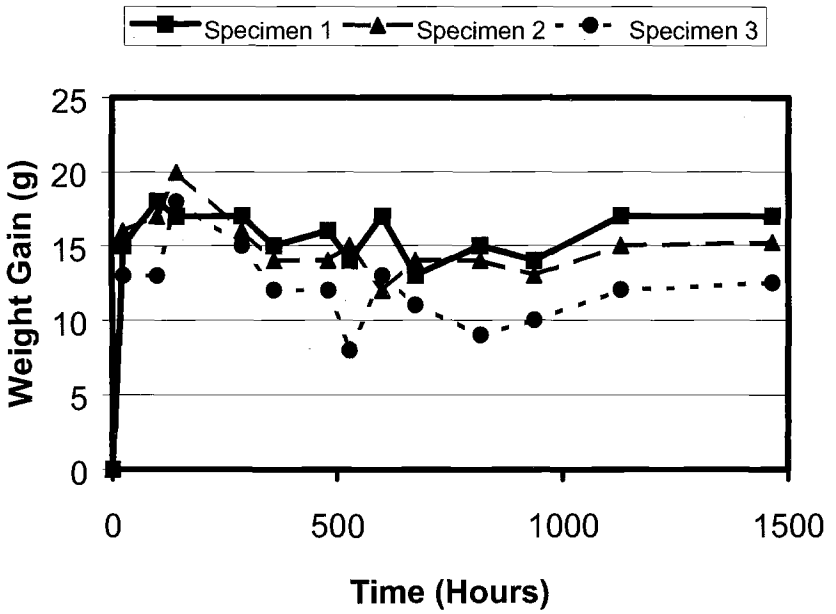

Figure 3 – *Measured Weight Gains versus Time for Specimens of Pipe Insulation Installed on a 35 F Pipe Loop and Exposed to Ambient Conditions of 90 F and 80% RH*

These data indicate that the steady state weight gain during the initial transient period is roughly 15 grams per section of pipe. Experiments have shown that, if fully saturated with water, the wick material has the capability to hold about 36 grams of water per section of pipe. From this we conclude that 1) the weight gain measured is confined to the wick material and 2) the wick material, under continuous severe conditions, is less than 50% saturated.

The measured rate of weight gain during the initial transient period can be used to determine an upper limit on the latent contribution. Since the slot is dry during this period, it is reasonable to assume that any water vapor ingress through the slot area will be maximized during this period.

Repeating the earlier calculations using the value of 15 gram per day per section of pipe to approximate the water vapor flow rate yields the following:

Table 2 – *Energy Gains based on Laboratory Measurements*

Pipe Size NPS	Pipe OD in.	Insul OD in.	Sensible Gain Btu/hr/ft	Latent Gain Btu/hr/ft	Total Heat Gain Btu/hr/ft	Percentage (Latent/Sens.)
0.75	1.05	2.88	5.89	0.471	6.36	8.00%
1	1.32	3.50	6.11	0.475	6.58	7.77%
2	2.38	4.50	9.30	0.481	9.78	5.17%
4	4.50	6.62	15.08	0.493	15.57	3.27%
12	12.75	15.00	37.16	0.541	37.70	1.46%

Based on the laboratory testing, it appears that the latent component during the initial transient period ranges from 1 to 8 % of the sensible heat flow. Since this testing represents a worst case condition (initial start-up with a hot/humid environment), we conclude that the latent contribution will be less than 10% of the sensible heat gain.

Commercial Installations

Field experience with wicking technology has identified a number of points worth highlighting.

Elbows, valves, and fittings have been successfully insulated by wrapping with wicking material prior to installing insulation. Various installation details have been developed to accomplish this but the key for installers is to utilize the wicking materials to transport condensed water to the lowest point in the system where it can be removed to the outside and evaporated.

Vertical runs are treated similarly, with the wicking material serving as the conduit to transport condensed water to a location where it can be removed from the system and evaporated.

The ability to install insulation on operating systems has proven to be a significant benefit. In some facilities, cooling systems are critical to operations and shutting down to install insulation is not feasible. Since the wicking products are designed to remove water from the cold surface to the environment, surfaces do not need to be dry during installation. A number of hospitals and data processing centers have chosen to use wicking products to reinsulate existing cold lines while maintaining operations.

Conclusions

Wicking technology has been successfully used to manage moisture in below-ambient insulation systems. Hydrophilic wicking material serves to absorb condensed water and transport it via capillary forces and gravity to the evaporator section where it can be evaporated to the ambient air. The insulation remains dry, allowing it to maintain it's initial thermal conductivity. Attention must be paid to limiting the latent component of heat flow. Calculations based on laboratory experiments indicate that the latent

component can be limited to 1 to 8% of the sensible load using a conventional vapor retarder.

References

[1] Mumaw, John., "Below-Ambient Piping Insulation Systems", *Insulation Outlook*, September 2001.

[2] 2001 ASHRAE Handbook of Fundamentals, American Society of Heating, Refrigerating, and Air Conditioning Engineers, Inc., Chapter 23, 2001

[3] Korsgaard, V., "Innovative Concept to Prevent Moisture Accumulation and Icing of Cold Pipe Insulation." *ASHRAE Transactions*, Volume 99, Part 1, 1993.

[4] Korsgaard, V., "Innovative Self-Drying Concept for Thermal Insulation of Cold Piping", *Insulation Materials: Testing and Applications: Third Volume*, STP 1320, R.S. Graves and R.R. Zarr, Eds., American Society for Testing and Materials, 1997.

[5] Korsgaard, V., U.S. Patent no. 5,441,083, Aug. 15, 1995.

[6] Brower, Glenn, "A New Solution for Controlling Water Vapor Problems in Low Temperature Insulation Systems." *Insulation Outlook*, September, 2000.

Andreas H. Holm[1] and Hartwig M. Künzel[1]

The Influence of Measurement Uncertainties on the Calculated Hygrothermal Performance

Reference: Holm, A. H. and Künzel, H. M., **"The Influence of Measurement Uncertainties on the Calculated Hygrothermal Performance,"** *Insulation Materials: Testing and Applications: 4th Volume, ASTM STP 1426*, A. O. Desjarlais and R. R. Zarr, Eds., ASTM International, West Conshohocken, PA, 2002.

Abstract

Ecological Insulation materials are getting more and more popular, but until now their share of the insulation market is e.g. in Europe below 10 %. One of the reasons is, that architects, engineers or designers are not well informed about the advantages of their use. With the use of advanced hygrothermal building simulation tools, like WUFI-ORNL/IBP the realistic heat and moisture performance of a wall or roof assembly can be predicted easily. Unfortunately the needed material properties for the ecological insulation materials are not completed or even unknown. This work is focused on the measurement of the hygrothermal material properties. Afterwards the results are used in order to calculated the hygrothermal performance for a roof construction under real climatic conditions. With the information about the stochastical deviation of the measured data and the help of the computational sensitivity analysis, one can study how sensitive the solution of a problem based on the data confidence input and its reaction to a single parameter of uncertainty. It may also provide us the basis for simplifying some of the hygrothermal analyses by allowing us to use material properties that are representative to materials with similar but not exactly the same properties.

Keywords

Monte Carlo Simulation; sensitivity approach, thermal conductivity, hygrothermal material properties, WUFI, uncertainty, pitched roof

[1]Doctor, Hygrothermical Department, Fraunhofer-Institute for Building Physics, Fraunhoferstr. 10, 83626 Valley, Germany

Nomenclature

a_k [-]	Short wave absorption coefficient
a_L [-]	Long wave emission coefficient
a_R [-]	Rain water absorption coefficient
A [kg/m$^2\sqrt{s}$]	A-Value
c [kJ/kgK]	Heat capacity
u_{80} [kg/m^3]	Water content at 80 % RH
u_{95} [kg/m^3]	Water content at 95 % RH
u_f [kg/m^3]	Capillary saturation
α [W/m^{2}K]	Heat transfer coefficient
λ [W/mK]	Heat conductivity
μ [-]	Wasserdampfdiffusionswiderstandszahl
ρ_w [kg/m^3]	Density

Introduction

Ecological insulation materials are getting more and more popular, but until now their share of the insulation market in Europe is below 10%. One of the reasons is that architects, engineers or builders have too little information about the advantages and the correct application of these materials. Because there is a lack of long-term experience with most of the ecological insulation materials, consumers can only be convinced to use them if scientific evidence can prove their suitability. However, most companies producing ecological building materials cannot afford extensive field testing; therefore alternative methods to assess the applicability of these products are required. Concerning the hygrothermal behavior of these materials, advanced hygrothermal building simulation tools, such as WUFI-ORNL/IBP, may be employed. Thus the realistic heat and moisture performance of a wall or roof assembly can be predicted in a cost-effective way. Unfortunately, the material parameters required for such simulations are for most ecological insulation materials incomplete or rough estimations.

This work is focused on the measurement of the hygrothermal material properties of ecological insulation materials, such as cellulose fiber, cork or sheep wool. The test results are used to calculate the hygrothermal performance of a roof and wall assembly under real climatic conditions. Because the production process of these materials is to a certain extent controlled by nature, the material data may be subject to considerable variations. Therefore, a sensitivity analysis will be carried out in order to assess the data confidence and reactions to a single parameter of uncertainty [1]. The technique applied in this case is the Differential Sensitive Analysis (DSA) and the Monte Carlo Analysis (MCA).

Material Property Tests

Compared to common insulation materials (mineral wool or polystyrene foam), the hygrothermal material properties of ecological insulation materials have been much less investigated. Furthermore, their parameters required for hygrothermal simulations cannot be found in any major database. Therefore, a complete set of these parameters had to be determined. This paper deals mainly with cellulose fiber, which is the most popular ecological insulation material in Europe. For hygrothermal calculations under transient conditions, the moisture storage function (in this case the sorption isotherm is sufficient), the liquid transport coefficients and the heat conductivity as a function of the water content should be known in addition to standard properties like bulk density, vapor permeability, etc.

Table 1 - *Water content of cellulose fiber at 23°C and different RH. For the reference water content at 80 % RH the temperature dependence is also given.*

Cellulose Fiber (Density: 50 kg/m³)	Water content [M.-%]					
	23 °C and 50%	23 °C and 80%	23 °C and 93%	5 °C and 80%	40 °C and 80%	Capillary saturation
Sample 1	5.1	11.3	14.9	12.4	9.5	850
Sample 2	6.0	10.9	14.6	12.3	11.2	854
Sample 3	5.2	10.9	14.4	11.9	9.5	850
Average	5.4	11.0	14.7	12.2	10.1	852

Table 1 shows the measured values of the sorption isotherm including the value for capillary saturation at 23°C. In order to assess the temperature dependency of the moisture retention function, the equilibrium water content at 80% R.H. is also given for 5° and 40° C. This equilibrium moisture content determined at different temperatures decreases with temperature confirming experimental results of Hansen [2] and Tveit [3]. The capillary saturation amounts to 850 M.-% or 420 kg/m³. However, during the measurement of the

capillary saturation when one surface of the material sample is submerged in water the dimensions of the sample are altered by a slow contraction process.

Figure 1 shows a sample of cellulose fiber before and after this test. This means that the material is severely affected by direct contact with liquid water which will impair the thermal performance of the assembly. Therefore, liquid water penetration into the insulation layer has to be avoided by all means.

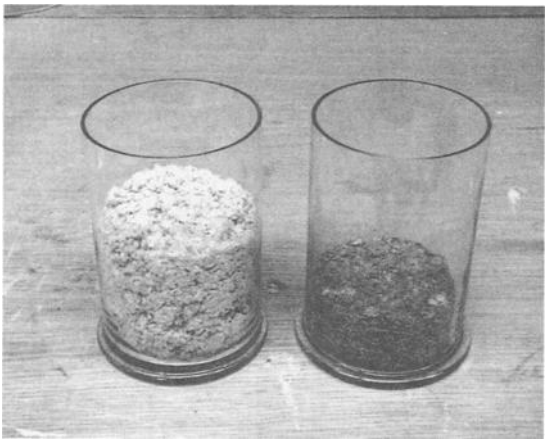

Figure 1 - *Picture of the cellulose fiber samples. The sample on the right side was dried after its capillary saturation. In contrast to its condition before the experiment (left side) it collapsed after the contact with water*

The most important material parameter is the thermal conductivity λ. In general λ is a function of moisture content which is determined by guarded hot plate measurements of dry samples and of samples conditioned in climatic chambers at 80 % R.H. In Figure 2 the temporal evolution of the thermal conductivity for cellulose fiber is plotted as determined from the transient heat flux in the guarded hot plate at different temperature levels. Due to the hygroscopic nature of cellulose fiber, the dry sample absorbs minor amounts of vapor from the ambient air. This effect will be included in the evaluation of the measured results. The bottom graph shows the extrapolation of the heat conductivity for the temperature range between 10 °C and 40 °C. From the difference of these two linear functions the moisture related increase of the heat conductivity can be calculated. The results show that the moisture supplement at 80% R.H. related to the dry conductivity attains 6 %. This is much less than the 20 % supplement assumed in the German standard for determining the design λ-value. The discrepancy can be explained as follows:

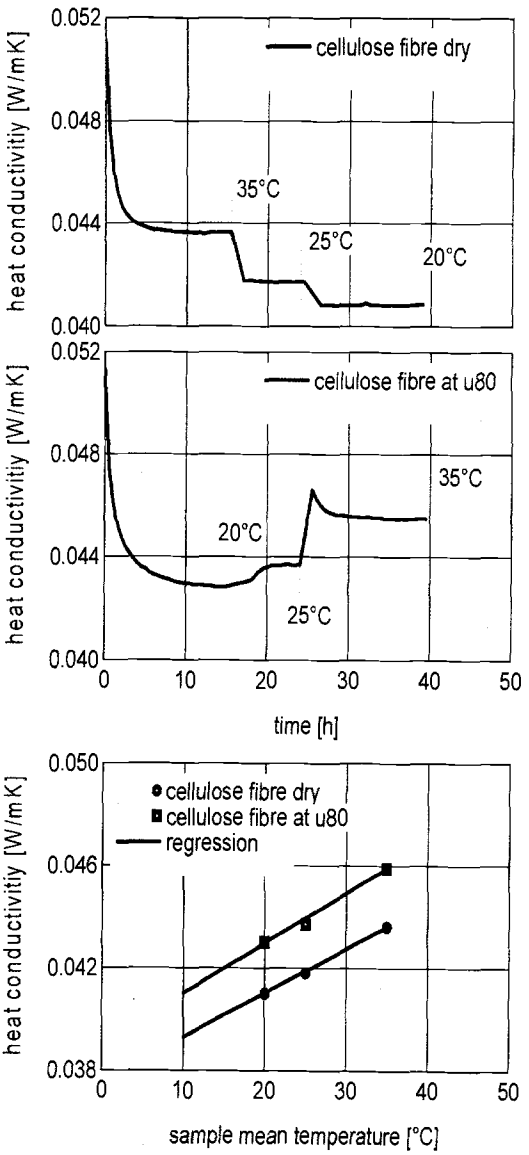

Figure 2 - *Measured development of the heat conductivity for cellulose fiber. The results of the top graph represent the measurement of a dry sample, the ones in the middle those of a sample conditioned at 80 %RH. The bottom graph shows the extrapolation of the heat conductivity for the temperature range between 10 °C and 40°C. From the difference of these two linear functions the moisture related supplement of the heat conductivity can be calculated.*

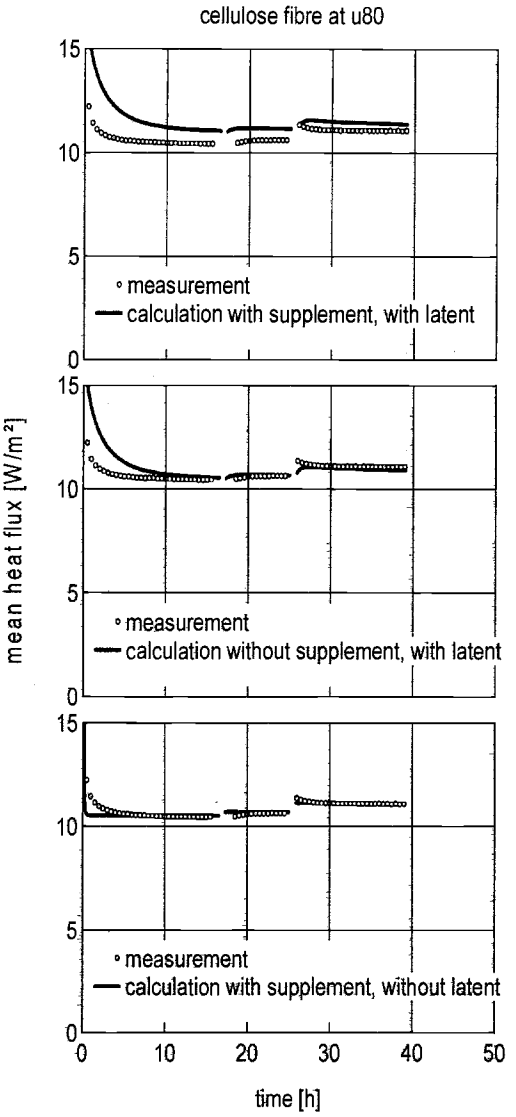

Figure 3 - *Comparison between measured and, with WUFI calculated average heat flux for a sample of cellulose fiber conditioned at 80 % RH.*
top: calculation, where the measured moisture supplement and latent heat effects are taken into consideration.
middle: calculation, where the measured moisture supplement is neglected but latent heat effects is taken into consideration.
bottom: calculation, where the measured moisture supplement is taken into consideration, but latent heat effects neglected.

Table 2

Surface parameter

Parameter		Exterior Value	E1	E2	Interior Value	E1	E2
$1/\alpha$	[m²K/W]	1/19 ± 15 %	-0,3	-4,4	1/8 ± 15 %		0,05
S_d	[m]	1000 ± 150			0,15± 0,05	-0,05	-0,02
A_K	[-]	0,6 ± 0,1	-0,25	-4,2			
A_L	[-]	0,3 ± 0,05					
A_R	[-]	0					

E1 ≡ Elasticity of the maximum moisture increase
E2 ≡ Elasticity of the moisture balance

Material properties

Parameter		Wooden Sheathing Value	E1	E2	Cellulose Fiber (160 mm) Value	E1	E2	Vapour retarder: s_d 2 m Value	E1	E2
ρ	[kg/m³]	400 ± 40	0,05	0,5	60 ± 10	-0,1	-0,25			
Por.	[-]	0,73 ± 0,1			0,95 ± 0,1					
C	[kJ/kgK]	1500 ± 250		0	2500 ± 250		0,07			
λ	[W/mK]	0,09 ± 0,03	0,07	0,4	0,04 ± 0,01		-0,5			
Δ λ	[%]	1,3 ± 0,25								
U_{80}	[kg/m³]	60 ± 10	-0,1	-1	10 ± 3	-0,1	-0,4			
U_{95}	[kg/m³]	90 ± 10[2)]	0,17	1,5	40 ± 10		0,2			
U_{cap}	[kg/m³]	575 ± 50			430 ± 25		0,07			
μ (φ)	[-]	μ (0): 200 ± 10% μ (25):150 ± 10% μ (70): 30 ± 10% μ (100):15 ± 10%			μ (0): 1,5 ± 10%	-0,14	-0,4	μ (0):2000 ± 10%	-0,9	-0,4

Figure 3 shows the measured and the calculated (WUFI-simulations) average heat flux through a sample of cellulose fiber conditioned at 80% RH. The calculations are carried out in three different ways. The first run includes latent heat effects by moisture evaporating at the hot plate and condensing at the cold plate as well as a moisture supplement of 6% on the thermal conductivity. In the second and third run only the latent heat affects or the moisture supplement is taken into account. It should be mentioned, that it is physically not correct to exclude latent heat effects during hygrothermal calculations, but here it is necessary in order to estimate its importance. From the results the conclusion can be drawn, that the measured moisture supplement of 6 % is only a latent heat effect. This means that the real thermal conductivity of the insulation material in equilibrium with 80% R.H. is not higher than in the dry state. But the temperature gradient in the insulation material during the test leads to a redistribution of the sorption moisture in the sample by vapor diffusion. This entails an enthalpy flow which affects the guarded hot plate test in a way similar as the heat flow by conduction. However, there is a distinct difference between the enthalpy flow and the conduction heat flux. The enthalpy flow is transient in nature and reversible. That means it ceases as soon as the local sorption equilibrium is achieved. When the temperature gradient is reversed the enthalpy flow changes direction and the lost energy is recovered. Therefore, the latent heat effects should not be included in the thermal conductivity.

Analyzed Construction and Boundary Conditions

For the calculations a pitched roof construction with non-ventilated cathedral ceiling insulation was chosen. The inclination is 50° and its ridge points west-east. Here the critical part concerning interstitial condensation, the north facing cathedral ceiling is considered. The cross section below the vapor tight covering is, from exterior to interior; as follows: 16 mm wooden sheathing, 160 mm insulation, polyethylene vapor retarder and a gypsum board. Hourly weather data measured in a typical year (1991) at Holzkirchen (located close to the Bavarian alps at 680 m altitude) represent the climatic conditions. The room climate varies in a sinousidal way between 20 °C, 40 % relative humidity in the winter and 22 °C and 60 % relative humidity in the summer. These values correspond to normal conditions in residential buildings of central Europe [4]. The heat transfer coefficient at the external surface is 19 W/m^2K, and 8 W/m^2K on the inside. The short-wave absorption coefficient a_s of the roof covering is 0.6. Rainwater absorption is neglected (the roof is rain tight). The starting point is the beginning of October with an initial moisture content corresponding to the equilibrium moisture content at 80% RH. The criterion to assess the influence of the different input parameters is the moisture balance after one year.

Stochastic Approach

In this paper, we will employ stochastic analysis to investigate the influence of the uncertainty of building material parameters. A similar approach was carried out by [5],[6].The fundamental equations used here in the 'stochastic' modeling are the same as in the deterministic modeling, no additional term or

noise is included in the original formulation of the system of equations, as for example in the building performance analyses of Hokoi et al. [7],[8],[9]. The stochastic method employed in this paper is based on the Monte-Carlo technique and is used in the following way. Material properties are assumed to have a certain range (individual range for each property). The probability of the existence of the values within this range follow normal distribution i.e. mean values are more likely to exist than the values close to the range limits.

Description of the Model used for the Simulations

WUFI-Star [10], a derivation of WUFI [11] and WUFI-ORNL/IBP, is a menu-driven PC program which calculates the transient hygrothermal behaviour of multi-layer building components exposed to a set of climatic conditions including the uncertainty of the input data. The model includes vapor diffusion and liquid transport in building materials. The model only requires standard material properties and approximation methods for the moisture storage and liquid transport functions [12],[13],[14]. During the past seven years the mathematical model was validated by numerous comparisons with experimental investigations.

Results

In order to figure out the sensitive material properties the, "Up-and-Down-Method", is applied [1]. In the beginning a standard case simulation is performed, in which the input parameters are set to the best estimates of the parameters under consideration. These results define the hygrothermal category. The calculation carried out with the "best" values leads to a equable moisture balance - the moisture balance is defined as the difference of the total moisture content in the construction after one year. A positive moisture balance means, that moisture is accumulated in the construction - with a maximum increase during the condensation period of about 0,5 kg/m^2. These two values will serve as the performance criteria [15].

Then the simulation is repeated with one input parameter changed from P to P + 10% respectively from P to P - 10%. This is done for each parameter in turn. In total 69 calculations are carried out. As an indicator for the sensitivity the so-called elasticity is calculated. The elasticity E(U, V) of an input parameter V in relation to the performance criteria U is defined as the ratio of the relative changes. $E(U,V) = (\Delta U/U)/(\Delta V/V)$. The results for each material parameter are shown in Table 2. For the moisture balance it can be seen, that the short wave absorption and the heat transfer resistance are the most sensitive input data. Both have a great influence on the temperature on the surface of the cladding. On the other hand, the maximum increase of the moisture content is mainly dominated by the performance of the vapour retarder. The most influential material properties are the moisture function and the thermal values of the wooden sheathing and the cellulose fiber.

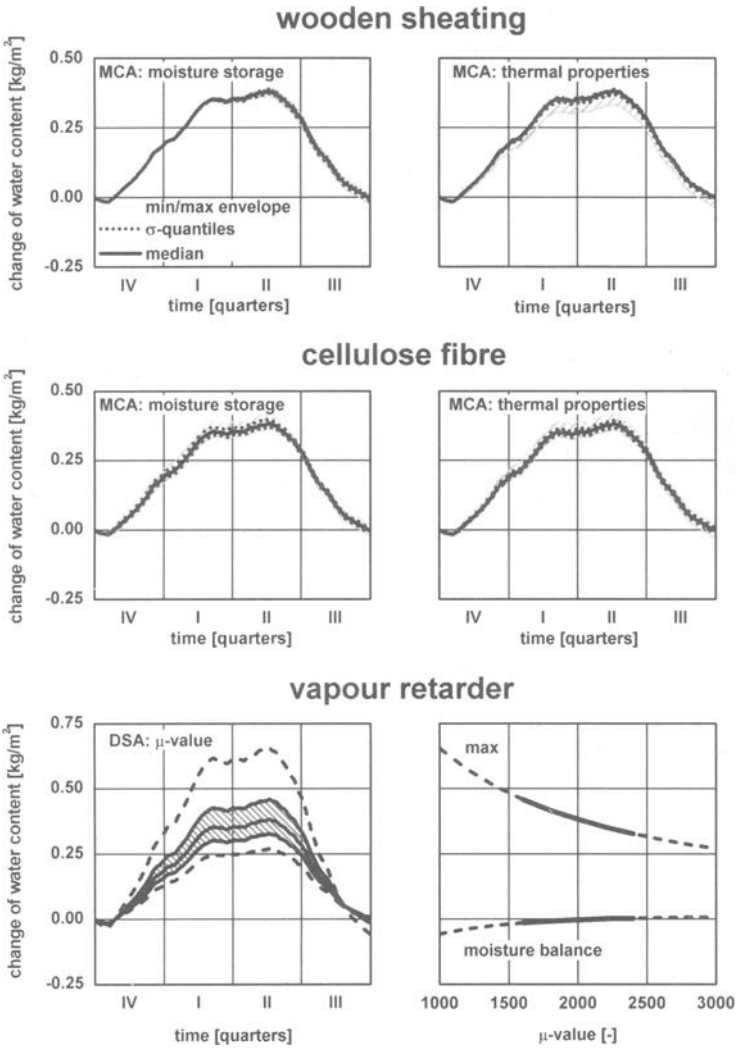

Figure 4 - *Evaluation of the change of water content since start (1. October) Top: Correlated Monte Carlo Analysis (MCA) of the sensitive material properties of the wooden sheathing.*
Middle: Correlated Monte Carlo Analysis (MCA) of the sensitive material properties of cellulose fiber.
Bottom: Differential Sensitivity Analysis (DSA) for the vapour permeability (μ-values) of the vapour retarder.

This method only analyzes which parameters have the greatest influence on the output results, but does not identify any interaction between the parameters.

Therefore Monte Carlo Analysis (MCA) with these sensitve data has been used, too. For all material and surface parameters a probability distribution is assumed (see Table 2). Two hundred random cases were generated simultaneously and later simulated. In order to study the influence of the uncertainty of the material properties the temporal evolution of the water content per unit area is shown in Figure 4. The top graphs represent the results of the MCA for the most sensitive properties of the wooden sheathing, the middle graphs those for cellulose fiber. In each graph the resulting average of all simulations including the σ quantiles is shown. The hatched area represents the envelope between minimum and maximum observed values. The evaluation of the results shows that the uncertainty of both is insignificant influencing the tendency of the calculated results. As mentioned before, the permeability of the vapor retarder is a very sensitive input parameter. In Figure 4 these results of the sensitivity analysis are shown, too. In contrast to the maximum increase of the total moisture content the moisture balance is not really dependent on the vapour permeability.

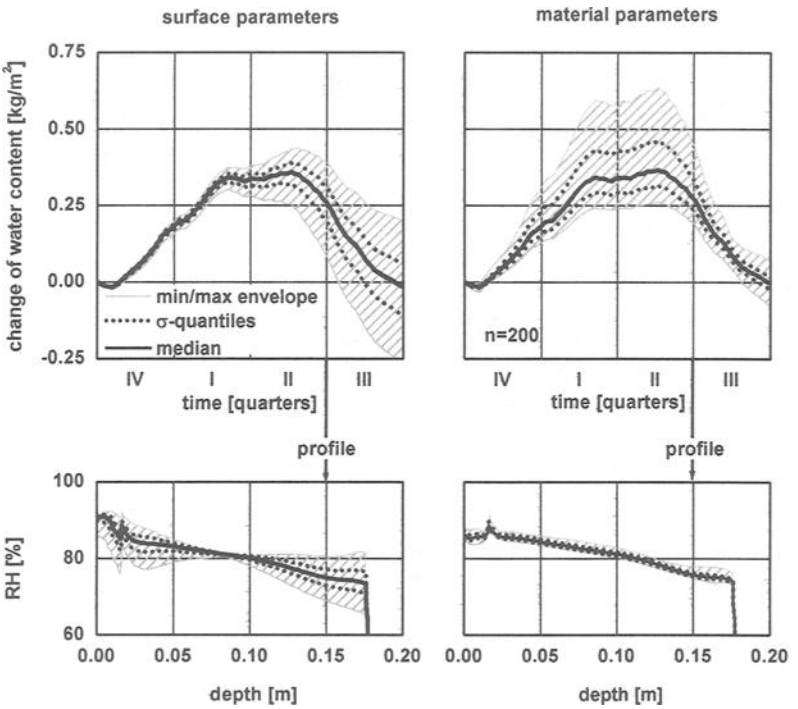

Figure 5 - *Monte-Carlo Analysis for all surface parameters (left) and all material properties (right)*

In order to get information about the accuracy of the calculation, a complete Monte Carlo Simulation for all sensitive input data can be carried out.

The same probability distribution for all material and surface parameters is assumed as described before. Two hundred random cases were generated simultaneously and later simulated. The bottom graph of Figure 5 shows the obtained results. The initial hygrothermal behavior for the "Surface parameter MCA" is nearly identical. The evaluation of the total moisture content starts to drift apart after the end of the first quarter. The main transport direction is then oriented inwards. The top σ-Quantile of the moisture balance after one year is around 0,1 kg/m^2; a critical value for the construction. With a probability of more then 50 % the construction is critical. The results of MCA for all material properties are shown in the same figure. The huge variation is due to the vast influence of the permeability of the vapour retarder, but under assumption of the values and its uncertainties the moisture balance after one year is even-tempered. Now the construction can be considered as safe.

Discussion and Conclusions

Computer calculations are increasingly used to determine the hygrothermal behavior in building components, since modern calculation methods achieve good agreement with measurements. It will be more and more important to know exactly each material or system property. Full and exact material properties are needed when investigating and trying to understand moisture transport in building materials and for validation purposes when developing the numerical models. However, materials are rarely homogeneous in nature and the probability of existence of the measured property values is often a question. This leads to the need for sets of material property values which then could be used in stochastic or Monte Carlo simulations. Statistical analysis methods can be powerful tools that can provide us with reliability ranges for the hygrothermal performance results. They may also provide us the basis for simplifying some of the hygrothermal analyses by allowing us to use material properties that are representative of materials with similar but not exactly the same properties.

Acknowledgments

The authors would like to thank Dr.-Ing Klaus Sedlbauer, Manfred Kehrer and Dr.- Ing Martin Krus for their support of this work, especially the experimental part.

References

[1] Holm, A., "Ermittlung der Genauigkeit von instationären hygrothermischen Bauteilberechnungen mittels eines stochastischen Konzeptes," *Dissertation*, Universität Stuttgart, 2001.

[2] Hansen, K. K., "Sorption Isotherms Catalogue," *Technical Report 162 / 86*, Technical University of Denmark, 1986.

[3] Tveit, A., "Measurements of moisture sorptions and moisture permeability of porous

materials," Norwegian Building Research Institute, Rapport 45, Oslo, 1966.

[4] Künzel, H.M., "Raumluftfeuchteverhältnisse in Wohnräumen," IBP-Mitteilung 24 (1997), Nr. 314.

[5] Karagiozis, A. and Salonvaara, M., "Parametric Study on Material Properties Using Stochastic Modeling," IEA Annex 24 Task1 Simplified Modeling.

[6] Nielsen, A., "Use of Statistics for Prediction of Risk for Condensation in a Wall Construction, Moisture Problems in Building Walls Porto CIB W40 Meeting in Porto September 1995.

[7] Hokoi S. and Matsumoto M., "Impact of the Stochastic Nature of Climate on Building Thermal Analysis," ASHRAE Trans. 1994, Vol.100, Part 2, pp. 787-797, 1994.

[8] Hokoi S. and Matsumoto M., "Condensation Process in External Concrete Walls under Random Fluctuation of Outdoor Temperature - Fundamental Study on Heat and Moisture Behaviour by Fokker-Planck Equation," International Journal of HVAC&R Research, ASHRAE, October 1996, vol.2, no.4, pp. 337-353, 1996.

[9] MacDonald, I. and Strachan, P., "Practical application of uncertainty analysis," Energy and Buildings, 33, S. 219-227, 2001.

[10] Holm, A., The computer Program WUFI-Star. Results not published yet.

[11] Künzel, H. M., "Verfahren zur ein- und zweidimensionalen Berechnung des gekoppelten Wärme- und Feuchtetransports in Bauteilen mit einfachen Kennwerten," Dissertation, Universität Stuttgart, 1994.

[12] Bednar, Th., "Beurteilung des feuchte- und wärmetechnischen Verhaltens von Bauteilen und Gebäuden," Technische Universität Wien, Dissertation, 2000.

[13] Krus, M., Holm, A., "Simple methods to approximate the liquid transport coefficients describing the absorption and drying process," Proceedings of the 5th Symposium 'Building Physics in the Nordic Countries', Gothenburg, S. 241-248, August 24-26, 1999.

[14] Holm, A. and Krus, M., "Bestimmung des Transportkoeffizienten für die Weiterverteilung aus einfachen Trocknungsversuchen und rechnerischer Anpassung," Internationale Zeitschrift für Bauinstandsetzen 4, H. 1, S. 33-52, 1998.

[15] Künzel, H.M., "Außen dampfdicht, vollgedämmt?" bauen mit holz, H. 8, S. 36-41, 1998.

Session 7: Foam Insulations

Phalguni Mukhopadhyaya,[1] Mark T. Bomberg,[2] M. Kumar Kumaran,[3] Michel Drouin,[4] John Lackey,[5] David van Reenen,[5] and Nicole Normandin[5]

Long-Term Thermal Resistance of Polyisocyanurate Foam Insulation with Impermeable Facers

Reference: Mukhopadhyaya, P., Bomberg, M. T., Kumaran, M. K., Drouin, M., Lackey, J., van Reenen, D., and Normandin, N., "**Long-Term Thermal Resistance of Polyisocyanurate Foam Insulation with Impermeable Facers**," *Insulation Materials: Testing and Applications: 4th Volume, ASTM STP 1426,* A. O. Desjarlais, Ed., ASTM International, West Conshohocken, PA, 2002.

Abstract: Polyisocyanurate (*polyiso*) foam insulation with impermeable facers is known for its superior insulating properties in building envelope applications. The impermeable facer on both sides of *polyiso* foam insulation board is designed to increase and maintain the long-term thermal resistance (LTTR) of the insulation. Currently, the Institute for Research in Construction (IRC)/National Research Council (NRC) of Canada, in association with the Canadian Polyisocyanurate Council, has embarked on a research project to develop a standard test methodology that would help to quantify the design LTTR value of *polyiso* foam insulation boards with impermeable facers. This paper outlines the research project and presents preliminary test results from experimental work. These preliminary results are discussed with a view to developing a methodology that will be used as the basis for a National Standard in Canada for the determination of LTTR of *polyiso* foam insulation with impermeable facers.

Keywords: long-term thermal resistance (LTTR), polyisocyanurate foam insulation, impermeable facer, accelerated aging, field test

[1]Research Officer, National Research Council, Ottawa, Ontario, Canada K1A OR6.
[2]Adjunct Professor, Concordia University, Montreal, Quebec, Canada H3G 1M8.
[3]Principal Research Officer, National Research Council, Ottawa, Ontario, Canada K1A OR6.
[4]Director of Technology, Roofing Systems Group, Johns Manville, Cornwall, Ontario, Canada K6H 5T1.
[5]Technical Officer, National Research Council, Ottawa, Ontario, Canada K1A OR6.

Introduction

Optimum use of energy is the keyword for success and survival in the 21st century. The socioeconomic health of a nation is now irrefutably related to its energy consumption and the effective management of it. Even at the dawn of this century, it is becoming very evident that in the coming decades the planet will experience an unprecedented demand for energy and an increasing desire to minimize the impact from unnecessary use of fossil fuels. In such a situation the importance of energy conservation in every aspect of life cannot be overemphasized [*1*].

The use of thermal insulation in various residential, commercial and industrial applications to save energy is a common practice in the developed as well as in the developing world. Quite naturally, a higher thermal resistance (R-value) of insulating material is very much a desirable characteristic. Apart from instant energy savings it can also help to render better long-term durability of materials and systems, more effective moisture management and improved fire protection [*2*]. However, the overall insulation benefit of these materials is dependent on their long-term thermal resistance (LTTR) or aging characteristics.

Closed-cell foam insulation products are extensively used in building envelope applications as they have high R-values, primarily due to the low thermal conductivity of the gas used as the blowing agent during the manufacturing of the foam. This type of insulation can contribute significantly to the global cause of energy conservation. However, aging of closed-cell foam insulation can occur due to inward diffusion of external air and outward diffusion of the blowing agent gas. Hence, the LTTR of closed-cell foam insulation remains the most important criterion for the design performance of thermal insulating systems and its contribution towards energy conservation.

One of the most widely used closed-cell foam insulation products is polyisocyanurate (referred to commonly as '*polyiso*') insulation. *Polyiso* is athermoset plastic foam manufactured from an aromatic polyester polyol, a polymeric isocyanate and a blowing agent. *Polyiso* foam insulation offers many advantages such as:

1. high R-value per unit thickness
2. excellent fire resistance
3. excellent moisture resistance and water repelling characteristics
4. desirable dimensional stability, and
5. resistance to solvents commonly found in construction adhesives.

Polyiso insulation products are made with facers in the form of a rigid board. Facers can be permeable or impermeable. The introduction of impermeable facers on the surface of *polyiso* rigid board is aimed at enhancing the LTTR properties of the foam insulation.

The LTTR of a foam product is defined, in the CAN/ULC Standard for Determination of Long-term Thermal Resistance of Closed-cell Thermal Insulating Foams (S770-98), as the value measured after a 5-year storage in a laboratory environment. Estimation of the LTTR of unfaced (e.g., extruded polystyrene) or permeable faced closed-cell foam insulation can be done using CAN/ULC S770-98 or ASTM Test Method for Estimating the Long-term Change in the Thermal Resistance of Unfaced Rigid Closed-Cell Plastic Foams by Slicing and Scaling Under Controlled Laboratory Conditions (C 1303). These standards provide means for LTTR prediction based on accelerated aging laboratory tests. However, these standard test procedures are not appropriate for estimating the LTTR

value of impermeably faced *polyiso* rigid board insulation products. A joint research project is currently in progress at the Institute for Research in Construction (IRC), National Research Council (NRC) of Canada, in association with Canadian Polyisocyanurate Council to address the aforesaid issue of the LTTR of impermeably faced *polyiso* foam insulation.

This paper presents the aims and objectives of this project, test programs in progress and preliminary results available from the laboratory and field tests.

Background

The low thermal conductivity of high molecular weight blowing agent gas is the primary reason for the higher thermal resistance of closed-cell foam insulation as compared to other generic insulation products. During the service life of the insulation, high molecular weight blowing agent gas starts to diffuse out of the cell or dissolve into the polymer matrix and at the same time comparatively light-weight air components (primarily nitrogen and oxygen) from the external environment start to enter into the closed foam cells. The blowing agent will diffuse out at a rate that is generally between one and two orders of magnitude lower than the rate of air diffusion into the foam [*3*]. These phenomena result in a continuous reduction of thermal resistance (i.e., aging) of the foam over a period of time. The rate of this aging process depends on the type of polymer used, foam structure, temperature, chemical composition of the blowing agent, and cell pressure [*4*].

Limited number of long-term performance studies on commercially available *polyiso* and polyurethane impermeably faced boardstock are available in the literature. The results of a five-year aging study on *polyiso* had been documented by Sherman [*5*]. Using the same *polyiso* test materials as in the five-year study, the results of an eleven-year aging study had been reported by Hagan and Miller [*6*]. A ten-year aging study on polyurethane had also been conducted by Sherman [*7*].

The complex multi-component inward and outward gas diffusion process, which reduces the thermal resistance of polymer foam as a function of time, was first depicted in the 1960s by a simplified isothermal, multi-component diffusion model developed by Norton [*8*]. A number of limitations [*9*] associated with Norton's approach, arising from simplified assumptions, were later addressed by researchers from MIT [*10-12*] in the early 1980s. Researchers at IRC/NRC had also worked during the second half of the 1980s and the early 1990s to develop a model that not only incorporates the basic approach of Norton and MIT but many improvements, including an extrapolative technique applicable to closed-cell foam insulation with facers [*9,13*]. The model is known as the distributed parameter continuum (DIPAC) model.

However, the aforementioned models require an extensive range of input parameters such as: gas diffusion coefficients, accurate determination of cell-gas composition at various stages, appropriate characterization of the blowing agent gas storage/solubility in the foam polymer, thermal conductivity of the various components of the gas and the foam polymer, characterization of various heat transfer mechanisms, cell-gas pressure distribution, temperature profile, etc. It is not always possible to obtain all these data for any particular insulation product. Furthermore, it is not only time consuming and expensive but also inherently difficult to measure these in the laboratory. Hence, in such

a situation, it is important and necessary to integrate the results from laboratory experiments, field observations and modeling [*14*] to achieve a reliable assessment of the LTTR of closed-cell foam insulation. This is the approach adopted in this study as described in the following sections.

Research Significance and Objectives

The main objective is to develop a comprehensive test procedure that can be used to predict the LTTR of *polyiso* foam insulation products with impermeable facers. Once the method has been developed, it would be applied to evaluate LTTR of three commonly used *polyiso* rigid insulation boards with impermeable facers.

More specifically, there are two major tasks involved in this project:

1. Laboratory and field tests on specimens, and
2. Analysis of the test observations/data with a numerical modeling tool (DIPAC)

It is envisaged that by combining the output from the above two tasks, a methodology would be developed that can be applied to estimate the LTTR characteristics of *polyiso* with impermeable facers.

Material

Three *polyiso* foam rigid insulation boards are under consideration in this study. These boards were obtained from three different North American sources and each one differs from the others in terms of the blowing agent or the manufacturing process; however, they have very similar physical properties, as shown in Table 1. The boards were dispatched to the laboratory from the manufacturing plant within a week of the manufacturing date. In this paper these three boards will be referred to as Product A, Product B and Product C.

Experimental Program and Modeling

The test program and modeling work are designed to complement each other. Laboratory and field tests are being carried out on full-thickness and thin-slice specimens. While thin-slice specimens are aged and tested only in the laboratory, full-thickness specimens are aged and tested both in the laboratory and in the field.

Laboratory Tests

Two types of specimens are considered in laboratory tests for all three products. Tests are done on (1) full-thickness specimens, and (2) thin-slice specimens. Table 2, and Figures 1 and 2 describe the size and other related information about the specimens.

Full-Thickness Specimens - Six full-thickness ($\geq$ 25 mm) specimens (610 mm $\times$ 610 mm) were cut from three different boards for each product from various locations of the boards. Initial heat transmission properties of these specimens were determined in the laboratory within ten days of arrival at the laboratory using a 'Heat Flow Meter Apparatus' according to the ASTM Test Method for Steady-State Thermal Transmission

Table 1 - *Physical Description of Materials*

Product / Material ID	Average thickness (mm)	Density (kg/m^3)	Full board size (mm × mm)	Remarks
A	24.8	35.9	1220 × 2440	Aluminum foil faced
B	25.6	36.9	1220 × 2440	Aluminum foil faced
C	24.8	34.3	1220 × 2440	Aluminum foil faced

Table 2 - *Details of Laboratory Test Specimens*

Specimen type	Dimension		Total no. of specimen	Comments
	Area (mm^2)	Thickness (mm)		
Full-thickness	610 × 610	≅25	6	
Thin-Slice - Test 1	305 × 305	6	4	(a) two each from top and bottom surface (b) two with slit on the facer and two without it (Figure 1a) (c) Totally encapsulated with glass plate and epoxy coating on edges (Figure 1b)
Thin-Slice - Test 2	305 × 305	6 or 12	4	(a) Core slices (Figure 2a) without facers (b) One-sided aging for 6 mm thin slices (Figure 2b) (c) Two-sided aging for 12 mm thin slices
Thin-Slice - Test 3	Same as Thin Slice - Test 1	Same as Thin-Slice - Test 1	Same as Thin Slice - Test 1	Same as Thin-Slice - Test 1
Thin-Slice - Test 4	Same as Thin-Slice - Test 2	Same as Thin-Slice - Test 2	Same as Thin-Slice - Test 2	Same as Thin-Slice - Test 2

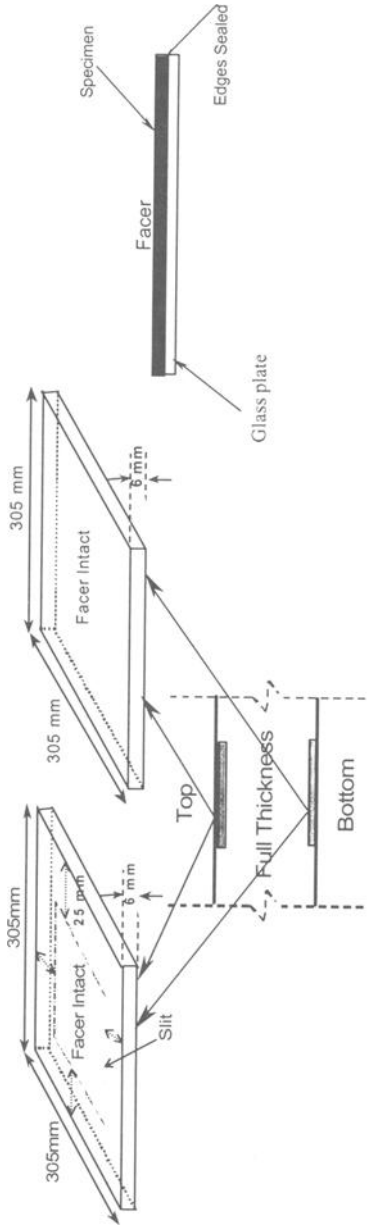

Figure 1a - *Specimens for ' Thin Slice - Test 1'*

Figure 1b - *Specimens for Thin Slice - Test 1'*

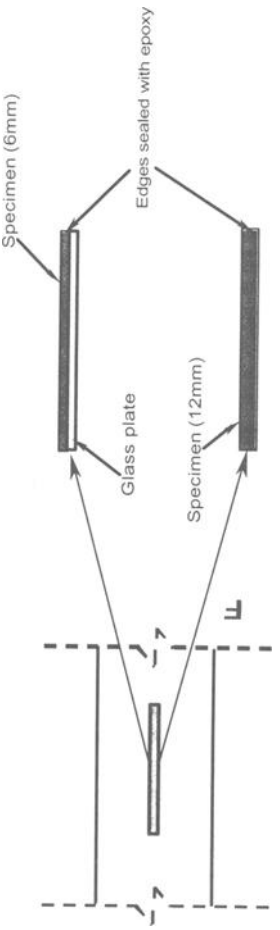

Figure 2 - *Specimens for ' Thin Slice - Test 2'*

Properties by Means of Heat Flow Meter Apparatus (C518). These specimens are currently exposed to a laboratory environment of 24° C (temperature) and 50% RH (relative humidity), and will be re-tested after about twelve months of exposure.

Thin-Slice Specimens - Four sets of tests are being conducted with thin-slice specimens for each of the three products. As shown in Table 2, these tests are identified as Test 1, Test 2, Test 3 and Test 4. The details of test specimens are given in Table 2 and Figures 1 and 2.

In Test 1, two 6 mm thick slices were cut from each surface (Figure 1a) (total of four) of the board and placed on an epoxy-coated glass substrate (Figure 1b). The edges of each specimen were sealed with epoxy coating to facilitate one-sided aging of the *polyiso* foam through the foil facer only. Two of these four specimens have the facer surface intact on the exposed side whereas the other two have a slit on the facer surface of about 25 mm from the edge (Figure 1a). The presence of the slit on the facer allows 2-D diffusion pattern, i.e., accounts also for diffusion parallel to the facer surface.

For Test 2, all the thin slices are taken from the core of the *polyiso* board (Figure 2a). Naturally, these core foam slices are without any facer. Two of the slices are 6 mm and the other two are 12 mm. The core slices of 6 mm thickness are subjected to one-sided aging on the glass plate and edges sealed with epoxy coating (Figure 2b). However, the 12 mm thick core slices are being tested without any kind of treatment on the two major surfaces, i.e., two-sided aging (Figure 2b).

Test 3 and Test 4 are repeat tests of Test 1 and Test 2, respectively. Preparation of thin-slice specimens is done within around 30 days of the date of delivery of the product to the laboratory. Thin-slice specimens are exposed in the laboratory and tested for heat transmission properties at different stages of aging, using 'Heat Flow Meter Apparatus' according to ASTM C518.

Field Test in the IRC/NRC Test Hut

Any long-term performance evaluation process is not complete without field exposure tests. In this research program, all three full-size *polyiso* rigid boards have been installed in a purpose-built test-hut (Figure 3a) at the IRC/NRC campus in Ottawa. The indoor environment of the test hut is controlled and exterior weather data are also available. As shown in Figure 3b, full-size boards of Product A and Product C are installed on the east wall of the test hut and Product B and Product C on the west wall. In this way, the field performance of all three *polyiso* products can be monitored and also the difference in performance due to wall orientation (east or west) can be identified. A typical cross-section of the wall, after installation of *polyiso* board in the test hut, is shown in Figure 4. The in-situ thermal properties of the *polyiso* foam boards are being monitored using the instrumentation set-up as described in the following paragraph.

Field Instrumentation of Specimens and Measurement - Each of the four insulation boards was instrumented with two heat flow sensors located as shown in Figures 5a and 5b. Around each heat flow sensor, seven thermocouples were installed in the locations shown in Figure 5a. The complete set-up consists of 56 type 'T' thermocouples and eight heat flow sensors. The data are collected by a Hewlett Packard mainframe data

acquisition system connected to a digital personal computer. Temperature and heat flow measurements are made at every three minutes.

Each of the heat flow sensors outputs an EMF voltage that is proportional to the heat flow through the sensor. Each of the sensors is calibrated separately, and the heat flow through the specimen is calculated from the output voltage of the sensor. The R-value is then calculated from the temperature distribution and the measured heat flow.

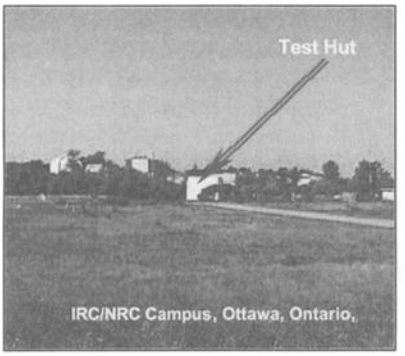

(a) *Test Site*

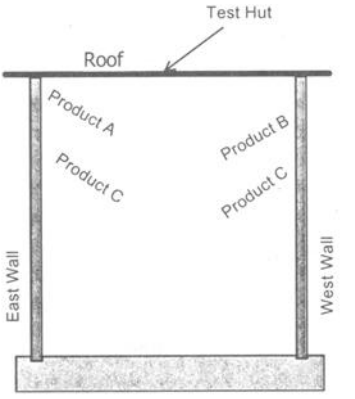

(b) *Specimen Placement Inside the Test Hut*

Figure 3 - *Field Test Facilities*

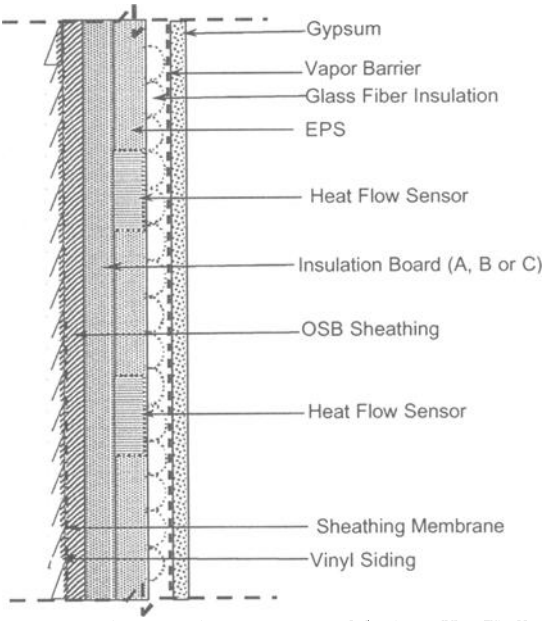

Figure 4 - *Schematic Cross-section of the Test Hut Wall*

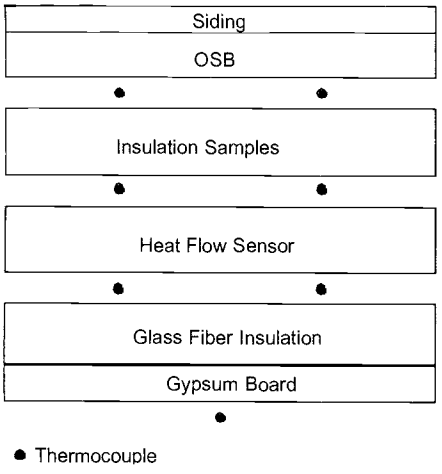

Figure 5a - *Cross-section of the Test Hut Wall with Instrumentation*

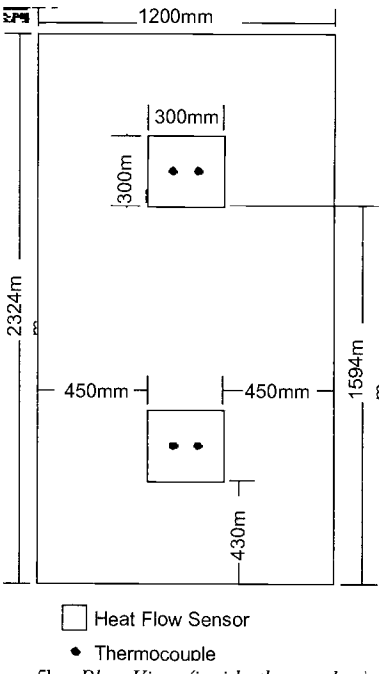

Figure 5b - *Plan View (inside the test hut) of Instrumentation*

Modeling Tool

The distributed parameter continuum or DIPAC model, developed at IRC/NRC, can be and had been used in the recent past [*13*] as an important tool for evaluating LTTR of foam insulation. Several publications are now available where the fundamentals of the DIPAC 1-D model have been discussed at length [*9,13*]. However, the DIPAC 1-D model does not have an effective provision for accommodating the lateral diffusion component of the blowing agent, i.e., the flow of gas parallel to the facer. It is envisaged that having a 2-D model of heat and gas transfer will facilitate the incorporation of the lateral diffusion component of the blowing agent into the DIPAC model.

The 2-D DIPAC model needs to include three different layers cut parallel to the facer [9,13]. The external layers represent foam with properties different from those in the central or core layer. This permits introduction of the lateral gas diffusion through the external layers. Furthermore, each external surface is provided with a contact resistance used to simulate an impermeable facer. The objective of DIPAC 2-D is to calculate the heat flux through a slab, provided with a facer on each side, as a function of aging time and boundary conditions. To achieve this, the facers and the slab are divided into a given number of layers and the aging time is counted as a number of time-steps. Some of the material characteristics used in these calculations, e.g., density, extinction coefficient for

infrared radiation or effective gas diffusion coefficient, may vary across the slab. Therefore, all the material characteristics used for the input are measured at three locations: at the middle and at each surface of the slab. Using a linear interpolation one may calculate material characteristics for each layer.

Work on the development of the DIPAC 2-D model is in progress and will be used to evaluate the LTTR values when experimental results from thin-slice experiments are available.

Preliminary Test Results

Laboratory and field tests currently in progress are generating an enormous amount of useful and interesting information. However, it is beyond the scope of this paper to present all these data in an objective manner at this stage of the project. Hence, only representative and pertinent sets of test results are presented and discussed in the following sections.

Full-Thickness Specimens

The average values for the initial thermal resistivity of the three products are shown in Figure 6. The initial values appear to be very close to each other. The results obtained from six specimens for each product also show that all observations are within ±2% of the average thermal resistivity values reported in Figure 6. Hence, it confirms the fact that the results are reproducible with the Heat Flow Meter used in this study and that the variation of the material properties at different locations of the board is insignificant. The specimens are currently exposed to laboratory condition (24°C; 50%RH) and further tests on these specimens will be carried out after a period of around twelve months.

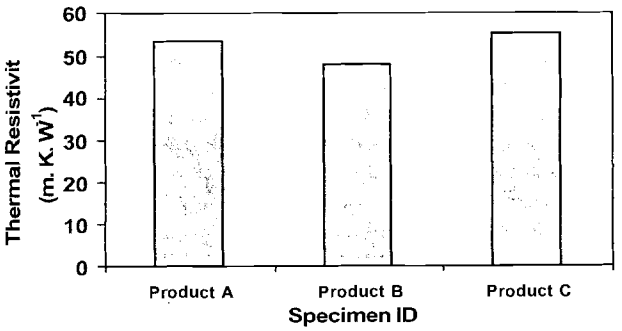

Figure 6 - *Initial Thermal Resistivity of Full Thickness Impermeably Faced Polyiso Foam Insulation*

Thin-Slice Specimens

As mentioned earlier, two types of thin slices are being tested in this research program. Surface slices are in Test 1 and core slices in Test 2.

Observations from Test 1 - Typical aging (i.e., reduction in thermal resistivity with time) curves of thin surface slice specimens, after up to six months of laboratory exposure from Test 1, with and without a slit on the facer, can be seen in Figures 7a to 7d. These results are for Product A (six months) and Product B (three months). Similar results are also available for Product C but for a much shorter time period and will be reported elsewhere in due course.

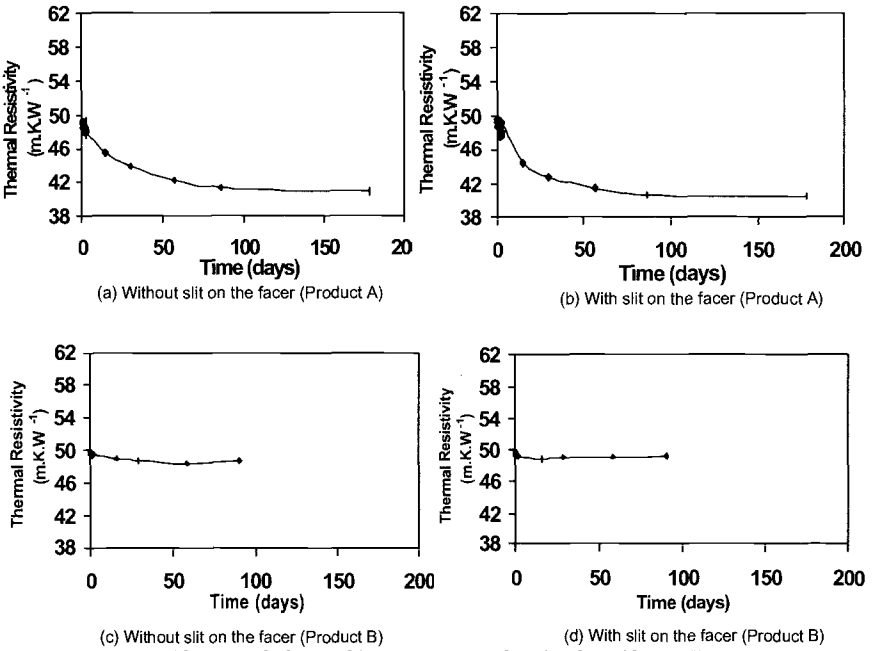

Figure 7 - *Change of Thermal Properties in Thin Surface Slices (Test-1)*

These aging curves clearly show rapid aging at the beginning of the exposure and then a reduction in the aging rate to a near stable value for Product A. In the case of Product B, however, these changes are less evident. The different aging characteristics of Products A and B imply that aging characteristics of one *polyiso* product can vary from another and it is necessary to investigate more that one *polyiso* product, as has been done in this project. There is also a clear indication that the presence of a slit on the facer in Product A results in a greater rate of aging in the initial stage but for Product B this effect is less visible at this stage. This phenomenon is more evident, for Product A, if the results are presented in terms of aging ratio (i.e., the ratio of the thermal resistivity at any specified time to the initial thermal resistivity), as shown in Figure 8. One possible explanation for the aging of the faced specimen is that in the presence of an inert cell gas the process of solubility of the blowing agent in the foam matrix will change the molar composition of the cell-gas and thereby reduce the effective thermal conductivity of the foam. Another possible explanation is the lateral diffusion of cell gases parallel to the facer. In addition, it is also possible that the facer is not effectively impermeable. The

rapid aging has almost stabilized the thermal resistivity of the thin slice after 110 days when there is a slit on the facer but without it, the aging process is still continuing at 180 days. Quite naturally, further exposure of the specimens is necessary and the process is ongoing. In general, these preliminary observations of Test 1 indicate that experimentally it is possible to identify the effect of the lateral flow of the blowing agent on the aging process of impermeably faced *polyiso* insulation foam board. Hence, this phenomenon now can be incorporated in the DIPAC 2-D model where exterior layers would resemble the thin layers of Test 1.

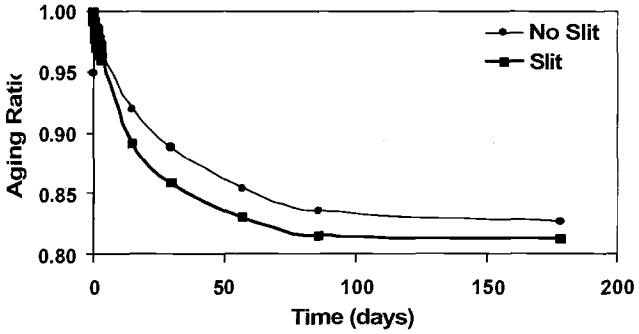

Figure 8 - *Aging Due to Lateral Flow of Blowing Agent Parallel to Facer (Product A)*

Observations from Test 2 - Figures 9a to 9d show the typical aging curves of core slices from Test 2 for Product A and Product B. These figures indicate that, as would be expected, the initial (up to 15-20 days) aging process is rapid but thereafter it slows down significantly. However, the aging process continues beyond the test period. Figure 10 shows the plot of aging ratio vs. time for the two core slices of Product A. The two-sided aging of a 12 mm thick core slice appears to be faster than the one-sided aging of the 6 mm core slice. It should be noted that the aging ratio represents a combination of many effects. The impact on aging caused by a few hours difference in the start of the test is proportional to the second power of the thickness of each layer (here a factor of 2) and the foam itself may have a gradient of physical properties. While an analysis of these differences requires the use of a computer model, the fact that tests on core slices showed much faster aging than the surface slices in the Test 1 signifies that the impermeable facer influences the rate of aging. The aging characteristics of these core slices will help to model core elements in the DIPAC 2-D model.

Field Test Observations

After installation of the specimens in the test hut (Figure 3), the data acquisition has just started. Typical, initial recorded results for Product B on the west wall of the test hut are presented in Figure 11. The similarity between field test data and laboratory observations on the same product at around the same time clearly indicates that the entire instrumentation system used for the field observation is reliable. These tests will continue for one year. The field observation data will complement the laboratory test data and the output from the DIPAC 2-D modeling.

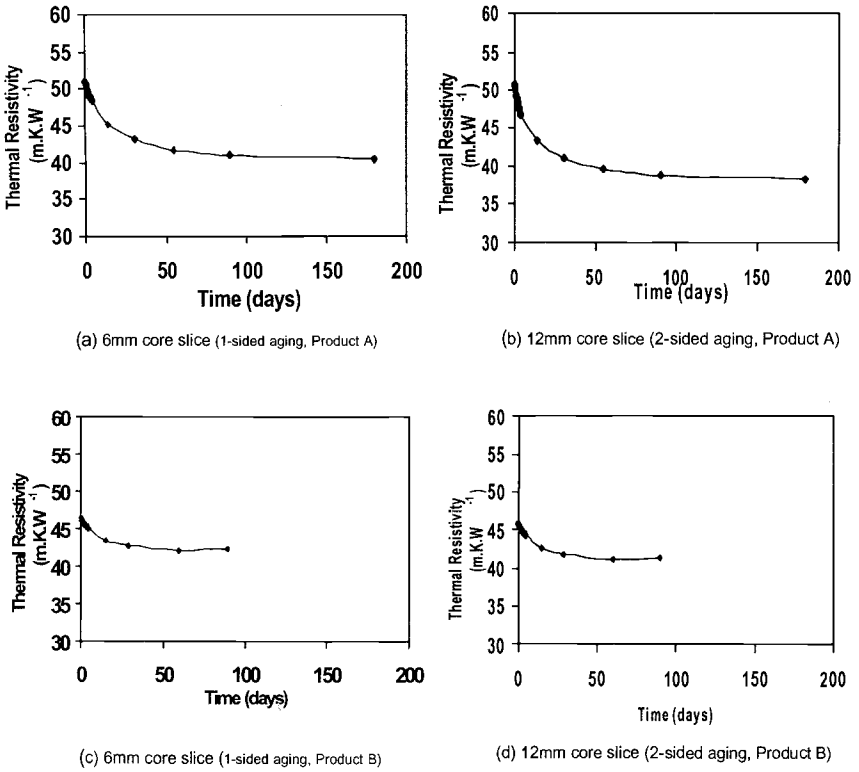

Figure 9 - *Change of Thermal Properties in Thin Core Slices (Test-2)*

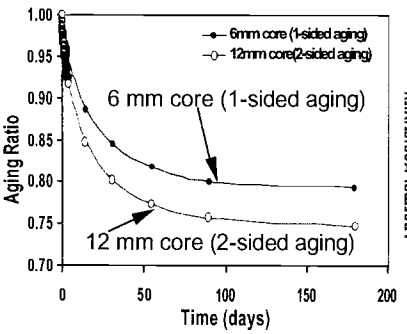

Figure 10 - *Aging of Core Slices*
(one-sided and two-sided aging - Product A)

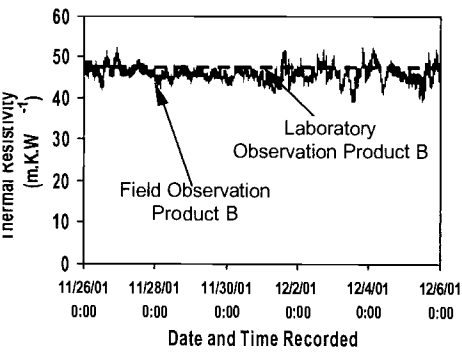

Figure 11 - *Typical Recorded Field Test Data*

Discussion

The work presented in the previous sections takes into account three distinct but complementary approaches, i.e., laboratory tests, field observations and numerical modeling. This comprehensive approach is designed to address the complex issue of the LTTR of impermeably faced *polyiso* foam insulation board.

The preliminary experimental observations show that the designed thin-slice tests can in fact identify the aging of the foam due to lateral diffusion of the blowing agent gas parallel to the facer. For appropriate quantification of this phenomenon, the ongoing series of tests need to be carefully monitored and carried to their logical end. The aging of core slices also indicate their own characteristics, which differ from those obtained from surface slices. On the other hand the preliminary results obtained from field tests show that laboratory and field observations could be correlated. However, continuous monitoring, collection of data and analysis of the data simultaneously still need to be completed in the coming days.

Summary of Observations

The following interim observations can be made at this stage from this ongoing research project.

1. A comprehensive research project to determine the long-term thermal resistance (LTTR) of polyisocyanurate (*polyiso*) foam insulation board with impermeable facers is currently in progress.
2. Thin-slice tests indicate that aging of *polyiso* foam does occur due to the lateral diffusion of the blowing agent gas parallel to the facer surface.
3. Core *polyiso* foam slices without any facer indicate a faster aging than surface *polyiso* foam slices with facer.
4. Field performance monitoring of full-size *polyiso* insulation board is currently in progress and preliminary test data are comparable to the laboratory observations.
5. Experimental observations from thin-slice tests show that the approach taken in the DIPAC 2-D model to divide the *polyiso* foam in three different layers is both reasonable and logical.

Acknowledgement

The authors would like to acknowledge the support and comments provided by the members of Canadian Polyisocyanurate Council for the preparation of this paper. Members of the Canadian Polyisocyanurate Council are: John Letts (Firestone Building Products), Rich Roe (Atlas Roofing), Sachi Singh and Paul Coleman (Huntsman Polyurethanes), Andy Lodge (IKO Industries), Michel Drouin (Johns Manville) and John Clinton (PIMA).

References

[1] Goodacre, C., Sharples, S. and Smith, P., 'Integrating Energy Efficiency with the Social Agenda in Sustainability,' *Energy and Buildings*, Vol. 34, 2002, pp. 53-61.

[2] *ASHRAE Handbook - Fundamentals*, American Society of Heating, Refrigerating and Air-Conditioning Engineers, Inc., N.E. Atlanta, GA 30329, Chapter 22, 1997.

[3] Alsoy, S., 'Modeling of Diffusion in Closed Cell Polymeric Foams,' *Journal of Cellular Plastics*, Vol. 35, May 1999, pp. 247-271.

[4] Isberg, J., 'Thermal Insulation – Conditioning of Rigid Cellular Plastics Containing a Gas with Lower Thermal Conductivity than Air Prior to Determination of Thermal Resistance and Related Properties,' Chalmers University of Technology, No. 698, Goteborg, Sweden, 1988.

[5] Sherman, M., 'Aged Thermal Resistance (R-value) of Foil-Faced Polyisocyanurate Foam Thermal Insulation Board,' *Proceedings of Conference on Thermal Performance of the Exterior Envelopes of Buildings*, 1979, pp. 952-964.

[6] Hagan, J. R. and Miller, R. G., 'Long-Term R-Values and Thermal Testing Requirements for Rigid Insulating Foams,' Insulation Materials, Testing, and Applications, *ASTM STP 1030*, D. L. McElroy and J. F. Kimpflen, Eds., ASTM, Philadelphia, 1990, pp. 205-217.

[7] Sherman, M., 'Sampling Faced Foam Insulation Board for Heat Flow Meter Thermal Performance Testing, 'Thermal Insulation Performance, *ASTM STP 718,* D. L. McElroy and R. P. Tye, Eds., ASTM, Philadelphia, 1980, pp. 298-306.

[8] Norton, F. J., 'Thermal Conductivity and Life of Polymer Foams,' *Journal of Cellular Plastics*, Jan. 1967, pp. 23-37.

[9] Bomberg, M., 'A Model of Aging for Gas-Filled Cellular Plastics,' *Journal of Cellular Plastics*, Vol. 24, July 1988, pp. 327-347.

[10] Ostrogorsky, A.G. and Glicksman L.R., 'Aging of Polyurethane Foams, the Influence of Gas Diffusion on Thermal Conductivity,' ORNL/SUB/84-9009/2,1986, pp.1-98.

[11] Schuetz, M. A. and Glicksman L.R. 'A Basic Study of Heat Transfer Through Foam Insulation,' *6th International Polyurethane Conference*, San Diego, CA, 1983, pp. 341-347.

[12] Glicksman, L.R., Ostrogorsky, A.G. and Chiapetta, S., 'Effective Conductivity of Aging of Polyurethane Foam,' ORNL/SUB/84-9009/1,1986, pp.1-56.

[13] Bomberg, M. and Kumaran, M. K., 'Use of the Distributed Parameter Continuum (DIPAC) Model for Estimating the Long-Term Thermal Performance of Insulating Foams,' *Thermal Performance of the Exterior Envelopes of Buildings VI*, Clearwater Beach, FL,1995, pp. 15-24.

[14] Bomberg, M. and Brandreth, D.A., 'Evaluation of Long-term Thermal Resistance of Gas-filled Foams: A State of the Art,' *ASTM STP 1030*, ASTM International, West Conshohocken, PA, 1990, pp. 156-173.

James Whalen[1]

Performance of Molded Expanded Polystyrene (EPS) Thermal Insulation in Below-Grade Applications

Reference: Whalen, J., **"Performance of Molded Expanded Polystyrene (EPS) Thermal Insulation in Below-Grade Applications,"** *Insulation Materials: Testing and Applications: 4th Volume, ASTM STP 1426*, A. O. Desjarlais and R. R. Zarr, Eds., ASTM International, West Conshohocken, PA, 2002.

Abstract: Molded expanded polystyrene (EPS) products are used for a wide variety of construction applications, including such applications as thermal insulation for below-grade foundations, frost-protected shallow foundations and floor slabs. The performance of EPS thermal insulation has been demonstrated in these applications for more than 40 years.

When used as below-grade insulation in building construction, EPS insulation is one component in a system whose purpose is to minimize heat loss and, in turn, energy consumption in that portion of the building envelope. As with any product, the successful use of EPS insulation depends upon its correct installation in accordance with good building practice.

Material properties required for the selection of the correct EPS insulation product for below-grade applications and performance characteristics are discussed in this paper. In addition to identifying material properties considered important in below-grade applications, current laboratory test methods used for measuring the property, where applicable, and references demonstrating performance of EPS product after defined in service periods are cited. The role each material property plays in the performance of EPS insulation is also highlighted.

Keywords: below-grade, building insulation, EPS, product performance, molded expanded polystyrene insulation, thermal insulation

1 Technical Marketing Manager, Registered Professional Engineer, Plasti-Fab, Division of PFB Corporation, Suite 270, 3015 – 5th Avenue NE, Calgary, Alberta T2A 6T8 Canada

Introduction

EPS is the acronym commonly used for molded expanded polystyrene insulation. EPS insulation is an air-filled, closed cell, rigid foam plastic insulation. That is, the closed cellular structure as delivered to the end-user does not contain any significant amount of blowing agent (see section on thermal resistance for further discussion of blowing agents in foam plastic insulation).

Dependent upon the specific product application, one or more of the following material properties for EPS thermal insulation may need to be considered for below-grade building applications:

- Thermal resistance
- Drainage capabilities
- Water absorption
- Water vapor permeance
- Compressive stress and stress distribution
- Durability

CAN/ULC-S701-01, *Standard for Thermal Insulation, Polystyrene, Boards and Pipe Covering* is the National Standard of Canada that specifies requirements for EPS insulation material. Only EPS insulation types and property values as specified in CAN/ULC-S701 (Table I) are cited in this paper for clarity. Minimum product density is not specified in CAN/ULC-S701. Nominal density values for the various product types are provided below for reference only[1].

Table I – *EPS Insulation Material Properties – CAN/ULC-S701-01*

Material Property	Test Method	Units	Type 1	Type 2	Type 3
Thermal Resistance *Minimum @ Mean temperature 24 C (75 F)*	ASTM C518	$m^2 \cdot °C/W \cdot 25\text{-mm}$ ($Ft^2 \cdot hr \cdot °F/BTU \cdot in$)	0.65 (3.75)	0. 70 (4.04)	0.74 (4.27)
Water Vapor Permeance *Maximum*	ASTM E96	$Ng/Pa \cdot s \cdot m^2$ (perms)	300 (5.2)	200 (3.5)	130 (2.3)
Compressive Strength *Minimum @ 10% Deformation*	ASTM D1621 Procedure A	kPa (psi)	70 (10)	110 (16)	140 (20)
Flexural Strength *Minimum*	ASTM C203 Procedure B	kPa (psi)	170 (25)	240 (35)	300 (44)
Dimensional Stability *Maximum*	ASTM D2126 7 Days @ 70 ± 2°C	% Linear Change	1.5	1.5	1.5

1

Nominal Density	C303 or D1622	kg/m^3 (pcf)	Type 1	Type 2	Type 3
			16 (1.0)	24 (1.5)	32 (2.0)

Water Absorption *Maximum*	ASTM D2842	% by volume	6.0	4.0	2.0
Limiting Oxygen Index *Minimum*	ASTM D2863	%	24	24	24

ASTM C578-01, Standard Specification for Rigid, Cellular Polystyrene Thermal Insulation, Vol. 04.06 Annual Book of ASTM Standards, is the product specification that covers the types, physical properties, and dimensions of cellular polystyrene intended for use as thermal insulation in the United States. Only EPS insulation types and property values as specified in C578 (Table II) are cited in this paper for clarity. C578 differs from the Canadian product standard in that *minimum* product densities are specified in this specification.

Table II – EPS Insulation Material Properties – ASTM C578-01

Material Property	Test Method	Units	Type I	Type VIII	Type II	Type IX
Density *Minimum*	C 303 or D 1622	kg/m^3 (pcf)	12 (0.90)	18 (1.15)	22 (1.35)	29 (1.80)
Thermal Resistance *Minimum @ Mean temperature 24 C (75 F)*	ASTM C518	$m^2 \cdot °C/W \cdot 25\text{-}mm$ ($Ft^2 \cdot hr \cdot °F/BTU \cdot in$)	0.63 (3.60)	0.67 (3.80)	0.70 (4.00)	0.74 (4.20)
Water Vapor Permeance *Maximum*	ASTM E96	$Ng/Pa \cdot s \cdot m^2$ (Perm-inch)	287 (5.0)	201 (3.5)	201 (3.5)	115 (2.0)
Compressive Strength *Minimum @ 10% Deformation*	ASTM D1621 Procedure A	kPa (psi)	69 (10.0)	90 (13.0)	104 (15.0)	173 (25.0)
Flexural Strength *Minimum*	ASTM C203 Procedure A	kPa (psi)	173 (25.0)	208 (30.0)	240 (35.0)	345 (50.0)
Dimensional Stability *Maximum 7 Days @ 70 ± 2°C*	ASTM D2126	% Linear Change	2.0	2.0	2.0	2.0
Water Absorption *Maximum*	ASTM C272	% By volume	4.0	3.0	2.0	2.0
Limiting Oxygen Index *Minimum*	ASTM D2863	%	24	24	24	24

It must be noted that the test methods used to determine the material properties in both CAN/ULC-S701 and C578 provide a means of comparing different cellular plastic thermal insulation. The material property values cited are generally intended for use in specifications, product evaluations and quality control. In many cases, they do not predict end-use product performance.

While CAN/ULC-S701 and ASTM C578 were developed mainly for thermal insulation applications in building construction, in many cases the material properties are applied to a much wider range of product applications.

Thermal Resistance

Heat Transfer Mechanisms

Thermal resistance of an insulation material is generally referenced as R-Value (also referred to RSI-Value in the SI System). The R-Value of an insulation material is a relative measure of the ability of the material to resist heat flow through it, with a higher R-Value indicating a greater resistance to heat flow.

In order to discuss thermal performance of EPS insulation, it is important to understand the mechanisms of heat transfer in cellular plastic insulations. Heat transfer in cellular foam plastics occurs through three distinct mechanisms: convection, conduction and radiation [*1*].

Heat transfer by convection occurs due to a temperature differential between two surfaces and, in the case of cellular plastics between the cell walls, in the direction of heat flow. Because EPS insulation cell size is small, the temperature differential is very small and heat transfer as a result of convection is minimal.

Heat transfer by conduction occurs in foam plastic insulation through both the gas and solid portions. Since gases occupy approximately 90 to 98 percent by volume of cellular foam plastics, conduction through the gas portion is by far the most significant. Some cellular plastics depend upon low thermal conductivity gases, such as CFCs, HFCs or HCFCs, inside their cells to maintain lower thermal conductivity. However, unless the foam plastic is enclosed within a gas impermeable barrier, eventually some of the gases in the cells will diffuse out and be replaced by air. This phenomenon is known as thermal aging. In the case of EPS thermal insulation, the closed cellular structure contains only air; therefore, the thermal resistance of EPS insulation does not decrease with age as a result of thermal aging.

Heat transfer by radiation occurs through cell walls in EPS insulation and is also an important consideration, although it is not as significant a heat transfer mechanism as conduction. Lighter density cellular plastics, as well as thinner sections, are especially subject to heat transfer through radiation, because the cell walls are more transparent to radiation. As density and thickness increase, however, the contribution to heat transfer as a result of radiation decreases. The thermal resistance of EPS insulation is closely related to the density of the finished product. Within the normal range of EPS thermal insulation densities, as product density insulation increases, thermal resistance values also increase.

In summary, the primary method of heat transfer in cellular plastics is through conductance and, since gases occupy 90 to 98 percent by volume of a cellular plastic insulation, it occurs mainly through the gas trapped within the foam. Heat transfer also occurs to a lesser degree through radiation. For this reason, the long-term thermal resistance of a cellular plastic will depend, to a large extent, upon the type of gas that remains within the cellular structure.

Drainage Capabilities

Absorbed moisture is known to reduce the thermal resistance of any cellular plastic insulation because it replaces the gas in the cellular structure and results in latent heat transfer through evaporation and condensation. As well, water in contact with insulation, in whatever phase, provides an additional factor to consider in heat transfer.

The importance of adequate drainage to remove liquid water present in the vicinity of below grade insulation can be seen by reviewing the thermal conductivities of moisture (Table III) in various phases [*2*] in comparison to air and EPS thermal insulation.

Table III – Thermal Conductivities of Moisture in Various Phases in Comparison to Air and EPS Thermal Insulation

Material	Mean Temperature		Thermal Conductivity	
	°F	°C	BTU· in/HR· ft^2· °F	**W/m· °C** *(1 meter thickness)*
Air	32	0	0.169	0.024
Water Vapor	32	0	0.171	0.025
Liquid Water	68	20	4.175	0.602
Snow	Freshly Fallen		4.147	0.598
	32	0	15.257	2.200
Ice	32	0	15.534	2.240
	-4	-20	16.921	2.440
EPS Insulation Nominal 16 kg/m^3 (1 pcf)	75	24	0.267	0.0384

The importance of removing any water in the vicinity of the insulation can be seen, by comparing the thermal conductivity of water vapor to that of either liquid water (approximately 25 times that of air or water vapor) and ice (approximately 100 times greater than that of water vapor and four times greater than that of liquid water) in contact with the insulation.

Capillary movement of moisture is eliminated in closed cellular plastic insulations such as EPS. Limited water absorption is possible as a result of redistribution of moisture through vaporization and condensation mechanisms as a result of the prevailing thermal gradient. However, when used as below-grade foundation wall insulation, the surface of EPS insulation will act as a capillary breaking layer between the soil and foundation. In other words, the closed cell structure of EPS insulation resists movement of water into the insulation.

Research conducted at the National Research Council in Ottawa, Ontario, Canada [*3*] as part of the Exterior Insulation Basement System (EIBS) project confirmed that if adequate provision for drainage were provided at the base of a foundation wall, the exterior surface of EPS insulation on the foundation wall would act as a capillary breaking layer providing a drainage plane to drainage tile at the base of the wall.

Water Absorption

The test parameters required by laboratory test procedures specified in material standards, such as CAN/ULC-S701 and ASTM C578, do not correlate to field

performance of EPS insulation in that they call for submersion of the test specimen under a head of water, which would not be encountered in normal applications. This lack of correlation is recognized in Appendix Clause X1.4 of ASTM C 578, which states that water absorption characteristics may have significance when end-use of the material requires exposure to water for extended periods of time. CAN/ULC-S701 highlights an excerpt from the '*Significance and Use*' section of ASTM D2842, Standard Test Method for Water Absorption of Rigid Cellular Plastics, which states the following:

> *The purpose of this test is to provide a means for comparing relative water absorption tendencies between different cellular plastics. It is intended for use in specifications, product evaluations, and quality control. It is applicable to specific end-use design requirements only to the extent that the end-use conditions are similar to the immersion period (normally 96 h) and 5.1 cm. (2 in.) head requirements of the test method.*

Field Performance in Comparison to Laboratory Test Methods

Measurements of moisture content after long-term exposure in below-grade applications confirm the performance of EPS insulation. A number of published reports demonstrate that water absorption by EPS insulation exposed in actual applications over extended periods of time is much less than values indicated by laboratory test methods.

In 1995, the Expanded Polystyrene Association of Canada (EPAC) initiated a joint research program with the National Research Council of Canada/Institute for Research in Construction (NRC/IRC), to evaluate the performance of EPS insulation in an exterior insulation basement system application. EPS insulation was attached to the exterior of a foundation wall exposed to a soil backfill for a period of 30 months. The moisture content of EPS insulation samples removed after 30 month exposure was in the range of 0.01 to 0.96% by volume [*4*].

The Norwegian Public Roads Administration (NPRA) has approximately 30 years of experience with the use of EPS as a lightweight fill material in road applications. The NPRA has monitored the performance of EPS lightweight fill material (Table IV) by extracting samples from a number of lightweight fill applications [*5*].

Table IV – Testing Frequencies on EPS Embankments

Fill Location	Constructed	Test Samples Retrieved			
National road 159 Flom bridges	1972/ 73	0	7	12	24
National road 154 Solbotmoan	1975	4	9	21	
County road 91 Lenken	1978	6			
County road 26 Langhus	1977	7			
National road 610 Sande – Osen	1982	9			

Tests performed on EPS lightweight fill samples retrieved from three of the above applications where the EPS blocks were placed in a drained condition (i.e. blocks located above the groundwater or flood level) confirmed all moisture contents were below 1% by

volume after almost 30 years in the ground. Furthermore, there was hardly any change in the moisture content with time.

A Finnish study comparing results from laboratory water absorption test methods to values from field applications (Table V) found that actual water absorption in below grade applications was less than half that predicted by laboratory test values.

Table V – Moisture Content of EPS Frost Insulation from Site Investigations and after 28-Day Immersion Tests Done for the Same Sets of Material [6]

Age (Years)	Dry Density (kg/m^3)	Moisture Content (%/Vol.)		Ratio Immersion Test/In the Field
		In the Field	Water Immersion	
5	15.0	1.8	5.2	2.9
6*	19.7	1.1	6.2	5.6
6*	19.7	0.03	6.2	>>max
7	14.5	5	3.1	0.6 min
8	13.4	0.5	4.3	8.6
8	13.7	1.7	5.1	3.0
8	14.1	1.7	5.1	3.0
8	24	2.1	2.1	1.1
9	16.6	2.5	3.8	1.5
11	10.7	2.4	1.9	0.8
11	11.4	1.3	3.9	3.0
14	24.1	1.8	5.1	2.8
15	15.4	6.8	---	---
16	15	2.8	---	---
18	17.8	0.6	---	---
Average	16.3	2.1	4.3	>2

Water Vapor Permeance

The ability of a material to resist water vapor movement through it depends upon its water vapor permeability characteristic. Water vapor permeability characteristics of rigid cellular plastic insulation are determined using ASTM E96-00, Standard Test Methods for Water Vapor Transmission of Materials, and are a function of product thickness.

Water vapor transmission through a material is the passage of water in the vapor phase through the material. Capillary movement of moisture is eliminated in closed cellular plastic insulation such as EPS insulation; therefore, redistribution of moisture

* Values are for two samples (double EPS boards 2 x 50 mm) taken from the same site with the first figure relating to upper board.

occurs through vaporization and condensation mechanisms as a result of the prevailing thermal gradient. For this reason, most moisture gain in field applications of EPS insulation is restricted to either the surface cells or as water vapor in the interstitial spaces, rather than absorbed moisture.

A significant vapor drive (i.e. temperature/vapor pressure differential) is required in order to induce water vapor movement into EPS insulation based upon the maximum water vapor permeability values specified for S701 and C578 EPS insulation product types. A 1986 University of Minnesota Underground Space Center study of existing research related to foam plastic used in below grade applications offered the following comment on water vapor pressure differentials encountered in typical below-grade insulation applications [*7*]:

Building/ground vapor pressure differentials should seldom exceed 0.30" Hg (1015 Pa vapor pressure) outwards and 0.50" Hg (1690 Pa vapor pressure) inwards. Laboratory test results at this level of vapor differential did not result in a significant absorption of moisture.

In comparison to other common building materials, EPS insulation has moderate water vapor permeability per unit of thickness.

Compressive Stress

EPS insulation compressive stress/strain characteristics are determined using ASTM D1621-00, Standard Test Method for Compressive Properties of Rigid Cellular Plastics, or ASTM C165-00, Standard Test Method for Measuring Compressive Properties of Thermal Insulations. Compressive strength values included in material standards and specifications for cellular plastics, including EPS insulation, are typically compressive stress characteristics at 10% strain (deformation from original thickness). The compressive stress at 10% strain is not failure strength, but rather is intended for product evaluations and quality control, as well as for comparing relative compressibility of different cellular plastics. Compressive stress characteristics for EPS insulation are closely related to product density.

EPS Design Principles

The compressive stress at 10% deformation is not used for design purposes when EPS insulation is to be subjected to short or long term compressive loads. If specific compressive loads are anticipated, the required compressive stress characteristic can be determined by a review of the type and duration of load (short or long term). As well, independent of the nature of the load, the loaded area must be calculated from the load contact area based upon the structure of the layer above the insulation (reinforced concrete slab or loose material such as composite paving on a sand or gravel bed).

Once the nature of the loading and type of stress distribution layer above the EPS insulation are known, a calculation flow diagram [*8*] (Figure 1) can be followed to assess:

- The type and magnitude of the load
- Load distribution from contact area through overlay material into EPS insulation
- Determination of the maximum load transferred to the insulation.

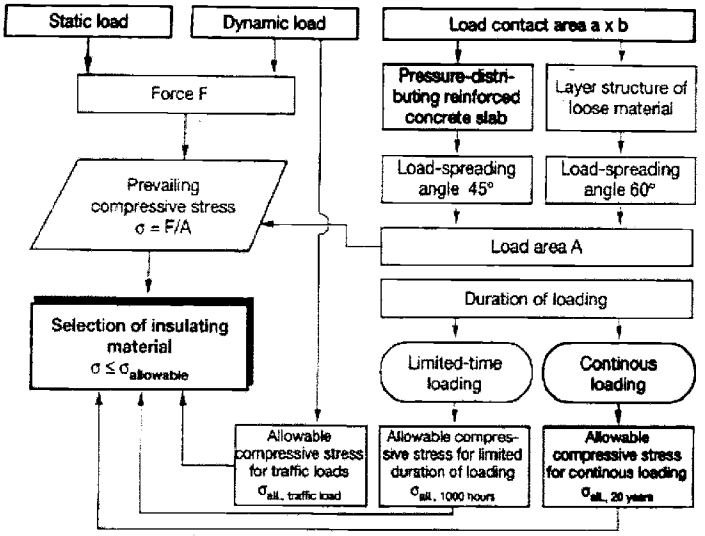

Figure I - Calculation Flow Diagram

EPS insulation type is then selected from a review of the stress calculation based upon compressive properties. Typically, compressive properties used for design purposes are either compressive stress within the elastic limit or compressive modulus.

Compressive properties of EPS insulation can be obtained from a variety of industry publications in order to enable designers to select a product density (Table VI) for *preliminary* design purposes. The range of compressive properties below is intended for *preliminary* design purposes only.

Table VI – Compressive Properties of EPS Insulation

Minimum density	kg/m^3 (pcf)	16 (1.0)	24 (1.5)	32 (2.0)
Compressive stress at 10 % compressive strain	kPa (psi)	65 to 100 (9.4 to 14.5)	110 to 140 (16.0 to 20.3)	170 to 200 (25.0 to 29.0)
Compressive stress for sustained loads	kPa (psi)	25 to 35 (3.6 to 5.1)	50 to 60 (7.2 to 8.7)	70 to 90 (10.2 to 13.0)
Modulus of elasticity (compressive test)	kPa (psi)	2,500 to 3,500 (362 to 508)	5,000 to 6,000 (725 to 870)	7,000 to 9,000 (1,015 to 1,305)

Designers should consult EPS insulation manufacturers in their market area in order to determine specific EPS product types available. Compressive properties of EPS insulation will vary to some extent dependent upon specific manufacturing techniques and raw materials employed.

Sub-Slab Design Considerations

When placed over a compressible or elastic subgrade such as soil or EPS insulation, factors such as load distribution and transfer to the sub-slab insulation are often controlled by the response of the concrete slab itself to loads. Floor loads cause deflection as a function of both the concrete slab properties and the compressibility of the subgrade.

The degree of deflection of the floor slab establishes the magnitude of unit load transferred to the subgrade material, in this case EPS insulation. Deflection is determined by the following factors based on current slab-on-grade design theory:

- Load exposure
- Slab strength characteristics
- Subgrade (soil and insulation) response to load transfer.

Selection of a sub-slab insulation product has typically been based upon its ability to respond to compressive loads transferred from the slab, without full and accurate determination of the load distribution characteristics of the slab. However, with proper slab design, EPS insulation can deliver cost-effective thermal performance to the specifier and building owner. The need for higher strength, less cost efficient sub-slab insulation products is eliminated.

The load factor used to evaluate subgrade response (soil or insulation) is referred to as the modulus of subgrade reaction (k) or, in other cases, foundation modulus, k modulus, k value, etc. EPS insulation moduli of subgrade reaction values (Table VII) are derived from modulus of elasticity values determined in accordance with D1621or C165. k @ design thickness is derived by dividing k @ 25-mm (k @ 1") by specified insulation thickness.

Table VII – EPS Insulation Modulus of Subgrade Reaction

Minimum density	kg/m^3 (pcf)	16 (1.0)	24 (1.5)	32 (2.0)
k @ 25-mm	N/mm^3	2500 to 3500	5,000 to 6,000	7,000 to 9,000
k @ 1"	lbs/in^3	25 to 35 (3.6 to 5.1)	725 to 870	1,015 to 1,305

EPS Insulation Durability

A modified version of ASTM C666-97, Standard Test Method for Resistance of Concrete to Rapid Freezing and Thawing, has been one laboratory test procedure used in the past to assess 'freeze-thaw' resistance for cellular foam plastic insulation. This modified procedure uses up to 600 cycles of full-thickness freezing of an insulation sample in air and thawing by complete submersion in water to assess durability. The results from this test procedure do not correlate to conditions encountered with typical

application for an insulation product. The question becomes how many cycles of an inappropriate test procedure are required to create a 'failure' of the product, rather than how an insulation product will perform in an application.

ASTM Committee C16 recently approved a new test method, ASTM C1512-01, Standard Test Method for Characterizing the Effect of Exposure to Environmental Cycling on Thermal Performance of Insulation Products, for assessing durability of insulation products. This test method was initially developed as a draft protocol as part of the 1995 EIBS joint research project conducted by NRC/IRC and funded by EPAC [*9*]. Testing conducted as part of the project confirmed that the test method provided valid comparative ratings for the products tested versus field performance. The draft protocol was then further developed under Sub-Committee C16.33, Task Group C16.33.2 and received final approval as C1512 after successful ballot at ASTM Committee C16 meetings in October 2001.

Durability Performance versus Laboratory Test Methods

The study cited previously of foam plastic insulation performance in below-grade applications as prepared by the University of Minnesota Underground Space Centre concluded that:

1. Freeze-thaw testing involving hundreds of full-thickness freeze-thaw cycles of a fully or partially submerged insulation is poorly related to the expected performance of insulation for below-grade applications over a reasonable economic life for a building.
2. The impact of freeze-thaw cycling in a drained, below-grade building foundation application should not be large since the annual number of freeze-thaw cycles is small below grade, and little of the insulation thickness will experience sub-freezing temperatures.

In addition, the durability of EPS insulation in a below-grade application was demonstrated as part of the EIBS joint research project conducted by NRC/IRC. The in-situ thermal performance of the EPS insulation material was monitored continuously over the 30-month exposure period and found to be constant. The thermal and mechanical properties of material samples tested after removal from the application were also unchanged [*10*].

Conclusion

In the introduction section of this paper, EPS insulation property values as specified in CAN/ULC-S701 and C578 were provided. As noted, the material properties in these two recognized North American documents provide a means of comparing different cellular plastic thermal insulation and are generally intended for use in specifications, product evaluations and quality control. However, in many cases, they do not predict end-use product performance. Many factors influence the choice of the correct below-grade insulation product type used for such applications as foundation walls, frost-protected shallow foundations and beneath floor slabs.

The benefits of full-height exterior insulation basement systems (EIBS) have been recognized for some time. Exterior insulation provides many benefits such as reducing

interior temperature fluctuations, reducing thermal stresses in foundation walls, and preventing condensation on the interior face of basement walls. A report issued by the Housing and Urban Development Association of Canada (HUDAC) investigated performance of EPS insulation material and concluded that it was suitable for this application [*11*]. A later HUDAC publication provided recommendations on products and installation procedures [*12*].

A 1987 report by Canada Mortgage and Housing Corporation (CMHC) and the Canadian Home Builders Association (CHBA) [*13*] concluded that the use of insulation partway down the interior of the basement walls actually increases heat loss to the adjacent soil. The report recommended full-height insulation since the upper zone insulation is appreciably short-circuited by the heat loss from below.

An externally insulated wall eliminates the possibility of concealed condensation, one problem that may be difficult to remedy with interior basement insulation. Because externally insulated basement walls remain warm during winter, the risk of condensation is eliminated. In addition, a CMHC sponsored study concluded that hidden moisture in finished basement wall assemblies of new homes could be traced to dissipation of moisture trapped within the concrete as a result of finishing the interior of the basement before the concrete foundation wall had sufficient time to dry [*14*].

Material properties required for the selection of the correct EPS insulation product for below-grade applications and performance characteristics are discussed in this paper. In addition to identifying material properties considered important in below-grade applications, current laboratory test methods used for measuring the property, where applicable, are cited. Actual EPS product performance is summarized from a number of publications highlighting the fact that molded expanded polystyrene (EPS) products have been used successfully for over 40 years in below-grade applications.

References

[1] Khanpara, J. C., and Sirdeshpande, G., 'Heat Transfer Through Elastomeric Foams – A Review', *Rubber and Chemistry Technology,* Volume 66.

[2] 1997 ASHRAE *Handbook of Fundamentals*, American Society of Heating, Refrigeration and Air-Conditioning Engineers, Atlanta, GA, Chapter 36, Tables 1, 2 and 3, pp 36.1 –36.4.

[3] Swinton, M.C., Bomberg, M.T., Kumaran and Maref, 'In situ Performance of Expanded Molded Polystyrene in the Exterior Basement Insulation System (EIBS)', *Journal of Thermal Envelope & Building Science*, Vol. 23, October 1999.

[4] Normandin, N., Maref, W., Bomberg, M. T., and Swinton, M.C., 'In-Situ Performance Evaluation of Exterior Insulation Basement Systems (EIBS) – EPS Specimens', NRC Report No. 3132.1, March 1999.

[5] Nordic Road Transport Research Report 1-2000, 'Long-Term Performance and Durability of EPS as a Lightweight Fill', Norwegian Public Roads Administration.

[6] Ojanen, T. and Kokko, E., 'Moisture Performance Analysis of EPS Frost Insulation,' *Insulation Materials: Testing and Applications: Third Volume, ASTM STP 1320*, R.S. Graves and R.R. Zarr, Eds., American Society for Testing and Materials, West Conshohocken, PA, pp. 442-455, 1997.

[7] A Review Analysis of Published Laboratory and Field Tests, 'Moisture Absorption and its Effect on the Thermal Properties of EPS Insulation for Foundation Applications', University of Minnesota Underground Space Centre, October 1986.

[8] BASF Technical Information, 'Styrodur in Load-Bearing Applications', Report JK/re/0002e, April 1993.

[9] Normandin, N., Bomberg, and M. T., Swinton, M.C., 'Development of a Draft Test Protocol for Evaluating Durability Under Environmental Cycling of Insulation Products for Exterior Basement Applications', NRC Report No. 3132.2, December 1999.

[10] Swinton, M.C., Bomberg, M.T., Kumaran, M.K., Normandin, N., and Maref, W. 'Performance of Thermal Insulation on the Exterior of Basement Walls', *NRC Construction Technology Update* No. 36.

[11] Housing and Urban Development Association of Canada (HUDAC), External Insulation of Basement Walls, Phase II Report, Project T79-44, September 1981.

[12] Housing and Urban Development Association of Canada (HUDAC), External Insulation of Basement Walls, Brochure published in 1982.

[13] Canada Mortgaging and Housing Corporation/Canadian Home Builders Association, 'Builder's Workshop Series, House Foundations', 1987.

[14] Unies Ltd. 'Basement Condensation, Field Study of New Homes in Winnipeg', December 1987.

Therese K. Stovall,[1] Barbara A. Fabian,[2] Gary E. Nelson,[1] and David R. Beatty[2]

A Comparison of Accelerated Aging Test Protocols for Cellular Foam Insulation

Reference: Stovall, T. K., Fabian, B. A., Nelson, G. E., and Beatty, D. R., **"A Comparison of Accelerated Aging Test Protocols for Cellular Foam Insulation,"** *Insulation Materials Testing and Applications, 4th Volume, STP 1426*, A. O. Desjarlais and R. R. Zarr, Eds., ASTM International, West Conshohocken, PA, 2002.

Abstract: Both the ASTM Standard Test Method for Estimating the Long-Term Change in the Thermal Resistance of Unfaced Rigid Closed-Cell Plastic Foams by Slicing and Scaling Under Controlled Laboratory Conditions (C 1303) and the Standard for Determination of Long-Term Thermal Resistance of Closed-Cell Thermal Insulating Foams (CAN/ULC-S 770) are based on accelerating the foam aging process by slicing the foam into thin specimens. This accelerates the diffusion process so that thermal conductivity for foam insulation of varying thickness can be determined in a short period of time, typically less than one year. The C 1303 process calls for a series of measurements to define a relationship between thermal conductivity and a scaled aging time which is then analyzed to calculate the time-average thermal conductivity over any given service life. The S 770 process also uses scaled aging time, but uses the projected thermal conductivity at precisely five years of age to represent the insulation's useful service value. There is also a difference in how the thermal results are reported. The S 770 protocol calls for very careful determination of the initial thermal resistivity of a full thickness board, to which an aging factor is applied to determine the five-year value. The C 1303 protocol calls for reporting both the average thermal resistance for the selected thickness and service life and the aging curve data from the thin specimens. During a round-robin exercise performed in support of the S 770 standard, parallel measurements were made on the same specimens to permit application of the C 1303 procedure. This paper presents the results of that comparison for several types of foam. This paper also gives more explicit instructions on the proper application of the C 1303 methodology than is found in that document.

Keywords: Insulation, Closed-Cell Foam, Accelerated Aging, Diffusion, Thermal Conductivity, Thermal Resistance

Introduction

[1] Oak Ridge National Laboratory, P.O. Box 2008, Oak Ridge, TN 37831.
[2] Owens Corning, 275 Southwest Ave, Tallmadge OH 44278.

Introduction

There are several different types of foam insulation products. Some contain only atmospheric gases and others are made with an open cellular structure. These types of insulation may show a change in thermal properties during a very short time period after fabrication, but are then stable over their service life. Other foam products consist of a closed cellular structure, which may be filled with a gas specially selected for its low thermal conductivity. However, over a long period of time, these low-conductivity gases diffuse through the thickness of the foam, and atmospheric gases diffuse into these same closed cellular volumes. Because of this gas movement, the overall thermal conductivity of the insulation product changes over time. This phenomenon is typically called "aging".

Both the American Society for Testing and Materials (ASTM) and the Underwriters' Laboratories of Canada (ULC) have recognized the foam-aging phenomenon and on-going efforts within these standards-setting organizations are seeking to improve the quality of information available about these products. The ASTM method is described in the ASTM Standard Test Method for Estimating the Long-Term Change in the Thermal Resistance of Unfaced Rigid Closed-Cell Plastic Foams by Slicing and Scaling Under Controlled Laboratory Conditions (C 1303). The ULC procedure is described in the Standard for Determination of Long-Term Thermal Resistance of Closed-Cell Thermal Insulating Foams (CAN/ULC-S 770).

Accurately identifying the thermal properties of the insulation products is important for several reasons. First, designers need accurate material specifications to determine the heating and cooling loads for buildings and appliances. If the insulation's thermal properties are not properly determined, the heating and cooling equipment could be undersized for the loads. Second, these insulation products are compared to other insulation products on both price and performance. It is important that the performance be accurately described and understood by the consumer.

Initial efforts to provide useful information resulted in the use of a 180-day aging period for foam insulation products subject to aging. However, as will be described here, that process is flawed in its ability to properly represent the thermal performance of many products.

Diffusion 101

In order to enhance its insulating qualities, foam products are often produced with low-conductivity gases. It is obviously desirable to maintain these gases within the foam's cells for as long a time as possible. However, diffusion processes continuously release these low-conductivity gases, and also allow the incursion of atmospheric gases.

The diffusion of multiple gases through foam products is well understood and described fully in reference [*1*], which in turn includes 50 references on the subject. First, the rate of gas movement through the foam is different for different gases. Two gas characteristics, molecular size and the relative solubility of the gas in the polymer matrix, affect the rate at which gases diffuse in and out of the foam. Smaller molecules, such as air molecules, migrate through the foam's cellular spaces at a much faster rate than larger molecules. Larger molecules, including some of the low-conductivity gases originally

placed in the cells, move through the foam at a much slower rate, sometimes requiring many years to fully diffuse out of the foam. Second, the rate of gas movement through the foam is proportional to the thickness of the material squared. For example, if one foam product is ½ as thick as another product manufactured from the same materials, it will reach its fully aged status in 1/4 the time required for the thicker specimen.

Because of this relationship between the foam's composition and thickness and the progress of the gas diffusion phenomena, the 180-day aging period produces vastly different results for different foam products. For example, a ½-in. thick foam insulation product may be very close to equilibrium properties at the end of 180 days. But a 2-in. thick foam insulation product would still be in the fast-changing portion of its aging process (when air is entering the cells), and would still show a much higher thermal resistance that it would ultimately provide to the customer. Similarly, depending on the polymer and gas composition, some foams will age much faster than others, so that some will have reached their equilibrium value in 180 days and others will not.

Defining Thermal Performance

The apparent thermal conductivity of the foam is affected by the gas composition within the foam. Because the gas composition is changing with time, the apparent thermal conductivity is also changing. This instantaneous apparent thermal conductivity will be referred to throughout this paper as λ. If you want to determine the amount of heat that passes through a layer of insulation over an extended period of time, you need a time-averaged apparent thermal conductivity, referred to in this paper as λ_{avg} and defined in Eq. 1, where SL is the service life and τ is time.

$$\lambda_{avg} = \frac{\int_0^{SL} \lambda d\tau}{SL} \tag{1}$$

The service life of a foam insulation product can vary depending on its application, from 15 to 20 years for a refrigerator to 30 years for a basement wall. However, it is not necessary to monitor the thermal conductivity over such a long period of time in order to determine λ_{avg}. The squared relationship between foam thickness and gas diffusion time makes it possible to accelerate the aging of a foam product by slicing the foam into thin pieces. Both C 1303 and S 770 take advantage of this acceleration method to provide a better characterization of the foam's thermal performance than is currently available with the 180-day aging period. An abbreviated summary of each procedure is shown in Table 1. A portion of the C 1303 procedure is not included in this summary. Specifically, the tests for homogeneity and the calculation of the thickness of the destroyed surface layer have been omitted. These omissions would not be acceptable if the foam was a new product of unknown characteristics. However, all the products tested here have been tested previously and these data show that the thickness of the destroyed surface layer has a negligible effect on the results for specimens thicker than about 0.8 cm.

Despite the fundamental similarity of their accelerated aging methods, there are some differences between the two approaches. The S 770 method selects a 15-year service life

and three product thicknesses as typical and uses λ at an age of five years to represent λ_{avg} for a 15-year service life. This relationship was derived using a logarithmic model for the aging phenomenon[2]. The C 1303 method defines λ_{avg} as a function of the product's service life and thickness, but doesn't specify a particular service life or thickness. Both methods are applicable to homogenous foam insulation products, and both define homogeneity by comparing the aging of surface slices to core slices. However, C 1303 bases its reported results on a stack of core slices or a mixed stack of core and surface slices, while S 770 bases its reported results on whichever type of specimen, core or surface, shows the least aging.

Another point of difference lies in the way the thin-slice thermal conductivity data are applied to determine λ at a given point in time. S 770 uses a ratio of the five-year thin-slice λ to the initial thin-slice λ, and applies that ratio to λ of a freshly-manufactured full thickness specimen. C 1303 discusses the application of an aged ratio to the freshly-manufactured full thickness value as a way to account for the effect of the destroyed

Table 1 – *An Abbreviated Comparison of C 1303 and S 770*

C 1303	S770
	Measure the as-manufactured λ of the full thickness product.
Cut the foam into pieces 30 x 30 cm (12 x 12 in). If using a rotary slicer, prepare one to two slices from the core of each piece. If using a band saw, prepare up to four slices from a five cm-thick specimen.	Slice the material with very smooth surfaces, meeting prescribed tolerances on the distribution of the specimen thicknesses. Produce both surface and core slices and test them separately.
Measure λ of a stack of several thin slices immediately after slicing and several times during the first few weeks. Take a minimum of ten measurements over the course of a year, with the latter few measurements spanning larger time steps.	Measure the initial λ of the surface and core specimen stacks within two hours of their production. Use the average specimen thickness for each stack to precisely determine the test time that corresponds to a full-thickness age of five years for three specified product thicknesses. Measure λ for both the core and surface stacks on the dates calculated.
Using the average slice thickness, the times of each test, and the measured λ, represent λ as a function of scaled time (time divided by the square of the average specimen thickness). Calculate λ_{avg} for the desired service life and product thickness. Report this value and the overall functional relationship.	Compare the ratios of the five-year λ to the initial (two-hour) λ for the surface and core stacks of specimens. Using the lower of the two ratios, multiply that ratio times the as-manufactured λ of the full thickness product. Report the reciprocal of this value.

surface layer. Based on experience with commonly used products and test specimen thicknesses, however, this practice has been eliminated, and the C 1303 results are based directly on the measured thin-slice values, without any use of an initial full-thickness value.

Results

Comparing C 1303 to Full-Thickness Aging Data

The C 1303 procedure was first published by ASTM in 1995, but was in development for some time before then. During that time there have been several instances where parallel data were taken to compare the predicted aging values from C 1303 to actual full-thickness aged specimens. Some of that data for extruded polystyrene (XPS) and polyisocyanurate (PIR) is presented in Table 2. The XPS specimens were aged under laboratory conditions, the PIR specimens were aged in a field installation. Although many of the full thickness specimens were measured after only one year, 53 specimens have been aged for five years, and show that C 1303 provides estimates of the five-year aged λ accurate to within 2%.

Comparing S 770 to C 1303

During a round robin exercise performed in support of the S 770 standard, parallel

Table 2 – *Comparison of Aged Full-Thickness Thermal Resistance to That Predicted by C 1303*

Data source	Foam type and thickness	Age (yr)	Number of specimens	Standard deviation (% of $1/\lambda_{\text{full thickness}}$)	$\lambda_{\text{full thickness}}/\lambda_{C1303}$ (or $R_{C1303}/R_{\text{full-thickness}}$)
Lab B*	XPS, 2.5 cm	1	11	2.6	1.01
Lab B*	XPS, 2.5 cm	5	12	2.4	1.02
Lab B*	XPS, 3.8 cm	1	11	2.5	1.01
Lab B*	XPS, 3.8 cm	5	12	2.4	1.01
Lab B*	XPS, 5.1 cm	1	26	2.0	1.01
Lab B*	XPS, 5.1 cm	5	29	1.9	1.01
Lab A [3]	CFC-11 PIR, 38 mm	1	1		1.00
Lab A [3]	HCFC-123 PIR, 38 mm	1	1		1.01
Lab A [3]	HCFC-141b PIR, 38 mm	1	1		0.99
Lab A [3]	HCFC-141b PIR, 38 mm	1	1		0.99

*Owens Corning data provided by author

Table 3 – *Comparing The S 770 Five-Year Aging Factor To The C 1303 15-Year Service Life Integrated Average. (All Measurements Lab A)*

Thickness (mm)	S 770 λ_0/λ_5 (equivalent to R_5/R_0) / C 1303 λ_0/λ_{avg} for 15 year service life		
	Product 1	Product 2	Product 3
50	**1.01**	**1.00**	**1.01**
75	**1.01**	**1.00**	**1.00**

measurements were made to permit application of the C 1303 procedure. A portion of these data are summarized in Table 3. This initial comparison considers only the thin-slice data, that is, it compares the S 770 "aging factor" to a similar ratio derived from the C 1303 λ_{avg}. For this comparison, the initial thin-slice λ was divided by the C 1303 λ_{avg} corresponding to a 15-year service life and the specified thickness (because the S 770 five-year λ values were selected to represent the λ_{avg} over a 15-year service life). There was insufficient data to calculate the C 1303 15-year service life λ_{avg} for the 25 mm product thickness. For the two thicknesses shown, the C 1303 ratios and S 770 aging factors agree within 1%.

The S 770 procedure, however calls for this ratio to be applied to the freshly-manufactured (between seven and 14 days old) full thickness λ. During this study, significant differences were noted between these full-thickness measurements and the initial (within two hours) thin-slice value. The λ of the full thickness specimens ranged between 3 to 7% lower than those for the thin slices at lab B, which used a band saw method and was therefore able to complete all the measurements within one day as specified in the S 770 procedure. Lab A used a slicer to prepare the thin slices, which is more time consuming, so that the thin slices were prepared one day after the full-thickness measurements were made. For Lab A, the full thickness λ values ranged from 0.4 to 2% lower than the initial thin slice measurements for the surface slices. When this portion of the S770 procedure (applying the ratio to the initial full-thickness slice) is included, S 770 can be compared to C 1303 as shown in Table 4. This table compares

Table 4 – *Compare Insulation R-Values Predicted By S 770 And C 1303 Five Years After Production, Values Shown are* $\lambda_{C\,1303}/\lambda_{S\,770}$ *(Equivalent to* $R_{S\,770}/R_{C\,1303}$*).*

	Lab A	**Lab B**	**Lab B**	**Lab B**
Product 1, 25 mm	1.03			
Product 1, 50 mm	1.03			
Product 1, 75 mm	1.03			
Product 2, 25 mm	0.95			
Product 2, 50 mm	1.01	1.03		
Product 2, 75 mm	1.08			
Product 3, 25 mm	1.09	1.06		
Product 3, 50 mm	1.08	1.14	1.04	1.11
Product 3, 75 mm	1.08	1.20		

the five-year λ values from the C 1303 curve to the S 770 five-year λ values.

This comparison of results from the two procedures shows much larger differences. A portion of the difference, on the order of 1-2% for products 1 and 2, and from 2-5% for product 3, comes from comparing the S 770 surface-slice measurement to the C 1303 core or mixed-slice values. But a large part of the difference is due to the application of the aging factor to the initial full-thickness value. The thermal conductivity of freshly manufactured foam changes much more rapidly than that of older foam products[*4*]. Figure 1 shows an aging curve, or λ vs. time, for polyurethane foam from an evaluation of alternative blowing agents (other curves shown on this figure are discussed in the appendix)[*5*]. This prototypical curve shows just how sensitive λ is during the early life of a foam product, and why it may be problematical to define the initial thermal conductivity with a single measurement. The S 770 procedure acknowledges this sensitivity by requiring a thin-slice λ measurement within two-h of slicing, and the full-thickness within a carefully defined seven-day period. The C 1303 integrated average approach is much less sensitive to this initial value, because λ_{avg} weights each λ measurement by the elapsed time at that value, and the foam is in this fast-changing state for a relatively short period of time.

Conclusions

There are advantages and disadvantages to each approach. The S 770 approach is more useful for product rating purposes, because it produces a single value for each

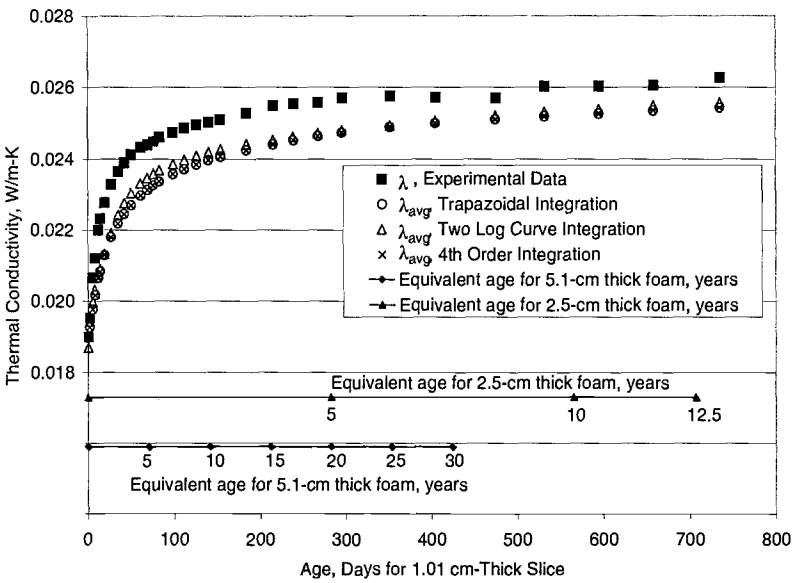

Figure 1. *Aging Data for Polyurethane Foam Blown with HCFC 141b, Aging in a 30 °C Environment [5]*

thickness. However, C 1303 is more useful in providing information necessary for application designs, because its curves give the fully aged value, as well as the average performance for *any* thickness or service life. The calculation procedures and data processing called for in S 770 are explicit and clear; the same cannot be said for the current version of C 1303. Also, given the C 1303 curve, the S 770 five-year value can usually be identified by interpolation. But the S 770 results cannot be used to calculate the C 1303 aging curve.

Although C 1303 tests usually involve a larger number of thermal conductivity measurements, that standard only calls for a minimum of 10 measurements. The S 770 calls for a total of 11 measurements and its test schedule can be challenging. As mentioned above, Lab A was unable to meet the requirements that the thin slices be prepared and measured during the same day as the full-thickness specimens are prepared and measured. Indeed, using a slicer, Lab A was just barely able to meet the two-h requirement for the initial thin-slice thermal conductivity measurement. There were also difficulties meeting the precise test dates, especially when one of the dates fell on December 31, 1999.

The significant differences reported here between the C 1303 five-year value and that produced by the S 770 procedure raise a number of questions and should be investigated more fully. These differences are partially attributable to the differing uses of core/surface slice values. There are also differences introduced by the use of the initial full-thickness R-value in S 770. It is hoped that a detailed examination of these results can lead to improvements in both methods, and perhaps a consensus approach to the identification of the insulation's service-life R-value.

Appendix: C 1303 Calculation Guide

One frequent complaint about the C 1303 method has been the lack of detailed data processing instructions within the standard itself. While processing the data for this analysis, a computer program was written to process the test data for the C 1303 calculations. Three different integrated average methods were included and are compared in Figure 1.

The two-log curve has traditionally been used for this procedure. In this method, the data for thermal conductivity are represented logarithmically and then regressed, over two regions, against the normalized time as shown in [2]. In performing these regressions, some judgment is necessary to distinguish between the two regions (the first region corresponds to the early rapid aging due to air diffusion into the cells and the second region to the later slower aging due to the diffusion of blowing agents out of the cells) and to decide which data should not be used because it is in the transition between these two regions. The coefficients identified in these regressions are used to define an exponential expression for λ (as a function of time and thickness) that can be analytically integrated using Eq. 1, for any selected thickness and service life, to produce λ_{avg}.

Two numerical integration methods were also explored. The first is a very simple trapezoidal method, shown in Eq. 2.

$$\lambda_{avg} = \frac{\left(\sum_{n=1}^{N} (\tau_n - \tau_{(n-1)}) \times \frac{(\lambda_n + \lambda_{(n-1)})}{2}\right)}{\tau_N} \qquad (2)$$

where

λ_{avg} = integrated average thermal conductivity over total time τ_N,
τ = time,
N = number of data points corresponding to time τ_N,
λ_n = apparent thermal conductivity measured at nth point, and
τ_n = time corresponding to λ_n.

This approach sums the area under the original data curve, assuming each point is connected to the next with a straight line. A simple interpolation of this integrated value, based on the normalized time corresponding to any selected thickness and service life, can then be used to determine the average thermal conductivity. An example of this calculation is shown in Table 5, again using experimental data from [*5*]. The first and third columns represent the experimental data. The second column represents the time for each data point, normalized by dividing the days since slicing by the average slice thickness squared. The average slice thickness for this experiment was 1.018 cm. The last column is calculated using Eq. 2, and represents the integrated average thermal conductivity up to that point in time. To use this data, first select the desired product thickness and service life. For this example, a 30-year service life and a five-cm product thickness were chosen. The normalized time corresponding to this selection is 438 days/cm^2 (= 30 x 365 / 5 / 5). This value has been inserted in Table 5 between the two bounding experimental data points. A linear interpolation was then used to calculate λ_{avg} from the two bounding experimental data points. This underlined value, 0.02525 W/m-K, represents the average thermal conductivity that this five-cm thick product can be expected to provide over its 30-year service life.

The second numerical integration method also treats the experimental data as a differential equation and uses a fourth-order variable mesh solution to find the area under the curve.[*6*] For this application, the first three data points are evaluated using the trapezoidal method, with all subsequent points evaluated using the variable mesh fourth-order equations. These equations are not shown here because, as will be shown, the added complexity gave results equivalent to those obtained using the simpler trapezoidal method.

Table 5 – *Example of the Application of the Trapezoidal Integration Method to Determine λ_{avg} for Any Selected Service Life and Product Thickness, Data from [5].*

Time Since Slicing (days)	Normalized Time (day/cm^2)	λ (W/m-K)	λ_{avg} (W/m-K)
0.05	0.05	.01899	
5.35	5.16	0.02067	0.02050
19	18.33	0.02277	0.02201
69	66.58	0.02440	0.02300
83	80.09	0.02461	0.02363
140	135.1	0.02501	0.02420
296	285.6	0.02570	0.02469
405	390.8	0.02572	0.02521
	438 = 30x365/5/5		*0.02525*
735	709.24	0.02628	0.02547

Table 6 – *A Comparison of* λ_{avg} (W/m-K) for a *15-Year Service Live for Varying Amounts of Test Data, for Polyurethane Foam Blown with HCFC 141b, Aging in a 32 °C Environment, Original Data from[5].*

Foam Thickness (mm)	32 Data Points	17 Data Points	9 Data Points
37.5	0.0250	0.0250	0.0250
50	0.0245	0.0245	0.0244
75	0.0236	0.0236	0.0235

Figure 1 shows λ_{avg} for all three of these methods, along with the experimental λ values used in the calculations. At most points, the λ_{avg} values from all three integration methods are so close as to be indistinguishable. The only region where there is a small difference is in the transition region, between the early rapid aging due to air diffusion into the cells and the later slower aging due to the diffusion of blowing agents out of the cells. The two-log curve method doesn't use the data collected during this transition period and would be expected to be less accurate in this region. The trapezoidal method is clearly the simplest of the three, is most adaptable to a spreadsheet environment, and doesn't require the intermediate regression step. An Excel spreadsheet with Visual Basic macros has been written to calculate these values and is available at the ASTM web site (www.astm.org). One criticism of the C 1303 procedure has been the perceived need for large numbers of tests. A further examination of the same data set from [5] was made to explore this issue. Figure 2 and Table 6 summarize the results of using one-half the data (or every other data point) and one-fourth of the data (or every fourth point). These results indicate that the minimum number of data points specified by C 1303 should be sufficient, so long as they are appropriately spaced. Obviously, the time intervals between data points need to be shorter during the initial period when the foam is changing more rapidly.

Any C 1303 data set can also be used to generate S 770-style rating values, as shown in Table 7 (using the same data from [5]). For example, S 770 calls for five-year λ values for three product thickness, 25, 50, and 75 mm. Table 7 shows how the data can be used to generate these values, again using an interpolation based on the normalized time. Remembering that the five-year λ values were selected to represent the 15-year λ_{avg} values, Table 7B shows a similar interpolation for λ_{avg} on a 15-year service life. A comparison of the example values generated in Tables 7A and 7B is shown in Table 7C. Considering the greater amount of data reflected by the λ_{avg} values, and the reduced sensitivity of these values to the earliest data measurements, the λ_{avg} results should be used when possible. However, as this example shows, data is required for a much longer period, especially for thinner products. In these cases, $\lambda_{5\text{-year}}$ should produce values within 1-2% of the 15-year λ_{avg} results.

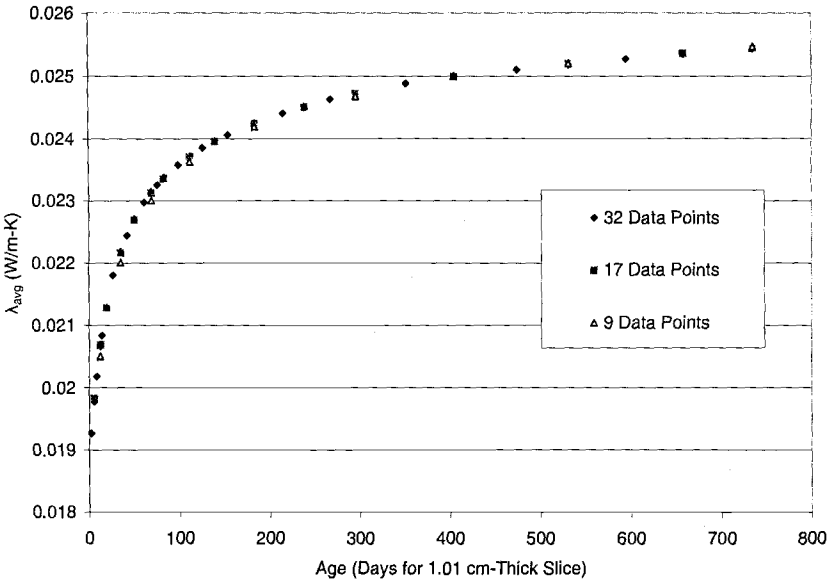

Figure 2. *A Comparison of the Average Apparent Thermal Conductivity for Varying Amounts of Test Data, for Polyurethane Foam Blown With HCFC 141b, Aging in a 32 °C Environment [5]*

References

[1] Bomberg, M.T., M. K. Kumaran, and Ascough, M., "Evaluation of Long-Term Thermal Performance of Cellular Plastics Revisited," *2nd International Workshop on Long-Term Thermal Performance of Cellular Plastics*, Niagara-on-the-Lake, Ontario, Canada, June 5-7, 1991.

[2] Graves, R. S., McElroy, D. L., Weaver, F. J., and Yarbrough, D. W., "Interlaboratory Comparison On Estimating The Long-Term Thermal Resistance Of Unfaced, Rigid, Closed-Cell, Polyisocyanurate (Pir) Foam Insulation – A Cooperative Industry/Government Project," ORNL/M-3976, Oak Ridge National Laboratory, Oak Ridge, TN, January, 1995.

[3] Christian, J. E., Courville, R. S., Linkous, R. L., McElroy, D. L., Weaver, F. J., and Yarbrough, D. W., "Thermal Measurement of In-Situ and Thin-Specimen Aging of Experimental Polyisocyanurate Roof Insulation Foamed with Alternative Blowing Agents," *Insulation Materials: Testing and Applications, 2nd Volume, ASTM STP 1116*, R. S. Graves and D. C. Wysocki, Eds., American Society for Testing and Materials, Philadelphia, 1991.

Table 7A – *Example of the Application of the Trapezoidal Integration Method to Determine $\lambda_{5\text{-year}}$ for S 770 Rating Conditions, Data from [5]*

Time Since Slicing (days)	Normalized Time (day/cm^2)	λ (W/m-K)	λ_{avg} (W/m-K)
0.05	0.05	.01899	
5.35	5.16	0.02067	0.02050
19	18.33	0.02277	0.02201
	32.4=5x365/7.5/7.5	**0.02325**	
69	66.58	0.02440	0.02300
	73.=5x365/5/5	**0.02450**	
83	80.09	0.02461	0.02363
140	135.1	0.02501	0.02420
296	285.6	0.02570	0.02469
	292=5x365/2.5/2.5	**0.02570**	
405	390.8	0.02572	0.02521
735	709.24	0.02628	0.02547

Table 7B – *Example of the Application of the Trapezoidal Integration Method to Determine λ_{avg} for S 770 Rating Conditions, Data from [5]*

Time Since Slicing (days)	Normalized Time (day/cm^2)	λ (W/m-K)	λ_{avg} (W/m-K)
0.05	0.05	.01899	
5.35	5.16	0.02067	0.02050
19	18.33	0.02277	0.02201
69	66.58	0.02440	0.02300
83	80.09	0.02461	0.02363
	97.3=15x365/7.5/7.5		**0.02356**
140	135.1	0.02501	0.02420
	219=15x365/5/5		**0.02400**
296	285.62	0.02570	0.02469
405	390.8	0.02572	0.02521
735	709.24	0.02628	0.02547
	876=15x365/2.5/2.5		**Extrapolation not recommended**

Table 7C– *Summary of Example Problem Using C 1303 Data Analysis to Produce S 770 Type Rating Values*

Product Thickness	Rating Based on $\lambda_{5\text{-year}}$ (W/m-K)	Rating Based on $\lambda_{avg,\ 15\text{-year}}$ (W/m-K)	Difference (%)
25 mm	0.02570	Not available	
50 mm	0.02450 (5.9 R/in.)	0.02400 (6.0 R/in.)	2.0
75 mm	0.02325 (6.2 R/in.)	0.02356 (6.1 R/in.)	1.3

[4] Hilyard, N.C., and Cunningham, A., *Low Density Cellular Plastics, Physical Basis of Behaviour, Chapman and Hall, London, 1994.*

[5] Wlkes, K. E., Gabbard, W. A., Weaver, F. J., and Booth, J. R., "Aging of Polyurethane Foam Insulation in Simulated Refrigerator Panels – Two-Year Results with Third-Generation Blowing Agents," *Proceedings of the Polyurethanes 2000 Conference, Boston, MA, Oct. 8-11, 2000, pp. 417-428.*

[6] Van Wyk, R., "Variable Mesh Methods for Differential Equations," NASA CR-1247, NTIS, Springfield, VA, November 1968.

Appendix

David L. McElroy[1] and John A. Scott[2]

ASTM C16 Survey for Heat Transfer Test Method Equipment

Reference: McElroy, D. L. and Scott, J. A., "**ASTM C16 Survey for Heat Transfer Test Method Equipment**," *Insulation Materials: Testing and Applications, 4th Volume, ASTM STP 1426*, A. O. Désjarlais and R. R. Zarr, Eds., ASTM International, West Conshohocken, PA, 2002.

Abstract: Committee C16 on Thermal Insulation has conducted two surveys to determine the availability of test equipment in North America that meets the requirements for the following five ASTM standards[3]:

1. Standard Test Method for Steady-State Heat Flux Measurements and Thermal Transmission Properties by Means of the Guarded-Hot-Plate Apparatus (C 177);
2. Standard Test Method for Steady-State Thermal Transmission Properties by Means of the Heat Flow Meter Apparatus (C 518);
3. Standard Test Method for Steady-State Heat Transfer Properties of Horizontal Pipe Insulation (C 335);
4. Standard Test Method for Steady-State Heat Transfer Properties of Pipe Insulation Installed Vertically (C 1033); and,
5. Standard Test Method for Steady-State Thermal Transmission Properties by Means of the Thin-Heater Apparatus (C 1114)

The surveys were conducted during 2000 and 2001 and the results will assist in the continued development of the above C16 test methods by identifying potential participants for future interlaboratory round robins.

Keywords: guarded hot plate, heat flow meter, heat flux, pipe insulation, steady state, survey, test equipment, thin heater

Introduction

In the late 1990s Committee C16 on Thermal Insulation formed a new task group to identify laboratories willing to participate in future interlaboratory studies conducted by ASTM Committee C16. This appendix describes the scope, history, and results of the surveys conducted by the task group.

[1] Consultant, 7914 Gleason Drive, Knoxville, TN, 37919
[2] Technical Services and Standards Manager, Roxul Inc, 551 Harrop Drive, Milton, ON, L9T3H3
[3] *Annual Book of ASTM Standards*, Vol. 04.06.

Scope

The scope for task group C16.30.1.6 on Test Equipment Inventory And Training is as follows: *Conduct a survey of C16.30 test methods equipment availability in North America. Initially, this will include equipment that meets five standards: C 177, C 518, C 335, C 1114, and C 1033. This information may benefit existing test method standards and future interlaboratory round robins.*

History

In June 2000, ASTM Headquarters distributed to C16 members the Equipment Survey (ES-2000) given in Addendum A. The survey was also distributed to NVLAP laboratories accredited for thermal insulation testing and purchasers of thermal insulation SRMs. Information was sought about apparatuses in North America that complied with the technical requirements of five standards: C 177, C 518, C 335, C 1033, and C 1114. Table 1 summarizes the results of responses to ES-2000.

Table 1 – *List of Nineteen (19) Responders to Equipment Survey - 2000 (ES-2000)*

Organization	Contact	C177	C518	C335	C1114	C1033
Anter Corporation	Peter Gaal	1	1	0	0	0
Armacell LLC	Paul Hough	0	1	0	0	0
Celotex Technical Center	R. Gerry Miller	0	7	0	0	0
Dow Chemical Co.	George Lennox	0	1	0	0	0
Geoscience Ltd	Heinz F. Poppendiek	7	7	5	3	0
Holometrix	Tim Kunz	4	2	1	0	0
Integrex Testing Systems	John R. Mumaw	2	3	1	1	0
Johns Manville	Michel Drouin	0	2	0	0	0
Knauf Fiber Glass GmbH	Timothy R. Jonas	2	2	2	0	0
L. L. Bean, Inc.	Daniel Otis	0	1	0	0	0
Mexmil Company	David Indyke	0	1	0	0	0
NIST	Robert Zarr	2	2	0	0	0
Owens Corning	Barbara Fabian[1]	0	3	0	0	0
Precision Measurement and Instrument Co.	Heng Wang	1	1	0	0	0
R&D Services, Inc.	Ronald S. Graves[1]	0	1	0	0	0
RADCO	Mike Zieman	0	1	0	0	0
Thermal Visions, Inc.	Dwight Musgrave	0	1	0	0	0
Tutco Scientific	F. B. Hutto	1	1	2	0	0
Underwriters Laboratory	Ken Rhodes	0	1	0	0	0
Total		*20*	*39*	*11*	*4*	*0*

[1]Also responded to ES-2001 (see Table 2)

To obtain additional responses, in April 2001 ASTM Headquarters distributed to C16 members ES-2001, a one-page Equipment Survey, given in Addendum B. Later, in July 2001, Kevin P. Collins from Lasercomp distributed the same survey to their customers for additional input to be included with the survey results from C16 membership. Table 2 summarizes the results of responses to ES-2001.

Table 2 – *List of Twenty-one (21) Responders to Equipment Survey - 2001 (ES-2001)*

Organization	Contact	C177	C518	C335	C1114	C1033
Architectural Testing, Inc.	Richard Troyer	0	2	0	0	0
BASF Corporation	Roy Pask	0	2	0	0	0
Dow Chemical Co. – GA	Stacy Blake	0	1	0	0	0
Dow Chemical Co. – IL	Robert Braun[1]	0	1	0	0	0
Dow Chemical Co. – IL	Jess Garcip[1]	0	2	0	0	0
Dow Chemical Co. – MI	Linda M. Hess	0	3	0	0	0
DuPont Co.	Joe Creazzo	0	0	0	0	0
Firestone Building Products	Tim Tackett	0	4	0	0	0
Foam Enterprises	Abbas Shekari	0	1	0	0	0
General Plastics Mfg. Co.	Kathy Devlin-LaFountaine	0	1	0	0	0
Huntsman Polyurethanes	John Bowers	0	5	0	0	0
Insultech Inc.	Les Truksa	0	1	0	0	0
Johns Manville, JMTC	Mark Albers	3	16	4	1	0
Lasercomp, Inc.	Kevin P. Collins	1	10	0	0	0
Mesa Insulation	Rick L. Dolin	0	0	1	0	0
NAHB Research Center	Thomas Kenney	0	4	0	0	0
OC Celfortec, Inc.	Micheline Roy	0	1	0	0	0
OSI Specialties	K. M. Stalnaker	0	2	0	0	0
Owens Corning	Barbara Fabian[2]	0	3	0	0	0
R & D Services, Inc.	Ronald S. Graves[1, 2]	0	3	0	0	0
Tennessee Technological University	David W. Yarbrough[1]	0	1	0	0	0
Total		*4*	*63 (58)*[3]	*5*	*1*	*0*

[1]Responder represents same laboratory facility.
[2]Also responded to ES-2000 (see Table 1).
[3]Total excludes duplications.

A total of 40 responses (addresses are given in Addendum C) were obtained from both ES-2000 and ES-2001; however, only 36 responses were considered unique because of some duplication as noted above. Table 3 summarizes the grand total for the 2000 and 2001 surveys (excluding duplications).

Table 3 – *Grand Total of Available Apparatus (By Test Method)*

	C 177	C 518	C 335	C 1114	C 1033
Number of Apparatus	24	97	16	5	0

Discussion

Of the responders, 36 were willing to participate in future round robins sponsored by ASTM C16. Table 4 lists their specific suggestions with regard to ASTM standards and apparatuses.

Table 4 – *Comments Given by Responders Concerning ASTM C16 Standards*

#	Comment
1	Too complicated. Most people do not take the time to read and understand. Not friendly.
2	C 1114 needs a round robin.
3	It would be beneficial to industry that NIST develop a user-friendly standard reference material one day that could be used over and over on C 335 apparatus.
4	Run round robin at more than one temperature.

The responders provided a variety of suggestions for potential materials to be used in future C16 interlaboratory studies and the comments are given in Table 5. The minutes of six meetings of this task group are given in Addendum D.

Table 5 – *Suggested Materials for Use in Future Interlaboratory Round Robins*

#	Comment
1	Fiberglass and Some type of foam.
2	C 1086 needled material for high temperature.
3	Reinforced plastics or resin plates for C 1114 (higher k @ 75 °F).
4	Vacuum insulation or foam.
5	Suggest each task group consult E 691 to plan test program, including materials.
6	Extruded polystyrene foam (XPS).
7	Aircraft grade fiberglass insulation (per ASTM C 800).
8	Extruded polystyrene insulation foam and bead board.
9	For C 335 or C 177 or C 518 Xonotlite PC (Xonotlite BD).
10	We use our apparatus primarily for clothing and bedding tests.
11	Pyroceram 9606, fused Silica, and alumina.
12	Noncellular polymers, evacuated panels.
13	(Polyurethane) Rigid closed cell foams from our company-various product lines and densities.
14	Batts, blown insulations, foam boards.

15	There is a need for standards in the 1 - 3 Btu-in/hr-ft^2-°F range to be used for computer simulation in the fenestration industry.
16	Expanded polystyrene/Xpanded polystyrene, Polyiso.
17	Non-aging foam board.
18	Polyurethanes.
19	Preformed mineral fiber, expanded polymer foams.
20	EPS thermal insulation.
21	Calsil, foam glass, mineral wool.
22	Rigid foam, 8 in. x 8 in. x 1 in. from boardstock mfg.
23	Polystyrene, polyurethane, polypropylene.
24	Rigid polyurethane "foam".
25	Rigid polyurethane foam, EPS board.
26	Polyisocyanurate cellular foam.

Conclusion

The results of these surveys indicate that there is considerable interest by C16 members and users in compiling (and maintaining) current data on the availability of equipment for Test Methods C 177, C 518, C 335, C 1114, and C 1033. The statistics of the surveys indicated that the largest number of apparatus in use were for C 518 (total of 97), followed by totals of C 177 (24), C 335 (16), and C 1114 (5). There were apparently no current users of Test Method C 1033. The responders also provided useful information on the test method standards and suggested materials for future interlaboratory round robins. The surveys identified several potential participants for future interlaboratory round robins. These results will assist ASTM C16 in planning future comparisons and for developing better standards.

Addendum A: Equipment Survey – 2000 (June 16, 2000)

Equipment Survey Questions - 2000***

Please complete this form. Thank you.

Name _____ Telephone _____

Company _____ Fax Number _____

Address _____ E-Mail Address _____

_____

_____

1. Are you willing to participate in future Interlaboratory Round Robins sponsored by ASTM C16?

_____

2. Can you suggest materials for consideration for an Interlaboratory Round Robin for your apparatus?

_____

_____

3. Do you have any specific suggestions about the ASTM standard that your apparatus(s) meet?

_____

_____

_____

4. Circle the Standard(s) that your apparatus(s) meet:

1. C177 (Guarded-Hot-Plate) 2. C518 (Heat-Flow-Meter) 3. C335 (Pipe-Insulation Apparatus)
4. C1033 (Vertical-Pipe Apparatus) 5. C1114 (Thin-Heater Apparatus)

Please proceed to the page of questions for your apparatus(s)

***Please return this form by October 1, 2000 to Ms. Melinda Long, ASTM, 100 Barr Harbor, West Conshohocken, PA 19428-2959. Thank You**

Addendum A1. C177 (Guarded-Hot-Plate Apparatus) Questions (April 16, 2000)

-Please use one page per apparatus-

1. Circle the items that describe your apparatus(s): Horizontal Plates Vertical Plates

Single Sided Double Sided Heat Flow Direction: Up Down Variable

Special (Please Describe) _____

2. Plate Dimensions (Please Do for Each Apparatus):

Total Plate Size (Guards + Meter) _____ in.

Plate Meter Size _____ in.

Guard(s) Size(s) _____ in.

Maximum Sample Thickness _____ in.

Minimum Sample Thickness _____ in.

3. Temperature Limits

Hot Face Maximum _____ Minimum _____

Cold Face Maximum _____ Minimum _____

Temperature Difference Across Specimen _____

Addendum A2. C518 (Heat-Flow-Meter Apparatus) Questions (April 16, 2000)
-Please use one page per apparatus-

1. Circle the items that describe your apparatus(s): Horizontal Plates Vertical Plates

Single Sided Double Sided Heat Flow Direction: Up Down Variable

2. Plate Dimensions (Please Do for Each Apparatus):

Total Plate Size _____ in.

Heat Flux Transducer Size _____ in.

Maximum Sample Thickness _____ in.

Minimum Sample Thickness _____ in.

Is Any Guarding Used? _____

3. Temperature Limits

Hot Face Maximum _____ Minimum _____

Cold Face Maximum _____ Minimum _____

Temperature Difference Across Specimen _____

Addendum A3. C335 (Pipe-Insulation Apparatus) Questions (April 16, 2000)
-Please use one page per apparatus-

1. Circle the items that describe your apparatus (s):

   Guarded-End Pipe Insulation Apparatus Calibrated-End Pipe Insulation Apparatus

   Horizontal Pipe Vertical Pipe

   Other (Please Describe)_____

2. Pipe and Sample Dimensions (Please Do for Each Apparatus):

Nominal Pipe Size _____in. Minimum Sample Outer Diameter _____in.

Exact Pipe Diameter _____in. Sample Length _____in.

Length of Each Guard _____in. Minimum Sample Thickness _____in.

Metered Length _____in. Maximum Sample Thickness _____in.

Total Length (Guards + Meter) _____in.

3. What is the minimum pipe surface temperature for testing with your apparatus?

   _____

4. What is the maximum pipe surface temperature for testing with your apparatus?

Addendum A4. C1033 (Vertical-Pipe Apparatus) Questions (April 16, 2000)
-Please use one page per apparatus-

1. Circle the items that describe your apparatus (s):

   Guarded-End Pipe Insulation Apparatus Vertical Pipe

   Other (Please Describe) _____

2. Pipe and Sample Dimensions (Please Do for Each Apparatus):

Nominal Pipe Size _____in. Minimum Sample Outer Diameter _____in.

Exact Pipe Diameter _____in. Sample Length _____in.

Length of Each Guard _____in. Minimum Sample Thickness _____in.

Metered Length _____in. Maximum Sample Thickness _____in.

Total Length (Guards + Meter) _____in.

3. What is the minimum pipe surface temperature for testing with your apparatus?

   _____

4. What is the maximum pipe surface temperature for testing with your apparatus?

   _____

Addendum A5. C1114 (Thin-Heater Apparatus) Questions (April 16, 2000)
-Please use one page per apparatus-

1. Circle the items that describe your apparatus(s): Horizontal Plates Vertical Plates

   Single-Sided Double-Sided Heat Flow Direction: Up Down Variable

   Special (Please Describe) _____

2. Heater Dimensions (Please Do for Each Apparatus):
   Heater Material _____

   Total Heater Size _____ in. Thickness _____ in.

   Meter Size _____ in. Guard(s) Size(s) _____ in.

   Minimum Sample Thickness _____ in. Maximum Sample Thickness _____ in.

3. Temperature Limits

   Hot Face Maximum _____ Minimum _____

   Cold Face Maximum _____ Minimum _____

   Temperature Difference Across Specimen _____

Addendum B: Equipment Survey - 2001* (April 17, 2001)**

Please complete this form. Thank you.

Name _____ Telephone _____

Company _____ Fax Number _____

Address _____ E-Mail Address _____

_____

_____

1. Are you willing to participate in future Interlaboratory Round Robins sponsored by ASTM C16?

_____

2. Can you suggest materials for consideration for an Interlaboratory Round Robin for your apparatus?

_____

3. Do you have any specific suggestions about the ASTM standard that your apparatus(s) meet?

_____

4. Circle the Standard(s) that your apparatus(s) meet and indicate the Number Owned:

Standard	Number Owned
1. C177 (Guarded-Hot-Plate)	_____
2. C518 (Heat-Flow-Meter Apparatus)	_____
3. C335 (Pipe-Insulation Apparatus)	_____
4. C1033 (Vertical-Pipe Apparatus)	_____
5. C1114 (Thin-Heater Apparatus)	_____

***Please return this form by September 1, 2001 to Mr. Timothy S. Brooke, ASTM, 100 Barr Harbor, West Conshohocken, PA 19428-2959. Thank You Very Much.**

Addendum C1: Addresses Of Nineteen Responders To ES - 2000

Name and Address	Telephone, Fax Number, and E-Mail Address
Peter Gaal Anter Corporation 1700 Universal Road Pittsburgh, PA 15235	(412) 795-6410 (412) 795-8225 (Fax) testing@anter.com
Paul Hough Armacell LLC P. O. Box 1038 Mebane, NC 27302	(717) 396-4195 (717) 396-4079 (Fax) pahough@armstrong.com
R. Gerry Miller Celotex Technical Center 10301 9th St. N St. Petersburg, FL 33716	(727) 563-5151 (727) 563-5180 (Fax) gmiller@celotex.com
George Lennox The Dow Chemical Company 200 Larkin, 1605 Joseph Drive Midland, MI 48674	(517) 638-4318 (517) 636-0194 (Fax) ghlennox@dow.com
Heinz F. Poppendiek Geoscience Ltd 6260-B Marindustry Drive San Diego, CA 92121	(858) 453-5483 (858) 453-4694 (Fax) ---
Tim Kunz Holometrix 25 Wiggins Avenue Bedford, MA 01730	(781) 275-3300 (781) 275-3705 (Fax) tkunz@holometrix.com
John R. Mumaw Integrex Testing Systems 2790 Columbus Rd., Rt 16 Granville, Ohio 43023-1200	(740) 321-7068 (740) 321-4067 (Fax) john.mumaw@owenscorning.com
Michel Drouin Johns Manville P. O. Box 398 Cornwall, Ontario, K6H 5T1, Canada	(613) 932-6352 (613) 932-8060 (Fax) drouinm@jm.com

Timothy R. Jonas
Knauf Fiber Glass Gmbh
240 Elizabeth Street
Shelbyville, IN 46176

(317) 398-4434
(317) 392-8181 (Fax)
trj1@knauffiberglass.com

Dan Otis
L. L. Bean, Inc
Casco Street
Freeport, ME 04033

(207) 552-2461
(207) 552-6851 (Fax)
dotis@llbeam.com

David Indyke
The Mexmil Company
2865 South Pullman Street
Santa Ana, CA 92705

(949) 250-4999
(949) 250-4556 (Fax)
david.indyke@mexmil.com

Robert Zarr
NIST
100 Bureau Drive, MS 8632
Gaithersburg, MD 20899-8632

(301) 975-6436
(301) 975-5433 (Fax)
rzarr@nist.gov

Barbara Fabian
Owens Corning
275 Southwest Ave.
Tallmadge, OH 44278

(330) 633-6735, x211
(330) 633-4939 (Fax)
barbara.fabian@owenscorning.com

Heng Wang
Precision Measurement and
Instrument Co.
3665 SW Deschutes Street
Corvallis, OR 97333

(541) 753-0607
(541) 753-0610 (Fax)
hengwang@pmiclab.com

Ronald S. Graves
R&D Services, Inc.
P. O. Box 2400
Cookeville, TN 38502-2400

(931) 372-8871
(931) 525-3896 (Fax)
rdserv2@charter.net

Mike Zieman
RADCO
3220 E. 59th St.
Long Beach, CA 90805

(562) 272-7241
(562) 529-7513 (Fax)
mzieman@radcoinc.com

Dwight Musgrave
Thermal Visions, Inc.
83 Stonehenge Rd.
Granville, OH 43023

(740) 587-4025
(740) 587-4025 (Fax)
dwight.musgrave@thermalvisions.com

F. B. Hutto, Jr.
Tutco Scientific
676 Peony Drive
Grand Junction, CO 81503

(970) 245-7763
(970) 245-7763 (Fax)
tutco@gj.net

Ken Rhodes
Underwriters Laboratories, Inc.
353 Pfingsten Road
Northbrook, IL 60062-2096

(847) 664-2211

Addendum C2: Addresses Of Twenty-One Responders To ES - 2001

Name and Address	Telephone, Fax Number, and E-Mail Address
Richard Troyer Architectural Testing, Inc. 130 Derry Ct. York, PA 17402-9405	(717) 764-7700 (717) 764-41229 (Fax) rtroyer@testati.com
Roy Pask BASF Corporation 1609 Biddle Avenue Wyandotte, MI 48192	(734) 324-6308 (734) 324-6301 (Fax) paskr@basf.corp.com
Stacy Blake Dow Chemical 1881 West Oak Parkway Marietta, GA 30062	(678) 269-1298 (770) 590-3539 (Fax) sjblake@dow.com
Robert Braun The Dow Chemical Co. 2050 N. Broadway Joliet, IL 60435	(815) 774-6500 (815) 774-3760 (Fax) bgbraun@dow.com
Jess Garcip Dow Chemical Company 2050 N. Broadway Joliet, IL 60435	(815) 727-1472 (815) 774-6542 (Fax) jmgarcip@dow.com
Linda M. Hess Dow Chemical 1605 Joseph Drive Midland, MI 48642	(989) 636-5069 (989) 636-0194 (Fax) lindahess@dow.com
Joe Creazzo DuPont Co. P. O. Box 80711 Wilmington, DE 19880-0711	(302) 999-4167 (302) 999-2093 (Fax) joseph.a.creazzo@usa.dupont.com
Tim Tackett Firestone Building Products 525 Congressional Blvd. Carmel, IN 46032	(317) 575-7109 (317) 575-7227 (Fax) tdtackett@firestonebp.com

Abbas Shekari
Foam Enterprises
1703 Crosspoint
Houston, TX 77054
(731) 796-9743
(731) 796-1530 (Fax)
abbas_shekari@foamenterprizes.com

Kathy Devlin-LaFountaine
General Plastics Mfg. Co.
4910 Burlington Way
Tacoma, WA 98404
(253) 473-5000
(253) 473-5104 (Fax)
Kathy_Devlin@generalplastics.com

John Bowers
Huntsman Polyurethanes
286 Mantua Grove Road
West Deptford, NJ 08066
(856) 423-8524
(856) 423-8502 (Fax)
john_d_bowers@hunstsman.com

Les Truksa
Insultech Inc.
100 Milvan Drive
Weston, Ontario, M9L 126, Canada
(416) 746-8989
(416) 746-4829 (Fax)
triska@ica.net

Mark Albers
Johns Manville
JMTC
10100 W. Ute Avenue
Littleton, CO 80127
(303) 978-5008
(303) 978-3123 (Fax)
albersm@jm.com

Kevin P. Collins
Lasercomp, Inc.
20 Spring Street
Saugus, MA 01906
(781) 233-1717
(781) 981-2484 (Fax)
www.lasercom.com

Rick L. Dobin/Max Lopez
Mesa Insulation
1110 16 Road
Fruita, CO 81521
(970) 858-6209
(970) 858-1018 (Fax)
dolinr@jm.com

Thomas Kenney
NAHB Research Center
400 Prince George's Blvd.
Upper Marlboro, MD 20774
(301) 430-6246
(301) 430-6246 (Fax)
tkenney@nahbrc.org

Micheline Roy
OC Celfortec, Inc.
542 Gaetan
Grande-Ile, Quebec, J6S 4V3 Canada
(450) 377-1725, x5025
(450) 377-2973 (Fax)
micheline.roy@owenscorning.com

K. M. Stalnaker
OSI Specialties
3200 Kanawha Turnpike
South Charleston, WVA 25303

(304) 746-1670
(304) 746-1801 (Fax)
stalnka@cromptoncorp.com

Barbara Fabian
Owens Corning
275 Southwest Ave
Tallmadge, OH 44278

(330) 633-6735, x211
(330) 633-4939 (Fax)
barbara.fabian@owenscorning.com

Ronald S. Graves
R & D Services, Inc.
P. O. Box 2400
Cookeville, TN 38502-2400

(931) 372-8871
(931) 525-3896 (Fax)
rdserv2@charter.net

David W. Yarbrough
Tennessee Technological University
TTU Box 5013
Cookeville, TN 38505

(931) 372-3494
(931) 372-6352 (Fax)
rdserv1@charter.net

Addendum D. Minutes of Meetings of C16.30.1.6 Test Equipment Survey Task Group

First Meeting: This Task Group met April 19, 1999 in Seattle with seven members: David L. McElroy, Kenneth E. Wilkes, Mark Leuthold, John Scott, Gerry Miller, Robert Zarr, and Cliffe Shirtliffe. The initial survey will focus on test equipment that meets C335 and C1033. The survey form will be similar to that used by Gerry Miller and Bill Goss in 1991 for the Hot Box Survey. We believe the survey will obtain information that will be beneficial to future revisions of Test Method Standards.

Second Meeting: This Task Group met from 4 to 5 PM on Monday, October 4, 1999, in San Antonio. Present were: Randi Gerrish, Francis Hutto, Tim Jonas, Gerry Miller, Dave McElroy, Roger C. Oxford, John Scott, and Bob Zarr. The Task Group reviewed ASTM equipment surveys and pipe insulation interlaboratory tests to obtain a limited questionnaire. This survey will be conducted in 2000 to identify: (1) Who has pipe tester insulation testers? and, (2) Are they willing to participate in interlaboratory tests?

Third Meeting: Task Group C16.30.1.6, Test Equipment Survey, met from 4 to 5 PM on Monday, April 10, 2000 in Toronto. Twelve Members were present: Mark Albers, Bill Brayman, Andre Désjarlais, Francis Hutto, Tim Jonas, Kumar Kumaran, Dave McElroy, Gerry Miller, John Mumaw, John Scott, Ken Wilkes, and Bob Zarr. The Task Group reviewed and modified a set of equipment survey questions for five standards: C177, C1114, C518. C335, and C1033. ASTM will mail this to all C16 members in May 2000. The forms are to be returned to M. Long, ASTM, by August 1, 2000. Others to be surveyed include: NVLAP Labs, SRM-1450 buyers, and Equipment Buyers by Equipment Manufacturers.

Fourth Meeting: Task Group C16.30.1.6, Test Equipment Survey, met from 4 to 5 PM on Monday, October 30, 2000 in Charlotte. Eight Members were present: Randi Gerrish, Tim Jonas, Tim Kunz, Gerry Miller, John Scott, Tom Whitaker, Ken Wilkes, and Bob Zarr. This meeting was chaired by John Scott in Dave McElroy's absence. The Task Group reviewed input from 13 responders on the thermal equipment survey of C518, 177, 1114, 335, and 1033 equipment. The Task Group agreed to ask C16 to again issue the survey to all C16 members to try to generate further input for the database. We will request further input by December 31, 2000. Equipment manufacturers will be asked to circulate the survey to their customers for input. It was suggested by the Task Group that the findings of the survey be documented in one or both of the following ways: 1. ASTM Research Report, 2. Electronic Storage on ASTM Web Site for future reference and up dating. This Task Group will require a table for the next C16.30 meeting.

Fifth Meeting: Task Group C16.30.1.6, Test Equipment Survey, met from 4 to 5 PM. on Monday, April 2, 2001 in Phoenix. Nine members were present: Mark Albers, Bill Brayman, Andre Désjarlais, Francis Hutto, Tim Jonas, Tim Kunz, Dave McElroy, Cliffe Shirtliffe, and Tom Whitaker. The history of the Equipment Survey (ES-2000) was reviewed. Mailouts totaling over 350 (C16: 320; NVLAP labs: 18; SRM purchasers: 24) has yielded 19 responses (about 5%). Causes for the low response are not known. Future plans include

thanking the 19 responders; distributing a much, much simpler Equipment Survey (ES-2001) with a reply date of September 1, 2001; and asking only: "Do you have equipment that meets C177, C518, C335, C1114, or C1033?"

Sixth Meeting: Task Group C16.30.1.6, Test Equipment Survey, met from 4 to 5 PM on Monday, October 15, 2001, in Deerfield Beach, FL. This meeting was chaired by John Scott. The task group met with six members present. A finished report on C177, 518, 335, 1033 and 1114 equipment availability and location was reviewed. One of the labs missing information will be added to the report. A cover page will be written for the report and will be issued to ASTM as a research report. This report can then be referenced within the respective standards for ease of finding equipment for round robin candidates. Valuable suggestions for standard improvement and round robin materials were also suggested. Copies of the report will also be circulated to the task group chairs. This task group has completed its' goal and will now be disbanded. The task group would like to thank Dave McElroy for his work on this report.

Author Index

Subject Index